



RESEARCH & DEVELOPMENT

Continuing Toward Implementation of Performance Engineered Concrete Mixtures for Durable and Sustainable Concrete

Tara L. Cavalline, Ph.D., P.E.

Brett Q. Tempest, Ph.D., P.E.

Peter Theilgard

David Alex Dillworth

Joseph OCampo

**Department of Engineering Technology and Construction
Management**

Department of Civil and Environmental Engineering

University of North Carolina at Charlotte

9201 University City Boulevard

Charlotte, North Carolina 28223-0001

NCDOT Project 2020-13

FHWA/NC/2020-13

February 2023

1. Report No. FHWA/NC/2020-13	2. Government Accession No.	3. Recipient's Catalog No.	
4. Title and Subtitle Continuing Toward Implementation of Performance Engineered Concrete Mixtures for Durable and Sustainable Concrete		5. Report Date February 7, 2023	
		6. Performing Organization Code	
7. Author(s) Tara L. Cavalline, Ph.D., P.E., Brett Q. Tempest, Ph.D., P.E., Peter Theilgard, David Alex Dillworth, Joseph OCampo		8. Performing Organization Report No.	
9. Performing Organization Name and Address Department of Engineering Technology and Construction Management Department of Civil and Environmental Engineering University of North Carolina at Charlotte 9201 University City Boulevard Charlotte, NC 28223-0001		10. Work Unit No. (TRAIS)	
		11. Contract or Grant No.	
12. Sponsoring Agency Name and Address North Carolina Department of Transportation Research and Development Unit 104 Fayetteville Street Raleigh, North Carolina 27601		13. Type of Report and Period Covered Final Report August 1, 2019 – June 30, 2022	
		14. Sponsoring Agency Code 2020-13	
Supplementary Notes:			
16. Abstract <p>Extensive research in recent decades has led to new understanding of concrete deterioration mechanisms, advancements in concrete mixture design, and development of better field and laboratory tests for QA and QC. With this new knowledge, an FHWA initiative is underway to improve the performance of concrete infrastructure through performance engineered concrete mixtures (PEM). Work included in this project leveraged progress from the <u>initial</u> efforts of NCDOT to move towards a specification for PEM initiated as part of NCDOT RP 2018-14 and RP 2019-41, along with the extension of findings from other ongoing related research on concrete materials to support specifications for and use of more durable and sustainable concrete mixtures in North Carolina highway infrastructure. This project included laboratory evaluation to expand the catalog of data available to refine specifications and targets for several PEM tests, including surface resistivity, shrinkage, Super Air Meter (SAM), and strength. Emphasis was placed on evaluating the potential benefits that could be achieved through use of optimized aggregate gradation mixtures and lower paste contents. Resources and tools to support quality assurance (QA) and quality control (QC) of structural and pavement concrete were developed, and the surface resistivity meter was also evaluated for use in evaluating the quality of overlay concrete. PEM tests were also used in the field as part of a second pilot project, which included construction of structures along an interstate widening project south of Charlotte, NC. The test results were analyzed, and recommendations regarding targets and PEM specification approaches were provided. Overall, this work should support 1) cost savings associated with longer service life and reduced maintenance costs for concrete pavements, bridges, and other infrastructure 2) an enhanced focus on quality during construction, driven by performance-based requirements, 3) guidance on interpretation of laboratory testing results and the impact on performance, 4) improved QA and QC testing particularly the use of new and emerging PEM tests from AASHTO PP 84 (now R 101), and 5) further implementation of PEM tests and specifications by NCDOT.</p>			
17.		18. Distribution Statement	
19. Security Classif. (of this report) Unclassified	20. Security Classif. (of this page) Unclassified	21. No. of Pages 232	22. Price

DISCLAIMER

The contents of this report reflect the views of the author(s) and not necessarily the views of the University. The author(s) are responsible for the facts and the accuracy of the data presented herein. The contents do not necessarily reflect the official views or policies of either the North Carolina Department of Transportation or the Federal Highway Administration at the time of publication. This report does not constitute a standard, specification, or regulation.

ACKNOWLEDGMENTS

This research project was sponsored by the North Carolina Department of Transportation (NCDOT) and their continued support is greatly appreciated. The research team would like to express their appreciation to the following:

- The NCDOT personnel serving on the Steering and Implementation Committee for this research study. In particular, we would like to thank Brian Hunter, Chair of the Steering and Implementation Committee for his insight, assistance, and support. Feedback received from all members of the Steering and Implementation Committee (Ben Chola, Joshua Law, Aaron Earwood, Cameron Cochran, Todd Whittington, Clark Morrison, and Jim Phillips) during the course of this project was greatly appreciated.
- NCDOT Research and Development personnel, particularly Mustan Kadhibhai and Neil Mastin.
- Material suppliers for their generous donations of aggregates, cementitious materials, and admixtures supporting this research.
- Wesley Maxwell, Research Operations Manager, UNC Charlotte Department of Engineering Technology and Construction Management.
- UNC Charlotte Graduate Research Assistant Allison Summers.
- UNC Charlotte Undergraduate Research Assistants Austin Yorke, Clarke Summers, Alex Nowatkowski, James Decker, Michael Wright, Brandon Ellis, and Kyle Stewart.
- Jake Leflore of Oklahoma State University for providing SAM training session to support the pilot project.
- The following individuals generously supported the pilot project effort:
 - Sam Lenoble, Stephan Marcella, and Jerry Queen - Blythe Construction
 - Kevin Cero, Darin Waller, Aaron Earwood, Michael Smith, Brian Davis, Sam Frederick, and Roman Loshinskiy - NCDOT
 - Rob Cousins, Jason Stafford, and Dylan Owen - Summit Design and Engineering
 - Joe Beato and Parker Guffey – RK&K
 - Kevin Bridges – SEPI, Inc.
 - Adam Neuwald, Patrick Baker, Dustin Heiland, TJ Harris, Jason Bradley - Concrete Supply Co.
 - Greg Williams - Wood

EXECUTIVE SUMMARY

The long service life expectations of pavements, bridges, and other components cannot be reliably met by using traditional tests for specification and acceptance, which center around three criteria: slump, air content, and compressive strength. These three criteria are only loosely related to deterioration phenomena and do not always ensure satisfactory field performance. Consistent with the focus of MAP-21 legislation on performance, the FHWA, public agencies, and industry are moving towards performance engineered construction materials for more durable and sustainable concrete infrastructure. Performance engineered mixtures (PEM) include optimized mixture designs (materials selection, gradation, cement content etc.) that provide improved durability and sustainability. FHWA has established the PEM Initiative, which focuses on state agency implementation of PEM guidance provided in AASHTO PP 84, “Standard Practice for Developing Performance Engineered Concrete Pavement Mixtures.” Recently, this provisional standard has been approved as a practice standard, renamed, AASHTO R 101, “Developing Performance Engineered Concrete Mixtures” (AASHTO 2022). Although developed for pavement concrete mixtures, the approach outlined in AASHTO PP 84 and R 101 could be extended to include specifications for PEMs utilized for other infrastructure, such as bridges, barriers, and lower grade uses.

There are tangible benefits to moving towards performance specifications for concrete, as seen in other states. However, each agency must do the groundwork necessary to identify the components of PEM concrete specifications appropriate for their agency and local stakeholders, including identification of desired tests and specification approaches, performance targets, and training/technology transfer for all stakeholders. Nationally, the PEM initiative is a dynamic effort that is a key, current focus of many state agencies, researchers, and industry partners. The FHWA, other state agencies, and academic institutions continue to make advancements in the basic science behind key PEM tests, identification of QA and QC and specification approaches, and links to performance data.

NCDOT’s preliminary work to support PEM included RP 2018-14 (Cavalline et al. 2020a) and RP 2019-41 (Cavalline et al. 2020b, Cavalline et al. 2022), which provided early steps towards performance specifications for concrete infrastructure and deployment of several PEM approaches in an interstate pavement project. Work included in this project leveraged progress from these initial efforts along with findings from other ongoing related research on concrete materials to support specifications for and use of more durable, sustainable concrete mixtures in North Carolina highway infrastructure. Laboratory evaluation to expand the catalog of data available to refine specifications and targets for several PEM tests, including surface resistivity, shrinkage, Super Air Meter (SAM), and strength, was performed. Emphasis was placed on evaluating the potential benefits that could be achieved through use of optimized aggregate gradation mixtures and lower paste contents. It was found that compressive and flexural strengths were roughly equivalent between optimized and non-optimized mixtures, indicating that current NCDOT specifications could reasonably be met by mixtures containing a 10% reduction in cementitious materials and a 2-3% reduction in paste volume. This could offer both economic and sustainability benefits. Durability performance benefits could be realized by optimized aggregate gradation mixtures as well, with later age shrinkage measurements showing improvements over conventional mixtures. Electrical tests to evaluate permeability appeared to be influenced by the additional interfacial transition zone (ITZ) of the optimized gradation mixtures, and performance targets may need to be adjusted. The freeze-thaw durability of both optimized gradation and non-optimized gradation concrete mixtures was excellent, and recommendations regarding air void system parameters and the SAM target are provided.

Resources and tools to support quality assurance (QA) and quality control (QC) of structural and pavement concrete were developed, and the surface resistivity meter was also evaluated for use in evaluating the quality of overlay concrete. A procedure using the surface resistivity meter was developed, and overlay thickness was successfully evaluated. Guidance regarding the influence of conditions such as edges, reinforcing steel, and voids on field surface resistivity measurements was also prepared.

PEM tests were also used in the field as part of a second pilot project, which included the construction of structures along an interstate widening project south of Charlotte, NC. The test results were analyzed, and recommendations regarding targets and PEM specification approaches are provided. Surface resistivity measurements reaffirmed the proposed targets for structural concrete developed as part of laboratory studies. SAM data continued to show variability, but the variability in this data is reduced from that observed in the initial pilot study. This is likely due to a training session held by the developer, use of selected technicians, and more frequent use of the SAM.

Overall, this work should support 1) cost savings associated with longer service life and reduced maintenance costs for concrete pavements, bridges, and other infrastructure 2) an enhanced focus on quality during construction, driven by performance-based requirements, 3) guidance on interpretation of laboratory testing results and the impact on performance, 4) improved QA and QC testing particularly the use of new and emerging PEM tests, and 5) further implementation of PEM tests and specifications by NCDOT.

TABLE OF CONTENTS

DISCLAIMER	iii
ACKNOWLEDGMENTS	iv
EXECUTIVE SUMMARY	v
LIST OF TABLES	ix
LIST OF FIGURES	xii
LIST OF ABBREVIATIONS	xvii
1.0 INTRODUCTION AND RESEARCH OBJECTIVES	1
1.1 Introduction	1
1.2 Performance Engineered Mixtures - Materials, Mixture Parameters, and Specifications	2
1.3 Construction QA and QC for Performance Engineered Mixtures	3
1.4 Implementation of Performance Engineered Mixtures	3
1.4.1 Implementation Efforts of Other State Highway Agencies	3
1.4.2 North Carolina DOT's PEM Implementation Efforts to Date	4
2.0 LITERATURE REVIEW - OVERVIEW	6
3.0 OPTIMIZED AGGREGATE GRADATION MIXTURES	6
3.1 Concrete Mixtures	6
3.2 Materials Description and Characterization	12
3.2.1 Cementitious Materials	12
3.2.2 Aggregates	13
3.2.3 Admixtures	13
3.3 Testing Program and Results	13
3.3.1 Fresh Concrete Properties	14
3.3.2 Mechanical Properties	14
3.3.2.1 Compressive Strength	14
3.3.2.2 Modulus of Rupture	18
3.3.2.3 Modulus of Elasticity	20
3.3.2.4 Poisson's Ratio	23
3.3.3 Durability Performance	24
3.3.3.1 Surface Resistivity	24
3.3.3.2 RCPT	31
3.3.3.3 Formation Factor	37
3.3.3.4 Volumetric Shrinkage	38
3.4 Summary of Laboratory Findings	41
4.0 PERFORMANCE TARGETS FOR FREEZE-THAW DURABLE CONCRETE	45
4.1 Introduction	45
4.2 Limitations	45
4.3 Methods and Test Results	45
4.3.1 Fresh Air vs. Spacing Factor	48
4.3.2 Fresh Air vs. Durability Factor	49
4.3.3 Fresh Air vs. SAM Number	50
4.3.4 Spacing Factor	51
4.3.5 Durability Factor	52
4.4 Development of Recommended SAM Specification	53
4.5 Conclusions	54

5.0 USE OF SURFACE RESISTIVITY METER TO EVALUATE BRIDGE DECK OVERLAYS	55
5.1 Test Specimen Preparation	55
5.2 Test Methods	59
5.3 Results	61
5.3.1 Reinforced Cylinder Specimens	62
5.3.2 Miniature Slab Specimens	66
5.3.3 Bridge Deck Mockups	67
5.4 Summary of Findings	72
5.5 Field Evaluation Procedure	73
6.0 TECHNOLOGY TRANSFER AND TRAINING TO SUPPORT PEM	74
7.0 PILOT PROJECT IMPLEMENTATION	76
7.1 Surface Resistivity	76
7.2 SAM	80
7.3 Shrinkage	81
7.4 Conclusions	82
8.0 SUMMARY AND CONCLUSIONS	83
9.0 VALUE OF RESEARCH FINDINGS AND RECOMMENDATIONS	85
9.1 Value of Research Findings	85
9.2 Recommendations	86
10.0 IMPLEMENTATION AND TECHNOLOGY TRANSFER PLAN	87
11.0 REFERENCES	89
APPENDICES	
APPENDIX A – LITERATURE REVIEW and REFERENCES	A-1
A.1 Introduction	A-1
A.1.1 Strength	A-1
A.1.2 Durability	A-1
A.1.3 Economy	A-3
A.1.4 Sustainability	A-4
A.1.5 AASHTO PP 84 and R 101	A-4
A.1.5.1 Overview	A-4
A.1.5.2 Strength Provisions	A-5
A.1.5.3 Durability Provisions	A-5
A.2 Optimized Aggregate Gradations (Material Supporting Chapter 3)	A-6
A.2.1 Particle Packing	A-6
A.2.2 Aggregate Gradation Methods	A-7
A.2.3 Tarantula Curve	A-9
A.3 Freeze-Thaw Durable Concrete (Material Supporting Chapter 4)	A-10
A.3.1 Freeze-Thaw Stresses	A-10
A.3.2 Deicing Salts	A-12
A.3.3 Concrete Deterioration Due to Freeze-Thaw Stresses	A-12
A.3.3.1 Theories of Freeze-Thaw Stress Action	A-12
A.3.3.1.1 Hydraulic Pressure Theory	A-12
A.3.3.1.2 Osmotic Pressure Theory	A-13
A.3.3.1.3 Ice-Lens Model Theory	A-13
A.3.4 Distress Mechanisms	A-14
A.3.4.1 Internal Cracking	A-14

A.3.4.2 Surface Scaling Due to Deicing Salts	A-14
A.3.5 Mitigation Strategies	A-15
A.3.5.1 Concrete Permeability	A-15
A.3.2.6 Air Entrainment	A-16
A.3.6 Tests to Evaluate Concrete Freeze-Thaw Durability	A-17
A.3.6.1 Total Air Content of Fresh Concrete	A-17
A.3.6.2 Super Air Meter	A-18
A.3.6.3 Freeze-Thaw Testing of Hardened Concrete	A-19
A.3.6.4 Hardened Air Void System Analysis	A-20
A.3.7 Research Needs for Freeze-Thaw Durable Concrete in North Carolina	A-21
A.4 Surface Resistivity for Use in Overlay Evaluation (Material Supporting Chapter 5)	A-21
A.4.1 Introduction	A-21
A.4.2 Bridge Deck Overlays	A-22
A.4.3 General Overview and Design Considerations	A-22
A.4.3.1 Materials	A-22
A.4.3.1.1 Latex Admixtures	A-23
A.4.3.1.2 Cementitious Materials	A-23
A.4.3.1.3 Aggregate	A-23
A.4.3.2 Construction Methods	A-24
A.4.3.2.1 Surface Demolition and Preparation Methods	A-24
A.4.3.2.2 Batching and Placement	A-24
A.4.3.3 Challenges	A-24
A.4.4 Quality Assurance and Quality Control Methods	A-25
A.4.4.1 Non-destructive Evaluation (NDE) for Construction Quality Assurance and Control	A-26
A.4.4.2 Introduction to NDE and Value to Construction	A-26
A.4.5 Surface Resistivity	A-26
A.4.6 Use of Surface Resistivity in Field Settings	A-28
A.4.6.1 Influences on Surface Resistivity	A-29
A.4.6.2 Use of Surface Resistivity on Bridge Deck Overlays	A-32
A.4.7 Research Needs	A-32
A.5 References	A-32
 APPENDIX B – SUPPORTING MATERIAL FOR LABORATORY TESTING PROGRAM AND RESULTS (Chapter 3)	 B-1
 APPENDIX C – SUPPORTING MATERIAL FOR IDENTIFICATION of PERFORMANCE TARGETS FOR FREEZE-THAW DURABLE CONCRETE (Chapter 4)	 C-1
 APPENDIX D – SUPPORTING MATERIAL FOR USE OF SURFACE RESISTIVITY METER TO EVALUATE BRIDGE DECK OVERLAYS (Chapter 5)	 D-1
 APPENDIX E – DRAFT FIELD EVALUATION PROCEDURE FOR USE OF SURFACE RESISTIVITY METER TO EVALUATE BRIDGE DECK OVERLAYS (Chapter 5)	 E-1
 APPENDIX F – SUPPORTING MATERIAL FOR PILOT PROJECT (Chapter 7)	 F-1

LIST OF TABLES

Table 3.1: Concrete mixtures with material proportions for RP 2018-14 (non-optimized aggregate gradations)	9
Table 3.2: Mixture proportions for non-optimized gradation mixtures (RP 2018-14) and optimized gradation mixtures (RP 2020-13)	12
Table 3.3: Testing program	13
Table 3.4: Average percent difference between average compressive strength for 700* pcy optimized mixtures vs 700 pcy non-optimized mixtures	17
Table 3.5: Average percent difference between average compressive strength for 700* pcy optimized mixtures vs 700 pcy non-optimized mixtures by w/cm ratio	18
Table 3.6: MOR, MOE, and Poisson's Ratio	19
Table 3.7: Average percent difference between optimized aggregate gradation mixtures MOR and companion mixtures	20
Table 3.8: Table 3.8. Average percent difference in MOE between optimized mixtures, non-optimized mixtures calculated per ACI 318 and AASHTO LRFD	22
Table 3.9: Average 28-day MOE of optimized aggregate gradation mixtures and non-optimized aggregate gradation mixtures by cementitious content	22
Table 3.10: Average percent difference in 28-day MOE by type of mixture	22
Table 3.11: Average percent difference between Poisson's ratios	23
Table 3.12: Average percent difference in Poisson's ratios between all optimized fly ash replacement mixtures and their companion mixtures, grouped by fly ash replacement rate	24
Table 3.13: AASHTO T 358 surface resistivity index	24
Table 3.14: Surface resistivity and RCPT results for optimized aggregate gradation and non-optimized aggregate gradation mixtures	25
Table 3.15: Average percent difference between surface resistivity of 700* pcy optimized mixtures and companion 700 pcy non-optimized mixtures	27
Table 3.16: Average percent difference between surface resistivity of 700* pcy optimized straight cement and fly ash replacement mixtures surface resistivity compared with companion 700 pcy non-optimized mixtures	27
Table 3.17: Average percent difference between 650* pcy optimized surface resistivity and their companion 650 pcy non-optimized mixtures	28
Table 3.18: Average percent difference between 650* pcy optimized straight cement and fly ash replacement mixtures surface resistivity compared with companion 650 pcy non-optimized straight cement and fly ash replacement mixtures	28
Table 3.19: Average percent difference in surface resistivity between 600* pcy optimized and companion 600 pcy non-optimized mixtures	29
Table 3.20: Average percent difference between 600* pcy optimized straight cement and fly ash replacement mixtures surface resistivity compared with companion 600 pcy non-optimized straight cement and fly ash replacement mixtures	30
Table 3.21: Average surface resistivity of all mixtures grouped by w/cm ratio, along with their average percent difference between pairs of optimized and non-optimized mixtures	30
Table 3.22: Average surface resistivity of all mixtures grouped by cementitious content (pcy) and the average percent difference between optimized and non-optimized mixtures	30
Table 3.23: Average surface resistivity and the average percent difference of all optimized aggregate gradation mixtures straight cement and fly ash mixtures grouped by w/cm ratio	31
Table 3.24: Average surface resistivity and the average percent difference of all optimized aggregate gradation mixtures straight cement and fly ash mixtures grouped by cementitious content (pcy)	31
Table 3.25: ASTM C1202 RCPT index	31
Table 3.26: Average percent difference between RCPT test results for optimized aggregate gradation and non-aggregate gradation mixtures grouped by cementitious content	33
Table 3.27: Average percent difference between RCPT test results of optimized aggregate gradation and non-aggregate gradation mixtures grouped by w/cm ratio	33
Table 3.28: Average percent difference between RCPT test results of optimized aggregate gradation and non-aggregate gradation straight cement and fly ash replacement mixtures grouped by w/cm ratio	33
Table 3.29: Surface area factor of aggregates	35

Table 3.30: Estimated surface area for optimized and non-optimized mixtures	35
Table 3.31: Surface resistivity, RCPT, and difference of surface area from aggregates of all mixtures	36
Table 3.32: Chloride ion penetrability associated with various formation factor values	37
Table 3.33: Volumetric shrinkage results and average percent difference of optimized and non-optimized straight cement and fly ash replacement mixtures microstrains by w/cm ratio	40
Table 3.34: Average volumetric shrinkage and average percent difference of optimized and non-optimized mixtures grouped by w/cm ratio	41
Table 3.35: Average volumetric shrinkage and average percent difference of optimized and non-optimized mixtures grouped by cementitious material content	41
Table 4.1: Results of durability testing for all mixtures	46
Table 4.2: Design Mix Performance Criteria (WVDOT)	53
Table 5.1: Concrete proportions for bridge deck overlay slabs	55
Table 5.2: Number of 6 in. x 12 in. cylinders for preliminary testing	55
Table 5.3: Change in surface resistivity (k Ω -cm) per change in cover depth (increments of 0.5 in.)	65
Table 5.4: Rate of change (ROC) correction factors that could be used to estimate the surface resistivity of each overlay material at different ages per 1 inch increment in thickness change	71
Table 7.1: Summary statistics for surface resistivity test results for QA cylinders for pilot project	45
Table A.1 Projected cost savings with 10% reduction in cementitious material	78
Table A.2: CO ₂ emission reduction per lane mile	A-3
Table A.3: Prescriptive testing requirements	A-3
Table A.4: AASHTO PP 84 prescriptive and performance requirements	A-5
Table A.5: Table A.5: Comparison between the permeability of rocks and cement pastes (Mehta and Montiero 2006, originally from Powers 1958)	A-6
Table A.6: Time required to achieve a discontinuous pore structure (Powers et al. 1959) values (LADOTD 2018)	A-16
Table A.7: Summary of agency specification RCPT and surface resistivity requirements	A-21
Table A.8: Surface resistivity geometry correction factor	A-21
Table A.9: NCDOT Equipment Load Restrictions for Bridges (NCDOT 2018)	A-28
Table A.10: MnDOT Curing Requirements for Concrete Bridge Elements (MnDOT 2018)	A-27
Table A.11: MnDOT Minimum Requirements for Opening Pavements to General Traffic (MnDOT 2018)	A-28
Table A.12: Minnesota Concrete Mix Design Requirements (MnDOT 2018)	A-28
Table A.13: Minnesota High Early Strength Design Requirements (MnDOT 2018)	A-29
Table A.14: New York Allowable Pozzolan Substitutions (NYSDOT 2019)	A-30
Table A.15: Minimum Time for Form Removal and Loading Limitations for Substructures in New York (NYSDOT 2019)	A-30
Table A.16: High Early Strength Concrete Requirements for New York (NYSDOT 2019)	A-31
Table A.17: Maximum Permissible Florida DOT Cementitious Materials and Mixture Proportions (%) (FDOT 2019)	A-31
Table A.18: Florida DOT Concrete Master Proportions (FDOT 2019)	A-32
Table A.19: Florida DOT Cement Use by Environmental Classification (FDOT 2019)	A-33
Table A.20: FDOT Concrete class, Compressive Strength, and Slump Requirements (FDOT 2019)	A-34
Table A.21: IowaDOT Cement Types and Substitution for Portland Cement Concrete with Class V Aggregates (IowaDOT 2015)	A-35
Table A.22: IowaDOT Maximum Allowable Substitution Rates for Concrete Bridge Decks (IowaDOT 2015)	A-35
Table A.23: IowaDOT Minimum Age Requirements for Loading Concrete Structures (IowaDOT 2015)	A-35
Table A.24: Minimum Flexural Strength for Opening Concrete Pavements (IowaDOT 2015)	A-36
Table A.25: Mix Design Criteria for IDOT (IDOT 2016)	A-36
Table B.1: Fresh concrete test results (average of two batches comprising a single mixture) for RP 2018-14 (non-optimized gradation mixtures) and RP 2020-13 (optimized gradation mixtures)	B-4
Table B.2: SAM test results for optimized aggregate gradation mixtures	B-5
Table B.3: 28-day compressive strength results	B-5
Table B.4: Average percent difference between average compressive strength for 650* pcy optimized mixtures vs 650 pcy non-optimized mixtures	B-8
Table B.5: Average percent difference between average compressive strength for 650* pcy optimized mixtures vs 650 pcy non-optimized mixtures by w/cm ratio	B-8

Table B.6: Average percent difference between average compressive strength for 600* pcy optimized mixtures vs 600 pcy non-optimized mixtures	B-8
Table B.7: Average percent difference between average compressive strength for 600* pcy optimized mixtures vs 600 non-optimized mixtures by w/cm ratio	B-8
Table B.8: 28- and 56-day surface resistivities and formation factors for optimized aggregate gradation mixtures	B-17
Table B.9: 28- and 56-day surface resistivities and formation factors for non-optimized aggregate gradation mixtures	B-17
Table B.10: Optimized and non-optimized aggregate gradation mixtures volumetric shrinkage (in microstrain) 28-day reading is used as initial reading	B-18
Table B.11: Optimized aggregate gradation mixtures volumetric shrinkage (in microstrain), 0-day reading is comparator reading per ASTM C157 standard	B-19
Table C.1 Fresh concrete test results for NCDOT RP 2015-03, RP 2016-06, RP 2018-14, and RP 2020-13	C-1
Table D.1: Equation of the line for each age and mixture (X = cover, Y =surface resistivity)	D-5
Table F.1: Testing program proposed for use on pilot project	F-1
Table F.2: Surface resistivity data collected by NCDOT regional laboratory personnel for selected structural concrete mixtures	F-2
Table F.3: Surface resistivity data from QC laboratory	F-9
Table F.4: Surface resistivity data from historical NCDOT projects at low (<0.39) w/cm ratios	F-10
Table F.5: Analysis of low (<0.39) w/cm mixtures meeting pavement and Class AA resistivity targets at selected ages	F-10
Table F.6: Surface resistivity data from historical NCDOT projects at moderate (0.41 to 0.43) w/cm ratios	F-11
Table F.7: Analysis of moderate (0.41 to 0.43) w/cm mixtures meeting pavement and Class AA resistivity targets at selected ages	F-11
Table F.8: Surface resistivity data from historical NCDOT projects at high (>0.47) w/cm ratios	F-12
Table F.9: Analysis of high (>0.47) w/cm mixtures meeting pavement and Class AA resistivity targets at selected ages	F-13
Table F.10: SAM data collected at pilot project	F-14

LIST OF FIGURES

Figure 3.1: Concrete mixture matrix from RP 2018-14 with supporting information	7
Figure 3.2: Concrete mixture matrix for RP 2020-13 with supporting information	8
Figure 3.3: Tarantula Curve recommended gradation boundaries	10
Figure 3.4: Particle sizes of non-optimized mixture H-700-0 on Tarantula Curve	10
Figure 3.5: Particle sizes of H-700*-0 optimized aggregate gradation mixture	11
Figure 3.6: Development of average compressive strength for 700/700* pcy cementitious material mixtures	15
Figure 3.7: Development of average compressive strength for 650/650* pcy cementitious material mixtures	15
Figure 3.8: Development of average compressive strength for 600/600* pcy cementitious material mixtures	16
Figure 3.9: Development of compressive strength for 700/700* pcy cementitious material mixtures at 0.47 w/cm ratio	16
Figure 3.10: Development of compressive strength for 700/700* pcy cementitious material mixtures at 0.42 w/cm ratio	17
Figure 3.11: Development of compressive strength for 700/700* pcy cementitious material mixtures at 0.37 w/cm ratio	17
Figure 3.12: MOR of optimized and non-optimized aggregate gradation mixtures by fly ash content	19
Figure 3.13: MOR of optimized and non-optimized aggregate gradation mixtures by w/cm ratio	20
Figure 3.14: Optimized and non-optimized aggregate gradation mixtures 28-day MOE by w/cm ratio	21
Figure 3.15: MOE vs. 28-day compressive strength, plotted with ACI and AASHTO LRFD calculated MOE	21
Figure 3.16: Poisson's ratio for optimized and non-optimized mixtures at 28-days	23
Figure 3.17: Average surface resistivity for 700/700* pcy cementitious material mixtures	25
Figure 3.18: Average surface resistivity test results for 700/700* pcy cementitious material mixtures at 0.47 w/cm ratio	26
Figure 3.19: Average surface resistivity test results for 700/700* pcy cementitious material mixtures at 0.42 w/cm ratio	26
Figure 3.20: Average surface resistivity test results for 700/700* pcy cementitious material mixtures at 0.37 w/cm ratio	26
Figure 3.21: Average surface resistivity for 650/650* pcy cementitious material mixtures	28
Figure 3.22: Average surface resistivity for 600/600* pcy cementitious material mixtures	29
Figure 3.23: 28-day RCPT results for optimized aggregate gradation and non-optimized aggregate gradation mixtures grouped by w/cm ratio	32
Figure 3.24: 90-day RCPT results for optimized aggregate gradation and non-optimized aggregate gradation mixtures grouped by w/cm ratio	32
Figure 3.25: Surface resistivity plotted against RCPT test results for optimized aggregate gradation and non-optimized aggregate gradation mixtures	34
Figure 3.26: Formation Factors for optimized aggregate gradation mixtures at 28- and 56-days	38
Figure 3.27: Volumetric shrinkage measurements (in microstrain) for optimized and non-optimized aggregate gradation mixtures, measurement after 28-day cure as initial reading	39
Figure 3.28: Volumetric shrinkage measurements (in microstrain) for optimized aggregate gradation mixtures (0-day reading is comparator reading per ASTM C157 standard)	39
Figure 3.29: 16-week volumetric shrinkage measurements (in microstrain) for optimized and non-optimized aggregate gradation mixtures, 28-day as initial reading	40
Figure 3.30: 32-week volumetric shrinkage measurements (in microstrain) for optimized and non-optimized aggregate gradation mixtures, 28-day as initial reading	40
Figure 4.1a: Specimen cast for hardened air void analysis	48
Figure 4.1b: Specimen sawcut, prior to polishing	48
Figure 4.1c: Specimen after face is polished using progressively finer grit	48
Figure 4.2a: Treated specimen prior to scanning.	48
Figure 4.2b: Treated specimen prior to scanning.	48
Figure 4.2c: Scanned image of sample with black and white contrast card (UNC Charlotte ID card) along with Bubble Counter system parameters	48
Figure 4.3: Fresh Air (%) vs. Spacing Factor (in.)	48
Figure 4.4: Fresh Air (%) vs. Spacing Factor (μm)	48
Figure 4.5: Fresh air (%) vs. spacing factor (μm) – OSU data from Ley et al. (2017) with NCDOT mixtures	49

(red data markers)	
Figure 4.6: Fresh air (%) vs. DF	49
Figure 4.7: Fresh air (%) vs. DF	49
Figure 4.8: Fresh air (%) vs. DF – OSU data from Ley et al. (2017) with NCDOT mixtures (red data markers)	50
Figure 4.9: Fresh air (%) vs. SAM number	50
Figure 4.10: Fresh air (%) vs. SAM number	50
Figure 4.11: Fresh air (%) vs. SAM number - OSU data from Ley et al. (2017) with NCDOT mixtures (red data markers)	51
Figure 4.12: Spacing factor (μm) vs. DF - OSU data from Ley et al. (2017) with NCDOT mixtures (red data markers)	51
Figure 4.13: SAM Number vs. Spacing Factor (μm) - OSU data from Appendix of Ley et al. (2017) with NCDOT mixtures overlaid (red data markers)	52
Figure 4.14: SAM Number vs. Spacing Factor (μm) – OSU data from Appendix of Ley et al. (2017) with NCDOT mixtures utilizing off spec fly ash overlaid (red data markers)	52
Figure 4.15: SAM Number vs. DF - OSU data from Ley et al. (2017) with NCDOT mixtures (red data markers)	53
Figure 5.1: Figure 5.1: 6 in by 12 in reinforced cylinder specimen	56
Figure 5.2: Miniature slab forms	56
Figure 5.3 Plan view of bridge deck mockups	57
Figure 5.4: Detail of reinforcing steel in bridge deck mockups	57
Figure 5.5 Typical bridge deck mockup section view	58
Figure 5.6a: Slab mockup forms	58
Figure 5.6b: Mockups after AA deck slab was placed, but prior to overlay placement	58
Figure 5.6c: Mockups with overlay slabs placed (rear three mockups)	58
Figure 5.7a, b, and c: Mockup void placement - (a) LMC, (b) VHES-LMC, and (c) VHES	59
Figure 5.8a: 6 in by 12 in cylinder cross section, with measurement positions labeled 1-4 and embedded rebar shown as blue circle.	59
Figure 5.8b: Typical miniature slab with location and orientation of rebar (shown in black) and test locations (shown in blue)	59
Figure 5.9a: Mockup surface showing grid layout spacing	60
Figure 5.9b: Testing sequence for surface resistivity of mockups	60
Figure 5.10: Typical surface moisture condition after wetting/preparation and attachment to allow surface resistivity measurements to be taken rapidly while standing.	60
Figure 5.11: Schematic showing the three different orientations used when measuring surface resistivity at the 169 measurement points.	60
Figure 5.12: Compressive strength of CC-RM, LMC, VHES, and VHES-LMC used in mockups	61
Figure 5.13: Surface resistivity of CC-RM, LMC, VHES, and VHES-LMC used in mockups	61
Figure 5.14a: Data, radar plot, and schematic of conventional concrete with no rebar	63
Figure 5.14b: Data, radar plot, and schematic of conventional concrete with standard rebar	63
Figure 5.14c: Data, radar plot, and schematic of conventional concrete with epoxy-coated rebar	63
Figure 5.15: Average surface resistivity of cylinders over time	64
Figure 5.16: Surface resistivity vs. concrete cover at selected concrete ages for the CC cylinders	64
Figure 5.17: Average surface resistivity of each mixture vs. concrete cover for each mixture, with specific value of 2.9" cover shown	66
Figure 5.18a: VHES miniature slab 7-day surface resistivity – no reinforcement	66
Figure 5.18b: VHES miniature slab 7-day surface resistivity – standard reinforcement	66
Figure 5.18c: VHES miniature slab 7-day surface resistivity – epoxy-coated reinforcement	66
Figure 5.19: Theoretical effects of edge of slab on surface resistivity meter current field	67
Figure 5.20: Graphical representation of edge effects on measured surface resistivity	68
Figure 5.21: 3-day surface resistivity readings of the LMC overlay mockup, showing edge effects on resistivity readings	69
Figure 5.22: 3-day surface resistivity readings on the VHES-LMC overlay mockup, showing the impact of the tapering overlay slab thickness on resistivity readings	70
Figure 5.23: Foam inclusions (“voids”) superimposed on 7-day surface resistivity readings of LMC mockup	71
Figure 5.24: Average surface resistivity of VHES mockup over time, with measurement points screened and grouped	72

Figure 7.1: Surface resistivity of QA cylinders for Class A mixtures	77
Figure 7.2: Surface resistivity of QA cylinders for Class AA mixtures	77
Figure 7.3: Surface resistivity of QA cylinders for drilled pier mixtures	77
Figure 7.4: Surface resistivity of all QA specimens measured at NCDOT's regional laboratory	77
Figure 7.6: Surface resistivity test results from QC laboratory for a Class A mixture, a Class AA mixture, and a drilled shaft mixture	78
Figure 7.7: Air content from Type B meter vs. SAM air content	80
Figure 7.8: Air content from SAM meter vs. SAM number. Red line shows proposed SAM target for NCDOT	80
Figure 7.9: SAM air content vs. SAM number for mixtures with air content > 5.5%	81
Figure 7.10: SAM air content vs. SAM number for mixtures with air content > 6.0%	81
Figure 7.11: SAM test results performed before and after pumping	81
Figure 7.12: Results of multi-laboratory shrinkage tests of a Class AA mixture and a drilled shaft mixture	82
Figure A.1: Power 0.45 curve (Ley and Cook 2014)	A-8
Figure A.2: Coarseness factor chart	A-8
Figure A.3: Tarantula Curve (Cook et al. 2013)	A-10
Figure A.4: 2D illustration of protective zone (gray) surrounding an air void (white)	A-11
Figure A.5: 2D illustration showing small evenly dispersed air voids	A-11
Figure A.6: 2D illustration showing a lower quality air void system	A-11
Figure A.7: Concrete microstructure (Tanesi and Meininger 2006 originally from Powers and Helmuth 1953)	A-11
Figure A.8: Salt Consumption (US) (Lilek 2017)	A-11
Figure A.9: Visualization of Spacing Factor (adapted from Ken Hover, Cornell)	A-14
Figure A.10: Time required to achieve a discontinuous pore structure (Powers et al. 1959)	A-18
Figure A.11: Spacing factor vs. SAM number (Ley et al. 2017)	A-18
Figure A.12: Correlation for spacing factor vs SAM number (Ley et al. 2017)	A-19
Figure A.13: Correlation for SAM number vs durability factor (Ley et al. 2017)	A-19
Figure A.14: Example of color modified sample	A-20
Figure A.15: Flatbed scanner used to scan samples	A-20
Figure A.16: Example of a color modified sample being scanned	A-20
Figure A.17: Finished scan of a prepared sample	A-20
Figure A.18: Proceq Resipod surface resistivity meter (Proceq 2017)	A-27
Figure A.19: Proceq Resipod measurement schematic (Proceq 2017)	A-27
Figure A.20: Probe configuration to reduce surface resistivity error	A-29
Figure A.21: Effect of contact spacing on resistivity measurement	A-31
Figure A.22: Four-probe square array principal (Lataste et al. 2003)	A-31
Figure B.1: Mill report for OPC	B-1
Figure B.2: Chemical analysis of fly ash	B-3
Figure B.3: Particle size analysis of aggregates used in RP 2018-14 and RP 2020-13	B-3
Figure B.4: Particle size analysis of aggregates used in RP 2020-13: No. 67, No. 89M, and fine aggregate	B-4
Figure B.5: Development of average compressive strength for 650/650* pcy cementitious material mixtures at 0.47 w/cm ratio	B-6
Figure B.6: Development of average compressive strength for 650/650* pcy cementitious material mixtures at 0.42 w/cm ratio	B-6
Figure B.7: Development of average compressive strength for 650/650* pcy cementitious material mixtures at 0.37 w/cm ratio	B-6
Figure B.8: Development of average compressive strength for 600/600* pcy cementitious material mixtures at 0.47 w/cm ratio	B-7
Figure B.9: Development of average compressive strength for 600/600* pcy cementitious material mixtures at 0.42 w/cm ratio	B-7
Figure B.10: Development of average compressive strength for 600/600* pcy cementitious material mixtures at 0.37 w/cm ratio	B-7
Figure B.11: Average surface resistivity test results for 650/650* pcy cementitious material mixtures at 0.47 w/cm ratio	B-9
Figure B.12: Average surface resistivity test results for 650/650* pcy cementitious material mixtures at 0.42 w/cm ratio	B-9
Figure B.13: Average surface resistivity test results for 650/650* pcy cementitious material mixtures at	B-9

0.37 w/cm ratio	
Figure B.14: Average surface resistivity test results for 600/600* pcy cementitious material mixtures at 0.47 w/cm ratio	B-10
Figure B.15: Average surface resistivity test results for 600/600* pcy cementitious material mixtures at 0.42 w/cm ratio	B-10
Figure B.16: Average surface resistivity test results for 600/600* pcy cementitious material mixtures at 0.37 w/cm ratio	B-10
Figure B.17: Surface resistivities of high w/cm ratio optimized concrete mixtures vs percent coarse aggregate volume	B-11
Figure B.18: Surface resistivities of medium w/cm ratio optimized concrete mixtures vs percent coarse aggregate volume	B-11
Figure B.19: Surface resistivities of low w/cm ratio optimized concrete mixtures vs percent coarse aggregate volume	B-12
Figure B. 20: Surface resistivities of high w/cm ratio optimized and non-optimized concrete mixtures vs percent coarse aggregate volume	B-12
Figure B.21: Surface resistivities of medium w/cm ratio optimized and non-optimized concrete mixtures vs coarse aggregate volume	B-13
Figure B.22: Surface resistivities of low w/cm ratio optimized and non-optimized concrete mixtures vs coarse aggregate volume	B-13
Figure B.23: RCPT results of high w/cm ratio optimized concrete mixtures vs coarse aggregate volume	B-14
Figure B.24: RCPT results of medium w/cm ratio optimized concrete mixtures vs coarse aggregate volume	B-14
Figure B.25: RCPT results of low w/cm ratio optimized concrete mixtures vs coarse aggregate volume	B-15
Figure B.26: RCPT results of high w/cm ratio optimized and non-optimized concrete mixtures vs coarse aggregate volume	B-15
Figure B.27: RCPT results of medium w/cm ratio optimized and non-optimized concrete mixtures vs coarse aggregate volume	B-16
Figure B.28: RCPT results of low w/cm ratio optimized and non-optimized concrete mixtures vs coarse aggregate volume	B-16
Figure B.29: 28-day formation factor vs resistivity	B-17
Figure B.30: 56-day formation factor vs resistivity	B-18
Figure D.1: Surface resistivity measurements of LMC cylinders	D-1
Figure D.2: Surface resistivity measurements of VHES cylinders	D-2
Figure D.3: Surface resistivity measurements of VHES-LMC cylinders	D-3
Figure D.4: Surface resistivity vs. concrete cover at selected concrete ages for the LMC cylinders	D-4
Figure D.5: Surface resistivity vs. concrete cover at selected concrete ages for the VHES cylinders	D-5
Figure D.6: Surface resistivity vs. concrete cover at selected concrete ages for VHES-LMC cylinders	D-5
Figure D.7: VHES miniature slabs – 1 and 2 hour surface resistivity measurements	D-6
Figure D.8: VHES miniature slabs - 4 hour and 1 day surface resistivity measurements	D-7
Figure D.9 VHES miniature slabs – 3 and 7 day surface resistivity measurements	D-8
Figure D.10: VHES miniature slabs - 14 and 28 day surface resistivity measurements	D-9
Figure D.11: VHES miniature slabs data - 56 and 90 day surface resistivity measurements	D-10
Figure D.12: VHES-LMC miniature slabs - 4 hour and 1 day surface resistivity measurements	D-11
Figure D.13: VHES-LMC miniature slabs - 3 and 7 day surface resistivity measurements	D-12
Figure D.14: VHES-LMC miniature slabs - 14 and 28 day surface resistivity measurements	D-13
Figure D.15: VHES-LMC miniature slabs - 56 and 90 day surface resistivity measurements	D-14
Figure D.16: Edge effects on surface resistivity measurements in each orientation	D-15
Figure D.17: Control mockup – diagonal orientation 7 day surface resistivity reading	D-16
Figure D.18: Control mockup – horizontal orientation 7 day surface resistivity reading	D-16
Figure D.19: Control mockup – vertical orientation 7 day surface resistivity reading	D-17
Figure D.20: Control mockup –average of orientations 7 day surface resistivity reading	D-17
Figure D.21: Control mockup – standard deviation of 7 day surface resistivity readings	D-18
Figure D.22: LMC mockup overlay thickness measurements	D-18
Figure D.23: LMC mockup void locations	D-19
Figure D.24: LMC overlay mockup – surface resistivity diagonal orientation at 7 days	D-19
Figure D.25: LMC overlay mockup – surface resistivity horizontal orientation at 7 days	D-20

Figure D.26: LMC overlay mockup – surface resistivity vertical orientation at 7 days	D-20
Figure D.27: LMC overlay mockup – surface resistivity average of orientations at 7 days	D-21
Figure D.28: LMC mockup – surface resistivity standard deviation at 7 days	D-21
Figure D.29: Voids superimposed on LMC mockup - 7 day average surface resistivity data	D-22
Figure D.30: VHES mockup overlay thickness measurements	D-22
Figure D.31: VHES mockup void locations	D-23
Figure D.32: VHES overlay mockup – surface resistivity diagonal orientation at 7 days	D-23
Figure D.33: VHES overlay mockup – surface resistivity horizontal orientation at 7 days	D-24
Figure D.34: VHES overlay mockup – surface resistivity vertical orientation at 7 days	D-24
Figure D.35: VHES overlay mockup – surface resistivity average of orientations at 7 days	D-25
Figure D.36: VHES mockup – surface resistivity standard deviation at 7 days	D-25
Figure D.37: Voids superimposed on VHES mockup - 7 day average surface resistivity data	D-26
Figure D.38: VHES-LMC mockup overlay thickness measurements	D-26
Figure D.39: VHES-LMC mockup void locations	D-27
Figure D.40: VHES-LMC overlay mockup – surface resistivity diagonal orientation at 7 days	D-27
Figure D.41: VHES-LMC overlay mockup – surface resistivity horizontal orientation at 7 days	D-28
Figure D.42: VHES-LMC overlay mockup – surface resistivity vertical orientation at 7 days	D-28
Figure D.43: VHES-LMC overlay mockup – surface resistivity average of orientations at 7 days	D-29
Figure D.44: VHES-LMC mockup – surface resistivity standard deviation at 7 days	D-29
Figure D.45: Voids superimposed on VHES-LMC mockup - 7 day average surface resistivity data	D-30
Figure D.46: LMC mockup - surface resistivity diagonal orientation with different exclusions	D-30
Figure D.47: LMC mockup - surface resistivity horizontal orientation with different exclusions	D-31
Figure D.48: LMC mockup - surface resistivity vertical orientation with different exclusions	D-31
Figure D.49: LMC mockup - surface resistivity average of orientations with different exclusions	D-32
Figure D.50: VHES mockup diagonal orientation with different exclusions	D-32
Figure D.51: VHES mockup horizontal orientation with different exclusions	D-33
Figure D.52: VHES mockup vertical orientation with different exclusions	D-33
Figure D.53: VHES mockup average of orientations with different exclusions	D-34
Figure D.54: VHES-LMC mockup diagonal orientation with different exclusions	D-34
Figure D.55: VHES-LMC mockup horizontal orientation with different exclusions	D-35
Figure D.56: VHES-LMC mockup vertical orientation with different orientations	D-35
Figure D.57: VHES-LMC mockup average of orientations with different exclusions	D-36
Figure E.1: Bridge deck area to be analyzed	E-1
Figure E.2: Proposed testing sequence for surface resistivity of mockups	E-2
Figure E.3: Measuring surface resistivity in the standing position	E-3
Figure E.4: surface resistivity (left) versus overlay thickness change in inches (right) (VHES-LMC 14 day average orientation)	E-4
Figure F.1: Datasheet for mixture 6011, Class A 3000 psi showing materials, proportions, fresh concrete test results, and compressive strength test results	F-6
Figure F.2: Datasheet for mixture 6012 (Class AA mixture) showing materials, proportions, fresh concrete test results, and compressive strength test results	F-7
Figure F.3: Concrete Supply datasheet for Mixture 6013 (Drilled Shaft Mixture) showing materials, proportions, fresh concrete test results, and compressive strength test results	F-8
Figure F.4: Training session for SAM with developer (Jake LeFlore, OSU)	F-13
Figure F.5: SAM air content vs. SAM number, comparing test results for Class A and Class AA mixtures	F-17

LIST OF ABBREVIATIONS

AASHTO	American Association of State Highway and Transportation Officials
ACI	American Concrete Institute
ACR	alkali-carbonate reaction
AEA	air entraining admixture
ASCE	American Society of Civil Engineers
ASR	alkali-silica reactivity
ASTM	American Society for Testing and Material
BME	Bridge Management Elements
CDOT	Colorado Department of Transportation
cf	cubic feet
cwt	hundred weight of cement
cy	cubic yard
DF	durability factor
DOT	Department of Transportation
dpi	dots per inch
FHWA	Federal Highway Administration
FFT	Fast Fourier Transform
FLDOT	Florida Department of Transportation
F-T	freeze-thaw
ft	foot
g	gram
gal	gallon
HPC	high performance concrete
hr	hour
ID	identification
IDOT	Illinois Department of Transportation
in	inch
IowaDOT	Iowa Department of Transportation
ITZ	interfacial transition zone
kg	kilogram
k Ω	kilo-ohm
LaDOTD	Louisiana Department of Transportation and Development
lb	pound
LCA	lifecycle assessment
LCCA	lifecycle cost analysis
LMC	latex-modified concrete
LWA	lightweight aggregate
m	meter
MAP	Moving Advancements into Practice
$\mu\epsilon$	microstrain
μm	micrometer
mL	milliliter
mm	millimeter
MnDOT	Minnesota Department of Transportation
MOE	modulus of elasticity
MOR	modulus of rupture
MRWR	mid-range water reducing admixture
NC	North Carolina
NCC	National Concrete Consortium
NCDOT	North Carolina Department of Transportation
NYSDOT	New York State Department of Transportation
Ω	ohm
OPC	ordinary portland cement

OSU	Oklahoma State University
oz	ounce
PC	polycarboxylate superplasticizing admixture
PCA	Portland Cement Association
PCC	portland cement concrete
pcf	pounds per cubic foot
pcy	pounds per cubic yard
PEM	performance engineered (concrete) mixtures
PLC	portland limestone cement
psi	pounds per square inch
PLC	portland limestone cement
PRS	performance-related specifications
PVA	polyvinylidene chloride
QA	quality assurance
QC	quality control
RCPT	rapid chloride permeability test
ROC	rate of change
RP	Research Project
SAM	Super Air Meter
SBR	styrene-butadiene rubber
SCM	supplementary cementitious material
SF	spacing factor
SG	specific gravity
SHA	state highway agency
SHRP	Strategic Highway Research Program
SSD	saturated surface dry
TRB	Transportation Research Board
US	United States
VDOT	Virginia Department of Transportation
VHES	very high early strength
VHES-LMC	very high early strength latex modified concrete
<i>w/cm</i>	water to cementitious materials ratio
WisDOT	Wisconsin Department of Transportation
WRA	water-reducing admixture
WROS	Wood rosin air entraining admixture
WVDOT	West Virginia Department of Transportation
yd	yard
°F	degrees Fahrenheit

1.0 INTRODUCTION AND RESEARCH OBJECTIVES

1.1 Introduction

In the past century, many changes have been made to concrete mixtures and materials. Concrete materials have become more complex, using a wide variety of admixtures and supplementary cementitious materials (SCMs), sometimes in combinations (Cackler et al. 2017a). Exposure conditions, including increased traffic, adverse chemical reactions from chlorides in sea environments, and increased use of deicing chemicals in winter environments have impacted long term durability and service lives of many concrete structures (Cavalline et al. 2016). Advances in construction technologies have resulted in changes in the way concrete is batched, placed, consolidated, and finished. Also, accelerated schedules are placing increased demands on the early-age performance of concrete. Due to the impacts of these various factors on long term concrete performance of concrete infrastructure, the Federal Highway Administration (FHWA), state highway agencies, and many industry stakeholders agree there is a need to readdress the way that concrete mixtures are specified and tested.

Extensive research in recent decades has led to new understanding of concrete deterioration mechanisms, advancements in concrete mixture design, and development of better field and laboratory tests for QA and QC. With this new knowledge, an FHWA initiative is underway to improve performance of concrete infrastructure through performance engineered concrete mixtures (PEM). This initiative has resulted in development of AASHTO specification and commentary, AASHTO PP 84, “Standard Practice for Developing Performance Engineered Concrete Pavement Mixtures,” which provides a framework and guidance for state highway agencies to develop a specification for performance engineered concrete mixtures that focuses on measurement and acceptance of concrete based on characteristics that have been linked to satisfactory long-term durability performance of the concrete (AASHTO 2020). Recently, this provisional standard has been approved as a practice standard, renamed, AASHTO R 101, “Developing Performance Engineered Concrete Mixtures” (AASHTO 2022). Although initially developed for pavement concrete mixtures, the approach outlined in AASHTO PP 84 and R 101 could be extended to include specifications for PEMs utilized for other infrastructure, such as bridges, barriers, and lower grade uses, as well.

Performance-related specifications provide agencies the ability to obtain the desired construction quality while allowing contractor greater control and flexibility (Ahlstrom 2016). For instance, current prescriptive specifications for minimum cement content and rate of strength gain may preclude the acceptance of mixtures that have superior economy, durability, and satisfactory mechanical performance, but contain high proportions of SCMs. The provisions included in AASHTO PP 84 and R 101 are presented in a format that allows state agencies flexibility in selecting the tests and requirements most applicable to their states. Recommended uses of the PEM tests, such as for mixture qualification or for acceptance, are also suggested. An appendix to the standard provides additional context, technical information, and guidance. It is noted that AASHTO PP 84 was modified almost yearly between 2016 and 2021, with slight changes to format, content, recommended testing protocol, and testing targets. AASHTO R 101 will also likely be updated frequently as research and deployment activities supporting the PEM initiative progress in the coming years.

Performance-related specifications require measurement of key properties and performance characteristics. In order for performance specifications to be successfully utilized, QA and QC tests should be performance related, rapid, effective, reliable, and inexpensive (Cackler et al. 2017b). Recent advancements in testing technologies have provided means of more directly measuring the properties of concrete mixtures that have been linked to successful field performance (Cackler et al. 2017b). A number of state agencies are using and evaluating new, rapid, early-age testing technologies such as resistivity, sorptivity, and air void system analysis that support development and use of performance-engineered concrete mixtures. Ongoing concrete materials research is providing state highway agencies data to support the use of PEMs. However, additional work is needed to identify appropriate performance measures, performance goals, and QA and QC protocol. The capabilities of these tests to evaluate the durability performance of concrete mixtures is improving as state highway agencies build sufficient data to correlate the test results with field performance.

1.2 Performance Engineering Mixtures – Materials and Mixture Parameters, and Specifications

As mentioned earlier, tests used for specification and acceptance of concrete mixtures have typically been tests for slump, air content, and strength. It has generally been believed that strength could be used as a “quasi-indicator of durability” (Cackler et al. 2017a). However, research and field experience has shown that slump, air, and strength are not reliable predictors of long-term performance. To endure stresses related to field exposure, concrete needs to exhibit characteristics that indicate good resistance to freezing and thawing, and chemical attack from corrosive deicing salts and chlorides, to the extent to which it will be exposed during its service life (Cavalline et al. 2016). Additionally, the concrete cannot be susceptible to deleterious alkali-aggregate interaction (such as alkali-silica reactivity, or ASR).

Although none of these characteristics are easily measured directly, it has long been known that durable concrete is associated with several performance characteristics measurable in a laboratory setting. Low permeability, resistance to cracking and transport of deleterious substances, aggregate stability, and an adequate air void system are examples of these performance characteristics (Cackler et al. 2017a, Taylor et al. 2013). Additionally, to mitigate placement defects that result in the poor durability of what would otherwise be a satisfactorily-performing concrete mixture, workability needs to be considered (Cackler et al. 2017a, Taylor 2016).

Conventional mixture designs using ordinary portland cements and quality aggregates, can provide good durability performance if they are properly proportioned with low w/c ratio, good workability, and take advantage of admixtures to create an adequately dispersed air void system (Taylor et al. 2013). Additionally, SCMs, such as fly ash and slag have been shown to provide enhanced durability performance (reduced permeability and mitigation of ASR). Established and emerging mixture proportioning and test methods included in AASHTO PP 84 and R101 will help to ensure that mixtures will meet performance expectations.

A key feature of the AASHTO PP 84 and R101 specifications is that they provide a menu of potential specification provisions that address six-key performance-related properties listed below, with recommended test methods that state highway agencies can select (or omit) as they desire. This approach allows state highway agencies to incorporate knowledge of local historical performance, risk tolerance, and agency preference into a durability-based specification. For many performance requirements, an agency can select from either a prescriptive or performance approach. The six key performance requirements included in AASHTO PP 84 and R101 include (AASHTO 2020, AASHTO 2022):

1. Concrete strength

Despite not always being directly indicative of long-term performance, the strength of concrete continues to be an important specification parameter. AASHTO PP 84 and R101 suggest use of either flexural or compressive strength (or both) for mixture qualification and for acceptance.

2. Reducing cracking due to shrinkage

AASHTO PP 84 and R 101 suggests several specification provisions to reduce cracking, including a prescriptive measure of limiting the volume of paste in a paving mixture to 25%. A performance test that could be selected includes the unrestrained volume change (AASHTO T160). Other conventional and emerging test methods such as the restrained ring tests and a probability of cracking method are discussed in the Appendix of the standard.

3. Durability of hydrated cement paste for freeze-thaw durability

AASHTO PP 84 and R 101 suggest use of a prescriptive w/c ratio limit (0.45), or acceptable performance using one of several other currently utilized or emerging rapid test methods. These methods include fresh air content using the conventional pressure or volumetric air meter (AASHTO T 152 and T 196), the Super Air Meter (SAM) (AASHTO TP 118), and tests related to time of critical saturation (ASTM C1585) and deicing salt damage. Other prescriptive specification provisions suggested for protecting concrete from deicing salts include use of SCMs at a suggested replacement rate of 30%, and application of sealers (AASHTO M 224). Measures to protect joints from damage caused by calcium oxychloride formation include tests to quantify the amount of calcium oxychloride in the cement paste (AASHTO T 365).

4. Transport properties

A prescriptive measure of maximum w/cm (limiting to less than 0.45 or 0.50) is suggested, based upon freeze-thaw conditions. Results from several research projects showed test results of the surface resistivity meter (AASHTO T 358) correlate with the well-established but time-consuming rapid chloride ion permeability test (ASTM C1202) (Rupnow and Icenogle 2011). However, both of these electrical tests have limitations associated with pore solution ionic concentration, temperature effects, sample geometry, degree of saturation, and storage. AASHTO PP 84 extends the use of resistivity meter by suggesting use of a formation factor (F-factor) to assist in normalizing the results of surface resistivity testing.

5. Aggregate stability

Prevention of deleterious aggregate-related issues such as D-cracking, alkali-silica reactivity (ASR), and alkali-carbonate reactivity (ACR) are addressed in AASHTO PP 84 and R 101. ASTM T 161 and ASTM C1646 are suggested for screening aggregates for D-cracking. AASHTO PP 84 and R 101 suggest use of the approaches outlined in AASHTO R 80 to prevent and mitigate ASR and ACR.

6. Workability

Although not a measure of durability performance, considerations for assessing workability are included in the AASHTO PP 84 and R 101 standards due to the linkage between inappropriate workability and construction-induced issues such as poor consolidation, edge slump, segregation, and degraded air void system quality. Two emerging methods of assessing concrete workability of low-slump paving mixtures suggested in AASHTO PP 84 and R 101 are the Box Test and the Modified V-Kelly test (AASHTO TP 129).

1.3 Construction QA and QC for Performance Engineered Mixtures

Properties of interest for performance engineered concrete mixtures will depend on the agency's goals, preferences, and risk tolerance, as well as the project constraints. Performance specifications allow the contractor flexibility to meet contract requirements, encouraging innovation and potential cost savings for the owner (Cackler et al. 2017a). Agencies will need to continue to review and approve performance engineered concrete mixtures as they would other types of concrete. Guidance for establishing a quality assurance program for performance engineered concrete mixtures is outlined in Cackler et al. (2017b). This publication also describes the importance of development and use of contractor QC plans, which serve as a means for the contractor to alert the agency about how specification provisions will be met.

AASHTO PP 84 and R101 provide mixture proportioning guidance to assist in developing PEM. Commentary provided within the standards and their Appendices provide insight into strategies to meet performance goals, such as optimizing aggregate gradation to assist in reducing paste volume, and meeting strength requirements while simultaneously economizing the mixture. Requirements for mixture qualification and mixture acceptance are presented.

Performance specifications tend to shift risk from the agency to the contractor, with the contractor in turn benefitting from the opportunity to innovate. AASHTO PP 84 and R101 detail the required QC activities to be performed by the producer, which include development, approval and implementation of a QC plan. This QC plan should include details on the methods and frequency of monitoring and testing, as well as data management and reporting tools such as control charts. The QC plan will communicate to the agency how the contractor intends to meet the specification requirements (Cackler et al. 2017b). A quality control plan to support PEM will reduce risk for all parties and can maximize the economic and performance benefits associated with the mixture. Education and training (of both agency and contractor personnel), use of shadow and pilot projects, a mixture qualification/verification procedure, and QC tools such as control charts are important parts of a quality assurance (QA) program for PEM (Cackler et al. 2017b).

With proper mixture design, control, and testing, construction considerations for use of performance engineered concrete mixtures in transportation infrastructure components should not differ significantly from construction considerations for conventional concrete mixtures. As with other types of concrete, appropriate construction techniques must be utilized and adequate curing must be performed in order to ensure development of the desired properties.

1.4 Implementation of Performance Engineered Mixtures

The approach outlined in AASHTO PP 84 was developed for pavement concrete mixtures. However, PEMs could be extended to include mixtures of other classes of concrete as well. For example, use of PEM specifications could be used to ensure placement of low permeability concrete in bridge decks, girders, piers and foundations, if desired.

Development and implementation of PEM specifications is an extensive undertaking, and the shift will impact all stakeholders in the construction process. The menu of specification provisions suggested by AASHTO PP 84 and R 101 have provided guidance for several state agencies to make initial movement towards PEM in a variety of means (examples include shadow testing using emerging test methods, pilot projects, and enhanced QC plans). At the time of preparation of this literature review (Summer 2022), PEM tests were being performed by a number of states, including Arkansas, California, Colorado, Georgia, Idaho, Illinois, Iowa, Kansas, Maine, Michigan, Minnesota, New York, North Carolina, Ohio, Oklahoma, Pennsylvania, South Dakota, and Wisconsin.

Although some states are currently utilizing some performance-related or performance-based specification provisions, implementation of PEM is an ongoing effort to improve specifications. Research is being performed at many universities and DOTs to enhance the knowledge of the basic science, emerging tests, and field performance data to support the specification. Evaluation of new technologies and equipment under field working conditions is ongoing, with a goal of providing feedback to researchers and agencies, as well as refining the technologies (Praul 2016).

Challenges facing agencies interested in moving towards PEM include ensuring stakeholders are aware of and are capable of performing the new tests, as well as properly interpreting the results. Some tests require purchase of new testing equipment by both agencies and contractors. Ongoing technology transfer efforts are focused on preparing guidance for specification approaches, tests, and quality control (Praul 2016). AASHTO PP 84 and R 101 also require an approved QC plan. This provision, although likely to improve the quality of concrete produced, may be viewed as an additional burden by some contractors. Overall, implementation of PEM should result in "higher quality concrete and more efficient construction practices, reducing long-term costs to the agency (Cackler et al. 2017b)."

1.4.1 Implementation Efforts of Other State Highway Agencies

Several state agencies have made advancements towards implementing performance specifications for concrete. These states include Minnesota DOT, New York State DOT, and Louisiana DOTD, among others. Each state agency has approached changes to their specifications in a manner that was consistent with agency preferences and stakeholder comfort

level. Although approaches vary by state, a review of these states' approaches to PEM implementation provides insight and guidance as NCDOT identifies future PEM studies and implementation efforts. For example, Minnesota DOT has made incremental changes to their concrete pavement and bridge specifications from 1996 to present day. Their pre-1996 concrete specifications focused on strength-based requirements. Over the next two decades, incremental changes were made to include (Sutter et al. 2018):

- 1) A reduction in maximum w/cm ratio from 0.46 to 0.40
- 2) Optimization of gradations from the gap graded to the well-graded aggregate
- 3) Increased pozzolan substitution for portland cement to lower the risk of alkali-silica reaction (ASR)
- 4) Improved curing materials and practices
- 5) Increase in plastic air content

As described by Sutter et al. (2018), these incremental changes in concrete material specifications have led to construction of pavements with lower permeability, higher strength, and increased air concrete. Potentially more importantly, the ride quality for pavements constructed using the new concrete specifications “appears to be better and the rate of degradation of ride quality appears to be slower (Sutter et al. 2018).” A marked decrease in permeability of Minnesota concrete pavements (as evidenced by an increase in measured resistivity) after implementation of concrete specification changes has been measured and is described in Sutter et al. (2018).

New York State DOT specification “ITEM 504.01010001 - Performance Engineered Concrete Mixture for Pavements” in 2015. To date, this specification has been implemented on 47 design-build projects, including bundled bridge projects, major paving projects, and train stations (Streeter 2018). With agency experience, this performance specification continues to be refined and updated, with the most recent revision issued April 25, 2019. The key performance provisions included in NYSDOT's PEM specification include surface resistivity requirements (to ensure low permeability concrete) for different applications of concrete mixtures. Prescriptive provisions include air content and minimum strength requirements. In the spirit of performance mixture design, no slump, w/c ratio, aggregate gradation, or pozzolan requirements are provided in this specification. The NYSDOT PEM specification also includes requirements for contractor QC, as well as agency QA requirements (NYSDOT 2019).

Other states, such as Iowa DOT have implemented PEM shadow specifications to gain field experience with new PEM tests, to refine shadow specifications and performance targets, and to identify requirements for contractor QC plans (Hanson 2018). Most of the states participating in the FHWA PEM pooled fund study have applied for (and received) implementation funding. Agency experiences with PEM shadow specifications is documented in a series of reports provided at the National Concrete Pavement Technology Center's Website (CP Tech Center 2022), providing agency lessons learned and stakeholder guidance. This literature includes experience gained during NCDOT's own initial PEM implementation study (Cavalline et al. 2020b, Cavalline et al. 2022), which provide insights into NCDOT's implementation path

As evidenced by several states' successful experiences, the benefits of moving towards performance specifications for concrete are tangible. However, each agency must do the groundwork necessary to identify the components of PEM concrete specifications appropriate for their agency and local stakeholders. Work performed as part of this project enhanced NCDOT's knowledge to support deployment of several approaches and testing targets for PEM, while also moving advancing implementation efforts as appropriate for NCDOT personnel and local industry.

1.4.2 North Carolina DOT's PEM Implementation Efforts to Date

In 2017, NCDOT initiated the first phase of this project focused on PEM, including support of FHWA's PEM Pooled Fund Study and funding a separate PEM research project. RP 2018-14, “Durable and Sustainable Concrete Through Performance Engineered Concrete Mixtures” was a first step towards implementation of PEM (Cavalline et al. 2020a). This project includes a data analysis of concrete mixtures used in NCDOT's projects to 1) identify trends in materials and proportions, and link to unacceptable, acceptable, and excellent performance, and 2) correlate mixture characteristics and QA and QC test results with observed condition data, if possible. The laboratory evaluation included in RP 2018-14 includes a mixture matrix of 24 mixtures typical of bridge deck (AA) and pavement mixtures at three water cement ratios, three cementitious contents, and two replacement rates of fly ash (20% and 30%). Three mixtures contained portland limestone cement (PLC) to aid in determining potential performance improvements that could result through use of ternary blends of cementitious materials. This laboratory program included a single source for each cementitious material, and aggregates utilized were representative of the Piedmont region (coarse aggregate sourced from Wake Stone's Triangle Quarry, and a natural sand from the Lemon Springs Pit).

Additionally, NCDOT applied for and received additional funds to support PEM implementation as part of FHWA's “Demonstration Project for Implementation of Performance Engineered Mixtures/AASHTO PP 84.” These funds were awarded to NCDOT in Spring 2018, and the UNC Charlotte research team was retained (as part of RP 2019-41) to assist

NCDOT in supporting the contractor at the PEM current implementation site (an I-85 pavement reconstruction project). Work contracted to UNC Charlotte as part of RP 2019-41 included support of contractor and NCDOT personnel at the current implementation site. Efforts also include preliminary technology transfer and training efforts focused on NCDOT regional and divisional personnel. This implementation project was successful, and findings are presented in (Cavalline et al. 2020b, Cavalline et al. 2022).

It is well understood by those involved in the PEM initiative that implementation of performance-related specifications is an extensive undertaking that includes identification of locally appropriate values, agency preferences, and training/technology transfer for all stakeholders. Nationally, the PEM initiative is a dynamic effort that is a key, current focus of many state agencies, researchers, and industry partners. FHWA, other state agencies, and academic institutions continue to make advancements in the basic science behind key PEM tests, identification of QA and AC and specification approaches, and links to performance data. NCDOT's preliminary work has provided early steps towards performance specifications for concrete infrastructure. However, additional work is needed in several areas to move closer to implementation of performance-based specifications for concrete. Specifically:

- The laboratory evaluation program in RP 2018-14 contains a matrix representing a portion of types of concrete mixtures used in NCDOT's projects, with a limited sample of materials and proportions. Additional work is needed to broaden the range of mixtures included in the PEM studies.
- Research support is needed to assist NCDOT personnel in identifying QA and QC advancements and approaches that can be used in local PEM implementation efforts. Implementation in the pavement pilot project broke ground in bringing PEM shadow specifications to North Carolina concrete paving project. However, additional implementation sites focused on bridge projects (for deck, superstructure, and substructure concrete) are needed in order to refine PEM targets and shadow specifications. Tests for structural concrete could be expanded to include shrinkage, which was not included in the pavement concrete pilot project.
- Technology transfer and tools should be enhanced and broadened to promote understanding and use of PEM approaches.

1.5 Research Objectives

Mindful of ongoing work and the dynamic nature of progress of the PEM initiative on many fronts, the objectives of this research project were as follows:

Objective 1) Supplemental laboratory evaluation to expand the catalog of data to support development and refinement of PEM specifications

- laboratory evaluation expanded the range of mixtures and materials providing data to support appropriate performance measures and target values
- mixture characteristics that reduce paste content through optimized aggregate gradation
- additional specification guidance regarding w/cm ratios, aggregate gradations, and/or paste contents

Objective 2) Development of resources, tools and guidance to support QA and QC

- evaluate the surface resistivity meter for use in evaluating the quality of concrete overlays
- provide guidance regarding use of SAM and other tests to support freeze-thaw durable concrete
- provide tools and training focused on enhancing QA and QC activities

Objective 3) Implementation of PEM tests and shadow specifications at additional existing highway projects

PEM tests were deployed during and after construction of many structures included in the I-485 widening project in south Charlotte, NC. The structural concrete was used for bridge decks, overlays, substructure components, superstructure components, barrier walls, approach slabs, drilled shafts, drilled piers, and culverts. Some non-structural (Class A) mixtures were also tested.

2.0 LITERATURE REVIEW - OVERVIEW

To present a concise report, the literature review is included Appendix A. The literature review performed to support this project focused on three key areas, listed below.

- Introduction to PEM and recent advancements (Appendix A.1)
- Optimized aggregate gradations (Appendix A.2 – this material supports Chapter 3)
- Freeze-thaw durable concrete (Appendix A.3 – this material supports Chapter 4)
- Surface resistivity and its potential use in overlay evaluation (Appendix A.4 – this material supports Chapter 5)

3.0 OPTIMIZED AGGREGATE GRADATION MIXTURES

3.1 Concrete Mixtures

The testing program for this work was designed to evaluate NCDOT structural (Class AA) and pavement mixtures with optimized aggregate gradations, and to identify targets for specifications for surface resistivity, shrinkage, and the SAM. Mixtures for this project were based upon the mixtures in the Phase I PEM study sponsored by NCDOT, RP 2018-14. The w/cm ratio, total cementitious content, and fly ash replacement percentage are highly influential in development of the integrity of the paste structure of concrete. These parameters were the primary focus in developing the mixture matrix for NCDOT RP 2018-14, shown in Figure 3.1.

- Three w/cm ratios – 0.37, 0.42, and 0.47
- Three cementitious contents – 700 pcy, 650 pcy, and 600 pcy
- Two fly ash replacement levels – 20% and 30% by weight

Higher cementitious content mixtures (700 pcy and 650 pcy, shown in orange and yellow, respectively in Figure 3.1) are typical of bridge mixtures (NCDOT Class AA). Lower cementitious content mixtures (600 pcy, shown in green) are typical of lower cementitious content AA mixtures and pavement mixtures. In RP 2018-14, 21 of the 24 mixtures contained OPC, while 3 lower cementitious content (low AA and pavement) mixtures contained PLC. For each mixture included in RP 2018-14, a companion mixture with an optimized aggregate gradation was developed. No PLC mixtures were developed as part of this study, RP 2020-13. Material types and sources were kept consistent between projects and within projects for all mixtures, including aggregates, fly ash, admixtures, and water.

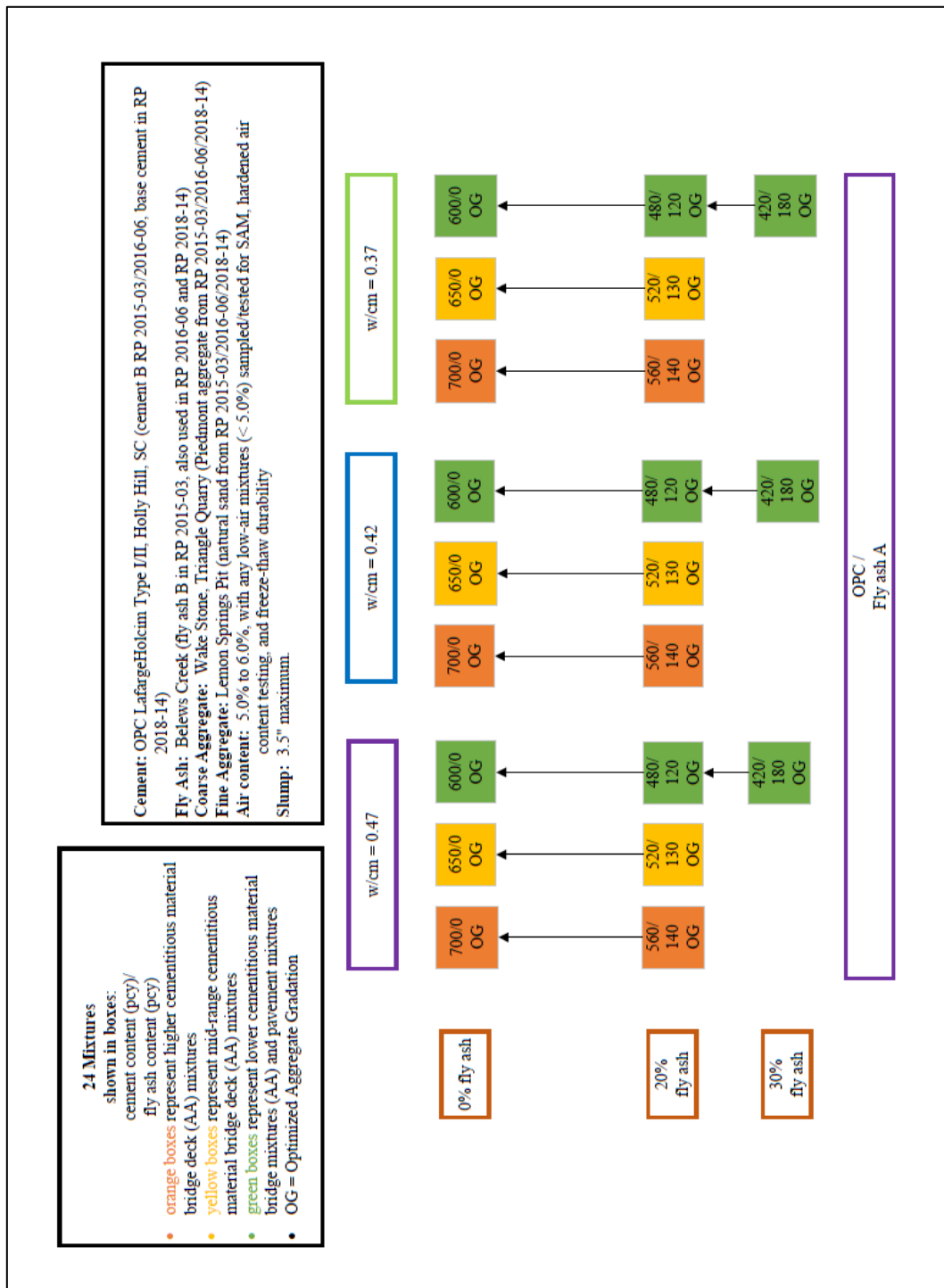


Figure 3.2: Concrete mixture matrix for RP 2020-13 with supporting information

Using the established w/cm and cementitious materials contents, along with the aggregate properties measured, the remainder of mixture proportions were computed using the ACI 211.1 methodology. Mixture materials and proportions for RP 2018-14 (minus the PLC mixtures which were not the focus of continued study) are shown in Table 3.1. The colors in the table correspond to the colors of the boxes in Figure 3.2. The concrete mixtures developed for this project were each given a mixture ID, with the convention W-XXX-YYY, which is summarized as follows:

- W is the w/cm ratio (H = high = 0.47, M = medium = 0.42, L = low = 0.37)
- XXX is the cement content in pcy
- YYY is the fly ash content in pcy

Table 3.1: Concrete mixtures with material proportions for RP 2018-14 (non-optimized aggregate gradations)

Mixture ID W-XXX-YYY, where W is w/cm ratio, XXX is cement content, YYY is fly ash content	Mixture Proportions, pcy							
	Mixture type	w/cm ratio	Fly ash replacement (%)	Cement	Fly ash	Coarse aggregate	Fine aggregate	Water
H-700-0	AA (high and medium cm content)	0.47	0	700	0	1659	1072	329.0
H-560-140			20	560	140	1659	1022	329.0
H-650-0			0	650	0	1659	1175	305.5
H-520-130			20	520	130	1659	1129	305.5
H-600-0			0	600	0	1659	1277	282.0
H-480-120			20	480	120	1659	1235	282.0
H-420-180			30	420	180	1659	1214	282.0
M-700-0		0.42	0	700	0	1659	1163	294.0
M-560-140			20	560	140	1659	1114	294.0
M-650-0			0	650	0	1659	1259	273.0
M-520-130			20	520	130	1659	1214	273.0
M-600-0			0	600	0	1659	1356	252.0
M-480-120			20	480	120	1659	1313	252.0
M-420-180			30	420	180	1659	1292	252.0
L-700-0	AA (low cm content) and Pavement	0.37	0	700	0	1659	1254	259.0
L-560-140			20	560	140	1659	1205	259.0
L-650-0			0	650	0	1659	1344	240.0
L-520-130			20	520	130	1659	1298	240.0
L-600-0			0	600	0	1659	1434	222.0
L-480-120			20	480	120	1659	1392	222.0
L-420-180			30	420	180	1659	1370	222.0

Implementation of the Tarantula Curve

AASHTO PP 84 suggests that mixtures should have a paste content of less than 25%, although this limit is intended for paving mixtures which are typically far less workable than structural mixtures. The non-optimized mixtures produced in RP 2018-14 had paste contents ranging from 24.5% to 33.8%, and an average paste content of 28.5%. To support development of optimized mixtures, a target cementitious material reduction of 10% was selected (while adjusting water content to hold the w/cm ratio consistent) so that a uniform reduction could be applied to each non-optimized aggregate gradation concrete mixture. Using this target to develop optimized aggregate gradation mixture designs facilitated a fairly uniform comparison between non-optimized aggregate gradation mixtures and their counterpart optimized aggregate gradation mixtures. Larger paste reductions may have been feasible for some mixtures. However, this approach was not used since optimized versions of the non-optimized mixtures with paste contents already below the 25% recommendation by AASHTO PP 84 would have paste contents close to 20%, causing workability concerns.

Applying a 10% cementitious material reduction to the RP 2018-14 paste contents, the paste contents of optimized mixtures ranged from 22.0% to 30.3%, with an average paste content of 25.6%. To facilitate easy comparison between companion mixtures, the previous study's name structure of W-XXX-YYY was maintained for optimized gradation mixtures, where W is the w/cm ratio, XXX is the cement content of the original non-optimized mixture and * denotes that the mixture has an optimized aggregate gradation with a reduced paste content, and YYY is the fly ash content of the mixture.

The quantities of each non-optimized mixture's materials were entered into a spreadsheet that projected gradations across the Tarantula Curve with percent retained limits for each sieve discussed in Chapter 2. The limits set by the Tarantula curve are: the 1-inch sieve should retain less than 16 percent, sieves #4 – 3/4" should retain between 4 – 20

percent, sieves #8 and #16 should retain less than 12 percent, sieves #30 and #50 should retain between 4 – 20 percent, and sieve #100 should retain between 0 – 10 percent (Cook et al. 2013). A graph of the recommended Tarantula Curve boundaries is shown in Figure 3.3.

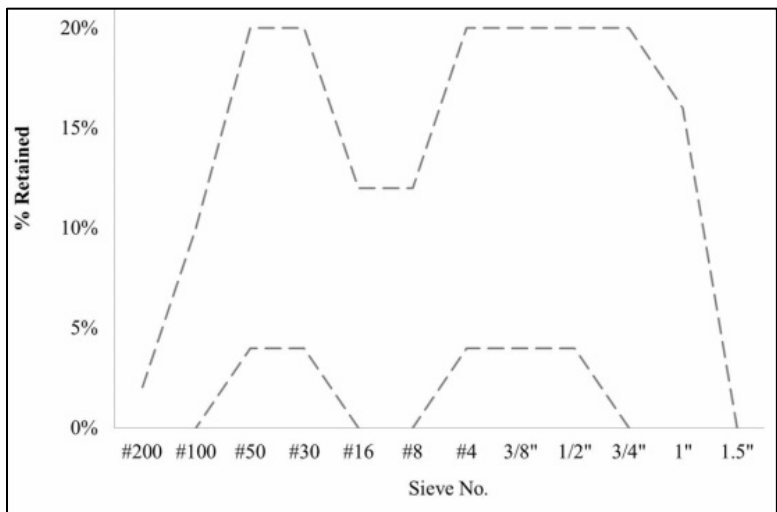


Figure 3.3: Tarantula Curve recommended gradation boundaries

The same materials used in concrete batched in RP 2018-14 (non-optimized gradation mixtures) were also used for this study’s optimized aggregate gradation mixtures, supporting direct comparison. Sieve analyses were performed on aggregates obtained from each study to verify consistency. The gradations of aggregates used from RP 2018-14 and this study were very similar, and can be seen in Figure B.1 in Appendix B. Sieve analysis results were entered into a spreadsheet developed to assess the combined aggregate gradations with the guidance of the Tarantula Curve. In Figure 3.4, the combined aggregate gradation for the aggregates used in the non-optimized mixture H-700-0 is shown with the Tarantula curve boundaries. The combined gradation exceeds the recommended percent retained on the 1/2” sieve.

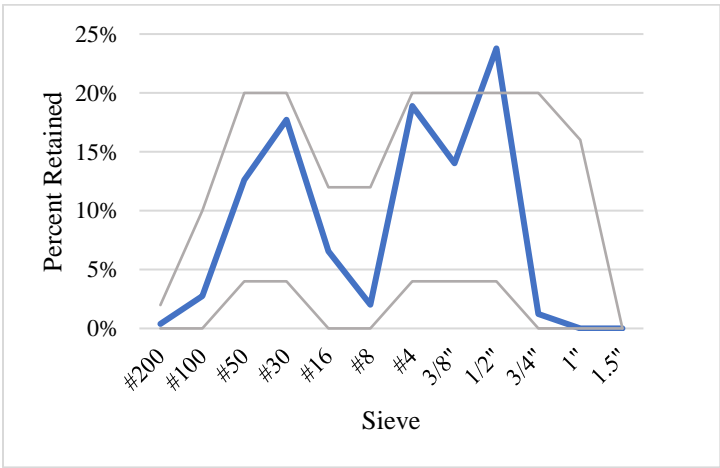


Figure 3.4: Particle sizes of non-optimized mixture H-700-0 on Tarantula Curve

Using information collected from the coarse aggregate supplier, several aggregate gradations (No. 8, No. 9, No. 78, and No. 89M) were explored to help identify an intermediate aggregate which, when paired with the coarse and fine aggregate, would best satisfy parameters of the Tarantula Curve while allowing for a reduction in cementitious materials. The No. 89M stone was selected because it had a peak percent retained distributed between the No. 4 and No. 8 sieves, shown in Appendix A. The quantity of this intermediate aggregate used in each optimized concrete mixture was adjusted in a manner that allowed the combined, optimized aggregate gradation to meet the Tarantula Curve recommendations while trying to minimize the reduction in fine aggregate removed. Figure 3.5 shows the combined aggregate gradation used in optimized mixture H-700*-0, contained within the boundaries of the Tarantula curve.

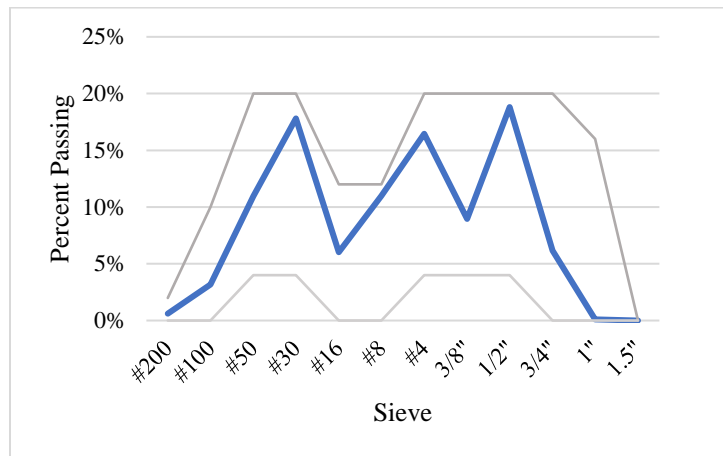


Figure 3.5: Particle sizes of H-700*-0 optimized aggregate gradation mixture

This process was repeated for all 21 OPC mixtures used in RP 2018-14. Cementitious material contents for non-optimized aggregate gradation mixtures varied from 600 pcy to 700 pcy while the cementitious material contents for optimized aggregate gradation mixtures varied between 378 pcy and 630 pcy after the 10% cementitious materials reduction. The final mixture matrix for this project, with the optimized aggregate gradation mixtures that utilized the Tarantula Curve can be seen next to their companion mixture in Table 3.2. Note that Mixture IDs are as follows: **W-XXX*-YYY**, where **W** is w/cm ratio, **XXX** is cement content where * denotes an optimized gradation, **YYY** is fly ash content

3.2. Materials Description and Characterization

3.2.1 Cementitious Materials

A Type I/II OPC meeting ASTM C150 was used in both RP 2018-14 and this study, RP 2022-13. This cement was produced in Holly Hill, South Carolina, and is a commonly used cement for the Coastal and Piedmont regions of NC. This OPC is sourced from the same production facility as the OPC used in RP 2016-06 and Cement B used in RP 2015-03, which supported development of initial PEM test targets. A mill report for the cement is provided in Appendix B as Figure B.1.

Fly ash used in this study was a Class F ash sourced from the Belews Creek Power Plant in Belews Creek, NC. Additional information is provided in Figure B.2. NCDOT Standard Specifications allow for substitution of 1 pound of Class F fly ash per pound of cement replaced up to 30%. In this project, percentages of 20% and 30% were used.

3.2.2 Aggregates

Aggregates for this project met the requirements of ASTM C33 and were selected as representative of many aggregates used for structural and paving concrete in the Piedmont area. The coarse aggregate was a granitic gneiss [SG of 2.63 (RP 2018-14) and 2.64 (RP 2020-13) and absorption of 0.40%] sourced from a quarry near Cary, NC. The coarse aggregate met the gradation requirements of No. 67 stone. A granitic gneiss intermediate aggregate, No 89M stone (SG of 2.66 and an absorption of 2.76%) from a quarry in Moncure, North Carolina was also used to produce the optimized aggregate gradation mixtures. The fine aggregate used for this study was a natural sand [SG 2.61 (RP 2018-14) and 2.62 (RP 2022-13), absorption 0.40%, and a fineness modulus of 2.65]. Sieve analysis results for the coarse and fine aggregates are shown in Appendix B, Figures B.3 and B.4.

3.2.3 Admixtures

A commercially available air entraining admixture (MasterAir AE 200 manufactured by BASF) and a mid-range water-reducing admixture (MasterPolyheed 997 manufactured by BASF) were used in all mixtures. The target slump for the mixtures was 3.5 inches, although reasonable variations to this target slump were accepted in order to achieve the target w/cm while maintaining the selected material proportions. NCDOT specifications allow an air content for pavement mixtures of $5.0\% \pm 1.5\%$, and for structural concrete $6.0\% \pm 1.5\%$. However, a relatively tight allowable air content tolerance of 5.0% to 6.0% was utilized for all batches in order to ensure consistency between test results and to ensure that differences in laboratory test results could be attributed to changes in materials, rather than changes in air content.

Table 3.2: Mixture proportions for non-optimized gradation mixtures (RP 2018-14) and optimized gradation mixtures (RP 2020-13)

Mixture ID	Mixture Type	Mixture Proportions, pcv						
		Fly Ash Repl. (%)	Cement	Fly Ash	No. 67 Coarse Aggregate	No. 89 Intermediate Aggregate	Fine Aggregate	Water
H-700-0	AA (high and medium cm content)	0	700	0	1659	0	1072	329.0
H-700-0*		0	630	0	1175	620	1065	296.1
H-560-140		20	560	140	1659	0	1022	329.0
H-560-140*		20	504	126	1158	615	1055	296.1
H-650-0		0	650	0	1659	0	1175	305.5
H-650-0*		0	585	0	1215	640	1105	275.0
H-520-130		20	520	130	1659	0	1129	305.5
H-520-130*		20	468	117	1204	632	1088	275.0
H-600-0		0	600	0	1659	0	1277	282.0
H-600-0*		0	540	0	1261	662	1130	253.8
H-600C-0		0	600	0	1659	0	1277	282.0
H-600C-0*		0	540	0	1261	662	1130	253.8
H-480-120		20	480	120	1659	0	1235	282.0
H-480-120*		20	432	108	1243	652	1125	253.8
H-420-180		30	420	180	1659	0	1214	282.0
H-420-180*		30	378	162	1227	652	1124	253.8
M-700-0		0	700	0	1659	0	1163	294.0
M-700-0*		0	630	0	1206	636	1107	264.6
M-560-140		20	560	140	1659	0	111	294.0
M-560-140*		20	504	126	1193	626	1093	264.6
M-650-0		0	650	0	1659	0	1259	273.0
M-650-0*		0	585	0	1248	658	1130	245.7
M-520-130		20	520	130	1659	0	1214	273.0
M-520-130*		20	468	117	1235	650	1115	245.7
M-600-0		0	600	0	1659	0	1356	252.0
M-600-0*		0	540	0	1284	678	1162	226.8
M-600C-0		0	600	0	1659	0	1356	252.0
M-600C-0*		0	540	0	1284	678	1162	226.8
M-480-120		20	480	120	1659	0	1313	252.0
M-480-120*		20	432	108	1277	672	1141	226.8
M-420-180		30	420	180	1659	0	1292	252.0
M-420-180*		30	378	162	1270	590	1211	226.8
M-600P-0		0	600	0	1659	0	1356	252.0
M-480P-120		20	480	120	1659	0	1313	252.0
M-420P-180		30	420	180	1659	0	1292	252.0
L-700-0	AA (low cm content and Pavement)	0	700	0	1659	0	1254	259.0
L-700-0*		0	630	0	1252	658	1122	233.1
L-560-140		20	560	140	1659	0	1205	259.0
L-560-140*		20	504	126	1224	650	1123	233.1
L-650-0		0	650	0	1659	0	1344	240.0
L-650-0*		0	585	0	1279	675	1159	216.0
L-520-130		20	520	130	1659	0	1298	240.0
L-520-130*		20	468	117	1270	668	1140	216.0
L-600-0		0	600	0	1659	0	1434	222.0
L-600-0*		0	540	0	1316	697	1186	199.8
L-600C-0		0	600	0	1659	0	1434	222.0
L-600C-0*		0	540	0	1316	697	1186	199.8
L-480-120		20	480	120	1659	0	1392	222.0
L-480-120*		20	432	108	1297	688	1177	199.8
L-420-180		30	420	180	1659	0	1370	222.0
L-420-180*		30	378	162	1293	684	1173	199.8

3.3 Testing Program and Results

The testing program for this project was identical to the testing program used in NCDOT RP 2018-14 (Cavalline et al. 2020a) to facilitate comparison of test results between conventional mixtures and optimized aggregate gradation mixtures. Testing was performed on fresh and hardened concrete in accordance with the AASHTO, ASTM, and other test procedures shown in Table 3.3. Since flexural strength tests are typically only required for pavement concrete, flexural strength (modulus of rupture) tests were only performed on the lower cementitious content mixtures, which were mixtures typical of pavement mixtures.

Table 3.3: Testing program

	Test name	Standard	Testing age(s) in days	Replicates
Fresh	Air content	ASTM C231	Fresh	1
	SAM number	AASHTO TP 118	Fresh	1
	Slump	ASTM C143	Fresh	1
	Fresh density (unit weight)	ASTM C138	Fresh	1
	Temperature	AASHTO T 309	Fresh	1
Hardened	Compressive strength	ASTM C39	3, 7, 28, 56, 90	3 each age
	Modulus of rupture (MOR, or flexural strength)	ASTM C78	28	2
	Modulus of elasticity (MOE) and Poisson's ratio	ASTM C469	28	2
	Surface Resistivity	AASHTO T 358	3, 7, 28, 56, 90	3 each age
	Rapid chloride permeability	ASTM C1202	28, 90	2
	Formation factor (via Bucket Test)	Protocol by J. Weiss, Oregon State University (Weiss 2018)	35	2
	Shrinkage	ASTM C157	Per standard	3
	Freeze-thaw durability	ASTM C666 (procedure A)	Per standard	3
	Hardened air content	ASTM C457 (automated)	N/A	2

Batching was performed in accordance with ASTM C685. For higher-cementitious material content (structural) mixtures, all specimens were produced from one batch, including concrete for fresh concrete tests, and test specimen for compressive strength/surface resistivity, modulus of elasticity, formation factor, rapid chloride penetration, hardened air void system, freeze-thaw durability, and shrinkage. Specimens for low-cementitious content (paving) mixtures were prepared in two batches. One mixture included concrete used for fresh tests and for preparation of test specimens for compressive strength/surface resistivity, modulus of elasticity, formation factor, and rapid chloride penetration tests. The second mixture included concrete used for fresh tests and for preparation of specimens for modulus of rupture, hardened air void system, shrinkage, and freeze-thaw durability tests.

3.3.1 Fresh Concrete Properties

Fresh concrete tests, including slump, air content, temperature, density, and SAM were performed immediately after mixing. To mitigate the influence of a wide range of air contents on the test results, the air content of all batches was restricted to a range between 5.0% to 6.0%. The target slump for mixtures in this project was 3.5 ± 1 inch. However, based on the objectives of the project, it was more important to ensure the desired w/cm ratios were maintained. Several mixtures had slumps that exceeded this target (H-700-0, H-700*-0, H-560-140, H-650-0, H-650*-0, H-520-130, M-700-0, M-560-140, M-560*-140) but this could be expected since these mixtures tended to be the higher w/cm ratio mixtures. Mixtures with slumps below 3.5 inches were deemed acceptable only if they could be adequately consolidated into the specimen molds. A summary of test results for each fresh concrete property test (average of the two batches for each mixture) is presented in Appendix B, Table B.1, with results of SAM tests for optimized aggregate gradation mixtures in Table B.2.

3.3.2 Mechanical Properties

Results for mechanical property tests are presented below, with results for optimized gradation mixtures compared to both NCDOT specifications and the companion non-optimized gradation mixtures. For all mechanical property tests, it should again be noted that the high (0.47) w/cm ratio mixtures were originally batched as non-optimized aggregate gradation mixtures to provide test results that are indicative of poor concrete mixtures that are not typical to NCDOT use. Optimized aggregate gradation concrete mixtures at the high w/cm ratio were batched and tested for a direct comparison between the optimized and non-optimized aggregate gradation mixtures. However, as these mixtures are representative of a higher w/cm ratio than typical NCDOT concrete mixtures, these results may not be as valuable.

3.3.2.1. Compressive Strength

Averaged test results for all test dates with test results for both non-optimized and optimized aggregate gradation mixtures can be found in Table B.3 and are graphically displayed in figures presented in this section. NCDOT's 2018 Standard Specifications require paving and Type AA bridge mixtures to have a minimum 28-day compressive strength of 4,500 psi. Of the 24 optimized aggregate gradation mixtures, only H-420*-180 did not meet this requirement. This mixture contained 30 percent fly ash, which is known to provide later-age strength gain later than mixtures with portland cement

alone, and did, however, meet the minimum requirement at 56 days. In the following sections, average compressive strength results are presented with mixtures sorted by cementitious material, comparing optimized and non-optimized aggregate gradation mixtures by w/cm ratio and fly ash rates to understand the differences between the aggregate types.

Figure 3. Figure 3.6 shows the compressive strength test results for pairs of optimized and non-optimized aggregate gradation mixtures developed with 700 pcy cementitious material. Similarly, Figures 3.7 and 3.8 show the compressive strength test results for pairs of optimized and non-optimized aggregate gradation mixtures developed with 650 pcy and 600 pcy of cementitious material, respectively. Optimized aggregate gradation mixtures and non-optimized aggregate gradation mixtures performed similarly on most test dates and had similar variability on each test date.

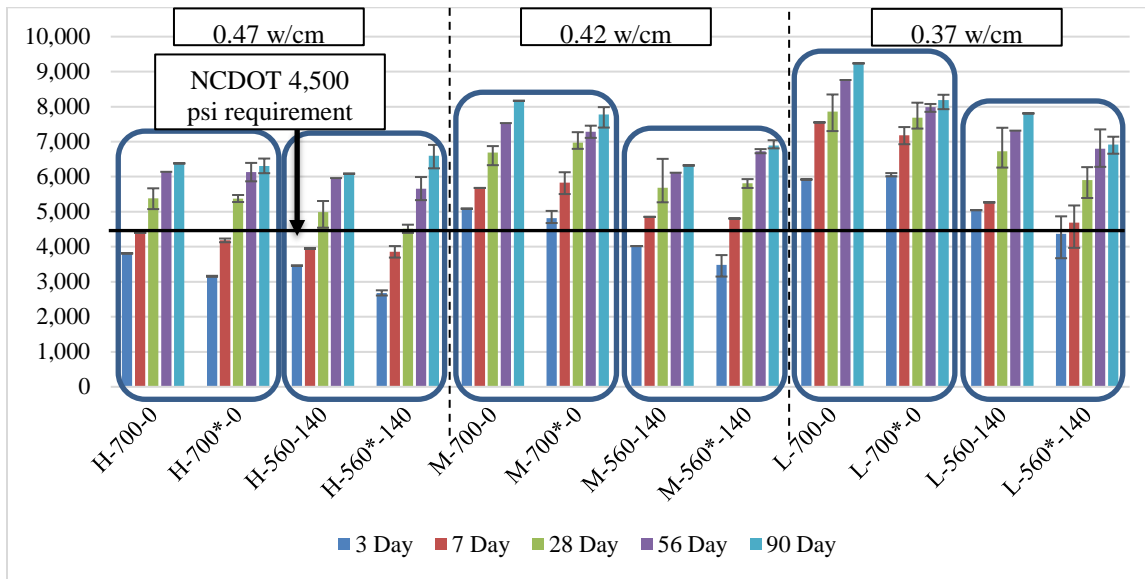


Figure 3.6: Development of average compressive strength for 700/700* pcy cementitious material mixtures

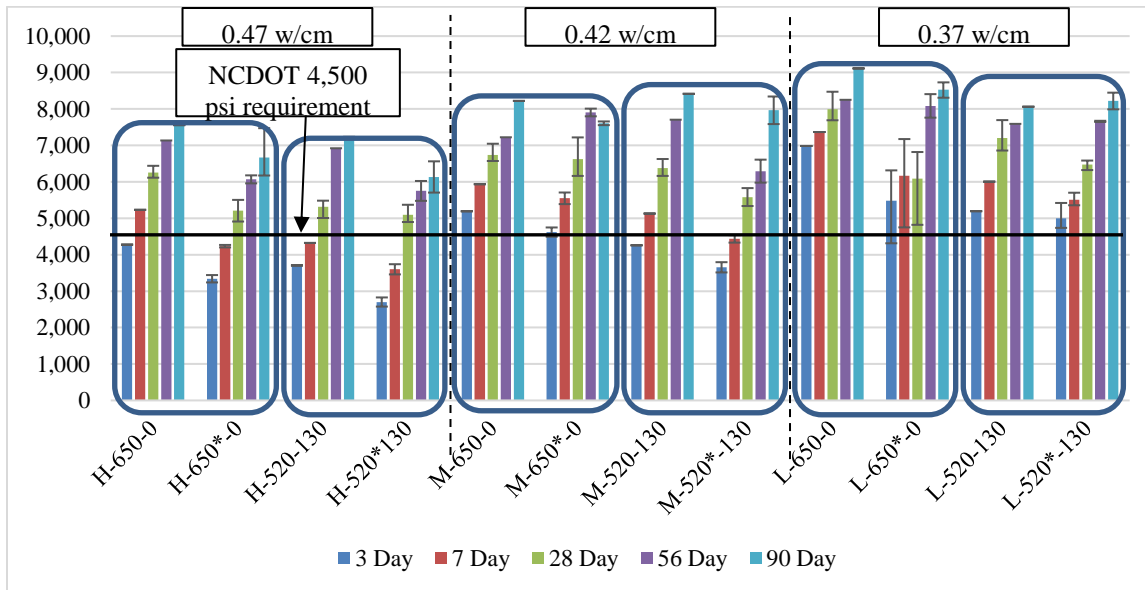


Figure 3.7: Development of average compressive strength for 650/650* pcy cementitious material mixtures

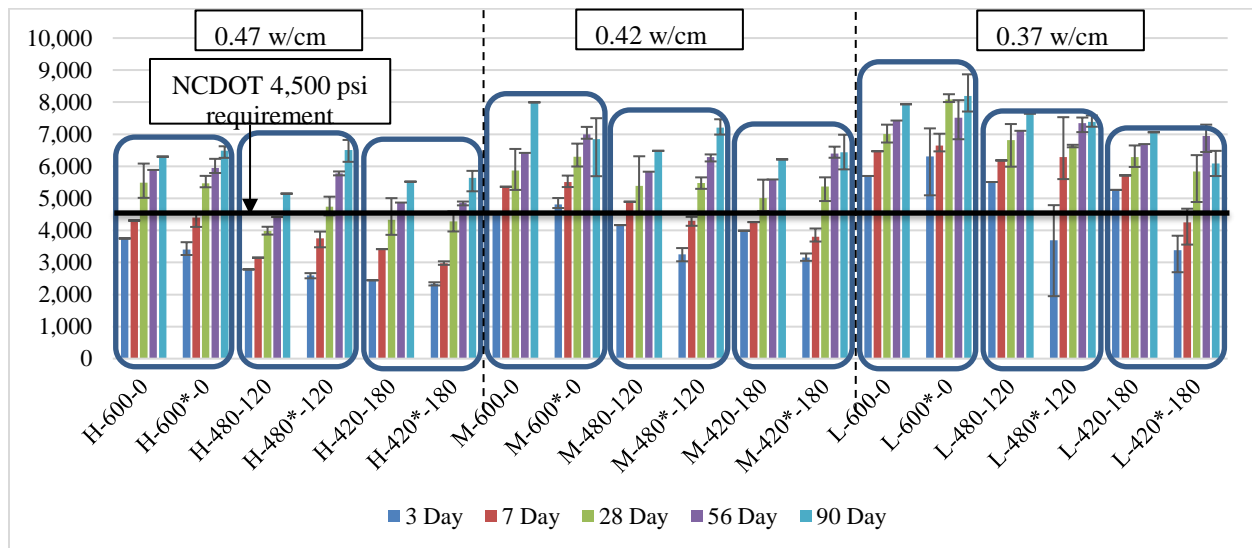


Figure 3.8: Development of average compressive strength for 600/600* pcy cementitious material mixtures

To further compare the strength gain of optimized vs. non-optimized mixtures with similar cementitious materials contents, a series of plots were created. Figures 3.9 through 3.11 illustrate the strength gain for pairs of mixtures with total cementitious contents of 700 pcy at each water cement ratio, and plots for other cementitious materials contents and w/cm ratios are provided in Appendix B in Figures B.5 through B.7 (for 650 pcy total cementitious content mixtures) and B.8 through B.10 (for 600 pcy total cementitious content mixtures). In Figures 3.9 through 3.11, as well as Figures B.5 through B.10, the optimized aggregate gradation mixtures tended to show similar strength gain over time, but often had slightly lower strength, particularly at later ages. However, as indicated previously, almost all mixtures readily met NCDOT's strength target of 4500 psi.

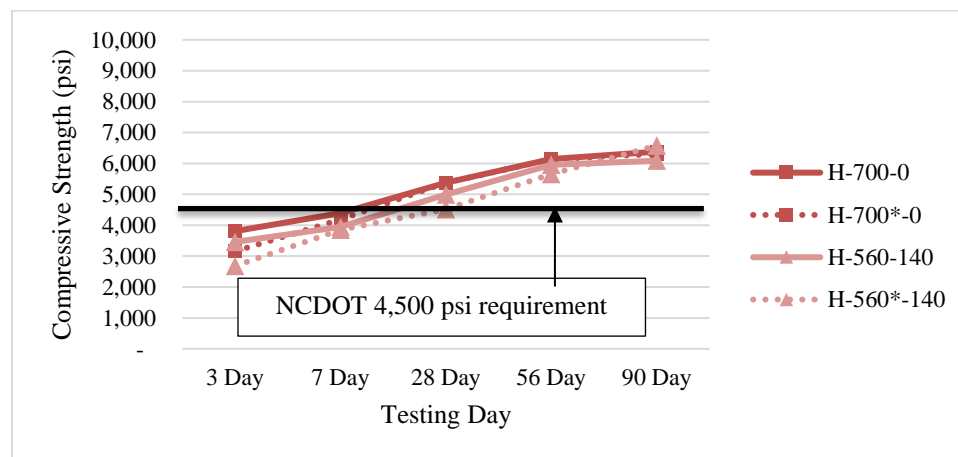


Figure 3.9: Development of compressive strength for 700/700* pcy cementitious material mixtures at 0.47 w/cm ratio

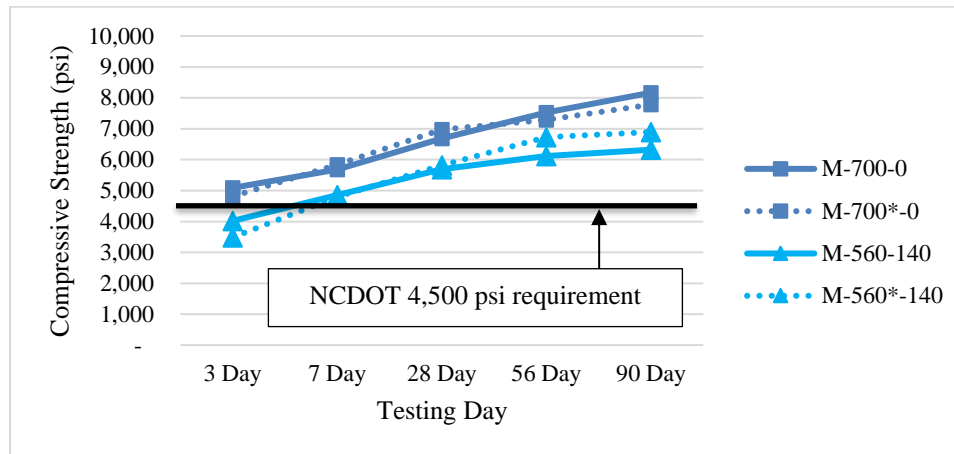


Figure 3.10: Development of compressive strength for 700/700* pcy cementitious material mixtures at 0.42 w/cm ratio

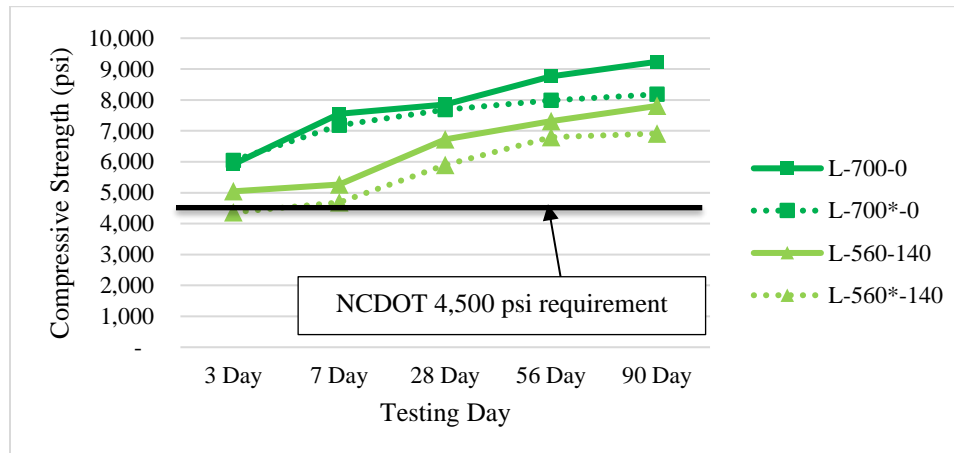


Figure 3.11: Development of compressive strength for 700/700* pcy cementitious material mixtures at 0.37 w/cm ratio

Table 3.4 shows the average compressive strength and the average percent difference of average compressive strengths between 700* pcy optimized aggregate gradation mixtures when compared to their 700 pcy non-optimized companion mixtures. The average percent difference was calculated by taking the average of all mixtures percent difference between optimized and non-optimized aggregate gradation mixtures compressive strength results. 700* pcy optimized aggregate gradation mixtures exhibited an average compressive strength noticeably lower for early age (3-day) testing. However, a fairly negligible difference (less than 10 percent different on average with all mixtures meeting the 28-day compressive strength requirement of 4,500 psi) was exhibited at all other ages.

Table 3.4: Average percent difference between average compressive strength for 700* pcy optimized mixtures vs 700 pcy non-optimized mixtures

Characteristic	Mixture Type	Test Day				
		3 Day	7 Day	28 Day	56 Day	90 Day
All 700* pcy mixtures	Non-optimized	4,557	5,282	6,222	6,971	7,334
	Optimized	4,091	5,091	6,044	6,764	7,110
	Average percent difference	-14.1%	-3.9%	-3.5%	-2.8%	-2.7%
Straight cement mixtures	Non-optimized	4,940	5,874	6,641	7,478	7,929
	Optimized	4,670	5,733	6,679	7,133	7,425
	Average percent difference	-8.1%	-2.5%	0.6%	-4.4%	-6.3%
Fly ash replacement mixtures	Non-optimized	4,175	4,690	5,804	6,464	6,739
	Optimized	3,511	4,449	5,409	6,396	6,794
	Average percent difference	-20.0%	-5.3%	-7.5%	-1.3%	0.9%

Table 3.5 shows the average compressive strength as well as their average percent difference of average compressive strengths between 700* pcy optimized aggregate gradations when compared to their 700 pcy non-optimized companion mixtures grouped by w/cm ratio. As previously described, early age (3-day) average compressive strengths were noticeably different, but pairs of mixtures tended to perform more similarly as the concrete aged. 700* pcy optimized aggregate gradation mixtures with a w/cm ratio of 0.47 and 0.42 performed more similarly to their companion non-optimized mixtures at later test dates than the 0.37 w/cm ratio optimized mixtures. However, all pairs with the exception of 0.37 w/cm ratio optimized mixtures showed a fairly negligible average percent difference (less than 10% different on average with all mixtures meeting the 28-day required compressive strength of 4,500 psi). Although the optimized aggregate mixtures at the 0.37 w/cm ratio exhibited a 90-day compressive strength average 12.9 percent lower than their companion non-optimized 0.37 w/cm ratio mixtures, it is noted that this difference was computed based upon the optimized aggregate gradation exhibiting a 90-day average compressive strength of 7,549 psi and was deemed negligible.

Table 3.5: Average percent difference between average compressive strength for 700* pcy optimized mixtures vs 700 pcy non-optimized mixtures by w/cm ratio

w/cm ratio	Mixture Type	Test Day				
		3 Day	7 Day	28 Day	56 Day	90 Day
0.47	Non-optimized	3,636	4,172	5,187	6,051	6,234
	Optimized	2,919	4,019	4,945	5,896	6,442
	Average percent difference	-24.9%	-3.8%	-5.3%	-2.7%	3.1%
0.42	Non-optimized	4,554	5,267	6,188	6,823	7,245
	Optimized	4,149	5,321	6,393	7,006	7,338
	Average percent difference	-10.5%	0.8%	3.1%	2.9%	1.7%
0.37	Non-optimized	5,483	6,409	7,293	8,039	8,523
	Optimized	5,204	5,933	6,793	7,391	7,549
	Average percent difference	-6.8%	-8.8%	-8.1%	-8.7%	-12.9%

Similar tables comparing the compressive strength gain of pairs of optimized and non-optimized mixtures with 650 and 600 pcy of cementitious material, at all w/cm ratios, are provided in Appendix B, Tables B.4 through B.7, and Tables B.8 through B.10. In general, optimized aggregate gradation mixtures and non-optimized aggregate gradation mixtures performed similarly on most test dates and had an expected variability on each test date. Although optimized aggregate gradation mixtures typically exhibited lower compressive strength than their companion optimized mixtures, the average 28-day compressive strengths almost always met the NCDOT standard specification target of 4,500 psi, and all mixtures exceeded the target by 56 days.

3.3.2.2 Modulus of Rupture

Modulus of rupture (MOR) testing was performed at 28-days for 600 pcy cementitious content (pavement) mixtures only, and results for optimized aggregate gradation and non-optimized aggregate gradation mixtures are presented in Table 3.6. MORs for optimized aggregate gradation mixtures ranged from 581 psi to 840 psi, with an average of 715 psi, while the 28-day MOR of non-optimized aggregate gradation mixtures ranged from 715 psi to 822 psi, with an average of 766 psi. All optimized aggregate gradation mixtures MOR test results were higher than the NCDOT required 28-day MOR of 650 psi, except for mixtures H-420*-180 and M-420*-120. The two mixtures that did not meet the requirement contained 30 percent fly ash, and significant additional strength gain after 28 days could be expected. H-420*-180 also did not meet the 28-day compressive strength requirement by the NCDOT but did by the 56-day test. As fly ash mixtures are known to gain strength later than straight cement mixtures, these mixtures may have met the requirement by a later testing date.

Table 3.6: MOR, MOE, and Poisson's Ratio

Mixture ID	Modulus of Rupture (psi)		Modulus of Elasticity (psi)		Poisson's Ratio	
	Non-Optimized	Optimized	Non-Optimized	Optimized	Non-Optimized	Optimized
H-700-0	-	-	3,045,000	3,266,000	0.21	0.21
H-560-140	-	-	2,675,000	2,894,000	0.20	0.20
H-650-0	-	-	3,650,000	3,862,000	0.21	0.20
H-520-130	-	-	3,056,000	3,349,000	0.23	0.24
H-600-0	745	720	2,980,000	3,733,000	0.19	0.19
H-480-120	808	704	2,527,000	3,230,000	0.20	0.22
H-420-180	724	581	2,461,000	2,995,000	0.22	0.20
M-700-0	-	-	3,569,000	3,975,000	0.24	0.18
M-560-140	-	-	3,363,000	4,260,000	0.18	0.18
M-650-0	-	-	3,706,000	3,842,000	0.20	0.14
M-520-130	-	-	3,620,000	3,921,000	0.20	0.18
M-600-0	822	748	3,398,000	4,294,000	0.21	0.17
M-480-120	726	683	3,076,000	3,942,000	0.20	0.20
M-420-180	726	637	3,131,000	3,700,000	0.19	0.20
L-700-0	-	-	3,826,000	3,838,000	0.17	0.15
L-560-140	-	-	3,656,000	4,492,000	0.20	0.19
L-650-0	-	-	4,317,000	4,588,000	0.19	0.17
L-520-130	-	-	3,632,000	3,992,000	0.21	0.15
L-600-0	817	840	3,761,000	4,932,000	0.19	0.19
L-480-120	718	808	3,087,000	3,949,000	0.22	0.17
L-420-180	815	713	3,241,000	3,942,000	0.20	0.17

Table 3.6: MOR, MOE, and Poisson's Ratio

Mixture ID	Modulus of Rupture (psi)		Modulus of Elasticity (psi)		Poisson's Ratio	
	Non-Optimized	Optimized	Non-Optimized	Optimized	Non-Optimized	Optimized
H-700-0	-	-	3,045,000	3,266,000	0.21	0.21
H-560-140	-	-	2,675,000	2,894,000	0.20	0.20
H-650-0	-	-	3,650,000	3,862,000	0.21	0.20
H-520-130	-	-	3,056,000	3,349,000	0.23	0.24
H-600-0	745	720	2,980,000	3,733,000	0.19	0.19
H-480-120	808	704	2,527,000	3,230,000	0.20	0.22
H-420-180	724	581	2,461,000	2,995,000	0.22	0.20
M-700-0	-	-	3,569,000	3,975,000	0.24	0.18
M-560-140	-	-	3,363,000	4,260,000	0.18	0.18
M-650-0	-	-	3,706,000	3,842,000	0.20	0.14
M-520-130	-	-	3,620,000	3,921,000	0.20	0.18
M-600-0	822	748	3,398,000	4,294,000	0.21	0.17
M-480-120	726	683	3,076,000	3,942,000	0.20	0.20
M-420-180	726	637	3,131,000	3,700,000	0.19	0.20
L-700-0	-	-	3,826,000	3,838,000	0.17	0.15
L-560-140	-	-	3,656,000	4,492,000	0.20	0.19
L-650-0	-	-	4,317,000	4,588,000	0.19	0.17
L-520-130	-	-	3,632,000	3,992,000	0.21	0.15
L-600-0	817	840	3,761,000	4,932,000	0.19	0.19
L-480-120	718	808	3,087,000	3,949,000	0.22	0.17
L-420-180	815	713	3,241,000	3,942,000	0.20	0.17

Figure 3.12 shows the MOR test results for all optimized aggregate gradation mixtures and non-optimized companion mixtures, grouped by fly ash content and Figure 3.13 shows the MOR of optimized gradation mixtures and non-optimized gradation mixtures grouped by w/cm ratio.

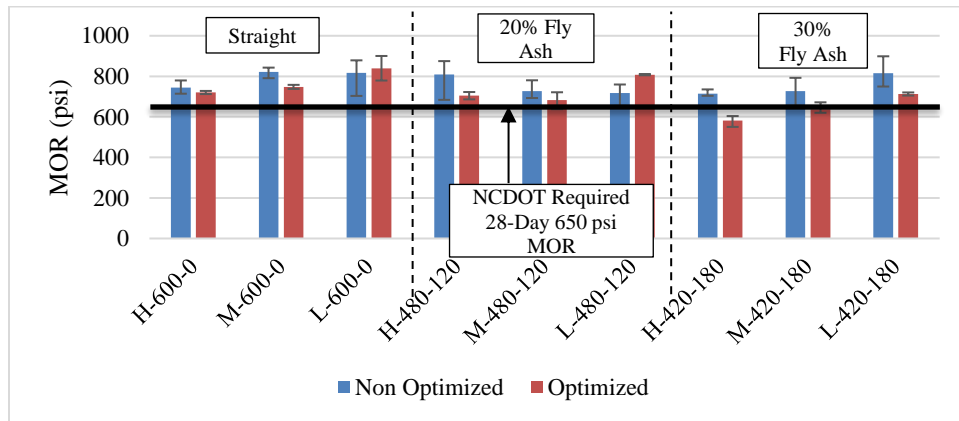


Figure 3.12: MOR of optimized and non-optimized aggregate gradation mixtures by fly ash content

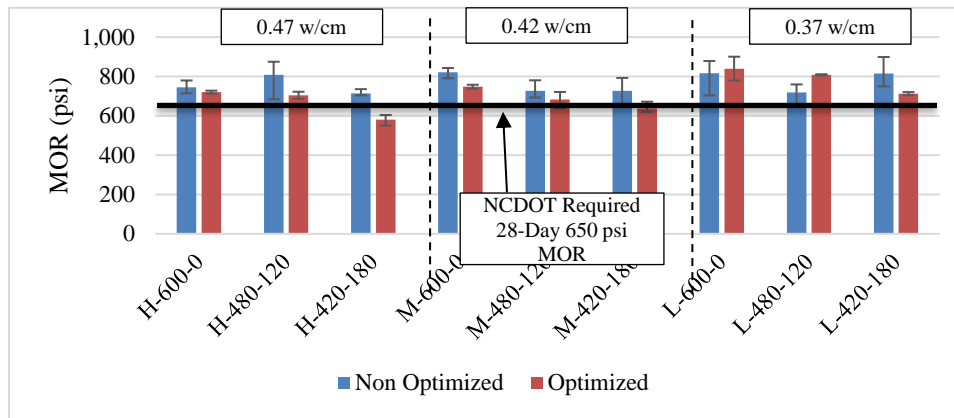


Figure 3.13: MOR of optimized and non-optimized aggregate gradation mixtures by w/cm ratio

Table 3.7 shows the average percent difference in MOR between optimized aggregate gradation mixtures and companion non-optimized mixtures. Optimized aggregate gradation mixtures with 20 percent fly ash replacement showed a negligible difference (while meeting the NCDOT 28-day required MOR of 650 psi) when compared with companion non-optimized 20% fly ash replacement mixtures, companion optimized straight cement mixtures, and companion non-optimized straight cement mixtures. Optimized aggregate gradation mixtures with 30% fly ash replacement did, however, show a significant decrease in their MOR values when compared to all of their companion mixtures.

As mentioned previously, two optimized 30% fly ash replacement mixtures did not meet the NCDOT 28-day requirement of 650 psi: H-420*-180 with an MOR of 581 psi and M-420*-180 with an MOR of 637. As the mixtures that contain the highest rate of fly ash replacement, it is possible they may have reached the required MOR of 650 psi at a later date due to the delayed strength gain attributed to fly ash mixtures. It also should be noted that while these mixtures did not meet the NCDOT 28-day requirement, they did meet the 28-day recommended AASHTO PP 84 target of 600 psi.

Table 3.7: Average percent difference between optimized aggregate gradation mixtures MOR and companion mixtures

Optimized mixture characteristic	Non-optimized companion mixture	Optimized straight cement companion mixture	Non-optimized straight cement companion mixture
Straight cement mixtures	-3.5%	-	-
20% fly ash replacement mixtures	-3.3%	-5.2%	-9.0%
30% fly ash replacement mixtures	-17.1%	-19.7%	-23.9%

3.3.2.3 Modulus of Elasticity

Modulus of Elasticity (MOE) results of both optimized aggregate gradation and non-optimized aggregate gradation mixtures are provided in Table 3.6. The 28-day MOE test results for optimized aggregate gradation mixtures ranged from approximately 2,890,000 psi to 4,930,000 psi with an average of approximately 3,840,000 psi. These values are greater than the 28-day MOE test results for non-optimized aggregate gradation mixtures, which ranged from approximately 2,460,000 psi to 4,320,000 psi with an average of approximately 3,320,000 psi. As could be expected, the mixtures with the lowest w/cm ratio had MOE values relatively higher than the mixtures with the highest w/cm ratio. MOE values for optimized aggregate gradation mixtures tended to be higher than their companion non-optimized mixtures. Figure 3.14 shows the results of the MOE tests for all pairs of non-optimized and optimized mixtures grouped by w/cm ratio.

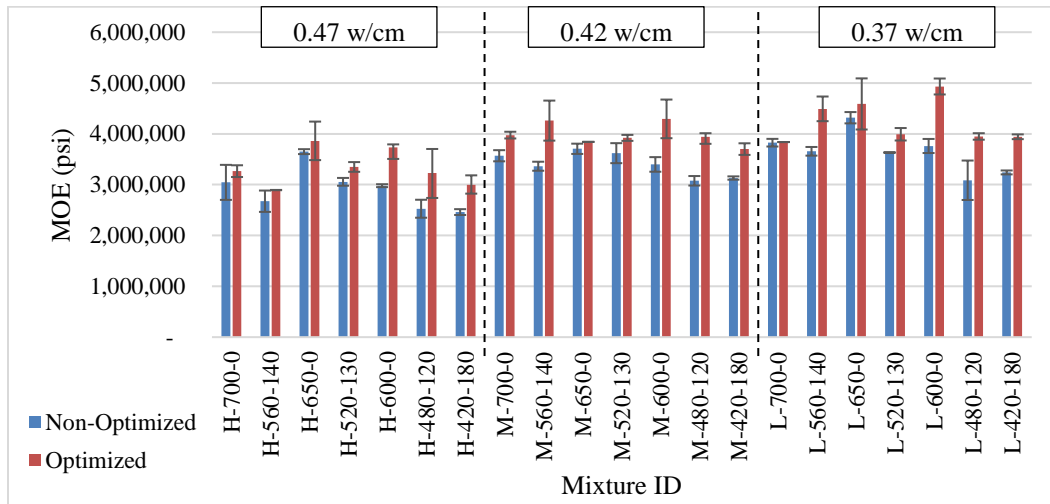


Figure 3.14: Optimized and non-optimized aggregate gradation mixtures 28-day MOE by w/cm ratio

Figure 3.15 displays the measured MOE values for both optimized and non-optimized mixtures plotted against their 28-day compressive strength in comparison with the ACI 318 calculated MOE value using equation 19.2.2.1b (Equation 3.1) and the MOE calculated using AASHTO LRFD equation C5.4.2.4-2 (Equation 3.2) (AASHTO 2017, ACI 2019). This figure displays optimized aggregate gradation mixtures and non-optimized aggregate gradations 28-day MOE values were lower than the calculated values using ACI 318, which is a finding similar to other concrete studies performed by the research team. Studies have shown that the type of aggregate used in concrete mixtures can affect the MOE (Beuhausen and Ditmer 2015), and this is the suspected primary cause of the difference.

$$E_c = 57,000 * \sqrt{f'_c} \quad \text{Equation 3.1}$$

$$E_c = 33,000 * K_1 * w_c^{1.5} * \sqrt{f'_c} \quad \text{Equation 3.2}$$

K_1 = correction factor for source of aggregate
 w_c = unit weight of concrete (kcf)

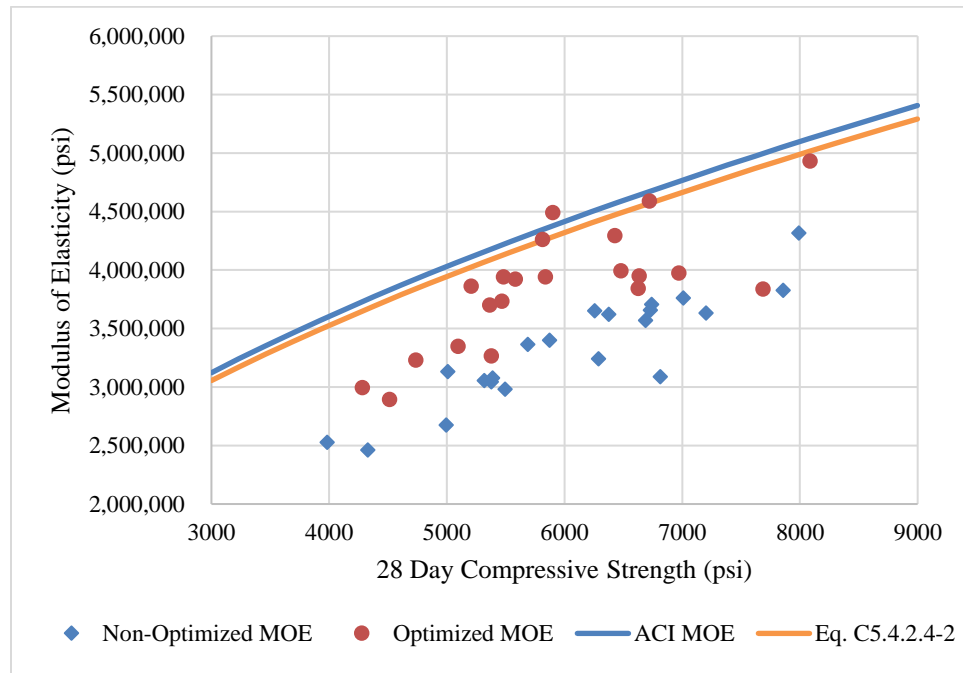


Figure 3.15: MOE vs. 28-day compressive strength, plotted with ACI and AASHTO LRFD calculated MOE

Table 3.8, the average percent difference between the measured 28-day MOE values of optimized mixtures are compared to their companion non-optimized mixtures, the ACI 318 calculated MOE and the AASHTO calculated MOE,

grouped by w/cm ratio and by cementitious content. As the w/cm ratio decreased in optimized aggregate gradation mixtures, their 28-day MOE values became closer to the calculated MOE using both ACI 318 and AASHTO LRFD equations but did not change significantly when compared to their companion non-optimized aggregate gradation mixtures. As cementitious content decreased in optimized aggregate gradation mixtures, their measured 28-day MOE became closer to the calculated MOE values using ACI 318 and ASHTO LRFD equations.

All optimized gradation mixtures had measured 28-day MOE values an average of 13.6% higher than their companion non-optimized gradation mixtures. As the w/cm ratio decreased in optimized aggregate gradation mixtures the average percent difference remained fairly consistent. As the cementitious content decreased in optimized aggregate gradation mixtures there was no trend in MOE change observed. However, medium and low cementitious content optimized aggregate gradation mixtures had the highest 28-day MOE, which could be expected (as shown in Table 3.9), while non-optimized aggregate gradation mixtures with low cementitious content mixtures had the lowest 28-day MOE.

Table 3.8. Average percent difference in MOE between optimized mixtures, non-optimized mixtures calculated per ACI 318 and AASHTO LRFD

Optimized mixture characteristic	Average % difference vs non-optimized companion mixture	Average % difference vs ACI 318 calculated MOE	Average % difference vs AASHTO calculated MOE
All mixtures	13.6%	-14.3%	-13.9%
0.47 w/cm ratio	12.6%	-21.0%	-19.8%
0.42 w/cm ratio	14.4%	-10.9%	-10.8%
0.37 w/cm ratio	13.9%	-10.9%	-11.0%
700* pcy of cementitious material	10.8%	-18.3%	-17.4%
650* pcy of cementitious material	6.7%	-12.4%	-12.1%
600* pcy of cementitious material	20.1%	-12.9%	-12.7%

Table 3.9: Average 28-day MOE of optimized aggregate gradation mixtures and non-optimized aggregate gradation mixtures by cementitious content

Cementitious content (pcy)	Mixture characteristic	Non-optimized	Optimized
700	All mixtures	3,356,000	3,788,000
	Straight cement	3,480,000	3,693,000
	Fly Ash replacement	3,231,000	3,882,000
650	All mixtures	3,664,000	3,926,000
	Straight cement	3,891,000	4,097,000
	Fly ash replacement	3,436,000	3,754,000
600	All mixtures	3,074,000	3,857,000
	Straight cement	3,380,000	4,320,000
	Fly ash replacement	2,921,000	3,626,000

Table 3.10 shows the percent difference in measured MOE test results between optimized aggregate gradation straight cement and fly ash mixtures when compared to companion non-optimized mixtures, companion optimized straight cement mixtures, companion non-optimized straight cement mixtures, and the calculated MOE using ACI 318 and AASHTO LRFD equations. Optimized aggregate gradation fly ash mixtures performed as expected, with an increase in fly ash replacement causing lower 28-day MOE values when compared to all mixtures.

Table 3.10: Average percent difference in 28-day MOE by type of mixture

Optimized mixture characteristic	Average % difference vs non-optimized companion mixture	Average % difference vs companion optimized straight cement mixture	Average % difference vs companion non-optimized straight cement mixture	Average % difference vs ACI 318 calculated MOE	Average % difference vs AASHTO calculated MOE
Straight cement mixtures	10.8%	-	-	-14.4%	-14.0%
All optimized fly ash mixtures	15.8%	-11.3%	4.5%	-14.2%	-13.8%
20% fly ash replacement	12.6%	-6.3%	3.7%	-11.2%	-10.8%
30% fly ash replacement	17.0%	-21.9%	4.4%	-15.9%	-15.6%

3.3.2.4 Poisson's Ratio

Poisson's ratios for both optimized aggregate gradation and non-optimized aggregate gradation mixtures are shown in Table 3.6. Optimized aggregate gradation mixtures exhibited Poisson's ratios in the range of 0.14 to 0.24, with an average of 0.19. Non-optimized aggregate gradation mixtures exhibited Poisson's ratios that ranged from 0.17 to 0.24 with an average of 0.20. Figure shows the Poisson's ratio for all pairs of non-optimized aggregate gradation mixtures and optimized mixtures, with mixtures grouped by the w/cm ratio of the mixtures. Poisson's ratios for optimized aggregate gradation mixtures and non-optimized aggregate gradation mixtures were similar on most test dates and had an expected variability on each test date.

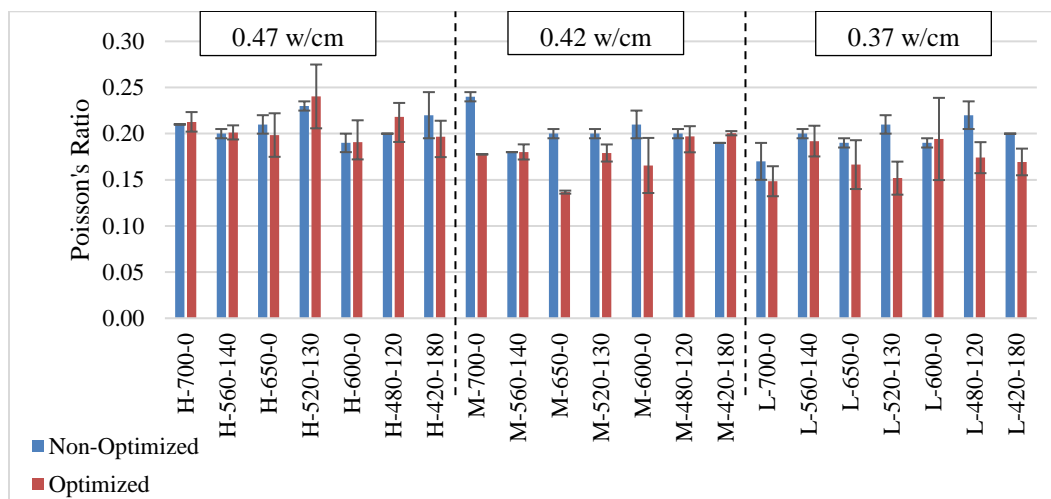


Figure 3.16: Poisson's ratio for optimized and non-optimized mixtures at 28-days

Table 3.11 shows optimized aggregate gradation mixtures 28-day Poisson's ratios compared with the 28-day Poisson's ratios for their companion non-optimized mixtures, grouped by w/cm ratio and cementitious content (pcy). As the w/cm ratio of optimized aggregate gradation mixtures decreased, the average Poisson's ratio for each w/cm ratio decreased from 0.21 to 0.17 while the average Poisson's ratio for non-optimized aggregate gradation mixtures decreased from 0.21 to 0.19. Optimized gradation mixtures with a cementitious material content of 700* pcy and 600* pcy had average Poisson's ratios negligibly different (less than 10 percent) when compared to companion non-optimized gradation mixtures, while optimized aggregate gradation mixtures with 650* pcy of cementitious material were noticeably different. The percent difference for 650/650* pcy mixtures could be skewed, as the two lowest Poisson's ratios for optimized aggregate gradation mixtures (M-650*-0, 0.14; and L-520*-130, 0.15) were from the 650*/650 pcy cementitious material content.

Table 3.11: Average percent difference between Poisson's ratios

Optimized mixture characteristic	Average % difference in Poisson's ratio vs non-optimized companion mixture
All mixtures	-11.1%
0.47 w/cm ratio	-0.4%
0.42 w/cm ratio	-16.6%
0.37 w/cm ratio	-16.2%
700* pcy of cementitious material	-8.6%
650* pcy of cementitious material	-18.7%
600* pcy of cementitious material	-7.6%

Table 3.12 shows the average percent difference between the Poisson's ratios of optimized aggregate gradation fly ash replacement mixtures compared to their companion non-optimized mixtures, companion optimized straight cement mixtures, and their companion non-optimized straight cement mixtures. Optimized aggregate gradation fly ash mixtures all exhibited a negligible difference (less than 10 percent) in measured Poisson's ratios when compared with their companion mixtures.

Table 3.12: Average percent difference in Poisson's ratios between all optimized fly ash replacement mixtures and their companion mixtures, grouped by fly ash replacement rate

Optimized mixture characteristic	Average % difference in Poisson's ratio vs non-optimized companion mixture	Average % difference in Poisson's Ratio vs companion optimized straight cement mixture	Average % difference in Poisson's Ratio vs companion non-optimized straight cement mixture
Straight cement mixtures	-15.4%	-	-
All optimized fly ash mixtures	-7.8%	6.0%	-5.6%
20% fly ash replacement	-6.3%	6.1%	-4.8%
30% fly ash replacement	-8.3%	1.9%	-4.5%

3.3.3 Durability Performance

Durability performance tests were performed using the methods listed in Table 3.3. A summary of these results (typically the average of two or three specimens) is provided in Table 3.13. The durability performance between non-optimized and optimized mixtures is compared using the average percent difference, which was calculated by taking the average of the percent difference between companion non-optimized and optimized aggregate gradation mixtures. Supporting information is presented in Theilgard (2022).

It should again be noted that the high (0.47) w/cm ratio mixtures were originally batched as non-optimized aggregate gradation mixtures to provide test results that are indicative of poor concrete mixtures that are not typical to NCDOT use. Optimized aggregate gradation concrete mixtures at the high w/cm ratio were batched and tested for a direct comparison between the optimized and non-optimized aggregate gradation mixtures. However, as these mixtures are representative of a higher w/cm ratio than typical NCDOT concrete mixtures, these results may not be as valuable.

3.3.3.1 Surface Resistivity

Surface resistivity test results can be qualitatively described with the permeability ratings included in AASHTO T 358, provided in Table 3.13. Results of surface resistivity tests are presented in Table 3.14, along with results from RCPT. Surface resistivity test results for optimized aggregate gradation mixtures tended to be lower than their companion non-optimized aggregate gradation mixtures. This does not necessarily mean less permeable mixtures and could be a function of reduced cement content, the increased volume of interfacial transition zone (ITZ) offered by the increased aggregate volume, the 10% paste reduction, or some other reason.

Table 3.13: AASHTO T 358 surface resistivity index

Resistivity measured with 4"x8" Cylinder (kΩ·cm)	Chloride Ion Permeability
<12	High
12-21	Moderate
21-37	Low
37-254	Very Low
>254	Negligible

Table 3.14: Surface resistivity and RCPT results for optimized aggregate gradation and non-optimized aggregate gradation mixtures

Mixture ID	Non-optimized mixtures - Surface Resistivity (k Ω *cm)		Optimized mixtures - Surface Resistivity (k Ω *cm)		Non-optimized mixtures – RCPT (coulombs passed)		Optimized mixtures – RCPT (coulombs passed)	
	28 Day	90 Day	28 Day	90 Day	28 Day	90 Day	28 Day	90 Day
H-700-0	7.3	14.0	8.0	8.2	4253	3070	6976	5080
H-560-140	6.6	18.8	7.1	13.1	3860	2118	7067	3407
H-650-0	8.7	9.8	6.8	8.1	4687	4018	6538	4832
H-520-130	10.6	21.8	6.2	12.3	4480	2879	7746	3575
H-600-0	8.1	17.6	8.4	9.6	4159	3439	6208	4922
H-480-120	9.5	17.1	7.0	13.5	3766	2266	7204	3358
H-420-180	11.2	20.7	6.0	15.9	3571	1980	6699	3148
M-700-0	10.9	12.5	8.6	11.5	4479	3822	5261	4275
M-560-140	6.4	18.4	7.5	16.8	4354	2148	6930	3356
M-650-0	10.7	11.9	8.6	12.7	3506	3008	5580	4355
M-520-130	12.1	26.9	6.5	12.8	4247	2154	5486	3439
M-600-0	10.0	22.7	8.5	9.2	3943	3087	5192	4450
M-480-120	9.4	20.3	7.3	13.4	3632	2132	7421	3377
M-420-180	6.1	19.6	8.8	22.0	3391	1768	5687	2362
L-700-0	9.3	15.7	10.2	13.7	4766	2947	4497	3332
L-560-140	12.3	20.2	10.6	26	4094	2136	3831	1559
L-650-0	14.8	18.6	9.1	14	4239	2197	4107	3293
L-520-130	13.1	23.3	9.5	27	2532	1409	4389	1848
L-600-0	9.9	17.0	10.0	16.5	3572	1962	4351	3227
L-480-120	9.1	19.8	12.0	29.3	2987	1840	3644	1441
L-420-180	8.4	18.7	10.2	30	2879	1557	4041	1648

700*/700 pcy of Cementitious Material Surface Resistivity

Figure 3.17 provides the surface resistivity test results for pairs of optimized and non-optimized mixtures for the 700 lb cementitious materials mixtures. Optimized aggregate gradation mixtures consistently exhibited surface resistivity values lower than their companion non-optimized aggregate gradation mixtures. Also shown on Figure 3.17 are the proposed surface resistivity targets for pavement mixtures (11 k Ω *cm), and bridge mixtures (15 k Ω *cm) developed as part of the previous study (Biggers 2019, Cavalline et al. 2020a). Although the proposed target for structural mixtures was not met by most mixtures at the high water-cement ratios, the target was met by 90 days for all mixtures containing fly ash (both optimized and non-optimized aggregate gradations) at moderate (0.42) and low (0.37) w/cm ratios.

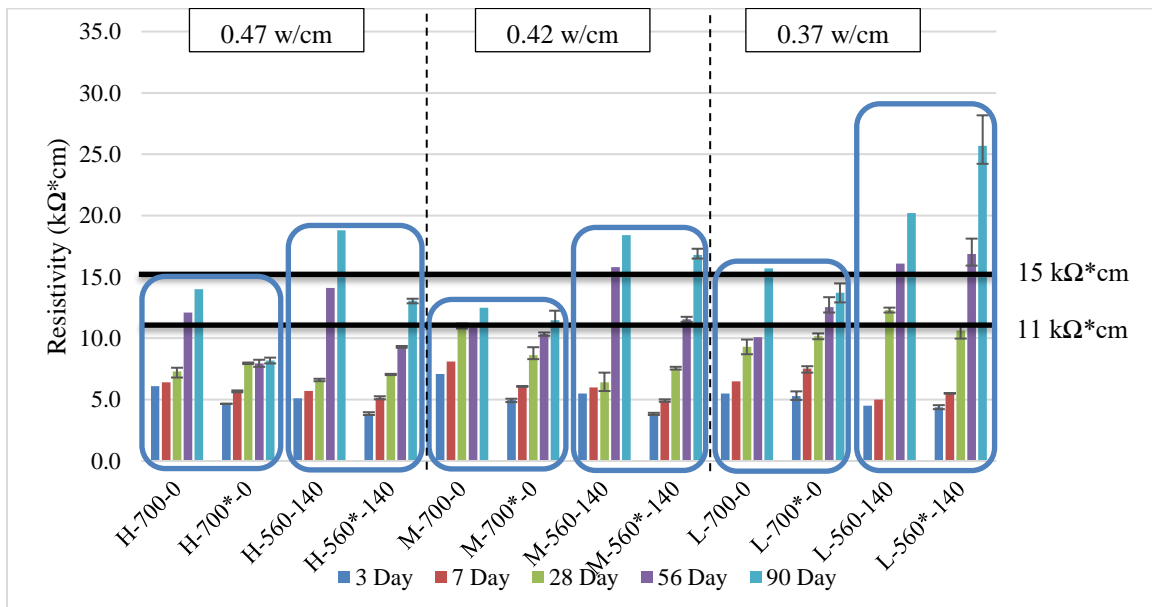


Figure 3.17: Average surface resistivity for 700/700* pcy cementitious material mixtures

Figure 3.18 through Figure 3.20 show the changes in surface resistivity measurements by testing date for mixture pairs at each w/cm ratio. From these plots, the similarities and differences in surface resistivities between pairs of optimized/non-optimized mixtures and between pairs of straight cement/fly ash replacement mixtures can be observed.

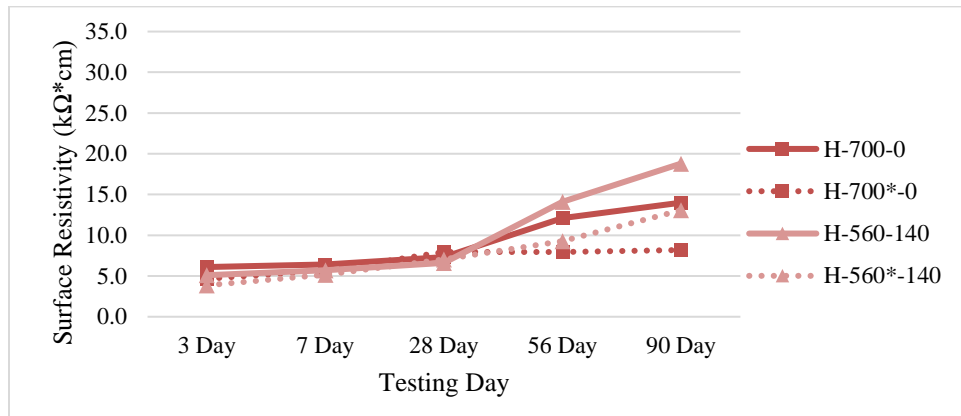


Figure 3.18: Average surface resistivity test results for 700/700* pcy cementitious material mixtures at 0.47 w/cm ratio

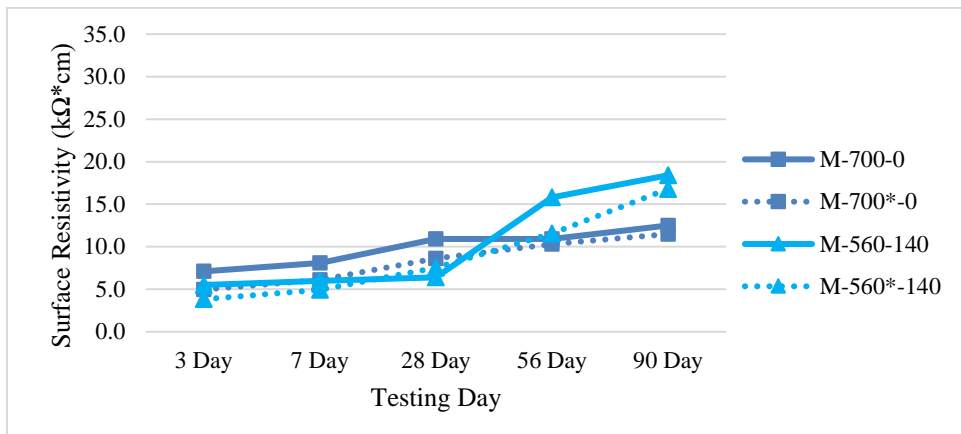


Figure 3.19: Average surface resistivity test results for 700/700* pcy cementitious material mixtures at 0.42 w/cm ratio

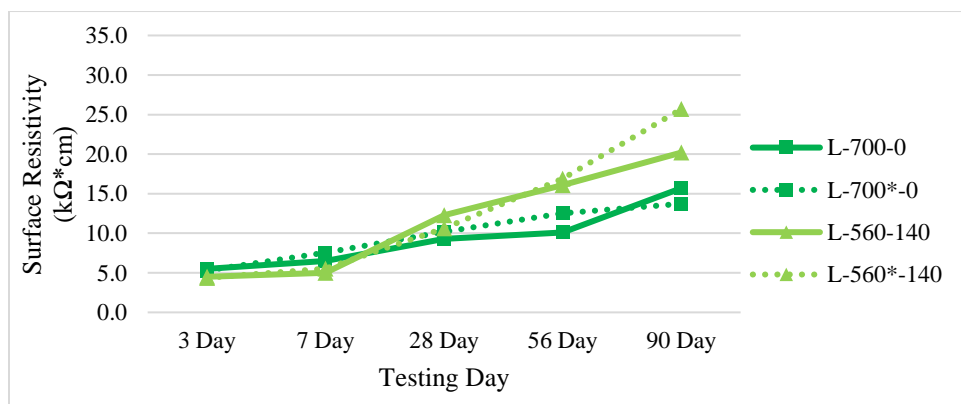


Figure 3.20: Average surface resistivity test results for 700/700* pcy cementitious material mixtures at 0.37 w/cm ratio

This trend could also relate to the 10% cementitious material reduction of the optimized aggregate gradation mixtures, as lower cementitious material mixtures. Table 3.15 shows the average percent difference between the average surface resistivities for the 700* pcy optimized aggregate gradation mixtures compared to their companion 700 pcy non-optimized mixtures, segmented by w/cm ratio. At most ages, and for most mixtures, there is an improvement (increase) in surface resistivity as the w/cm ratio decreases at later ages (after 28 days of age). This trend reinforces the importance of controlling (reducing) the w/cm ratio as the primary tool for producing quality concrete. This trend could also relate to the

10 percent cementitious material reduction of the optimized aggregate gradation mixtures, as lower cementitious material mixtures have demonstrated improved durability performance.

Table 3.15: Average percent difference between surface resistivity of 700* pcy optimized mixtures and companion 700 pcy non-optimized mixtures

w/cm ratio	Test Day				
	3 Day	7 Day	28 Day	56 Day	90 Day
0.47	-31.4%	-11.7%	7.4%	-51.8%	-57.4%
0.42	-43.4%	-27.5%	-5.7%	-21.1%	-9.2%
0.37	-3.4%	11.5%	-3.7%	12.0%	3.5%

Table 3.16 shows the average percent differences between the average surface resistivities of the 700* pcy optimized aggregate gradation straight cement and fly ash replacement mixtures compared to their companion 700 pcy non-optimized aggregate gradation straight cement and fly ash replacement mixtures. Both straight cement mixtures and fly ash replacement mixtures with 700* pcy of cementitious material performed similarly to their companion non-optimized 700 pcy mixtures. This is consistent with findings from previous studies performed by the research team, where 700 pcy non-optimized straight cement mixtures outperformed 700 pcy non-optimized fly ash mixtures at the 28-day tests, with fly ash replacement mixtures outperforming straight cement mixtures at 56- and 90-day tests. As mentioned previously, the 700* mixture series has a cementitious content typical of structural concrete mixtures, and the proposed surface resistivity target is 15 kΩcm. Of the 700* pcy optimized mixtures, only L-560*-140 met the recommended 15 kΩcm structural concrete surface resistivity target by the 56-day test, and M-560*-140 met the recommended 15 kΩcm surface resistivity target by the 90-day test. Of the 700 pcy non-optimized mixtures only M-560-140 and L-560-140 met the recommended 15 kΩcm surface resistivity target by the 56-day test, with H-560-140 and L-700-0 meeting the recommended 15 kΩcm surface resistivity target by the 90-day test.

Table 3.16: Average percent difference between surface resistivity of 700* pcy optimized straight cement and fly ash replacement mixtures surface resistivity compared with companion 700 pcy non-optimized mixtures

Mixture Characteristic	Test Day				
	3 Day	7 Day	28 Day	56 Day	90 Day
All mixtures	-26.1%	-9.2%	-0.7%	-20.3%	-21.0%
Straight cement mixtures	-25.9%	-10.7%	-3.2%	-12.6%	-31.4%
Fly ash replacement mixtures	-26.3%	-7.8%	1.9%	-27.9%	-10.6%

650*/650 pcy of Cementitious Material Surface Resistivity

Figure 3.21 shows the surface resistivity test results for pairs of optimized and non-optimized mixtures for the 650 lb cementitious content series of mixtures. It can be observed that optimized aggregate gradation mixtures again consistently exhibited lower surface resistivity values than their companion non-optimized mixtures. However, some non-optimized aggregate gradation mixtures exhibited low surface resistivity values at early ages and high w/cm ratios as well. Figures showing the surface resistivity changes by testing age by mixture pairs for the 650 pcy cementitious content mixtures are provided in Appendix B, Figures B.11 through B.13.

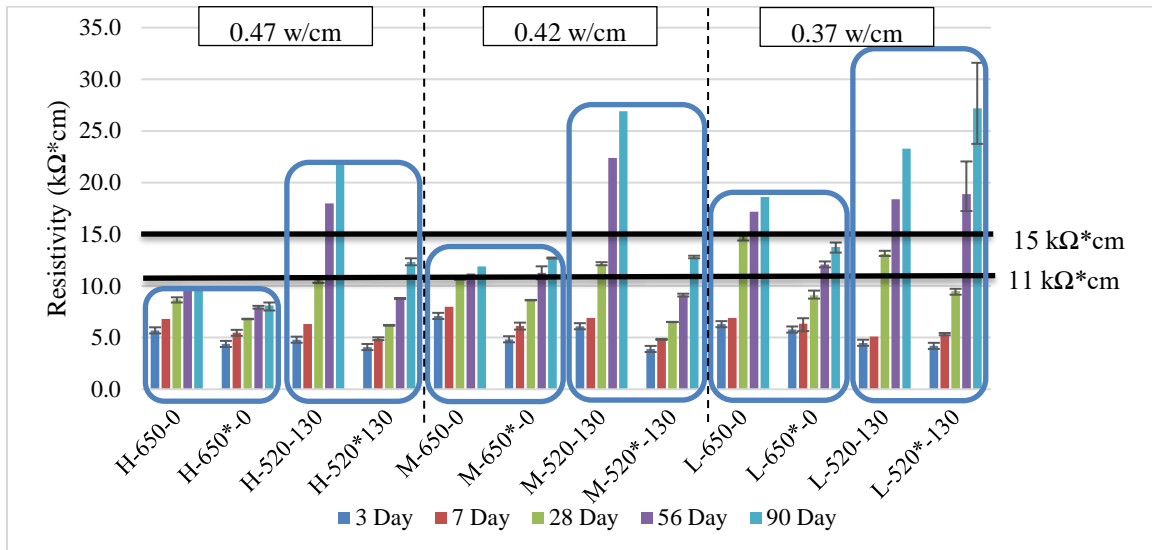


Figure 3.21: Average surface resistivity for 650/650* pcy cementitious material mixtures

Table 3.17 shows the average percent difference in the average surface resistivities between the 650* pcy optimized aggregate gradation mixtures compared to their companion 650 pcy non-optimized mixtures grouped by w/cm ratio. Similar to the 700 pcy cementitious content mixtures, optimized 650 pcy cementitious content mixtures exhibited surface resistivity similar to their companion non-optimized mixtures as the w/cm ratio decreased. However, this trend is notably deviated by two fly ash mixtures, where H-520*-130 had a resistivity 71.2 percent lower than H-520-130, M-520*-130 had a resistivity 85.8 percent lower than M-520-130, and one straight cement mixture, L-650*-0 had a resistivity 65.6 percent lower than L-650-0. For 56- and 90-day tests, mixtures H-520*-130 and M-520*-130 continued to be outperformed by their companion non-optimized mixtures. Of note, mixture L-650*-0 showed the opposite trend, with higher surface resistivity than its companion non-optimized mixture.

Table 3.17 Average percent difference between 650* pcy optimized surface resistivity and their companion 650 pcy non-optimized mixtures

w/cm ratio	Test Day				
	3 Day	7 Day	28 Day	56 Day	90 Day
0.47	-23.7%	-26.7%	-49.6%	-63.5%	-48.7%
0.42	-51.6%	-36.9%	-54.9%	-72.6%	-51.9%
0.37	-8.0%	-2.6%	-50.1%	-19.9%	-10.4%

Table 3.18 shows the average percent difference in the average surface resistivities between 650* pcy optimized aggregate gradation straight cement and fly ash replacement mixtures compared to their companion 650 pcy non-optimized straight cement and fly ash replacement mixtures. The previously observed trend where optimized fly ash replacement mixtures outperformed straight cement optimized mixtures at later dates is not present for this series of mixtures. As mentioned before, H-520*-130 and M-520*-130 were significantly outperformed by their non-optimized companion mixtures. Despite the fly optimized aggregate gradation fly ash replacement mixtures at high and medium w/cm ratios exhibiting lower resistivity, L-520*-130 was the only optimized aggregate gradation mixture to meet the recommended 15 kΩ*cm target for bridge mixtures by the 56-day test at the low w/cm ratio.

Table 3.18: Average percent difference between 650* pcy optimized straight cement and fly ash replacement mixtures surface resistivity compared with companion 650 pcy non-optimized straight cement and fly ash replacement mixtures

Mixture Characteristic	Test Day				
	3 Day	7 Day	28 Day	56 Day	90 Day
All mixtures	-27.8%	-22.1%	-51.5%	-52.0%	-37.0%
Straight cement mixtures	-28.5%	-21.4%	-38.2%	-21.3%	-16.5%
Fly ash replacement mixtures	-27.0%	-22.7%	-64.9%	-82.7%	-57.5%

600*/600 pcy of Cementitious Material Surface Resistivity

Figure 3.22 provides the surface resistivity test results for pairs of optimized and non-optimized mixtures for the 600 lb cementitious content mixtures. It can be observed that optimized aggregate gradation mixtures again consistently exhibited surface resistivity values lower than their companion non-optimized aggregate gradation mixtures especially at later testing dates. Figures showing the surface resistivity changes by testing age by mixture pairs for the 600 pcy cementitious content mixtures are provided in Appendix B, Figures B.14 through B.16.

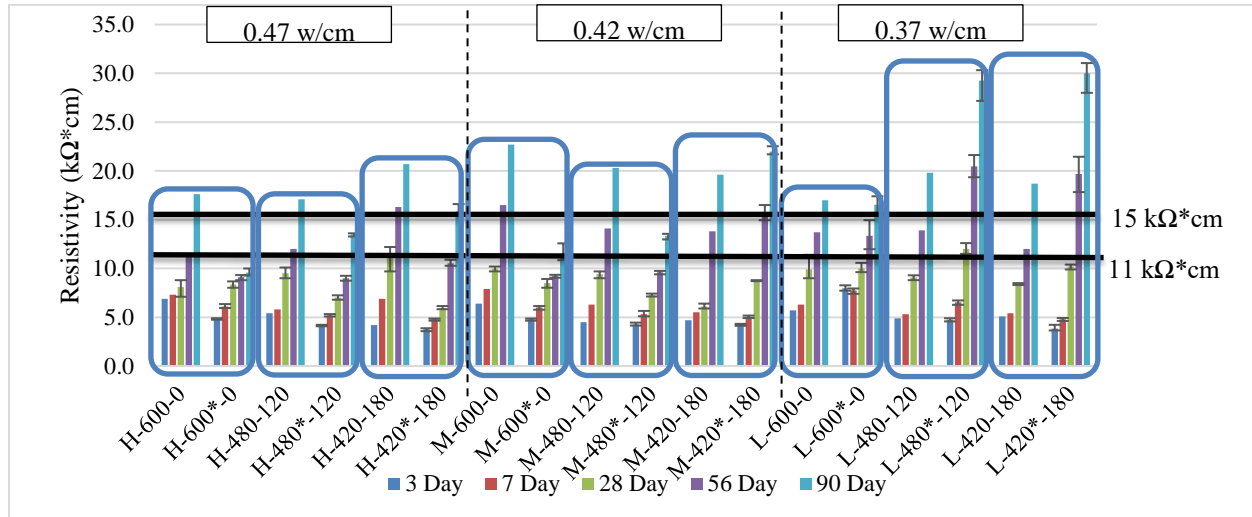


Figure 3.22: Average surface resistivity for 600/600* pcy cementitious material mixtures

Table 3.19 shows the average percent difference between the average surface resistivities of the 600* pcy optimized aggregate gradation mixtures compared to their companion 600 pcy non-optimized mixtures grouped by w/cm ratio. The previously observed trend of optimized aggregate gradation mixtures performing similarly to their companion non-optimized mixtures as w/cm ratio decreases is present, again reinforcing the importance of controlling (reducing) the w/cm ratio as the primary tool for producing quality concrete.

Table 3.19: Average percent difference in surface resistivity between 600* pcy optimized and companion 600 pcy non-optimized mixtures

w/cm ratio	Test Day				
	3 Day	7 Day	28 Day	56 Day	90 Day
0.47	-28.5%	-25.3%	-40.2%	-37.0%	-47.0%
0.42	-16.9%	-19.8%	-5.5%	-38.0%	-46.5%
0.37	-2.2%	8.2%	14.4%	22.8%	22.4%

Table 3.20 shows the average percent difference in average surface resistivities of the 600 pcy optimized aggregate gradation straight cement and fly ash replacement mixtures when compared to their companion 600 pcy non-optimized straight cement and fly ash replacement mixtures. The previously observed trend of the optimized aggregate gradation fly ash replacement mixtures exhibiting surface resistivities similar to their companion non-optimized fly ash replacement mixtures at later ages (56- and 90-day tests) is present. As mentioned previously, the 600 pcy cementitious material mixtures could be more representative of pavement concrete mixtures, which have a proposed target resistivity of 11 k Ω *cm. Of the 600* optimized mixtures, mixtures M-420*-180, L-600*-0, L-480*-120, and L-480*-120 met the recommended 11 k Ω *cm surface resistivity target by the 56-day test. H-480*-120, H-420*-180, M-600*-0, and M-480*-120 met the recommended 11 k Ω *cm surface resistivity target by the 90-day test. H-600*-0 was the only 600* optimized mixture to not meet the proposed target. All 600 pcy cementitious material non-optimized mixtures met the recommended 11 k Ω *cm surface resistivity values by the 56-day test.

Table 3.20: Average percent difference between 600* pcy optimized straight cement and fly ash replacement mixtures surface resistivity compared with companion 600 pcy non-optimized straight cement and fly ash replacement mixtures

Mixture Characteristic	Test Day				
	3 Day	7 Day	28 Day	56 Day	90 Day
All mixtures	-15.9%	-12.3%	-10.4%	-17.4%	-23.7%
Straight cement mixtures	-16.3%	-10.7%	-4.4%	-34.8%	-61.6%
Fly ash replacement mixtures	-15.7%	-13.1%	-13.5%	-8.7%	-4.8%

The previously observed trend that optimized aggregate gradation mixtures perform similarly to their companion non-optimized mixtures as the w/cm decreases holds true across all cementitious contents, and is highlighted in Table 3.21, where the average surface resistivity values are shown for optimized aggregate gradation mixtures, non-optimized aggregate gradation mixtures, along with the percent difference between companion mixtures. This trend reinforces that producing low w/cm ratio mixtures is very important to support the production of quality concrete. However, it should be noted that by reducing the cementitious materials by 10% in optimized aggregate gradation mixtures, the cementitious paste systems of optimized and non-optimized aggregate gradations are not identical and could have resulted in the varying surface resistivity results.

Table 3.21: Average surface resistivity of all mixtures grouped by w/cm ratio, along with their average percent difference between pairs of optimized and non-optimized mixtures

w/cm ratio	Mixture type	3 Day	7 Day	28 Day	56 Day	90 Day
0.47	Non-optimized	5.5	6.5	8.9	13.3	17.1
	Optimized	4.2	5.3	7.0	8.9	11.5
	Average percent difference	-28.0%	-21.8%	-29.3%	-48.8%	-50.5%
0.42	Non-optimized	5.9	7.0	9.4	15.0	18.9
	Optimized	4.4	5.5	8.0	11.0	14.4
	Average percent difference	-34.4%	-26.9%	-19.7%	-43.1%	-37.4%
0.37	Non-optimized	5.2	5.8	11.0	14.5	19.0
	Optimized	5.2	6.2	10.2	16.3	22.3
	Average percent difference	-4.2%	6.1%	-9.2%	7.5%	7.6%

Table 3.22 shows the average surface resistivity test results between optimized aggregate gradation mixtures and their companion non-optimized aggregate gradation mixtures and their average percent difference. As cementitious material contents (pcy) decreased in optimized aggregate gradation mixtures there was no noticeable trend that showed optimized mixtures performing similarly to their companion non-optimized mixtures. However, the 600* pcy optimized aggregate gradation mixtures did perform slightly better than the 700* pcy optimized mixtures at later ages, and significantly better than the 650* pcy optimized mixtures at all ages. This could be related to additional ITZ volume that is added when optimizing the gradation of a concrete mixture. As the cementitious material content increases in a mixture, so does the volume of the ITZ, likely causing its surface resistivity measurements to decrease. This is discussed later in this report.

Table 3.22: Average surface resistivity of all mixtures grouped by cementitious content (pcy) and the average percent difference between optimized and non-optimized mixtures

Cementitious material (pcy)	Mixture type	3 Day	7 Day	28 Day	56 Day	90 Day
700*/700	Non-optimized	5.6	6.3	8.8	13.2	16.6
	Optimized	4.5	5.8	8.7	11.4	14.8
	Average percent difference	-26.1%	-9.2%	-0.7%	-20.3%	-21.0%
650*/650	Non-optimized	5.8	6.7	11.7	16.2	18.7
	Optimized	4.5	5.5	7.8	11.3	14.5
	Average percent difference	-27.8%	-22.1%	-51.5%	-52.0%	-37.0%
600*/600	Non-optimized	5.3	6.3	9.1	13.7	19.3
	Optimized	4.7	5.7	8.7	13.0	17.9
	Average percent difference	-15.9%	-12.3%	-10.4%	-17.4%	-23.7%

Table 3.23 shows the average percent difference of the average surface resistivity measurements of optimized aggregate gradation straight cement and fly ash replacement mixtures. The previously observed trend where w/cm ratio decreases as surface resistivity values improve is visible in optimized fly ash replacement mixtures. Additionally, the

trend where the surface resistivity measurements for optimized fly ash replacement mixtures improve at later ages is also visible in optimized fly ash replacement mixtures. By the 56-day test all optimized aggregate gradation fly ash replacement mixtures had an average surface resistivity higher than their companion optimized aggregate gradation straight cement mixtures.

Table 3.23: Average surface resistivity and the average percent difference of all optimized aggregate gradation mixtures straight cement and fly ash mixtures grouped by w/cm ratio

w/cm ratio	Mixture type	3 Day	7 Day	28 Day	56 Day	90 Day
0.47	Optimized Straight Cement mixtures	4.6	5.8	7.7	8.3	8.6
	Optimized Fly Ash Replacement mixtures	4.0	5.0	6.6	9.4	13.7
	Average percent difference	-18.2%	-17.1%	-20.8%	9.0%	34.9%
0.42	Optimized Straight Cement mixtures	4.9	6.1	8.6	10.3	11.9
	Optimized Fly Ash Replacement mixtures	4.1	5.0	7.5	11.5	16.2
	Average percent difference	-19.6%	-20.7%	-15.3%	8.0%	23.7%
0.37	Optimized Straight Cement mixtures	6.4	7.2	9.8	12.7	14.7
	Optimized Fly Ash Replacement mixtures	4.3	5.5	10.6	19.0	28.0
	Average percent difference	-58.4%	-34.3%	6.8%	32.1%	46.1%

As cementitious content decreases in optimized aggregate gradation fly ash mixtures, there is no noticeable trend. However, when optimized aggregate gradation fly ash mixtures are compared with their companion optimized straight cement mixtures in Table 3.24 below, the previously mentioned trend that optimized fly ash mixtures do not perform as well until their later age tests (56- and 90-day tests) can be observed.

Table 3.24: Average surface resistivity and the average percent difference of all optimized aggregate gradation mixtures straight cement and fly ash mixtures grouped by cementitious content (pcy)

w/cm ratio	Mixture type	3 Day	7 Day	28 Day	56 Day	90 Day
700*	Optimized Straight Cement mixtures	5.0	6.4	8.9	10.3	11.1
	Optimized Fly Ash Replacement mixtures	4.0	5.2	8.4	12.6	18.5
	Average percent difference	-24.0%	-23.5%	-7.8%	16.9%	38.5%
650*	Optimized Straight Cement mixtures	5.0	6.0	8.2	10.4	11.5
	Optimized Fly Ash Replacement mixtures	4.1	5.0	7.4	12.3	17.4
	Average percent difference	-23.0%	-19.3%	-12.6%	7.3%	28.1%
600*	Optimized Straight Cement mixtures	5.9	6.6	9.0	10.6	12.5
	Optimized Fly Ash Replacement mixtures	4.2	5.3	8.5	14.2	20.7
	Average percent difference	-40.6%	-26.6%	-9.3%	20.7%	36.5%

3.3.3.2 RCPT

RCPT can be evaluated using the index provided in ASTM C1202, shown in Table 3.25. Results for 28- and 90-days tests are shown in Table 3.13. Figure 3.23 and Figure 3.24 display the 28- and 90-day test results for optimized aggregate gradation and non-optimized aggregate gradation mixtures, grouped by w/cm ratio. These figures show the typical decrease in chloride permeability as the concrete specimens age for both optimized and non-optimized aggregate gradation mixtures. With a few exceptions, optimized aggregate gradation mixtures typically exhibited higher chloride permeability than their companion non-optimized aggregate gradation mixtures indicating more permeability, particularly at early ages and at higher w/cm ratios. However, optimized aggregate gradation mixtures exhibited chloride permeability closer to their companion non-optimized aggregate gradation mixtures as the w/cm ratio decreases, further reinforcing that producing low w/cm ratio mixtures is important to support the production of quality concrete.

Table 3.25: ASTM C1202 RCPT index

Charge Passed (Coulombs)	Chloride Ion Permeability
>4,000	High
2,000-4,000	Moderate
1,000-2,000	Low
100-1,000	Very Low
<100	Negligible

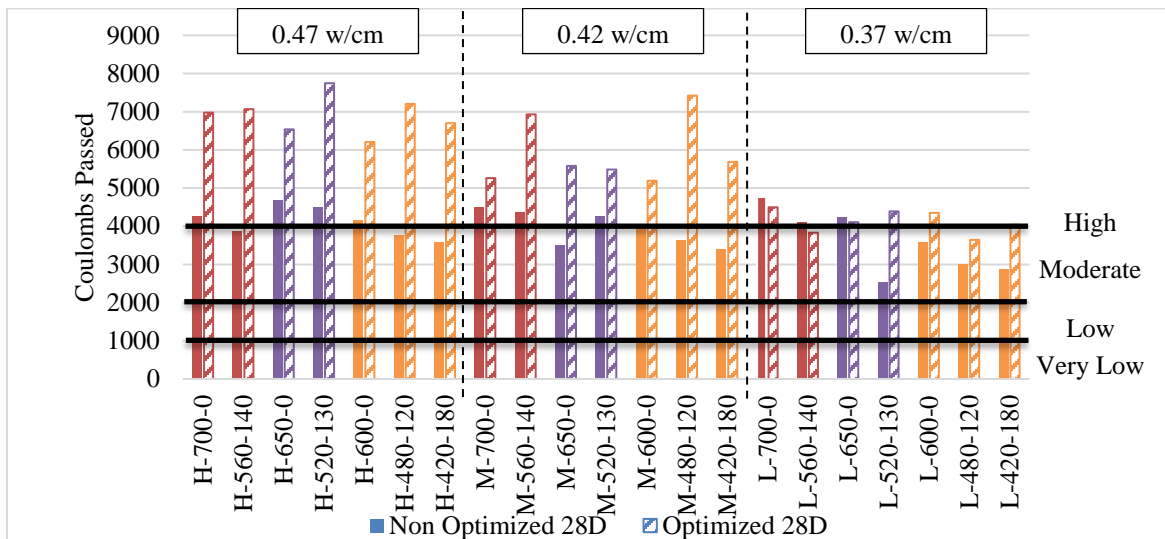


Figure 3.23: 28-day RCPT results for optimized aggregate gradation and non-optimized aggregate gradation mixtures grouped by w/cm ratio

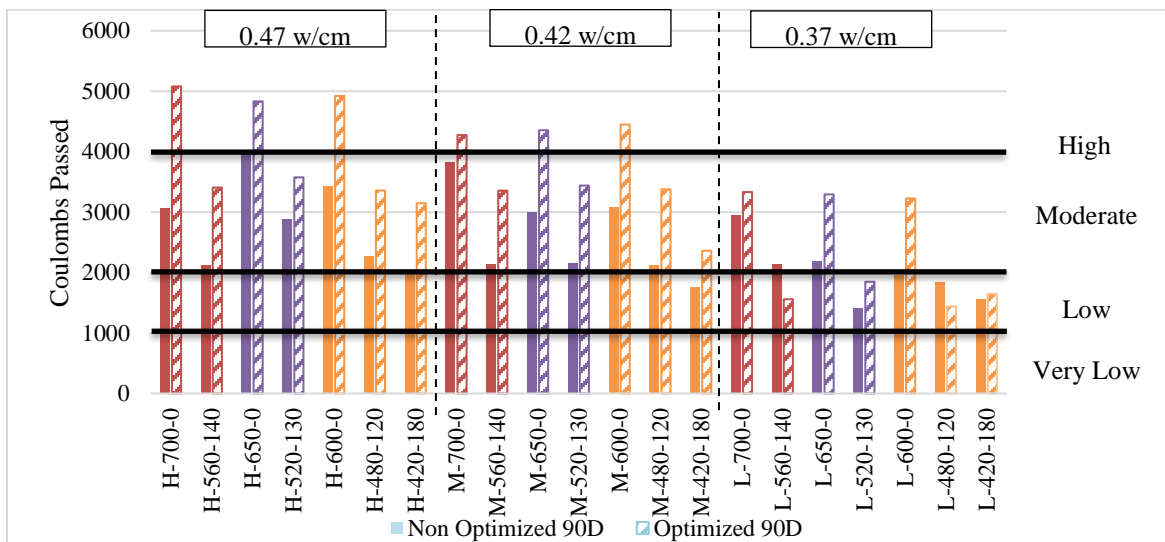


Figure 3.24: 90-day RCPT results for optimized aggregate gradation and non-optimized aggregate gradation mixtures grouped by w/cm ratio

Table 3.26 shows average RCPT results for optimized aggregate gradation mixtures and non-optimized mixtures, grouped by cementitious content (pcy). There was no noticeable trend as the cementitious content decreased in optimized aggregate gradation mixtures. However, regardless of the w/cm ratio used, optimized aggregate gradation mixtures did show improvement when compared to their non-optimized aggregate gradation mixtures by the 90-day test.

Table 3.26: Average percent difference between RCPT test results for optimized aggregate gradation and non-aggregate gradation mixtures grouped by cementitious content

Cementitious Content (pcy)	Mixture Type	Test Day	
		28 Day (Coulombs)	90 Day (Coulombs)
700	Non-optimized	4301	2707
	Optimized	5760	3501
	Average percent difference	20.6%	16.4%
650	Non-optimized	3949	2611
	Optimized	5641	3557
	Average percent difference	28.2%	26.9%
600	Non-optimized	3544	2226
	Optimized	5605	3104
	Average percent difference	34.2%	23.3%

Table 3.27 shows average RCPT results for optimized aggregate gradation mixtures and non-optimized gradation mixtures, grouped by w/cm ratio. As the w/cm ratio decreased, there was a noticeable improvement in the chloride ion penetrability of optimized mixtures (a lower number of coulombs was measured). This trend again reinforces that producing low w/cm ratio mixtures is very important to ensure quality concrete is produced. Additionally, this trend may indicate a higher w/cm ratio mixture combined with the added aggregate likely increases the volume of the ITZ, leading to permeability, as exhibited by the charge passed in the RCPT.

Table 3.27: Average percent difference between RCPT test results of optimized aggregate gradation and non-aggregate gradation mixtures grouped by w/cm ratio

w/cm Ratio	Mixture Type	Test Day	
		28 Day (Coulombs)	90 Day (Coulombs)
0.47	Non-optimized	4111	2824
	Optimized	6920	4046
	Average percent difference	20.6%	16.4%
0.42	Non-optimized	3936	2588
	Optimized	5937	3659
	Average percent difference	28.2%	26.9%
0.37	Non-optimized	3581	2007
	Optimized	4123	2335
	Average percent difference	34.2%	23.3%

Table 3.28 shows average RCPT results for optimized aggregate gradation straight cement mixtures and optimized aggregate gradation fly ash replacement mixtures, grouped by w/cm ratio. As previously observed, there was no improvement in permeability of these mixtures as cementitious content decreased. Both optimized straight cement mixtures and optimized fly ash replacement mixtures did show reduced permeability as the w/cm ratio decreased. As the concrete aged, optimized fly ash replacement mixtures outperformed their companion optimized straight cement mixtures as would be expected from fly ash replacement mixtures due to the later-age hydration and pozzolanic effects.

Table 3.28: Average percent difference between RCPT test results of optimized aggregate gradation and non-aggregate gradation straight cement and fly ash replacement mixtures grouped by w/cm ratio

w/cm Ratio	Mix Type	Test Day	
		28 Day (Coulombs)	90 Day (Coulombs)
0.47	Optimized straight cement	6574	4945
	Optimized fly ash replacement	7179	3372
	Average percent different	8.4%	-46.6%
0.42	Optimized straight cement	5344	4360
	Optimized fly ash replacement	6381	3133
	Average percent different	16.2%	-39.1%
0.37	Optimized straight cement	4318	3284
	Optimized fly ash replacement	3976	1624
	Average percent different	-8.6%	-102.2%

Figure 3.25 indicates that the surface resistivity (kΩcm) vs the RCPT test results (charge passed in coulombs) for both non-optimized and optimized mixtures exhibit a similar correlation, supporting the findings of RP 2018-14 (the non-optimized aggregate gradation mixtures) in Biggers (2019) and Cavalline et al. (2019). As can be seen in Figure 3.25, the correlation between surface resistivity tests and RCPT is best modeled using a power-curve, as indicated in a seminal study on surface resistivity by Rupnow and Icenogle (2012). As previously observed, optimized aggregate gradation mixtures in this study routinely exhibited electrical test results that indicated more permeable mixtures compared to their companion non-optimized aggregate gradation mixtures. This is possibly due to the additional aggregate introducing additional ITZ volume and is discussed subsequently in this report. Additionally, the higher RCPT results could be attributed to the use of admixtures such as AEA and WRA or fly ash that was used in the mixtures.

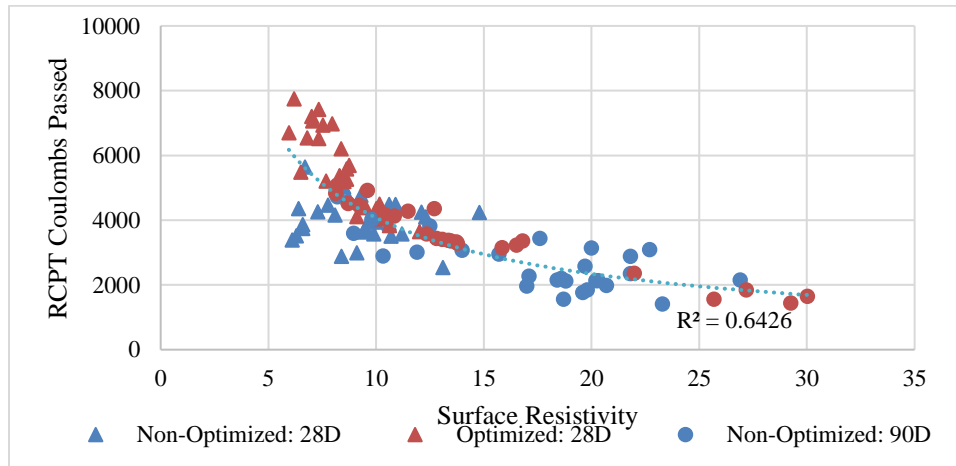


Figure 3.25: Surface resistivity plotted against RCPT test results for optimized aggregate gradation and non-optimized aggregate gradation mixtures

Influence of the Interfacial Transition Zone on Electrical Tests

In almost all optimized aggregate gradation mixtures, the surface resistivity and RCPT results showed increased permeability (lower surface resistivity and higher RCPT results) than their companion non-optimized mixtures. This reduction in surface resistivity (and commensurate increase in RCPT charge passed) is likely due to four causes: 1) the reduction in cementitious content of 10 percent between companion mixture pairs, 2) the influence of the additional interfacial transition zone (ITZ) in the paste due to the additional aggregate content, and 3) the potential for the resistivity of the additional aggregate volume to influence the measurement of electrical tests 4) the influence of different quantities of admixtures across non-optimized and optimized aggregate gradation mixtures.

To examine a potential influence of the volume of the ITZ in mixtures, the ITZ volume in each mixture was estimated. To compute this estimate, it was assumed that all ITZ around each aggregate would have a unit thickness, enabling a calculation of the surface areas of aggregates to be used to compare the ITZ volume between optimized and non-optimized aggregate gradation mixtures. The surface area of the coarse (#67) and intermediate (#89M) aggregate was estimated using a method developed at the National Center for Asphalt Technology (NCAT) at Auburn University, used when calculating the asphalt film thickness. See the formula and table below (NCAT 2009). Because the added ITZ volume is of interest, and the volume of sand was fairly consistent between companion mixtures, only the surface area of the coarse and intermediate aggregates were considered. Table 3.29 shows the surface area factors used by the NCAT procedure, while Table 3.30 shows the estimated surface area of each mixture, computed using the NCAT procedure.

$$SA = \sum P_i * FA_i \quad \text{Equation 3.3}$$

P_i = percent passing sieve

FA_i = surface area factor of aggregates from Table 3.29)

Table 3.29: Surface area factor of aggregates

Sieve opening size	Surface area factor, m ² /kg (ft ² /lb)
1"	0.41 (2)
3/4"	0.41 (2)
1/2"	0.41 (2)
3/8"	0.41 (2)
#4	0.41 (2)
#8	0.82 (4)
#16	1.64 (8)
#30	2.87 (14)
#50	6.14 (30)
#100	12.29 (60)
#200	32.77 (160)

Table 3.30: Estimated surface area for optimized and non-optimized mixtures

Mixture ID	Non-optimized mixture estimated surface area (ft ² /yd ³)	Optimized mixture estimated surface area (ft ² /yd ³)
H-700-0	1,367	1,818
H-560-140	1,369	1,794
H-650-0	1,367	1,875
H-520-130	1,368	1,855
H-600-0	1,367	1,944
H-480-120	1,368	1,914
H-420-180	1,369	1,901
M-700-0	1,375	1,863
M-560-140	1,368	1,838
M-650-0	1,367	1,928
M-520-130	1,368	1,906
M-600-0	1,367	1,984
M-480-120	1,368	1,970
M-420-180	1,369	1,853
L-700-0	1,367	1,931
L-560-140	1,369	1,895
L-650-0	1,367	1,977
L-520-130	1,369	1,959
L-600-0	1,367	2,035
L-480-120	1,368	2,009
L-420-180	1,369	1,997

Once the surface areas were calculated, the percent difference between optimized aggregate gradation mixtures and non-optimized aggregate gradation mixtures was calculated. Table 3.31 shows the 28-day and 90-day surface resistivities and RCPT results for pairs of mixtures, along with the percent difference between the estimated ITZ volumes of the optimized aggregate gradation mixtures and the non-optimized aggregate gradation mixtures.

Table 3.31: Surface resistivity, RCPT, and difference of surface area from aggregates of all mixtures

Mixture ID	Test Day	Optimized RCPT Results (Coulombs)	Non-Optimized RCPT Results (Coulombs)	Optimized Surface Resistivity (k Ω *cm)	Non-Optimized Surface Resistivity (k Ω *cm)	% Difference in Surface Area
H-700-0	28 Day	4235	6976	8.0	7.3	25%
	90 Day	3070	5080	8.2	14	
H-560-140	28 Day	3860	7067	7.1	6.6	24%
	90 Day	2118	3407	13.1	18.8	
H-650-0	28 Day	4687	6538	6.8	8.7	27%
	90 Day	4018	4832	8.1	9.8	
H-520-130	28 Day	4480	7746	6.2	10.6	26%
	90 Day	2879	3575	12.3	21.8	
H-600-0	28 Day	4159	6208	8.4	8.1	30%
	90 Day	3439	4922	9.6	17.6	
H-480-120	28 Day	3766	7204	7.0	9.5	29%
	90 Day	2266	3358	13.5	17.1	
H-420-180	28 Day	3571	6699	6.0	11.2	28%
	90 Day	1980	3148	15.9	20.7	
M-700-0	28 Day	4479	5261	8.6	10.9	26%
	90 Day	3822	4275	11.5	12.5	
M-560-140	28 Day	4354	6930	7.5	6.4	26%
	90 Day	2148	3356	16.8	18.4	
M-650-0	28 Day	3506	5580	8.6	10.7	29%
	90 Day	3008	4355	12.7	11.9	
M-520-130	28 Day	4247	5486	6.5	12.1	28%
	90 Day	2154	3439	12.8	26.9	
M-600-0	28 Day	3943	5192	8.5	10	31%
	90 Day	3087	4450	9.2	22.7	
M-480-120	28 Day	3632	7421	7.3	9.4	31%
	90 Day	2132	3377	13.4	20.3	
M-420-180	28 Day	3391	5687	8.8	6.1	26%
	90 Day	1768	2362	22.0	19.6	
L-700-0	28 Day	4766	4497	10.2	9.3	29%
	90 Day	2947	3322	13.7	15.7	
L-560-140	28 Day	4094	3831	10.6	12.3	28%
	90 Day	2136	1559	26.0	20.2	
L-650-0	28 Day	4239	4107	9.1	14.8	31%
	90 Day	2197	3293	14.0	18.6	
L-520-130	28 Day	2532	4389	9.5	13.1	30%
	90 Day	1409	1848	27.0	23.3	
L-600-0	28 Day	3572	4351	10.0	9.9	33%
	90 Day	1962	3227	16.5	17	
L-480-120	28 Day	2987	3644	12.0	9.1	32%
	90 Day	1840	1441	29.3	19.8	
L-420-180	28 Day	2879	4041	10.2	8.4	31%
	90 Day	1557	1648	30.0	18.7	

Figures B.17 through B.28 in Appendix B show the relationships between the estimated ITZ volume and surface resistivity and RCPT test results. Figures B.17 through B.19 show the percent aggregate by volume plotted against the surface resistivity of optimized aggregate gradation mixtures only against the surface resistivity results grouped by w/cm ratio. Figures B.20 through B.22 plot the percent aggregate by volume against the surface resistivity results of optimized and non-optimized aggregate gradation mixtures grouped by w/cm ratio. Figures B.23 through B.25 plot the percent aggregate by volume against the RCPT results of optimized aggregate gradation mixtures grouped by w/cm ratio. Figures B.26. through B.28 plot the percent aggregate by volume against the RCPT test result of optimized and non-optimized

aggregate gradation mixtures. These figures were created to provide a potential explanation for the discrepancy in electrical test results for optimized and non-optimized aggregate gradation mixtures. However, it should be noted that by changing the cementitious material content in the optimized aggregate gradation mixtures, the cementitious matrix of the mixtures was changed as well, making a direct comparison between the mixtures inaccurate.

As the w/cm ratio decreases, the quality of the ITZ likely decreases as well since there is less water present to increase the thickness and permeability of the ITZ. This could explain the difference between electrical test results (surface resistivity and RCPT) between optimized and non-optimized mixtures. The increase in ability to carry electrical current does not necessarily mean optimized aggregate gradation mixtures are more permeable (and inherently less durable). Instead, it may indicate that performance targets for optimized aggregate gradation mixtures may need to be adjusted. Additional discussion is presented following these figures, and research into the relationship between the ITZ and electrical test results is recommended.

Research has been performed on the influence of recycled aggregate concrete by a team at Rowan University suggesting that the additional mortar contained in recycled concrete aggregates influences electrical tests, and that target thresholds for chloride ion penetrability classifications should be lower (Lomboy 2021). Research has also been performed at Oklahoma State University (OSU) that presented the idea that the gradation of aggregate used in a concrete mixture impacts the surface resistivity (Govindbhai 2012). Trends observed in this research indicated that the resistivity of the cylinder could be thought of as a composite resistivity: influenced by the resistivity of the paste, the resistivity of the fine aggregate, and the resistivity of the coarse aggregate. The study performed at OSU found a relationship that was inverse to the relationship findings in this study. However, the research performed by Dr. Lomboy at Rowan University on recycled aggregate concrete seems to support the findings of this study, showing that an increased ITZ decreases electrical resistivity, and the electrical tests on this concrete were also influenced by the w/cm ratio and the volume of coarse aggregate in the concrete mixture. More research on the relationship between coarse aggregate volume and electrical tests is recommended.

While the optimized aggregate gradation mixtures electrical durability testing indicates more permeable concrete mixtures, factors such as introducing additional aggregate and possibly increasing the ITZ may be causing these deviations. Additionally, as the cementitious material of optimized aggregate gradation mixtures was reduced by 10%, the cementitious paste system in the non-optimized aggregate gradation mixtures has been changed as mentioned before. This change, in addition to changes in chemical admixture dosages for the optimized aggregate gradation mixtures, may have played a role in the skewed surface resistivity results of the optimized aggregate gradation mixtures.

3.3.3.3 Formation Factor

Testing to support the evaluation of the use of the formation factor (per AASHTO PP 84) instead of using an unmodified surface resistivity value was performed. Ongoing research using the Bucket Test method helped to provide insight into the role of pore solution chemistry and pore structure on bulk resistivity and surface resistivity measurements. Table 3.32 shows the formation factors associated with various levels of chloride ion penetrability, as found in AASHTO PP 84.

Table 3.32: Chloride ion penetrability associated with various formation factor values

Chloride ion classification	Formation factor value
High	520
Moderate	520 – 1,040
Low	1,040 – 2,080
Very low	2,080 – 20,700
Negligible	20,700

Two samples per mixture were tested using the procedure developed by Dr. W. Jason Weiss at Oregon State University at intervals ranging from 2 hours to 91 days. Surface resistivity and bulk resistivity tests were performed on the cylinders after being removed from buckets filled with a solution designed to mimic concrete pore solution. The average test result from the two specimens was calculated and used to compute the formation factor. Table B.8 provides 28- and 56-day test results for surface resistivity, Bucket Test, and Formation Factor for optimized aggregate gradation mixtures calculated using the assumed resistivity of the pore solution of 0.127 Ωm from AASHTO PP 84. It is noted that the assumed resistivity of the pore solution has changed between the 2017 and 2020 versions of AASHTO PP 84 used for NCDOT RP 2018-14 and RP 2020-13 (this study), respectively. Table B.9 shows a sample of the test results for 28- and 56-day surface resistivity, Bucket Test, and the calculated formation factor using the assumed resistivity of the pore solution of 0.10 Ωm used previously by the research team (Cavalline et al. 2018). It is noted that Bucket Test and Formation Factor calculations

for optimized aggregate gradation mixtures H-700*-0, H-560*-140, and H-650*-0 were not obtained due to a lack of specimens.

Figure 3.26 shows all optimized mixtures Formation Factor plotted in comparison to the chloride ion penetrability classification from AASHTO PP 84. Figures B.29. and B.30 display the 28- and 56-day optimized aggregate gradation mixture formation factors plotted against the same testing days surface resistivity, showing reasonably strong correlation between the results of the two tests. All mixtures showed improved performance at later testing dates, similar to the surface resistivity and RCPT test results. The average formation factors for optimized mixtures with fly ash were only slightly higher than their companion optimized straight cement mixtures at 28 days (1.4%). However, the formation factors improved at the 56-day test mark considerably with an average formation factor 27.7 percent higher than their companion optimized straight cement mixtures.

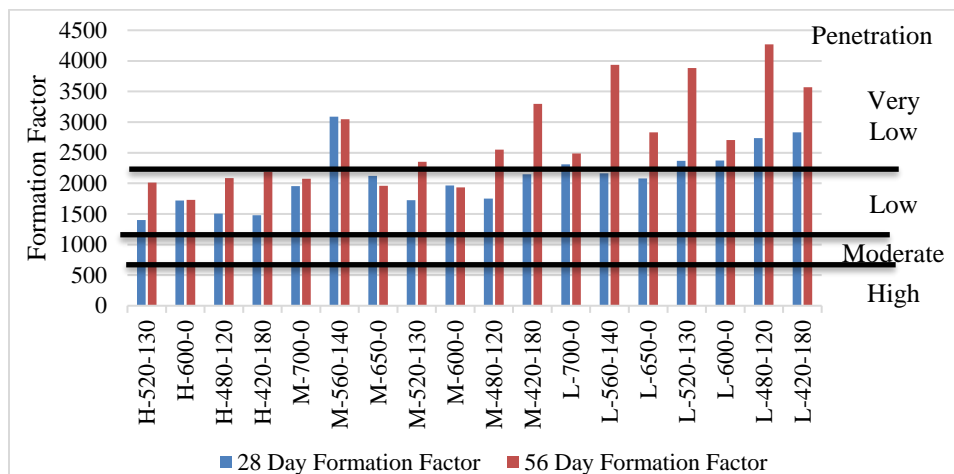


Figure 3.26: Formation Factors for optimized aggregate gradation mixtures at 28- and 56-days

Based on the limited test data gathered as part of this study (which only utilizes two cements and one SCM), as well as ongoing current developments in the PEM initiative at the national level, use of the formation factor in NCDOT specifications is not recommended at this time. However, data found as part of this laboratory testing program shows a correlation between the chloride penetrability classifications given in AASHTO PP 84 for formation factor and RCPT, surface resistivity, and bulk resistivity. Ongoing developments associated with use of the formation factor, as well as related tests such as the Bucket Test, should be monitored and included in future PEM studies supported by NCDOT.

3.3.3.4 Volumetric Shrinkage

Shrinkage tests were performed per ASTM C157, using concrete beam specimens consisting of 4 inch by 4 inch by 11¼ inch prisms. Measurements were made at 4, 7, 14, and 28 days, and at later ages, and results are provided in Appendix B in Table B.10. During RP 2018-14, shrinkage measurements were computed using the measurement directly after curing as the initial measurement, which deviated from ASTM C157 which uses the measurement after demolding as the initial measurement. Therefore, to facilitate comparison, volumetric shrinkage measurements in microstrain for optimized and non-optimized mixtures are reported in Table B.10 for 28day, 8-week, 16-week, and 32-week testing days (after a 28 day curing period) using shrinkage values calculated using the measurement directly after curing as the initial comparator reading. Table B.11 provides the microstrain of optimized aggregate gradation mixtures with the microstrains for 28day, 8-week, 16-week, and 32-week testing days, but has been calculated using the initial reading directly after demolding as the comparator reading as per ASTM C157. For optimized aggregate gradation mixtures, the difference in the two methods with comparator reading at 28 days and 0 days directly after demolding resulted in an average difference of 78 microstrain across all mixtures and test dates.

Since AASHTO PP 84 suggests that a 28-day shrinkage target (focusing on *timely* performance criteria) be used, so analysis of this data focused on 28-day test results. Figure 3.27 displays the volumetric shrinkage results for the 28-day test for both optimized and non-optimized gradation mixtures, with the values calculated using the measurement taken directly after curing as the initial comparator reading. Figure 3.28 displays the volumetric shrinkage results for the 28-day test for the optimized gradation mixtures using the shrinkage values calculated using the measurement directly after demolding as the initial comparator reading per the ASTM C157 standard. The 28-day maximum shrinkage target of 420 µε suggested by AASHTO PP 84-20 is shown by the solid black line (AASHTO 2020). When using the measurement after

curing as the comparator reading, optimized aggregate gradation mixtures did not perform as well as their companion non-optimized mixtures at the early age testing requirements as shown in Figure 3.27. However, all optimized aggregate gradation mixtures did meet the AASHTO PP 84 420 microstrain recommended target at their 28-day test except for H-520*-130, which had a 28-day microstrain of 440. All mixtures did meet the AASHTO PP 84 420 microstrain requirement at their 28-day test when using the measurement directly after demolding per ASTM C157.

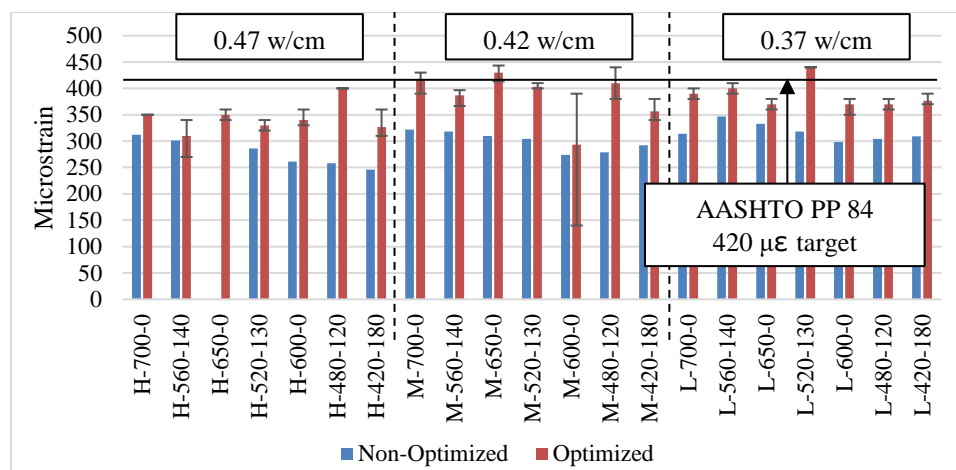


Figure 3.27: Volumetric shrinkage measurements (in microstrain) for optimized and non-optimized aggregate gradation mixtures, measurement after 28-day cure as initial reading

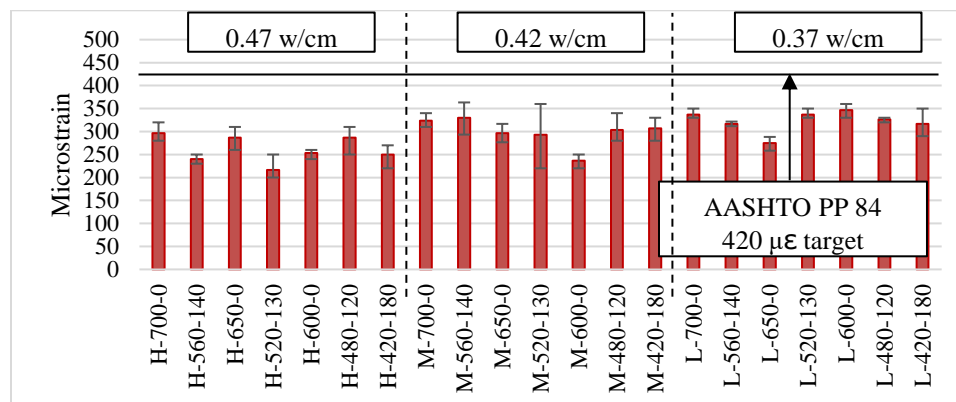


Figure 3.28: Volumetric shrinkage measurements (in microstrain) for optimized aggregate gradation mixtures (0-day reading is comparator reading per ASTM C157 standard)

Table 3.33 shows the average shrinkage (in microstrain) and the percent difference between optimized aggregate gradation mixtures and non-optimized mixtures, for all mixtures, straight cement mixtures, and fly ash replacement mixtures. As the concrete continues to age, optimized aggregate gradation mixtures began to exhibit less shrinkage (lower microstrain) when compared to their companion non-optimized mixtures. These optimized mixtures eventually showed less shrinkage (outperforming) their non-optimized mixtures by 32-weeks, shown in Figure 3.29 and 3.30.

Table 3.33: Volumetric shrinkage results and average percent difference of optimized and non-optimized straight cement and fly ash replacement mixtures microstrains by w/cm ratio

Mixture Characteristic	Mixture type	28 Day (microstrain)	8 Week (microstrain)	16 Week (microstrain)	32 Week (microstrain)
All	Non-optimized	299	373	445	763
	Optimized	372	487	552	603
	Average percent difference	19.1%	23.1%	18.9%	-29.8%
Straight cement	Non-optimized	303	375	452	728
	Optimized	368	497	562	611
	Average percent different	17.5%	24.4%	18.9%	-24.8%
Fly ash replacement	Non-optimized	298	375	440	795
	Optimized	379	482	544	593
	Average percent different	20.1%	22.2%	19.0%	-34.8%

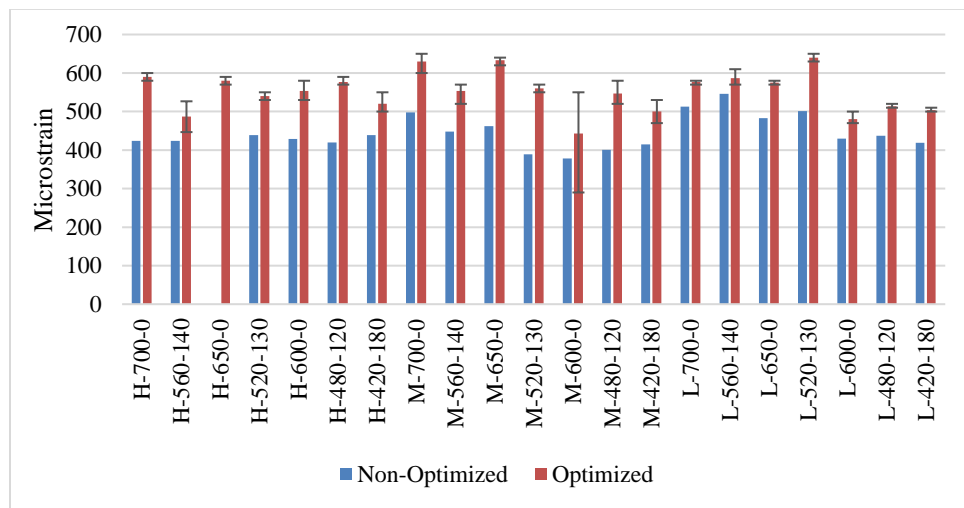


Figure 3.29: 16-week volumetric shrinkage measurements (in microstrain) for optimized and non-optimized aggregate gradation mixtures, 28-day as initial reading

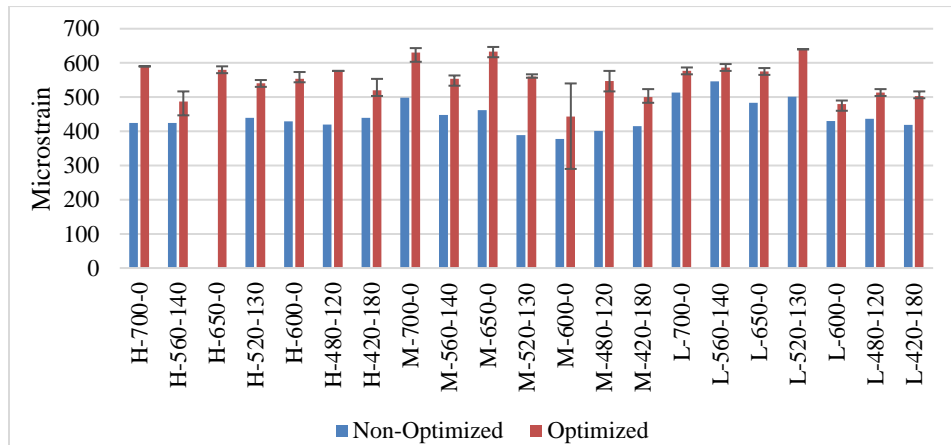


Figure 3.30: 32-week volumetric shrinkage measurements (in microstrain) for optimized and non-optimized aggregate gradation mixtures, 28-day as initial reading

Table 3.34 shows the average volumetric shrinkage (in microstrain), along with the percent difference in volumetric shrinkage between optimized aggregate gradation mixtures and non-optimized mixtures grouped by cementitious content. Optimized aggregate gradation mixtures exhibited lower shrinkage at later dates, and both optimized and non-optimized mixtures exhibited lower shrinkage as the cementitious material content decreased. However, optimized aggregate gradation mixtures with 650* pcy of cementitious material had slightly more volumetric shrinkage than the average shrinkage of optimized 700* pcy mixtures until the 32-week test date.

Table 3.34: Average volumetric shrinkage and average percent difference of optimized and non-optimized mixtures grouped by w/cm ratio

Cementitious material (pcy)	Mixture type	28 Day (microstrain)	8 Week (microstrain)	16 Week (microstrain)	32 Week (microstrain)
700	Non-optimized	319	401	476	798
	Optimized	373	496	571	627
	Average percent difference	13.8%	18.4%	16.5%	-29.4%
650	Non-optimized	310	385	455	828
	Optimized	387	513	588	622
	Average percent difference	20.7%	25.5%	22.8%	-37.0%
600	Non-optimized	280	348	419	733
	Optimized	360	464	515	572
	Average percent difference	21.7%	24.8%	18.4%	-27.7%

Table 3.35 shows the average volumetric shrinkage (in microstrain) and the percent difference in shrinkage between optimized aggregate gradation mixtures and non-optimized mixtures grouped by w/cm ratio. The trend that optimized aggregate gradation mixtures exhibit lower shrinkage than non-optimized mixtures at later dates is again visible. Non-optimized aggregate gradation mixtures showed an increase in average shrinkage as the w/cm decreased. This trend was also evident in optimized aggregate gradation mixtures at 28-day and 8-week testing dates, however, the volumetric shrinkage stabilized at the 16-week testing date with average volumetric shrinkage results being very similar across all w/cm ratios.

Table 3.35: Average volumetric shrinkage and average percent difference of optimized and non-optimized mixtures grouped by cementitious material content

w/cm ratio	Mixture type	28 Day (microstrain)	8 Week (microstrain)	16 Week (microstrain)	32 Week (microstrain)
0.47	Non-optimized	277	348	429	709
	Optimized	342	470	550	617
	Average percent difference	17.7%	24.9%	20.8%	-17.3%
0.42	Non-optimized	300	369	427	750
	Optimized	385	502	552	592
	Average percent difference	21.4%	26.0%	22.3%	-29.5%
0.37	Non-optimized	318	398	476	852
	Optimized	388	490	554	587
	Average percent difference	18.0%	18.5%	14.0%	-94.3%

When using the measurement after curing as the comparator reading, optimized aggregate gradation mixtures did not perform as well as their companion non-optimized mixtures at the early age tests. However, all optimized aggregate gradation mixtures did meet the AASHTO PP 84 420 microstrain requirement at the 28-day test except for H-520*-130, which had a 28-day microstrain of 440. All mixtures did meet the AASHTO PP 84 420 microstrain recommended performance target at their 28-day test when using the measurement directly after demolding per ASTM C157.

3.4 Summary of Laboratory Findings

Overall, the analysis demonstrated that the cementitious content of concrete mixtures could be reduced by 10 percent and still meet current NCDOT specification provisions. For moderate (w/cm = 0.42) and low (w/cm = 0.37) mixtures, many optimized gradation mixtures produce mechanical property test results that were similar to concrete mixtures that did not have a reduction in cementitious material. Electrical tests indicated greater permeability in optimized aggregate gradation mixtures, but the influence of the additional aggregate content, ITZ, and the 10% reduction in cementitious materials effectively changing the cement paste structure may have influenced the results. Such indirect measurements may require adjustments to performance targets for optimized mixtures. The use of optimized aggregate mixtures may reduce costs and emissions of greenhouse gases via the reduction of cement, and additionally may result in mixtures with improved durability characteristics, a longer service life, and lower cracking through volumetric shrinkage. While this research provided test results where optimized aggregate gradation mixtures with reduced cementitious materials demonstrated more permeable characteristics, it does not mean that these mixtures are actually less durable.

Specific laboratory findings of this project are:

Fresh Properties

- Low (0.37) w/cm ratio and low (600* pcy) cementitious material content optimized aggregate gradation mixtures required the most WRA to achieve acceptable workability.
- Optimized aggregate gradation concrete mixtures had lower slumps than the companion non-optimized mixtures, with higher cement content mixtures requiring less WRA to achieve target slump.
- Low (0.37) w/cm ratio and low (600* pcy) cementitious material content optimized aggregate gradation mixtures required the most AEA to achieve the target range for entrained air.
- Unit weights of optimized aggregate gradation mixtures increased as the w/cm ratio decreased; this trend is also present in non-optimized aggregate gradation mixtures. As could be reasonably expected due to the denser aggregate packing, the optimized aggregate gradation mixture unit weights were slightly higher (ranging from 140.9 pounds per cubic foot (pcf) to 145.8 pcf and averaging 143.6 pcf) than their companion non-optimized aggregate gradation unit weights (which ranged from 136.1 pcf to 143.9 pcf and averaged 139.9 pcf).
- Optimized aggregate gradation mixtures typically had a slightly higher unit weight than the companion non-optimized aggregate gradation mixtures.

Mechanical Properties

- Mechanical properties of both non-optimized and optimized aggregate gradation mixtures improved as the w/cm ratio decreased.
- Mechanical properties of optimized aggregate gradation straight cement mixtures with reduced paste showed a negligible impact at all testing dates.
- Mechanical properties of optimized aggregate gradation mixtures of fly ash mixtures at 20% replacement rates showed a negligible impact to mechanical properties for tests at ages greater than 3-days, and mechanical properties of fly ash mixtures at 30% replacement rates showed negligible impact to mechanical properties for tests past 28-days. These findings may indicate that NCDOT should continue to encourage the use of SCMs at replacement rates of up to 30%.

Compressive and Flexural Strength

- **Compressive strengths were roughly equivalent between optimized and non-optimized mixtures, indicating that current NCDOT specifications could reasonably be met by mixtures containing a 10% reduction in cementitious materials and a 2-3% reduction in paste volume. This could offer both economic and sustainability benefits.**
- The flexural strength test results for optimized gradation of 20% fly ash mixtures were roughly 2.1% less than their identical non-optimized, 7.8% less than the non-optimized straight cement mixtures, and about 4.9% less than the optimized straight cement mixtures. **This roughly equivalent performance between optimized and non-optimized mixtures indicates that current NCDOT specifications could reasonably be met by mixtures containing a 10% reduction in cementitious materials and a 2-3% reduction in paste volume, offering both economic and sustainability benefits.**
- Optimized aggregate gradation straight cement mixtures aged 3-days had average compressive strengths 9.7% lower than companion non-optimized aggregate gradation straight cement mixtures. Optimized aggregate gradation straight cement mixtures exhibited compressive strengths that were similar at later ages.
 - Average compressive strength test results of optimized aggregate gradation straight cement mixtures as the w/cm ratio decreased were closer to the companion non-optimized aggregate gradation straight cement mixtures. Average compressive strengths of high (0.47) w/cm ratio straight cement optimized aggregate gradation mixtures were 19.7% lower at 3-day tests but were within 10% of non-optimized mixtures at all other test ages.
 - Average compressive strength test results of optimized aggregate gradation straight cement mixtures with 650* pcy of cementitious material were noticeably lower than their companion non-optimized aggregate gradation straight cement mixtures at the ages of 3- and 7-day tests (22.6% and 16.7% respectively) but performed closer to the non-optimized straight cement mixtures at later ages. However, the 700* pcy and 600* pcy optimized aggregate gradation straight cement mixtures did not exhibit this trend and were within 10% at all ages, sometimes outperforming non-optimized companion mixtures.

- Average 28-day MOR test results of optimized aggregate gradation straight cement mixtures showed essentially no difference in flexural strength than companion non-optimized aggregate gradation straight cement mixtures (3.5% lower).
- Optimized aggregate gradation mixtures with fly ash did not perform as well as their companion non-optimized aggregate gradation mixtures with fly ash at early test dates. However, the average compressive strength of all optimized aggregate gradation mixtures with fly ash did perform as well (within in 1%) as their companion non-optimized aggregate gradation fly ash mixtures at later testing dates.
 - The average compressive strength of optimized aggregate gradation fly ash (20% and 30% replacement rates) mixtures was 24.0% lower than companion non-optimized aggregate fly ash mixtures at 3-day tests. Optimized aggregate gradation mixtures with 20% fly ash showed a negligible difference compared to their companion non-optimized mixtures by the 7-day tests (6.3% lower), optimized aggregate gradation mixtures with 30% fly ash average compressive strengths were almost equivalent to non-optimized companion mixtures by the 28-day tests (0.7% lower).
 - Average compressive strengths of high (0.47) w/cm ratio optimized and non-optimized aggregate gradation 30% fly ash mixtures did not meet the 28-day NCDOT 4,500 psi requirement, but both mixtures had average compressive strength results above the 4,500 psi requirement by 56-day tests.
 - The 28-day MOR of optimized aggregate gradation 20% fly ash mixtures showed no difference in flexural strength when compared to the companion non-optimized aggregate gradation 20% fly ash mixtures (3.3% lower). However, optimized aggregate gradation 30% fly ash mixtures had 28-day MOR 17.1 % lower than companion non-optimized aggregate gradation 30% fly ash mixtures, with two mixtures not meeting the 28-day NCDOT requirement of 650 psi.

Modulus of Elasticity

- Measured 28-day MOE values of optimized aggregate gradation mixtures were 13.6% higher than companion non-optimized aggregate gradation mixtures
 - Average 28-day MOE values of optimized aggregate gradation mixtures were 14.3% lower than the MOE calculated using the ACI 318 equation; 11.9% lower than the MOE calculated with AASHTO LFRD equation C5.4.2.4-2. These differences were roughly consistent across all optimized aggregate gradation straight cement and fly ash mixtures.
 - The 28-day MOE of optimized aggregate gradation mixtures with fly ash showed similar trends of decreasing average 28-day MOE as fly ash content increased when compared to their companion non-optimized mixtures. The average 28-day MOE of optimized aggregate gradation mixtures with 20% and 30% fly ash decreased by 6.8% and 13.8% respectively when compared to their companion optimized straight cement mixtures. The average 28-day MOE of non-optimized aggregate gradation mixtures with 20% and 30% fly ash decreased by 12.4% and 21.7% respectively when compared to their non-optimized straight cement mixtures.

Durability Performance

- Durability performance test results improved as the w/cm ratio decreased in both optimized and non-optimized aggregate gradation mixtures, suggesting the NCDOT may want to further explore prescriptive specification provisions to reduce the w/cm ratio of their mixtures. This prescriptive change could result in less permeable concrete, lower shrinkage, potentially lower paste contents, and overall improved durability performance.
- Optimized aggregate gradation mixtures with fly ash exhibited improved durability performance characteristics at later ages when compared to companion optimized and non-optimized aggregate gradation mixtures, suggesting the NCDOT may want to explore prescriptive specifications to encourage the use of SCMs at replacement rates up to 30 percent to improve durability performance.

RCPT and Surface Resistivity

- RCPT results of optimized aggregate gradation mixtures were typically higher than the companion non-optimized aggregate gradation mixtures at both 28- and 90-day tests.
- These electrical test results may be influenced by the increased volume of the ITZ, the increased aggregate volume, or other factors. Additional study is recommended to better understand these results.
 - Results for both optimized and non-optimized aggregate gradation mixtures improved as the w/cm decreased.
 - The optimized aggregate mixtures with fly ash had higher RCPT results than straight cement mixtures at 28-day tests (5.1% higher than optimized straight cement mixtures and 25.1% higher than non-optimized straight

cement mixtures) but had lower RCPT results than companion straight cement mixtures by the 90-day tests (64.4% lower than companion optimized straight cement mixtures and 16.7% lower than non-optimized straight cement mixtures).

- Average surface resistivity test results for optimized aggregate gradation mixtures were typically lower than the companion non-optimized aggregate gradation mixtures.
 - Average surface resistivity results of optimized and non-optimized aggregate gradation mixtures improved as the w/cm ratio decreased at later age tests. Non-optimized aggregate gradation mixtures exhibited this trend by the 28-day tests while optimized aggregate gradation mixtures exhibited this trend at all test dates.
 - Average surface resistivity results of optimized aggregate gradation mixtures with fly ash had similar resistivities than the companion non-optimized aggregate gradation straight cement mixtures by the 56-day tests (4.5% lower) and had higher average surface resistivities by the 90-day tests (7.2% higher).

Formation Factor

- Preliminary formation factor results show trends similar to other electrical resistivity tests. It should be noted that the testing and calculation method for formation factor testing is still being revised and improved, therefore these values are relevant only for preliminary observations.
- Additional study on formation factor tests should be considered as NCDOT begins using mixtures with an increased range of cementitious materials and ternary blends.

Volumetric Shrinkage

- Volumetric shrinkage of all optimized aggregate gradation mixtures met the AASHTO PP 84 suggested limit of 420 microstrain at 28-days.
- In the previous study, the research team used the measurement after the 28-day wet curing period as the initial measurement. Therefore, comparisons were made between companion optimized and non-optimized aggregate gradation mixtures using this approach, despite ASTM C157 indicating that the measurement immediately following demolding should be used as the initial measurement.
 - Optimized aggregate gradation mixtures had higher average 28-day volumetric shrinkage (in microstrain) than companion non-optimized aggregate gradation mixtures.
 - Optimized aggregate gradation mixtures had lower average volumetric shrinkage (in microstrain) than non-optimized aggregate by the 32-week measurement.

4.0 PERFORMANCE TARGETS FOR FREEZE-THAW DURABLE CONCRETE

4.1 Introduction

The Super Air Meter (SAM) is a relatively new test method that evaluates the dispersion of an air void system within fresh concrete. The SAM number has been shown to correlate with spacing factor and durability factor (DF) from the ASTM C666 freeze-thaw test (Ley et al. 2017). This test uses a modified Type B pressure meter (SAM) that undergoes a set of sequential pressure steps. The equilibrium pressure difference between the first and second steps of pressurization provides the SAM number. The goals of this research were to evaluate how the materials and mixture proportions commonly used by NCDOT affect the SAM number, as well as to identify SAM numbers that are indicative of durable concrete based on the performance specifications of the NCDOT.

Mixtures from this project, as well as four past NCDOT projects, that used a variety of w/cm, fly ash types and replacement percentages, and cementitious material content were included in this study. SAM numbers obtained from fresh concrete tests were correlated to freeze-thaw durability test results (ASTM C666, method A) and air void system parameters determined using manual point count methods (ASTM C457). This analysis provided insight into the performance of NCDOT mixtures in the freeze-thaw durability test, the relationship between the air void system spacing factor of the hardened concrete and historically used performance targets, and a potential SAM number performance target that could be used in shadow specifications by NCDOT in future concrete construction.

4.2 Limitations

The research study supporting this effort was configured to support evaluation of optimized aggregate gradation concrete mixtures and identification of performance targets for multiple PEM tests, including surface resistivity and shrinkage in addition to SAM. Data from other research projects included in this analysis also had different objectives. To support these objectives, fresh air contents for mixtures produced were limited to a tight range (5 to 6%) to minimize the variation in the mechanical properties and durability performance test results both within this current project and between projects. Since NCDOT specifications require air contents of $5.5 \pm 1.5\%$, the range of 5.0% to 6.0% air should encompass many mixtures being accepted on job sites across North Carolina's highway system. With such a narrow band of fresh air encompassed by the project mixtures the spacing factors associated with these air contents are also a narrower band than in other projects dealing with the SAM. Therefore, it is likely that the limited range of air contents allowed in the mixtures included in this work did not allow for the full spectrum of spacing factors seen in similar evaluations of the SAM or hardened air void systems. Nevertheless, this chapter presents an analysis of the air void systems of a range of NCDOT structural and pavement concrete mixtures, comparing test results of different mixtures to one another and to published data on air void systems from previous research studies.

It is noted that the SAM test results included in this analysis were obtained over the course of approximately 8 years using two SAM devices and approximately 10 different operators. Additionally, over the course of the project, both SAM devices received service from the OSU technician at several points, including reprogramming of the gauge with updated software as it became available. Lightweight sand used in RP 2016-06 (Cavalline et al. 2018) as an internal curing agent was porous and may have influenced the SAM measurements for these mixtures. These changes in equipment, operator, materials, and computational algorithm each likely influenced the accuracy and the uncertainty of SAM number measurements. Evaluating the influence of these changes on the SAM measurements was not included in the scope of this study, but the likely influence of these changes is acknowledged.

4.3 Methods and Test Results

SAM tests were performed using the AASHTO TP 118 procedure as part of three past research studies for NCDOT: RP 2015-03 (Cavalline et al. 2017), RP 2016-06 (Cavalline et al. 2018), and RP 2018-14 (Cavalline et al. 2020a). Due to space limitations in this report, the reader is referred to the project reports for the previous studies, as well as a thesis published on this work (OCampo 2022) for further details on mixture proportions, materials, and fresh and hardened property test results. Data from these studies was paired with new SAM and freeze-thaw test results from RP 2020-13 (this study), and additional hardened air void analysis was performed on specimens from all four studies. All SAM numbers of 0.60 or greater were discarded as these high values were likely the result of a leak during the test than a true SAM number, given that almost all mixtures had a total air content measured with the Type B meter between 5.0 and 6.0%. AASHTO TP 118-17 recommends a range of 0.01 to 0.82 for acceptable SAM numbers so to ensure the integrity of the SAM testing was upheld a more conservative threshold of 0.60 was used as the upper limit.

SAM test results used in this analysis are provided in Appendix C, Table C.1, along with other fresh property test results for these mixtures.

Results of durability testing, including SAM measurements are shown in Table 4.1. Freeze-thaw testing was performed using ASTM C666, Procedure A. For each mixture, 3 replicate beam specimens were tested. Fundamental transverse frequency measurements were made using a Rigol DS1052E digital oscilloscope and Omega Engineering ACC-PS2 accelerometer. The digital oscilloscope was set to Fast Fourier Transform (FFT) mode and the fundamental transverse frequency was determined in accordance with ASTM C215, “Standard Test Method for Fundamental Transverse, Longitudinal, and Torsional Resonant Frequencies of Concrete Specimens” (ASTM 2019). It should be noted that during the course of RP 2020-13 (this study) the settings on the oscilloscope were such that the fundamental frequency measurements were only captured to the hundredths of a kHz (e.g., 2.1 kHz) rather than additional resolution (e.g., 2.13 kHz). This source of resolution loss is acknowledged as a limitation of the DF computed for specimens tested in this study, many of which were greater than 100 at the completion of the study. A full analysis of the impact of this change in measurement resolution on the uncertainty of the measurements was beyond the scope of this study but would likely also need to consider the combined uncertainty of all sources (calibration, frequency, length, mass, etc.). The fundamental transverse frequencies were used to compute DF per ASTM C666.






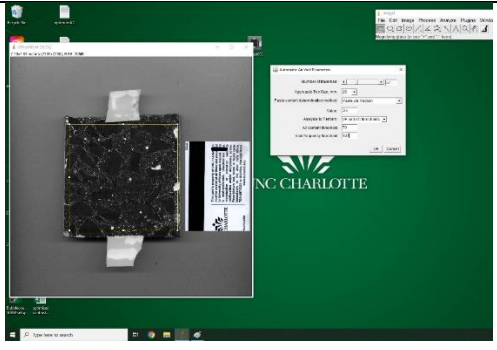
Table 4.1: Results of durability testing for all mixtures

Project Number	Mixture ID	DF	Mass Loss (%)	SAM	SF (in.)	SF (μm)
2015-03	Piedmont coarse aggregate					
	PANM	95.73	-0.08%	0.19	0.0212	539
	PAAM	95.59	0.79%		0.0217	552
	PABM	94.65	1.51%	0.29	0.0313	794
	PANN	81.7	0.94%	0.1	0.0239	608
	PBLNM	100.06	-0.27%	0.28	0.0409	1040
	PBLBM	94.34	1.11%	0.19	0.0175	444
	PBLAM	94.65	2.43%	0.29	0.02	508
	PBLNN	74.2	1.60%	0.19	0.016	407
	PBAM	95.9	1.25%	0.42	0.0196	497
	PBBM	94.65	0.72%	0.22	0.0179	454
	PBNM	98.02	-0.29%	0.23	0.0217	551
	PBNN	81.03	1.09%	0.27	0.0221	560
	Coastal coarse aggregate					
	CANM	96.63	0.52%		0.0186	472
	CBNM	99	-0.09%	0.35	0.0215	545
	CBLNM	98.99	0.00%	0.19	0.0187	474
	Mountain coarse aggregate					
	MANM	77.92	1.41%		0.0413	1048
	MBNM	78.69	2.22%		0.0226	575
	MBLNM	79.52	2.48%		0.0198	503
2016-06	Conventional concrete, no fly ash					
	CC	85.22	-0.39%	0.32	0.0243	617
	Internally cured concrete, no fly ash					
	I1M	88.39	-0.17%	0.4	0.0211	536
	I2M	100.96	0.23%	0.12	0.0219	557
	I1H2*	91.67	-0.20%	0.24	0.0215	546
	I2H	83.8	-0.48%	0.39	0.0323	821
	Internally cured pavement mixture					
	IP	84.39	0.66%	0.3	0.0138	351
	Conventional concrete, fly ash					
	CF	80.15	-0.29%	0.3	0.0221	560
	Internally cured concrete, fly ash					
	I1MF	87.2	-0.23%	0.25	0.016	408
	I2MF	38	1.57%	0.19	0.0242	615
	I1HF	83.19	0.39%	0.29	0.0196	497
	I2HF 2	52.26	2.99%	0.27	0.023	585

2018-14	H-series (high w/cm ratio, 0.47)					
	H-560-140			0.19	0.0228	580
	H-650-0			0.38	0.0227	576
	H-480-120			0.28	0.0111	281
	H-420-180			0.22	0.0167	424
	M Series (moderate w/cm ratio, 0.42)					
	M-700-0			0.25	0.0237	601
	M-650-0			0.23	0.0208	528
	M-420-180			0.24	0.0159	403
	L Series (low w/cm ratio, 0.37)					
	L-600-0			0.06	0.0196	499
2020-13	H-series (high w/cm ratio, 0.47)					
	H-700*-0	103.46	1.22%	0.29		
	H-560*-140	105.19	0.96%	0.4	0.0246	626
	H-650*-0	103.46	1.12%	0.13	0.0209	532
	H-520*-130	101.73	1.03%	0.3	0.0204	519
	H-600*-0	100	2.05%		0.0236	599
	H-480*-120	103.46	1.93%	0.18	0.0158	402
	H-420*-180	103.46	1.22%	0.24	0.0209	530
	M Series (moderate w/cm ratio, 0.42)					
	M-700*-0	100	1.28%		0.022	559
	M-560*-140	93.65	1.08%		0.026	660
	M-650*-0	103.25	-0.15%	0.43	0.0156	395
	M-520*-130	100	2.30%	0.41	0.0205	520
	M-600*-0	100	1.93%		0.0124	315
	M-480*-120	100	3.20%	0.53	0.0116	295
	M-420*-180	100	3.49%		0.0197	502
	L Series (low w/cm ratio, 0.37)					
	L-700*-0	100	0.98%	0.2	0.031	786
	L-560*-140	96.83	0.54%	0.39	0.0226	574
	L-650*-0	100	0.17%	0.42	0.0208	529
	L-520*-130	106.5	0.41%	0.27	0.0195	496
	L-600*-0	100	1.37%		0.0214	544
	L-480*-120	98.53	0.50%	0.51	0.0205	520
	L-420*-180	100	3.20%		0.0206	523
	CNT Series, containing carbon nanotube mixtures, w/cm designated H, M, L as defined above					
	H-600C-0	96.71	1.77%	0.55	0.0157	400
	M-600C-0	100	0.11%	0.38	0.0248	630
	L-600C-0	98.9	0.15%	0.5	0.0197	500
	CNT Series, containing carbon nanotube mixtures, w/cm designated H, M, L as defined above contains Non-Optimized Aggregate Gradation					
	HNO-600C-0	95.06	0.57%		0.031	788
	MNO-600C-0	95.06	0.31%		0.0176	447
	LNO-600C-0	100	0.09%		0.0241	612

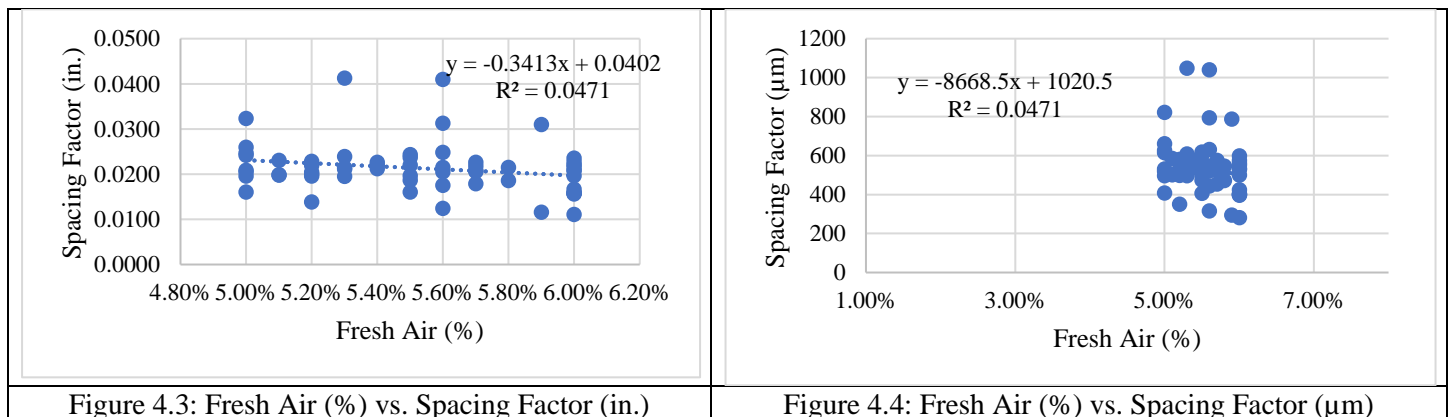
Hardened air void analysis was performed using the scanner procedure developed by Michigan Technological University (Peterson et al. 2001, Peterson et al. 2002, Carlson et al. 2005, Sutter et al. 2007). Development of the calibration set of specimens for use of the system is described in Ojo (2018). To minimize sawcutting, specimens cast for hardened air analysis used cardboard takeout food cartons as molds (Figure 4.1a). To perform the hardened air analysis, specimens were sawcut (Figure 4.1b), polished to roughly 800 grit (Figure 4.1c), and treated with black ink. After the black ink dried, white powder was pressed into the air voids (Figure 4.2a and b). Each specimen was inspected closely, and any entrapped air voids or voids within aggregates were painted with black ink so that they were not “counted” as entrained air voids. The prepared concrete surface was then scanned on a flatbed scanner. The characteristics of the air

void system were then determined using the Bubble Counter software developed by researchers at Michigan Tech (Peterson et al. 2001) (Figure 4.2c).

		
<p>Figure 4.1a: Specimen cast for hardened air void analysis</p>	<p>Figure 4.1b: Specimen sawcut, prior to polishing</p>	<p>Figure 4.1c: Specimen after face is polished using progressively finer grit</p>
		
<p>Figure 4.2a: Treated specimen prior to scanning. Note the limited number of white air voids visible</p>	<p>Figure 4.2b: Treated specimen prior to scanning. Note the presence of more air voids than in the specimen shown in Figure 4.2a</p>	<p>Figure 4.2c: Scanned image of sample with black and white contrast card (UNC Charlotte ID card) along with Bubble Counter system parameters</p>

4.3.1 Fresh Air vs. Spacing Factor

Figure 4.3 shows a downward trend of the spacing factor as the fresh air content (%) increases. This is consistent with findings of other researchers. When Figure 4.3 is compared to a similar figure from Ley et al. (2017) a trend in the spacing factor decreasing as the percentage of fresh air increases can be observed. If a wider ranging fresh air content had been allowed in these studies, a broader range of spacing factor values may have been provided and the trend could have potentially been more strongly exhibited.



To explore whether the data obtained as part of this NCDOT study align with that obtained by OSU, the data provided in the Appendix of Ley et al. (2017) was mined and plotted. Data from this NCDOT-funded study was then plotted with the data from Ley et al. (2017) in the same figure to facilitate comparison. The first of these graphs is shown

below in Figure 4.5, where comparing the data obtained from the OSU data sets is shown with data obtained from NCDOT mixtures (red markers). As seen in Figure 4.5, the data gathered from this NCDOT study are contained fully within an air content range of 5% to 6%. While the spacing factors from some NCDOT mixtures are within the range seen in the OSU data most mixtures spacing factors are between 2 and 3 times the average seen by the data plotted from Ley et al. (2017). There are several factors that could be affecting the difference in spacing factors seen between the data provided by Ley et al. (2017) and the NCDOT projects such as different AEAs used, using a different class of fly ash, and differing WRAs being used for the different studies. Determining the causes of the general increase in spacing factor was not within the scope of this study and as such will not be evaluated at this time.

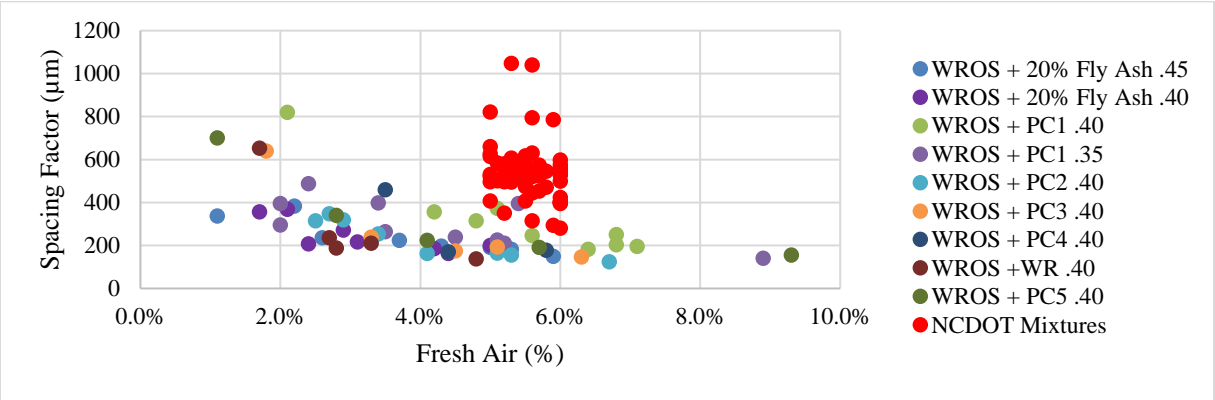


Figure 4.5: Fresh air (%) vs. spacing factor (µm) – OSU data from Ley et al. (2017) with NCDOT mixtures (red data markers)

For similar mixtures dispersion in the SAM numbers could be attributed to the change in users, change in SAM device, different temperatures, or changes in cementitious material chemistry. Interactions between the admixtures may also have coarsened the air voids system, causing larger air bubbles and therefore larger spacing factors. For the mixtures included in this study, the rodding procedure was used to consolidate the concrete into the base of the SAM unit. In recent years, the developer of the SAM has recommended a vibration procedure that could potentially be used to improve the quality of SAM data collected. A daily leak check procedure has also been developed recently and could also be used to improve the accuracy of SAM measurements.

4.3.2 Fresh Air vs. Durability Factor

Figures 4.6 and 4.7 include plots of data from the NCDOT mixtures, with the DF of each mixture plotted against the measured percentage of fresh air. One trend setting the NCDOT mixtures batched and tested for this project apart from the OSU data published in Ley et al. (2017) is the fact that NCDOT mixtures exhibited particularly good durability performance in this test. In fact, only 2 NCDOT mixtures included in this analysis had DF lower than the recommendation provided by Ley et al. (2017), while only 6 NCDOT mixtures fell below a more conservatively recommended DF of 80. In both graphs there is a trend upwards in the DF as the fresh air content percentage increases, as could be expected. Figure 4. shows the same data from Figure 4.6 with a broader range of air contents, showing the limitations in this dataset due to mixture air contents maintained between 5 and 6%.

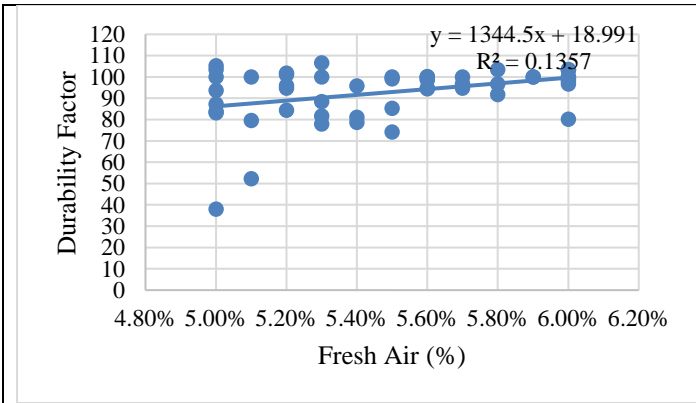


Figure 4.6: Fresh air (%) vs. DF

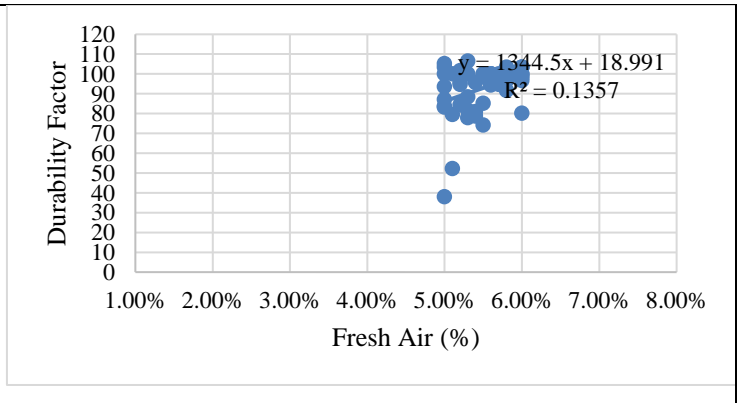


Figure 4.7: Fresh air (%) vs. DF

The test results for mixtures used for this NCDOT project have been overlayed on the test results of the mixtures used by Ley et al. in Figure 4.8. The NCDOT mixtures used for this project (plotted using red markers in Figure 4.8) align well with the OSU data based on the expectations from the data provided by Ley et al. (2017) in this category.

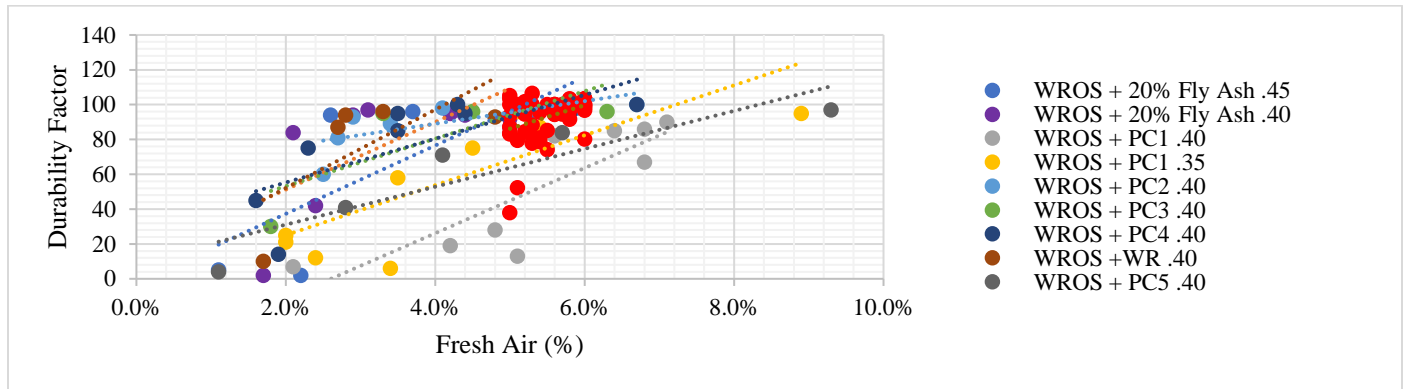


Figure 4.8: Fresh air (%) vs. DF – OSU data from Ley et al. (2017) with NCDOT mixtures (red data markers)

4.3.3 Fresh Air vs. SAM Number

Figures 4.9 and 4.10 show a slight increase in the SAM number as the fresh air percentage increases for NCDOT mixtures. Figure 4.11 displays the same data that is shown in Figure 4.10; however, the data is plotted using a broader range of air contents. As previously stated, the mixtures used for all NCDOT project analysis were designed with mechanical properties and other durability concerns in mind (e.g. evaluating surface resistivity, shrinkage, and mechanical properties). This focus, along with a guiding criterion of maintaining a tight air content range to facilitate comparisons of mixture properties/test performance without undue effects of air content, has left the range of fresh air allowed as a very narrow range. Based on the limitations of this dataset, and the dispersion that could be expected based on the wide range of mixtures tested, the poor correlation shown in Figure 4.10 could be expected.

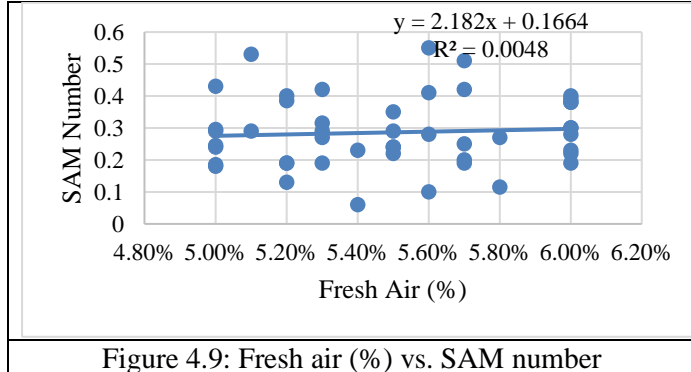


Figure 4.9: Fresh air (%) vs. SAM number

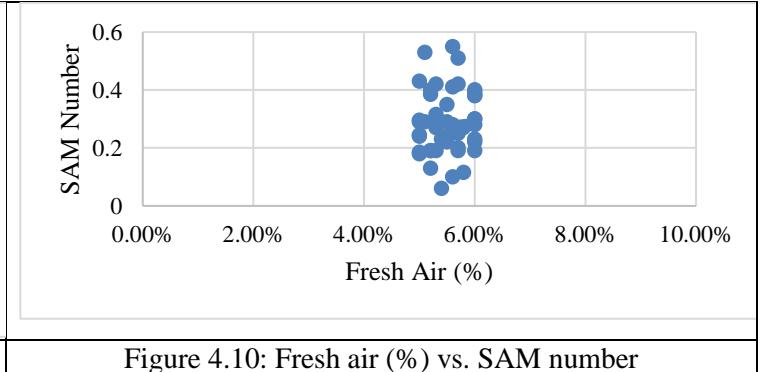


Figure 4.10: Fresh air (%) vs. SAM number

As can be seen in Figure 4.11, where test results for the NCDOT mixtures used in this project (red data markers) are plotted along with the OSU data from Ley et al. (2017). A fairly wide range of SAM numbers was measured for NCDOT mixtures containing between 5 and 6% air content. This variability in the data may be the result of issues arising from use of the device (such as leaks), variability induced by different mixtures, materials, operators, environmental conditions, or other reasons. Riding and Albahtiti (2016) found that between one SAM test to the next within the same site the coefficient of variation was 154% higher than that of the air content tests on average. Overall, the SAM test had a coefficient of variation of 56% throughout all of the samples taken while the air content had a coefficient of variation of 22% (Riding and Albahtiti 2016). The number of SAM operators used to collect UNC Charlotte's dataset is estimated to be approximately 10 people, likely contributing to the dispersion of the data. Although some users received training from the SAM developer, others learned via the online videos or from other users. Many agencies have reported improved results after additional training from the developer (Hall et al. 2019), and it is acknowledged that the change in user and device played a role in the dispersion observed in the data. It is also noted, however, that the spacing factors measured for the NCDOT mixtures were also greater than those obtained by Ley et al. (2017), and the increase in measured SAM number could therefore be expected.

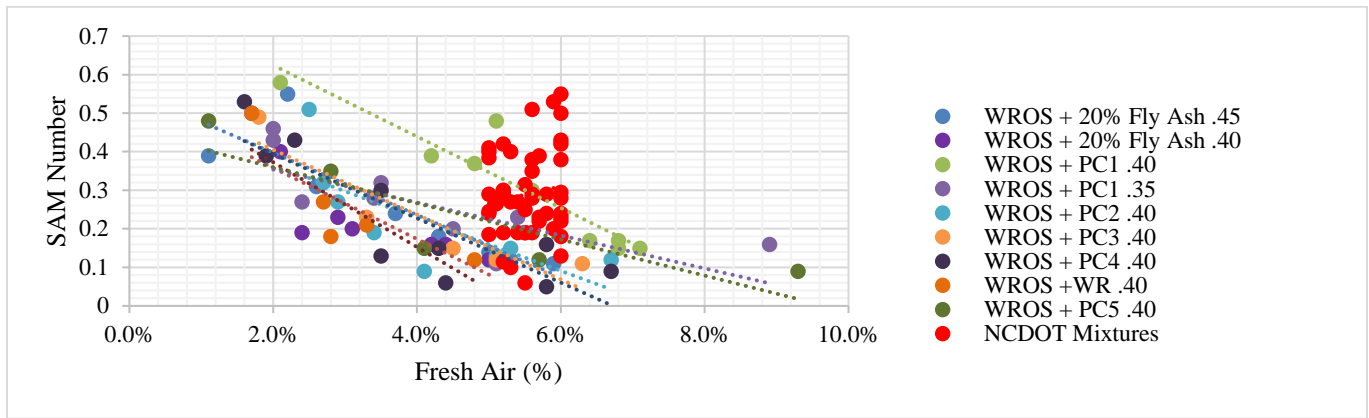


Figure 4.11: Fresh air (%) vs. SAM number - OSU data from Ley et al. (2017) with NCDOT mixtures (red data markers)

4.3.4 Spacing Factor

ASTM C457 testing was performed on two samples per mixture. Of the 65 samples which had a spacing factor calculated, 29 were above the average of 0.0213 in. Of the samples which had above the average spacing factor 8 of 29 utilized fly ash while the variable w/cm ratio mixtures from 2018-14 and 2020-13 accounted for 10 of the 29 mixtures. Figure 4.12 shows the spacing factor (μm) graphed against the DF using data from Ley et al. (2017) and NCDOT mixtures (red markers). For the OSU data, the DF can be seen to decrease rapidly in the space between 200 μm and 400 μm with most mixtures at or before 200 μm having a DF above 80. The mixtures measured with a spacing factor of above 200 μm rapidly descend in the DF measured until they hit a general low at 400 μm and above with only random mixtures displaying a DF above 80 and the majority of mixtures being measured below 40. As noted before, only a few of the NCDOT mixtures performed poorly the ASTM C666 test. Note that the data shown with hollow red markers is from RP 2020-13 specimens where the DF was measured to be slightly greater than 100 due to the oscilloscope settings used.

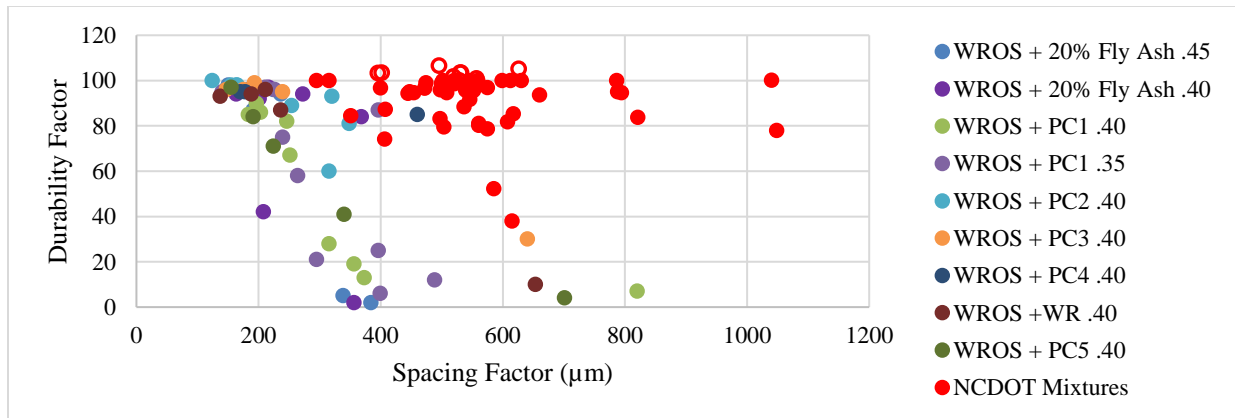


Figure 4.12: Spacing factor (μm) vs. DF - OSU data from Ley et al. (2017) with NCDOT mixtures (red data markers)

Figure 4.13 shows a plot of SAM number vs. spacing factor, with mixtures from OSU from Ley et al. (2017) plotted with NCDOT data (red markers). The data found from the NCDOT mixtures notably exhibits spacing factors higher in general when compared to the data acquired from OSU. This correlates with work by Ojo (2018) using mixtures with North Carolina materials and NCDOT paving mixtures.

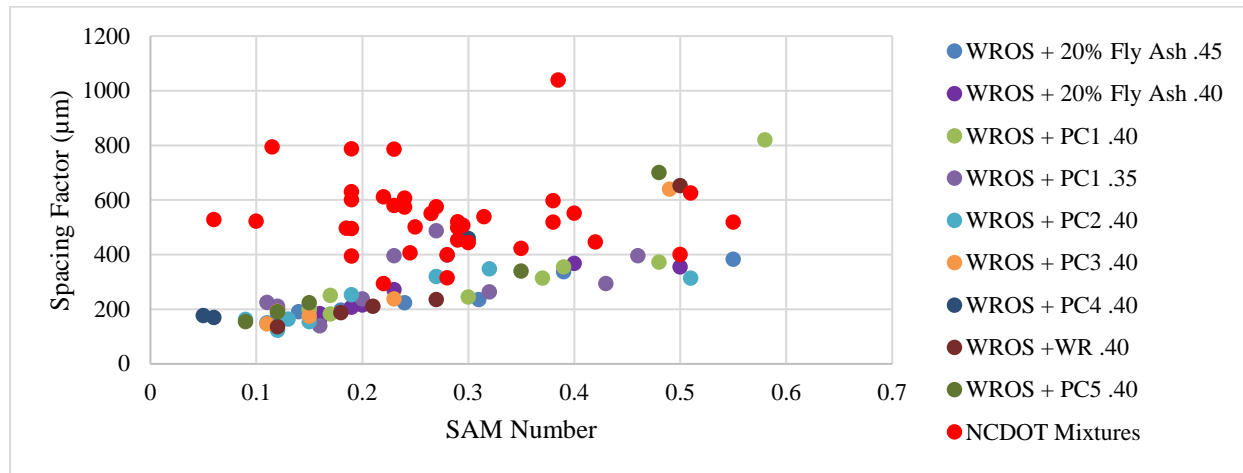


Figure 4.13: SAM Number vs. Spacing Factor (μm) - OSU data from Appendix of Ley et al. (2017) with NCDOT mixtures overlaid (red data markers)

Figure 4.14 shows the SAM number plotted against spacing factor for a study completed for a private entity using NCDOT mixtures (Ojo 2018). It is noted that some mixtures contained fly ashes that did not meet ASTM C168 in several mixtures. These findings align more closely with the relationships between the SAM number and spacing factor suggested by OSU (Ley et al. 2017).

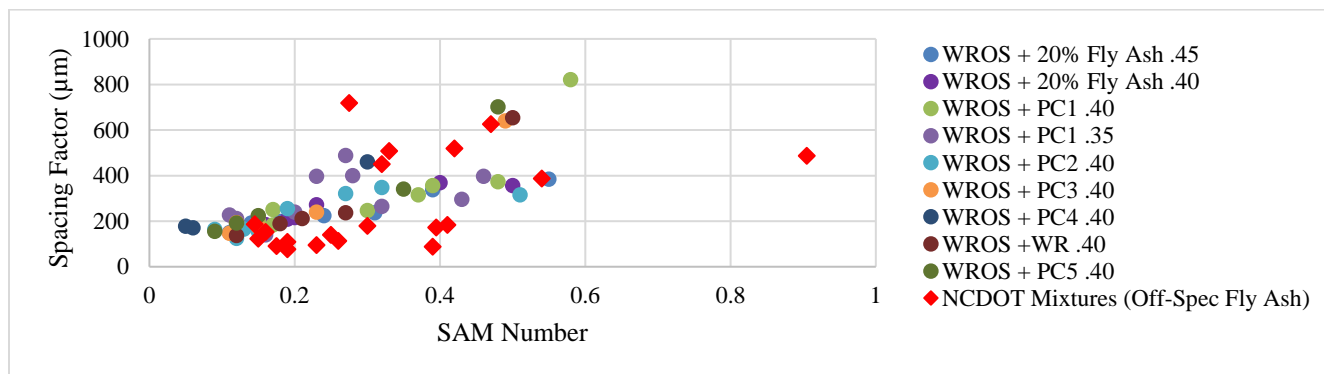


Figure 4.14: SAM Number vs. Spacing Factor (μm) – OSU data from Appendix of Ley et al. (2017) with NCDOT mixtures utilizing off spec fly ash overlaid (red data markers)

4.3.5 Durability Factor

For all NCDOT studies included in this work, ASTM C666 testing was performed on three specimens per mixture, and the averages are plotted in Figure 4.15 (red markers) with data from OSU for comparison (Ley et al. 2017). As described earlier, a change in the oscilloscope settings during RP 2020-13 resulted in a loss of resolution on the fundamental frequency of these samples. Therefore, several samples from the RP 2020-13 project had a final (after 300 cycle) relative dynamic modulus higher than that of the initial reading, and therefore DF slightly greater than 100. These samples will be shown as having a DF of 100 but are marked with a hollow red circle to show which exceeded this limit.

The data from OSU shows a general drop in the DF as the SAM number approaches 0.4, which is similar to the drop measured when graphing the spacing factor (μm) vs the DF for this data. The NCDOT mixtures did not exhibit a drop in DF with only 6 of the 57 mixtures with a DF being under a DF of 80. Of these 6 mixtures that fell under a DF of 80 only 2 were below a DF of 70. According to Brian Hunter, State Laboratory Engineer at NCDOT, North Carolina's bridge and pavement concrete mixtures have historically exhibited good freeze-thaw durability. UNC Charlotte's freeze-thaw laboratory tests of NCDOT mixtures have indeed supported this field observation.

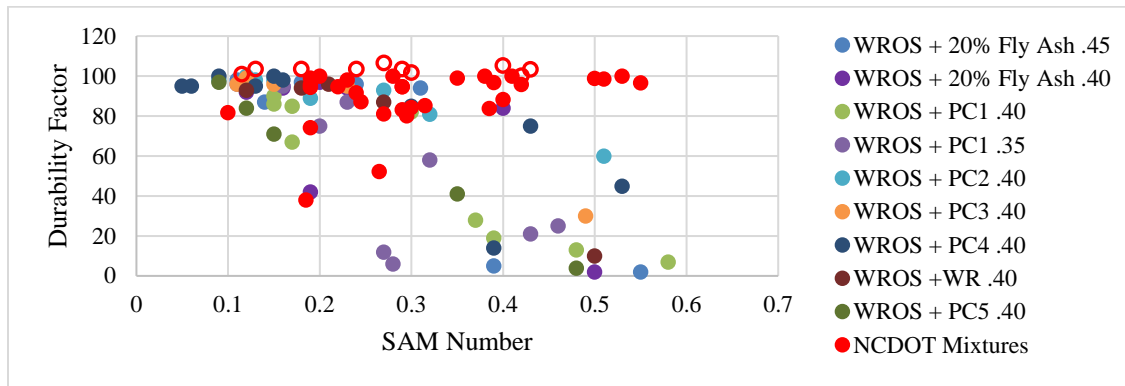


Figure 4.15: SAM Number vs. DF - OSU data from Ley et al. (2017) with NCDOT mixtures (red data markers)

Previous work by Ojo (2018) using NCDOT-type mixtures with a variety of in-spec and off-spec fly ash more closely aligned with the findings from Ley et al. (2017), but also aligned with NCDOT studies in that a majority of concrete mixtures that passed ASTM C666 testing. It is noted that many mixtures in Ojo (2017) contained off-spec fly ash from several sources, some treated with a chemical compound to assist with air entrainment. Although the performance of mixtures containing fly ash from each source was different, mixtures containing air contents greater than 5% all had high (typically >90%) DFs at the end of 300 freeze-thaw cycles (Ojo 2018).

4.4 Development of Recommended SAM Specification

To support use of the results from this research project in future work and to develop a preliminary SAM specification for NCDOT, a review of existing SAM specifications was undertaken. Findings of this review are published in Ocampo (2022) and are summarized here.

Currently the SAM is being utilized in several states as well as some Canadian provinces. However, of the state specifications reviewed for this project, only Wisconsin had SAM requirements included in the standard specifications as a mixture design approval requirement (WisDOT 2022). At the time of this review, the Wisconsin DOT standard specifications includes a quality management plan requiring the SAM test be performed at least once per lot with the following exceptions: lots less than 4 sublots, high early strength concrete, special high early strength concrete, concrete pavement approach slabs, concrete masonry culverts, concrete masonry retaining walls, crash cushions, and concrete-filled steel grid floor. While the SAM number was a required measurement, no pay adjustment was required for an unsatisfactory test result, and recommendations for an acceptable SAM number were not included (WisDOT 2022).

At the time of this review, the New York DOT did not have a standard specification calling for the use of the SAM test but did include a special provision for SAM testing during mixture design phase in section 501-3 (NYSDOT 2022). A SAM number of 0.20 was typically recommended, or a DF > 90%. Colorado DOT has also created a special provision for the SAM test where all air entrained concrete produced for their projects will also need to have a SAM number reported when air testing is conducted for mixture design (CODOT 2021). This provision has been placed into section 601.05 of the standard specifications for projects that include a special provision. West Virginia approved of using the SAM as a project specific special provision for mixture design acceptance. The criteria required for the mixture design is shown in Table 4.2 below.

Table 4.2: Design Mix Performance Criteria (WVDOT)

SAM Number	Required Action
Less than 0.25	Accept Concrete
0.25 to 0.30	Accept with Corrective Action Needed
Greater than 0.30	Reduced payment for concrete

The original lab work completed by Ley et al. (2017) showed that above a SAM number of 0.30, a steep decline occurred in the ability of the concrete to provide a DF above 80 in the ASTM C666 freeze-thaw test. With such a steep decline exhibited by the mixtures included to date, the OSU research team established a recommended of a SAM number of 0.20 to ensure adequate freeze-thaw performance of most mixtures. Other laboratories performing research on different types of concrete mixtures using materials from different geographic areas have had results that indicate a different SAM number may correlates to a recommended spacing factor and/or DF.

In a study aimed to evaluate the SAM in Poland, Dabrowski et al. (2019) found that a SAM number of 0.40 provided a more accurate correlation to the desired spacing factor of 200 μm . These researchers indicated that a SAM

number target of 0.20 was too restrictive, with only one of the tested mixtures included in their study achieving a SAM number of 0.20 or below while mixtures with a SAM number greater than 0.20- but less than 0.40 still exhibiting a desirable spacing factor. European countries do not use a rapid freeze-thaw test such as ASTM C666, so this study did not provide data to allow comparisons to be made with the DF. However, a SAM number of 0.40 had an apparent correlation to the content of microvoids deemed acceptable. Microvoids are air voids that are under 300 μm in size and have been shown to be a useful parameter in determining the quality of the microstructure of the air void system (Dabrowski et al. 2019).

Work done by Ojo (2018) at UNC Charlotte indicated that a SAM number of 0.30 was found to encompass all but three mixtures that had a DF of 60 or higher which is the failure threshold for ASTM C666. As a disclaimer, the mixtures used by Ojo (2018) used fly ash that did not meet ASTM C618 in some mixtures. However, the mixtures and materials did provide useful insights into a wider range of air contents which the NCDOT-sponsored research did not provide due to the study design.

In studies of NCDOT concrete mixtures by UNC Charlotte, freeze-thaw tests performed on mixtures with a wide range of w/cm, SCM contents, aggregate sources, and other factors showed that these mixtures exhibited favorable freeze-thaw durability performance in the laboratory, with DF typically greater than 80 at 300 cycles. With these favorable DFs in the ASTM C666 test, supported by typically good freeze-thaw durability of concrete in service, a less conservative SAM number (e.g., greater than 0.20) should be an appropriate preliminary target for NCDOT project special provisions for the SAM until additional field and laboratory data is collected and analyzed. It is therefore recommended that NCDOT use a SAM number of 0.30 in shadow specifications for future projects, along with requirements for total air content aligned with their current specifications $6.0\% \pm 1.5\%$. In environments experiencing significant freeze-thaw, such as in the mountains, it could be worthwhile to for NCDOT to consider specifying a higher air content range of 6 to 8%, consistent with other states with similar environments.

4.5 Conclusions

- NCDOT structural and pavement mixtures batched and tested as part of a series of research studies are very resistant to freeze-thaw stresses. After 300 cycles of ASTM C666 testing, only 6 of the 56 mixtures exhibited a DF below 80 and only 2 falling below ASTM C666's performance threshold DF of 60.
- The historically used spacing factor limit of 0.008 in (200 μm) appears to be too conservative for use of NCDOT in specification development. Many mixtures exhibiting good to excellent freeze-thaw durability performance in the ASTM C666 test had spacing factors that exceeded this target. Since most concrete mixtures included in this study exhibited DFs greater than 80, a proposed target spacing factor could not be identified.
- Fresh air content exhibited a reasonable correlation to the spacing factor and DF found during testing.
- The SAM numbers obtained during studies of NCDOT concrete at UNC Charlotte exhibited a lesser correlation to the DF. The strong relationship between SAM number and spacing factor observed in other studies was not observed based on findings of this work. Variability in the SAM measurements was likely increased due to use of multiple devices, operators, and materials. Variability also exists in the spacing factor measurements, which could have affected the ability to observe meaningful correlations.
- The findings of this study were significantly limited by the range of air contents (5 to 6%) used in the mixtures. A more comprehensive study should be performed using a wider range of air contents (such as 2% to 10%). Analysis of field-produced concrete should also be paired with additional laboratory testing of to further explore the SAM number, in hopes of expanding the types of materials and mixtures used to identify the performance target. Future research projects to support NCDOT's PEM initiatives could further explore the spacing factor, SAM number and DF that correlates to adequate performance in both the field and laboratory.

5.0 USE OF SURFACE RESISTIVITY METER TO EVALUATE BRIDGE DECK OVERLAYS

Also included as part of the laboratory evaluation was an investigation of the potential for the surface resistivity meter to be used as a QA tool for bridge deck overlays. Although the resistivity meter shows strong promise for field applications, the influence of a number of factors such as overlay thickness, influence of reinforcing steel, and influence of polymeric mixture additives on surface resistivity measurements is not yet fully understood. To explore the potential for use of the surface resistivity meter for use in bridge deck overlay QA, several laboratory mockups were constructed. Mockups were designed and constructed in a manner that allowed the impact of a variety of factors on the measured resistivity to be explored. As constructed, variables to be explored using these mockups include: overlay mixture type (conventional, polymer modified, very high early strength), overlay thickness, rebar depth/size, voids/defects, edge effects, and moisture content.

The concrete mixtures used to construct the test specimens replicated common mixtures employed by NCDOT for bridge deck construction, bridge deck overlays, and bridge deck repair patches. Mixture designs met Class AA bridge deck specifications which require a minimum 4,500 psi 28-day compressive strength and a cement content of between 639-715 pounds per cubic yard. Details on the materials used are provided in Dillworth (2021). The concrete mixtures are described in Table 5.1 and included those listed below.

- A conventional bridge deck mixture (CC)
- A conventional ready-mix bridge deck mixture (CC-RM)
- A latex-modified bridge deck overlay mixture (LMC)
- A very high early strength overlay mixture (VHES)
- A very high early strength latex-modified overlay mixture (VHES-LMC)

Table 5.1: Concrete proportions for bridge deck overlay slabs

Mixture		lb/cy				gal/cy	oz/100# cement	
	w/c	Cement	Water	CA	FA	Latex	MRWR	AEA
CC	0.37	715	265.5	1720	1113	0	7.66	3.65
CC-RM	0.39	572	288.6	1825	1014	-	-	-
LMC	0.39	658	177	1304	1510	17.5	5.55	0
VHES	0.45	658	299	1304	1510	0	15	2.56
VHES-LMC	0.45	658	222	1304	1510	17.5	5.55	0

5.1 Test Specimen Preparation

Previous research by Polder (2002) had found a 2x to 6x reduction in surface resistivity measurements when the probe is placed on top of and parallel to the epoxy-coated steel reinforcement. This work was performed using early version of the surface resistivity meter. To better understand the effect of different types of reinforcing steel embedded in concrete at different depths on resistivity measurements a preliminary investigation was carried out on concrete cylinders and miniature slabs cast from CC, LMC, VHES, and VHES-LMC.

For cylinder specimen, concrete mixtures shown in Table 5.2 were cast into 6 in. x 12 in. cylinders. A single No. 6 (3/4 in.) rebar was embedded longitudinally into selected cylinders as follows (1) with a single standard rebar - two cylinders per mixture, (2) with a single epoxy-coated rebar - two cylinders per mixture, and (3) no reinforcement - two cylinders per mixture.

Table 5.2: Number of 6 in. x 12 in. cylinders for preliminary testing

Type of reinforcement	Number of Cylinders			
	CC	LMC	VHES	VHES-LMC
Standard rebar	2	2	2	2
Epoxy coated rebar	2	2	2	2
No rebar	2	2	2	2

In cylinders containing reinforcement, the No. 6 bar was placed off-center longitudinally through the cylinder, providing differing cover dimensions for the surface resistivity testing, depending on where the meter was placed longitudinally along the cylinder to take a reading. Rebar was placed approximately 1.5 in. from the outside surface of the cylinders, as shown in Figure 5.1.

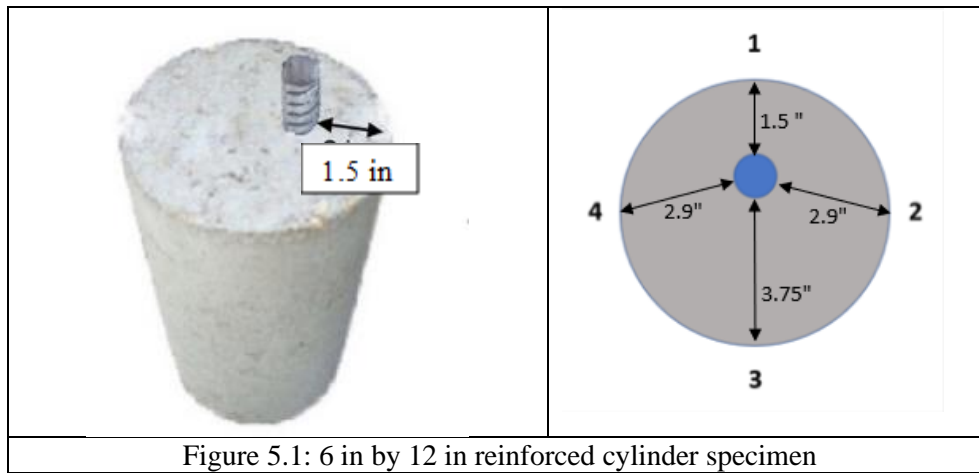


Figure 5.1: 6 in by 12 in reinforced cylinder specimen

After the concrete cylinders were cast, they were covered with plastic to promote curing without moisture loss. Cylinders cast from the two conventional (non-VHES) concrete mixtures were allowed to cure for 24 hours in laboratory conditions prior to demolding, then were tested for surface resistivity at 1 day (24 hours). After the 1-day tests, cylinders were placed in the moist curing room and removed only for the 3, 7, 14, 28, 56, and 90-day surface resistivity tests.

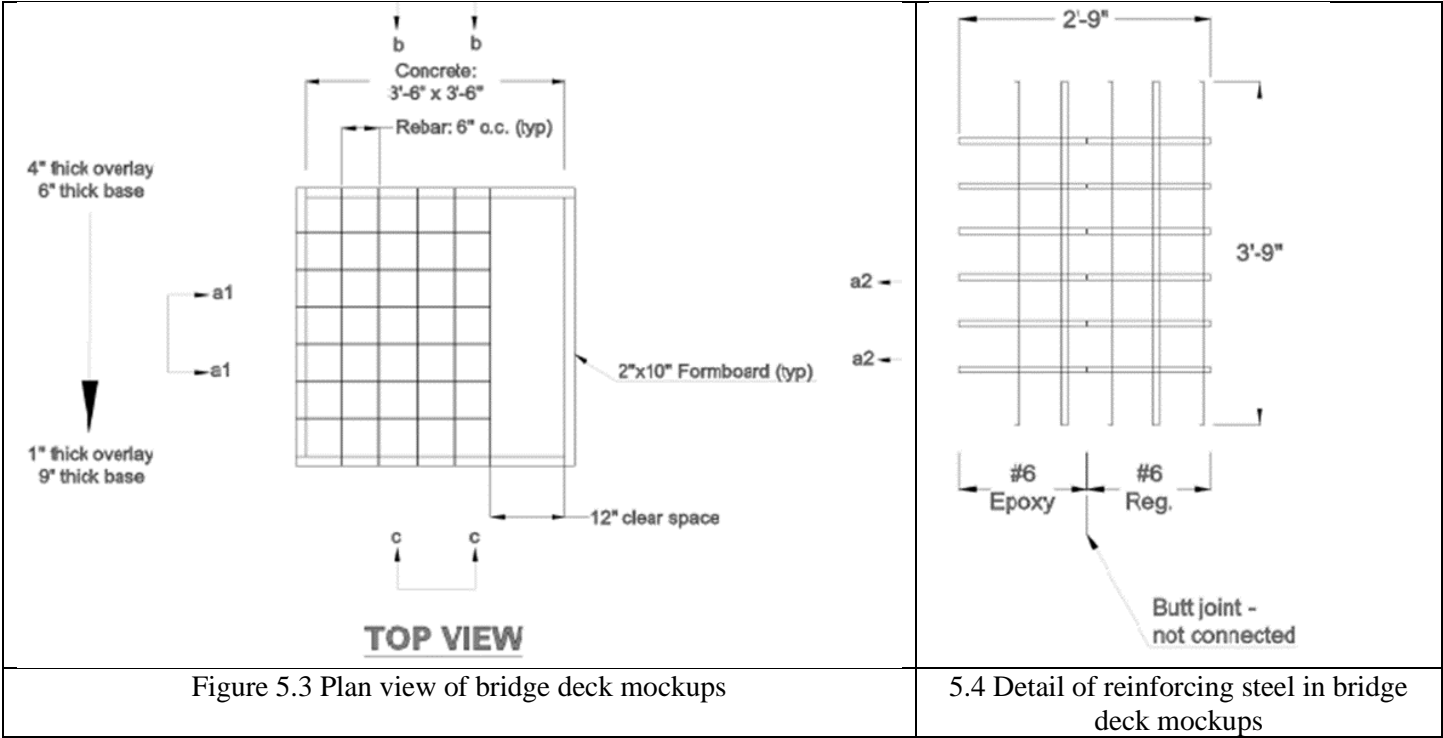
Cylinders cast from the two VHES mixtures were also covered with plastic to promote curing without moisture loss. At 1 hour, the cylinders were demolded, and surface resistivity tests were performed at 1 hour, 2 hours, and 4 hours. The VHES cylinders were then placed in the moist curing room to follow the same testing schedule utilized for the conventional (non-VHES) concrete test specimens. At 120 days, all cylinders (CC, LMC, VHES-LMC, VHES-non latex) were relocated to an environmental chamber programmed to retain a constant temperature of $73 \pm 3^\circ\text{F}$ with a relative humidity of $50 \pm 4\%$ to allow them to reach a steady yet unsaturated state, and surface resistivity testing resumed.

As an intermediate-sized test specimen between the preliminary 6 in. x 12 in. cylinders and the more extensive bridge deck mockups, miniature slabs were constructed and tested as part of this preliminary work. The miniature slabs served to better understand the influence of reinforcing steel, edge, and orientation of test on measured surface resistivity. Figure 5.2 shows the containers used as concrete forms for the miniature slabs with the three reinforcing conditions – unreinforced (at top), uncoated rebar (middle) and epoxy-coated rebar (bottom). The No. 6 reinforcement was placed 6 in.-on-center to maintain the same spacing as the bridge deck mockups. The forms at the left of Figure 5.2 were filled with VHES concrete, the forms on the right of Figure 5.2 were filled with VHES-LMC. After being filled with concrete, the boxes were placed on a vibrating table to assist with consolidation of the concrete around the reinforcement. Miniature slabs cast using the two conventional (non-VHES) mixtures were cured in the curing room and tested following the schedule used for the non-VHES cylinders. VHES concrete miniature slabs were cured and tested following the schedule and procedure previously used for the VHES cylinders (1, 2, 4 hours, then 1, 3, 7, 14, 28, 56, and 90 days).

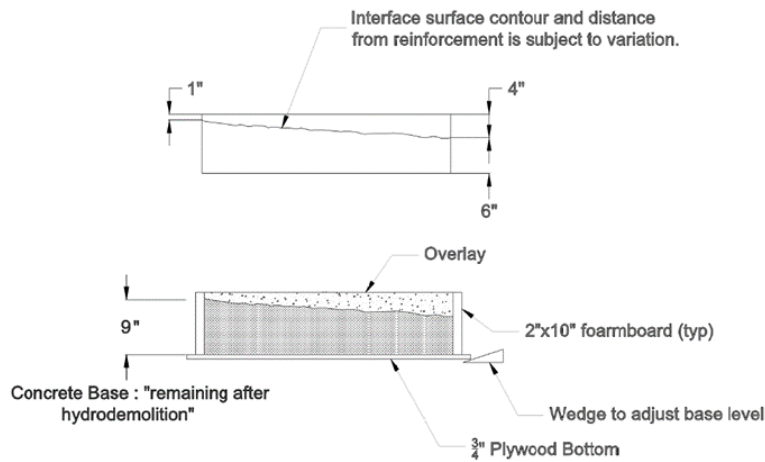


Figure 5.2: Miniature slab forms

Four bridge deck mockups were also developed and constructed, each resembling a 10-inch-thick section of a typical cast-in-place reinforced concrete bridge deck. In developing the mockups, consideration was given to steel reinforcement diameter and spacing as set forth by typical bridge deck construction practices, except for the inclusion of only the top steel reinforcement mat. The steel reinforcement that would typically be found in the lower portion of bridge decks was omitted due to the fact that the reach of the surface resistivity meter’s current field is limited with respect to depth. It is suspected that the lower reinforcement mat would not influence surface resistivity readings. Figure 5.3 shows the plan view schematic of a typical bridge deck mockup form including the top reinforcement mat and the 12-inch clear space for control measurements and does not display the placed void material. Figure 5.4 provides additional detail for the steel reinforcement mat, showing the division line between the epoxy-coated and non-coated steel reinforcement, as well as dimensioning. At the reinforcement division line, the reinforcement is simply butted end-to-end, without connection. The steel reinforcement mat within each mockup was composed of No. 6 epoxy coated and standard or non-coated transverse and lateral reinforcement strands spaced at 6 inches on center.



Each mockup contained a different concrete mixture configuration. The single control mockup was filled entirely with a CC bridge deck mixture CC-RM, and the remaining three mockups contain the CC-RM only as the base layer, then a different overlay concrete mixture was poured on top of each. To create a varying thickness overlay, the base concrete was intentionally poured and finished out of level. Figure 5.5 shows a section view of a typical bridge deck mockup. As depicted in the figure, the base concrete and overlay concrete thickness varies from left-to-right.



SIDE b

Figure 5.5: Typical bridge deck mockup section view

The bridge deck mockup forms were built using 2-in x 10-in lumber for the sides and plywood on the bottom (Figure 5.6a). To provide a moisture loss barrier, the mockup forms were lined with 3 mil. polyethylene sheeting. Once the forms were built, the steel reinforcement was placed and supported through predrilled holes on three of the four form walls then tied with standard reinforcement ties. The mockups were built to be carted around the laboratory on a pallet jack. Figure 5.6a shows a typical completed mockup form containing epoxy-coated reinforcement (left), standard reinforcement (middle), and a non-reinforced section (right).

The control mockup and overlay bases were all poured together on the same day using concrete supplied by a local ready-mixed concrete company. During placement, an electric handheld concrete vibrator was utilized to assist with consolidation. After pouring the conventional concrete for the control mockup and the base sections for the three overlay mockups, the mockups were moist cured outdoors for 7 days to allow for curing per NCDOT's specifications. Therefore, the 1 day and 3-day surface resistivity testing of the control mockup was performed outside of the laboratory in ambient conditions. On the 7th day, the moist curing concluded, and the mockups were relocated inside for the duration of the testing program.



Figure 5.6a: Slab mockup forms



Figure 5.6b: Mockups after AA deck slab was placed, but prior to overlay placement



Figure 5.6c: Mockups with overlay slabs placed (rear three mockups)

The LMC mockup was prepared by including six pieces of foam to simulate voids as depicted in Figure 5.7a. An additional void (bottom left-hand corner of Figure 5.7b) was included on the VHES-LMC mockup for a total of seven voids, and the VHES mockup contained two additional voids ([1] bottom left-hand corner and [2] top right-hand corner of Figure 5.7c) for a total of eight voids.

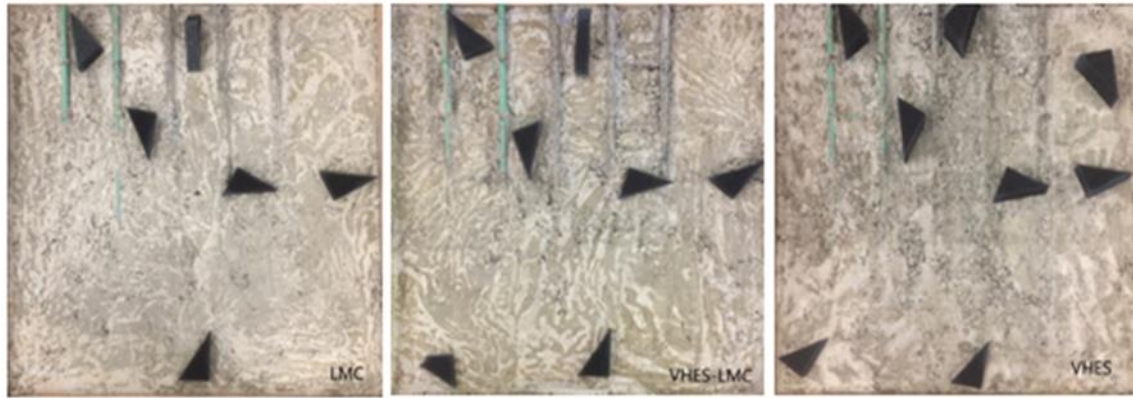


Figure 5.7a, b, and c: Mockup void placement - (a) LMC, (b) VHES-LMC, and (c) VHES

The three overlay mixtures, LMC, VHES-LMC, and VHES, were batched in the laboratory and placed on top of the CC-RM base concrete a later date, after 7 days of curing of the base. The bridge deck mockups containing Type I/II cement (conventional concrete, latex modified concrete) were cured after finishing with wet burlap under polyethylene sheets in an effort to maintain the desired moist conditions for the 7-day curing period (NCDOT 2018). The overlay concrete containing the VHES cement were cured similarly to non-VHES mockups except for the curing duration was reduced from 7 days to a one hour curing period, as recommended by the cement manufacturer. Cylinders for each overlay concrete mixture were also cast and were measured for surface resistivity (Figure 4b) and compressive strength at 1, 3, 7, 14, 28, 56, and 90 days. The VHES and VHES-LMC mixtures were also tested at 1 hour and 4 hours. All data is provided in Dillworth (2021).

5.2 Test Methods

The Resipod surface resistivity meter manufactured by Proceq was used for this study. Surface resistivity measurements were made on the preliminary 6 in. x 12 in. specimens following the AASHTO T 358 standard method. Resistivity measurements were made on two replicates of each concrete type and reinforcement configuration at the four circumferential points shown in Figure 5.8a. The influence of mixture type, reinforcement type, and depth of cover on surface resistivity measurements were evaluated with attention given to the comparison of measurements at quadrant 1 with other quadrants. For miniature slab specimens, resistivity measurements were made using the meter placed at 22 locations on the top surface of the miniature slabs. Figure 5.8b shows a typical miniature slab, with the rebar locations shown in black. Testing locations and alignment of the surface resistivity meter are shown in blue.

<p>A diagram of a circular cross-section of a 6 in by 12 in cylinder. A blue circle in the center represents the embedded rebar. Four measurement points are labeled 1, 2, 3, and 4 around the perimeter. The distance from the center to point 1 is 1.5". The distance from the center to points 2 and 4 is 2.9". The distance from the center to point 3 is 3.75".</p>	<p>A photograph of a miniature slab with a grid of black lines representing rebar locations. Blue lines and arrows indicate the test locations and the orientation of the surface resistivity meter.</p>
<p>Figure 5.8a: 6 in by 12 in cylinder cross section, with measurement positions labeled 1-4 and embedded rebar shown as blue circle.</p>	<p>Figure 5.8b: Typical miniature slab with location and orientation of rebar (shown in black) and test locations (shown in blue)</p>

Surface resistivity measurements of the bridge deck mockups were measured over a series of selected time periods (1, 3, 7, 14, 28, 56, and 90 days for conventional mixtures; 1, 2, and 4 hr, 1, 3, 7, 14, 28, 56, and 90 days for VHES mixtures) at designated points arranged in a 13 x 13 cell grid (169 points) across the top surface (Figure 5.9a and

b). Each of the 169 points was measured with the meter held at a certain orientation (horizontal, vertical, or diagonal) before beginning the next orientation. The points were measured in a sequence from left-to-right, top-to-bottom starting with the top left point in the following orientations, diagonal, horizontal, then vertical.

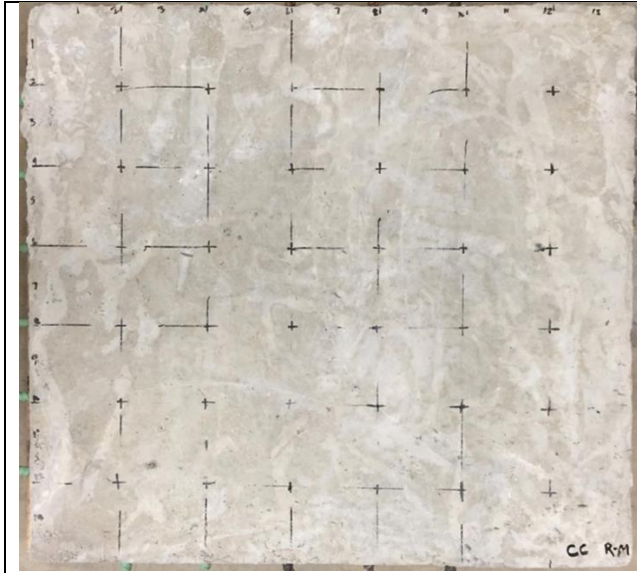


Figure 5.9a: Mockup surface showing grid layout spacing

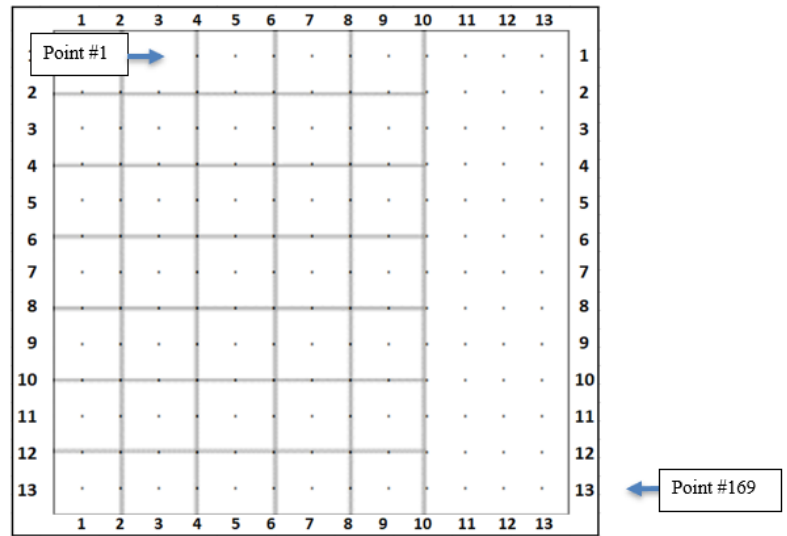


Figure 5.9b: Testing sequence for surface resistivity of mockups

For the meter's current to successfully enter and pass through the pore liquid water must be added to the mockups surface. Roughly 1 gallon of water divided into three pours was used to saturate the 3.5 ft. by 3.5 ft. testing area per orientation. The water was poured onto the surface so that it is fully covered without spillover, allowing it to absorb and reapplying several times to account for evaporation. An extension was temporarily attached to the meter to facilitate easier data collection from the standing position (Figure 5.10). The desired saturation was achieved when the surface resistivity measurement no longer drifted and remained stable. The points were measured with the surface resistivity meter positioned in three different orientations with respect to image of Figure 5.11.

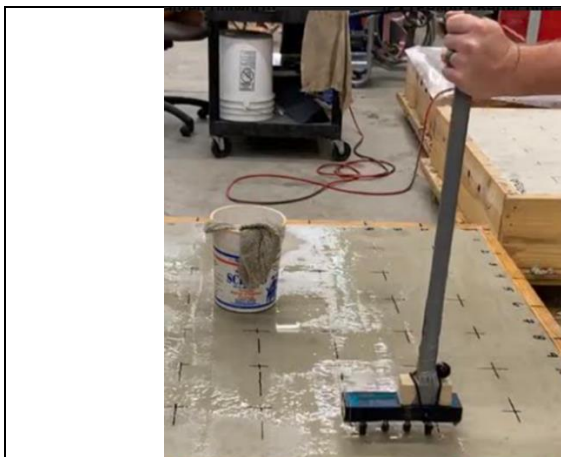


Figure 5.10: Typical surface moisture condition after wetting/preparation and attachment to allow surface resistivity measurements to be taken rapidly while standing.

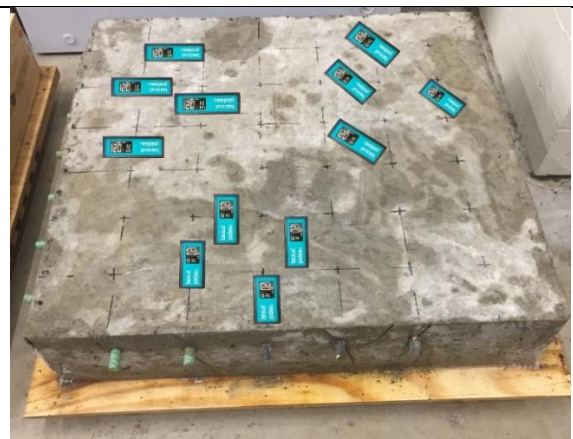


Figure 5.11: Schematic showing the three different orientations used when measuring surface resistivity at the 169 measurement points.

5.3 Results

Surface resistivity measurements were made on unreinforced 4 in by 12 in cylinders cast from the CC-RM and the three overlay mixtures, which were cured in a moist curing room. A summary of the compressive strength of these mixtures is shown in Figure 5.12, with the surface resistivity shown in Figure 5.13.

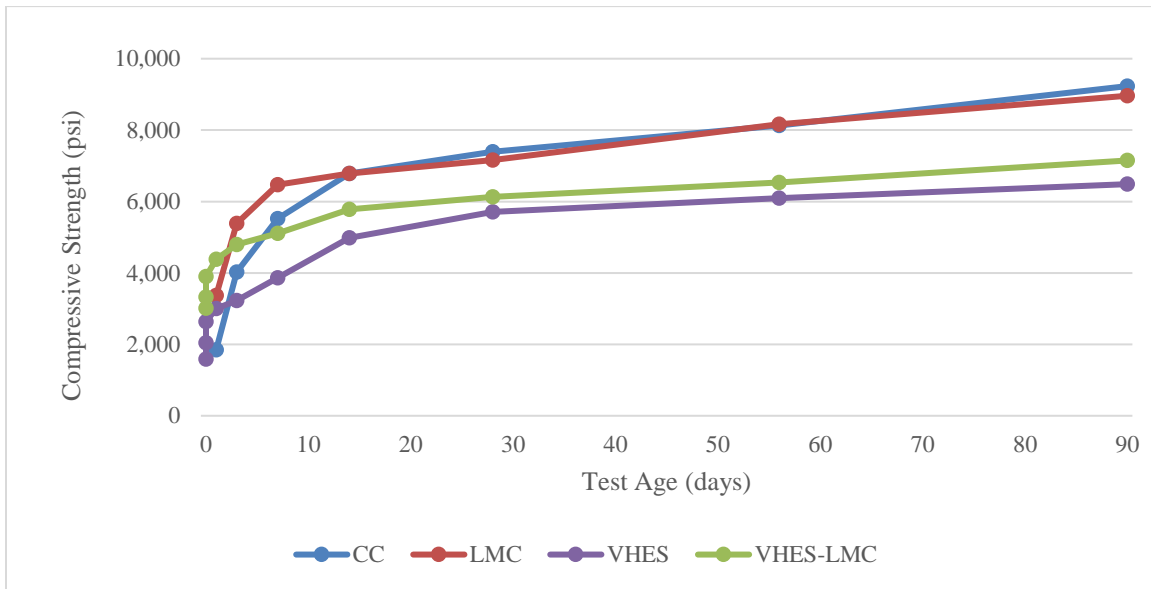


Figure 5.12: Compressive strength of CC-RM, LMC, VHES, and VHES-LMC used in mockups

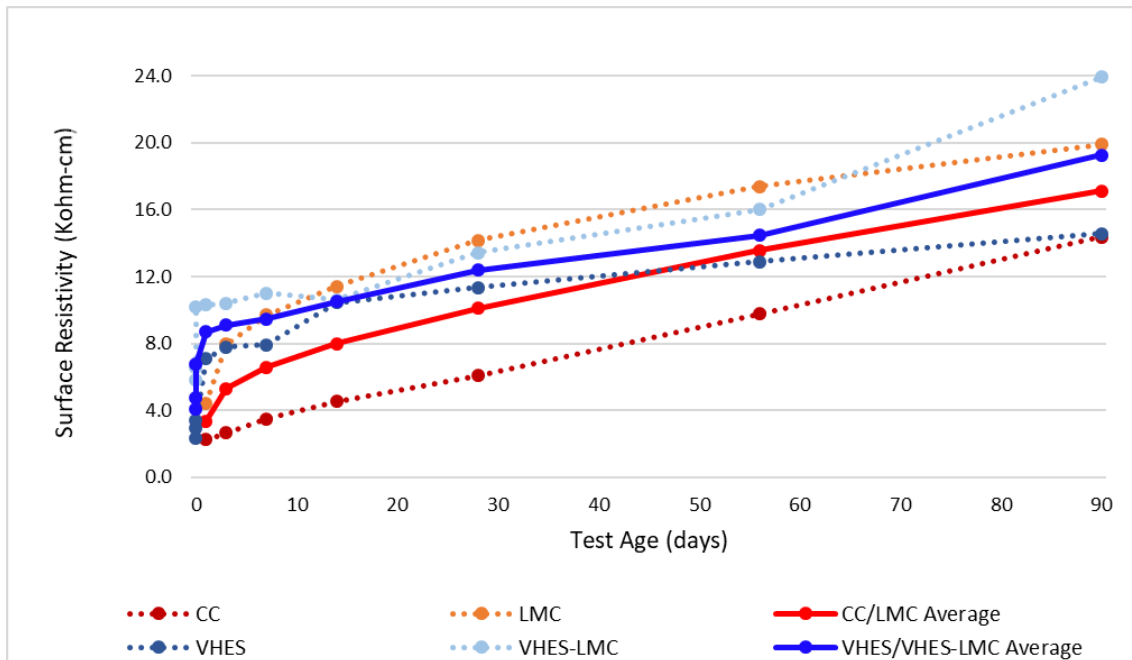


Figure 5.13: Surface resistivity of CC-RM, LMC, VHES, and VHES-LMC used in mockups

5.3.1 Reinforced Cylinder Specimens

Results for tests on the reinforced cylinder specimen are shown in Figure 5.14. Figures 5.14a, 5.14b, and 5.14c show the surface resistivity measurement at each point (1-4) around the circumference of the cylinders cast from the conventional concrete mixture. As shown in Figure 5.14b and c, the rebar is offset towards point 1 on the cylinder. The radar chart represents the end view of the cylinders with the numbers 1-4 correlating the circumferential positions on the diagrams. If the radar plots in Figure 5.14a, 5.14b, and 5.14c are compared, the influence of the standard rebar on the resistivity measurement can be readily observed, particularly near position 1 (where the reinforcement is closest to the surface). This drop in surface resistivity is evident in both the data tables and the radar plots. Readings at position 1 for the conventional rebar (Figure 5.14b) are lower than those at position 1 for the unreinforced cylinder (Figure 5.14a) and for the cylinder with epoxy-coated rebar (Figure 5.14c).

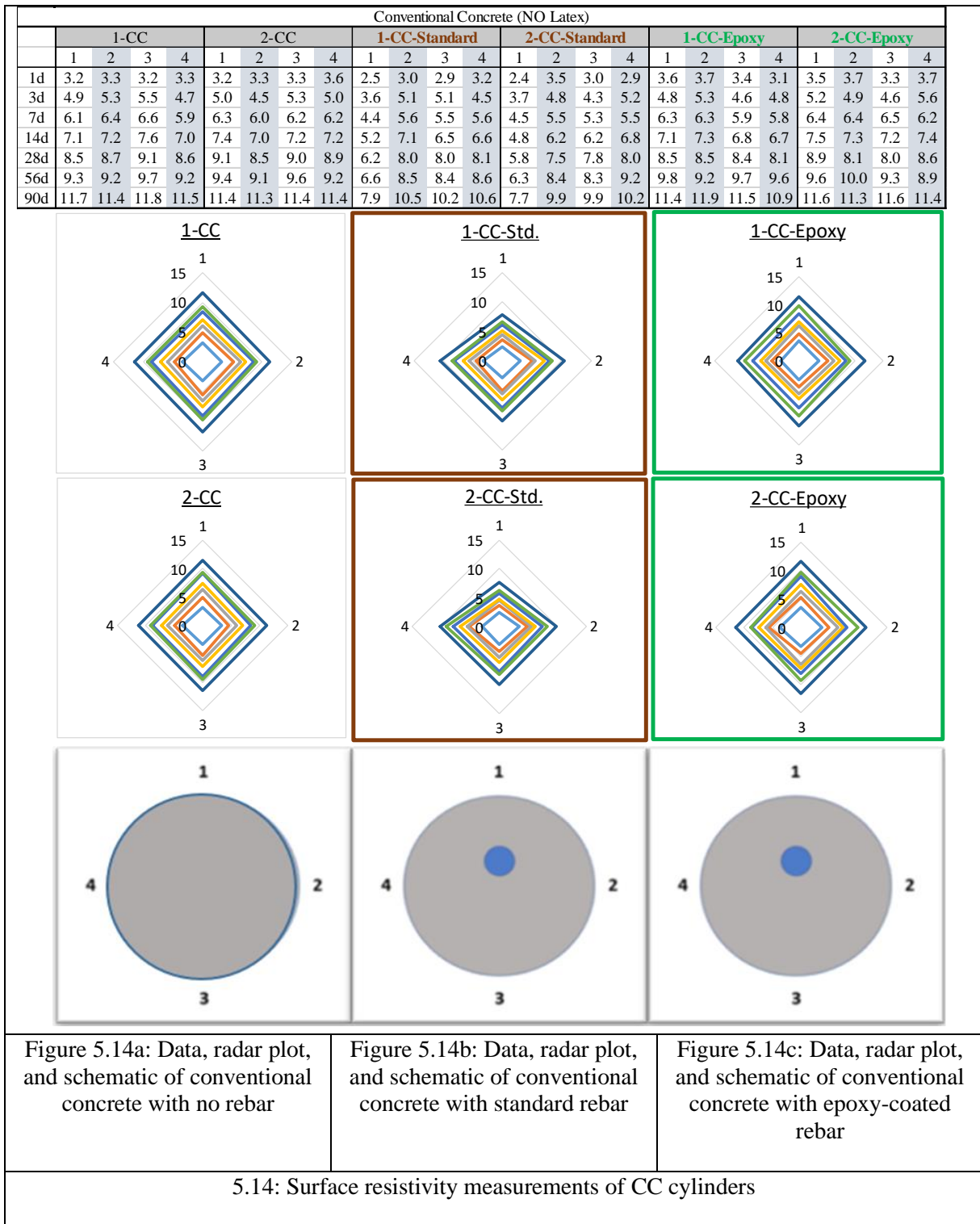
This testing showed that uncoated reinforcement will influence (decrease) surface resistivity measurements and that the proximity of the reinforcement to the meter influences the decrease in the resistivity measurement. However, the radar chart showing resistivity tests of the unreinforced cylinders (Figure 5.14a) and of cylinders with epoxy-coated reinforcement (Figure 5.14c) appear to be similar. It therefore appears that the surface resistivity measurement is not influenced by the epoxy-coated reinforcement. This is likely due to an insulating effect of the epoxy coating.

Plots similar to those shown in Figure 5.11 are provided for LMC, VHES, and VHES-LMC cylinders in Appendix D. A similar trend can be observed in measurements for the LMC, shown in Appendix D, Figures D.1 through D.3. For LMC mixtures (Figures D.1a through D.1c), the influence of the uncoated reinforcement on resistivity readings was also evident in the radar plots, particularly at location 1 where the bar is closest to the surface of the cylinder. Similar to the CC cylinder, the epoxy coated rebar did not appear to influence the resistivity readings. There was also an overall increase in resistivity measurements for all LMC mixtures, indicating a lower permeability and higher durability performance of this mixture compared to the conventional concrete mixture.

The influence of the uncoated reinforcement on the resistivity of the VHES concrete cylinders (Figures D.2a through D.2c) is again evident when compared to the unreinforced cylinder and the cylinder containing the epoxy coated reinforcement. Of note, the surface resistivity values of the VHES concrete are generally much higher than those of the conventional concrete and LMC up to 28 days, but the readings dropped after this time to levels more on the order of the CC and LMC mixtures by 90 days. The resistivity values for the VHES concrete at 7 days were lower than the measurements at 3 days, indicating the start of the decrease in resistivity. It is suspected that this reduction in resistivity is the result of the VHES cylinders increasing in humidity/moisture content due to being stored in the moist curing room.

The influence of the uncoated reinforcement on the surface resistivity of the VHES LMC cylinders (Figures D.3a through D.3c) is again evident when compared to the unreinforced cylinder and the cylinder containing the epoxy coated reinforcement. Of note, the surface resistivity values of the VHES-LMC concrete are substantially higher than those of the conventional concrete, the LMC, and the VHES concrete. Similar to the trends observed in the VHES mixture, the resistivity values appeared to peak at 3 days, and then lower readings were measured at 7 days and 14 days.

Figure 5.15 shows surface resistivity versus time for the cylinders (dashed lines) that illustrates the peak in surface resistivity of the VHES-LMC and VHES concrete mixtures. The two solid trendlines in Figure 5.15 are the average of similar mixtures (CC averaged with LMC and VHES averaged with VHES-LMC). It is suspected that this peak in surface resistivity at 3 day is the result of the rapid hydration taking place within the VHES and VHES-LMC cylinders which increases the water requirements during early curing, resulting in a dehydrated medium when compared to non-VHES concrete mixtures. As discussed in the literature, heat and low moisture content both inversely correlated to surface resistivity. In a sense, the VHES containing concretes may be in a state of low moisture content (dehydrated) during this time, and due to being stored in the moist curing room, over time the moisture content stabilizes, resulting in the leveling off of the surface resistivity readings.



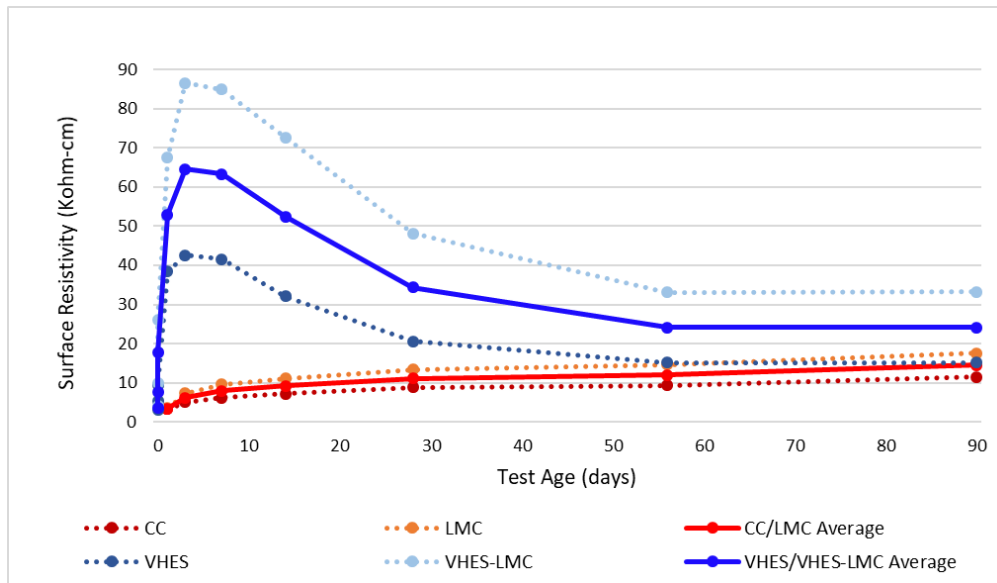


Figure 5.15: Average surface resistivity of cylinders over time

As shown in Figure 5.8a, the cover of the rebar varied based upon the position of the measurement on the cylinder. In Figures 5.16 and Figures D.4 through D.6 in Appendix D, the resistivity measurements are plotted for 1.5 in. (quadrant 1) and 3.75 in. (quadrant 3) of cover at each age, and a trendline connects the pair of measurements. In each figure, the plot shown includes measurements for one concrete mixture and the bold black trendline with arrow endpoints as well as the equation of the line shows the average of those trendlines. These trendlines are expected to demonstrate how the surface resistivity measurement is influenced by variable of cover depth on uncoated reinforcing steel. Of note, the dotted lines in these figures are of the later ages (14 days and older) and the solid lines are of early ages (7 days and earlier). The magnitude of surface resistivity in the CC and LMC mixtures (Figure 5.16 and D.4) increases with age, while the VHES and VHES-LMC mixtures (Figures D.5 and D.6) exhibit the increasing then decreasing resistivity described previously. Additionally, the 56 and 90 day trendlines are virtually identical in the VHES and VHES-LMC mixtures.

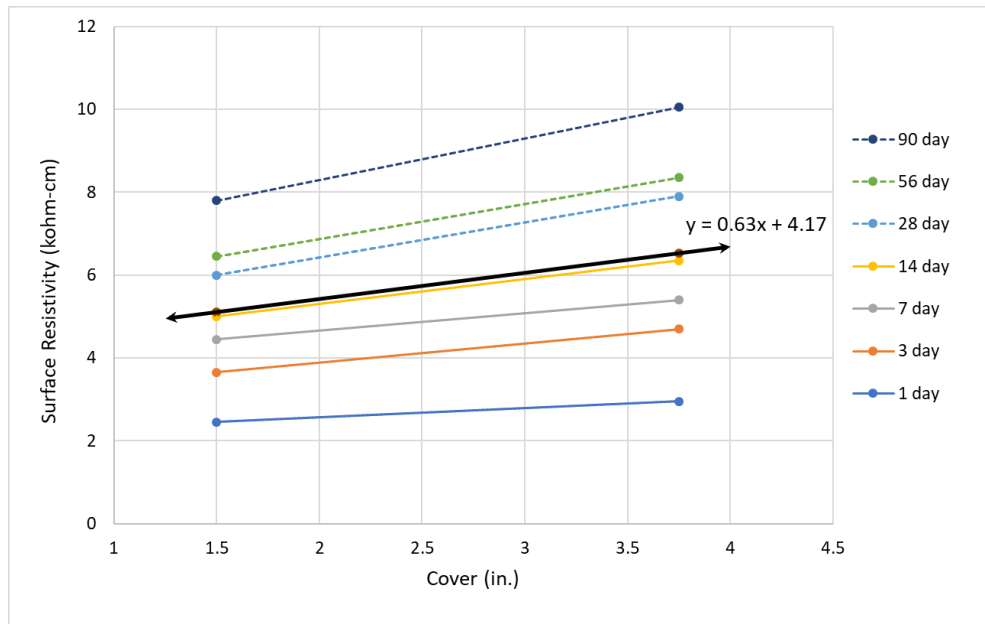


Figure 5.16: Surface resistivity vs. concrete cover at selected concrete ages for the CC cylinders

Table D.1 provides all of the trendline equations for Figures 5.16 and D.4 through D.6, where the x- variable represents the concrete cover distance (in.) and the y variable represents surface resistivity ($k\Omega\text{-cm}$). These trendline

equations can be used to estimate the degree of influence of cover on surface resistivity measurements. For example, in regard to the CC mixture at 1 day ($y = 0.22x + 2.1$), the cover depth (x variable) can be estimated by entering the measured surface resistivity value (measured on top of and parallel) into the y variable of the equation. So, if surface resistivity is measured to be 2.5 k Ω -cm at 1 day, the cover depth may be near 1.8 in., or if the surface resistivity was measured to be 2.8 k Ω -cm, the cover depth may be near 3.2 in. Or in regard to the VHES-LMC mixture at 56 day ($y = 3.7x + 16$), if the surface resistivity is measured to be 21 and 24 k Ω -cm, the cover depths can be estimated to be 1.4 and 2.2 in. respectively. As the surface resistivity value increases when compared to another measurement when measured directly on top of and parallel to the same steel reinforcement bar of the same condition, it is hypothesized that the cover depth is increasing at the rate provided in Table D.1. The estimated change in surface resistivity per each 0.5 in. increment of cover depth is arranged by mixture and age in Table 5.3.

These findings are specific to the concrete mixtures (materials and proportions) used for this study. However, a similar simple set of experiments could be performed with other materials and mixture proportions to identify trendlines and changes in surface resistivity for different cover depths. Similar to other resistivity tests, this approach assumes the concrete is homogeneous with regard to material, moisture, and temperature. Also, it is helpful to knowing the average surface resistivity of an unreinforced cylinder of the concrete being evaluated (per the standard AASHTO T358 test protocol) to indicate that the measured resistivity is within reason, and not an outlier. This research was also conducted on cover depths between 1.5 in. and 3.75 in., so cover depths beyond this range may not be supported by this work.

Table 5.3: Change in surface resistivity (k Ω -cm) per change in cover depth (increments of 0.5 in.)

Age	CC	LMC	VHES	VHES-LMC
1 hour			0.2	0.2
2 hour			0.2	0.5
4 hour			0.4	1.0
1 day	0.1	0.1	0.2	3.1
3 day	0.2	0.3	2.0	4.1
7 day	0.2	0.5	2.2	3.2
14 day	0.3	0.5	1.9	3.7
28 day	0.4	0.6	1.2	2.7
56 day	0.4	0.9	0.8	1.9
90 day	0.5	0.9	0.9	1.8

Figure 5.17 compares the bold black lines from the previous plots of surface resistivity vs. concrete cover (CC, LMC, VHES, and VHES-LMC) and similarly, the bold black trendline with arrow endpoints and equation of the line is the average of each mixture. As a confirmation of the accuracy of the trendlines, the 2.9 in. cover depth was introduced by averaging the surface resistivity measurements of all ages of quadrant 2 and 4. The average surface resistivity measurement of the 2.9 in. (quadrant 2 and 4) cover is plotted on Figure 5.14 for each concrete mixture. Of note, the 2.9 in. cover plots very closely to each respective trendline, with the closest one being the average (bold black trendline). This infers that due to the circular distribution of the surface resistivity meter's field, objects are detectable to the same degree whether they are centrically or eccentrically located below the measuring point.

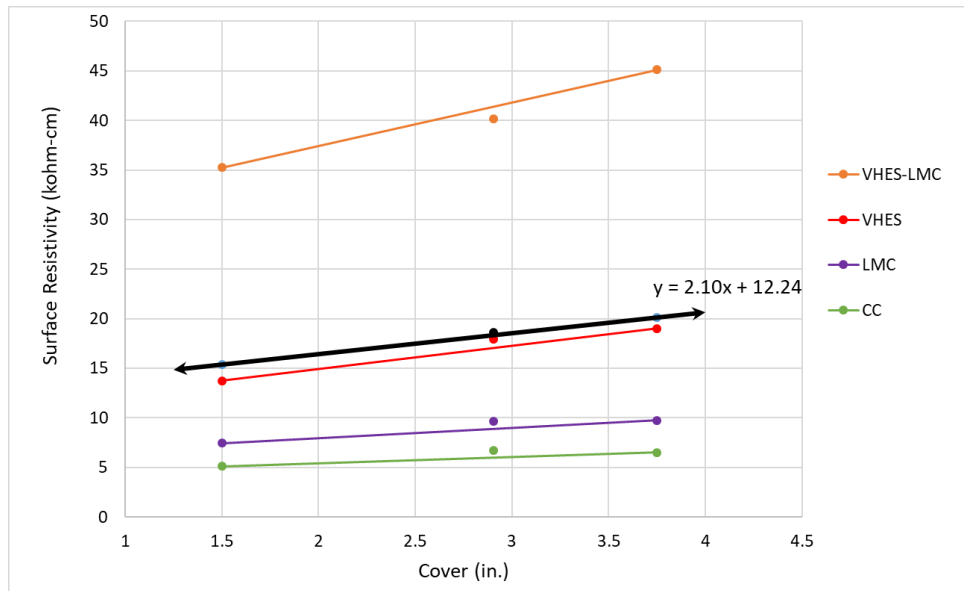


Figure 5.17: Average surface resistivity of each mixture vs. concrete cover for each mixture, with specific value of 2.9” cover shown

5.3.2 Miniature Slab Specimens

In Figures 5.18a through 5.18c, the results of surface resistivity testing of the VHES miniature slab at 7 days are shown in the following reinforcement conditions, without reinforcement (Figure 5.15a), with uncoated steel reinforcement (Figure 5.15b), and with epoxy-coated reinforcement (Figure 5.15c). The blue highlight in Figures 5.18b and 5.18c show the location of rebar. It was found that the resistivity readings of the remaining ages of the VHES miniature slabs as well as all the miniature slabs cast using other concrete mixtures have a similar distribution in the change in resistivity. All miniature slab measurement results are provided in Appendix D, Figures D.7 through D.15. The groups of cells where each number is repeated 4-5 times represents one resistivity measurement along that group of cells.

Surface resistivity readings taken around the perimeter of each box were found to have the highest magnitude at each testing age. Areas near the center of the box and on top of the rebar positioned in the y-axis direction tended to have the lowest resistivity measurements at each testing age. The rebars in the y-axis direction are closer to the testing surface than the rebars in the x-axis direction, which may explain some of the changes in magnitude in the readings in perpendicular directions. The lower resistivity observed when measurements were made on top of the rebar closer to the surface (in the y-axis direction) correlates to the findings from the preliminary reinforced concrete cylinder tests. Surface resistivity test results for the miniature slabs clearly indicated the potential for edge effects to notably increase resistivity measurements. Also, they provided an early indication of the influence of the reinforcement mat, identified by a decrease in measured resistivity.

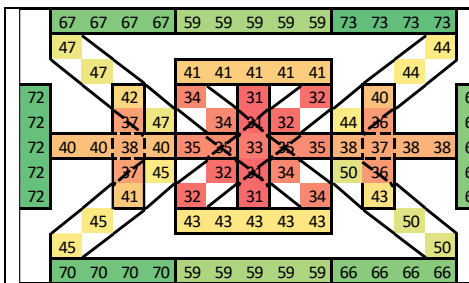


Figure 5.18a: VHES miniature slab 7-day surface resistivity – no reinforcement

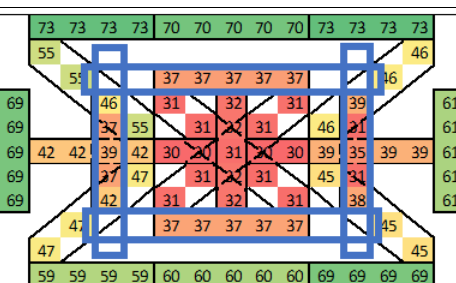


Figure 5.18b: VHES miniature slab 7-day surface resistivity – standard reinforcement

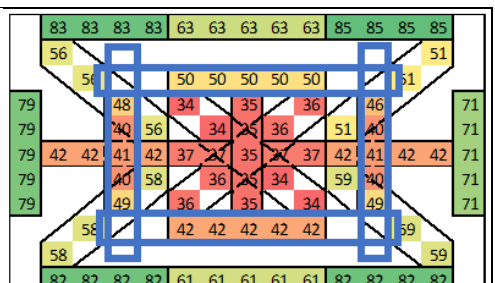


Figure 5.18c: VHES miniature slab 7-day surface resistivity – epoxy-coated reinforcement

5.3.3 Bridge Deck Mockups

For the larger slab mockups, surface resistivity measurements were compiled on an Excel table with color conditioning formatting ranging from green (high) to red (low) to help better visualize areas of different surface resistivity magnitudes. The three orientations were averaged at each age per cell and the standard deviation was calculated. The standard deviation aspect of the data analysis was computed at each point to reveal where the different orientations per cell will differentiate between one another.

Due to the 3-dimensional nature of the current field induced by the resistivity meter during measurement, consideration should be given to the fact that the meter's current field can be influenced by the edge of a homogeneous material such as concrete ('the edge effect'). The literature mentions this phenomenon and general reasoning, yet it has not been found to be quantified with respect to the orientation of the meter with respect to the edge in question. In Gowers and Milliard (1999), it is stated that the user shall keep a distance of at least twice the probe spacing from the specimen's edge to eliminate edge effects. The Resipod used in this study has a probe spacing of 1.5 in., requiring a 3 in. setback from the edge using the recommendations of Gowers and Millard (1999).

An experiment to better quantify this influence was performed on the control mockup at 90 days within the zone of the mockup not containing reinforcing steel. This experiment, detailed in Dillworth (2021) included measurement of resistivity at locations near the edge of the unreinforced control slab (no overlay), with the orientations of the meter shown in Figure 5.19. The current field for each orientation is illustrated, with the four linear dots representing the electrodes and the ovals representing the lines of current flow. The experiments revealed that use of the meter in the horizontal orientation (parallel to the edge) in Figure 5.19 displays the most obvious influence of edge effects. It is hypothesized that when the meter is positioned in this manner, more of the current field comes into contact with the edge, resulting in an increase in resistivity. In the diagonal orientation, less of the current field contacts the edge, resulting in less of a prominent influence. Lastly, the vertical orientation, where the current field is perpendicular to the edge, even less of an influence is observed. The results of this experiment are shown in Figure 5.20, indicating that to avoid these effects in the field, it may be recommended to stay at least 5 in. away from the edge when the parallel or diagonal orientation is used and at least 4 in. away when the perpendicular (vertical) orientation is being used to avoid edge effects.

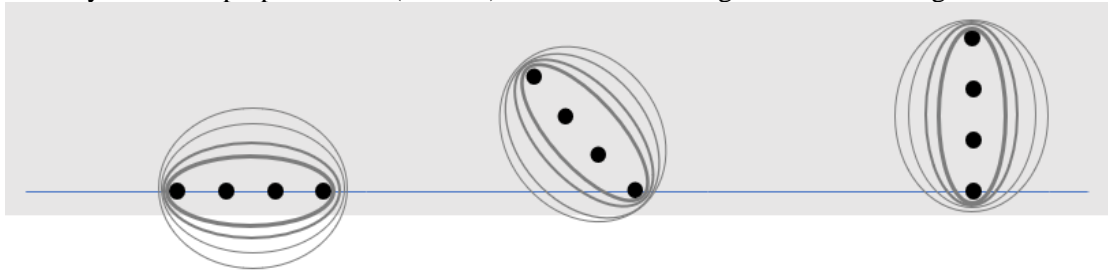


Figure 5.19: Theoretical effects of edge of slab on surface resistivity meter current field

The effects of slab edges were also evident in the time-series resistivity measurements made on each mockup slab over the first 90 days after casting. A sample of the data, clearly showing the edge effects on the resistivity readings of the LMC overlay mockup is shown in Figure 5.21. Note the relatively greener measurements around the perimeter of the slabs. In some of the analysis, further detailed in Dillworth (2021), rows 1 and 13 and columns 1 and 13 were removed in order to eliminate the edge effects from evaluation of the data.

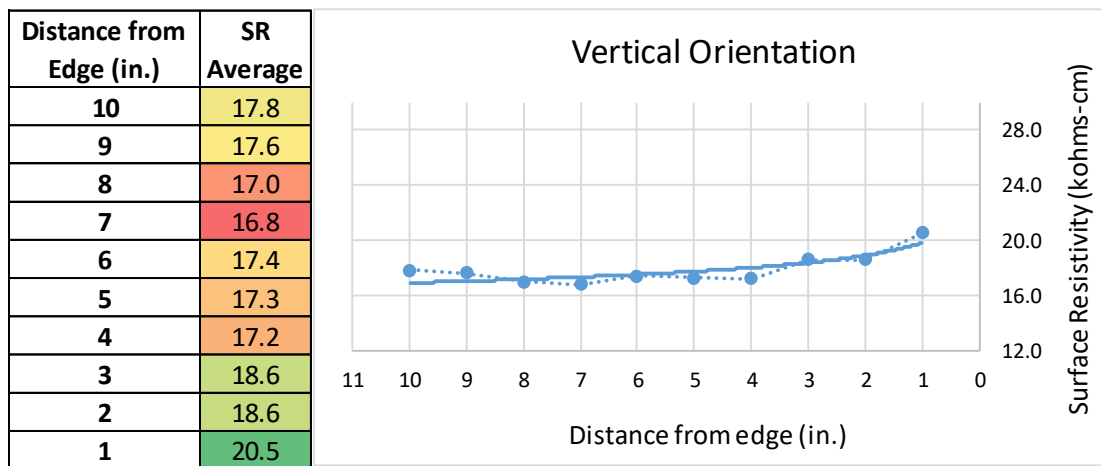
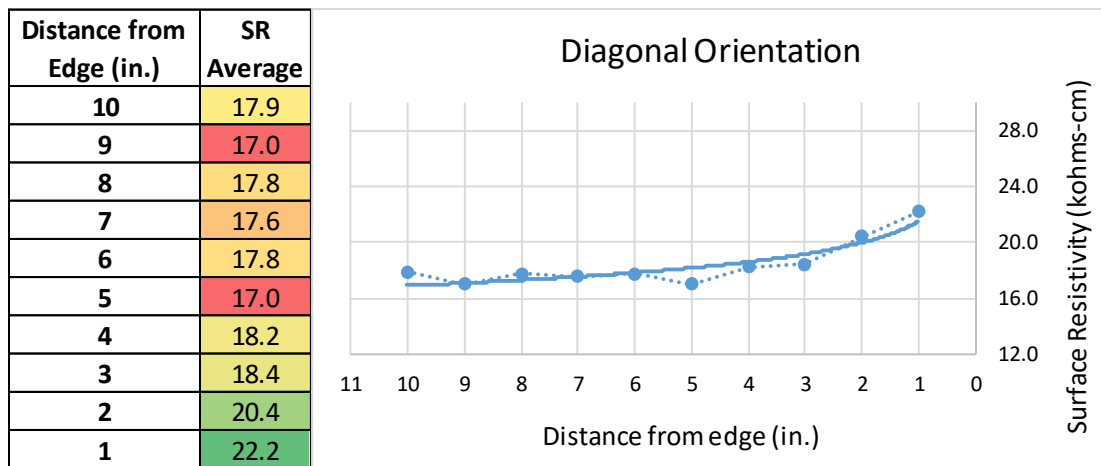
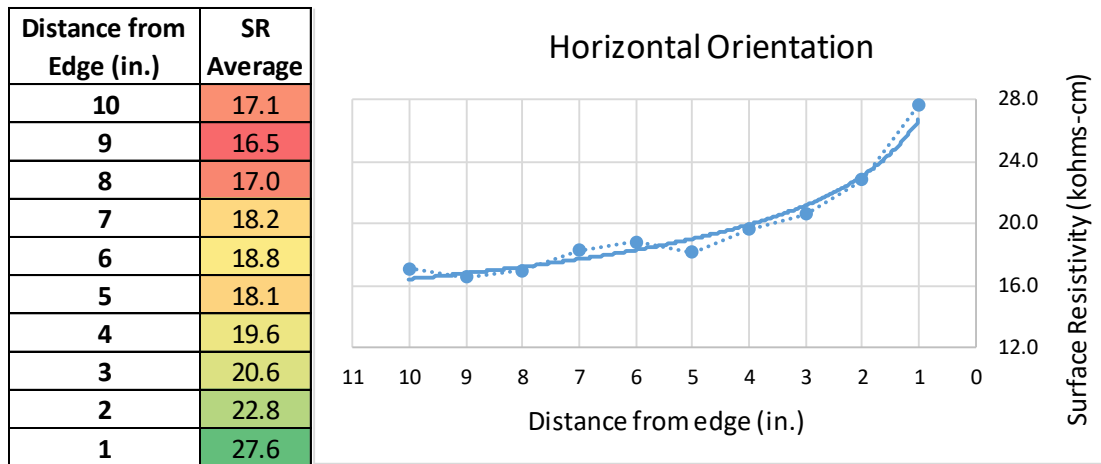


Figure 5.20: Graphical representation of edge effects on measured surface resistivity

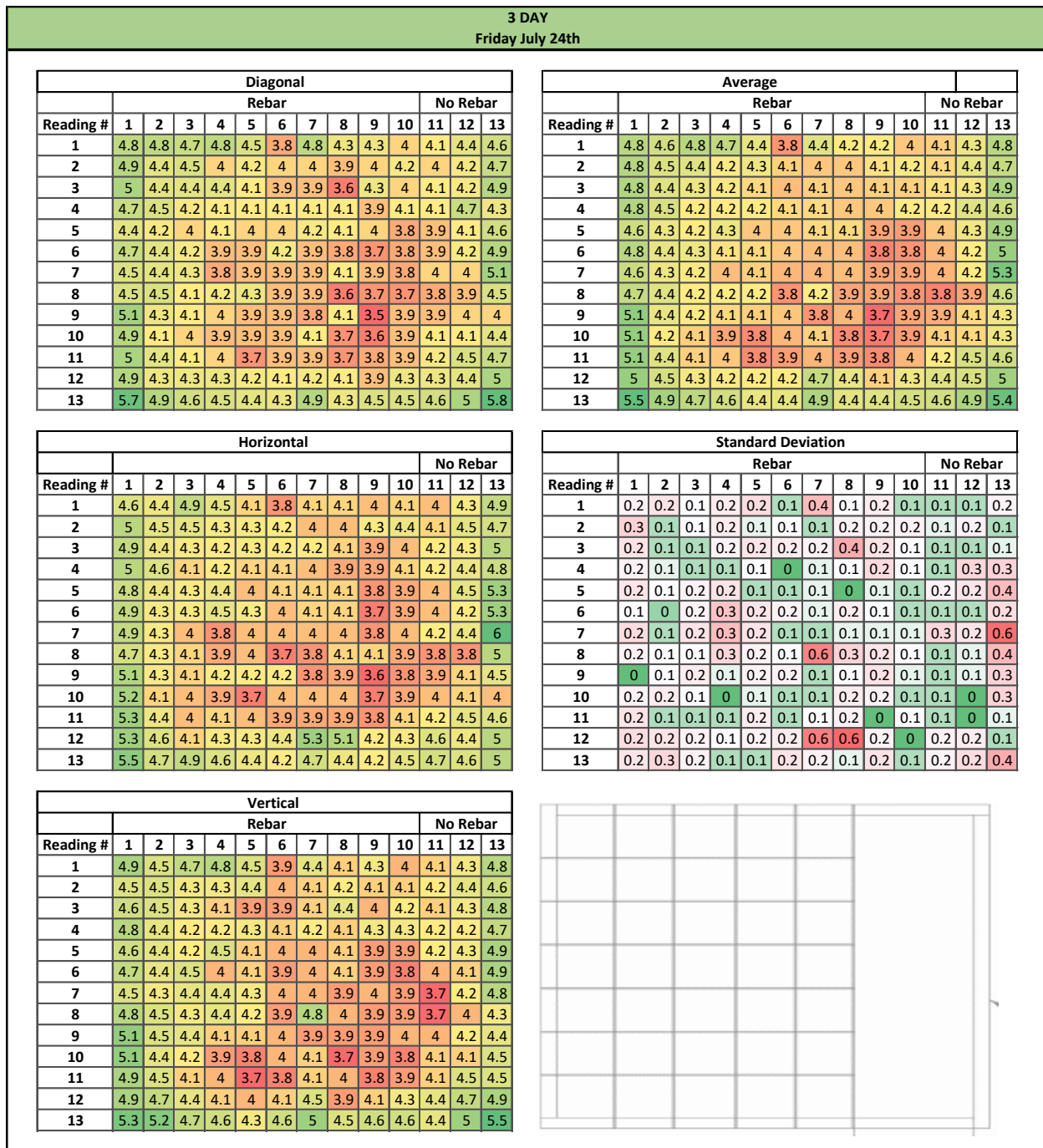


Figure 5.21: 3-day surface resistivity readings of the LMC overlay mockup, showing edge effects on resistivity readings

The surface resistivity meter was useful in evaluating the thickness of the overlay. This is shown in Figure 5.22, where tapering thickness of the VHES-LMC overlay slab from one side of the slab to the other (from row 13 readings to row 1 readings) can clearly be observed in the 3-day surface resistivity measurements. Note that the outer row of readings has been eliminated due to the edge effects in this dataset. An analysis of the surface resistivity vs. overlay thickness at different ages is presented in Dillworth (2021). In this analysis, Dillworth (2021) calculated rate of change (ROC) correction factors that could be used to estimate the surface resistivity of each overlay material at each age as the overlay thickness changes in 1 inch increments. A summary of these findings is provided in Table 5.4. For example, at 7 days and 28 days, as the LMC overlay thickness increased by 1 in., the surface resistivity can be expected to increase by 0.2 and 0.4 k Ω -cm respectively. It is noted that this is a fairly small change.

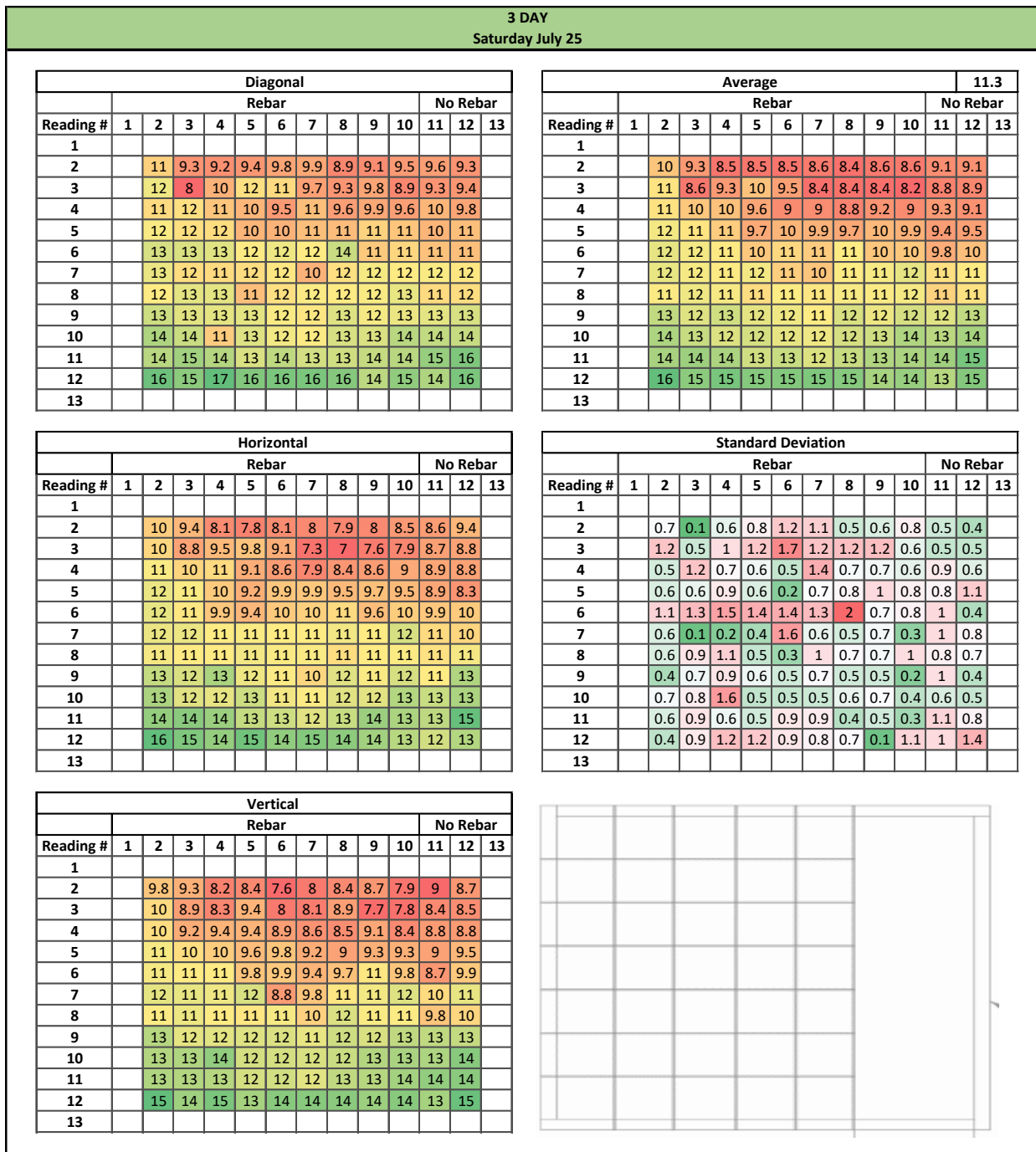


Figure 5.22: 3-day surface resistivity readings on the VHES-LMC overlay mockup, showing the impact of the tapering overlay slab thickness on resistivity readings

Table 5.4: Rate of change (ROC) correction factors that could be used to estimate the surface resistivity of each overlay material at different ages per 1 inch increment in thickness change

Age	LMC Overlay		VHES Overlay		VHES-LMC Overlay	
	Line slope equation	ROC	Line slope equation	ROC	Line slope equation	ROC
1 hour			$y = -0.15x + 1.74$	-0.2	$y = -0.28x + 3.31$	-0.3
4 hour			$y = -0.1x + 2.0$	-0.1	$y = -0.37x + 4.75$	-0.4
1 day	$y = 0.03x + 2.00$	0.0	$y = -1.75x + 12.25$	-1.8	$y = -2.54x + 15.61$	-2.5
3 day	$y = 0.09x + 4.02$	0.1	$y = -1.99x + 13.53$	-2.0	$y = -3.41x + 20.36$	-3.4
7 day	$y = 0.24x + 5.18$	0.2	$y = -1.62x + 12.80$	-1.6	$y = -3.81x + 22.77$	-3.8
14 day	$y = 0.16x + 7.78$	0.2	$y = -1.06x + 11.70$	-1.1	$y = -3.97x + 26.64$	-4.0
28 day	$y = 0.35x + 9.69$	0.4	$y = -0.60x + 9.86$	-0.6	$y = -2.17x + 24.84$	-2.2
56 day	$y = 0.29x + 12.36$	0.3	$y = -0.70x + 12.44$	-0.7	$y = -0.16x + 24.44$	-0.2
90 day	$y = 0.31x + 13.41$	0.3	$y = -1.51x + 15.92$	-1.5	$y = 0.07x + 27.74$	-0.1

Detailed analysis of the surface resistivity measurements of each mockup slab at a range of ages is presented in Dillworth (2021), and key measurements are included in Appendix D of this report, Figures D.17 through D.45. Results for the control slab are shown in Figures D.17 through D.21, results for the LMC mockup are shown in D.22 through D.29, results for the VHES mockup are shown in Figures D.22 through D.37, and results for the VHES-LMC mockup are shown in Figures D.38 through D.45. Analysis was performed using a range of approaches to average rows and columns, eliminating points with foam inclusions and rebar as necessary to help isolate variables and discern trends.

Of note, the surface resistivity meter was not particularly effective at identifying the foam inclusions embedded in the overlays to simulate voids. This is shown in Figure 5.23, where the triangles representing the voids in the LMC mockup are overlaid on the average (3-orientation) 7-day surface resistivity measurements. No discernable change in readings can be observed in the vicinity of the voids. A few of the placed foam inclusions could be identified by the readings, but this was not typical.

Average													
	Rebar										No Rebar		
	1	2	3	4	5	6	7	8	9	10	11	12	13
1	6.7	6.4	5.7	6.4	6.1	5.4	5.3	5.9	6	5.7	5.5	6.1	6.3
2	6.9	6.3	5.6	6	5.9	5.5	5.1	5.8	5.6	5.7	5.7	5.9	6.1
3	6.6	6.4	5.9	5.8	5.6	5.5	5.5	5.1	5.6	5.7	5.8	5.8	6.7
4	6	6.1	5.7	5.6	5.9	5.6	5.6	5.7	5.5	5.9	5.9	5.9	6.3
5	6.5	6.1	6	5.7	5.8	5.8	5.7	5.7	5.5	5.5	5.8	6	6.3
6	6	5.7	5.8	5.6	5.5	5.7	5.6	5.6	5.4	5.4	5.4	6.1	6.9
7	6.1	5.9	5.9	5.6	5.4	5.4	5.4	5.5	5.3	5.4	5.6	5.7	6.4
8	6.6	5.9	5.9	5.6	5.4	5.3	5.4	5.4	5.1	5.3	5.2	5.6	6
9	6.8	6	5.6	5.5	5.4	5.4	5.3	5.4	5.2	5.3	5.4	5.7	6
10	6.8	6	5.6	5.4	5.1	5.5	5.6	5.2	4.9	5.1	5.4	5.7	5.5
11	6.8	6.1	5.5	5.3	5.2	5.3	5.4	5	5.2	5.4	5.8	5.6	6
12	6.8	6	5.7	5.7	5.6	5.7	5.8	5.7	5.3	5.7	5.9	5.8	6.5
13	7.2	6.3	6.3	6.2	6	5.9	6.5	5.9	5.9	6.1	5.9	6.5	7.4

Figure 5.23: Foam inclusions (“voids”) superimposed on 7-day surface resistivity readings of LMC mockup

An analysis of time-series surface resistivity data grouped by eliminating specific variables was also performed to aid in assessing the influence of rebar oriented vertically (longitudinally), horizontally (transverse), and foam “voids” on the measurements. Plots were created similar to that shown in Figure 5.24 for all four mockups, using each of the three surface resistivity meter measurement orientations, plus the average of the three orientations (as shown in Figure 5.24).

Although there were some variations in the results, typically the average measurements taken over the vertical (longitudinal) reinforcing steel were lowest at a given age, with the measurements not taken over reinforcing steel or voids being highest. Plots for the LMC, VHES, and VHES-LMC mockup are shown in Figures D.46 to D.49, Figures D.50 to D.53 and Figures D.54 to D.57, respectively.

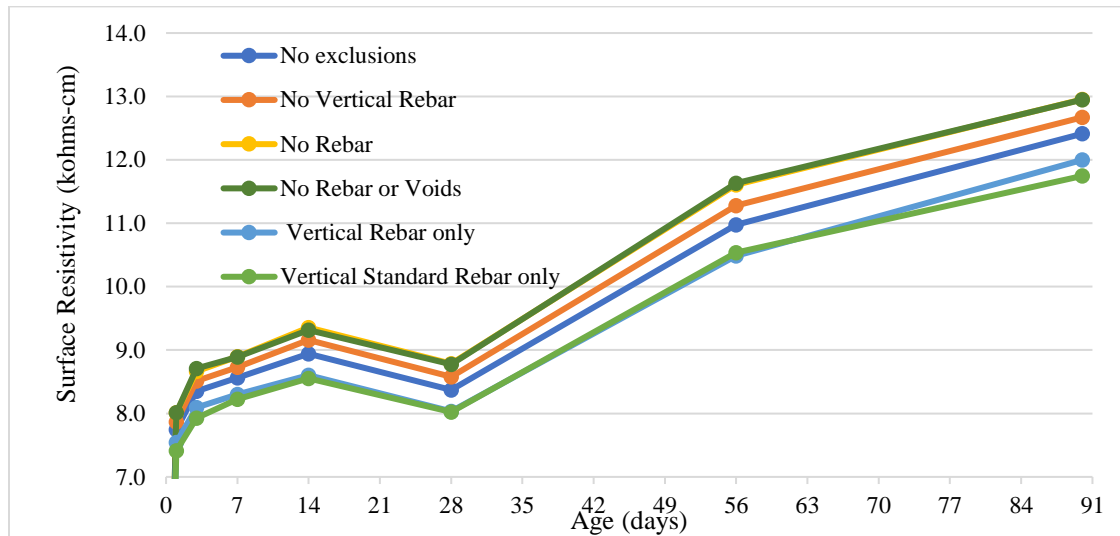


Figure 5:24: Average surface resistivity of VHES mockup over time, with measurement points screened and grouped

5.4 Summary of Findings

Findings From Reinforced Concrete Cylinder Tests

- Concrete mixtures with latex admixtures tend to produce slightly higher, yet similar surface resistivity measurements than that of concrete mixtures without the latex admixture at each of the test ages.
- The two concrete mixtures with very high early strength cement, VHES-LMC and VHES, produce very high and rapid surface resistivity gain within the first three days, where they reach a peak of approximately 85 kΩ-cm and 40 kΩ-cm respectively, compared to approximately 10 kΩ-cm 3 day measurement for the LMC and CC mixtures. The LMC and CC mixtures do not exhibit this peak at 3 days, rather the expected gradual surface resistivity gain.
- It is theorized that this peak in surface resistivity at 3 day is the result of the rapid hydration taking place within the VHES and VHES-LMC cylinders which increases the water demand during early curing, resulting in a relatively low humidity concrete at this time, when compared to non-VHES concrete mixtures. As discussed in the literature, temperature and moisture content are both inversely correlated to surface resistivity.
- As expected, the non-coated steel reinforcement significantly influences the surface resistivity measurement as depicted in the radar graphs. Table 5.3 shows the expected surface resistivity change for each mixture as the cover depth changes in 0.5 in increments. As an example, with regard to the VHES mixture at day 3, it is estimated that surface resistivity will be about 2.0 kΩ-cm higher when measured over steel reinforcement with 1.5 in. of cover versus 1 in. of cover (0.5 in. difference). It is noted that the anticipated changes in surface resistivity for cover depth are specific to these mixtures. However, a similar approach could identify these trends for other mixtures with different materials and proportions. The stark difference between the different types of mixtures, however, illustrates that significantly different behavior can be expected for different cover depths for different mixtures.
- Surface resistivity was not influenced by the epoxy-coated steel embedded into selected cylinders, as the radar graphs of these cylinders closely resemble graphs of cylinders with no steel reinforcement.

Findings from Miniature Slab Tests

- Surface resistivity values were always lower in the center of the miniature slabs (surrounded by the reinforcement mat), compared to the perimeter, for all mixtures at each age of testing. This is likely due to edge effects and the influence of the reinforcement mat density, which was analyzed in previous sections.
- Similar to the preliminary cylinders, the miniature slabs containing very high early strength cement and or latex admixtures were higher than that of the conventional concrete mixture at each of the test ages.

Findings from Tests of the Bridge Deck Mockups

The following is a summary of the findings resulting from this research in order of greatest to least significant:

- The overlay thickness change was found to be very detectable in the heatmaps of surface resistivity measurements made in each orientation and in analysis of row averages (presented in Dillworth 2021). Furthermore, it was apparent in the row average analysis of many of the mockups and correction factors were developed for each mixture in Table 5.4. These correction factors are specific to only these mixtures/materials/proportions. However, additional work could be done to explore the role of materials and proportions for each type of mixture on those correction factors.
- The edge effect analysis demonstrated that surface resistivity is influenced by the edge of a concrete member and to a differing degree depending on the orientation of the meter with respect to the edge. The rank of orientation influence of edge effects on surface resistivity is horizontal, diagonal, then vertical, with horizontal being the most influential. As a general rule of thumb, it is recommended to stay at least 5 in. away from the edge when the parallel or diagonal orientation is used and at least 4 in. away when the perpendicular orientation is being used to avoid edge effects. The non-coated steel reinforcement influenced surface resistivity at depths of 2.5 in. rather than the maximum depth of 1.18 in. as published by (Proceq 2017). Although, this finding was not observed in the heat maps as expected, the graphical trendlines of characteristic inclusion/exclusions was necessary to support this finding (presented in Dillworth 2021).
- A few of the placed voids in some of the mockups were confirmed using surface resistivity. Although this finding was not strongly observed in the heat maps, review of the graphical trendlines of void inclusion/exclusions provided the ability to show these voids, supporting this finding.
- Overall, it was hoped that the surface resistivity meter could be found useful to identify intentionally placed voids in the slabs. There is a chance that the material utilized to produce the artificial voids was influenced by the mix water, prewetting water, or other moisture, influencing the readings. The 6 inch spacing of the reinforcing grid may have also influenced the surface resistivity readings to the extent that voids were not discernable. Future work could attempt to utilize another type of material, or different sizes/shapes of voids, to further explore the potential of the surface resistivity meter to locate the voids.

5.5 Field Evaluation Procedure

A **field evaluation procedure** was also prepared to support evaluation of bridge deck overlays with the surface resistivity meter. This draft field evaluation procedure is presented in **Appendix E**.

6.0 TECHNOLOGY TRANSFER AND TRAINING TO SUPPORT PEM

Movement towards performance specifications is a significant undertaking and will require the support of a variety of stakeholders. All parties involved in design, construction, and testing of NCDOT's concrete infrastructure could benefit from technology transfer and training to support PEM. As part of RP 2019-14, simplified test procedures compatible with NCDOT's Concrete Field Technician Study Guide were produced and published in the project final report (Cavalline et al. 2020b). Also part of RP 2019-14, a series of three PEM training videos was produced by UNC Charlotte and provided to Mr. Brian Hunter, NCDOT State Laboratory Operations Manager, for dissemination to NCDOT personnel and other stakeholders.

For this project, additional technology transfer tools were prepared, including spreadsheets to support data collection for targeted testing technologies. The spreadsheets were transferred to Mr. Brian Hunter as well as partners at the pilot project included in RP 2020-13 (described in Chapter 7). In addition to these materials, other resources and tools could be used to help guide both NCDOT and contractor personnel in implementing the targeted PEM approaches. Some of these resources are described below, and links are provided to most.

Performance Engineered Mixtures (PEM) resources at the National Concrete Pavement Technology Center website
<https://cptechcenter.org/performance-engineered-mixtures-pem/>

This website is a central location for PEM information, resources, tools, and updates. The website includes up to date guidance on the Pooled Fund study supporting the PEM initiative, PEM test methods, information on PEM implementation projects, and a list of PEM sponsors.

1. Optimized aggregate gradations

- Brief overview – www.tarantulacurve.com/publications.html
- Guidance to developing specifications and limits – www.tarantulacurve.com/tarantula-curve.html
- Spreadsheets to support use of Tarantula Curve for assessing/optimizing aggregate gradations for bridge decks are available at www.tarantulacurve.com/tarantula-curve.html.

2. Surface resistivity

- Brief overview - https://intrans.iastate.edu/app/uploads/2020/08/PEM_test_resistivity_sheet.pdf
- Resistivity testing: What do I need to know? How do I use it? Presentation by Dr. Jason Weiss (2022). <https://intrans.iastate.edu/app/uploads/sites/7/2022/04/PEM-Resistivity-Slides.pdf>
- Spreadsheet to support resistivity/formation factor with temperature and geometry corrections, developed by Oregon State university is available at: <https://cptechcenter.org/performance-engineered-mixtures-pem/>. The specific link is not provided so that the user downloads the most recent version. There are also instructions for using this spreadsheet posted at the link above.
- A spreadsheet for data collection and analysis per AASHTO T 358 developed by UNC Charlotte for use on the pilot project was provided to Mr. Brian Hunter.

3. SAM

- Brief overview - https://intrans.iastate.edu/app/uploads/2020/08/PEM_test_SAM_sheet.pdf
- Background information – www.superairmeter.com
- Series of videos providing test background, test procedure, equipment checks and maintenance, and use of auxiliary equipment - <https://www.superairmeter.com/videos>
- Spreadsheet for data collection and analysis, including predicted response (“likely correct” report for test validity) is available at: <https://intrans.iastate.edu/app/uploads/sites/7/2019/09/SAM-Predicted-Response-V3-6-30-19.xlsx>.

4. Volumetric Shrinkage

- “Guidance to Reduce Shrinkage and Restrained Shrinkage Cracking” – report sponsored by FHWA (Weiss 2022)-
https://intrans.iastate.edu/app/uploads/2022/08/guidance_to_reduce_shrinkage_and_restrained_shrinkage_cracking_w_cvr.pdf
- A spreadsheet for data collection and analysis per AASHTO PP 84-20 and ASTM C157 developed by UNC Charlotte for use on the pilot project was provided to Mr. Brian Hunter of NCDOT.

5. Workability Tests

- Contractors interested in using PEM approaches to ensure workability can find resources on both the Box Test and the Vibrating Kelly Ball (VKelly) Test at <https://cptechcenter.org/performance-engineered-mixtures-pem/>

6. Quality Control for Paving, including PEM approaches

- Quality Control for Concrete Paving: A Tool for Agency and Industry (Cavalline et al. 2021) – includes information on integration of PEM tests into the mixture development, construction, and acceptance phases of concrete pavement projects. Also includes guidance on using control charts and other QC tools to support PEM and conventional tests. Available at: https://intrans.iastate.edu/app/uploads/2021/12/QC_for_concrete_paving.pdf

7.0 PILOT PROJECT IMPLEMENTATION

Previous PEM research for NCDOT included a pilot project to evaluate several PEM tests and targets in a concrete pavement project (Cavalline et al. 2020b, Cavalline et al. 2022). To continue to advance use of PEM approaches in field applications, as well as to broaden the number and types of stakeholders experienced with PEM, a pilot project to evaluate structural concrete was targeted. The I-485 Widening project (I-5507 Design Build) was selected, since the project included a number of types of structures including bridge decks, overlays, substructure components, superstructure components, barrier walls, approach slabs, drilled pier and culverts. Concrete specimens cast from mixtures used for each of these types of structural components, as well as some non-structural (Class A) mixtures, were tested. The three targeted PEM tests were surface resistivity, SAM, and shrinkage.

Participants in the pilot project effort included the prime contractor, several testing firms, NCDOT personnel from the central office and divisional office/laboratory, and a concrete supplier. A testing program was prepared, providing the test method, sampling location, testing frequency/number of specimens, and data collection and reporting approach to be used for each type of concrete. This table is provided in Appendix F, Table F.1. Although the testing program was not followed exactly (due to resource limitations and the quantity of concrete being used at the site), the table provided information needed to support deployment of the activities and could serve as a template for future PEM pilot studies.

7.1 Surface Resistivity

RP 2018-14 (Cavalline et al. 2020a) identified initial targets for surface resistivity for structural (Class AA) and pavement concrete. To produce a preliminary specification for possible implementation by the NCDOT, field performance verified RCPT targets from Virginia, a state with similarities to NC, were evaluated against the resistivity test results from NC Concrete mixtures to identify potential resistivity targets. For Class AA mixtures, a surface resistivity target of 15.0 k Ω -cm or 16.0 k Ω -cm (corresponding to RCPT values of 2,800 and 2,700 coulombs respectively) is recommended. Both targets appeared to reasonably discern between mixtures with higher and lower durability performance potential, with the target of 16.0 k Ω -cm providing an aggressive, but realistically feasible performance target for structural mixtures. In the existing coastal corrosive zones, a higher resistivity target could be warranted. Findings from RP 2019-22, a study of NCDOT's corrosive sites policy should help identify target values for these critical zones. For pavement mixtures, a target surface resistivity value of 11.0 k Ω -cm was identified, roughly corresponding to an RCPT of approximately 3,300 coulombs. Targets were not established for Class A or drilled pier mixtures as part of that study.

Laboratory test results indicated that NCDOT concrete mixtures may not meet some of the more aggressive RCPT and surface resistivity targets utilized by other states at early ages (28 days). At later ages, such as 56 days, some other state specification targets are achievable by typical NC mixtures, particularly by fly ash mixtures. NCDOT regional laboratories generally do not have the capacity to cure cylinders for durations longer than 28 days, and therefore it is necessary to identify a 28-day surface resistivity target that shows a strong likelihood that the concrete will meet resistivity targets at later ages (such as 56 days).

NCDOT Regional Laboratory personnel in Matthews, NC performed surface resistivity testing on a limited number of cylinders retained for QA purposes. All surface resistivity data is provided in Appendix F, Table F.2, and Figures 7.1, 7.2, and 7.3 show the surface resistivity measurements for Class A, Class AA, and drilled pier mixtures respectively. A summary of all measurements made by the NCDOT personnel is provided in Figure 7.4. Class A mixtures have a minimum 28-day compressive strength of 3,000 psi, while Class AA mixtures and drilled pier mixtures have a minimum 28-day compressive strength of 4,500 psi.

Summary statistics for each type of mixture at selected ages are provided in Table 7.1. Note that limited (or no) data was provided for certain ages, and in these cases statistics are not provided. Note that early age tests were made for Class A and Class AA mixture specimens, but only 28-day data was obtained for drilled pier mixtures. Therefore, trend lines could only be established for Class A and Class AA mixture data. Fairly strong correlations were obtained for Class A and Class AA mixtures using a power curve. Many Class AA mixtures met the 16 k Ω -cm resistivity target by 28 days, with most others showing a good likelihood of meeting the target by 56 days.

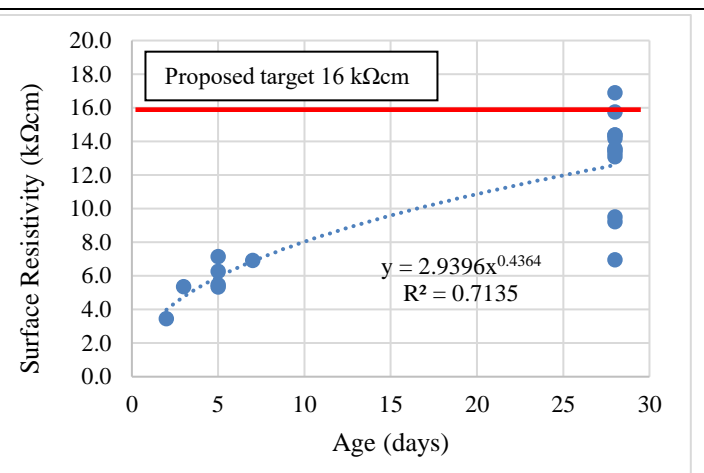
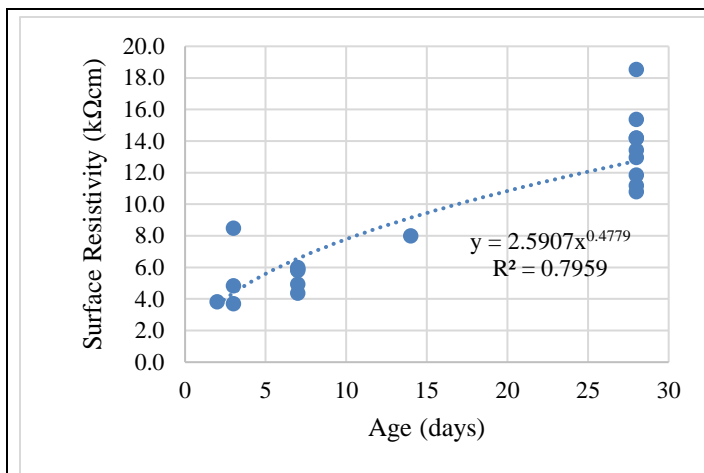


Figure 7.1: Surface resistivity of QA cylinders for Class A mixtures

Figure 7.2: Surface resistivity of QA cylinders for Class AA mixtures

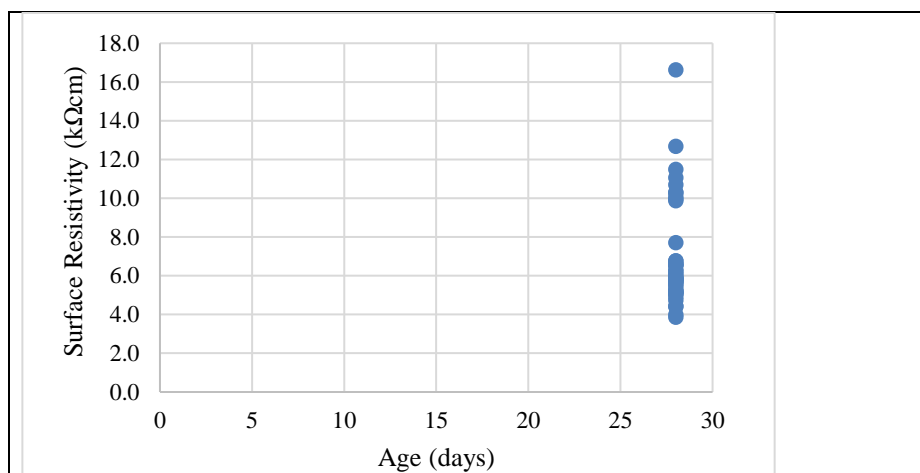


Figure 7.3: Surface resistivity of QA cylinders for drilled pier mixtures

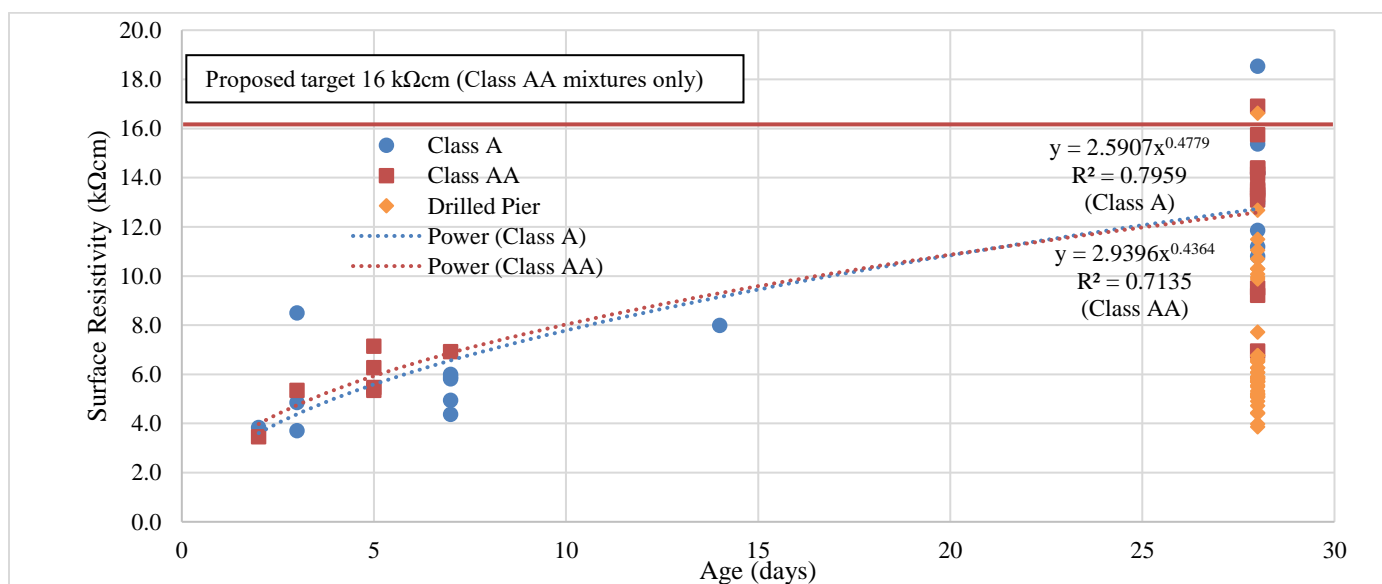


Figure 7.4: Surface resistivity of all QA specimens measured at NCDOT's regional laboratory

Table 7.1: Summary statistics for surface resistivity test results for QA cylinders for pilot project

Age/Statistic		Class A		Class AA		Drilled Pier	
3-day	Avg	5.69	n=3	---	---	---	---
	Std Dev	2.50		---		---	
7-day	Avg	5.27	n=6	---	---	---	---
	Std Dev	0.71		---		---	
28-day	Avg	13.62	n=9	12.89	n=12	6.91	n=35
	Std Dev	2.38		2.89		2.65	

Surface resistivity tests were also performed on selected mixtures batched and tested in the QC lab of the ready-mixed concrete supplier that produced concrete for structures in the pilot project. A Class A mixture, a Class AA mixture, and a drilled shaft mixture were tested. Mixture materials, proportions, and compressive strength test results for each of these mixtures is provided in Appendix F, Figures F.1. through F.3. All resistivity data collected by the QC personnel is provided in Table F.3. A plot of the QC test results is shown below in Figure 7.6. The Class AA mixture met the 16 k Ω -cm target by 28-days. The 3,000 psi Class A and drilled shaft mixtures almost met the 16 k Ω -cm Class AA resistivity target by 28 days (at 15.87 and 15.90 k Ω -cm, respectively), and far exceeded it at 56 days. Per AASHTO T 358, the chloride ion penetration of the Class A and drilled shaft mixtures is classified as “low,” while the chloride ion penetration of the Class AA mixture is “very low.”

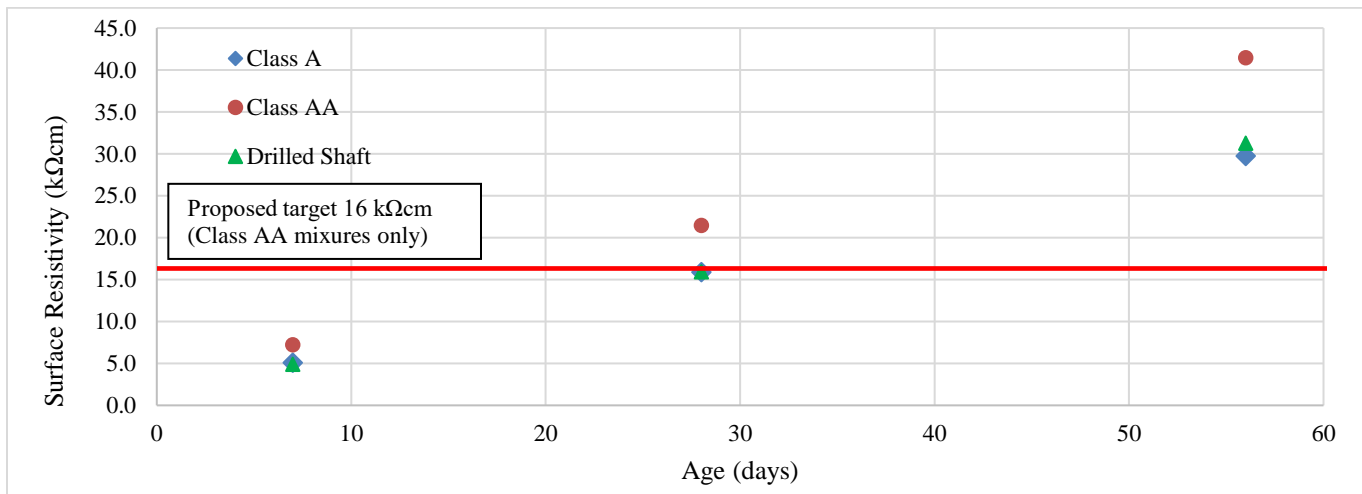


Figure 7.6: Surface resistivity test results from QC laboratory for a Class A mixture, a Class AA mixture, and a drilled shaft mixture

Space limitations at many NCDOT laboratories limits the ability to cure and test specimens at 56 days. Effort was made to review historical data from the series of NCDOT research studies performed at UNC Charlotte to identify 28-day resistivity targets that could provide strong probability that mixtures would meet the 11 k Ω -cm pavement target and 15 or 16 k Ω -cm target for Class AA mixtures at later ages. Data from across projects was combined, and although sample sizes are relatively small a few trends were discerned, described below. It is noted that only the two control mixtures from the internal curing study (RP 2016-06) to reduce any influence of lightweight aggregate on the analysis. Due to some later age measurements being made at either 56 days or 90 days (but not both), some interpolation and extrapolation was performed, as shown in Tables F.4 through F.9, where a summary of data used for the analysis is presented, and resistivities of mixtures meeting targets are highlighted in green.

Low w/cm mixtures (0.37 or less) – Tables F.4 and F.5

Pavement mixtures (n=6, 2 with fly ash 4 without fly ash)

- No mixtures met the target by 28 days.
- All pavement mixtures met the target by 56 days, regardless of whether or not they contained fly ash.

- Straight cement mixtures meeting the target at later ages typically had resistivities of 10 or greater at 28 days, while 20% fly ash had 28-day resistivities of 9 k Ω -cm or greater and 30% fly ash mixtures had 28-day resistivities of 8.4 k Ω -cm or greater.

Structural mixtures (n=10, 5 with fly ash, 5 without fly ash)

- Two mixtures (one with fly ash, one without fly ash) met the target at 28 days.
- All fly ash mixtures met the targets of 15 k Ω -cm and 16 k Ω -cm by 56 days. Two straight cement mixtures met the 15 k Ω -cm target by 56 days, and three straight cement mixtures met the 15 k Ω -cm target by 90 days. Only two of the straight cement mixtures met the 16 k Ω -cm target by 90 days. These typically were the higher cement contents mixtures.
- Structural mixtures meeting the target at later ages typically had 28-day resistivity of 9 k Ω -cm or greater.

Moderate w/cm mixtures (0.41 to 0.43) – Tables F.6 and F.7

Pavement mixtures (n=9, 3 without fly ash, 6 with fly ash)

- No mixtures met the target by 28 days.
- Seven pavement mixtures met the target by 56 days, 2 straight cement mixtures and 5 fly ash mixtures.
- All pavement mixtures met the target by 90 days, regardless of whether or not they contained fly ash.
- Straight cement mixtures meeting the target at later ages typically had resistivities of 10 k Ω -cm or greater at 28 days, while 20% fly ash had 28-day resistivities of 6.6 k Ω -cm or greater and 30% fly ash mixtures had 28-day resistivities of 6.1 k Ω -cm or greater.

Structural mixtures (n=8, 4 with fly ash, 4 without fly ash)

- No mixtures met either the 15 k Ω -cm or 16 k Ω -cm target at 28 days.
- Two fly ash mixtures met the target of 15 k Ω -cm by 56 days, one of which met the 16 k Ω -cm by 56 days.
- Three fly ash mixtures met both the 15 k Ω -cm and 16 k Ω -cm targets at 90 days.
- No straight cement mixtures met either of the target at any age.
- Fly ash mixtures meeting the target at later ages typically had 28-day resistivity of 9 k Ω -cm or greater.

High w/cm mixtures (0.47 or greater) – Tables F.8 and F.9

Pavement mixtures (n=27, 14 without fly ash, 13 with fly ash)

- Six mixtures met the target by 28 days, all containing fly ash.
- Ten mixtures met the target by 56 days, 1 straight cement mixture (600 pcy) and 9 fly ash mixtures.
- Fourteen mixtures met the target by 90 days, 1 straight cement mixture (600 pcy) and 13 fly ash mixtures.
- Straight cement mixtures with high water cement ratios typically did not meet the target, indicating the ability of fly ash to offset the negative effects of a high w/cm ratio.
- Fly ash mixtures meeting the target typically had resistivities of 9 k Ω -cm or greater at 28 days

Structural mixtures (n=8, 4 with fly ash, 4 without fly ash)

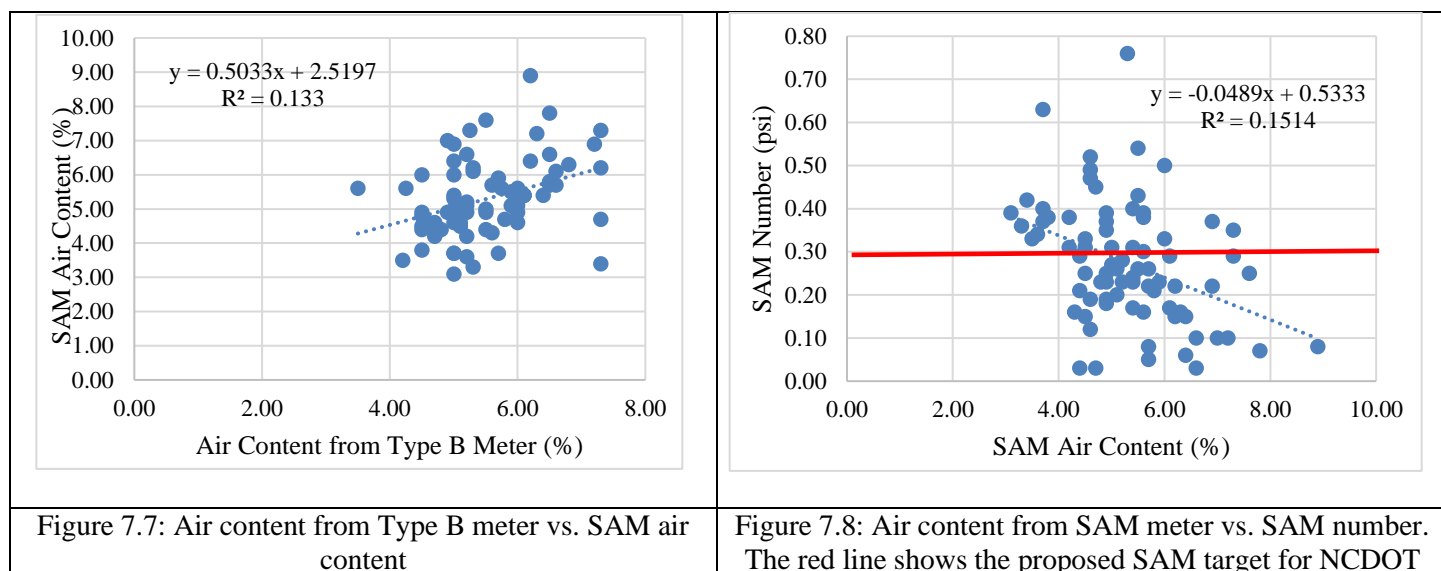
- No mixtures met either the 15 k Ω -cm or 16 k Ω -cm target at 28 days.
- One fly ash mixture met both the 15 k Ω -cm and 16 k Ω -cm targets by 56 days.
- Two fly ash mixtures and one straight cement mixture (700 pcy) appear to meet both the 15 k Ω -cm and 16 k Ω -cm targets at 90 days.
- The two fly ash mixtures meeting the target at later ages had 28-day resistivities of 6.6 and 10.6 k Ω -cm at 28 days. The straight cement mixture meeting the target at later ages had a 28-day resistivity of 12.1 k Ω -cm. Therefore, a 28-day resistivity target for high w/cm structural mixtures is difficult to identify from this limited dataset.

Although this exercise provided some insight into potential 28-day resistivity targets providing good odds of meeting the 11 k Ω -cm pavement target and 15 or 16 k Ω -cm target for Class AA mixtures at later ages, the limited number of mixtures supporting the analysis does not provide confidence in the findings. Therefore, it is recommended that additional studies be performed, obtaining later age resistivities of targeted mixtures (possibly through another pilot study) to gain more confidence in the 28-day early resistivity targets.

7.2 SAM

As part of participation in the PEM Pooled Fund, NCDOT was eligible for an on-site SAM training session by the device developer. UNC Charlotte worked with the developers of the SAM (Oklahoma State University) to arrange this training session, which was held at the contractor's site offices. A number of NCDOT and partnering consulting agency and testing laboratory personnel attended the training. However, three technicians attending the training were targeted users of the device on a regular basis, and each participated extensively in the training (Figure F.4). A fourth technician also performed SAM tests over the course of the work. Senior Assistant Resident Engineer on the project compiled the data and forwarded it to UNC Charlotte for analysis.

SAM data collected at the pavement PEM pilot project was quite variable (Cavalline et al. 2022), and a training session held prior to this pilot project was part of this effort's recommendations. The training session held prior to this pilot project appears to have supported technicians in obtaining far more consistent data. Figure 7.7 shows a plot of the air content (%) measurements obtained from the SAM and the Type B meter. All SAM data collected during this pilot project is provided in Appendix F in Table F.10. Figure 7.8 shows the relationship between the SAM number and SAM Air Content (%). It is noted that although there is not a strong correlation between SAM number and SAM air content, this could be a function of the data representing many different mixtures at multiple structures over the past several months. In general, SAM numbers for many mixtures fell below the preliminary target of 0.30 (discussed in Chapter 4), and very high SAM number measurements indicating leaks or other errors were not recorded.



Mixtures with total air contents greater than 5.5% (measured by SAM) tended to have a strong chance (72.7%) of meeting the proposed SAM target of 0.30 (Figure 7.9). Mixtures with total air contents greater than 6.0% (measured by SAM) had an even stronger chance (80.0%) of meeting the proposed SAM target of 0.30 (Figure 7.10). This may support recommendations to require an entrained air content greater than 6.0% for NCDOT concrete mixtures where excellent freeze-thaw durability is desired.

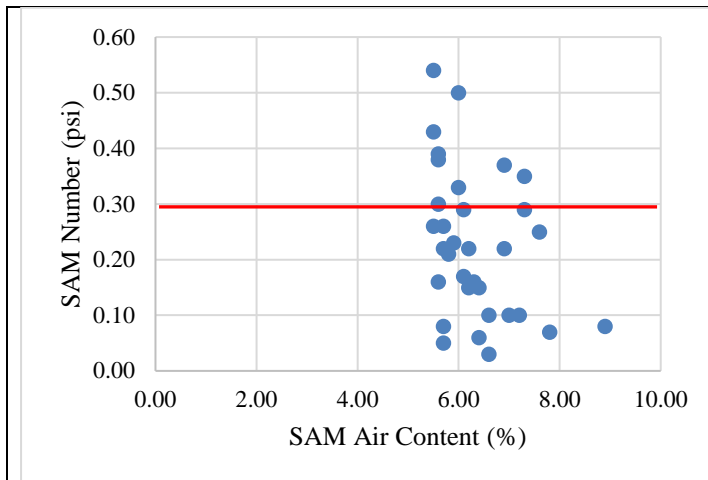


Figure 7.9: SAM air content vs. SAM number for mixtures with air content > 5.5%

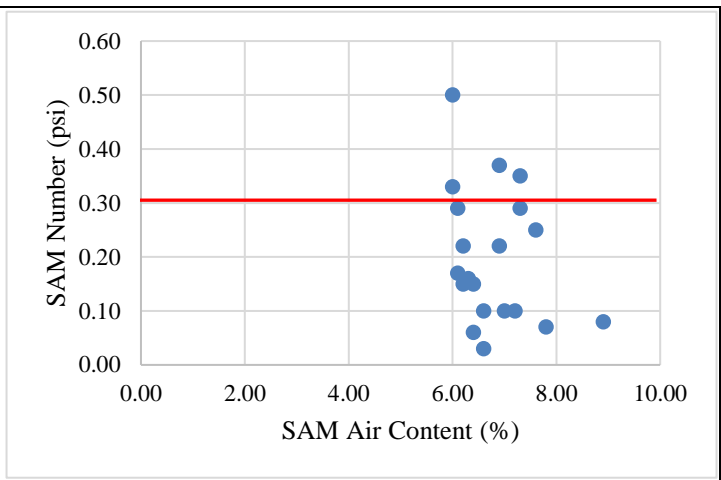


Figure 7.10: SAM air content vs. SAM number for mixtures with air content > 6.0%

Samples of concrete for pumped mixtures were obtained both before pumping and after pumping. It is noted that typically only one SAM test was performed for each placement, and sets of “before and after pumping” on the same mixture during the same placement were not made. However, test results for pumped mixtures (Figure 7.11) do show several general trends. The total air content and SAM numbers measured before pumping tended to be higher, with the SAM numbers showing more variability. When SAM tests were performed after pumping, the total air content tended to be lower, and SAM numbers exhibited slightly less variability. A plot of SAM air content vs. SAM number was also prepared in a manner that compared results for Class A and Class AA mixtures (Figure F.5 in Appendix F). Class A mixtures exhibited a stronger correlation between air content and SAM number, but this appeared to be due to the broader range of air contents accepted (some greater than 7.5%).

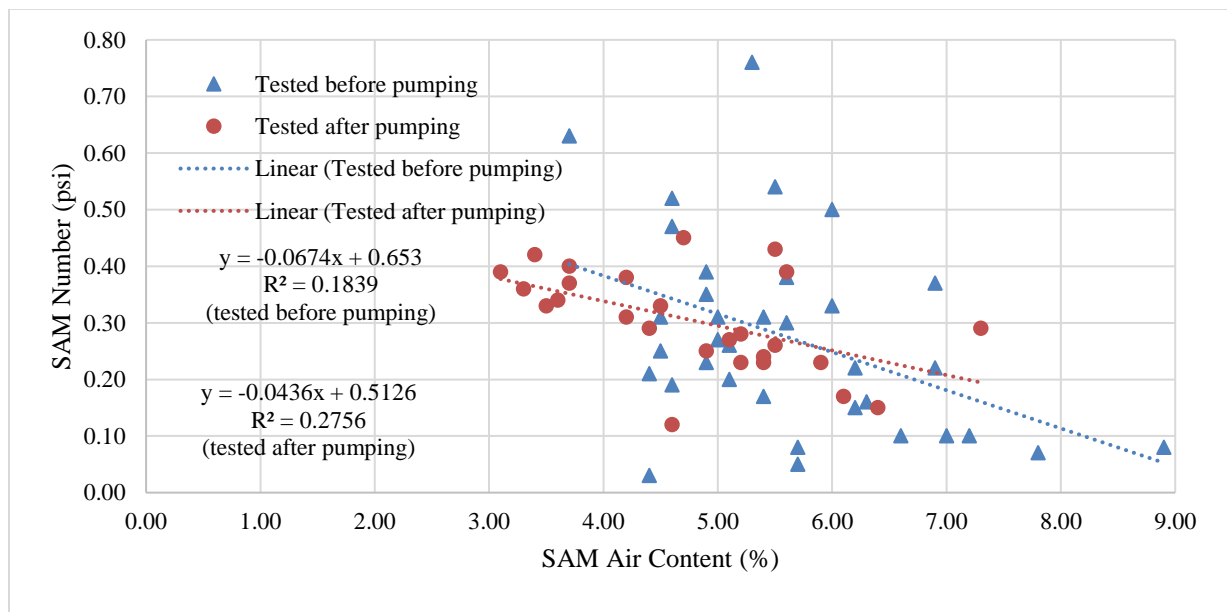


Figure 7.11: SAM test results performed before and after pumping

7.3 Shrinkage

Shrinkage testing was performed per ASTM C157 using mixtures batched by a ready-mix concrete producer. The supplier initially raised concerns regarding variability in test results between local laboratories. Therefore, these tests were performed on replicate specimens at NCDOT, UNC Charlotte, and a third-party testing laboratory. Shrinkage beams for two project mixtures (Mixture 6012 – a structural AA mixture and Mixture 6013 – a drilled shaft mixture). Mixture information, including materials, proportions, and compressive strength test results is presented in Appendix F, Figures F.2 and F.3, and results are summarized in Figure 7.12. As can be observed in Figure 7.12, the results for UNC

Charlotte’s laboratory and the third-party testing laboratory were very close in both magnitude of shrinkage measured for each mixture and in variability. Values were reasonably close to those for similar structural mixtures included in previous testing at UNC Charlotte (see Chapter 3). Data collected at the NCDOT laboratory indicated much greater shrinkage and a greater range of variability. Discussions indicated that additional training and experience may be needed for NCDOT personnel prior to deploying shrinkage tests in a more widespread use.

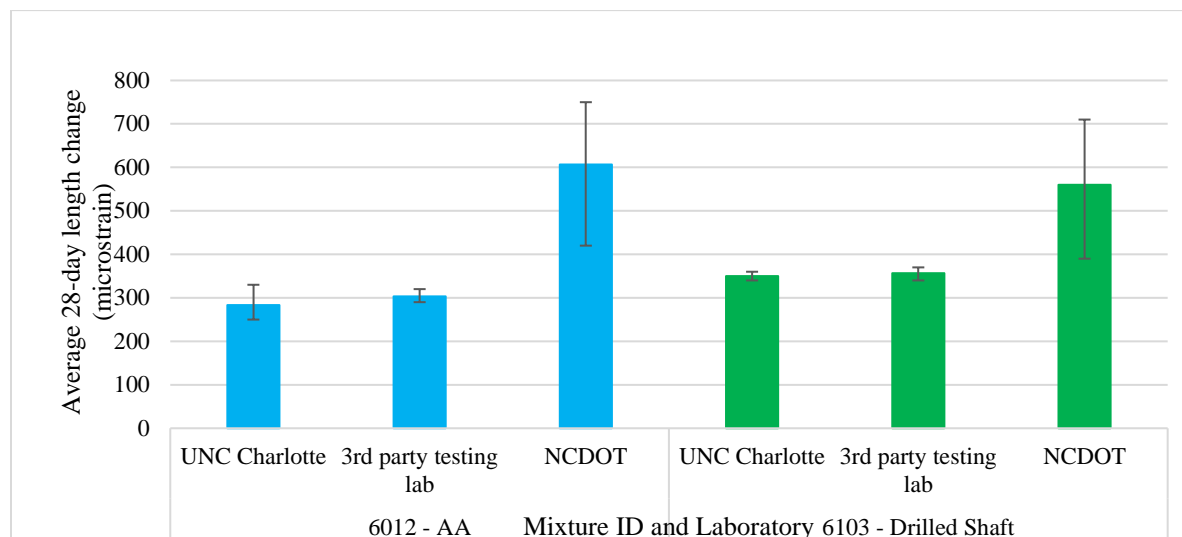


Figure 7.12: Results of multi-laboratory shrinkage tests of a Class AA mixture and a drilled shaft mixture

7.4 Conclusions

Surface Resistivity

- Surface resistivity tests on selected mixtures performed by the QC laboratory indicated that the Class A, Class AA, and drilled shaft mixture used on this project exhibit low to very low permeability to chloride ions. The proposed target of 16 kΩcm was readily met by the Class AA mixture by 28 days, and was nearly met by the other two mixtures at 28 days. All three mixtures well exceeded the target by 56 days. These mixtures included approximately 20% fly ash by weight.
- Surface resistivity tests performed by NCDOT as part of this work were taken up to ages of 28 days due to limitations in curing storage. The 28-day resistivity measurements provide reasonable confidence that the 16 kΩcm will be met by these mixtures used on pilot project components sometime after 28 days.
- An analysis of historical data provides some insights into potential 28-day resistivity targets that provide a strong probability that a mixture with a given w/cm ratio and fly ash content will meet the later age proposed pavement and bridge targets. Due to the limited amount of data to support this analysis, additional study is needed to have confidence in these suggested “early” 28-day resistivity targets.

SAM

- The quality of data obtained from the SAM improved as part of this pilot project, with lower variability observed than during the previous pilot project. This improvement was likely the result of a training session provided by the device developer, with focus on training the technicians responsible for testing. A limited number of technicians also obtained the data.
- The proposed SAM target of 0.30 appears to have been reasonably met with mixtures with air contents greater than 6%.

Shrinkage

- ASTM C157 28-day shrinkage targets (less than 400 microstrain) appeared to be reasonably met by the two structural mixtures, as tested by UNC Charlotte and a third-party laboratory.
- Additional training may be needed to support deployment of this PEM test on a wider basis.

8.0 SUMMARY AND CONCLUSIONS

This research project included four major areas of work. A detailed summary of findings for each of these areas of work was presented at the end of the following chapters of this report:

- Chapter 3 – Optimized Aggregate Gradation Mixtures
- Chapter 4 – Performance Targets for Freeze-Thaw Durable Concrete
- Chapter 5 – Use of Surface Resistivity Meter to Evaluate Bridge Deck Overlays
- Chapter 7 – Pilot Project Implementation

Although the reader is referred to the appropriate chapters for a summary of findings, key conclusions from each of the areas of work are provided below.

Optimized Aggregate Gradation Mixtures (Chapter 3)

- For moderate ($w/cm = 0.42$) and low ($w/cm = 0.37$) mixtures, many optimized gradation mixtures produced mechanical property test results that were similar to concrete mixtures that did not have a reduction in cementitious material.
- Compressive and flexural strengths were roughly equivalent between optimized and non-optimized mixtures, indicating that current NCDOT specifications could reasonably be met by mixtures containing a 10% reduction in cementitious materials and a 2-3% reduction in paste volume. This could offer both economic and sustainability benefits.
- Volumetric shrinkage of all optimized aggregate gradation mixtures met the AASHTO PP 84 suggested limit of 420 microstrain at 28-days.
- Electrical tests indicated greater permeability in optimized aggregate gradation mixtures, but the influence of the additional aggregate content, ITZ, and a 10% reduction in cementitious materials effectively changing the cement paste structure may have influenced the results. Such indirect measurements may require adjustments to performance targets for optimized mixtures. While this research provided test results where optimized aggregate gradation mixtures with reduced cementitious materials demonstrated more permeable characteristics, it does not mean that these mixtures are actually less durable.
- The benefits of using fly ash in concrete mixtures were again verified by this study, in which significant later-age reductions in permeability were observed.
- Durability performance test results improved as the w/cm ratio decreased in both optimized and non-optimized aggregate gradation mixtures, suggesting the NCDOT may want to further explore prescriptive specification provisions to reduce the w/cm ratio of their mixtures. This prescriptive change could result in less permeable concrete, lower shrinkage, potentially lower paste contents, and overall improved durability performance.
- Optimized aggregate gradation mixtures with fly ash exhibited improved durability performance characteristics at later ages when compared to companion optimized and non-optimized aggregate gradation mixtures, suggesting the NCDOT may want to explore prescriptive specifications to encourage the use of SCMs at replacement rates up to 30 percent to improve durability performance.
- The use of optimized aggregate mixtures may reduce costs and emissions of greenhouse gases via the reduction of cement, and additionally may result in mixtures with improved durability characteristics, a longer service life, and lower cracking through volumetric shrinkage.

Performance Targets for Freeze-Thaw Durable Concrete (Chapter 4)

- NCDOT structural and pavement mixtures batched and tested as part of the series of research studies performed by UNC Charlotte are very resistant to freeze-thaw stresses. After 300 cycles of ASTM C666 testing, only 6 of the 56 mixtures exhibited a DF below 80 and only 2 falling below ASTM C666's performance threshold DF of 60.
- The historically used spacing factor limit of 0.008 in (200 μm) appears to be too conservative for use of NCDOT in specification development. Many mixtures exhibiting good to excellent freeze-thaw durability performance in the ASTM C666 test had spacing factors that exceeded this target. Since most concrete mixtures included in this study exhibited DFs greater than 80, a proposed target spacing factor could not be identified.
- Fresh air content exhibited a reasonable correlation to the spacing factor and DF found during testing.

- The findings of this study were significantly limited by the range of air contents (5 to 6%) used in the mixtures. A more comprehensive study should be performed using a wider range of air contents (such as 2% to 10%). Analysis of field-produced concrete should also be paired with additional laboratory testing of to further explore the SAM number, in hopes of expanding the types of materials and mixtures used to identify the performance target. Future research projects to support NCDOT's PEM initiatives could further explore the spacing factor, SAM number and DF that correlates to adequate performance in both the field and laboratory.

Use of Surface Resistivity Meter to Evaluate Bridge Deck Overlays (Chapter 5)

- The surface resistivity meter could potentially be used as a tool to assist in evaluating bridge deck overlay quality. A procedure to do so was developed and is presented in Appendix E.
- Surface resistivity readings were influenced by conventional steel reinforcement, and an approach to help correlate changes in surface resistivity versus reinforcing steel bar distance was presented. The surface resistivity meter measurements were not influenced by the epoxy coating on steel reinforcement.
- Concrete mixtures with latex admixtures tend to produce slightly higher, yet similar surface resistivity measurements than that of concrete mixtures without the latex admixture at each of the test ages.
- Latex-modified and very high early strength latex modified mixture exhibit a trend of an early peak in surface resistivity, and then a gradual decrease.
- Changes overlay thickness were to be detectable using the surface resistivity meter and the approach provided in Appendix E.
- Edge effects were also evident and a minimum offset distance of 4 inches from an edge was found to be appropriate using the approach described in Appendix E.
- The surface resistivity meter was not effective in detecting voids intentionally placed in the mockup slabs constructed as par to this work. Future work could attempt to utilize another type of material, or different sizes/shapes of voids, to further explore the potential of the surface resistivity meter to locate voids or other defects.

9.0 VALUE OF RESEARCH FINDINGS and RECOMMENDATIONS

9.1 Value of Research Findings

Research products produced from this work included:

- Test data on a broadened range of highway concrete mixtures, including Class AA, A, drilled shaft, conventional overlay, latex-modified, and high-early strength mixtures to support movement towards performance specifications.
- Confirmation that performance criteria for the targeted technologies (surface resistivity, SAM, and shrinkage) from previous studies appear reasonable for use in future PEM projects.
- Indication that prescriptive specification measures such as w/cm ratio or cementitious materials content could be adjusted in upcoming specification revisions. The benefits of limiting w/cm ratio were confirmed through mechanical and durability performance tests. Benefits that could be achieved using reduced cementitious materials contents and paste volumes through optimized aggregate gradations were also identified.
- Additional confirmation of the benefits that could be achieved using fly ash and the importance of SCMs such as fly ash to achieving the desired performance from NCDOT's concrete infrastructure.
- Spreadsheet tools and other resources that can be used by NCDOT personnel, Resident Engineers, contractors and other stakeholders potentially involved in PEM.
- NCDOT and contractor insight from implementation of PEM shadow specifications and PEM tests at a structural concrete pilot project.
- A protocol for use of the surface resistivity meter to evaluate the quality of bridge deck overlays.

The success of this project could be measured by document documenting an increased number of stakeholders using PEM tests and improving QC processes. However, quantifying of true value of this research is challenging. Benefits of implementing PEM will most likely include cost savings, improved specifications, and improved performance of concrete bridge/pavement infrastructure. Specifically, benefits will be associated with:

- Cost savings associated with longer service life and reduced maintenance costs for concrete pavements, bridges, and other infrastructure
- An enhanced focus on quality during construction, driven by performance-based requirements
- Guidance on interpretation of laboratory testing results and the impact on performance
- Improved QA and QC testing and acceptance, particularly use of new and emerging PEM tests from AASHTO PP 84 (now R 101)
- Technology transfer tools and training sessions to aid NCDOT in implementation of PEM tests and specifications

As the North Carolina cement supply increasingly moves towards PLC (in lieu of traditional Type I and I/II cements), increased use of SCMs and PLC should also allow for lower cementitious materials contents to achieve the same durability performance. This would result in initial cost savings as well as cost savings over the life cycle of infrastructure components, which should achieve longer service lives and will require reduced maintenance and rehabilitation actions. Increased use of SCMs and PLC, along with lower cement contents will also result in a reduction in greenhouse gas emissions, allowing NCDOT to demonstrate progress towards MAP-21 goals.

The true measure of the economic benefits of movement towards use of the proposed specification provisions, along with increased use of sustainable materials such as PLC and SCMs will become evident only after infrastructure components are constructed in this manner, and then the life cycle costs compared to similar components constructed without use of PLCs, higher SCM contents and use of PEM technologies. As previously described in the report for the first phase of this project (Cavalline et al. 2020a), several future methods for quantification of the value of this research could include:

- A life cycle cost analysis (LCCA) on a roadway or structure constructed using the provisions recommended in this report, comparing it to a previously constructed roadway or structure. An LCCA would provide a measure of the economic (cost) savings associated with findings and recommendations presented herein. The cost savings could be computed on a materials-alone basis (cost per cubic yard of as-constructed concrete), on an annual basis, or on a percent cost savings per lane-mile basis. A history of maintenance actions (or a reliable estimate of anticipated maintenance actions) and expected service life would be needed to complete this analysis. Ongoing work to identify or predict these inputs to the LCCA is being performed by many researchers and could be supplemented by data obtained from an increasing number of pilot project studies planned and ongoing.

- A life cycle assessment (LCA) on a roadway or structure constructed using the provisions recommended in this report, comparing it to a previously constructed roadway or structure. FHWA’s recently published “Pavement Life-Cycle Assessment Framework” should be used (Harvey et al. 2016). An LCA would provide a measure of the sustainability benefits, including economic (cost) savings, reduced environmental impact, and reduced societal impacts associated with findings and recommendations presented herein. Many inputs required for the LCA could likely be reasonably assumed using previous research. However, limitations would still include information on required maintenance actions and expected service life as described above.

9.2 Recommendations

Following are the recommendations pertaining to the findings of this study:

- NCDOT should encourage the use of optimized aggregate gradation approaches to achieve the durability and sustainability benefits associated with reduced cementitious materials and paste contents.
- Increased use of SCMs such as fly ash at higher replacement rates would provide improved durability performance and hence, long-term economic and environmental benefits. It is recommended that NCDOT encourage increased use of SCMs such as fly ash on their concrete infrastructure projects.
- Prescriptive specification provisions such as w/cm ratios and cementitious materials contents should be revisited. The importance of controlling w/cm in achieving the desired mechanical properties and durability performance was demonstrated by this study, as well as previous studies. NCDOT currently requires minimum cementitious contents for many mixtures. Some states moving towards PEM are removing minimum cementitious contents or changing to specifying maximum cementitious contents to achieve durability and sustainability benefits.
- Surface resistivity is a promising technology for rapid evaluation of durability performance that is easy to perform, uses specimen already cast for compressive strength tests, and has been reasonably linked to long-term performance of existing infrastructure via the RCPT and field experience of other states currently utilizing resistivity in their specifications. Surface resistivity testing should be promoted by NCDOT, and it is recommended that NCDOT move towards adoption a resistivity specification to support more durable, sustainable concrete infrastructure.
- Future research to study the permeability of optimized aggregate gradation mixtures using non-electrical permeability tests such as the Germann Water Permeation Test (GWT) could be useful. The GWT is a non-electrical test that measures the permeation of water into the surface under an applied pressure. By comparing concrete mixtures with a varying volume of coarse aggregates electrical test results with a non-electrical test, more accurate targets for surface resistivity test results could be developed.
- To establish 28-day surface resistivity targets that provide a high likelihood of meeting resistivity targets at later ages, additional longer-term (56 to 90 day) test results are needed for different types of mixtures. This effort may temporarily require additional curing capabilities at a regional NCDOT laboratory, coordination with a testing firm, or other provisions, but would support deployment of surface resistivity specifications without requiring storage for longer term than currently used (28 days) at most NCDOT laboratories.
- Specifying volumetric shrinkage testing would provide a means for NCDOT to promote construction of less permeable infrastructure that is less prone to cracking. The shrinkage specification target presented in the prior study and confirmed as part of this study could be used in pilot studies to explore the benefits of such specification provisions in promoting enhanced performance.
- Additional PEM pilot projects should be encouraged for both pavement and structural concrete. Information obtained from the pilot projects should be used to evaluate the shadow specifications and performance targets developed as part of RP 2018-14 and this study.
- Gaining stakeholder buy-in is critical to success of the PEM initiative. Activities that support stakeholder education, training, and use of the PEM technologies should be continued. Presentations on PEM at the North Carolina Concrete Pavements Conference (as well as similar meetings) could help engage local/regional industry in the PEM effort. Outreach to consulting companies that are hired by NCDOT for design, testing, project management, and other activities should also increase at events for local/regional chapters of entities including the American Council of Engineering Companies (ACEC), American Society of Civil Engineers (ASCE), American Concrete Institute (ACI) National Society of Professional Engineers (NSPE) and others.
- Efforts to grow and improve FHWA’s PEM initiative are ongoing in many areas, including research, pilot projects, and development of technology transfer tools. NCDOT should continue to stay engaged in this initiative through the Pooled Fund Studies, the National Concrete Consortium, and other avenues that may emerge.

10.0 IMPLEMENTATION AND TECHNOLOGY TRANSFER PLAN

Key to success of the FHWA PEM initiative is technology transfer to stakeholders. This project directly supported implementation efforts through training and use of PEM tests by agency and contractor personnel at the I-485 PEM pilot project. In addition to the activities specifically performed as part of this project, technology transfer activities supported by this work could also include dissemination of the results of PEM research and implementation at NCDOT Construction conferences, training sessions for local NCDOT/industry personnel, and development of technology transfer literature as part of the project. Additional, specific technology transfer actions for the products of this research project are listed below.

Research Product 1	Digital database of test results from laboratory testing.
Suggested User	Materials & Tests Unit, Pavement Design & Collection Unit, Structures Management Unit
Recommended Use	Information contained in this database could serve as reference data for evaluation of concrete mixtures and/or test methods in future work. Data could also be used to supplement additional databases on maintained by the Materials and Tests Unit.
Recommended Training	None recommended at this time.

Research Product 2	Laboratory test data indicating that use of optimized aggregate gradations could reduce cementitious materials contents and paste contents, providing sustainability benefits.
Suggested User	Materials & Tests Unit, Pavement Design & Collection Unit, Structures Management Unit
Recommended Use	This information could be used to support design decisions and specification provisions that encourage or support use of optimized aggregate gradation mixtures.
Recommended Training	None recommended at this time.

Research Product 3	Laboratory test data providing performance targets for surface resistivity, SAM, and shrinkage.
Suggested User	Materials & Tests Unit, Pavement Design & Collection Unit, Structures Management Unit
Recommended Use	This information could be utilized in PSPs or shadow specifications to promote movement towards PEM.
Recommended Training	None recommended at this time.

Research Product 4	Draft procedure for use of surface resistivity meter for evaluating bridge deck overlay quality.
Suggested User	Construction Unit, Materials & Tests Unit, Structures Management Unit
Recommended Use	This procedure could be used to evaluate bridge deck overlay quality in lieu of conventional methods.
Recommended Training	The draft procedure is included in Appendix E of this report. UNC Charlotte personnel could meet with Materials & Tests Unit personnel to assist in training, if requested.

Research Product 6	Testing program template and spreadsheets for use of PEM tests at pilot projects
Suggested User	Materials & Tests Unit, Pavement Design & Collection Unit, Structures Management Unit
Recommended Use	These tools could be used to support upcoming PEM pilot projects on other projects as desired by NCDOT.
Recommended Training	None recommended at this time.

Research Product 7	Data from PEM pilot project for structural concrete.
Suggested User	Materials & Tests Unit, Structures Management Unit
Recommended Use	Information gathered as part of this pilot project can be used by NCDOT to support LCCA or LCA of the structural components to evaluate the benefits of PEM
Recommended Training	None recommended at this time.

11.0 REFERENCES

Note: References listed below are cited in the body of the report. A full list of references used to support this work is provided at the end of Appendix A, which contains the complete Literature Review for this project.

- Ahlstrom, G. (2016). "FHWA's Vision for Performance Engineered Concrete Mixtures and Quality Assurance Program." Presented at National Concrete Consortium, April 2015 meeting. Available at: <http://www.cptechcenter.org/ncc/Sp2016%20NC2/FHWA%20Combined%20for%20NCC%20April%202016%20Final%204-18-16%20pptx.pdf>
- American Association of State Highway and Transportation Officials (AASHTO). (2019). "Standard Practice for Developing Performance Engineered Concrete Pavement Mixtures." PP 84-19, American Association of State Highway and Transportation Officials, Washington, DC.
- American Association of State Highway and Transportation Officials (AASHTO). (2020). "Standard Practice for Developing Performance Engineered Concrete Pavement Mixtures." PP 84-20, American Association of State Highway and Transportation Officials, Washington, DC.
- American Association of State Highway and Transportation Officials (AASHTO). (2022). "Developing Performance Engineered Concrete Mixtures."
- American Association of State Highway and Transportation Officials (AASHTO). (2020). "Standard Method of Test for Compressive Strength of Cylindrical Concrete Specimens." AASHTO T 22M/T 22, American Association of State Highway and Transportation Officials, Washington, DC.
- American Association of State Highway and Transportation Officials (AASHTO). (2020). "Standard Method of Test for Flexural Strength of Concrete (Using Simple Beam with Third- Point Loading)." AASHTO T 97, American Association of State Highway and Transportation Officials, Washington, DC.
- American Association of State Highway and Transportation Officials (AASHTO). (2019). "Standard Method of Test for Air Content of Freshly Mixed Concrete by the Pressure Method." T 152-19, American Association of State Highway and Transportation Officials, Washington, DC.
- American Association of State Highway and Transportation Officials (AASHTO). (2017). "Standard Method of Test for Length Change of Hardened Hydraulic Cement Mortar and Concrete." T 160-17, American Association of State Highway and Transportation Officials, Washington, DC.
- American Association of State Highway and Transportation Officials (AASHTO). (2019). "Standard Method of Test for Air Content of Freshly Mixed Concrete by the Volumetric Method." T 196M/T 196-11, American Association of State Highway and Transportation Officials, Washington, DC.
- American Association of State Highway and Transportation Officials (AASHTO). (2020). "Standard Method of Test for Estimating the Cracking Tendency of Concrete." T 334-08, American Association of State Highway and Transportation Officials, Washington, DC.
- American Association of State Highway and Transportation Officials (AASHTO). (2015). "Standard Method of Test for Temperature of Freshly Mixed Portland Cement Concrete." T 309-15, American Association of State Highway and Transportation Officials, Washington, DC.
- American Association of State Highway and Transportation Officials (AASHTO) (2017). Standard Method of Test for Surface Resistivity Indication of Concrete's Ability to Resist Chloride Ion Penetration. AASHTO T 358-17 American Association of State Highway and Transportation Officials. Washington, D.C.
- American Association of State Highway and Transportation Officials (AASHTO). (2017). "Standard Method of Test for Evaluating Stress Development and Cracking Potential due to Restrained Volume Change Using a Dual Ring Test." T 363-17, American Association of State Highway and Transportation Officials, Washington, DC.
- American Association of State Highway and Transportation Officials (AASHTO). (2017). "Standard Method of Test for Characterization of the Air-Void System of Freshly Mixed Concrete by the Sequential Pressure Method." TP 118-17, American Association of State Highway and Transportation Officials, Washington, DC.
- American Association of State Highway and Transportation Officials (AASHTO). (2017). "Electrical Resistivity of a Concrete Cylinder Tested in a Uniaxial Resistance Test." TP 119-15, American Association of State Highway and Transportation Officials, Washington, DC.
- American Concrete Institute (ACI) 211.1 (2002). Standard Practice for Selecting Proportions for Normal, Heavyweight, and Mass Concrete. American Concrete Institute, Farmington Hills, MI.
- American Concrete Institute (ACI). 318-19 (2019). Building Code Requirements for Structural Concrete and Commentary. American Concrete Institute, Farmington Hills, MI.
- American Society for Testing and Materials (ASTM). (2018). ASTM C33/C33M-18 "Standard Specification for Concrete Aggregates." ASTM International, West Conshohocken, PA. DOI: 10.1520/C0033_C0033M-18. www.astm.org

- American Society for Testing and Materials (ASTM). (2021). ASTM Standard C39/C39M-21 “Standard Test Method for Compressive Strength of Cylindrical Concrete Specimens.” ASTM International, West Conshohocken, PA. DOI: 10.1520/C0039_C0039M-21. www.astm.org
- American Society for Testing and Materials (ASTM). (2021). ASTM Standard C78/C78M-21 “Standard Test Method for Flexural Strength of Concrete (Using Simple Beam with Third-Point Loading).” ASTM International, West Conshohocken, PA. DOI: 10.1520/C0078_C0078M-21. www.astm.org
- American Society for Testing and Materials (ASTM). (2017). ASTM C138/C138M-17a “Standard Test Method for Density (Unit Weight), Yield, and Air Content (Gravimetric) of Concrete.” ASTM International, West Conshohocken, PA. DOI: 10.1520/C0138_C0138M-17A. www.astm.org
- American Society for Testing and Materials (ASTM). (2020). ASTM C143/C143M-20 “Standard Test Method for Slump of Hydraulic-Cement Concrete.” ASTM International, West Conshohocken, PA. DOI: 10.1520/C0143_C0143M-20. www.astm.org
- American Society for Testing and Materials (ASTM). (2020). ASTM C150/C150M-20 “Standard Specification for Portland Cement.” ASTM International, West Conshohocken, PA. DOI: https://doi.org/10.1520/C0150_C0150M-20
- American Society for Testing and Materials (ASTM). (2017). ASTM C157/C157M-17 “Standard Test Method for Length Change of Hardened Hydraulic-Cement Mortar and Concrete.” ASTM International, West Conshohocken, PA. DOI: 10.1520/C0157_C0157M-17. www.astm.org
- American Society for Testing and Materials (ASTM). (2018). ASTM C192/C192M-18 “Standard Practice for Making and Curing Concrete Test Specimens in the Laboratory.” ASTM International, West Conshohocken, PA. DOI: 10.1520/C0192_C0192M-18. www.astm.org
- American Society for Testing and Materials (ASTM). (2019). ASTM C215-19 Standard Test Method for Fundamental Transverse, Longitudinal, and Torsional Resonant Frequencies of Concrete Specimens. ASTM International, West Conshohocken, PA. DOI: <https://doi.org/10.1520/C0215-19>
- American Society for Testing and Materials (ASTM). (2017). ASTM C231/C231M-17a “Standard Test Method for Air Content of Freshly Mixed Concrete by the Pressure Method.” ASTM International, West Conshohocken, PA. DOI: 10.1520/C0231_C0231M-17A. www.astm.org
- American Society for Testing and Materials (ASTM). (2016). ASTM Standard C457/C457M-16 “Standard Test Method for Microscopical Determination of Parameters of the Air-Void System in Hardened Concrete.” ASTM International, West Conshohocken, PA. DOI: 10.1520/C0457_C0457M-16. www.astm.org
- American Society for Testing and Materials (ASTM). (2021). ASTM C469/C469M-14e1 “Standard Test Method for Static Modulus of Elasticity and Poisson's Ratio of Concrete in Compression.” ASTM International, West Conshohocken, PA. DOI: 10.1520/C0469_C0469M-14E01. www.astm.org
- American Society for Testing and Materials (ASTM). (2019). ASTM C511-19 “Standard Specification for Mixing Rooms, Moist Cabinets, Moist Rooms, and Water Storage Tanks Used in the Testing of Hydraulic Cements and Concretes.” ASTM International, West Conshohocken, PA. DOI: <https://doi.org/10.1520/C0511-19>
- American Society for Testing and Materials (ASTM). ASTM C618-19 “Standard Specification for Coal Fly Ash and Raw or Calcined Natural Pozzolan for Use in Concrete.” ASTM International, West Conshohocken, PA. DOI: <https://doi.org/10.1520/C0618-19>
- American Society for Testing and Materials (ASTM). (2016). ASTM C666/C666M-15 “Standard Test Method for Resistance of Concrete to Rapid Freezing and Thawing.” ASTM International, West Conshohocken, PA. DOI: 10.1520/C0666_C0666M-15. www.astm.org
- American Society for Testing and Materials (ASTM). (2018). ASTM C685/C685M-17 “Standard Specification for Concrete Made by Volumetric Batching and Continuous Mixing.” ASTM International, West Conshohocken, PA. DOI: 10.1520/C0685_C0685M-17. www.astm.org
- American Society for Testing and Materials (ASTM). (2019). ASTM C1202-19 “Standard Test Method for Electrical Indication of Concrete’s Ability to Resist Chloride Ion Penetration.” ASTM International, West Conshohocken, PA. DOI: 10.1520/C1202-19. www.astm.org
- American Society for Testing and Materials (ASTM). (2021). ASTM C1260-21 “Standard Test Method for Potential Alkali Reactivity of Aggregates (Mortar-Bar Method).” ASTM International, West Conshohocken, PA. DOI: 10.1520/C1260-21. www.astm.org
- American Society for Testing and Materials (ASTM). (2020). ASTM C1293-20a “Standard Test Method for Determination of Length Change of Concrete Due to Alkali-Silica Reaction.” ASTM International, West Conshohocken, PA. DOI: 10.1520/C1293-20A. www.astm.org
- American Society of Civil Engineers (ASCE). (2021). 2021 Infrastructure Report Card. Available at: <https://www.infrastructurereportcard.org>. Accessed October 2021.
- American Society of Civil Engineers (ASCE). (2021). Policy statement 418 – The role of the civil engineer in sustainable development. Reston, VA.
- Biggers, R.B. (2019). “Development of a Surface Resistivity Specification for Durable Concrete” (Master’s thesis). University of North Carolina at Charlotte, Charlotte, NC.

- Blanchard, E. H. (2016). "Determination and Evaluation of Inputs for Portland Cement Concrete Pavement to Support Local Calibration of MEPDG for North Carolina" (Master Thesis), University of North Carolina at Charlotte
- Cackler, T., Harrington, D. and Taylor, P.C. (2017a). "Performance Engineered Mixtures (PEM) for Concrete Pavements." CP Road Map Brief, April 2017. National Concrete Pavement Technology Center. Ames, IA.
- Cackler, T., Praul, M. and Duval, R. (2017b). "Developing a Quality Assurance Program for Implementing Performance Engineered Mixtures for Concrete Pavements." CP Road MAP Brief, July 2017. National Concrete Pavement Technology Center. Ames, IA.
- Cavalline, T.L., Tempest, B.Q., Biggers, R.B., Lukavsky, A.J., McEntyre, M.S., and Newsome, R.A. (2020a). Durable and Sustainable Concrete through Performance Engineered Concrete Mixtures. Report No. FHWA/NC/2018-14. North Carolina Department of Transportation, Raleigh, NC.
- Cavalline, T.L., Tempest, B.Q., Blanchard, E.H., Medlin, C.D., and Chimmula, R.R. (2018). Improved Data for Mechanistic-Empirical Pavement Design for Concrete Pavements. Report No. FHWA/NC/2015-03. North Carolina Department of Transportation, Raleigh, NC.
- Cavalline, T.L., Tempest, B.Q., Hunter, B.J., White, F.D., and Ange, C.M. (2020b). "Post Construction Report for North Carolina Demonstration Project, Implementation of Performance Engineered Concrete Mixtures (PEM)/AASHTO PP 84." Final Report Project FHWA/NC/2019-41, North Carolina Department of Transportation. Submitted to Federal Highway Administration, April 2020.
- Cavalline, T. L., Tempest, B. Q., Leach, J. W., Newsome, R. A., Loflin, G. D., and Fitzner, M. J. (2019). Internal Curing of Concrete Using Lightweight Aggregate. Report No. FHWA/NC/2016-06. North Carolina Department of Transportation, Raleigh, NC.
- Cavalline, T.L., White, F.D., Tempest, B.Q., Hunter, B.J., Ange, C.M., and Simpson, R.P. (2022). "Performance Engineered Concrete Mixtures: Implementation at an Interstate Rigid Pavement Project." Transportation Research Record: Journal of the Transportation Research Board, 2676(5), 450-459. <https://doi.org/10.1177%2F03611981211067981>
- Colorado Department of Transportation (CDOT). (2021). Standard Special Provisions: Section 601: Concrete Mix Designs.
- Cramer, S.M., Hall, M., Parry, J. (1995). "Effects of Optimized Total Aggregate Gradation on Portland Cement Concrete for Wisconsin Pavements." Transportation Research Record No. 1478, Concrete and Concrete Pavement Construction. 100-106. <http://worldcat.org/issn/03611981>
- Dillworth, D.A. (2020). "Quality Assurance of Bridge Deck Concrete Overlays Using Surface Resistivity Testing." Master Thesis. University of North Carolina at Charlotte. Charlotte, NC.
- Hall, H., LeFlore, J., Staffileno, C., Fennell, M., and Ley, T. (2019). "Update on the Super Air Meter." Presented at the Spring 2019 meeting of the National Concrete Consortium. April 25, 2019. Denver, Colorado. Available at: <https://intrans.iastate.edu/events/spring-2019-national-concrete-consortium/>
- Ley, M.T., Welch, D., Peery, J., and LeFlore, J. (2017). Determining the Air Void Distribution in Fresh Concrete with the Sequential Air Method. Construction and Building Materials, 9(150), 723-737. <https://doi.org/10.1016/j.conbuildmat.2017.06.037>.
- Mehta, P.K. and Monteiro, P.J.M. (2014). Concrete: Microstructure, Properties, and Materials Fourth Edition. McGraw Hill Education.
- National Concrete Pavement Technology Center (2022). Performance Engineered Mixtures website. Available at: <https://cptechcenter.org/performance-engineered-mixtures-pem/>
- New York Department of Transportation (NYSDOT). (2019). Item 504.00000011 – Performance Engineered Concrete Mixture for Pavements. Albany, NY
- New York Department of Transportation (NYSDOT). (2022). Special Specifications: Section 501: Portland Cement Concrete – Performance Mixture Design and Quality Control. Albany, New York.
- North Carolina Department of Transportation (NCDOT). (2018). Standard Specifications for Roads and Structures: Division 10: Materials. Raleigh, North Carolina.
- Ocampo, J. (2022). "Freeze-Thaw Durability Specification for Highway Concrete." Master Thesis. University of North Carolina at Charlotte. Charlotte, NC.
- Ojo, T., O. (2018). "Performance of Portland Cement Concrete Containing Chemically Beneficiated High Loss on Ignition Fly Ashes with Air Entrainment." Master Thesis. University of North Carolina at Charlotte. Charlotte, NC.
- Peterson, K. W., Swartz, R. A., Sutter, L. L., and Van Dam, T. J. (2001). "Hardened Concrete Air Void Analysis with a Flatbed Scanner" Transportation Research Record, 1775, 36-43.
- Praul, M.F. (2016). "Quality Assurance and the Move to Performance Concrete Specifications." Presentation at the 11th International Conference on Concrete Pavements, San Antonio, TX, August 28-31, 2016. San Antonio, TX.
- Rupnow, T. and Icenogle, P. (2012). "Evaluation of Surface Resistivity Measurements as an Alternative to the Rapid Chloride Permeability Test for Quality Assurance and Acceptance." Transportation Research Record: Journal of the Transportation Research Board, 2290, 1, 30-37.
- Shilstone, J.M., Sr. and Shilstone J.M., Jr. (2002). Performance-Based Concrete Mixtures and Specifications for Today. *Concrete International*. 24(2), 80-83.

- Shilstone, J.M. (1990). "Concrete Mixture Optimization." Concrete international. 12(6). ACI Farmington Hills, MI. 33-39.
- Streeter, D. (2018). "QC/QA Implementation: NY." Presented at National Concrete Consortium, September 2018 meeting.
- Sutter, L., Moulzolf, G., and Masten, M., (2018). "Impact of Water/Cementitious-Based Concrete Mix Design Specification Changes on Concrete Pavement Quality." Report No. MN/RC 2018-25. Minnesota Department of Transportation, St. Paul, MN. July 2018.
- Taylor, P., Tennis, P., Obla, K., Ram, P., Van Dam, T. and Dylla, H. (2013). Durability of Concrete. Transportation Research Circular No. E-C171. TRB Committee AFN30. Transportation Research Board, Washington, DC.
- Taylor, P., Van Dam, T., Sutter, L., and Fick, G. (2019). "Integrated Materials and Construction Practices for Concrete Pavement: A State-of-the-Practice Manual." Second Edition. National Concrete Pavement Technology Center, Iowa State University, Ames, IA.
- Theilgard P. (2022). "Optimized Aggregate Gradation Concrete Mixtures with Cementitious Material Reduction" Masters Thesis, University of North Carolina at Charlotte, Charlotte, NC.

APPENDICES

FOR FINAL REPORT

**North Carolina Department of Transportation
Research Project No. 2020-13**

Durable and Sustainable Concrete Through Performance Engineered Concrete Mixtures

By

Tara L. Cavalline, Ph.D., P.E.
Associate Professor

Brett Q. Tempest, Ph.D., P.E.
Associate Professor

Peter Theilgard
Graduate Research Assistant

David Alex Dillworth
Graduate Research Assistant

Joseph OCampo
Graduate Research Assistant

University of North Carolina at Charlotte
9201 University City Boulevard
Charlotte, NC 28223

February 2023

APPENDIX A – LITERATURE REVIEW AND REFERENCES

A.1 Introduction

The quality of a concrete mixture's cementitious materials, aggregates, and the bond created between the materials directly impacts the quality of the concrete (Wilson and Tennis 2021). Specifications from multiple agencies have been written to help mitigate risks of choosing inadequate materials such as ASTM, AASHTO, and ACI. State agencies choose from these specifications according to their needs for particular applications. Mixture proportioning is the process of selecting the materials and appropriate proportions to be used in a concrete mixture to meet the requirements (air content, workability, compressive strength, and other characteristics) established by the concrete design (Mehta and Monteiro 2014). Concrete mixture design and proportioning is typically performed with the intent of simultaneously meeting several goals, including strength, durability, economy, and sustainability, described in the following sections.

A.1.1 Strength

The strength of a material is defined as “the ability to resist stress without failure” (Mehta and Monteiro 2014). Historically, concrete mixtures have been proportioned based upon a stakeholder's previous experience, using available materials that were subject to extensive variability (Dolen 2008). Development of mixture design protocols and material quality control procedures have resulted in great improvements in concrete quality over the past century. In 1918, Duff Abrams established a relationship between the water-cement ratio (w/cm) and compressive strength, a characteristic of concrete mixtures that is still critical to the control of quality today (Abrams 1918). Current mixture designs are more technical and practical than in the early 1900s and incorporate specifications to maximize the strength and durability of the mixture. The most widely used mixture proportioning standard is ACI 211.1, “Standard Practice for Selecting Proportions for Normal, Heavyweight, and Mass Concrete” (ACI 2002).

The quality of a concrete mixture has traditionally been evaluated through its compressive strength. It is imperative that a concrete mixture used for a structure or pavement have adequate strength to meet the design criteria. However, it is recognized that in aggressive environments, concrete strength is not as reliable an indicator of durability as permeability and other durability performance characteristics (Armaghani et al. 1992). Most DOTs have specifications that require more cementitious material than would be required to meet design strength. Excess cement quantities can result in adverse durability effects (Taylor et al. 2019). Although responsible for strength gain, the cementitious content of a concrete mixture is also responsible for other undesirable characteristics, including heat generation during curing and shrinkage. Additionally, higher cement paste renders the concrete more permeable to water carrying aggressive agents such as chlorides and sulfates (Mehta and Monteiro 2014).

To reduce the cementitious material required in concrete mixtures, some state agencies are moving towards using optimized aggregate gradations that reduce the paste content of a mixture by improving the particle packing. These mixtures have been shown to provide adequate strength, workability, and can, in some cases, improve the mixture's durability performance. There are many different computational mixture proportioning methods currently available, all aimed at allowing the designer to determine the best combination of materials to maximize the particle packing density and reducing the voids (Jones 2002). The most commonly used methods to optimize aggregate gradations in concrete mixtures will be discussed subsequently in this literature review.

Water is required in concrete mixtures to hydrate the cement. A challenge facing optimized mixture designs is how to reduce the cementitious material while holding the w/cm ratio constant without adversely impacting the workability of the mixture. To be able to achieve the low w/cm ratios desired for strength and durability properties, the use of water reducing admixtures (WRA) is often required. Control of the water content of concrete mixtures is critical to achieving both the desired mechanical properties and durability performance (Taylor et al. 2019).

A.1.2 Durability

While concrete mixture designs must meet their prescriptive requirements for characteristics such as required compressive strength, the concrete's durability performance ultimately determines the potential life span of the concrete structure or pavement. Durability is not a singular material characteristic of concrete, but rather “a series of properties required for the particular environment to which concrete will be exposed to during its service life” (Taylor et al 2013). In its circular, TRB's Standing Committee on Concrete Durability indicated the primary concrete characteristics that define durability are: 1) resistance to freeze thaw cycles, 2) compressive strength of at least 4,000 psi, 3) resistance to effects of alkali-silica reaction (ASR) and/or sulfate attack, 4) resistance from damage by abrasion, and 5) resistance from damage from steel corrosion (Taylor et al. 2013). These criteria are similar to the ones identified by the American Concrete Institute

(ACI) in 201.2R-16 Guide to Durable Concrete, which identifies mass transport, freeze thaw cycles, alkali-aggregate reaction, sulfate attack, chemical attack, corrosion of metals or materials embedded in the concrete, and abrasion as major contributing factors that can limit a concrete's lifespan by impacting its durability (ACI 2016). Many of these factors can be attributed to the climate in which the concrete is in service, exposure conditions such as moisture and aggressive agents, and how the environment will interact with the material.

ACI 318's Chapter 19 is designated to address durability concerns for structural concrete, and how the risks can be mitigated with required maximum w/cm ratios, compressive strength, and air content (ACI 2019). Similarly, AASHTO PP 84 focuses on concrete pavements, allowing for state highway departments to select criteria that they know from professional experience to have an impact on the durability of concrete in their state. Although initially developed to support use in concrete pavement application, the approach prescribed by AASHTO PP 84 and many provisions can be adapted to structural concrete mixtures as well (Cavalline et al. 2020a).

Producing durable concrete that provides adequate performance in a given service environment requires consideration of a variety of material and mixture characteristics to minimize the risk of chemical attacks by deleterious substances in the materials used. Aggregates typically comprise up to 60-75 percent by volume of a concrete mixture and must possess the qualities required to withstand the loading and environmental exposure the concrete mixture will face in its service life (Wilson and Tennis 2021). Studies have shown that using an optimized aggregate gradation can allow for an increase in aggregate content while reducing the paste content, minimizing chemical reactions, and increasing dimensional stability (Taylor et al. 2013). Aggregates selected for a concrete mixture should be non-reactive, meaning they are resistant to alkali-silica reaction (ASR). Typically, aggregates are prequalified for use, using testing standards to determine the potential reactivity through ASTM and AASHTO standardized methods, such as ASTM C1293, "Standard Test Method for Determination of Length Change of Concrete due to Alkali-Silica Reaction (Concrete Prism Test)," and ASTM C1260 (AASHTO T 303), "Potential Alkali-Reactivity of Aggregates (Mortar-Bar Method)." ASTM C1293 is a more accurate but longer (one year) test, while ASTM C1260 is an accelerated (16 day test) but less accurate method (Wilson and Tennis 2021).

Since most aggregates used in concrete mixtures are dense and virtually impermeable, water and other liquids move through the hardened concrete's paste. The area within a concrete mixture where the aggregates and cementitious materials form a bond is called the interfacial transition zone (ITZ). The ITZ is generally considered as the strength limiting factor in the concrete and has the greatest influence on the elastic modulus of the concrete. It is a direct contributing cause to damage due to permeability-related attacks because of the presence of microcracks within the ITZ's structure (Mehta and Monteiro 2014). In addition to the type and amount of cementitious materials used in a mixture, several factors have an influence on the ITZ's properties. For example, the thickness of the ITZ increases with increasing w/c ratio and aggregate/cement ratio (Crumbie 1994) and longer mixing times may create more a pronounced ITZ (Katz et al. 1998, Leeman et al., 2005).

It is well known and accepted fact that concrete mixtures with lower w/cm ratios are less permeable and more durable than those with higher w/cm ratios. However, the cement type used affects concrete durability, as well as the type and amount of supplementary cementitious (SCM) materials used. To improve a mixture's durability, the cement type used should be resistant to sulfate attack while also having an adequate strength to resist damage due to abrasion (Taylor et al., 2013). SCMs such as fly ash, slag, metakaolin, or silica fume, may be used in a concrete mixture as a replacement for a certain percentage of cement. Some SCMs are used to increase economy, but most SCMs can also enhance a concrete mixture's durability properties if proportioned with the other materials in the mixture. One drawback of some commonly used SCMs, such as fly ash and slag, are that they may reduce the early strength of the concrete. Longer-term strength is often similar to or improved over mixtures without SCMs, and these SCMs provide the benefits of lower heat of hydration, a denser paste microstructure resistant to moisture and aggressive chemicals, and reduced shrinkage (Taylor et al., 2013).

Chemical admixtures, such as WRAs and air entraining admixtures (AEA), can also help to achieve desired properties in fresh and hardened concrete (Wilson and Tennis 2021). AEAs are used to entrain a matrix of air bubbles in the concrete mixture, helping to resist risks of damage due to freeze-thaw cycles. WRAs are used to reduce the w/cm ratio in a concrete mixture while maintaining the workability. Additionally, they can help to influence the rates of cement hydration and early strength development of concrete mixtures (Mehta and Monteiro, 2006). By reducing the w/cm ratio of a mixture through the use of WRAs, there is typically an increase in compressive strength development, and a decrease in susceptibility to chloride ion and sulfate penetration, although there is a possible increase in drying shrinkage (Wilson and Tennis 2021). WRAs function by influencing the electrostatic and steric repulsive forces of the cement by giving the particles a slight negative charge to repel one another and releasing the water reducing the viscosity of the concrete (Wilson and Tennis 2021).

A.1.3 Economy

The American Society of Civil Engineering's (ASCE) 2021 report on American infrastructure, reports that 7.5 percent of highway bridges were designated as structurally deficient, and the total percentage of bridge deck area that is designated as structurally deficient is 5.5 percent (ASCE 2021). While these numbers are an improvement relative to previous report cards, which designated 12.1 percent of highway bridges as structurally deficient in 2009 and 6.3 percent of total percentage of bridge deck area as structurally deficient in 2016, the annual rate of reduction of structurally deficient bridges has reduced to 0.1 percent with an increasing number of bridges moving from good-to-fair condition to "poor" condition (ASCE 2021). Repair, rehabilitation, maintenance, and replacement of these bridges, as well as our highway pavements, will require a significant investment in materials.

Our infrastructure is aging, and resources to repair, rehabilitate, and maintain its components are limited. A 2010 report to the Federal Highway Administration (FHWA), estimated that one 12-inch-thick lane-mile of concrete can require about 4,800 tons of material with 10 – 14 percent by volume being cementitious materials (Tayabji et al. 2010). Economic considerations have, and will continue to play, a role in development and use of concrete mixture designs for structures and pavements.

Typically, aggregates are the lowest cost component of a concrete mixture. The cost of cement, cementitious materials, and admixtures is often significantly higher. Using an estimate for cement and fly ash costs obtained from a paving contractor performing work for NCDOT, an assumed concrete depth of 11 inches, lane width of 11 feet, and an additional 15 percent for waste, reducing the cementitious materials in a concrete mixture by 10 percent would reduce the cost per lane mile by \$8,980 - \$10,567 depending on quantities of cement and fly ash used. These savings are displayed in Table A.1

Table A.1: Projected cost savings with 10% reduction in cementitious material

Original Cement Content (pcy)	Reduced 10% Cement Content (pcy)	Fly Ash Replacement (%)	Cost Savings (\$/CY)	Cost Savings per Lane Mile
700	630	0	\$ 4.66	\$ 10,567
560	504	20	\$ 4.19	\$ 9,501
650	585	0	\$ 4.32	\$ 9,796
520	468	20	\$ 3.89	\$ 8,821
600	540	0	\$ 3.99	\$ 9,048
480	432	20	\$ 3.59	\$ 8,141
420	378	30	\$ 3.96	\$ 8,980

Producing concrete that is economical is also sustainable, since using optimized concrete mixtures reduces the amount of portland cement which reduces the amount of CO₂ released. On average, the cement industry produces 0.92 tons of CO₂ for every ton of cement produced (Wilson and Tennis 2021). Using 0.92 pounds of CO₂ emitted per pound of cement produced, an assumed concrete depth of 11 inches, lane width of 11 feet, and an additional 15 percent for waste, CO₂ emissions associated with concrete mixtures could be reduced by 87,621 – 146,035 pounds per lane mile by reducing the cement used by 10 percent, depending on the mixture characteristics, shown in Table A.2

Table A.

Table A.2: CO₂ emission reduction per lane mile

Original Cement Content (pcy)	Reduced 10% Cement Content (pcy)	Fly Ash Replacement (%)	CO ₂ Emission Reduction (lbs/cy)	CO ₂ Emission Reduction per Lane Mile (lbs)
700	630	0	64.4	146,035
560	504	20	51.5	116,828
650	585	0	59.8	135,604
520	468	20	47.8	108,483
600	540	0	55.2	125,173
480	432	20	44.2	100,139
420	378	30	38.6	87,621

A.1.4 Sustainability

ASCE defines sustainability as “a set of economic, environmental, and social conditions in which all of society has the capacity and opportunity to maintain and improve its quality of life without degrading the quantity, quality, or the availability of economic, environmental, and social resources” (ASCE 2021). Concrete mixtures have a public perception that they are major contributor to the amount of carbon dioxide in the atmosphere. It was estimated in 2007, 1.5% of carbon dioxide (CO₂) generated in the United States resulted from the manufacture of portland cement, and that portland cement is responsible for 90 – 95 percent of CO₂ emission associated with concrete (Taylor and Van Dam 2009). However, advancements in cement production have greatly decreased these impacts (Van Dam et al. 2012).

Using SCMs such as fly ash or silica fume while utilizing optimized aggregate gradations can reduce the traditionally required amount of Portland cement in concrete mixtures, potentially improving fresh concrete performance and improving durability characteristics. Additionally, these materials are industrial byproducts, and beneficially reusing them in concrete saves landfill space and can provide other sustainability benefits associated with energy use, hauling, and water quality (Van Dam et al. 2012). Use of optimized aggregate gradations can also improve the sustainability of a mixture. Studies have shown the volume of paste in a concrete mixture is correlated with plastic shrinkage and cracking (Shaeles and Hover 1988, Darwin et al. 2004). By implementing the use of high quality SCMs in optimized aggregate gradation mixtures, the amount of portland cement used can be reduced, potentially improving permeability of the concrete while reducing plastic shrinkage (Van Dam et al. 2012).

There are emerging technologies in the concrete industry aimed at improving the sustainability of concrete mixtures. One of these technologies is the use of high-volume SCM/portland limestone cement paving mixtures to potentially reduce the greenhouse gas emissions significantly (Van Dam et al. 2012). Portland limestone cement (PLC) is a cementitious material that allows up to 15 percent limestone replacement of portland cement clinker per AASHTO M240 (AASHTO 2020). Using a PLC cement at that replacement level can reduce the CO₂ emissions by roughly 10 percent (Van Dam et al. 2012). Photocatalytic cements can be used to degrade pollutants like nitrogen oxides by as much as 60 percent (Van Dam et al. 2012). Low carbon and carbon sequestering cementitious systems, which sequester carbon dioxide as they harden, lowering the carbon footprint (Van Dam et al. 2012). Photocatalytic cement and carbon sequestering cementitious systems have promising results but require additional research to become viable options for large scale operations (Van Dam et al. 2012).

A.1.5 AASHTO PP 84 and R 101

AASHTO R101 (formerly AASHTO PP 84), “Developing Performance Engineered Concrete Pavement Mixtures” is a guidance document that allows DOT’s and other state transportation agencies to adopt tests and quality control measures described in the provision to best fit their needs. AASHTO PP 84 focuses on six primary characteristics that influence concrete performance. These characteristics are strength, susceptibility to slab warping and shrinkage cracking, freeze-thaw durability, transport properties, requirements for aggregate stability, and workability (AASHTO 2020). Depending on the exposure conditions and climate the concrete is likely to be subjected to, AASHTO PP 84 has recommended tests and performance targets for each characteristic that should be considered throughout the concrete’s lifespan, from mixture qualification testing to acceptance testing during and after construction.

A.1.5.1 Overview

AASHTO PP 84-20 outlines existing, alternative, and emerging methods to evaluate concrete performance for concrete pavement life in the range of 30 years, providing states DOTs with the ability to evaluate and choose which methods will work best for their climates and uses (AASHTO 2020). The aim of the document is to assist state agencies in moving from prescriptive specifications for concrete mixtures to performance specifications by implementing tests and quality assurance control measures to better understand the quality of a mixture for the specific climate and/or failure mechanisms it will be exposed to throughout its service life. Performance specification provisions should help ensure satisfactory performance of concrete in the fresh and hardened state, and therefore support implementation of Performance Engineered Mixtures (PEMs) (Cackler et al. 2017).

The movement towards PEMs does not mean that state highway departments will abandon the specification provisions that they have been using. In fact, many of the requirements of performance engineered concrete outlined in AASHTO PP 84 are similar to requirements already in place with the NCDOT and are outlined in (AASHTO 2020, NCDOT 2018). Table A.3 provides prescriptive testing requirement recommendations from AASHTO PP 84.

Table A.3: AASHTO PP 84 prescriptive testing requirement suggestions

Test	AASHTO PP 84 Suggestion	NCDOT Requirement
Flexural Strength	600 psi at 28 days	650 psi at 28 days
Compressive Strength	4,000 psi at 28 days	4,500 psi at 28 days
Air Content	5 – 8%	5.0% ± 1.5%

The goal of moving towards performance specifications is to support agencies in amending and/or revising their specifications to help meet their design goals, as well as their durability and sustainability performance targets.

A.1.5.2 Strength Provisions

AASHTO PP 84 Section 6.3.1 recommends that concrete mixtures have a flexural design strength of 600 psi at 28 days using AASHTO T 97 “Standard Method of Test for Flexural Strength of Concrete” (AASHTO 2020). Section 6.3.2 states that concrete mixtures should achieve compressive strength of 4,000 psi at 28 days using AASHTO T 22 “Standard Method of Test for Compressive Strength of Cylindrical Concrete Specimens” (AASHTO 2020). Both sections 6.3.1 and 6.3.2 state that agencies may consider flexural strength and compressive strength either alone or in combination and acknowledges that it is not uncommon for agencies to have different target values at different ages (AASHTO 2020).

A.1.5.3 Durability Provisions

Section 6.4 of PP 84 “Susceptibility to Slab Warping and Shrinkage Cracking,” identifies the volume of paste in a mixture, unrestrained length change, and cracking potential as factors to be controlled to prevent damage from shrinkage or slab warping, recommending that only one be selected for project QC purposes (AASHTO 2020). One prescriptive approach is recommended in section 6.4. Section 6.4.1 states that if slab warping or drying shrinkage cracking is a concern, a maximum paste content of 25 percent should be allowed in a mixture. Alternatively, performance tests include measurement of the unrestrained length change (AASHTO 2020). AASHTO T 160 (harmonized with ASTM C157) is the test standard to be used for testing the unrestrained length change. In this test method, three 3-in x 3-in x 11-in specimens are tested and averaged, with 420 microstrain at 28 days as a target (AASHTO 2020).

Section 6.4.2 provides performance specifications for shrinkage cracking caused by water-related volume change if cracking is a concern (AASHTO 2020). Section 6.4.2.1 states that estimated cracking potential can be determined using a Restrained Ring Test, and that cracking tendency of restrained concrete can be estimated using T 334, “Standard Method of Test for Estimating the Cracking Tendency of Concrete,” or AASHTO T 363, “Standard Method of Test for Evaluating Stress Development and Cracking Potential due to Restrained Volume Change Using a Dual Ring Test.” Section 6.4.2.1.1 states cracking tendency estimated using AASHTO T 334 is to be tested without cracking before 180 days (AASHTO 2020). Section 6.4.2.1.2 states cracking tendency estimated using T 363 should have an average stress less than 60 percent of the splitting tensile strength when tested in the dual ring at the standard relative humidity and temperature in T 363 for 7 days (AASHTO 2020). Both methods are based on limits set for bridge decks and are considered conservative for pavement applications (AASHTO 2020). Cracking potential may also be estimated using numerical models as detailed in section 6.4.2.2, which states that the unrestrained volume change (determined using T 160) at 91 days should result in a probability of cracking of less than 5, 20, or 50 percent depending on the mixture design and application (AASHTO 2020).

The influence of freeze-thaw cycles on a concrete mixture’s durability is impacted by w/cm ratio, fresh air content, entrained air void system characteristics, time and duration of critical saturation, and presence of deicing solutions in joints (Li et al. 2012). Section 6.5.2 of AASHTO PP 84 provides recommended prescriptive specifications for w/cm ratio, air content, and Super Air Meter (SAM) to qualify concrete mixtures as freeze-thaw resistant (AASHTO 2020). Section 6.5.1.1 states the w/cm ratio of a mixture should not exceed 0.45 (AASHTO 2020). Section 6.5.1.2 states the air content should be within 5 to 8 percent, as determined using T 152 “Standard Method of Test for Air Content of Freshly Mixed Concrete by the Pressure Method,” T 196, “Standard Method of Test for Air Content of Freshly Mixed Concrete by the Volumetric Method,” or TP 118, “Standard Method of Test for Characterization of the Air-Void System of Freshly Mixed Concrete by the Sequential Pressure Method,” (AASHTO 2020). Section 6.5.1.3 states air content that is 4 percent or greater as determined in accordance with specifications listed in section 6.5.1.2, must have a SAM number less than or equal to 0.20 determined using TP 118 (AASHTO 2020). Section 7.1.2 provides construction acceptance requirements, stating a SAM number of 0.25 or lower may be accepted, a SAM number between 0.25 and 0.30 will require the concrete mixture to be modified, and a SAM number 0.30 and above will result in rejection (AASHTO 2020). Performance specifications for freeze-thaw durability are found in section 6.5.2.1, detailing “the properties of a mixture required to reach a critical

saturation at 30 years,” (AASHTO 2020). Section 6.5.3 details two prescriptive specifications for reducing joint damage due to deicing chemicals when CaCl_2 or MgCl_2 is used; either using a SCM to replace the cement with a mass of at least 30 percent or applying a topical sealer in accordance with M 224, “Standard Specification for Use of Protective Sealers for Portland Cement Concrete,” (AASHTO 2020).

Transport properties refer to the ability of ions and fluids to move through the material, potentially damaging the concrete and/or steel embedded in it. AASHTO PP 84 recommends that the w/cm ratio, formation factor, and the penetration of ionic species in concrete be used as key indicators of transport properties influencing a concrete mixtures durability (AASHTO 2020). Prescriptive specifications for transport properties are in Section 6.6.1. Section 6.1.1 states that the w/cm ratio shall be less than 0.50 if the concrete mixture is not subjected to freeze-thaw cycles or deicing applications, and less than 0.45 if the concrete mixture is subjected to freeze-thaw cycles or deicing applications (AASHTO 2020). The performance specification for a transport related property states that the formation factor will be determined and used in the determination of a service life (AASHTO 2020). The formation factor is determined by dividing the resistivity at 91 days according to TP 119-15, “Standard Method of Test for Electrical Resistivity of a Concrete Cylinder Tested in a Uniaxial Resistance Test,” with conditioning option A by a pore solution resistivity of $0.127 \text{ k } \Omega$. Section 6.6.1.2 states that the formation factor (F factor) must be greater than 500 if the concrete mixture is not subjected to freeze-thaw cycles or deicing applications and must be greater than 1000 if the concrete mixture is subjected to freeze-thaw cycles or deicing applications (AASHTO 2020).

These specifications have been provided in Table A.2 and show both prescriptive and performance specifications of AASHTO PP 84, with performance specifications highlighted in green.

Table A.2: AASHTO PP 84 prescriptive and performance requirements

AASHTO PP 84 Section	Provision	Specification
6.3	Flexural Strength	600 psi at 28 days
	Compressive Strength	4,000 psi at 28 days
6.4	Susceptibility to Slab Warping and Shrinkage Cracking (choose one)	Volume of paste shall not exceed 25%
		Unrestrained length change less than 420 microstrain at 28 days
		Estimated cracking tendency estimated using T 334
		Estimated cracking tendency estimated using T 363
6.5	Freeze-Thaw Durability	Maximum w/cm ratio of 0.45
		Air content between 5 - 8%
		Air content greater than 4% and a SAM number less than 0.20
		Model calculations that show a mixture will reach critical saturation at 30 years
6.6	Transport Properties (choose one)	w/cm less than 0.50 if concrete is not subjected to freezing and thawing or deicer application
		w/cm less than 0.45 if concrete is not subjected to freezing and thawing or deicer application
		Formation Factor greater than 500 if concrete is not subjected to freezing and thawing or deicer application
		Formation Factor greater than 1000 if concrete is not subjected to freezing and thawing or deicer application

A.2 Optimized Aggregate Gradations (Material Supporting Chapter 3)

Historically, concrete mixtures consist of two aggregate gradation types: a fine aggregate and coarse aggregate. Optimized aggregate gradations (also known as “optimized gradations”) generally require the presence of at least three or more aggregate gradation types (often a fine aggregate, a mid-size aggregate, and a coarse aggregate) to maximize the packing potential in the mixture. By maximizing the packing potential of aggregates in a mixture, the amount of cement paste used can be minimized to the amount needed to meet workability requirements of the mixture (Lindquist et al. 2015). Studies have shown that optimized aggregate gradation mixtures can have the same or improved workability and finishability with reduced particle segregation during vibration (Cramer et al. 1995).

A.2.1 Particle Packing

Optimized aggregate gradations seek to maximize the particle packing of the aggregates, in turn reducing the aggregate voids in a concrete mixture. To reduce voids, models have been developed in order attempt to maximize the packing density, or the ratio of the solid volume of the aggregates in a concrete mixture to the volume of the concrete

mixture itself (Mangulkar and Jamkar 2013). Packing density models assume that voids between larger aggregates will be filled by smaller aggregates (Mangulkar and Jamkar 2013). There are different types of models that attempt to maximize the packing density, but these models can generally be grouped into discrete and continuous models.

Discrete particle packing models examine two or more unique particle sizes, where the voids from the largest particles are filled by smaller particles (Kumar and Santhanam 2003). Discrete models may be classified as binary, which assumes the ideal packing of two particle sizes, ternary, which assumes the ideal particle packing of three particle sizes, or multimodal. (Kumar and Santhanam 2003). Continuous models assume all possible sizes are in the particle distribution system with no gaps between particle sizes (Kumar and Santhanam 2003).

Most particle packing models assume that the particles are spherical. However, studies have shown shape factor and convexity of the aggregate are the most important geometric factors, while mean size, specific gravity, and the voids ratio of the aggregate are the most important size parameters influencing the packing of the aggregate (Mangulkar and Jamkar 2013). Historically, concrete mixtures have used two aggregate types (coarse and fine) in a blended mixture. This combination has been shown to produce voids that are larger than necessary, which require more cementitious material to fill than mixtures with less voids. Particle packing methods and other methods that seek to optimize aggregate gradations, are an attempt to minimize the voids remaining in aggregate gradations, and to reduce the cementitious material by introducing one or more intermediate size aggregates that will fill voids left by traditional aggregate combination gradations.

A.2.2 Aggregate Gradation Methods

The aggregate gradation(s) selected for use in a mixture depends on a variety of factors, including the element thickness, reinforcing details, required workability, and available aggregate types and gradations. A wide range of aggregate gradations have been used in different concrete applications. However, historically only one coarse and one fine aggregate, have typically been used in a mixture design, with the gradation of each considered separately (not combined and evaluated with the design process). Coarse aggregates consist of one aggregate type with particles predominantly larger than 0.2 in, and fine aggregates consist of natural sand or crushed stone with particles smaller than 0.2 in. ASTM C 33 is a standard written to ensure aggregates meet specified grading requirements, sourcing requirements, and limits on the amount of deleterious substances allowable in both fine and coarse aggregate (ASTM 2018). An aggregate gradation can be determined by performing a sieve analysis (ASTM C 136) on a representative sample. The results of the gradation analysis are used to understand the sizes of aggregates contained in a certain supply of material. Results are expressed as a percent retained on a sieve or percent passing a sieve, and then are compared to predetermined aggregate size numbers and their percentages passing each sieve in ASTM C 33 (ASTM 2018, ASTM 2020).

Gradations can be considered to be uniformly graded, well graded, or gap-graded. Essentially, concrete mixtures that historically use a single coarse aggregate and a single fine aggregate function as “gap-graded” combined aggregate gradations. Gap-gradations contain a relatively small percent retained on the mid-size sieves, theoretically allowing larger voids between the larger aggregates to be filled by the much smaller aggregates. Gap-graded mixtures could achieve desired workability levels, however, would require more cementitious material to achieve the workability due to the larger surface area of the smaller-sized aggregates. In addition, gap-graded combined aggregate gradations have proved to have problems with edge slump, segregation during vibration, and wear resistance (Richardson 2005).

Well-graded, or dense aggregate gradations, are typically desirable for concrete mixtures because they reduce the volume of voids between aggregates. Well-graded aggregate gradations aim at maximizing the density of the gradation by maintaining a similar percentage of aggregates being retained on each sieve to minimize voids between aggregates. By minimizing the voids between the aggregates in the concrete mixtures, there is also a decreased amount of paste (and therefore total cementitious content) required to fill gaps between the aggregate within the concrete mixture (Obla et al. 2007). Dense aggregate gradations were originally developed by Fuller and Thompson in the early 1900’s. However, studies suggested maximum aggregate methods may not always provide the maximum strength or density of a concrete mixture, and that they produced mixtures that contained too little paste and were difficult to place (Wig et al. 1916, Talbot and Richart 1923, Richardson 2005).

Several approaches were developed to help optimize aggregate gradations and improve concrete performance. The Power 0.45 Curve gradation approach (Figure A.1) aims to identify an aggregate gradation that will maximize the density of the mixture by plotting the cumulative percent passing of sieve sizes to the 0.45 power (Kennedy et al. 1994). A gradation that creates a straight line on the Power 0.45 Chart between the smallest particle size and the largest particle size will create a gradation with the highest density and minimize the voids in a mixture. Although this method has provided success for some, there have also been studies that show this is not possible for particles smaller than the #30 sieve, and this method can create workability issues (Ley and Cook 2014).

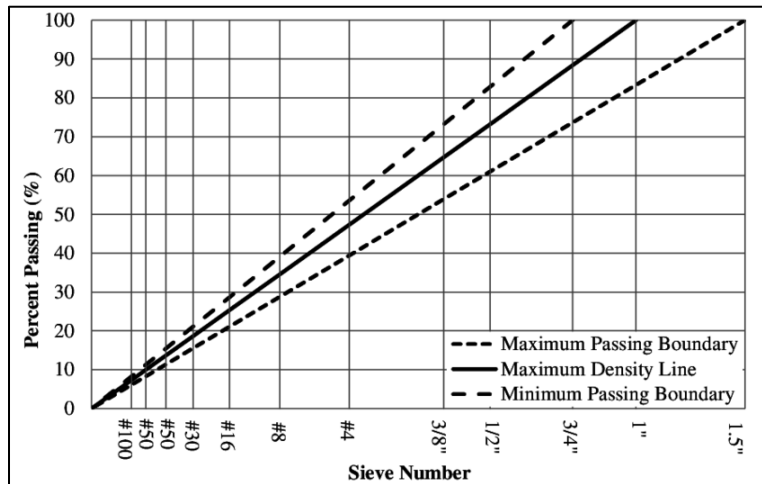


Figure A.1: Power 0.45 curve (Ley and Cook 2014)

The Coarseness factor chart (also known as the Shilstone Chart, the Workability Chart) was developed by James Shilstone, and is an empirical approach on reducing segregation in mixtures (Shilstone 2002). This chart plots the workability factor, indicative of the amount of sand and cementitious material in a mixture, on the x-axis versus the coarseness factor, the ratio of large to intermediate aggregate, on the y-axis. The plot is segmented into 5 zones shown in Figure A.2. The equations supporting the use of the Workability Factor chart are shown as Equations A.1 and A.2.

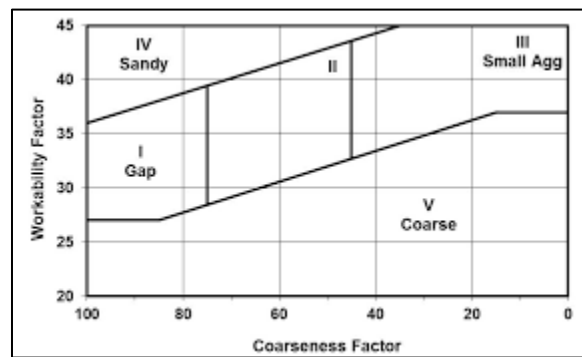


Figure A.2: Coarseness factor chart

$$\text{Workability factor} = P + \frac{2.5 * (M - 564)}{94} \quad \text{Equation A.1}$$

$$\text{Coarseness factor} = \frac{R}{S} * 100 \quad \text{Equation A.2}$$

$$P = \text{cululative percent passing the number 8 sieve} \quad \text{Equation A.3}$$

$$M = \text{cementitious material content} \left(\frac{\text{lb}}{\text{yd}^3} \right) \quad \text{Equation A.4}$$

$$R = \text{cumulative percent retained on the } \frac{3}{8} \text{'' sieve} \quad \text{Equation A.5}$$

$$S = \text{culative percent retained on the number 8 sieve} \quad \text{Equation A.6}$$

Zone II is the desirable area on the chart, indicating a well-graded design for a concrete mixture. Zone I indicates aggregate blends that are gap-graded, and include little amounts of intermediate aggregate – these blends result in mixtures that tend to segregate during placement. Zone III also indicates aggregate blends that are gap-graded but have very little coarse aggregate. Zone IV indicates aggregate blends that contain a large amount of sand and can be expected to have low strength and segregate during vibration. Zone V is indicative of aggregate blends that are heavy in coarse aggregates and can be considered “very rocky” (Shilstone 2002).

The 8-18 Band Gradation, an aggregate gradation recommendation that is typically credited to Holland, requires the total percentage of fine and coarse aggregate retained on any sieve to be between 8 percent and 18 percent to prevent

gap-gradations and prevent gradations from being too coarse or fine (Holland 1990). There are different variations of the 8-18 Band Gradation published in literature. For example in a subsequent revision, ACI 302.1R-96 “Guide for Concrete Floor and Slab Construction” section 5.4.3 recommended that smaller maximum size aggregate gradations (3/4 in or 1 in) have 8-22 percent retained on sieves ranging from the #100 – the maximum size aggregate (ACI 1996). In a subsequent revision, ACI 302.1R-15 has modified this in section 8.5.4, recommending a band gradation without setting particular limits requiring certain percentages to be retained on each sieve (ACI 2015).

A.2.3 Tarantula Curve

The Tarantula Curve was developed by researchers at Oklahoma State University, and is based on a modification to the 8-18 band gradation chart (Cook et al. 2013). It was developed by using five different aggregate types from different quarries in Oklahoma, designing mixtures with a constant w/cm ratio, and creating specific gradations to investigate the impacts of varying amounts of aggregates retained on each sieve. Proportions were identified based on three points of the Coarseness Factor chart (Shilstone Chart), one point in the middle of zone II, one point on the border of zone II and V in between zones I and II, and one point on the border of zone I and II in between zones IV and V (Cook et al. 2013).

To determine the sieve limits required for coarse aggregates, the gradation of sand was held constant while varying the amounts retained on each sieve and charting the amount of WRA required to pass the Box Test, which is indicative of the workability of the mixture (Cook et al. 2013). It was determined that when intermediate or coarse aggregate retained on a single or multiple sieves became excessive, the amounts of WRA required to achieve the desired workability increased drastically, indicating the mixture had poor workability. Ultimately, it was determined that coarse and intermediate aggregates should be limited to 20 percent retained for sieves #4 – 3/8 inch. Additionally, the gradation with the lowest intermediate aggregate retained and highest coarse aggregate retained required the most WRA and had segregation and edge slumping issues (Cook et al. 2013).

The impact of gap-gradation was investigated using mixtures with varying amounts of intermediate and coarse aggregate, while maintaining a constant volume and gradation of sand (Cook et al. 2013). A minor gap created on the 3/8 inch sieve and found to help the user achieve the desired workability with a typical amount of WRA. The gap moved from the 3/8 inch sieve to the #4 sieve. A gap on the #4 sieve achieved the desired workability with no added WRA, but was deemed to be on a borderline of acceptable due to the lack of required WRA. The aggregate size fractions were then redistributed to the 3/8 inch and 1/2 inch sieves, reducing the aggregate retained on the intermediate sieve sizes, causing a large increase in the required amount of WRA added to the mixture to achieve the desired workability (Cook et al. 2013).

Several aggregate gradations used in mixtures in the research study were designed to purposely contain low amounts of aggregate retained, or “valleys” which are thought to reduce workability. These were included in the study to explore their impact on a mixture’s workability (Cook et al. 2013). To understand the impact of valleys on the 3/8 inch sieve, gradations were created by varying the amount of aggregate retained on the 3/8 inch sieve between 0 – 15 percent while restricting the aggregate retained on all other sieves to less 20 percent, as previously discussed. The results of these mixtures showed a single valley did not negatively affect the workability of a mixture and did not require an excessive amount of WRA to attain the desired workability. Valleys were further studied by creating three aggregate gradations with troughs on the #4 and 3/4 inch sieves, and a valley on the 3/8 inch sieve. The mixture with the largest amount of aggregate retained on the #4 and 3/4 inch sieve and no aggregate retained on the 3/8 inch and 1/2 inch sieves required a jump in the required WRA to achieve desired workability. The results of studying valley gradations demonstrated that mixtures perform satisfactorily as long as a single sieve does not retain too much aggregate (Cook et al. 2013).

The impact of the maximum aggregate size on concrete workability was investigated by creating concrete using three gradations with a maximum aggregate size of 1/2 inch, 3/4 inch, and 1 inch, where no sieve retained more than 20 percent and had a similar volume of sand in each mixture (Cook et al. 2013). The mixture with the largest maximum aggregate size of 1 inch required the least amount of WRA to achieve desired workability. However, the difference in WRA required of all mixtures was not large enough to deem that the maximum aggregate size led to an improvement in workability. While the difference was not great enough to deem significant, it was noted that having a larger maximum aggregate size allows for an easier optimization of aggregate gradation, since it allows for a larger number of sieves to be used, effectively preventing any one sieve from retaining an excessive amount (Cook et al. 2013).

To determine the sieve limits for sand, coarse (#4 through #30 sieves) and fine (#30 through #200 sieves) sand were investigated separately, using the same method as with the coarse aggregates. The WRA required for concrete mixtures produced using different aggregate gradations to pass the Box Test were tracked (Cook et al. 2013). To investigate the sand limits for each sieve for coarse sand, mixtures were designed to investigate the impacts of varying amounts of aggregate retained on each sieve individually. Amounts of aggregate retained on the sieve being investigated varied between 0 percent and 12 percent retained. All sieves smaller were held constant in their percent retained, and coarse aggregates held as

constant as possible but requiring they be limited to the previously established maximum 20 percent retained per sieve. Using this method, a recommendation was developed that at least 15 percent of the aggregate should be retained on the #8 through #30 sieves to maximize workability (Cook et al. 2013).

To investigate the influence that fine sand has on the workability of a mixture, mixtures were designed to investigate the influence of varying amounts of aggregate retained on each individual sieve (Cook et al. 2013). Aggregate gradations were designed by holding 1 inch through #16 sieves consistent and investigating each sieve size individually by altering the percent retained on the sieve being investigated to determine how much WRA was required to produce a workable mixture. The recommendation for percent retained for fine sand, or sieves #30 - #200, is 24-34 percent retained, and the recommendation for percent retained for coarse sand, or sieves #8 - #30, is a minimum of 15 percent retained (Cook et al. 2013).

Ultimately, the research effort resulted in the development of a recommended framework for the combined gradation of aggregates. The recommended framework also includes guidance on what issues may occur if the gradation curve falls outside the framework. The Tarantula Curve does not provide a unique gradation aggregate gradation to optimize a concrete mixture. However, it provides range with multiple possible gradations to allow users to develop an optimized aggregate gradation. A figure of the framework (which resembles the shape of a Tarantula, spawning the name of the approach) can be found in Figure A.3 (Cook et al. 2013).

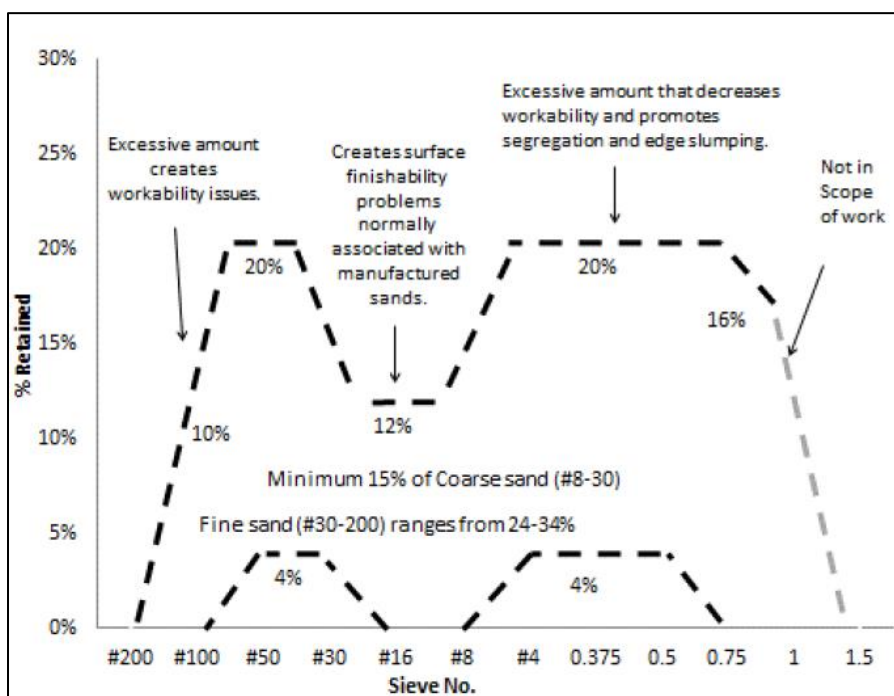


Figure A.3: Tarantula Curve (Cook et al. 2013)

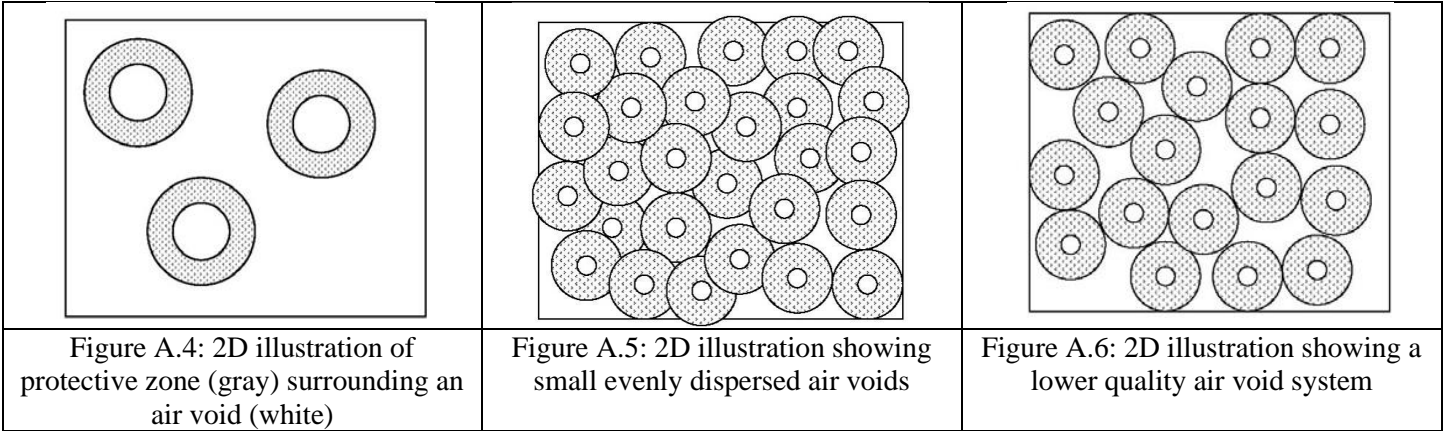
A.3 Freeze-Thaw Durable Concrete (Material Supporting Chapter 4)

A.3.1 Freeze-Thaw Stresses

The durability of concrete to freeze-thaw stresses will largely depend on what conditions it is subjected to, and this is no different for when it is being subjected to a freezing environment. Freezing environments can cause concrete to deteriorate in several different ways, but the most common deterioration method is cracking and spalling from being subjected multiple times to freezing conditions followed by a warm period that thaws the ice located within the concrete. The other deterioration methods that a freezing environment can produce are surface scaling when concrete freezes in the presence of deicing salts and D-cracking when the aggregates within the concrete crack, usually at edges and joints. These other methods will also be discussed in this document, however, when discussing freeze-thaw stresses in this document it will strictly be about cracking and spalling due to water freezing and thawing affecting the hardened paste of concrete (Mehta and Montiero 2006).

The current specifications from NCDOT require an air content of $5\% \pm 1.5\%$ in freshly mixed concrete for all concrete pavement and have an air content of $6\% \pm 1.5\%$ for all concrete that will be used for structures (NCDOT 2018). This specification has supported the construction of many concrete structures across North Carolina that have exhibited

adequate freeze-thaw performance for many years. However, the air content alone does not provide a strong correlation with adequate frost resistance, since the individual air voids still need to be dispersed within the paste closely enough to mitigate damage from water freezing within air voids contained within the paste. For a given total air content (volume %), attaining adequately close spacing between voids requires that the volume of air be dispersed in a network of many small, closely spaced air voids, rather than a network of larger, more distantly spaced air voids. For a given air content, a network of fine air voids will protect far more paste than a network of large, coarse air voids. Figures A.4, A.5, and A.6 illustrate the area of protection surrounding the air void as well as the differences between a well-developed air-void system and a poorly developed system.



Every concrete mixture includes air whether it was intentionally mixed into the concrete or was simply entrapped by the mixing process. Void space also exists in the network of pores contained in the paste. However, to resist freeze-thaw distress an appropriate air-void network requires the use of an air-entraining admixture to stabilize the smaller air voids and ensure they are not forced out of the (hydrated) cement paste by the act of mixing or placing the concrete. Entrained air voids are generally spherical and smaller than entrapped air voids which can be much larger and coarser (Hover 1993). Figure A.7 shows an enlarged view of the boundary between an air void and the other components that comprise the hardened cement paste system. These components are calcium silicate hydrate (CSH) gel, calcium hydroxide (CH), calcium sulfoaluminate, and capillary pores.

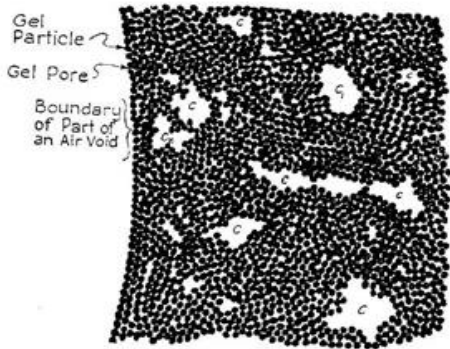


Figure A.7: Concrete microstructure (Tanesi and Meininger 2006 originally from Powers and Helmuth 1953)

The damage to concrete in freezing conditions comes not from the temperature but from the water held in the voids of the (hydrated) cement paste. This water contained within the cement paste will freeze within the air voids and exert stresses on the surrounding cement paste. This mechanical damage to the concrete caused by freezing water does not necessarily come from the water freezing within the concrete, but from the rate with which water is being expelled overloading what the concrete can handle. This is influenced by the rate of cooling, permeability, and degree of saturation of the concrete (Mehta and Montiero 2006). Out of these factors only the permeability can be influenced with the other factors being influenced by the environment that the concrete will be placed into.

Permeability not only controls the hydraulic pressure that comes about from the movement caused by water freezing within the concrete but also is the major factor affecting the critical saturation of the concrete (Mehta and Montiero, 2006). When the environmental temperature surrounding hardened concrete is below the threshold for water to freeze, freeze-thaw

damage to the concrete will not occur until the concrete hits the critical saturation level. This level is dependent on many factors. However, in the critical saturation theory that was proposed by Powers, the critical saturation level of cement paste is reached when the capillary pores of the cement paste are more than 91.7% full of water. This is based on the fact that water expands approximately 9% when frozen (Tanesi and Meininger 2006). Once the critical saturation level has been achieved the concrete will be damaged through the pressures developed by water freezing within the concrete.

The most accurate factor in determining the freeze-thaw resistance of a particular batch of concrete is the spacing factor as determined by ASTM C457 (Pigeon and Pleau 1995), which will be discussed in a subsequent section.

A.3.2 Deicing Salts

In the 1960's the United States started increasing the use of deicing salts to maintain clean roads after snowfall (Lilek 2017). This rapidly increased the amount of deicing salts that were being applied to the roadways. Figure A.8 shows graphically the increase in deicing salts used from 1940 to 2014 (Lilek 2017). This increase in roadway deicing is a cause of deterioration in the roadway due to the interaction between the concrete and the deicing salts within a freezing climate.

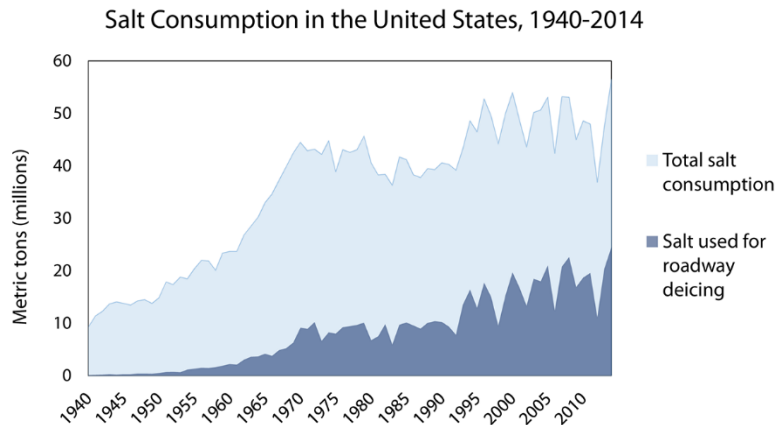


Figure A.8: Salt Consumption (US) (Lilek 2017)

A.3.3 Concrete Deterioration Due to Freeze-Thaw Stresses

The true mechanism behind freeze-thaw deterioration is not fully understood; however, there are several theories which may partially explain the forces and could also allow separate theories to work together to better explain the phenomenon (Pigeon and Pleau 1995).

A.3.3.1 Theories of Freeze-Thaw Stress Action

The first theory that will be discussed is Powers' hydraulic pressure theory. The next theory being discussed is the osmotic pressure theory put forth by Powers and Helmuth and expanded upon by Litvan to include the physics involved with supercooled water. The final theory this paper will go over is the ice lens growth. These three theories are perhaps the most complete and widely used theories explaining the mechanisms of frost damage in concrete.

A.3.3.1.1 Hydraulic Pressure Theory

The hydraulic pressure theory was developed by Powers in 1945 and further modified in 1949. This theory used a series of equations that related the air void spacing to properties of the cement paste and to the rate at which the temperature is decreasing. All of these equations are based upon the simple mechanism of freezing water expanding and forcing all non-frozen water out of the pore into the paste. Darcy's law of water flow through porous bodies is used to calculate how much pressure the expelled water will exert for the water to travel to the next open-air void.

$$\Delta h = \frac{\eta}{k} Q \frac{l}{A}$$

Equation A.7 Darcy's Law (pressure gradient)

Equation A.7 shows Darcy's Law as it is applied in Powers' hydraulic pressure theory where, Δh is the pressure gradient, η is the fluid viscosity, k is the permeability of the paste, Q is the flow rate, l is the length of the flow path, and A is the flow area (Tanesi and Meininger 2006).

It is this pressure exceeding the tensile strength of the paste that causes the internal cracking of the concrete. The pressure involved with the hydraulic pressure theory is increased through the distance the expelled water must travel to enter into the next air void and through an increase in the freezing rate (Pigeon and Pleau, 1995).

Powers would reconfigure Darcy's Law based on the flow length to create an equation for the maximum theoretical length of the flow path from one air void to another that would not cause the pressure gradient to be greater than the tensile strength of the cement paste. This maximum spacing between the air voids is called the spacing factor and is shown in Equation A.8 below (Tanesi and Meininger 2006).

$$l = \Delta h \frac{k A}{\eta Q}$$

Equation A.8: Spacing factor

A.3.3.1.2 Osmotic Pressure Theory

The hydraulic pressure theory could not explain every phenomenon that occurred within a sample that was undergoing freeze-thaw cycles such as the shrinkage that accompanies freezing concrete samples that have entrained air and some responses the samples had to the change in the rate of cooling they were undergoing (Powers and Helmuth 1953). While Powers and Helmuth saw evidence that the hydraulic pressure theory had a basis in reality, they also saw evidence that it was not the only phenomena that was causing all of the changes they had observed in the samples that were being tested. The theory they developed from their observations regarding the experimental results was that diffusion of water was occurring towards the freezing sites instead of water flowing away from the freezing sites.

A theory supplied by Litvan to supplement the osmotic pressure theory is based on the differences between supercooled water and ice particles. When adsorbed water (water that is held as a thin film on the outside of an internal material) is brought to below its freezing point cannot freeze without redistribution. Adsorbed supercooled water also cannot have freezing initiated by nucleation. These two properties cause the adsorbed water to remain as a liquid when the temperature falls below the freezing point of water. This causes there to be liquid water in the gel pores and ice outside which throws the system out of equilibrium because supercooled water has a higher vapor pressure than ice. Equilibrium is restored to the system by water being expelled out of the gel pore system so that it can freeze in the larger capillaries in the surrounding area. Further cooling of the concrete will cause more water to be expelled as the difference in vapor pressure is increased with a decreasing temperature (Litvan 1973).

A.3.3.1.3 Ice-Lens Model Theory

The ice-lens model or segregation ice model is a known principle cause of frost heave within soils (Peppin and Style 2013), however most of these models focus on a moving boundary and assume the matrix of the material to be infinitely rigid (Setzer 2001). The micro-ice-lens model created by Setzer was based on a shift in the triple-phase condition, a state where vapor, liquid, and solid water exist simultaneously in a stable condition, and a non-infinitely rigid system (Setzer 2001).

During the freezing stage the pore water will generate a negative pressure following the triple-point shift and the gel matrix will be compressed due to this negative pressure formed. This compression will cause the matrix to shrink in volume and to account for this decrease in volume water will flow out and into the ice forming in the air voids and capillary pores surrounding the gel matrix. If there is still space within the air voids surrounding the gel matrix then the degree of saturation will increase, and the micro-ice-lenses will grow without expansion of the pore. However, if a critical degree of saturation is reached the growth of the ice will cause damage to the pore further speeding up the transport of water to the ice lens forming (Setzer 2001).

During the thawing stage the pressure difference between water and ice starts to decrease with an increase in the temperature and the ice is transported back into water. This transformation back into water is a slower process than the transportation of water to ice that took place by the gel matrix squeezing out its water during the freezing phase. While the transportation of water from the micro-ice-lenses is not quick the gel matrix can be replenished by an external source if water is available through the much faster process of viscous flow. While thawing the micro-ice-lenses stay frozen within the pores keeping the saturation constant while the gel matrix increases in the degree of saturation if external water is available (Setzer, 2001).

A.3.4 Distress Mechanisms

There are two primary distress mechanisms that occur due to concrete freezing and thawing: internal cracking and surface scaling. Internal cracking is the more serious of the two as it can weaken the concrete significantly while not showing outward signs that the concrete is weakening. Surface scaling involves the surface layer of concrete flaking off which can lead to the ingress of water and other deleterious materials into the concrete.

A.3.4.1 Internal Cracking

The air-void system within the hardened concrete is an important factor when discussing deterioration due to the freeze-thaw cycle. The air-void system includes all of the air within the hardened concrete, this includes the microscopic and evenly shaped air voids as well as the much larger irregularly shaped air voids (Hover 2006). A properly established system of air voids within hardened concrete consists mainly of microscopic air voids that have been evenly dispersed throughout the mortar fraction of the mixture. According to Hover, an air-void system that will effectively provide frost resistance must have a total volume of empty air voids that is equal or exceeds the overflow volume of water or ice from the capillary pore system. Another factor that is just as important for frost resistance is how well dispersed the air voids are throughout the hardened cement paste. The exact requirements for volume, dispersion, and spacing of the air voids is dependent upon the environment the concrete will be placed in as well as the properties of the concrete.

This air-void system will generally increase the workability, cohesion, and frost resistance of the finished concrete product. However, this can influence the density and strength of the finished concrete by displacing some of the other components within the concrete and by creating a more porous cement paste.

Spacing factor is very important for internal micro cracking. The 0.008 in spacing factor that is generally accepted as durable is a conservative parameter and a spacing factor of up to 0.02 in could be considered durable with regard to internal cracking due to freeze-thaw cycles (Pigeon and Pleau 1995). Figure A.9 shows a visualization of how the space within real concrete is laid out along with a visualization of how a perfect air void spacing would look like. In the perfect version the space from each void is spaced such that any water being expelled from the capillary void system will have an empty air void to fill rather than increase the pressure exerted on the paste system (Hover 2006).

Spacing factor

$\frac{1}{2}$ of the average distance of an average sized void uniformly distributed in the paste

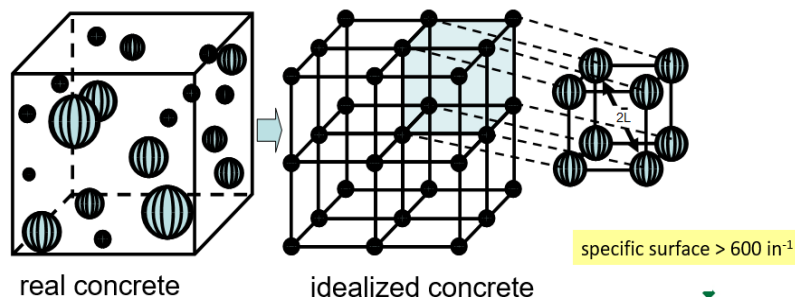


Figure A.9: Visualization of Spacing Factor (adapted from Ken Hover, Cornell)

A.3.4.2 Surface Scaling Due to Deicing Salts

Deicing salts affect the concrete in two ways: drawing water to the surface layer of the concrete surface and the leaching of $\text{Ca}(\text{OH})_2$. The suggested sequence of events for deicing salt damage is as follows. The deicing salt will melt the snow or ice that it comes into contact with while the surrounding ice and snow keeps the water pooled in that area. The melted ice and snow now have all of the deicing salts dissolved within it turning it into a salt solution which will lower the freezing point of the solution. This solution now gets absorbed into the surface layers of the concrete slab increasing the saturation level of the concrete. The ice surrounding the concrete slab will continue to melt diluting the salt solution within the concrete slab. This dilution will raise the temperature at which the solution can freeze until the solution freezes. This sequence of events can have as many or more freeze-thaw cycles when compared to a slab that has not been treated with deicing salts. Along with the freeze-thaw cycles caused by deicing salts there is a thermal shock that can occur in the subsurface concrete when the surface ice melts and extracts the latent heat of the concrete (Neville 2013).

A lower spacing factor is necessary to aid in creating a concrete that can resist surface scaling, although it alone is not sufficient to ensure that the concrete will be able to resist surface scaling (Pigeon and Pleau 1995). The lower spacing factor with regards to surface scaling is mostly due to the decrease in permeability the paste will have with a much smaller spacing factor.

A.3.5 Mitigation Strategies

The three most important factors concerning the prevention of frost damage are reducing freezable water, having a robust entrained air-void system, and proper design protocols. This thesis will only discuss ways to reduce freezable water and acquire a proper entrained air-void system as design protocols are not within the purview of this work. Reducing freezable water can be achieved by reducing the w/cm which will likely have the added benefits of a higher strength and lower permeability in the hardened concrete. In order to lower the w/cm and still maintain a proper workability supplementary cementitious materials and admixtures can be added that will increase the workability of the concrete without sacrificing the strength required (ACI 2016).

While reducing the amount of freezable water works to mitigate freeze-thaw damage the best way to mitigate freezing damage is to have a proper air-void network in the hardened concrete. A proper air-void network not only encompasses having enough air within the hardened paste to allow for any water within the concrete to flow to when in a freezing environment but also the quality and spacing of air voids involved. To achieve an entrained air-void system an air entraining admixture needs to be used to ensure that the air within the concrete is entrained and not entrapped air which does not help the concrete resist freezing damages (ACI 2016).

A.3.5.1 Concrete Permeability

According to Mehta and Montiero “Permeability is defined as the property that governs the rate of flow of a fluid into a porous solid.” The coefficient of permeability, simply called permeability in this paper, is governed by Darcy’s expression in Equation A.9 below:

$$\frac{dq}{dt} = K \frac{\Delta H A}{L \mu}$$

Equation A.9: Coefficient of permeability

Where dq/dt = rate of fluid flow

μ = viscosity of the fluid

ΔH = pressure gradient

A = surface area

L = thickness of the solid

In hardened cement paste, permeability is controlled indirectly by the mixing water used for the mixture as this determines the total space in the hardened cement paste once the mixing water has either hydrated the cement grains or evaporated out during the curing process. As concrete is a composite material the materials that are bound within the hardened cement paste will also affect the permeability of the concrete. Aggregates that are used in typical concrete mixtures will have a porosity, percentage of total volume that consists of voids, of 3 to rarely exceeding 10 percent whereas cement paste has a typical porosity of 30 to 40 percent. With such a difference in porosity it would be expected that the permeability of the aggregates would be much lower than that of the hardened cement paste, however that is often not the case. The reason for this is the size of the capillary pores in aggregates compared to the hardened cement paste, with the capillary pores in aggregates being much larger than those typically found in hardened cement paste. Table A.5 shows the permeability of some common types of rocks along with how that permeability compares to a matured cement paste (Mehta and Montiero 2006).

Table A.5: Comparison between the permeability of rocks and cement pastes (Mehta and Montiero 2006, originally from Powers 1958)

Type of Rock	Coefficient of permeability (cm/s)	Water-cement ratio of mature paste with the same coefficient of permeability
Dense trap	2.47×10^{-12}	0.38
Quartz diorite	8.24×10^{-12}	0.42
Marble	2.39×10^{-11}	0.48
Marble	5.77×10^{-10}	0.66
Granite	5.35×10^{-9}	0.70
Sandstone	1.23×10^{-8}	0.71
Granite	1.56×10^{-8}	0.71

As concrete continues to cure and produce more CSH and other products the porosity of the concrete will decrease. This decrease in porosity will also generally decrease the permeability with the capillary pores within the hardened paste becoming more disconnected overtime until every mixture that has a w/cm of 0.70 and under will eventually have a discontinuous pore structure. Table A.6 shows the time required for several w/cm to achieve a discontinuous pore structure along with the hydration that is needed during the curing process to achieve a discontinuous pore structure in these times (Hearn et al. 2006).

Table A.6: Time required to achieve a discontinuous pore structure (Powers et al. 1959)

w/cm ratio	Time required	Approximate degree of hydration required
0.40	3 days	0.50
0.45	7 days	0.60
0.50	14 days	0.70
0.60	6 months	0.95
0.70	1 year	1.00
>0.70	Impossible	>1.00

The freeze-thaw durability of a sample of concrete largely depends upon its level of saturation and whether its current saturation level is above its critical degree of saturation. The critical degree of saturation is the point at which a concrete sample will be damaged by the stresses generated by freezing. The degree of saturation can be seen expressed as Equation A.10. At a degree of saturation below the critical level there will be little to no frost damage if concrete freezes (Fagerlund 2004).

$$S = \frac{V_W}{V_P}$$

Equation A.10: Degree of saturation

where S = degree of saturation
 V_W = volume of evaporable water
 V_P = total pore volume

A.3.5.2 Air Entrainment

“Air is always present in concrete mixes. It is intentionally or unintentionally trapped in fresh concrete as a result of mixing and placing. About the only way to avoid trapping some air would be to mix, transport, and place concrete in a vacuum (Hover 1993).” As all concrete is not made in a vacuum the air that is mixed into a concrete mixture must be mixed in with precision and care to the final product.

Air entrainment first began by accident in the 1930s when some mills had been using beef tallow as a grinding aid when preparing cement. The cement used from these mills produced a less dense concrete that better survived the freezing and thawing cycles that the concrete was placed into (ACI 2012). Most common air entraining agents (AEA) act as a

surfactant, molecules that reduce the surface tension of the water, this allows the bubbles formed by mixing to become stabilized within the concrete (Neville 2013).

Air voids are put into two categories depending upon the size of the void with air voids larger than 0.04 in. (1 mm) being considered entrapped air and all voids smaller than 0.04in. (1 mm) being classified as entrained air. The amount and type of air voids is dependent upon many factors such as cement content and characteristics, coarse and fine aggregate size, w/cm ratio, SCMs used, chemical admixtures, and the characteristics of the water itself (Wilson and Tennis 2021). Along with those factors involved in the mixture design several production procedures and construction practices can also have a drastic effect on the air void system. The production factors include how the concrete is batched, the mixing time, speed, and capacity when compared to batched amount. The construction factors include transport and delivery, placement methods, finishing methods, and the environment during placement (Wilson and Tennis 2021).

When the air content of a concrete sample increases it causes the percentage of air voids that are filled to decrease, thus lowering the degree of saturation which will delay the sample from reaching a critical degree of saturation.

A.3.6 Tests to Evaluate Concrete Freeze-Thaw Durability

The current tests used to evaluate the freeze-thaw durability of a mixture have allowed for durable concrete to be made. However, these tests either provide a very loose correlation to durability or are expensive and take a long time to get results. The tests performed on fresh concrete currently only provide a total air amount and do not provide information about how the air-void system is physically established, which would provide a better look at how the hardened concrete might handle the stresses involved once it starts freezing and thawing in its environment. The tests run on hardened concrete provide a better correlation to the mixture's durability to the freeze-thaw cycle, however, these tests require hardened samples and take much longer to run the tests then the tests done to fresh concrete

A.3.6.1 Total Air Content of Fresh Concrete

There are three current ASTM approved tests to determine the air content of concrete while it is fresh: ASTM C138 (gravimetric method), ASTM C173 (volumetric method), and ASTM C231 (pressure method) (Concrete.org 2021). Table A.7 is based on earlier work done by Klieger which recommends an air content of 18 percent in the paste. These recommendations are based on using a Vinsol resin air-entraining admixture. These air content recommendations consider not only the exposure class that the concrete will be placed into but also the paste content of the concrete mixture and smaller nominal aggregate size will result in more paste content within the concrete mixture (ACI 2016).

Table A.7: Recommended air contents (ACI 2016)

Nominal maximum aggregate size, in. (mm)	Air content, percent	
	Exposure Class F1	Exposure Class F2 and F3
3/8 (9.5)	7	7.5
1/2 (12.5)	7	7
3/4 (19)	6.5	7
1 (25)	6.5	6.5
1-1/2 (37.5)	6	6.5
2 (50)	6	6
3 (75)	5	5.5

Research done by Felice et al. (2014) has shown that these air contents might be excessive with current modern air-entraining admixtures to achieve durable concrete mixtures. Concrete tested with modern AEAs were shown to be durable with a minimum air content of 3.5 percent when tested using ASTM C666/C666M. Research done by Ley et al. (2017) on mixtures that are identical except for one including a water reducer shows that the air content of fresh concrete does not line up with the spacing factor of both concrete mixtures. The mixture with only AEA had a linear trend that it would be under a spacing factor of 200 μm at around 4.5 percent air while the mixture with the water reducing admixture showed a linear trend of being under 200 μm at 7.5% air. Figure A.10 shows all of the data points used to acquire the linear trend and determine the estimated fresh air percentage to obtain an adequate spacing factor. This same shift between the two mixtures

was also observed when comparing the durability factor using the percentage of air within the fresh concrete (Ley et al. 2017).

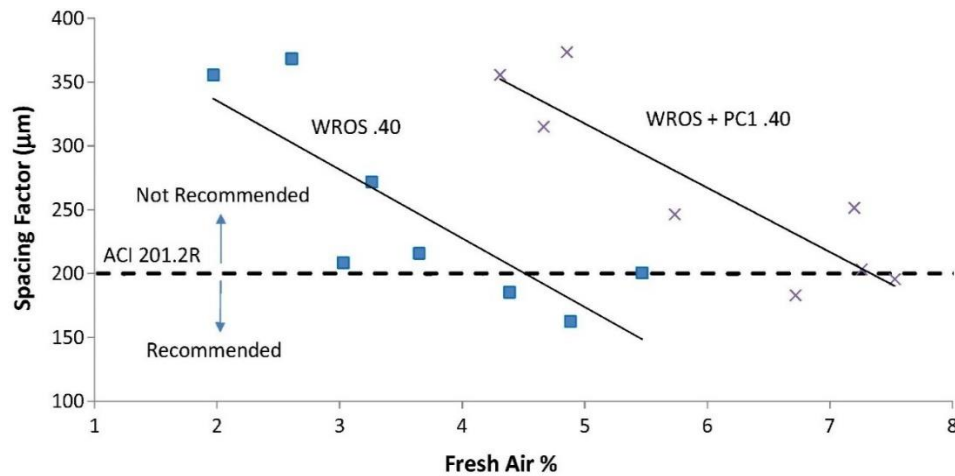


Figure A.10: Spacing factor vs. fresh air content (Ley et al. 2017)

A.3.6.2 Super Air Meter

While finding the air content in fresh concrete can provide a measure of understanding for how likely the concrete mixture will withstand the environment it will be placed in it cannot provide a measure of the quality of the air-void system. The Super Air Meter (SAM) uses a device similar to the ASTM C231 Type B pressure meter, however the Super Air Meter has six clamps to contain the increased pressure required during the test and a digital pressure gauge. Previous studies done by Ley and Tabb (2014), Ley et al. (2017), and Dabrowski et al. (2019) have found a correlation between the SAM number and factors that have been shown to affect the durability of concrete.

The SAM test goes through three pressurization steps (14.5 psi, 30 psi, and 45 psi) before allowing the chambers to depressurize and the pressurization steps are repeated to the same levels. This multi-step pressurization allows for the equilibrium pressure to be found for each run of pressurizations. The SAM number is the difference between the first and second pressurization's equilibrium pressure (Ley and Tabb 2014). When the SAM number was used instead of the percentage of air in the fresh concrete both mixtures used by Ley et al. had a better correlation between the SAM number and the spacing factor as show in Figure A.11. The durability factor created a similar graph when compared to the SAM number with both mixtures having a much closer trend line when compared to using the fresh air content (Ley et al. 2017).

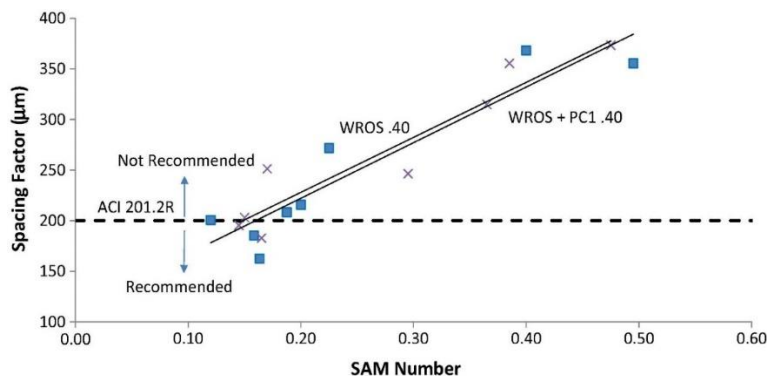


Figure A.11: Spacing factor vs. SAM number (Ley et al. 2017)

A correlation between the SAM number and spacing factor was then completed for 303 mixtures that came from both laboratory settings as well as field data all from the state of Oklahoma. From this data a SAM number of 0.20 was found to have the most data points fall at or below the spacing factor of 200 μm that is recommended to have the best chance of producing durable concrete in an environment that will undergo freezing and thawing. A SAM number of 0.20 was found to have approximately 88 percent of data points fall at or below 200 μm which is shown visually in Figure A.12 (Ley et al 2017).

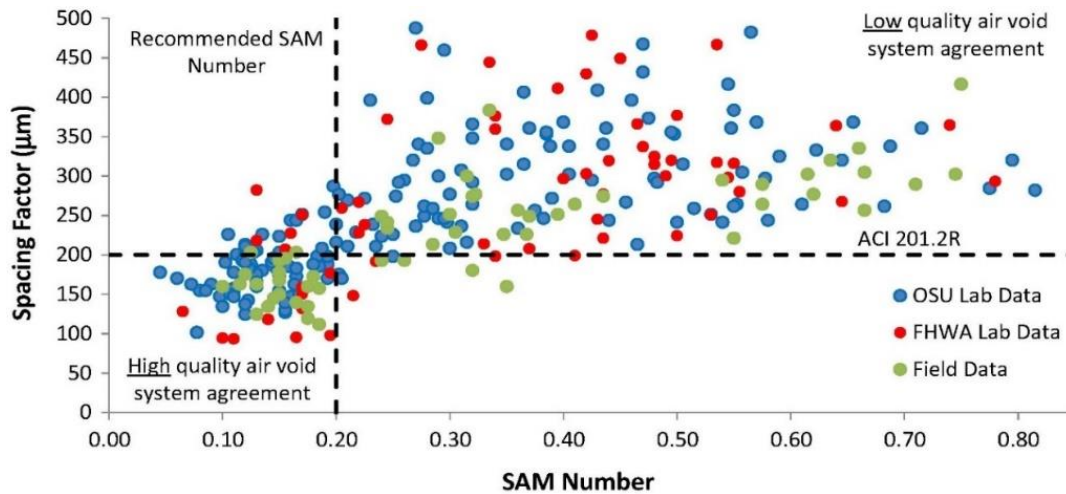


Figure A.12: Correlation for spacing factor vs SAM number (Ley et al. 2017)

When creating a correlation between the durability factor and SAM number Ley et al. chose a SAM number of 0.32 as it was accurate in the correlation for approximately 90 percent of the mixtures, and it was a more conservative choice over 0.35 which had nearly identical results (Ley et al. 2017). Figure A.13 details the durability factor of all of the chosen mixtures and compares their durability factor to the SAM number of the mixture. After a SAM number of 0.35 the durability factor of the chosen mixtures has a steep decline with almost none of the mixtures having a durability factor recommended for durable concrete (Ley et al 2017).

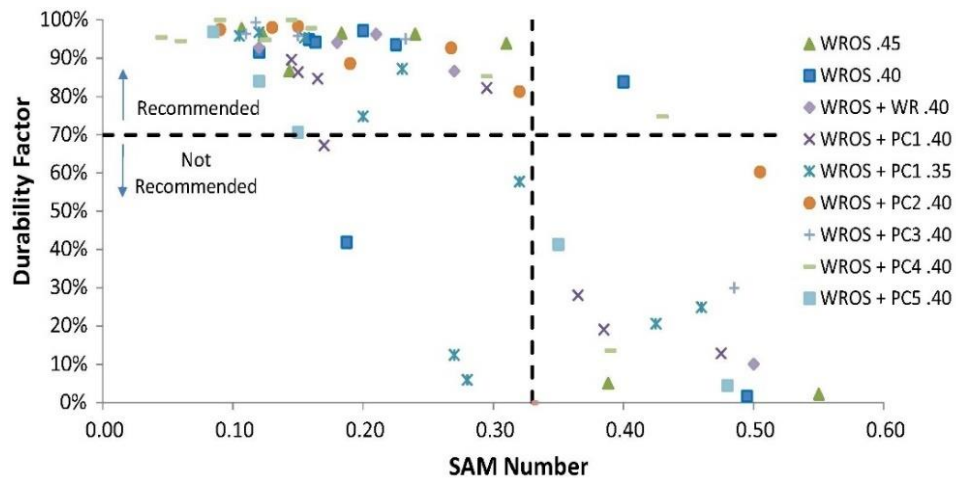


Figure A.13: Correlation for SAM number vs durability factor (Ley et al. 2017)

A.3.6.3 Freeze-Thaw Testing of Hardened Concrete

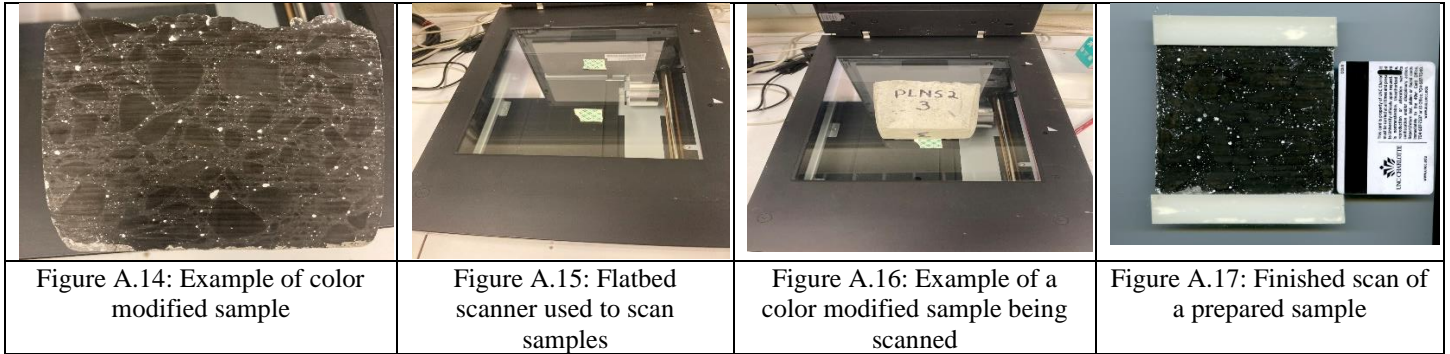
ASTM C666/C666M is currently and historically the definitive test used to determine the resistance to internal damage of concrete going through freeze-thaw cycles. While ASTM C672/C672M is used to evaluate the surface scaling resistance of a concrete mixture. ASTM C672/C672M relies on a visual inspection and numerical rating system and was not used within this study. Several researchers have criticized these tests for not providing an accurate look into what the actual conditions will be for the sample in its placed environment. This disconnects between field conditions and laboratory conditions necessitates heightened caution when using the results from these tests to determine the possible resistance of a particular concrete mixture to freeze-thaw damage (Hallet et al. 1991, ACI 2016).

A.3.6.4 Hardened Air Void System Analysis

Most of the generally accepted parameters to determine if a sample of concrete has an adequate air-void system come from the hardened air void analysis determined by ASTM C457/C457M (ACI 2016). ASTM C457/C457M can be used to determine the air content, paste content, void frequency, specific surface, spacing factor, and the paste-air ratio if desired. However, most often it is used to determine the hardened air content, spacing factor, and the specific surface in a concrete sample (ASTM 2016, ACI 2016).

There are several procedures that can be followed in ASTM C457/C457M to determine the parameters of the air-void system with this paper using Procedure C which is the contrast enhanced method using a flatbed scanner. This procedure was created by a team of researchers at Michigan Technological University as a way to automate determining the size distribution and volume fraction of air voids, which already had automated methods, along with the volume fraction of hardened cement paste (Peterson et al. 2001).

This procedure uses a number of hand-counted samples to provide a basis for the automated program to run off of to determine each component of the concrete sample accurately. The results from these hand-counted samples are used to create an optimization file for the software used. The software used for this study is called BubbleCounter which is based off of an open-source National Institute of Health (NIH) software program called ImageJ. The software works on samples that have been colored black and white to allow for easier contrast an example of which can be seen in Figure A.14. A black and white balance card is used to determine the intensity of the sections colored black and white. This will then be used to normalize the images so that the errors produced by slight variations in the scanning conditions can be reduced (BubbleCounter 2021). Figure A.15 shows an example of a flatbed scanner that can be used to analyze samples using Procedure C in ASTM C457. To protect the scanner from damage padded tape is placed on the scanning surface so that the sample is not in direct contact with the surface as seen in Figure A.16. An example of a scanned sample can be seen in Figure A.17.



Once the image has been normalized a section is chosen to be analyzed and the software will remove strips of pixels from the base image to comply with the point and length traversal requirements from ASTM C457. These strips taken from the base image are used to create a composite image that will then be analyzed by the program. Each pixel within the composite image is scanned and will be separated into either solid or air void depending upon values determined by calibrating the program using the hand counted samples (BubbleCounter 2021).

The formula used to determine the spacing factor is based on whether the paste-air ratio is greater than or less than or equal to 4.342. If greater than 4.342 the formula will be Equation A.11:

$$4.342L = \frac{3}{\alpha} \left[1.4 \left(1 + \frac{p}{A} \right)^{\frac{1}{3}} - 1 \right]$$

Equation A.11: Spacing factor for $p/A > 4.342$

where:

- L = Spacing Factor
- α = Specific Surface
- p = Paste Content, in %
- A = Air Content, in %

The formula used to determine the spacing factor if p/A is less than 4.342 is shown in Equation A.12:

$$4.342L = \frac{T_p}{4N}$$

Equation A.12: Spacing factor for $p/A < 4.342$

where:

L = Spacing Factor

T_p = traverse length through paste

N = total number of air voids intersected

All calculations and equations to determine the spacing factor have been laid out in ASTM C457 (ASTM, 2016).

A.3.7 Research Needs for Freeze-Thaw Durable Concrete in North Carolina

The durability of a concrete sample depends upon many different factors with the most important factor being the quality of the air-void system within the paste of the concrete. Historically there have been two primary ways to determine the likely durability of a concrete sample, ASTM C666 and ASTM C457. However, both of these tests are time consuming and can only be performed on hardened concrete samples after the concrete has already been placed and cured on site. Currently the only test performed on fresh concrete that is used to evaluate the possible durability of the concrete mixture is determining the total air content (volume %) within the mixture. As evidence from Ley et al. (2017) shows that the dispersion of this air is highly dependent upon the mixture itself. Only by evaluating the characteristics of this air void system (dispersion, coarseness) will actually provide an indication if the air void system of high enough quality to withstand the environment it will be placed in.

The Super Air Meter (and associated test method, AASHTO TP 118) have provided a reasonable means of testing fresh concrete to evaluate the air void system characteristics. Research has shown correlation with both the air void spacing factor and freeze-thaw durability tests via ASTM C666. However, the characteristics of an air void system and, ultimately, the performance of hardened concrete under freeze-thaw cycles depends on materials and mixture proportions, which vary across the country. In an effort to develop specifications for freeze-thaw durable concrete, many states have been performing work to determine the SAM number corresponding to adequate freeze-thaw performance via ASTM C666. North Carolina has not yet performed this work, which is the subject of this project.

A.4 Surface Resistivity for Use in Overlay Evaluation (Material Supporting Chapter 5)

A.4.1 Introduction

Critical transportation infrastructure components such as highway pavements and bridges experience harsh environmental and physical attack from freeze-thaw (F/T) cycles, deleterious chemicals, and vehicle traffic. Rather than replacing bridges that exhibit moderate to severe deterioration of the road surface, rehabilitation using concrete overlays is often the most economical approach to extend the useful life of a bridge. Concrete overlays are one strategy that can help to reduce the costs associated with maintenance and repair that state agencies would otherwise have to fund. Some of the rehabilitation objectives are to waterproof the road surface, repair cracks and spalled concrete, structural strengthening, replace visibly deteriorated concrete, and provide protection for corroded reinforcement (Haber et al. 2017). When concrete overlays are designed using an appropriate concrete mixture, installed properly, and proven curing methods are followed, they can extend a bridge's lifetime 30 years or more (Harrington and Fick 2014).

The Federal Highway Administration (FHWA) has estimated the cost of rehabilitating and replacing structurally deficient highway bridges throughout the U.S. to be near \$86 billion (FHWA 2019). The estimate includes bridges from the National Highway System (NHS) and non-NHS bridges. Due to the higher level of exposure, 50-85% of all expenditures for highway bridges go towards deck maintenance, repair, and replacement (Gucunski et al. 2010). That being said, the deck is often the first component of the bridge to be compromised. Visual inspection, the chain drag method, and hammer sounding have historically been the most commonly utilized non-destructive evaluation techniques utilized by state DOTs to detect the occurrence of deterioration and defects within the local medium of concrete pavements and bridge decks. Visual inspection and chain dragging are the initial inspection techniques to identify potential defects or delamination. Those areas are marked for further investigation (Gucunski et al. 2011).

A.4.2 Bridge Deck Overlays

Overlays can vary in thickness from 2-10 inches, or greater. There are two types of concrete overlays: bonded, which range from 2-4 in. thick, and unbonded, normally ranging from 6-10 in. thick. Bonded concrete overlays attach to the existing pavement or bridge deck and when in service act integrally as one monolithic slab, in the sense that the overlay becomes a part of the section thickness (Harrington and Fick 2014). The existing deck and overlay must behave monolithically in order to achieve the intended structural integrity. This will mitigate cracking due to the effects of loading and not compromise the durability and service-life requirements of the bridge (Lemieux et al. 2005). For a proper bond to be achieved, care must be given to surface preparation. These bonded overlays require that the existing surface be of sound material, either in-situ or after surface preparation. Alternatively, unbonded concrete overlays do not require that the existing pavement be free of deterioration, as the overlay does not rely on the existing material for to achieve the desired performance and structural capacity (Harrington and Fick 2014). For this research, bonded concrete overlays will be investigated as they are more suitable for bridge deck restoration projects.

NCDOT has completed an average of 25 overlays each year for the last five years using latex-modified concrete (LMC) or very early high strength (VHES) LMC mixtures (NCDOT 2018). Thorough testing of bridge deck concrete overlays must be further developed and employed to ensure that the quality at completion meets or exceeds specifications and guarantee that the overlay will last for the predicted duration.

A.4.3 General Overview and Design Considerations

When a bridge deck experiences excessive wear, corrosion, or deterioration, the application of an overlay is often used as the most cost-effective means to extend its useful life. Apart from a full replacement of the bridge deck, the unsound wearing surface can be removed by hydrodemolition, milling, and other techniques that leave the underlying steel reinforcement intact, and an overlay can be placed. These overlays are most commonly made of highly engineered mixtures which contain polymer admixtures to increase durability. For a specific bridge deck restoration need, there are a variety of bridge deck overlay solutions such as multi-layer polymer overlay, which restores skid value and seal cracks and concrete overlays. Concrete overlays can be used to match new surface profiles, add structural value, and provide chloride/corrosion protection (Beer 2018).

ElBatanouny (2012) explains that determining the optimum time for rehabilitating a bridge with one of these overlay methods will conserve the limited department maintenance resources. Bridge deck sealers are often used 3 to 6 months after construction but before any deicing salts have been applied. These sealers will generally provide an additional 5 years of service to the bridge deck. Polymer overlays are utilized on bridge decks that are in good to moderate condition and at a median age of 20 years. Polymer overlays provide additional cover for reinforcement and can increase the service life of a bridge deck 25 years. Polymer overlays not only increase the service life of the deck but also improve the skid resistance, appearance, and ride quality (ElBatanouny et al. 2017).

A.4.3.1 Materials

The selection of constituent materials and their proportions, along with mechanical and durability performance measures, is vital for the production of quality concrete structures. Class AA Concrete is commonly specified for the cast-in-place construction of each essential parts of a bridge (deck, beams, pile cap, barrier rails, end posts, etc.). The requirements for this class of concrete as defined by NCDOT in their Standard Specifications (2018) are as follows:

- Min. 28 day compressive strength: 4,500 psi
- Cement content range: 639-715 pcy
- Max. w/cm: 0.426 (angular aggregate, air-entrained)
- Max. Slump: 3.5 in.

The requirements for LMC mixtures as defined in the specification differ substantially, most notably the age requirement for compressive strength and slump. Those requirements are listed below:

- Min. 7 day compressive strength: 3,000 psi
- Min. cement content: 658 pcy
- Max. w/cm: 0.40
- Max. Slump: 6 in.

The objective of rehabilitating bridges is not only to restore them to their original condition, but often to exceed the standard specification at the time of former construction. The selection of proven concrete constituent materials intended to extend the bridge's useful life must be made with improved long-term durability performance in consideration. In addition to the variety of durability performance parameters, workability, shrinkage resistance, curing characteristics, and strength can be improved with informed material selection. Furthermore, overlay materials must be selected with thermal expansion

in consideration. To prevent cracking resulting from expansion and contraction, the concrete mixture of the overlay shall have an equal or lesser coefficient of thermal expansion than the existing concrete material (Harrington and Fick 2014).

A.4.3.1.1 Latex Admixtures

Performance concrete mixtures (PCM) containing polymer emulsion, or simply referred to as latex, offer improved durability protection from the infiltration of deleterious materials that may otherwise find its way to corrosion-sensitive reinforcement steel. Doty (2004) describes LMC as being composed of approximately 1 million-trillion tiny hydrophobic polymer beads that attach to all nonaqueous surfaces and infiltrate the existing microstructure of the hydrodemolished bridge deck. This phenomenon creates a waterproof coating once the overlay is fully hydrated. It is supposed that the water-resistant effect is accomplished by the act of the latex film creating a protective barrier to microcracks and the capillary pore structure within the concrete (Doty 2004).

By replacing part of the mixing water within an overlay mixture with a latex admixture, not only is workability greatly improved, but more importantly, durability is achieved by way of a virtually impermeable bridge deck (Mehta and Monteiro 2016). Mehta and Monteiro (2016) state that the LMC's ability to bond to existing concrete as another impressive characteristic which make it the essential admixture for bridge deck overlay rehabilitation projects, especially in corrosive environments. As a durability related measure, NCDOT typically uses latex admixtures in concrete mixtures for bridge deck overlays (NCDOT 2018).

LMC have been commercially available and utilized since the 50s, beginning with polyvinyl acetate (PVA) or polyvinylidene chloride (PVDC). However, those earlier products have widely been discontinued from concrete overlays due to low wet strength with PVA mixtures, and the suspicion of PVDC as being a leading cause of steel reinforcement corrosion (Mehta and Monteiro 2016). Therefore, styrene-butadiene rubber (SBR) is commonly preferred for LMC overlay materials, suitable for deck rehabilitation and occasionally new deck construction.

Assaad (2018) found that SBR latex admixtures increase the cohesiveness of the mixture which results in a reduction in flow velocity, passing ability, and reduction of bleeding and segregation. The findings determined that the compressive strength was increased due to the improved bond at the reinforcing steel-concrete and mortar-aggregate interfacial transition zone (ITZ). Further, the reduction of voids in the microstructure produced a concrete with a lower porosity than that of concretes without SBR latex admixtures (Assaad and Issa 2018). LMC also has improved ductility, abrasion and impact resistance, shear bond strength, tensile and flexural strength, and excellent freeze-thaw durability. Furthermore, some latexes provide resistance to acids, alkalis and organic solvents (Wilson and Tennis 2021).

As recommended by ACI Committee 584 (1992) and also required by NCDOT (2006), LMC mixtures shall have a minimum latex admixture content of 24.5 gal/cy and a maximum water content of 18.9 gal/cy. Also, it is imperative that latex materials be stored at moderate temperatures between 40-85° F to avoid freezing or excessive heat.

A.4.3.1.2 Cementitious Materials

In many cases, Type I/II portland cement is specified for bridge deck construction. This is a general-purpose hydraulic cement with moderate sulfate resistance due to its chemical composition. The selection of hydraulic cement has a significant influence on concrete properties due to the changes in matter and energy resulting from the chemical reaction that it has with the mixing water during hydration. In addition to cement selection, the proportional content of cement greatly affects the hydration process which affects setting time, durability and strength (Mehta and Monteiro 2014).

Rehabilitation effort of bridges and pavements require early stiffening of the concrete and a faster return to service; therefore, rapid hardening or Type III hydraulic cement is essential to producing VHES concrete which is often utilized for bridge deck concrete overlays.

A.4.3.1.3 Aggregate

Due to the fact that aggregates occupy the largest amount of space within a volume of concrete, typically between 60-75% by volume (70-85% by mass) and have a substantial impact on concrete's freshly mixed and hardened properties, as well as mixture proportions, the selection of quality fine and coarse aggregates is critical (Wilson and Tennis 2021). And since aggregates are relatively inexpensive, they are utilized as a filler material intended to minimize the volume of cementitious materials, resulting in a more economical concrete with a decreased paste content (Mehta and Monteiro 2014). Along with economy and improved long-term durability associated with a reduced paste content, constructability is also improved by the selection of the right aggregate characteristics which include grading, absorption, and proportions. No. 67 coarse aggregates (0.75 in. maximum size) have been widely used in conventional concrete for bridge decks. As concrete overlays can be as thin as 1 in., a smaller aggregate, No.78 (0.5" maximum size), is more functional. The aggregate

proportions in concrete overlay mixtures differ as well. NCDOT requires that the percent of fine aggregate as a percent of total aggregate by weight shall be between 50-55, assuming SSD condition (NCDOT 2018).

A.4.3.2 Construction Methods

The construction methods for installing a concrete overlay begins with the removal of unsound concrete, then the surface, including exposed reinforcement must be cleaned and prepared, then the overlay is batched and placed, and finally the overlay is cured. This general summary is detailed in the following sections.

A.4.3.2.1 Surface Demolition and Preparation Methods

Depending on the extent of deterioration, anticipated added service-life, and budget, there are two degrees of bridge deck surface demolition preparation for overlay installation: 1) with removal of existing concrete cover; or 2) without removal of existing concrete cover. The concrete cover can be completely removed to expose the reinforcement, and in situations where the concrete surrounding the reinforcement is unsound, that concrete shall be undermined to allow the reinforcement to be encased by the overlay concrete. If the reinforcement is found to be severely corroded and unsound, replacement is required. Hydrodemolition is often the primary method for removal of the unsound or deteriorated concrete cover when applying method 1 (Haber 2017). To secure the bond of the concrete overlay to exposed reinforcement, the concrete surrounding the reinforcing steel must be removed to a minimum clearance of ½ inch (TDOT 2014). Method 2 is followed when the removal of cover concrete is unnecessary. When this degree of surface demolition is selected, milling of the existing deck is utilized to provide a rough bondable interface appropriate for the overlay. On a single bridge deck overlay project, both methods can potentially be utilized on a case-by-case basis.

For both cases, hydrodemolition is preferred over milling or jackhammering because it leaves a clean, rough application surface, as well as undamaged and rust-free reinforcement. Another benefit of hydrodemolition is that it does not induce harmful microcracking of the remaining concrete (Lemieux et al. 2005). This demolition technique breaks down the concrete into gravel-sized pieces for removal without damaging the reinforcement. High-pressure hydrodemolition equipment can convey jets of water at 20-40 gal/min and with pressures of 10,000-35,000 psi. The precision of hydrodemolition equipment allows for concrete removal at depths ranging from 1/8 – 3 inches per pass. Demolition trials of sound and unsound concrete should be performed prior to starting the work to determine the necessary speed, pressure, and overlapping passes required to complete the demolition sufficiently. Once those parameters are determined, the equipment is calibrated, and the removal can begin (Bissonnette et al. 2012).

In construction environments where high chloride levels are present, epoxy-coated reinforcing bars will likely be present. If these bars become nicked or damaged, they must be recoated or touched up with an approved epoxy coating (McDonald 2011). Also, the rebar must be properly supported if dislodged.

The deck surface must remain wet with broomed mortar for the overlay placement but have no standing water or puddling. During minor delays, wet burlap can be used to protect the interface from drying, but delays shall not exceed 30 minutes (PennDOT 2019). Sprinkel (2000) explains that in order to achieve the highest possible bond strength and reach the expected useful life of the overlay, more attention should be directed to surface preparation, proficient placement, and sufficient cure time of the overlay.

A.4.3.2.2 Batching and Placement

The use of a mobile volumetric mixer is vital to producing these high-quality mix designs. Volumetric mixers allow for the contractor to mix onsite, directly within reach of the bridge deck. CemenTech (2019) states that volumetric mixers protect the integrity of the mix by reducing the age of the fresh concrete, reducing tempering water, and reducing segregation of the concrete caused by excessive drum revolutions. The minimum thickness of a latex-modified concrete overlay is 1 inch, not including the surface texturing depth. Concrete overlays shall not span across existing deck expansion joints and be sawcut, rather the overlay must have a discrete expansion joint constructed at the existing expansion joint (Beer 2018).

A.4.3.3 Challenges

Bridge decks sealed with epoxy resin or high molecular-weight methacrylate are sometimes overlaid with microsilica-modified, latex-modified, or super-dense plasticized concretes for complete overlay or repair jobs. The sealers are necessary for prevention of further chloride penetration into the deck, but when it is time for an overlay, the sealers should be removed. Gillum (2001) has found that when a sealer is present at the deck-overlay interface, the expected available bond strength is reduced more than 50%. The determination was made by the direct shear test, tension test, SHRP interfacial bond test, and flexural beam test. Gillum says that the bond strength can be secured if proper surface preparation techniques are implemented.

In an investigation on the behavior of reinforced concrete slab-like elements which utilized ultra-high-performance concrete (UHPC) overlays, Iowa State University determined that by increasing the roughness of the application surface, the bond strength at the interface will be increased. It was suggested that the minimum surface roughness be 0.08 in (2mm) in order to achieve this (Aaleti et al. 2013). Additional to the preparation of the overlay application, proper curing techniques must be followed such as the application of curing compounds and the placement of wet burlap and poly sheeting. The overlay surface must not be excessively textured and must have a flat plane transition at deck joints to reduce vehicle impact on those joints. Sufficient road surface drainage slopes should be planned to eliminate standing water and encourage immediate runoff (Carter et al. 2002).

Cracks formed in overlays provide a pathway for deleterious materials to ingress into the matrix and harm the longevity of the pavement. Cracking of overlays is a common problem but can be mitigated with the proper surface preparation and curing practices suggested by the Texas Department of Transportation (TDOT) (Beer 2018). Cracking may be caused by a cumulation of effects. Other cracking issues are due to the overlay thickness. In a study conducted by Michigan State University which utilized a modified ring shrinkage test (AASHTO PP 34-99), it was found that cracking of overlays can be caused by overlay thickness. For example, as the thickness of an overlay increases, interfacial shear stresses increase and debonding tended to occur, while crack producing tension stresses within the overlay decrease. This occurrence is largely due to shifts in the location of the neutral axis and is most prominent on overlays completed on bridge decks greater than 10 in thick (Shann 2012). Shann (2012) recommends that overlays not be applied to bridge decks that have an original thickness greater than 10 inches.

Very high early strength latex-modified concretes (VHES-LMC) are utilized in bridge deck overlays and pavement repairs to improve construction production efficiency and provide a durable and lasting product. VHES-LMC overlays have increased workability and provide early strength suitable to open for traffic after three hours of concrete placement. VHES-LMC typically has little to no bleed water and reduced water-cement ratio, so plastic shrinkage is likely. In a study performed by Yun and Choi (2014) it was determined that air temperature, relative humidity, concrete temperature, wind speed, and evaporation rate all influence the lack of bleed water during cement hydration and results in map cracking. This type of concrete is most commonly at risk of early age thermal cracking such as map cracking and transverse cracking. Map cracking is caused when water evaporates from the surface of freshly placed concrete faster than it can be replaced by bleed water. Other causes of map cracking are alkali-silica reaction (ASR), F/T reaction, and initial plastic shrinking which results from improper curing methods or use of curing compound that was delayed until after skid-resistant surface texturing or tinting (Yun and Choi 2014). The curing compound should be applied once between placement and surface texturing and reapply after surface texturing to mitigate the issue. Other crack reducing techniques are decreasing the hydration temperature, minimize cement paste volume, and reducing free shrinkage (Yun and Choi 2014).

Furthermore, low slump concrete mixtures are more likely to crack. The existing bridge deck acts as a confinement for the overlay so when excessive volumetric changes occur in the overlay, cracking occurs. Transverse cracking is caused by the combination of thermal stresses and drying shrinkage (Yun and Choi 2014).

Quality management in the field prevents poor overlay construction. The quality of the overlay placement work by the constructors is directly correlated to the performance and life span of bridge deck overlays. Premature debonding of high-density concrete overlays can be eliminated when proper care is given to the preparation of the existing deck-overlay interface, especially in regard to rotomilling, sandblasting, and the application of debonding agents at the demolition phase of the repair and providing a dry surface for the application. Haber et al. (2017) noted that corrosion of existing steel reinforcement can be the cause of delamination below the overlay but within the existing concrete. Delamination can also occur either within the overlay or at the overlay and substrate concrete interface, yet the former is highly unlikely. This is often due to poor preparation of the substrate concrete or poor consolidation (Haber et al. 2017). Additional to the preparation of the overlay application, proper curing techniques must be followed.

A.4.4 Quality Assurance and Quality Control Methods

When a bridge is identified for repair, appropriate specification provisions should be provided by agencies (or their contracted designers) and followed by contractors to provide the best possible solution. Recipe specifications or prescriptive specifications are established by state agencies to be strictly followed, which prevents the contractor from altering or improving the process. This is disadvantageous because there is no opportunity for innovation in the changing environment that exists on construction sites or variations in the material resource. Many of today's QA specifications are a combination of materials and methods specifications and QA requirements. The prescriptive measures of materials and methods specifications include specifying the procedures to follow and the equipment and materials to use. QA specifies the desired level of quality. Performance-related Specifications (PRS) specify the desired performance or serviceability level of the

concrete mixture and final product. With PRS, the desired level of quality, and the long-term performance can be predicted from acceptance tests (Taylor et al. 2013).

Highway agencies have an interest in ensuring that their pavements meet critical mixture performance requirements, and a QA program provides the specifications for constructing highway components with satisfactory service life. The 28-day strength benchmark used in the past is found to no longer determine quality of construction or durability, nor will it predict length of service life (Cackler et al. 2017). It is necessary to implement a quality monitoring testing program that can be performed during production and construction of concrete so that beneficial mix alterations can be made along the way. Cackler (2017) states the 6 Critical Performance Engineering Mixture Properties adopted from AASHTO 84-17 which includes aggregate stability, transport properties, paste durability, shrinkage, strength, and workability. Rather than agencies prescribing specifications such as minimum or maximum cement content, the contractor is given authority to develop the mixture design to meet the performance requirements of the Quality Control (QC) specifications. Cackler (2017) states that since this approach authorizes the contractor to control the process, they are able to innovate and be more effective. One of the tests proposed to be included into the PEM efforts for bridge deck rehabilitation is the surface resistivity test (Cackler et al. 2017).

A.4.4.1 Non-destructive Evaluation (NDE) for Construction Quality Assurance and Control

NDE techniques are valuable QA and QC methods for use on structures because they provide information about the quality of concrete components such as strength evolution, deterioration, cracks and other internal defects such as honeycombing without causing significant harm to the strength and durability of the concrete. Furthermore, NDE techniques are effective in assessing the durability of concrete, determining the position of reinforcement steel, determining the uniformity of concrete, and monitoring long-term changes within the medium (Lorenzi et al. 2012). NDE techniques typically also requires less effort than other approaches, which leads to a reduction of resources and expenditures. The drawback to some NDE techniques include the cost of some NDE tools, the rigor of the analysis required to analyze the data for some tools/techniques, and the level of training required of the technician performing the NDE tasks and data analysis. For example, with regard to data analysis, it should not be assumed that NDE test results will consistently correlate with traditional destructive testing techniques such as compressive strength without developing empirical correlation factors (Taylor et al. 2013).

A.4.4.2 Introduction to NDE and Value to Construction

Nondestructive evaluation (NDE) of reinforced concrete is complex due to its composite material nature, and a combination of preparation and placement variables such as mixture design, batching, mixing, and non-uniformity of aggregate supplies. (Gucunski et al. 2011)

A number of research studies have been performed over the past several decades to identify and refine the utility of different NDE tools and techniques for use in the field. For example, a research study by Gucunski et al. (2011) involved the use of a variety of NDE methods to determine the condition of a bridge deck. The evaluation program was conducted at a rate of about 2,500-3,000 square feet per workday. The following methods were utilized, listed in the order of their relative speed of data collection: ground penetrating radar, electrical resistivity, half-cell potential, impact echo, and ultrasonic surface waves. The NDE results were validated using drilled cores and by comparing to records from previous overlay projects (Gucunski et al. 2011). Gucunski et al. (2013), concluded in their research that in order to determine all occurrences of deterioration or defects, the use of more than a single NDE technology is required. Of the 10 NDE technologies utilized in their research detecting the health of concrete bridge decks, ultrasonic surface wave testing was the only technology found to provide information on vertical cracks. Surface wave testing was regarded as just a “fair” technology for that purpose, with the authors stating, “ultrasonic surface wave testing was also the only technology validated as having good potential in concrete deterioration detection and characterization”. Electrical resistivity was one of the four viable technologies that had a fair-to-good potential for corrosion detection (Gucunski et al. 2013).


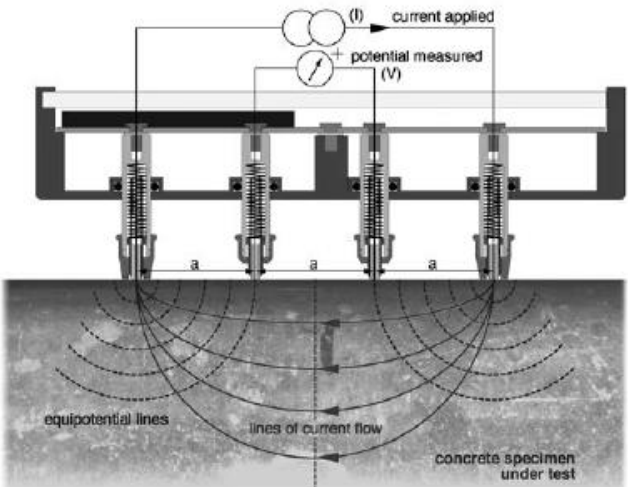
A.4.5 Surface Resistivity

Electrical resistivity is the ability for a material to resist the transfer of ions when subjected to an electrical field. It is mainly influenced by the pore size and interconnectivity of the pore structure (Layssi et al. 2015). Electrical resistivity testing is a method used to detect cracks or paths of moisture within a material’s microstructure (Growers and Millard 1999). Additionally, electrical resistivity equipment with the potential to estimate the thickness of concrete pavement slabs is being developed (Taylor et al. 2013).

Resistivity of reinforced concrete is directly associated with the likelihood of corrosion in reinforcing steel and corrosion of the concrete due to chloride diffusion (Proceq 2017). Concrete is an ion conductor, meaning that the electrical

conduction happens through the interconnected pore structure. The permeability of the concrete is an indication of its ability to resist chloride ion penetration (AASHTO 2017) and is the most important criteria for determining the long-term durability of concrete (Kevern 2015, Taylor et al. 2013).

A surface resistivity meter (Figure A.18) is a hand-held, non-destructive evaluation testing tool which has the ability to quickly determine the permeability or the connectivity of a concrete's pore structure. For this research study, the 38 mm (1.5") probe spacing Proceq Resipod surface resistivity meter was used to determine the electrical resistivity of concrete (Figure A.18). The Resipod uses a spring-loaded four pin array and applies an electrical current that is carried by ions in pore liquid from the outer probes, and the potential difference is measured between the inner probes. Figure A.19 shows a schematic of the surface resistivity meter with the probes engaged demonstrating the applied current and measurement of potential difference. The measurement result is displayed in kilohm-centimeters ($k\Omega\text{-cm}$) on the device (Proceq 2017).

	
<p>Figure A.18: Proceq Resipod surface resistivity meter (Proceq 2017)</p>	<p>Figure A.19: Proceq Resipod measurement schematic (Proceq 2017)</p>

The Resipod has the ability to read the resistivity of a concrete specimen within the range of 1-1000 $k\Omega\text{cm}$. Surface resistivity is calculated with the following equation, $\rho = 2\pi aV/I$ [$k\Omega\text{-cm}$], where ρ = resistivity [$\Omega\text{-m}$], a = electrode separation [m], V = voltage [V], I = current [A]. Proceq, the manufacturer of the Resipod list the following application examples, demonstrating its versatility:

- Estimation of the likelihood of corrosion
- Indication of corrosion rate
- Correlation to chloride permeability
- On site assessment of curing efficiency
- Determination of zonal requirements for cathodic protection systems
- Identification of wet and dry areas in a concrete structure
- Indication of variations in the water/cement ratios within a concrete structure
- Identification of areas within a structure most susceptible to chloride penetration
- Correlation to water permeability of rock

Since surface resistivity testing is a relatively simple and straightforward approach compared to many other NDE tools/techniques, it has a fairly small margin of error between users. In a study done by Icenogle and Rupnow (2012), where two tests were conducted by different laboratories on the same material, it was found that the surface resistivity readings did not differ by more than 11% (Icenogle and Rupnow 2012).

The approach of surface resistivity testing with the Wenner Probe has provided a fairly easy and time efficient method for determining important characteristics about the durability of hardened concrete. Today, the Wenner probe is a well-accepted tool for determining the quality of composition, likelihood of corrosion based on chloride permeability, degree of hydration, and characterization of transport properties as all of the above relate to electrical resistivity of concrete. Compared to previous methods such as rapid chloride permeability test (RCPT) that require intensive specimen preparation and may take days to perform, surface resistivity can be measured in minutes, and can be performed in the laboratory or on the jobsite.

The CNS Farnell Concrete Resistivity Meter was one of the early versions of the Wenner probe on the market for testing the electrical resistance of a concrete's pore structure and obtaining understanding of the risk of permeability and corrosion risk of concrete members. The manufacturers state that field use of this device investigates whether or not the embedded steel reinforcement is exhibiting corrosion, the internal structure is compromised, or the rate of chloride penetration resistance of the concrete member is of acceptable levels (CNS Farnell n.d.). Furthermore, electrical resistivity has been used to detect moisture, flaws, and pollution in porous media (Gucunski et al. 2011). Additionally, electrical resistivity was found to detect the presence of cracking during curing and determine the connectivity of the concrete's microstructure (Rajabipour et al. 2004). Recently, other types of Wenner probe devices have become commercially available for use in measuring surface resistivity. One of these devices is the Resipod manufactured by Proceq. As quoted by Proceq (2017), "The Resipod is an evolution of the industry standard CNS Farnell RM MKII resistivity meter, operating on the principle of the Wenner probe."

Due to the field pattern of the electrical current flow of the Wenner probe, the geometry of the specimen affects the surface resistivity measurement, so correction factors were implemented by Florida DOT (2004) to convert readings from a cylindrical specimen to flat surfaces, such as a slab or bridge deck. However, differing values were reported by Kansas Department of Transportation (Jenkins 2015). For example, Jenkins's (2015) findings considered concrete to have a high tendency for chloride penetration to have a surface resistivity measurement lower than 7.0 kΩ-cm rather than 12.0 kΩ-cm for a 4 in. x 8 in. cylinder. Table A.8 shows the correlation of surface resistivity of various sample geometries when tested with a Wenner probe with 1.5 in. spacing (Florida DOT 2004).

A.8: Surface resistivity geometry correction factor

Chloride Ion Permeability	Surface Resistivity (kΩ-cm)		
	4 in. x 8 in. Cylinder	6 in. x 12 in. Cylinder	Semi-Infinite Slab (Real)
High	< 12.0	< 9.5	< 6.7
Moderate	12.0 - 21	9.5 - 16.5	6.7 - 11.7
Low	21 - 37	16.5 - 29	11.7 - 20.6
Very Low	37 - 254	29 - 199	20.6 - 141.1
Negligible	> 254	> 199	> 141.1

The geometry correction factor (k) for 4 in. x 8 in. cylinders was established by Spragg et al. (2013) with the utilization of Morris et al.'s (1996) simulations which resulted in the formula below (Equation 2.1). The formula should be used only when the ratio of the diameter to the electrode spacing is less than or equal to 6 or if the ratio of the length to the electrode spacing is less than or equal to 6 ($d/a \leq 6$ or $L/a \leq 6$, where d = diameter, L= length, and a = electrode spacing) (Spragg et al. 2013):

$$k = 1.10 - \frac{0.730}{\frac{d}{a}} + \frac{7.34}{\left[\frac{d}{a}\right]^2}$$

Equation A.13: Geometry correction factor for surface resistivity

According to Growers and Millard's (1999) experimental findings, to mitigate misleading resistivity measurements, the spacing of the electrode shall be less than 25% of any dimension of the specimen and half the contact area distance from the specimen's edge as there is a restriction of the current flow near the edge. Not following these parameters can result in an overestimation of surface resistivity.

A.4.6 Use of Surface Resistivity in Field Settings

The primary objective of surface resistivity testing is to evaluate the potential of concrete to resist chloride ingress or susceptibility of corrosion to initiate in steel reinforcement. When testing specimens in a laboratory setting or specimens in the field, efforts are made to manipulate both settings to resemble one another in order to produce a one-to-one relationship (Presuel-Moreno et al. 2010). Gucunski et al. (2013) determined that electrical resistivity was not a favorable method for detecting the depth and width of vertical cracks but was somewhat favorable (1 out of 5 rating) for determining characteristics pertaining to delamination of overlays and concrete degradation in bridge decks. In this study, by ranking the overall value of several NDE technologies, it was determined that electrical resistivity was most valuable for evaluating the potential for corrosion in bridge decks.

A.4.6.1 Influences on Surface Resistivity

There are two groups of factors that influence electrical resistivity of concrete, intrinsic factors and factors that affect the resistivity measurement. Intrinsic factors that influence electrical resistivity of concrete include water to cementitious materials ratio (w/cm), characteristics of the pore structure, and aging. Factors that affect the resistivity measurement include moisture content, temperature, specimen geometry, electrode spacing, and the existence of rebar. Larger pores within the concrete and higher temperatures decrease the resistivity reading (Polder 2001).

The permeability of concrete, as well as a number of other properties, can be defined by its w/cm ratio. The higher the w/cm ratio, the more porous the microstructure. This concludes with a lower electrical resistivity of concretes (that do not contain supplementary cementitious materials such as slag) (Rupnow and Icenogle 2012). Chen et al. (2014) reported a 15-20% decrease in electrical resistivity when the w/cm ratio increased from 0.4 to 0.6.

Reinforcement steel embedded within the concrete conducts electrical current more efficiently than the surrounding concrete. Due to that, the current field within reinforced concrete can become distorted, particularly when the cover depth is less than 30 mm (1.18 in) (Proceq 2017). Weydert and Gehlen (1999) determined that when concrete is tested for surface resistivity on top and in the parallel orientation of rebar embedded at 10 or 20 mm deep, errors by magnitude of two to six times reduction of the actual resistivity could result. Even when one of the four probes are within 10-20 mm distance of the rebar, the results will contain errors. The error involving rebar will produce resistivity measurements lower than typical or expected. It was also found that the electrical current induced by a Wenner probe can travel through the concrete at a depth approximate to the electrode spacing (Polder 2001).

Sengul and Gjrv (2009) studied the effects of probe spacing on wet-cured slabs with and without steel reinforcement and found minimal differences when measured with varying probe spacings less than 30 mm. However, when electrode spacing increased from 20 mm to 70 mm an approximate resistivity increase of 26% resulted in slabs without embedded reinforcement. When tested on slabs with rebar, a 33% increase was found from testing perpendicular to the rebar and 26% decrease when testing with the meter oriented parallel to the rebar (Sengul and Gjrv 2009).

For reinforcement spacing that is greater than the space between the outer probes (4.5"), the optimum orientation of the meter to the bars is diagonal. When the reinforcement can't be avoided, it is best to position the meter perpendicular to the bars to minimize its influence. For each location, it is recommended to take 5 readings a few mm apart and then reporting the median of those 5 values (Proceq 2017, Polder 2001). Salehi et al. (2016) performed a study of the effects of different characteristics of concrete specimens containing rebar mesh being tested with the four-point Wenner probe and found that when the densities of the reinforcement mesh increased, the resistivity decreased, and that the effects of rebar diameter are negligible. It was also concluded that when the probe is setup on top of and perpendicular to the bottom rebar and parallel to and between top reinforcement bars, the smallest error would result, as illustrated in Figure A.20 (Salehi et al. 2016).

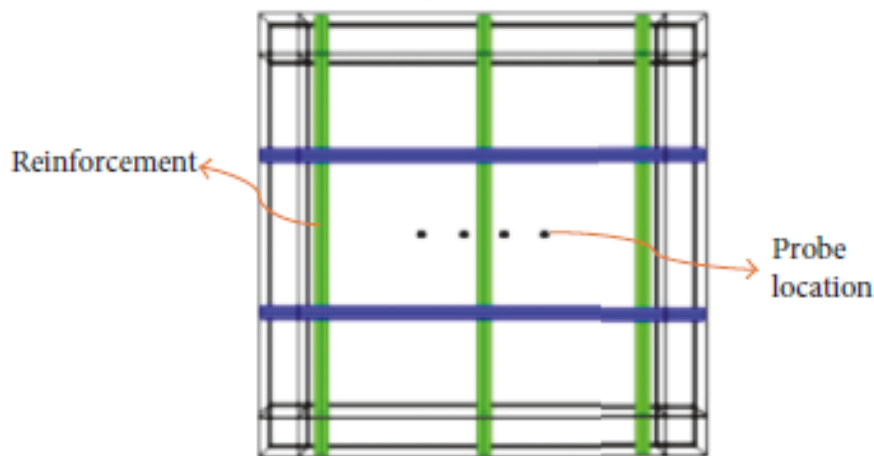


Figure A.20: Probe configuration to reduce surface resistivity error

Garzon et al.'s (2014) experimental study of the effects of rebar presence on cylindrical and rectangular prism mortar specimen's electrical resistivity using the four-point Wenner probe confirms those findings. When resistivity measurements are taken directly above the rebar of a double layer mesh, an error will result due to polarization at the concrete and steel interface which acts as a resistance capacitor (Garzon et al. 2014).

The influence that temperature has on the surface resistivity of concrete is significant. As the temperature of the concrete increases by one degree, the resistivity measurement can decrease by 3% for saturated concrete and 5% for dry

concrete (Proceq 2017), and if the ambient temperature is much higher than the specimen's temperature, the surface resistivity will be much lower than expected (Spragg et al. 2013). The effects of temperature on resistivity are due to the fact that electrons move faster at higher temperatures, which causes a higher electrical conductivity, resulting in a decrease in resistivity (Azarsa and Gupta 2017). Another contributing factor of temperature's influence on resistivity is that higher temperatures tend to decrease moisture content which indirectly affects resistivity (Poyet 2009). To help mitigate the influence of temperature, the concrete's temperature and ambient temperature should be monitored and recorded with the resistivity measurements. Reference values of surface resistivity are typically quoted for 68°F (Proceq 2017). Millard et al. (1991) and Gowers and Millard (1999) developed a correction factor of $0.33 \text{ K}\Omega\text{-cm}/^{\circ}\text{C}$ to compensate for temperature variation. It is noted, however, that this study only included testing at a limited temperature range.

Due to an increase in ion mobility that is accompanied by increased electrical conductivity, concrete's moisture content has an inverse effect on the surface resistivity measurements (Liu and Presuel-Moreno 2014, Larsen et al. 2006). Concrete specimens that were immersed in either water or lime water will likely have a different resistivity than those that were cured in a high humidity setting (Larsen et al. 2006). Larsen et al.'s (2006) research concluded that concrete's resistivity nearly doubled when the degree of saturation decreased from 88% to 77% and the resistivity increased an average of six times when the moisture degree decreased from 88% to 66%. Concrete in an air-dry state will have a higher than expected resistivity reading and sometimes make it impossible to collect the reading (Rupnow and Icenogle 2013). Sengul (2014) found a 50% increase in resistivity of concrete when air-dried versus concrete tested in a saturated condition. Due to less restricted electrical flow of a saturated pore solution, increasing the water content of concrete results in a lower resistivity. For example, fully saturated concrete has a resistivity on the order of 100-1000 ohm-m, while the resistivity of oven-dried concrete can be as high as 10^6 ohm-m. Care should also be given to surface saturation, as static ponding and the application of pressurized water can lead to inaccurate resistivity measurements of over 30% compared to full laboratory saturation (Marquez 2015).

Gjørsv et al. (1977) found that w/cm ratio has an inverse relationship on the electrical resistivity of concrete and later Gucunski et al. (2011) confirmed that finding. This was true of substantially cured concrete and freshly made concrete (Gucunski et al. 2011). In a study performed by Icenogle and Rupnow (2012) where five mixtures at three different w/cm ratios (0.35, 0.50, and 0.65) were tested for surface resistivity, it was found that the resistivity meter (Resipod) successfully identified differences in concrete with different w/cm ratios.

The size of aggregate in the concrete mixture is known to have an impact on surface resistivity. Normal weight aggregates will generally be more dense and less porous than the hardened cement paste, thus having a higher resistivity. In a study performed by Sengul (2014) where the effects of two different aggregates sizes were compared, it was found that increasing the aggregate nominal size and content results in a higher resistivity measurement. Morris et al. (1996) reports that concrete with a larger maximum aggregate size will result in a variability of resistivity readings within one specimen. This is likely caused by the size and shape of the interconnected pores, or tortuosity effect, and the amount of interfacial transition zones (ITZ). Aggregates with a higher percentage of smaller particle sizes will develop more ITZ occurrences within the concrete. This is also true of aggregates that have a rough surface texture or irregular particle shape. The ITZ has a greater porosity when compared to the hardened cement paste, which leads to a lower resistivity (Morris et al. 1996). When the nominal aggregate size within the concrete mixture is larger than the resistivity meter's probe spacing, the resistivity reading will likely be impacted (Proceq 2017). In a study performed by Gowers and Millard (1999) where specimens of a constant maximum aggregate size were measured for resistivity at changing probe spacings, a 10% increase in the standard deviation was observed as the probe spacing decreased approaching the maximum aggregate size. Figure A.21 is a graph developed by Gowers and Millard 1999 showing the rate in which the standard deviation percentage increases as the ratio of the contact spacing to maximum aggregate size decreases. To reduce the variance in measurement with the resistivity meter, Gowers and Millard (1999) recommends using a device with a probe spacing 1.5 times greater than the maximum nominal aggregate size.

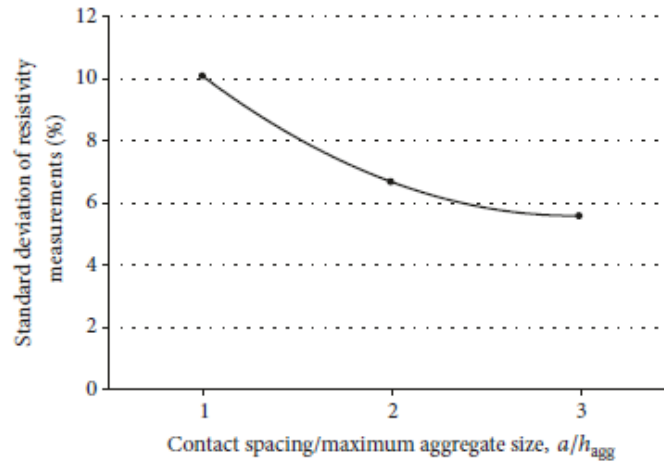


Figure A.21: Effect of contact spacing on resistivity measurement

Resistivity of concrete is also affected by the curing conditions. The curing and/or storage conditions of concrete specimens have a great influence on degree of saturation, degree of hydration, and the pore solution and structure through leaching (Spragg et al. 2013). Weiss et al. (2013) performed a study to determine the curing effects on resistivity. Mortar specimens of the same mixture were subject to three curing conditions: (1) sealed during curing and testing, (2) sealed during curing and saturated during testing, and (3) saturated during curing and testing. Specimens that were sealed both during curing and testing had the highest resistivity. In contrast, specimens that were sealed during curing but saturated during testing had the lowest resistivity. Curing a specimen under water will likely cause a completely different degree of hydration than what would occur in concrete from a field structure (Weiss et al. 2013). Azarsa and Gupta (2017) recommends wetting the specimen prior to performing the resistivity testing.

Resistivity testing is contingent on the initial assumption that concrete is isotropic and homogeneous with semi-finite geometry. When cracks are present within the reach of the imposed current, the electrical resistivity measurement may vary (Azarsa and Gupta 2017). Lataste et al. (2003) performed a study in an effort to locate and identify crack characteristics such as the opening of the crack and bridging degree between the opening and depth of the crack.

The experiment was performed on two reinforced concrete members, a slab in a field setting and beams in a laboratory setting. Rather than a linear electrode orientation of a Wenner probe, an instrument was built where the four electrodes are positioned at the four corners of a square. This instrument is shown in Figure A.22. The built instrument allows for measuring the resistivity in two orthogonal directions without requiring to rotate the probe ninety degrees between measurements. It was found that when the imposed electrical current was taken orthogonal to the visible water filled cracks, known as conductive cracks, there was no impact on the reading but when tested parallel to the crack a reduction in resistivity was observed. When tested on an insulated crack (air-filled cracks without bridging), an overestimation of resistivity was observed when the imposed current was in the orthogonal orientation, and an underestimation was observed when measured parallel with respect to the crack. In addition, it was also concluded that as the depth of a crack increased, the resistivity measurement also increased.

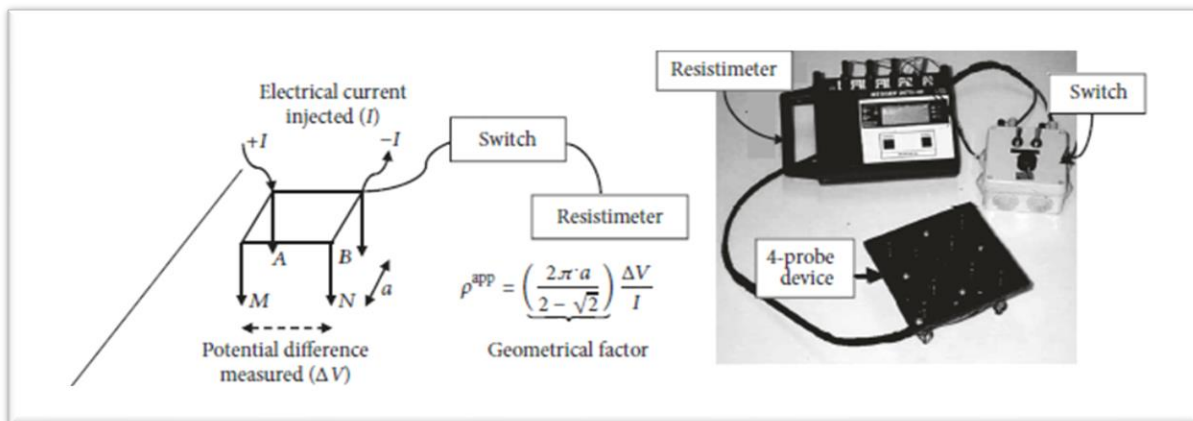


Figure A.22: Four-probe square array principal (Lataste et al. 2003)

Lataste et al.'s (2003) research was based on the assumption that the rebar's influence on the resistivity reading was independent of the presence of cracks. Also, it is possible that the small scale of the concrete specimen could exaggerate the crack's impact on the resistivity reading, and lastly the four corner setup of the probe utilized in the study could possibly produce other measurement errors when compared to the commonly accepted linear Wenner probe configuration (Azarsa and Gupta 2017). Shah and Ribakov's (2008) research on crack assessment and defect detection of concrete structures found that resistivity measurements in the vicinity of insulated cracks produced higher values than that of conductive cracks. Salehi et al. (2015) determined that the depth of cracks did not significantly impact the resistivity measurement on conductive cracks. Furthermore, when the two inner electrodes spanned an insulated crack, the maximum error occurred. The electrical resistivity in this orientation led to about 200% higher results than what was expected of the concrete's resistivity. Microcracking did not significantly affect the resistivity measurement (Morales 2015). Other characteristics that influence the resistivity of concrete are fluid salinity, cement chemistry, admixtures, and defects within the concrete (Gucunski et al. 2011).

4.6.2 Use of surface resistivity on bridge deck overlays

The Louisiana Department of Transportation has recently accepted surface resistivity as a viable quality assurance tool for new and existing concrete and has predicted a savings of over \$1.5 million each year by replacing RCPT with surface resistivity (Rupnow and Icenogle 2011; Rupnow and Icenogle 2012). Although this seminal study was primarily performed in the laboratory, other studies have focused on use of surface resistivity as a field tool, particularly to replace the more intensive and costly RCPT (ASTM 2009). RCPT testing requires that the technicians have significant training and sample preparation is very time consuming (Kevern 2015). Additionally, if evaluating field concrete, cores must be taken, which is a time-consuming, destructive process that can require traffic control, and certainly requires repair of the structure where the cores were removed. Surface resistivity is showing promise in field applications. For example, Kevern (2016) attempted to use the resistivity meter in field applications and was able to detect the presence of silane and lithium silicate sealers on bridge decks with surface resistivity.

Gucunski et al. (2011) explains that manual surface resistivity testing along a grid on large-scale surfaces areas such as bridge decks can get tedious and that there are no automated measurement systems on the market at the time of the research to provide a solution. Furthermore, electrodes need galvanic coupling to the surface of the concrete. To provide galvanic coupling, pre-wetting is necessary but over-wetting is a concern. Over-wetting may adversely affect the measurement because the device can possibly be detecting probe-to-probe current flow along the surface of the concrete and not within. To mitigate some of this current leakage from probe to probe, the surface should have a light coating of water and never puddling (Gucunski et al. 2011).

A.4.7 Research Needs

As overlays are often placed quickly with the intention of avoiding traffic delays, and the accompanying fact that overlay concrete mixtures often contain VHES which have a tendency to lose workability and consistency before anticipated, if the overlay gets away from the workers then construction errors are likely to occur. These construction errors can result in unwanted voids or an overlay thickness that does not provide sufficient reinforcement cover. As discussed in previous sections, surface resistivity testing of concrete has many benefits including cost, ease of use, and measurements are displayed immediately. Further research is necessary to investigate the potential of surface resistivity testing as QA inspection and testing protocol for concrete overlays. Surface resistivity testing of overlays could possibly be utilized to determine the quality of placement and act as verification or acceptance measure for newly placed bridge deck concrete overlays. Currently, no guidance or standard method exists to support use of the surface resistivity meter to evaluate the consistency and integrity of a bridge deck overlay and/or determine its thickness. Additionally, there is only limited information on the effects of different types of reinforcing steel, edges, interfaces between two materials that occur at different depths, and voids on surface resistivity readings. Guidance on corrections to surface resistivity readings due to these embedded items and voids, as well as edges and discontinuities, would be useful to practitioners hoping to use the surface resistivity meter as a QA device for these types of projects.

A.5 References

- Aaleti, Sriram, Sritharan, S. and Abu-Hawash, A. (2013) "Innovative UHPC-Normal Concrete Composite Bridge Deck." RILEM-fib-AFGC International Symposium on Ultra-High Performance Fiber-Reinforced Concrete
- Abrams, D. A. (1918). Design of Concrete Mixtures, Structural Materials, Research Laboratory. Lewis Institute, Chicago. *Bulletin, 1.*

- American Association of State Highway and Transportation Officials (AASHTO). (2020). “Standard Specification for Blended Hydraulic Cement.” M 240M/M 240, American Association of State Highway and Transportation Officials, Washington, DC.
- American Association of State Highway and Transportation Officials (AASHTO). (2019). “Standard Practice for Developing Performance Engineered Concrete Pavement Mixtures.” PP 84-19, American Association of State Highway and Transportation Officials, Washington, DC.
- American Association of State Highway and Transportation Officials (AASHTO). (2020). “Standard Practice for Developing Performance Engineered Concrete Pavement Mixtures.” PP 84-20, American Association of State Highway and Transportation Officials, Washington, DC.
- American Association of State Highway and Transportation Officials (AASHTO). (2022). “Developing Performance Engineered Concrete Mixtures.”
- American Association of State Highway and Transportation Officials (AASHTO). (2020). “Standard Method of Test for Compressive Strength of Cylindrical Concrete Specimens.” AASHTO T 22M/T 22, American Association of State Highway and Transportation Officials, Washington, DC.
- American Association of State Highway and Transportation Officials (AASHTO). (2020). “Standard Method of Test for Flexural Strength of Concrete (Using Simple Beam with Third- Point Loading).” AASHTO T 97, American Association of State Highway and Transportation Officials, Washington, DC.
- American Association of State Highway and Transportation Officials (AASHTO). (2019). “Standard Method of Test for Air Content of Freshly Mixed Concrete by the Pressure Method.” T 152-19, American Association of State Highway and Transportation Officials, Washington, DC.
- American Association of State Highway and Transportation Officials (AASHTO). (2017). “Standard Method of Test for Length Change of Hardened Hydraulic Cement Mortar and Concrete.” T 160-17, American Association of State Highway and Transportation Officials, Washington, DC.
- American Association of State Highway and Transportation Officials (AASHTO). (2019). “Standard Method of Test for Air Content of Freshly Mixed Concrete by the Volumetric Method.” T 196M/T 196-11, American Association of State Highway and Transportation Officials, Washington, DC.
- American Association of State Highway and Transportation Officials (AASHTO). (2020). “Standard Method of Test for Estimating the Cracking Tendency of Concrete.” T 334-08, American Association of State Highway and Transportation Officials, Washington, DC.
- American Association of State Highway and Transportation Officials (AASHTO). (2015). “Standard Method of Test for Temperature of Freshly Mixed Portland Cement Concrete.” T 309-15, American Association of State Highway and Transportation Officials, Washington, DC.
- American Association of State Highway and Transportation Officials (AASHTO) (2017). Standard Method of Test for Surface Resistivity Indication of Concrete’s Ability to Resist Chloride Ion Penetration. AASHTO T 358-17 American Association of State Highway and Transportation Officials. Washington, D.C.
- American Association of State Highway and Transportation Officials (AASHTO). (2017). “Standard Method of Test for Evaluating Stress Development and Cracking Potential due to Restrained Volume Change Using a Dual Ring Test.” T 363-17, American Association of State Highway and Transportation Officials, Washington, DC.
- American Association of State Highway and Transportation Officials (AASHTO). (2017). “Standard Method of Test for Characterization of the Air-Void System of Freshly Mixed Concrete by the Sequential Pressure Method.” TP 118-17, American Association of State Highway and Transportation Officials, Washington, DC.
- American Association of State Highway and Transportation Officials (AASHTO). (2017). “Electrical Resistivity of a Concrete Cylinder Tested in a Uniaxial Resistance Test.” TP 119-15, American Association of State Highway and Transportation Officials, Washington, DC.
- American Concrete Institute (2012). Chemical Admixtures for Concrete. ACI Education Bulletin E4-12. Farmington Hills, MI.
- American Concrete Institute (ACI) 201.2R-16 (2016). Guide to Durable Concrete. American Concrete Institute, Farmington Hills, MI.
- American Concrete Institute (ACI) 211.1 (2002). Standard Practice for Selecting Proportions for Normal, Heavyweight, and Mass Concrete. American Concrete Institute, Farmington Hills, MI.
- American Concrete Institute (ACI) 228.2R-98 (1998). Nondestructive test methods for evaluation of concrete in structures. American Concrete Institute, Farmington Hills, MI.

- American Concrete Institute (ACI) 302.1R-96 (1996). Guide for Concrete Floor and Slab Construction. American Concrete Institute, Farmington Hills, MI.
- American Concrete Institute (ACI). 302.1R-15 (2015). Guide for Concrete Floor and Slab Construction. American Concrete Institute, Farmington Hills, MI.
- American Concrete Institute (ACI). 318-19 (2019). Building Code Requirements for Structural Concrete and Commentary. American Concrete Institute, Farmington Hills, MI.
- American Concrete Institute (ACI) 548. (1992) Standard Specification for Latex-Modified Concrete (LMC) Overlays (ACI 548.4) Materials Journal, 89(5), 521-526.
- American Society for Testing and Materials (ASTM). (2018). ASTM C33/C33M-18 “Standard Specification for Concrete Aggregates.” ASTM International, West Conshohocken, PA. DOI: 10.1520/C0033_C0033M-18. www.astm.org
- American Society for Testing and Materials (ASTM). (2021). ASTM Standard C39/C39M-21 “Standard Test Method for Compressive Strength of Cylindrical Concrete Specimens.” ASTM International, West Conshohocken, PA. DOI: 10.1520/C0039_C0039M-21. www.astm.org
- American Society for Testing and Materials (ASTM). (2021). ASTM Standard C78/C78M-21 “Standard Test Method for Flexural Strength of Concrete (Using Simple Beam with Third-Point Loading).” ASTM International, West Conshohocken, PA. DOI: 10.1520/C0078_C0078M-21. www.astm.org
- American Society for Testing and Materials (ASTM). (2017). ASTM C138/C138M-17a “Standard Test Method for Density (Unit Weight), Yield, and Air Content (Gravimetric) of Concrete.” ASTM International, West Conshohocken, PA. DOI: 10.1520/C0138_C0138M-17A. www.astm.org
- American Society for Testing and Materials (ASTM). (2020). ASTM C143/C143M-20 “Standard Test Method for Slump of Hydraulic-Cement Concrete.” ASTM International, West Conshohocken, PA. DOI: 10.1520/C0143_C0143M-20. www.astm.org
- American Society for Testing and Materials (ASTM). (2020). ASTM C150/C150M-20 “Standard Specification for Portland Cement.” ASTM International, West Conshohocken, PA. DOI: https://doi.org/10.1520/C0150_C0150M-20
- American Society for Testing and Materials (ASTM). (2017). ASTM C157/C157M-17 “Standard Test Method for Length Change of Hardened Hydraulic-Cement Mortar and Concrete.” ASTM International, West Conshohocken, PA. DOI: 10.1520/C0157_C0157M-17. www.astm.org
- American Society for Testing and Materials (ASTM). (2018). ASTM C192/C192M-18 “Standard Practice for Making and Curing Concrete Test Specimens in the Laboratory.” ASTM International, West Conshohocken, PA. DOI: 10.1520/C0192_C0192M-18. www.astm.org
- American Society for Testing and Materials (ASTM). (2019). ASTM C215-19 Standard Test Method for Fundamental Transverse, Longitudinal, and Torsional Resonant Frequencies of Concrete Specimens. ASTM International, West Conshohocken, PA. DOI: <https://doi.org/10.1520/C0215-19>
- American Society for Testing and Materials (ASTM). (2017). ASTM C231/C231M-17a “Standard Test Method for Air Content of Freshly Mixed Concrete by the Pressure Method.” ASTM International, West Conshohocken, PA. DOI: 10.1520/C0231_C0231M-17A. www.astm.org
- American Society for Testing and Materials (ASTM). (2016). ASTM Standard C457/C457M-16 “Standard Test Method for Microscopical Determination of Parameters of the Air-Void System in Hardened Concrete.” ASTM International, West Conshohocken, PA. DOI: 10.1520/C0457_C0457M-16. www.astm.org
- American Society for Testing and Materials (ASTM). (2021). ASTM C469/C469M-14e1 “Standard Test Method for Static Modulus of Elasticity and Poisson's Ratio of Concrete in Compression.” ASTM International, West Conshohocken, PA. DOI: 10.1520/C0469_C0469M-14E01. www.astm.org
- American Society for Testing and Materials (ASTM). (2019). ASTM C511-19 “Standard Specification for Mixing Rooms, Moist Cabinets, Moist Rooms, and Water Storage Tanks Used in the Testing of Hydraulic Cements and Concretes.” ASTM International, West Conshohocken, PA. DOI: <https://doi.org/10.1520/C0511-19>
- American Society for Testing and Materials (ASTM). ASTM C618-19 “Standard Specification for Coal Fly Ash and Raw or Calcined Natural Pozzolan for Use in Concrete.” ASTM International, West Conshohocken, PA. DOI: <https://doi.org/10.1520/C0618-19>
- American Society for Testing and Materials (ASTM). (2016). ASTM C666/C666M-15 “Standard Test Method for Resistance of Concrete to Rapid Freezing and Thawing.” ASTM International, West Conshohocken, PA. DOI: 10.1520/C0666_C0666M-15. www.astm.org

- American Society for Testing and Materials (ASTM). (2018). ASTM C685/C685M-17 “Standard Specification for Concrete Made by Volumetric Batching and Continuous Mixing.” ASTM International, West Conshohocken, PA. DOI: 10.1520/C0685_C0685M-17. www.astm.org
- American Society for Testing and Materials (ASTM). (2019). ASTM C1202-19 “Standard Test Method for Electrical Indication of Concrete’s Ability to Resist Chloride Ion Penetration.” ASTM International, West Conshohocken, PA. DOI: 10.1520/C1202-19. www.astm.org
- American Society for Testing and Materials (ASTM). (2021). ASTM C1260-21 “Standard Test Method for Potential Alkali Reactivity of Aggregates (Mortar-Bar Method).” ASTM International, West Conshohocken, PA. DOI: 10.1520/C1260-21. www.astm.org
- American Society for Testing and Materials (ASTM). (2020). ASTM C1293-20a “Standard Test Method for Determination of Length Change of Concrete Due to Alkali-Silica Reaction.” ASTM International, West Conshohocken, PA. DOI: 10.1520/C1293-20A. www.astm.org
- American Society of Civil Engineers (ASCE). (2021). 2021 Infrastructure Report Card. Available at: <https://www.infrastructurereportcard.org>. Accessed October 2021.
- American Society of Civil Engineers (ASCE). (2021). Policy statement 418 – The role of the civil engineer in sustainable development. Reston, VA.
- Appropedia.org. 2021. BubbleCounter - Appropedia: The sustainability wiki. [online] Available at: <<https://www.appropedia.org/BubbleCounter>> [Accessed 7 April 2021].
- Aragoncillo, A.M.M., and Lomboy, G.R. (2021). “Correlation of Electrical Resistivity and Formation Factor with Chloride and Water Permeability of Recycled Aggregate Concrete.” Manuscript submitted for publication.
- Armaghani, J.M., Larsen, T.J., and Romano, D.C. (1992). Aspects of Concrete Strength and Durability. Transportation Research Record.
- Ashraf, W., and Noor, M.A. (2011). Performance-Evaluation of Concrete Properties for Different Combined Aggregate Gradation Approaches. *Procedia Engineering*, 14, 2627-2634.
- Assaad, J. and Issa, C. (2018). “Stability and Bond Properties of Latex-Modified Semi-Lightweight Flowable Concrete.” *American Concrete Institute (ACI) Materials Journal*, 4(115), 519-530.
- Azarsa, P. and Gupta, R. (2017) “Electrical Resistivity of Concrete for Durability Evaluation: A Review.” *Advances in Material Science and Engineering*, 2017, Hindawi Publishing Corporation.
- Beer, D. (2010) Bridge Deck Concrete Overlays. Challenges and Inspections. Texas Department of Transportation.
- Bissonnette, B., Vaysburd, A. and Fay, K. (2012) “Best Practices for preparing Concrete Surfaces Prior to Repairs and Overlays.” *Reclamation Managing Water in the West*. U.S. Department of the Interior Bureau of Reclamation Technical Service Center. Denver, CO. Report Number: MERL 12-17.
- Beushausen, H., Dittmer, T. (2015). “The Influence of Aggregate Type on Strength and Elastic Modulus of High Strength Concrete.” *Construction and Building Materials*, 74, 132-139. <https://doi.org/10.1016/j.conbuildmat.2014.08.055>
- Biggers, R.B. (2019). “Development of a Surface Resistivity Specification for Durable Concrete” (Master’s thesis). University of North Carolina at Charlotte, Charlotte, NC.
- Blanchard, E. H. (2016). “Determination and Evaluation of Inputs for Portland Cement Concrete Pavement to Support Local Calibration of MEPDG for North Carolina” (Master Thesis), University of North Carolina at Charlotte
- Brown, E. R., Kandhal, P. S., Roberts, F. L., Kim, Y. R., Lee, D.-Y., and Kennedy, T. W. (2009). *Hot Mix Asphalt Materials, Mixture Design, and Construction* (3ed ed.). National Asphalt Pavement Research and Education Foundation.
- Cackler, T., Harrington, D. and Taylor, P.C. (2017a). “Performance Engineered Mixtures (PEM) for Concrete Pavements.” CP Road Map Brief, April 2017. National Concrete Pavement Technology Center. Ames, IA.
- Cackler, T., Praul, M. and Duval, R. (2017b). “Developing a Quality Assurance Program for Implementing Performance Engineered Mixtures for Concrete Pavements.” CP Road MAP Brief, July 2017. National Concrete Pavement Technology Center. Ames, IA.
- Carter, P., Gurjar, S. and Wong, J. (2002) “Debonding of Highway Bridge Deck Overlays.” *Concrete International*, 24(7), 51-58.
- Cavalline, T.L., Tempest, B.Q., Biggers, R.B., Lukavsky, A.J., McEntyre, M.S., and Newsome, R.A. (2020a). Durable and Sustainable Concrete through Performance Engineered Concrete Mixtures. Report No. FHWA/NC/2018-14. North Carolina Department of Transportation, Raleigh, NC.

- Cavalline, T.L., Tempest, B.Q., Blanchard, E.H., Medlin, C.D., and Chimmula, R.R. (2018). Improved Data for Mechanistic-Empirical Pavement Design for Concrete Pavements. Report No. FHWA/NC/2015-03. North Carolina Department of Transportation, Raleigh, NC.
- Cavalline, T.L., Tempest, B.Q., Hunter, B.J., White, F.D., and Ange, C.M. (2020b). “Post Construction Report for North Carolina Demonstration Project, Implementation of Performance Engineered Concrete Mixtures (PEM)/AASHTO PP 84.” Final Report Project FHWA 2019-41, North Carolina Department of Transportation. Submitted to Federal Highway Administration, April 2020.
- Cavalline, T. L., Tempest, B. Q., Leach, J. W., Newsome, R. A., Loflin, G. D., and Fitzner, M. J. (2019). Internal Curing of Concrete Using Lightweight Aggregate. Report No. FHWA/NC/2016-06. North Carolina Department of Transportation, Raleigh, NC.
- Cavalline, T.L., White, F.D., Tempest, B.Q., Hunter, B.J., Ange, C.M., and Simpson, R.P. (2022). “Performance Engineered Concrete Mixtures: Implementation at an Interstate Rigid Pavement Project.” *Transportation Research Record: Journal of the Transportation Research Board*, 2676(5), 450-459. <https://doi.org/10.1177%2F03611981211067981>
- Chen, C.-T., Chang, J.-J. and Yeh, W.-C. (2014) “The effects of specimen parameters on the resistivity of concrete,” *Construction and Building Materials*, 71, 35–43.
- Claisse, P. A. (2014). *Transport Properties of Concrete: Measurements and Applications*, Elsevier.
- CNS Farnell Limited. Concrete Resistivity Meter. Hertfordshire, England. Retrieved from: www.cnsfarnell.com
- Colorado Department of Transportation (CDOT). (2021). Standard Special Provisions: Section 601: Concrete Mix Designs.
- Conway Sr., R., Corrigan, M., Duval, R. (2019). “Performance Engineered Pavements.” Technical Brief, November 2019. Federal Highway Administration. Washington, DC.
- Cook, M.D., Ley, M.T. (2014). “Aggregate Gradations for Concrete Pavement Mixtures.” CP Road Map MAP Brief, October 2014. National Concrete Pavement Technology Center. Ames, IA.
- Cook, M.D., Ley, M.T., Russell, B.W., and Seader, J.N. (2015). “Investigation of Optimized Graded Concrete for Oklahoma – Phase 2.” Final Report. FHWA-OK-15-07. Oklahoma Department of Transportation. October 2015.
- Cook, M.D., Ghazizadeh, A., Ley, M.T., and Russell, B. (2013). “Investigation of Optimized Graded Concrete for Oklahoma – Phase 1.” Final Report. FHWA-OK-13-12. Oklahoma Department of Transportation. October 2013.
- Cook, M.D., Ghazizadeh, A., and Ley, M.T. (2018). Impacts of Coarse-Aggregate Gradation on the Workability of Slip-Formed Concrete. *Journal of Materials in Civil Engineering*. 30(2). [https://doi.org/10.1061/\(ASCE\)MT.1943-5533.0002126](https://doi.org/10.1061/(ASCE)MT.1943-5533.0002126)
- Concrete.org (2021). How is the air content of freshly mixed concrete determined?. Available at: <https://www.concrete.org/tools/frequentlyaskedquestions.aspx?faqid=823> [Accessed 17 February 2021].
- Cramer, S.M., Hall, M., Parry, J. (1995). “Effects of Optimized Total Aggregate Gradation on Portland Cement Concrete for Wisconsin Pavements.” *Transportation Research Record No. 1478*, Concrete and Concrete Pavement Construction. 100-106. <http://worldcat.org/issn/03611981>
- Ćwirzeń, A., and Penttala, V.E. (2005). Aggregate-cement paste transition zone properties affecting the salt-frost damage of high-performance concretes. *Cement and Concrete Research*, 35(4), 671-679. doi: 10.1016/j.cemconres.2004.06.009
- Dabrowski, M., Glinicki, M. A., Dziedzic, K., and Anotlik, A. (2019). “Validation of sequential pressure method for evaluation of the content of microvoids in air entrained concrete,” *Construction and Building Materials*, 227, 1-12.
- Darwin, D., Browning, J.P., and Lindquist, W.D. (2004). Control of Cracking In Bridge Decks: Observations From The Field. *Cement Concrete and Aggregates*, 26, 1-7. <https://doi.org/10.1520/CCA12320>
- Dolen, T.P. (2008). “Historical Development of Durable Concrete for the Bureau of Reclamation.” Bureau of Reclamation, Denver, CO.
- Economic Development Research Group, Inc. (2016). “Failure to Act: Closing the Infrastructure Investment Gap for America’s Economic Future.” American Society of Civil Engineers. Reston, VA.
- ElBatouny, M., Nadelman, E., Kurth, J. and Krauss, P. (2017). “Use of Polymer Overlays or Sealers on New Bridges.” Final Report. WJE Associates Inc. The Iowa Highway Research Board TR-717.
- Fagerlund, G. (2004). “A service life model for international frost damage in concrete.” Rep. TVBM-3119, Div. of Building Technology, Lund Institute of Technology, Lund, Sweden.
- Federal Highway Administration (FHWA) (2019). “Bridge Replacement Unit Cost 2019”, Safety & Management, Bridge Inspection, National Bridge Inventory. Available at: <https://www.fhwa.dot.gov/bridge/nbi/sd2019.cfm>

- Felice, R., Freeman, J. M., and Ley, M. T. (2014). "Durable Concrete with Modern Air-Entraining Admixtures," *Concrete International* 36(8), 37-45.
- Garzon, A. J., Sanchez, J., Andrade, C., Rebolledo, N., Menéndez, E. and Fullea, J. (2014). Modification of four point method to measure the concrete electrical resistivity in presence of reinforcing bars," *Cement and Concrete Composites*, vol. 53, pp. 249–257
- Gillum, A., Shahrooz, B. and Cole, J. (2011). Bond Strength between Sealed Bridge Deck and Concrete Overlays. American Concrete Institute (ACI). *Structural Journal*, 98(6), 872-879.
- Gjorv, O. E., Vennesland, Ø, and El-Busiady, A. H. S. (1977). "Electrical Resistivity of Concrete in the Oceans" 9th Annual Offshore Technology Conference, Houston TX, USA, 581-588.
- Govinbdbhai, M.G. (2012). "Statistical Analysis of Strength and Resistivity of Optimized Graded Concrete." Master's thesis, Government College of Engineering, Aurangabad.
- Gowers, K. R. and Millard, S. G. (1999). Measurement of Concrete Resistivity for Assessment of Corrosion Severity of Steel Using Wenner Technique. *ACI Materials Journal*, 96(5), 536–542.
- Gucunski, N., Nazarian, S., Wiggenshauser, H., and Kutrubes, D. (2010). "Nondestructive Testing to Identify Concrete Bridge Deck Deterioration", SHRP 2-FEHRL Workshop R06-A, Brussels, Belgium.
- Gucunski, N. (2011). Comprehensive Bridge Deck Deterioration Mapping of Nine Bridges by Nondestructive Evaluation Technologies. Report SPR-NDEB(90)-8H-00, Federal Highway Administration U.S. Department of Transportation, Washington, D.C.
- Gucunski, N. (2013). Nondestructive Testing to Identify Concrete Bridge Deck Deterioration. Report S2-R06A-RR-1, U.S. Department of Transportation, Washington, D.C.
- Gudimettla, J. and Crawford, G. (2016). "Resistivity tests for concrete—recent field experience," *ACI Materials Journal*, 113(4)
- Haber, Z. B., Munoz, J. F. and Gaybeal, B. A. (2017). Field Testing of an Ultra-High Performance Concrete Overlay. Publication No. FHWA-HRT-17-096. U.S. Department of Transportation Federal Highway Administration. McLean, VA.
- Hall, H., LeFlore, J., Staffileno, C., Fennell, M., and Ley, T. (2019). "Update on the Super Air Meter." Presented at the Spring 2019 meeting of the National Concrete Consortium. April 25, 2019. Denver, Colorado. Available at: <https://intrans.iastate.edu/events/spring-2019-national-concrete-consortium/>
- Hallet, B., Walder, J. S., and Stubbs, C. W. (1991). "Weathering by Segregation Ice Growth in Microcracks at Sustained Sub-zero Temperatures: Verification from an Experimental Study Using Acoustic Emissions" *Permafrost and Periglacial Processes*, 2, 283-300.
- Harrington, D. and Fick, G. (2014) Guide to Concrete Overlays: Sustainable Solutions for Resurfacing and Rehabilitating Existing Pavements, 3rd Edition. ACPA Publication TB021.03P. National Concrete Pavement Technology Center. Iowa State University, Ames, IA.
- Hearn, N., Hooton, R. D., and Nokken, M. R. (2006). "Pore Structure, Permeability, and Penetration Resistance Characteristics of Concrete" ASTM 169C. Significance of Tests and Properties of Concrete & Concrete-Making Materials, ASTM International, West Conshohocken, PA, 238-252.
- Holland, J.A. (1990). "Mixture Optimization." *Concrete International*. 12(10) p. 10.
- Hover, K. (1993). 'Why is there Air in Concrete', http://www.concreteconstruction.net/_view-object?id=00000153-964c-dbf3-a177-967ddaf60000
- Hover, K. C. (1998). "Concrete Mixture Proportioning with Water-reducing Admixtures to Enhance Durability: A Quantitative Model." *Cement and Concrete Composites*, 20(1998), 113-119.
- Icenogle, P. and Rupnow T. (2012). Surface Resistivity Measurements for Quality Assurance Pave the Way to Savings in Louisiana. Louisiana Transportation Research Center. Baton Rouge, LA.
- Jenkins, A. (2015). "Surface resistivity as an alternative for rapid chloride permeability test of hardened concrete," Tech. Report FHWA-KS-14-15, Kansas Department of Transportation Bureau of Research, Topeka, KS.
- Jones, R. (1962). Non-destructive testing of concrete. Cambridge University Press, London
- Jones, M.R., Zheng, L., and Newlands, M.D. (2002). Comparison of particle packing models for proportioning concrete constituents for minimum voids ratio. *Materials and Structures*. 35. 301-309. 10.1007/BF02482136.
- Joshi, P., and Chan, C. (2002). "Rapid Chloride Permeability Testing. Hanley-Wood LLC. Publication #C02L037



- Katz, A., Bentur, A., Alexander, M., and Arliguie, G. (Eds.). (1998). “The Interfacial Transition Zone in Cementitious Composites.” E FN Spon.
- Kennedy, T., Huber, G.A., Harrigan, E.T., Cominsky, R.J., Hughes, C.S., Von Quintus, H., Moulthrop, J.S. (1994). “Superior Performing Asphalt Pavements (Superpave): The Product of the SHRP Asphalt Research Program.” National Research Council.
- Kevern, J., Halmen, C., Hudson, D. and Trautman, B. (2016). “Evaluation of Surface Resistivity for Concrete Quality Assurance in Missouri.” Transportation Research Record: Journal of the Transportation Research Board. 2577(1), 53-59.
- Larsen, C. K., Sellevold, E. J., Østvik, J.-M., and Vennesland, Ø. (2006). “Electrical resistivity of concrete—Part II: influence of moisture content and temperature,” in Proceedings of the 2nd International RILEM Symposium on Advances in Concrete through Science and Engineering.
- Lataste, J. F., Sirieix, C., Breysse, D., and Frappa, M. (2003). “Electrical resistivity measurement applied to cracking assessment on reinforced concrete structures in civil engineering,” NDT & E International, 36(6), 383–394.
- Layssi, H., Ghods, P., Alizadeh, A. R. and Salehi, M. (2015). “Electrical resistivity of concrete,” Concrete International, 37, 41–46.
- Lee, Y. H. and Oh, T. (2016). “The measurement of P-, S-, and R-wave velocities to evaluate the condition of reinforced and prestressed concrete slabs,” Advances in Material Science and Engineering, 2016, Article ID 1548215, Hindawi Publishing Corporation.
- Leemann, A, Muench, B, Gasser, P, and Holzer, L. (2006). Influence of compaction on the interfacial transition zone and the permeability of concrete. United States. <https://doi.org/10.1016/j.cemconres.2006.02.010>
- LeFlore, J. (2016). “Super Air Meter Test Video” [Video]. https://www.youtube.com/watch?v=xAcHqMz_m3I&t=485s
- Lemieux, M., R. Gagné, B. Bissonnette, and M. Lachemi. (2005). Behavior of Overlaid Reinforced Concrete Slab Panels Under Cyclic Loading—Effect of Interface Location and Overlay Thickness. ACI Structural Journal, 102(3), 454–461.
- Ley, M.T. and Tabb, B., 2014. “A Test Method to Measure the Freeze Thaw Durability of Fresh Concrete using Overpressure,” T&DI Congress 2014: Planes, Trains, and Automobiles, 79-87.
- Ley, M.T., Welchel, D., Peery, J., and LeFlore, J. (2017). Determining the Air Void Distribution in Fresh Concrete with the Sequential Air Method. Construction and Building Materials, 9(150), 723-737. <https://doi.org/10.1016/j.conbuildmat.2017.06.037>.
- Li, W., Pour-Ghaz, M., Castro, J., & Weiss, J. (2012). Water Absorption and Critical Degree of Saturation Relating to Freeze-Thaw Damage in Concrete Pavement Joints. Journal of Materials in Civil Engineering, 24(3), 299–307. doi:10.1061/(asce)mt.1943-5533.0000383
- Lilek, J. (2017). “Roadway deicing in the United States: How a few industrial minerals supply a vital transportation service.” American Geosciences Institute. Alexandria, VA. Available at: https://www.americangeosciences.org/sites/default/files/CI_Factsheet_2017_3_Deicing_170712.pdf
- Lindquist, W., Darwin, D., Browning, J., McLeod, H.A.K., Yuan, J., and Reynolds, D. (2015). Implementation of Concrete Aggregate Optimization. *Construction and Building Materials*. 74, 49-56. <https://doi.org/10.1016/j.conbuildmat.2014.10.027>
- Liu, Y. and Presuel-Moreno, F. J. (2014). “Normalization of temperature effects on concrete resistivity by method using Arrhenius law,” ACI Materials Journal, 111(4), 433-443.
- Lorenzi A., Fonseca Caetano L., Campagnolo J. L. and Silva Filho LCP (2012). Analyzing two different data processing strategies for monitoring concrete structures using ultrasonic pulse velocity. Revista Alconpat Int., 2(3), 182–194
- Mangulkar, Madhuri & Jamkar, Sanjay. (2013). Review of Particle Packing Theories Used for Concrete Mix Proportioning. Int. J. Sci. Eng. Res. 4. 143-148.
- Marquez, J. M. S. (2015). Influence of saturation and geometry on surface electrical resistivity measurements. M.S. thesis. Concordia University, Montreal, Canada
- McDonald, D. (2011). “Guidelines for Inspection and Acceptance of Epoxy-Coated Reinforcing Steel at the Jobsite.” Epoxy Interest Group. Available at: http://www.epoxyinterestgroup.org/index.cfm/_api/render/file/?method=inline&fileID=9C0262EF-BFDB-0C20-74CCB04EFC53D686
- Mehta, P.K. and Monteiro, P.J.M. (2014). Concrete: Microstructure, Properties, and Materials Fourth Edition. McGraw Hill Education.

- Moini, M. (2015). “The Optimization of Concrete Mixtures for use in Highway Applications.” Master’s thesis. University of Wisconsin Milwaukee. Milwaukee, WI.
- Moini, M. (2015). The optimization of aggregate blends for sustainable low cement concrete. *Construction and Building Materials*, 93, 627–634. 10.1016/j.conbuildmat.2015.06.019.
- Millard, S. G., Harrison, J. A. and Gowers, K. R. (1991). “Practical measurements of concrete resistivity,” *British Journal Non-destructive Testing*, 33, 59-63.
- Morales, M. (2015). “Experimental investigation of the effects of embedded rebar, cracks, chloride ingress and corrosion on electrical resistivity measurements of reinforced concrete,” Masters Thesis. Oregon State University, Corvallis, OR.
- Morris, W., Moreno, E.I. and Sagues, A.A. (1996). “Practical evaluation of resistivity of concrete in test cylinders using a Wenner array probe,” *Cement and Concrete Research*, 26(12), 1779–1787.
- National Ready Mixed Concrete Association (NRMCA). (2019). P2P initiative. Available at: <https://www.nrmca.org/association-resources/research-and-engineering/p2p/>. Accessed November 2021.
- National Ready Mixed Concrete Association (NRMCA). (2005). “The P2P Initiative: A Shift to Performance Specifications for Concrete Focuses on Innovation, Quality and Customer Satisfaction.” NRMCA, Silverspring, MD.
- Neville, A. M. (2013). *Properties of Concrete*. Pearson Education Limited, London, UK.
- New York Department of Transportation (NYSDOT). (2022). *Special Specifications: Section 501: Portland Cement Concrete – Performance Mixture Design and Quality Control*. Albany, New York.
- New York Department of Transportation (NYSDOT). (2019). Item 504.00000011 – Performance Engineered Concrete Mixture for Pavements. Albany, NY
- North Carolina Department of Transportation (NCDOT). (2018). *Standard Specifications for Roads and Structures: Division 10: Materials*. Raleigh, North Carolina.
- Obla, K.H., Kim, H., and Lobo, C.L. (2007). “Effect of Continuous (Well-Graded) Combined Aggregate Grading on Concrete Performance, Phase A: Aggregate Voids Content (Packing Density).” National Ready Mixed Concrete Association (NRMCA). https://www.nrmca.org/wp-content/uploads/2020/06/D340AGR_report_phaseA2.pdf
- OECD (2018), “Climate-resilient infrastructure”, OECD Environment Policy Papers, No. 14, OECD Publishing, Paris, <https://doi.org/10.1787/4fdf9eaf-en>.
- Ojo, T., O. (2018). “Performance of Portland Cement Concrete Containing Chemically Beneficiated High Loss on Ignition Fly Ashes with Air Entrainment.” Master Thesis. University of North Carolina at Charlotte. Charlotte, NC.
- Peppin, S. S. L. and Style, R. W. (2013). “The Physics of Frost Heave and Ice-Lens Growth,” *Vadose Zone Journal* 12(1), 1-12. <https://doi.org/10.2136/vzj2012.0049>
- Peterson, K. W., Swartz, R. A., Sutter, L. L., and Van Dam, T. J. (2001). “Hardened Concrete Air Void Analysis with a Flatbed Scanner” *Transportation Research Record*, 1775, 36-43.
- Pigeon, M. and Pleau, R. (1995). *Durability of Concrete in Cold Climates*. E & FN Spon, London, UK
- Powers, T.C. (1958). Structure and Physical Properties of Hardened Portland Cement Paste. *Journal of the American Ceramic Society*, 41 1-6. <https://doi.org/10.1111/j.1151-2916.1958.tb13494.x>
- Polder, R. B. (2001). “Test methods for onsite measurement of resistivity of concrete—a RILEM TC-154 technical recommendation,” *Construction and Building Materials*, 5(2-3), 125–131.
- Powers, T. C., and Helmuth, R. A. (1953). “Theory of Volume Changes in Hardened Portland Cement Paste During Freezing,” *Proceedings, Highway Research Board*, 32, 285-297.
- Powers, T.C., Copeland, L.E., and Mann, H.M. (1959). “Capillary continuity or discontinuity in cement pastes”. *Journal of the PCA Research and Development Laboratories*. 1(2), 38-48.
- Poyet, S. (2009) “Experimental investigation of the effects of temperature on the first desorption isotherm of concrete,” *Cement and Concrete Research*, 39(11), 1052-1059.
- Rached, M., De Moya, M., and Fowler, D.W. (2009). “Utilizing Aggregates Characteristics to Minimize Cement content in Portland Cement Concrete.” Final Report, International Center for Aggregates Research Project No. ICAR 401, February 2009.
- Rajabipour, F., Weiss, J., and Abraham, D. M. (2004). “Insitu electrical conductivity measurements to assess moisture and ionic transport in concrete (A discussion of critical features that influence the measurements),” School of Civil Engineering, Purdue University, West Lafayette, IN.

- Ram, P., Dam, T. V., Sutter, L., Anzalone, G., and Smith, K. (2012). Field Study of Air Content Stability in the Slipform Paving Process. Report No. WHRP 0092-11-06. Wisconsin Highway Research Program and Wisconsin Department of Transportation.
- Rixom, R. and Mailvaganam, N. (1999). "Chemical Admixtures for Concrete 3rd ed. E & FN Spon, London, UK.
- Richardson, D.N. (2005). Aggregate Gradation Optimization -- Literature Search. Report RDT 05-001. Missouri Department of Transportation. Jefferson City, MO.
- Rupnow, T. and Icenogle, P. (2011). "Surface Resistivity Measurements Evaluated as Alternative to the Rapid Chloride Permeability Test for Quality Assurance and Acceptance." Final Report, Report No. FHWA/LA.11/479. Louisiana Department of Transportation and Development, Baton Rouge, LA.
- Rupnow, T. and Icenogle, P. (2012). "Evaluation of Surface Resistivity Measurements as an Alternative to the Rapid Chloride Permeability Test for Quality Assurance and Acceptance." Transportation Research Record: Journal of the Transportation Research Board, 2290, 1, 30-37.
- Rupnow, T. and Icenogle, P. (2011) "Surface Resistivity Measurements Evaluated as Alternative to the Rapid Chloride Permeability Test for Quality Assurance and Acceptance." Final Report, Report No. FHWA/LA.11/479. Louisiana Department of Transportation and Development, Baton Rouge, LA.
- Salehi, M., Ghods, P. and Isgor, O. B. (2015). "Numerical study on the effect of cracking on surface resistivity of plain and reinforced concrete elements," Journal of Materials in Civil Engineering, 27(12), Article ID 04015053.
- Salehi, M., Ghods, P. and Isgor, B.O. (2016). "Numerical investigation of the role of embedded reinforcement mesh on electrical resistivity measurements of concrete using the Wenner probe technique," Materials and Structures, 49,(1-2), 301–316.
- Sansalone, M. J., and Streett, W. B. (1999). "The Impact-Echo Method", NDTnet, 3(2). Available at: <https://www.ndt.net/article/0298/streett/streett.htm#author>
- Santhanam, M., and Talbot, S.V. (2003). Particle packing theories and their application in concrete mixture proportioning: A review. The Indian Concrete Journal, 77, 1324-1331.
- Sengul, O. (2014). "Use of electrical resistivity as an indicator for durability," Construction and Building Materials, 73, 434–441.
- Sengul, O. and Gjrv, O. E. (2009). "Effect of embedded steel on electrical resistivity measurements on concrete structures," ACI Materials Journal, 106 (1), 11-18.
- Setzer, M. J. (2001). "Micro-Ice-Lens Formation in Porous Solid," Journal of Colloid and Interface Science 243, 193–201. doi: 10.1006/jcis.2001.7828
- Shaeles, C.A., Hover, K.C. (1988). Influence of mix proportions and Construction Operations on Plastic Shrinkage Cracking in Thin Slabs. American Concrete Institute Materials Journal, 85(6), 495-514.
- Shah, A.A., and Ribakov, Y. (2008). "Non-destructive measurements of crack assessment and defect detection in concrete structures," Materials and Design, 29(1), 61–69.
- Shann, S. V. (2012). Application of Ultra High Performance Concrete (UHPC) as a Thin-Bonded Overlay for Concrete Bridge Decks. M.S. Thesis. Michigan Technological University, Houghton, MI.
- Shilstone, J.M., Sr. and Shilstone J.M., Jr. (2002). Performance-Based Concrete Mixtures and Specifications for Today. *Concrete International*. 24(2), 80-83.
- Shilstone, J.M. (1990). "Concrete Mixture Optimization." *Concrete international*. 12(6). ACI Farmington Hills, MI. 33-39.
- Scrivener, K.L., Crumbie, A.K., and Laugesen, P. (2004). The Interfacial Transition Zone (ITZ) Between Cement Paste and Aggregate in Concrete. *Interface Science*. 12(4), 411-421. <http://dx.doi.org/10.1023/B:INTS.0000042339.92990.4c>
- Sharifi, N., Chen, S., You, Z., Van Dam, T., & Gilbertson, C. G. (2019). A review on the best practices in concrete pavement design and materials in wet-freeze climates similar to Michigan. *Journal of Traffic and Transportation Engineering*. <http://doi.org/10.1016/j.jtte.2018.12.003>
- Smyl, D. (2013). "Methods of Predicting Aggregate Voids." Final Report. FHWA-KS-12-8. Kansas Department of Transportation. Topeka, KS.
- Spragg, R., Bu, Y., Snyder, K., Bentz, D. and Weiss, J. (2013). "Electrical testing of cement-based materials: role of testing techniques, sample conditioning," Tech. Rep. FHWA/IN/JTRP-2013/28, Purdue University, West Lafayette, IN.

- Spragg, R., Villani, C., Snyder, K., Bentz, D., Bullard, J. and Weiss, J. (2013) “Factors that influence electrical resistivity measurements in cementitious systems,” Transportation Research Record: Journal of the Transportation Research Board, 2342, 90–98.
- Sprinkel, M. (2000). Evaluation of Latex-Modified and Silica Fume Concrete Overlays Placed on Six Bridges in Virginia. Virginia Transportation Research Council. Charlottesville, VA.
- Talbot, A.N., and Richart, F.E. (1923). “The Strength of Concrete and it’s Relation to the Cement, Aggregate, and Water.” University of Illinois Engineering Experiment Station Bulletin no. 137.
- Tanesi, J. and Meininger, R. (2006). Freeze-Thaw Resistance of Concrete with Marginal Air Content. Report No. FHWA-HRT_06-117. Federal Highway Administration, Washington, DC.
- Tayabji, S.D., Smith, K.D., Dam, T., & Tyson, S.S. (2010). Advanced High-Performance Materials for Highway Applications: A Report on the State of Technology.
- Taylor, P. (2015). Blended Aggregates for Concrete Mixture Optimization Best Practices for Jointed Concrete Pavements: Tech Brief, July 2015. Federal Highway Administration. Washington, DC.
<http://www.fhwa.dot.gov/pavement/concrete/pubs/hif15019.pdf>
- Taylor, P., Tennis, P., Obla, K., Ram, P., Van Dam, T. and Dylla, H. (2013). Durability of Concrete. Transportation Research Circular No. E-C171. TRB Committee AFN30. Transportation Research Board, Washington, DC.
- Taylor, P., Van Dam, T., Sutter, L., and Fick, G. (2019). “Integrated Materials and Construction Practices for Concrete Pavement: A State-of-the-Practice Manual.” Second Edition. National Concrete Pavement Technology Center, Iowa State University, Ames, IA.
- Theilgard P. (2022). “Optimized Aggregate Gradation Concrete Mixtures with Cementitious Material Reduction” Masters Thesis, University of North Carolina at Charlotte, Charlotte, NC.
- Van Dam, T., and Taylor., P. (2009). “Building Sustainable Pavements with Concrete: Briefing Document.” InTrans Project Reports. 154. http://lib.dr.iastate.edu/intrans_reports/154
- Van Dam, T., Taylor, P., Fick, G.J., Van Geem, M.G., & Lorenz, E.B. (2012). Sustainable Concrete Pavements: A Manual of Practice. National Concrete Pavement Technology Center, Iowa State University, Ames, IA.
- Weiss, W.J., Ley, M.T., Isgor, O.B., and Van Dam, T. (2017). “Toward Performance Specifications for Concrete Durability: Using the Formation Factor for Corrosion and Critical Saturation for Freeze-Thaw.” Transportation Research Board 96th Annual Meeting, Washington, DC.
- Weiss, J., Snyder, K., Bullard, J. and Bentz, D. (2013). “Using a saturation function to interpret the electrical properties of partially saturated concrete,” Journal of Materials in Civil Engineering, 25(8), 1097–1106.
- Welchel, D. (2014). “Determining the Air-Void Distribution of Fresh Concrete with the Sequential Pressure Method.” Masters Thesis. Oklahoma State University, Stillwater, OK. Available at: <https://hdl.handle.net/11244/299670>
- Weydert, R. and Gehlen, C. (1999). “Electrolytic Resistivity of Cover Concrete: Relevance, Measurement and Interpretation.” Eighth Int. Conf. on Durability of Materials and Components. Vancouver, Canada.
- Wig, R.J., Williams, G.M., and Gates, E.R. (1916). “Strength and other properties of concretes as affected by materials and methods of preparation.” Bureau of Standards no. 58.
- Wilson, M., and Tennis, P. (2021). Design and Control of Concrete Mixtures, 17th edition. Portland Cement Association. Skokie, IL.
- Wisconsin Department of Transportation (WisDot). (2022). Standard Specification for Highway and Structure Construction: Section 715: QMP Concrete Pavement and Structures. Madison, Wisconsin.
- Yun, K., Choi, P. (2014). “Cause and controls of cracking at bridge deck overlay with very-early strength latex-modified concrete.” Construction and Building Materials, 56, 53-62. DOI: 10.1016/j.conbuildmat.2014.01.055

APPENDIX B – SUPPORTING MATERIAL FOR LABORATORY TESTING PROGRAM AND RESULTS (Chapter 3)

Material: Portland Cement

Type: I-II (MH)

Material Certification Report


Test Period: 18-Sep-2019 to 19-Sep-2019

Date Issued: 14-Oct-2019

Certification					
This cement meets the specifications of ASTM C150 and AASHTO M85 for Type I-II (MH) cement.					
General Information					
Supplier: Holcim (US) Inc. d/b/a LafargeHolcim US		Source Location: Holly Hill Plant Silo: 18			
Address: 8700 West Bryn Mawr Ave Chicago, IL 60631		2173 Gardner Blvd Holly Hill, SC 29059			
Contact:		Contact: Scott Poaps / (803) 496-2995			
The following is based on average test data during the test period. The data is typical of product shipped from this source; individual shipments may vary.					
Test Data on ASTM Standard Requirements					
Chemical			Physical		
Item	Limit *	Result	Item	Limit *	Result
SiO ₂ (%)	-	20.1	Air Content (%)	12 max	7
Al ₂ O ₃ (%)	6.0 max	4.8	Blaine Fineness (m ² /kg)	260-430	404
Fe ₂ O ₃ (%)	6.0 max	3.5	Autoclave Expansion (%) (C151)	0.80 max	-0.04
CaO (%)	-	63.6	Compressive Strength MPa (psi)		
MgO (%)	6.0 max	1.4	3 day	10.0 (1450) min	31.0 (4500)
SO ₃ (%) *	3.0 max	3.2	7 day	17.0 (2470) min	38.4 (5570)
Loss on Ignition (%) *	3.5 max	1.9	28 day (previous month's data)	-	46.9 (6800)
Insoluble Residue (%)	1.50 max	0.35	Initial Vicat (minutes)	45-375	125
CO ₂ (%)	-	1.0	Mortar Bar Expansion (%) (C1038)	0.020 max	0.003
CaCO ₃ in Limestone (%)	70 min	88			
Potential Phase Compositions *:					
C ₃ S (%)	-	56			
C ₂ S (%)	-	15			
C ₃ A (%)	8 max	7			
C ₄ AF (%)	-	11			
C ₃ S + 4.75C ₃ A (%)	100 max	88			
Test Data on ASTM Optional Requirements					
Chemical			Physical		
Item	Limit *	Result	Item	Limit *	Result
Equivalent Alkalies (%)	-	0.48	Heat of Hydration kJ/kg (cal/g)	-	267 (64)
			(ASTM C1702) 3 Days *		
Notes (*1-9)					
1 - Dashes in the Limit / Result columns mean Not Applicable.					
2 - It is permissible to exceed the specification limit provided that ASTM C1038 Mortar Bar Expansion does not exceed 0.020% at 14 days.					
3 - Adjusted per Annex A1.6 of ASTM C150 and AASHTO M85.					
4 - Test results represent the most recent value and is provided for information only.					
5 - Limit = 3.0 when limestone is not an ingredient in the final cement product					
9/18/2019					
Grind 261					
Additional Data					
Item	Limestone	Inorganic Processing Addition	Base Cement Phase Composition	Result	
Amount (%)	2.6	0.7	C ₃ S (%)	58	
SiO ₂ (%)	2.7	30.3	C ₂ S (%)	15	
Al ₂ O ₃ (%)	0.7	11.0	C ₃ A (%)	7	
Fe ₂ O ₃ (%)	0.8	0.7	C ₄ AF (%)	11	
CaO (%)	50.1	41.4			
SO ₃ (%)	0.6	2.0			

Printed: 10/14/2019 3:10:27 PM

Version: 180412



Scott Poaps,
Quality Manager

Figure B.1: Mill report for OPC



June 4, 2020

Ms. Tara Cavalline
UNC Charlotte
9201 University City Blvd.
Charlotte, NC 28223-0001

Phone: 704-687-2305
Fax: 704-687-6653
Email: tcavalline@uncc.edu

Subject: **Report of Results for Product Testing**
Product Name: Roxboro DS 11/23-12/11 (2015)
TEC Services Project #: 20-1612
TEC Laboratory #: 20-461

Dear Ms. Cavalline:

SGS TEC Services is an AASTHO R18, ANS/ISO/IEC 17025:2005 and Army Corp of Engineers accredited laboratory. SGS TEC Services is pleased to present this report of our test results on the submitted material designated as "Roxboro DS 11/23-12/11 (2015)". Our services were performed in accordance with the terms and conditions of our Service Agreement TEC-PRO-20-1612. The test results presented only pertain to the samples tested.

The Roxboro material was delivered to our Lawrenceville, GA facility on April 14, 2020. At the request of UNC Charlotte, testing was performed on the material per ASTM C618-19 *Standard Specification for Coal Fly Ash and Raw or Calcined Natural Pozzolan for Use in Concrete*. The chemical analysis test results are reported in attached Table 1.

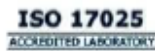
SGS TEC Services appreciates the opportunity to provide our professional services for this important project. If you have any questions regarding this report, or if we can be of further assistance please contact us at 770-995-8000.

Sincerely,

SGS TEC SERVICES

Dean T. Roosa
Project Manager

Shawn P. McCormick
Laboratory Principal



SGS TEC SERVICES
235 Buford Drive | Lawrenceville GA 30046
770-995-8000 | www.tecservices.com



Table 1 – Results of the Chemical Analysis

Oxides	Results Weight (%)
Silicon Dioxide (SiO ₂)	52.7
Aluminum Oxide (Al ₂ O ₃)	26.7
Iron Oxide (Fe ₂ O ₃)	11.12
Sum (SiO ₂ + Al ₂ O ₃ + Fe ₂ O ₃)	90.5
Calcium Oxide (CaO)	2.1
Magnesium Oxide (MgO)	1.1
Sodium Oxide (Na ₂ O)	0.34
Potassium Oxide (K ₂ O)	2.24
Equivalent Alkalies (Na ₂ O+0.658 K ₂ O)	1.81
Titanium Dioxide (TiO ₂)	1.42
Manganic Oxide (Mn ₂ O ₃)	0.026
Phosphorus Pentoxide (P ₂ O ₅)	0.21
Sulfur Trioxide (SO ₃)	0.75
Loss on Ignition	1.9
Moisture Content	0.38

Figure B.2: Chemical analysis of fly ash

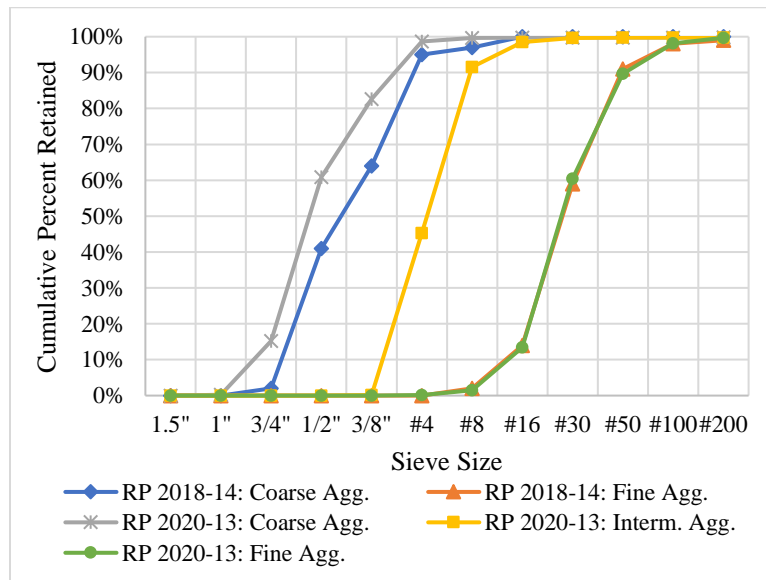


Figure B.3: Particle size analysis of aggregates used in RP 2018-14 and RP 2020-13

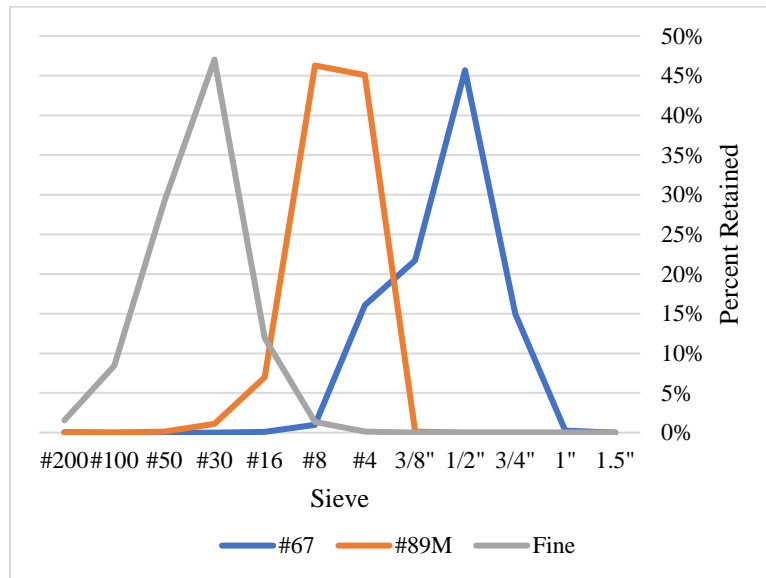


Figure B.4: Particle size analysis of aggregates used in RP 2020-13: No. 67, No. 89M, and fine aggregate

Table B.1: Fresh concrete test results (average of two batches comprising a single mixture) for RP 2018-14 (non-optimized gradation mixtures) and RP 2020-13 (optimized gradation mixtures)

Mixture ID	Slump (in.)		Air Content (%)		Unit Weight (pcf)	
	Non-Optimized	Optimized	Non-Optimized	Optimized	Non-Optimized	Optimized
H-700-0	8.0	5.0	5.2%	5.8%	137.1	144.5
H-560-140	8.0	3.5	5.2%	5.0%	136.4	142.3
H-650-0	6.5	5.0	6.0%	6.0%	141.4	140.9
H-520-130	7.0	2.3	5.5%	5.2%	138.0	143.1
H-600-0	2.5	0.0	5.8%	6.0%	138.7	144.3
H-480-120	3.0	3.3	6.0%	5.9%	139.4	142.9
H-420-180	3.8	1.9	6.0%	5.0%	136.1	142.9
M-700-0	5.0	3.8	5.5%	5.5%	141.6	142.9
M-560-140	4.3	6.0	6.0%	5.0%	136.6	142.1
M-650-0	2.5	2.5	5.7%	6.0%	142.4	144.2
M-520-130	3.0	1.8	5.5%	5.0%	139.7	145.8
M-600-0	1.0	0.8	6.0%	5.7%	140.5	143.0
M-480-120	1.5	0.9	5.0%	5.7%	139.6	144.9
M-420-180	2.0	0.8	6.0%	5.1%	138.1	144.3
L-700-0	2.3	1.5	6.0%	5.9%	143.9	144.5
L-560-140	1.8	0.5	5.0%	5.7%	140.3	142.9
L-650-0	1.0	1.0	6.0%	6.0%	141.8	144.2
L-520-130	1.0	0.5	5.0%	5.3%	141.6	144.1
L-600-0	1.0	0.0	5.5%	5.7%	142.6	144.3
L-480-120	0.8	0.0	5.5%	5.6%	142.0	144.0
L-420-180	1.0	0.0	5.2%	5.5%	142.0	144.0

Table B.2: SAM test results for optimized aggregate gradation mixtures

Mixture ID	Batch 1	Batch 2
H-700*-0	0.29	-
H-560*-140	0.40	-
H-650*-0	0.13	-
H-520*-130	0.30	-
H-600*-0	0.24	Error
H-480*-120	Error	0.18
H-420*-180	0.08	0.24
M-700*-0	0.62	-
M-560*-140	0.74	-
M-650*-0	0.43	-
M-520*-130	0.41	-
M-600*-0	Error	Error
M-480*-120	0.21	0.53
M-420*-180	Error	Error
L-700*-0	0.20	-
L-560*-140	0.39	-
L-650*-0	0.42	-
L-520*-130	0.27	-
L-600*-0	0.77	Error
L-480*-120	Error	0.51
L-420*-180	0.47	Error

Table B.3: 28-day compressive strength results

Mixture ID	Compressive Strength (psi)									
	Non-Optimized					Optimized				
	3 Day	7 Day	28 Day	56 Day	90 Day	3 Day	7 Day	28 Day	56 Day	90 Day
H-700-0	3,810	4,394	5,379	6,140	6,381	3,156	4,182	5,377	6,131	6,309
H-560-140	3,461	3,950	4,994	5,961	6,087	2,682	3,855	4,513	5,661	6,574
M-700-0	5,088	5,679	6,688	7,531	8,168	4,813	5,835	6,972	7,283	7,782
M-560-140	4,019	4,854	5,688	6,114	6,322	3,485	4,806	5,814	6,729	6,894
L-700-0	5,921	7,550	7,856	8,762	9,237	6,042	7,181	7,686	7,984	8,184
L-560-140	5,045	5,267	6,729	7,316	7,808	4,367	4,685	5,900	6,797	6,915
H-650-0	4,276	5,232	6,256	7,135	7,556	3,340	4,234	5,207	6,068	6,668
H-520-130	3,705	4,323	5,319	6,921	7,233	2,701	3,599	5,094	5,751	6,134
M-650-0	5,192	5,935	6,739	7,223	8,221	4,621	5,548	6,624	7,903	7,607
M-520-130	4,258	5,129	6,375	7,705	8,416	3,654	4,435	5,582	6,293	7,964
L-650-0	6,984	7,367	7,991	8,251	9,113	5,483	6,164	6,722	8,084	8,529
L-520-130	5,194	6,005	7,203	7,591	8,062	5,002	5,508	6,478	7,659	8,219
H-600-0	3,750	4,309	5,494	5,887	6,302	3,399	4,398	5,468	5,951	6,492
H-480-120	2,784	3,150	3,982	4,418	5,148	2,598	3,750	4,736	5,779	6,509
H-420-180	2,446	3,417	4,328	4,869	5,521	2,339	2,979	4,282	4,861	5,638
M-600-0	4,526	5,362	5,873	6,418	7,995	4,806	5,507	6,296	7,000	7,422
M-480-120	4,167	4,895	5,390	5,832	6,483	3,256	4,304	5,482	6,286	7,210
M-420-180	3,991	4,260	5,007	5,590	6,216	3,151	3,807	5,365	6,401	7,210
L-600-0	5,698	6,471	7,010	7,427	7,936	6,310	6,651	8,087	7,513	8,189
L-480-120	5,510	6,184	6,814	7,107	7,650	3,697	6,287	6,633	7,342	7,383
L-420-180	5,264	5,716	6,288	6,693	7,063	3,381	4,254	5,837	6,949	6,087

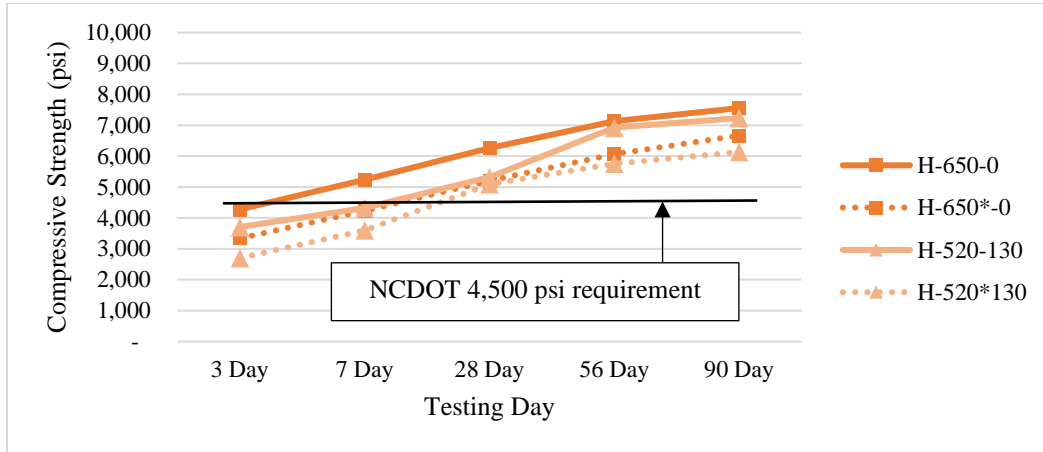


Figure B.5: Development of average compressive strength for 650/650* pcy cementitious material mixtures at 0.47 w/cm ratio

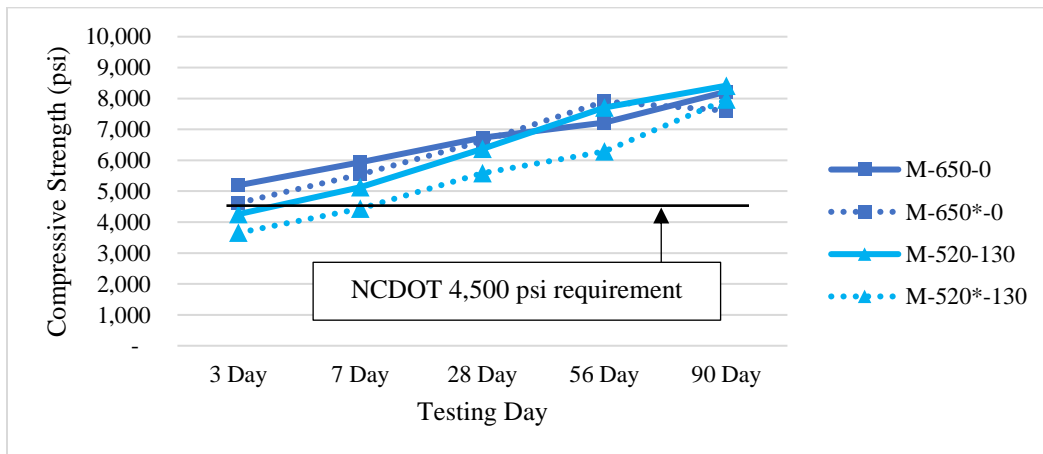


Figure B.6: Development of average compressive strength for 650/650* pcy cementitious material mixtures at 0.42 w/cm ratio

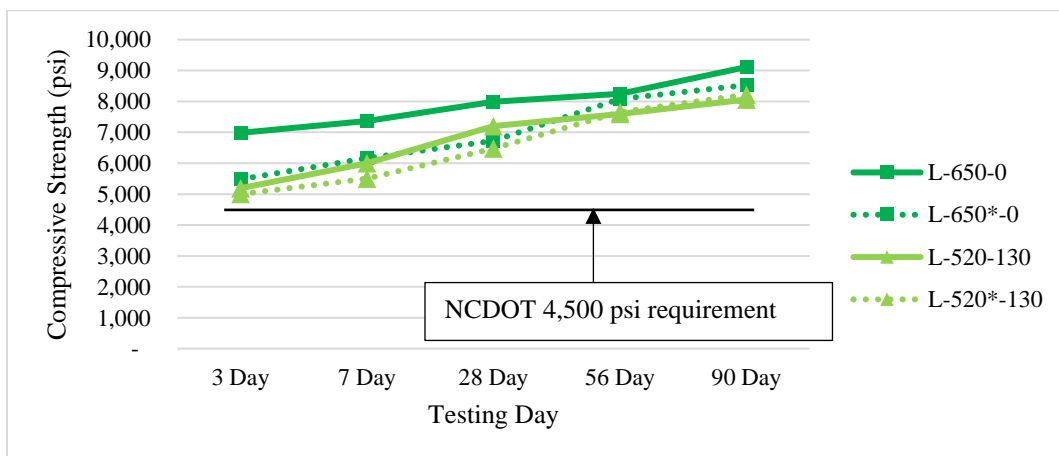


Figure B.7: Development of average compressive strength for 650/650* pcy cementitious material mixtures at 0.37 w/cm ratio

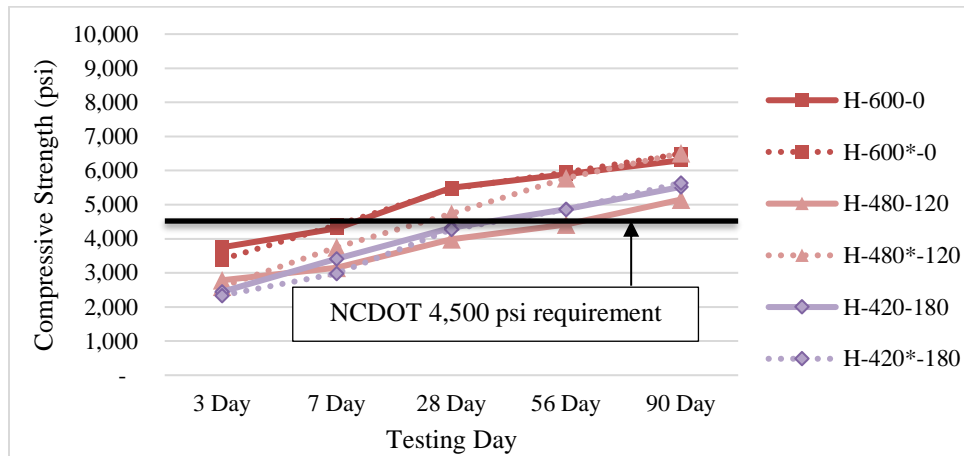


Figure B.8: Development of average compressive strength for 600/600* pcy cementitious material mixtures at 0.47 w/cm ratio

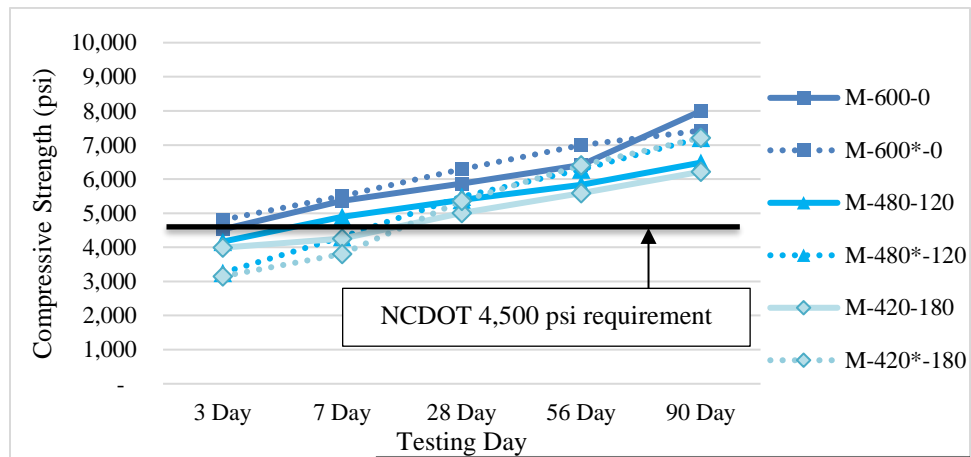


Figure B.9: Development of average compressive strength for 600/600* pcy cementitious material mixtures at 0.42 w/cm ratio

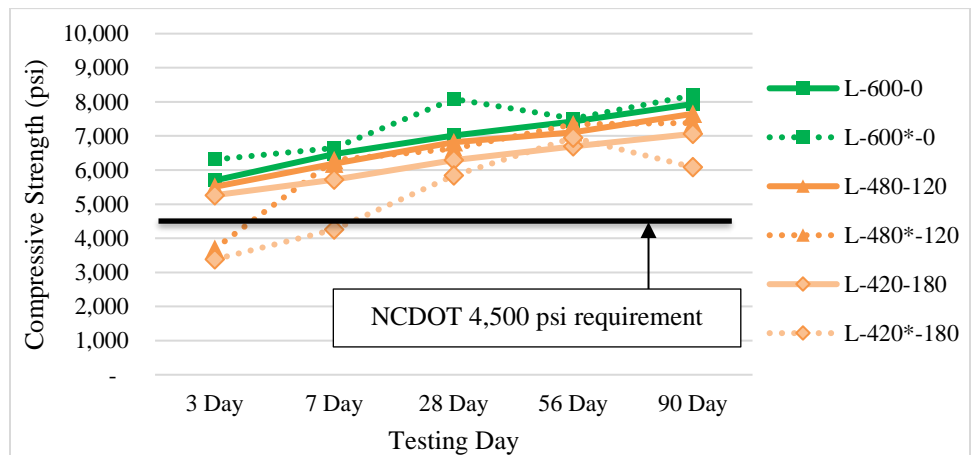


Figure B.10: Development of average compressive strength for 600/600* pcy cementitious material mixtures at 0.37 w/cm ratio

Table B.4: Average percent difference between average compressive strength for 650* pcy optimized mixtures vs 650 pcy non-optimized mixtures

Characteristic	Mixture Type	Test Day				
		3 Day	7 Day	28 Day	56 Day	90 Day
All 650* pcy mixtures	Non-optimized	4,935	5,665	6,647	7,471	8,100
	Optimized	4,133	4,915	5,951	6,960	7,520
	Average percent difference	-20.9%	-15.8%	-11.8%	-8.8%	-8.3%
Straight cement mixtures	Non-optimized	5,484	6,178	6,995	7,536	8,297
	Optimized	4,481	5,315	6,185	7,352	7,601
	Average percent difference	-22.6%	-16.7%	-13.6%	-3.7%	-9.4%
Fly ash replacement mixtures	Non-optimized	4,386	5,152	6,299	7,406	7,904
	Optimized	3,786	4,514	5,718	6,568	7,439
	Average percent difference	-19.2%	-14.9%	-9.9%	-14.0%	-7.2%

Table B.5: Average percent difference between average compressive strength for 650* pcy optimized mixtures vs 650 pcy non-optimized mixtures by w/cm ratio

w/cm ratio	Mixture Type	Test Day				
		3 Day	7 Day	28 Day	56 Day	90 Day
0.47	Non-optimized	3,991	4,778	5,788	7,028	7,395
	Optimized	3,021	3,917	5,151	5,909	6,401
	Average percent difference	-32.6%	-21.8%	-12.3%	-19.0%	-15.6%
0.42	Non-optimized	4,725	5,532	6,557	7,464	8,319
	Optimized	4,137	4,991	6,103	7,098	7,785
	Average percent difference	-14.4%	-11.3%	-8.0%	-6.9%	-6.9%
0.37	Non-optimized	6,089	6,686	7,597	7,921	8,588
	Optimized	5,242	5,836	6,600	7,872	8,374
	Average percent difference	-15.6%	-14.3%	-15.0%	-0.6%	-2.5%

Table B.6: Average percent difference between average compressive strength for 600* pcy optimized mixtures vs 600 pcy non-optimized mixtures

Characteristic	Mixture Type	Test Day				
		3 Day	7 Day	28 Day	56 Day	90 Day
All 600* pcy mixtures	Non-optimized	4,237	4,863	5,576	6,027	6,702
	Optimized	3,660	4,660	5,798	6,454	6,905
	Average percent difference	-18.4%	-5.5%	3.6%	6.7%	2.8%
Straight cement mixtures	Non-optimized	4,658	5,381	6,126	6,577	7,411
	Optimized	4,838	5,519	6,617	6,821	7,368
	Average percent difference	1.7%	2.5%	6.5%	3.5%	-0.6%
Fly ash replacement mixtures	Non-optimized	4,027	4,604	5,302	5,752	6,347
	Optimized	3,070	4,230	5,389	6,270	6,673
	Average percent difference	-28.5%	-9.5%	2.1%	8.4%	4.5%

Table B.7: Average percent difference between average compressive strength for 600* pcy optimized mixtures vs 600 non-optimized mixtures by w/cm ratio

w/cm ratio	Mixture Type	Test Day				
		3 Day	7 Day	28 Day	56 Day	90 Day
0.47	Non-optimized	2,993	3,625	4,601	5,058	5,657
	Optimized	2,778	3,709	4,829	5,530	6,213
	Average percent difference	-7.4%	1.1%	4.8%	8.2%	8.6%
0.42	Non-optimized	4,228	4,839	5,423	5,947	6,898
	Optimized	3,738	4,539	5,714	6,563	7,281
	Average percent difference	-16.3%	-7.7%	5.0%	9.4%	5.4%
0.37	Non-optimized	5,491	6,124	6,704	7,076	7,550
	Optimized	4,463	5,731	6,852	7,268	7,220
	Average percent difference	-31.7%	-10.0%	1.0%	2.7%	-5.5%

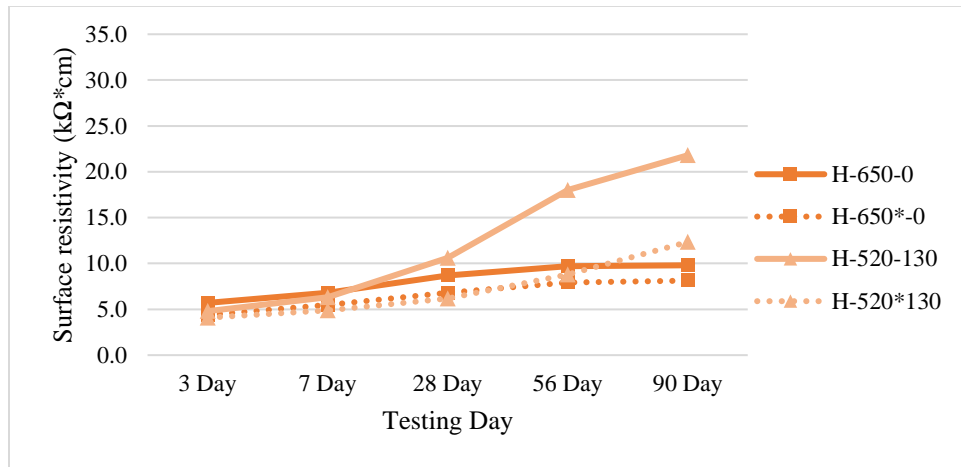


Figure B.11: Average surface resistivity test results for 650/650* pcy cementitious material mixtures at 0.47 w/cm ratio

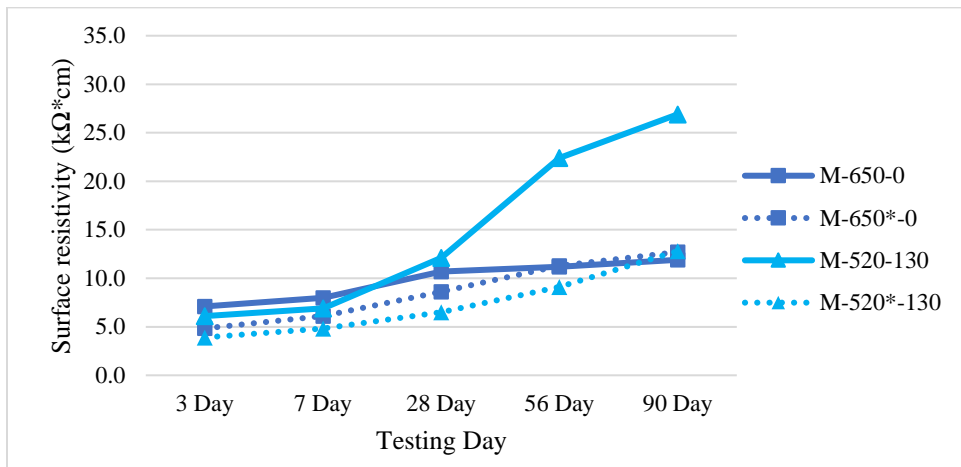


Figure B.12: Average surface resistivity test results for 650/650* pcy cementitious material mixtures at 0.42 w/cm ratio

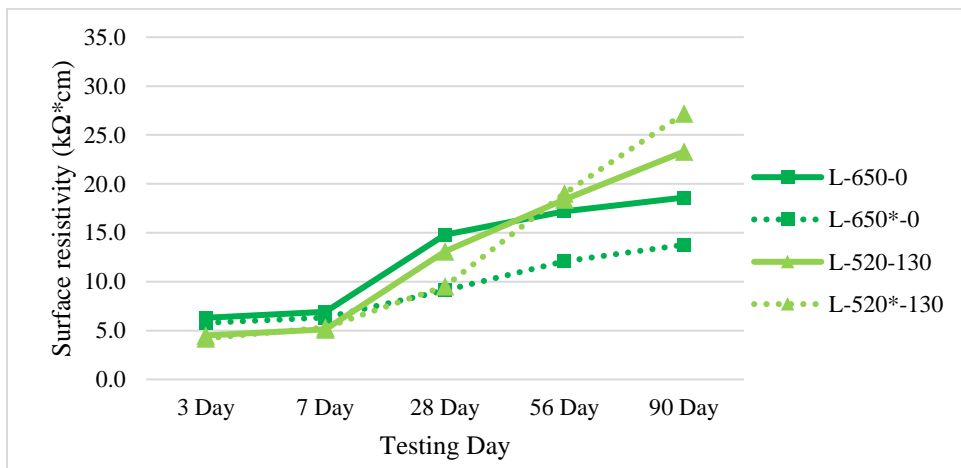


Figure B.13: Average surface resistivity test results for 650/650* pcy cementitious material mixtures at 0.37 w/cm ratio

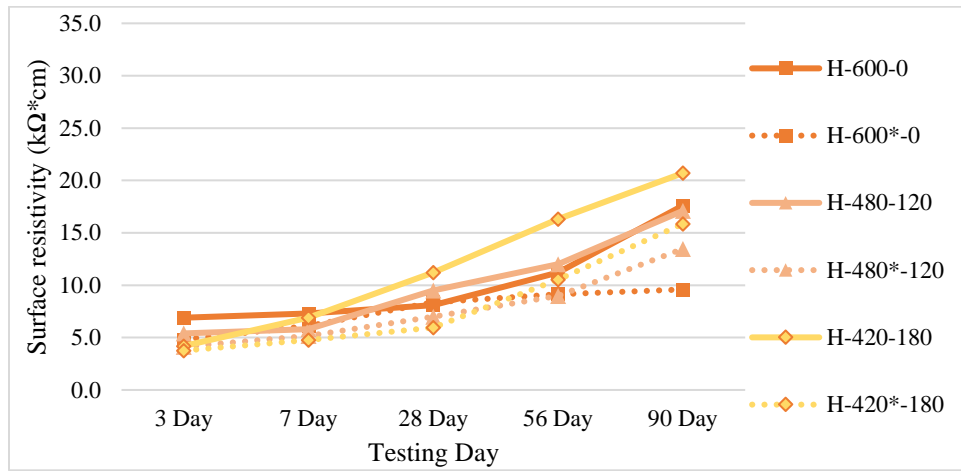


Figure B.14: Average surface resistivity test results for 600/600* pcy cementitious material mixtures at 0.47 w/cm ratio

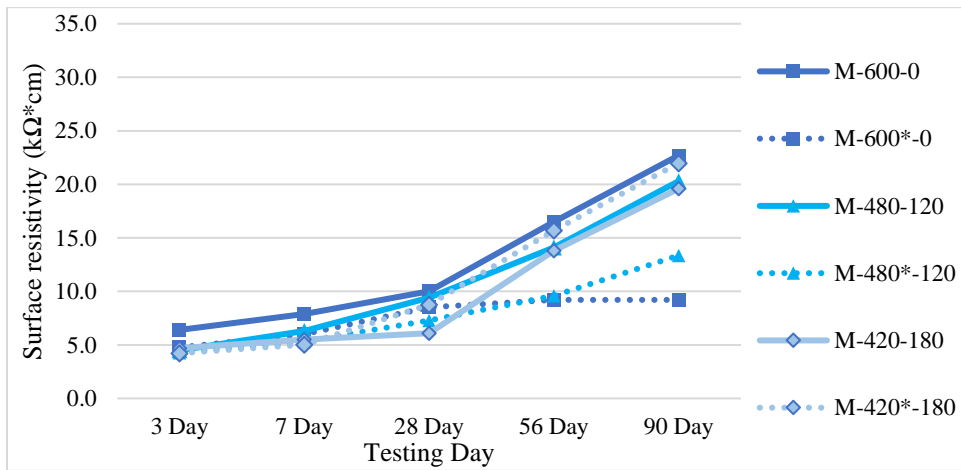


Figure B.15: Average surface resistivity test results for 600/600* pcy cementitious material mixtures at 0.42 w/cm ratio

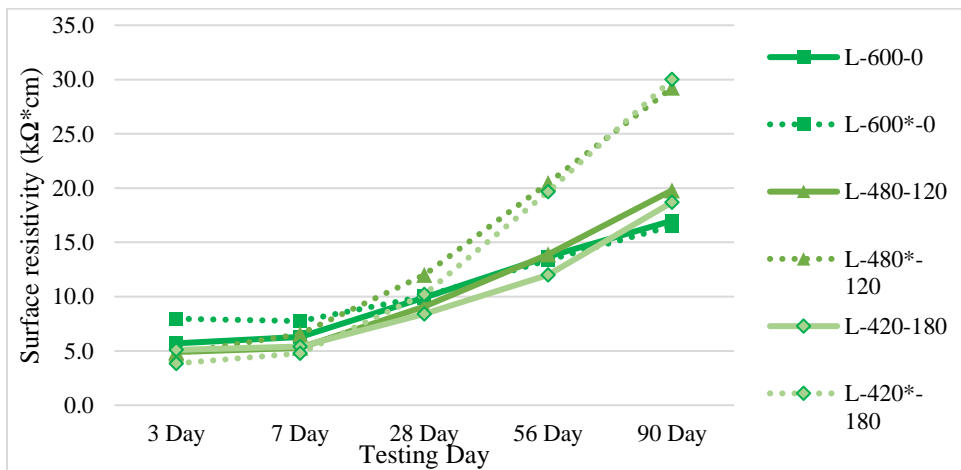


Figure B.16: Average surface resistivity test results for 600/600* pcy cementitious material mixtures at 0.37 w/cm ratio

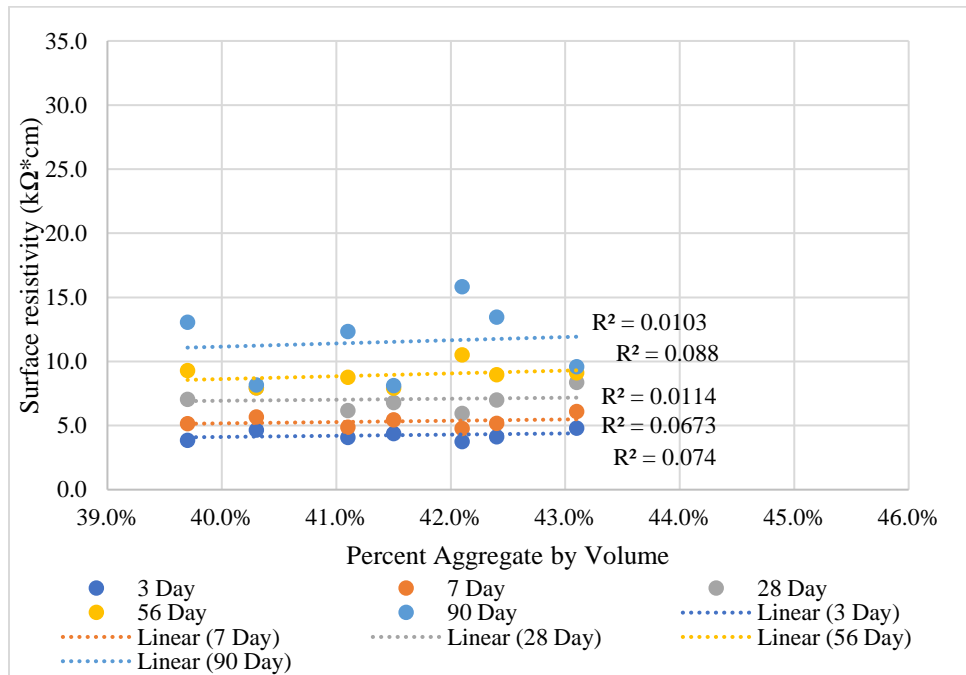


Figure B.17: Surface resistivities of high w/cm ratio optimized concrete mixtures vs percent coarse aggregate volume

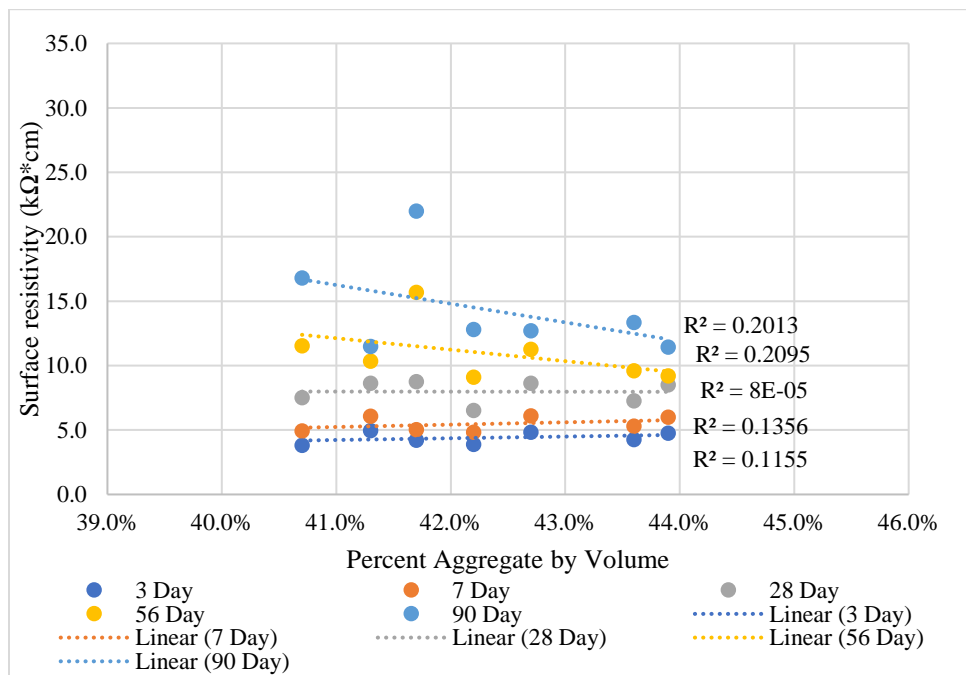


Figure B.18: Surface resistivities of medium w/cm ratio optimized concrete mixtures vs percent coarse aggregate volume

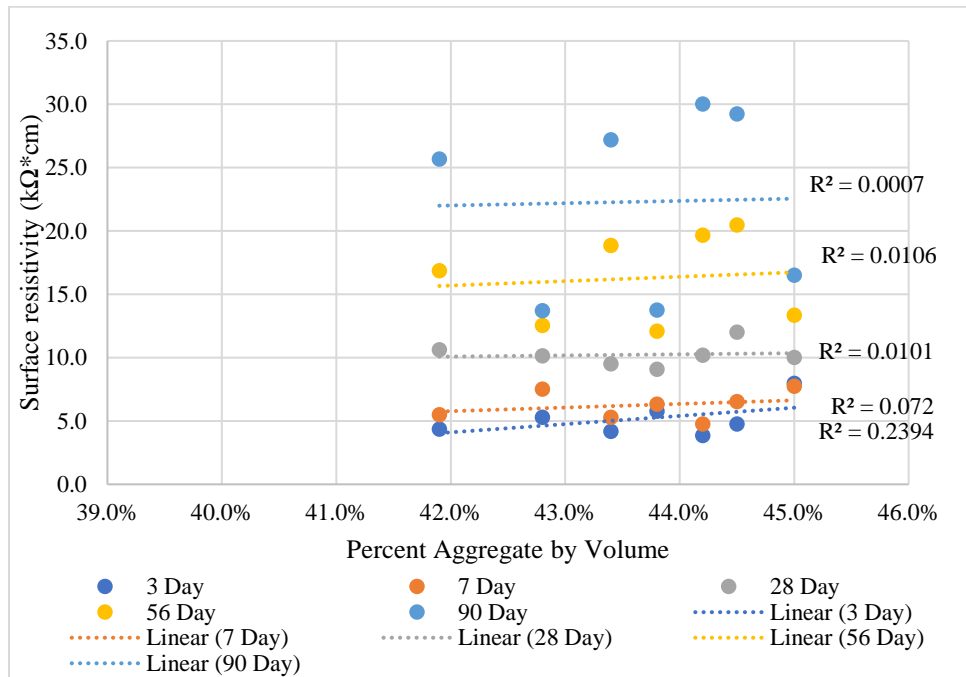


Figure B.19: Surface resistivities of low w/cm ratio optimized concrete mixtures vs percent coarse aggregate volume

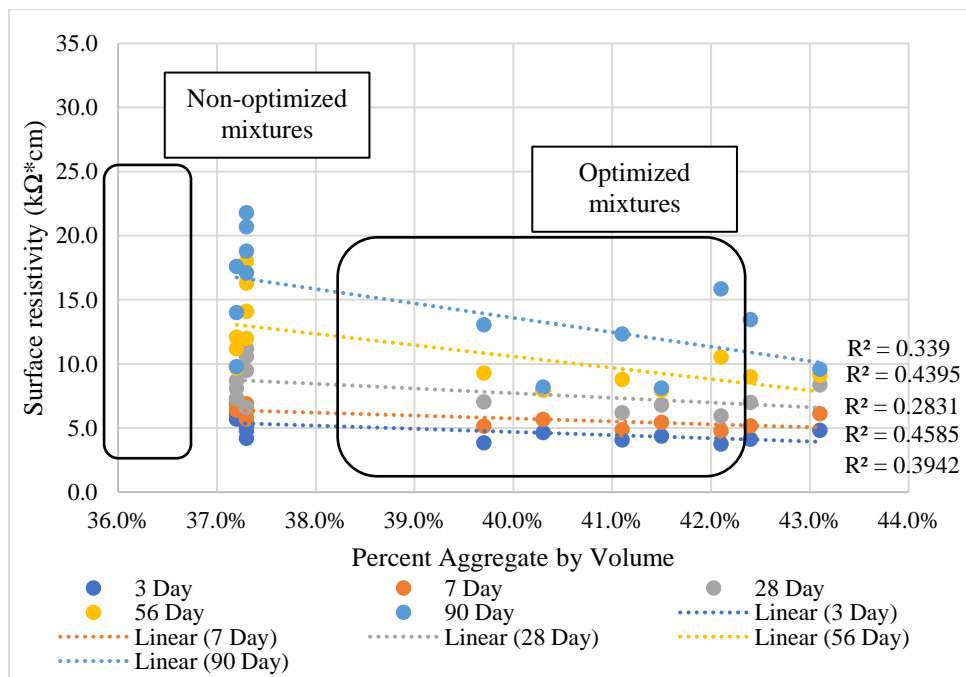


Figure B. 20: Surface resistivities of high w/cm ratio optimized and non-optimized concrete mixtures vs percent coarse aggregate volume

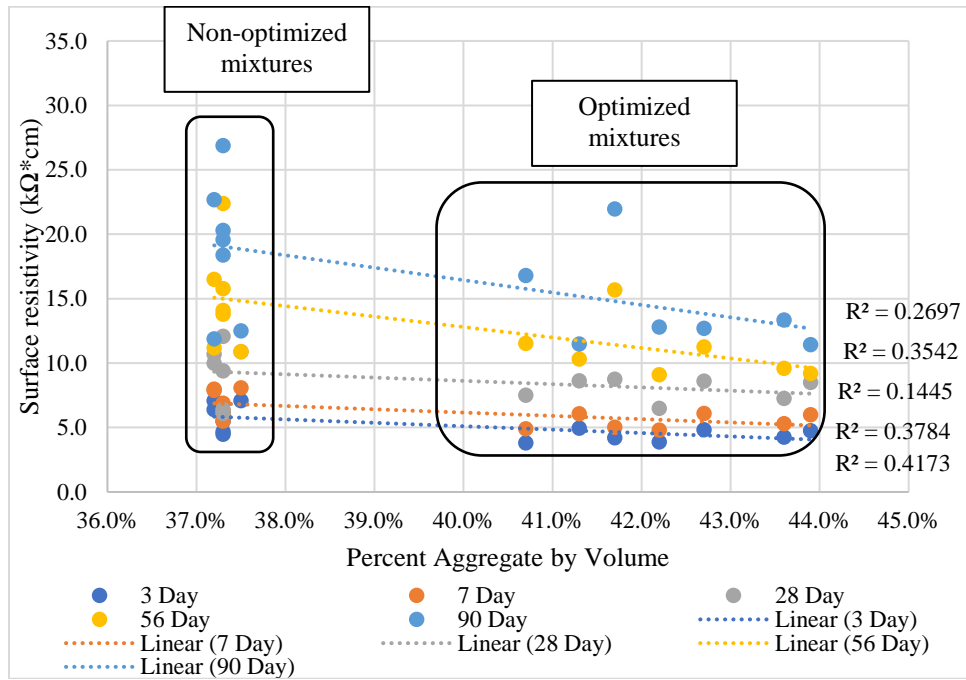


Figure B.21: Surface resistivities of medium w/cm ratio optimized and non-optimized concrete mixtures vs coarse aggregate volume

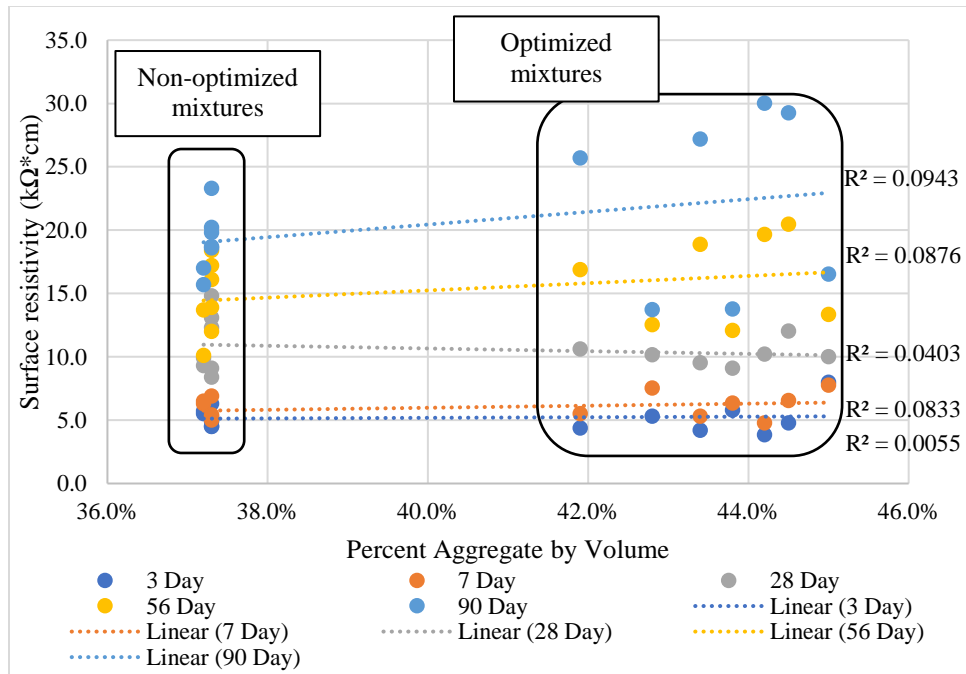


Figure B.22: Surface resistivities of low w/cm ratio optimized and non-optimized concrete mixtures vs coarse aggregate volume

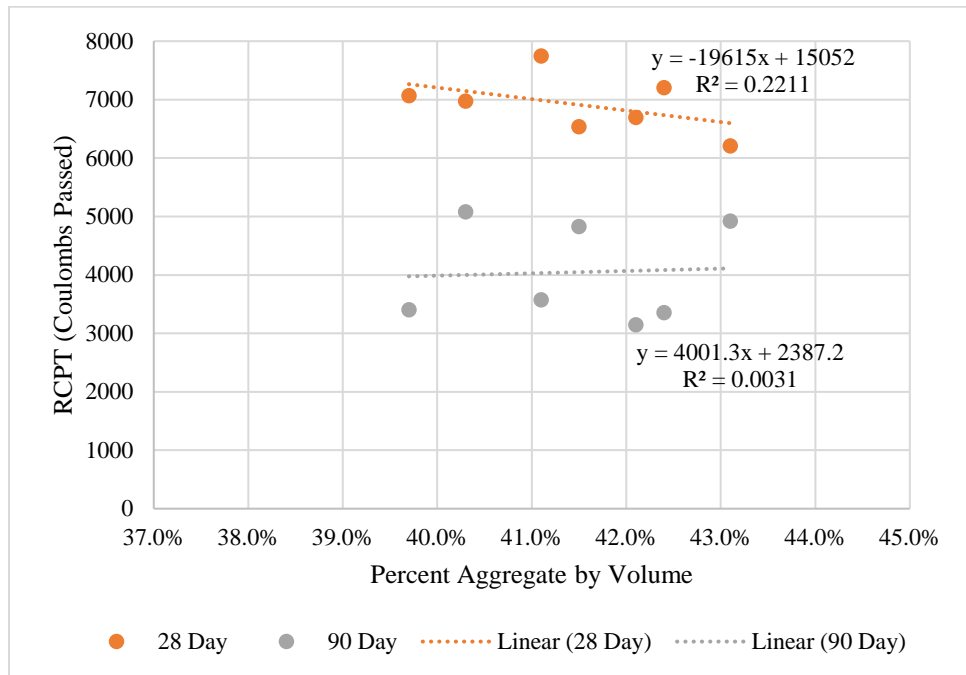


Figure B.23: RCPT results of high w/cm ratio optimized concrete mixtures vs coarse aggregate volume

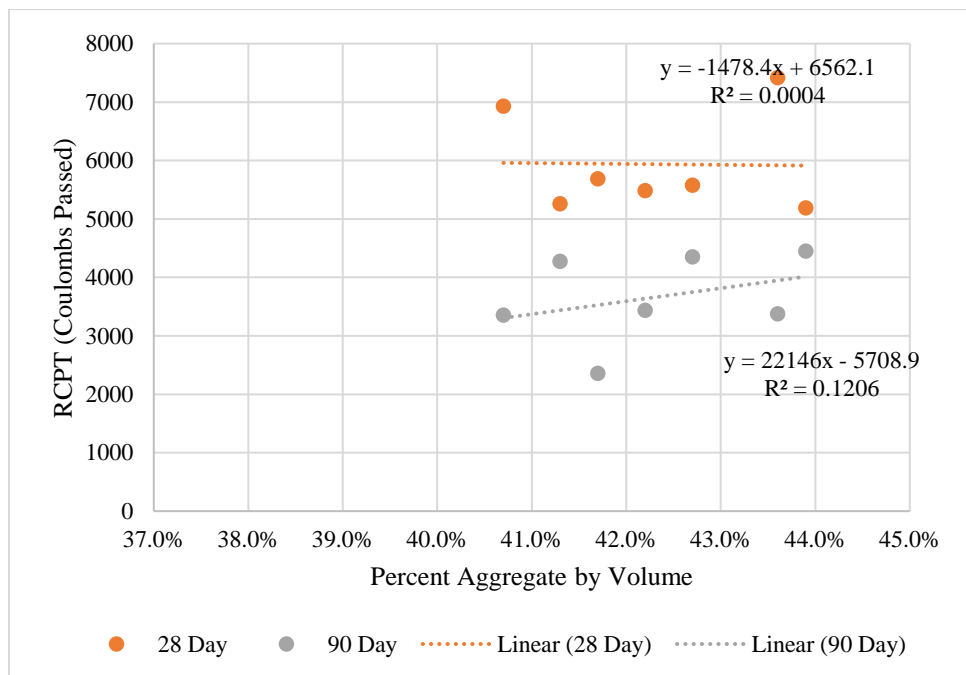


Figure B.24: RCPT results of medium w/cm ratio optimized concrete mixtures vs coarse aggregate volume

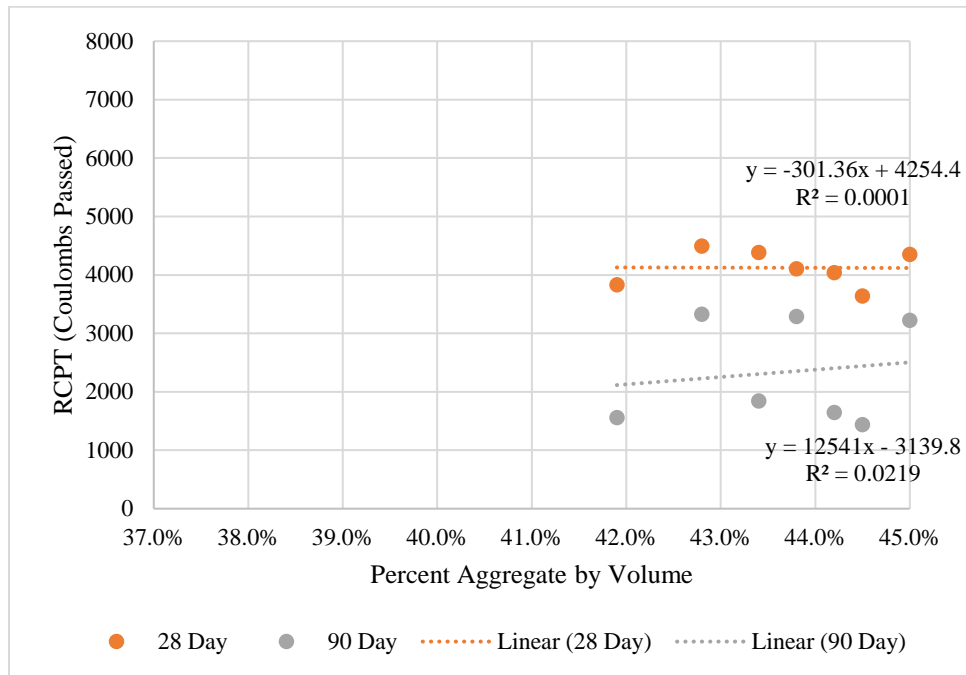


Figure B.25: RCPT results of low w/cm ratio optimized concrete mixtures vs coarse aggregate volume

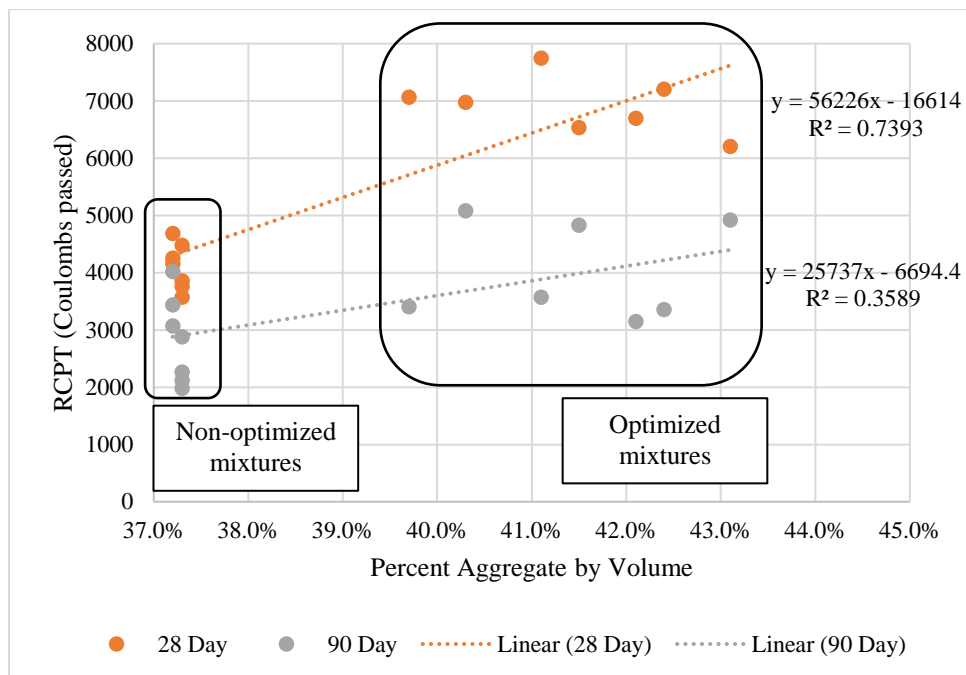


Figure B.26: RCPT results of high w/cm ratio optimized and non-optimized concrete mixtures vs coarse aggregate volume

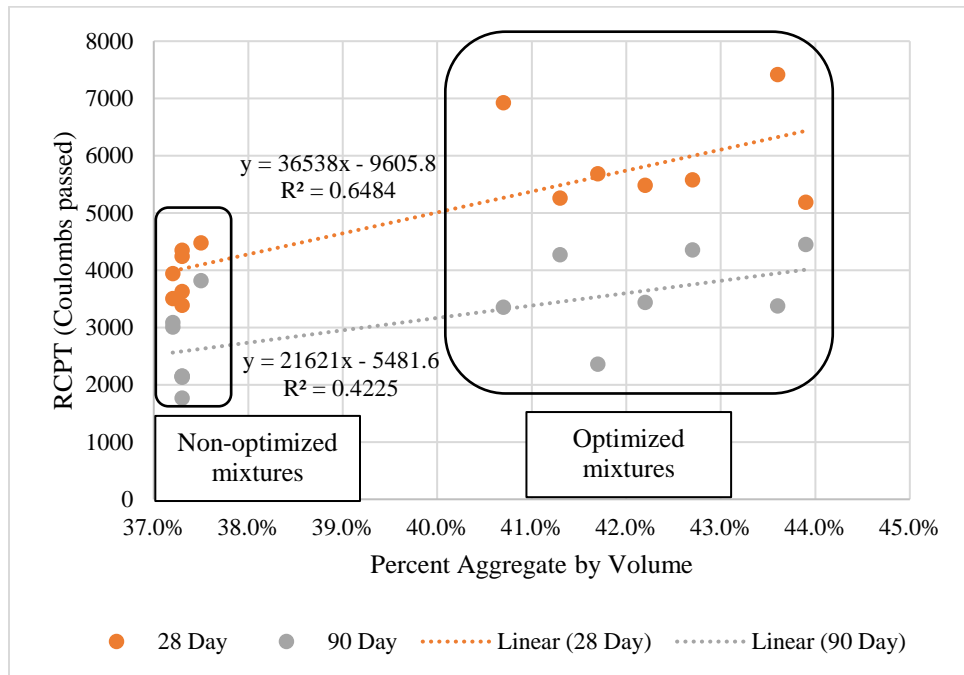


Figure B.27: RCPT results of medium w/cm ratio optimized and non-optimized concrete mixtures vs coarse aggregate volume

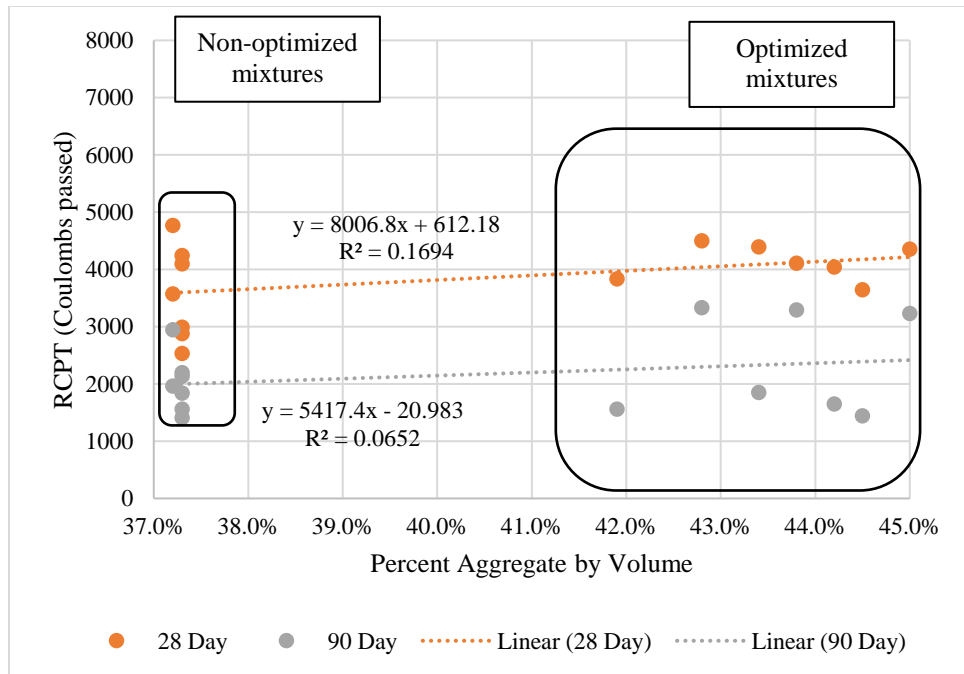


Figure B.28: RCPT results of low w/cm ratio optimized and non-optimized concrete mixtures vs coarse aggregate volume

Table B.8: 28- and 56-day surface resistivities and formation factors for optimized aggregate gradation mixtures

Mixture ID	28 Day Surface resistivity (k Ω -cm)	28 Day Bucket Test (k Ω -cm)	28 Day Formation Factor	56 Day Surface resistivity (k Ω -cm)	56 Day Bucket Test (k Ω -cm)	56 Day Formation Factor
H-700*-0	8.0	-	-	8.0	-	-
H-560*-140	7.1	-	-	9.3	-	-
H-650*-0	6.8	-	-	7.9	-	-
H-520*-130	6.2	17.8	1398	8.8	25.6	2012
H-600*-0	8.4	21.9	1720	9.1	22.0	1728
H-480*-120	7.0	19.1	1504	9.0	26.5	2087
H-420*-180	6.0	18.8	1480	10.5	27.8	2189
M-700*-0	8.6	24.8	1953	10.3	26.4	2075
M-560*-140	7.5	39.2	3087	11.6	38.7	3047
M-650*-0	8.6	27.0	2122	11.3	24.9	1961
M-520*-130	6.5	21.9	1724	9.1	29.9	2350
M-600*-0	8.5	25.0	1965	9.2	24.6	1933
M-480*-120	7.3	22.2	1748	9.6	32.4	2551
M-420*-180	8.8	27.3	2150	15.7	41.9	3299
L-700*-0	10.2	29.3	2307	12.5	31.6	2488
L-560*-140	10.6	27.5	2161	16.9	50.0	3933
L-650*-0	9.1	26.4	2079	12.1	36.0	2831
L-520*-130	9.5	30.1	2366	19.0	49.3	3882
L-600*-0	10.0	30.2	2374	13.4	34.4	2705
L-480*-120	12.0	34.8	2736	20.5	54.2	4268
L-420*-180	10.2	36.0	2835	19.7	45.4	3571

Table B.9: 28- and 56-day surface resistivities and formation factors for non-optimized aggregate gradation mixtures

Mix ID	Bucket Test					
	28 Day Surface resistivity (k Ω -cm)	28 Day Bucket Test (k Ω -cm)	28 Day Formation Factor	56 Day Surface resistivity (k Ω -cm)	56 Day Bucket Test (k Ω -cm)	56 Day Formation Factor
H-700-0	7.3	9.3	930	12.1	15.5	1550
H-420-180	11.2	12.5	1250	16.3	19.1	1910
M-700-0	10.9	12.2	1220	10.9	12.4	1240
M-420-180	6.1	7.8	780	13.8	14.4	1450
L-700-0	9.3	10.4	1040	10.1	10.5	1050
L-420-180	8.4	10.1	1010	12.0	13.2	1320

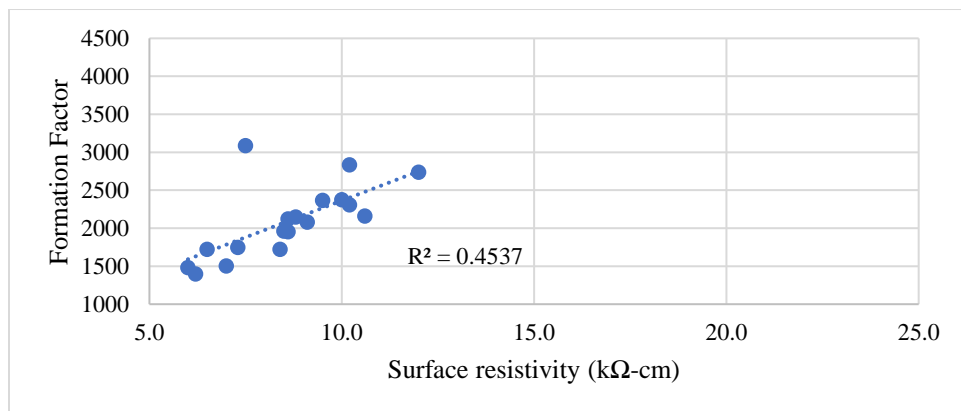


Figure B.29: 28-day formation factor vs resistivity

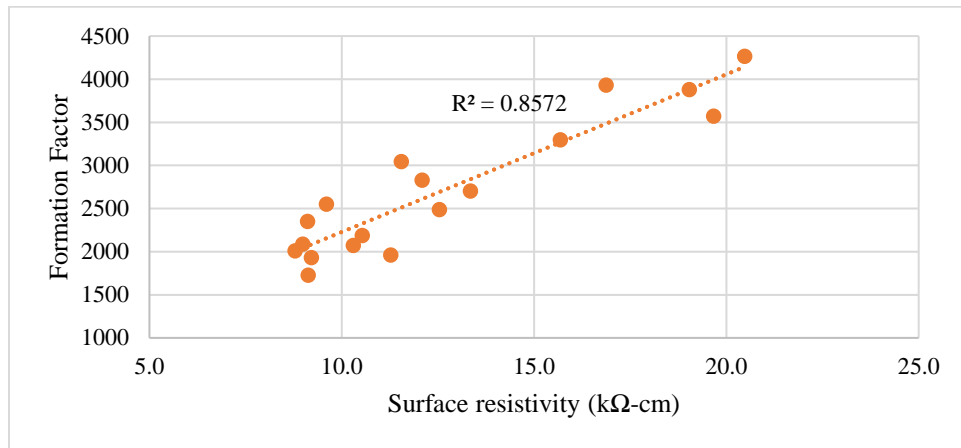


Figure B.30: 56-day formation factor vs resistivity

Table B.10: Optimized and non-optimized aggregate gradation mixtures volumetric shrinkage (in microstrain), 28-day reading is used as initial reading

Mixture ID	Non-Optimized				Optimized			
	28 Day	8 Week	16 Week	32 Week	28 Day	8 Week	16 Week	32 Week
H-700-0	312	382	424	504	350	493	590	667
H-560-140	301	376	424	937	297	397	487	583
H-650-0	-	-	-	-	350	480	580	653
H-520-130	286	342	439	-	330	460	540	613
H-600-0	261	322	429	829	340	473	553	603
H-480-120	258	329	420	683	400	527	577	640
H-420-180	246	336	439	592	327	457	520	557
M-700-0	322	401	498	567	417	577	630	643
M-560-140	318	387	448	1185	387	497	553	613
M-650-0	310	380	462	515	430	580	633	647
M-520-130	304	389	389	-	403	497	560	610
M-600-0	274	328	378	835	293	423	443	480
M-480-120	279	339	401	778	410	493	547	603
M-420-180	292	361	415	618	357	450	500	547
L-700-0	314	414	513	-	390	510	577	653
L-560-140	347	447	546	-	400	503	587	643
L-650-0	333	401	483	1140	370	495	575	587
L-520-130	318	414	501	-	440	567	640	707
L-600-0	298	371	430	703	370	440	480	550
L-480-120	304	375	437	964	370	463	513	587
L-420-180	309	367	419	599	377	453	503	577

Table B.11: Optimized aggregate gradation mixtures volumetric shrinkage (in microstrain), 0-day reading is comparator reading per ASTM C157 standard

Mixture ID	28 Day	8 Week	16 Week	32 Week
H-700*-0	297	440	537	613
H-560*-140	240	350	450	477
H-650*-0	287	417	517	590
H-520*-130	217	347	427	500
H-600*-0	253	387	467	517
H-480*-120	287	413	463	527
H-420*-180	250	380	443	480
M-700*-0	323	483	537	550
M-560*-140	330	440	497	557
M-650*-0	297	447	500	513
M-520*-130	293	387	450	500
M-600*-0	237	367	387	423
M-480*-120	303	387	440	497
M-420*-180	307	400	450	497
L-700*-0	337	457	523	600
L-560*-140	317	420	503	560
L-650*-0	275	400	480	477
L-520*-130	337	463	537	603
L-600*-0	347	417	457	527
L-480*-120	327	420	470	543
L-420*-180	317	393	443	517

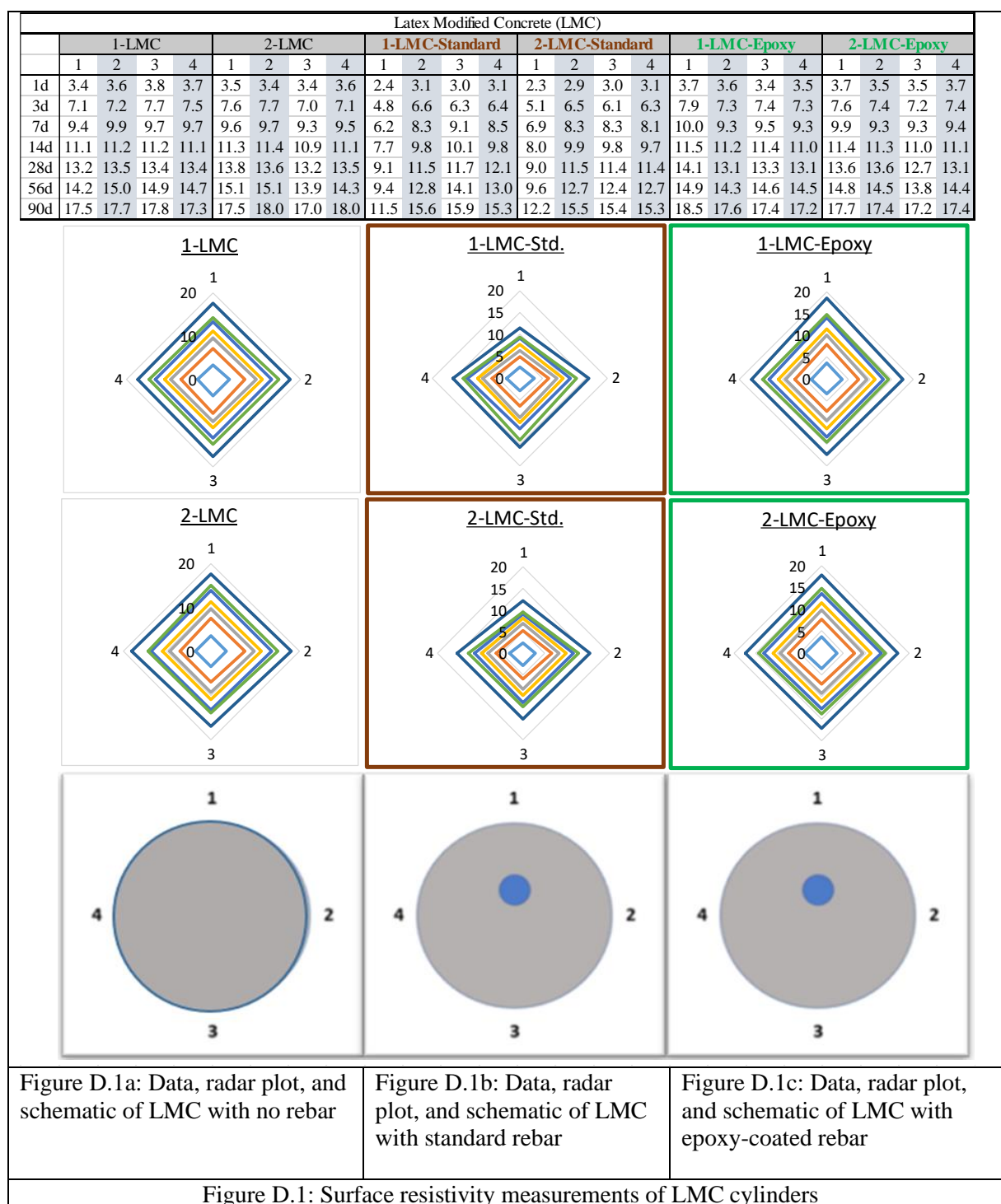
**APPENDIX C – SUPPORTING MATERIAL FOR IDENTIFICATION of PERFORMANCE TARGETS FOR
FREEZE-THAW DURABLE CONCRETE (Chapter 4)**

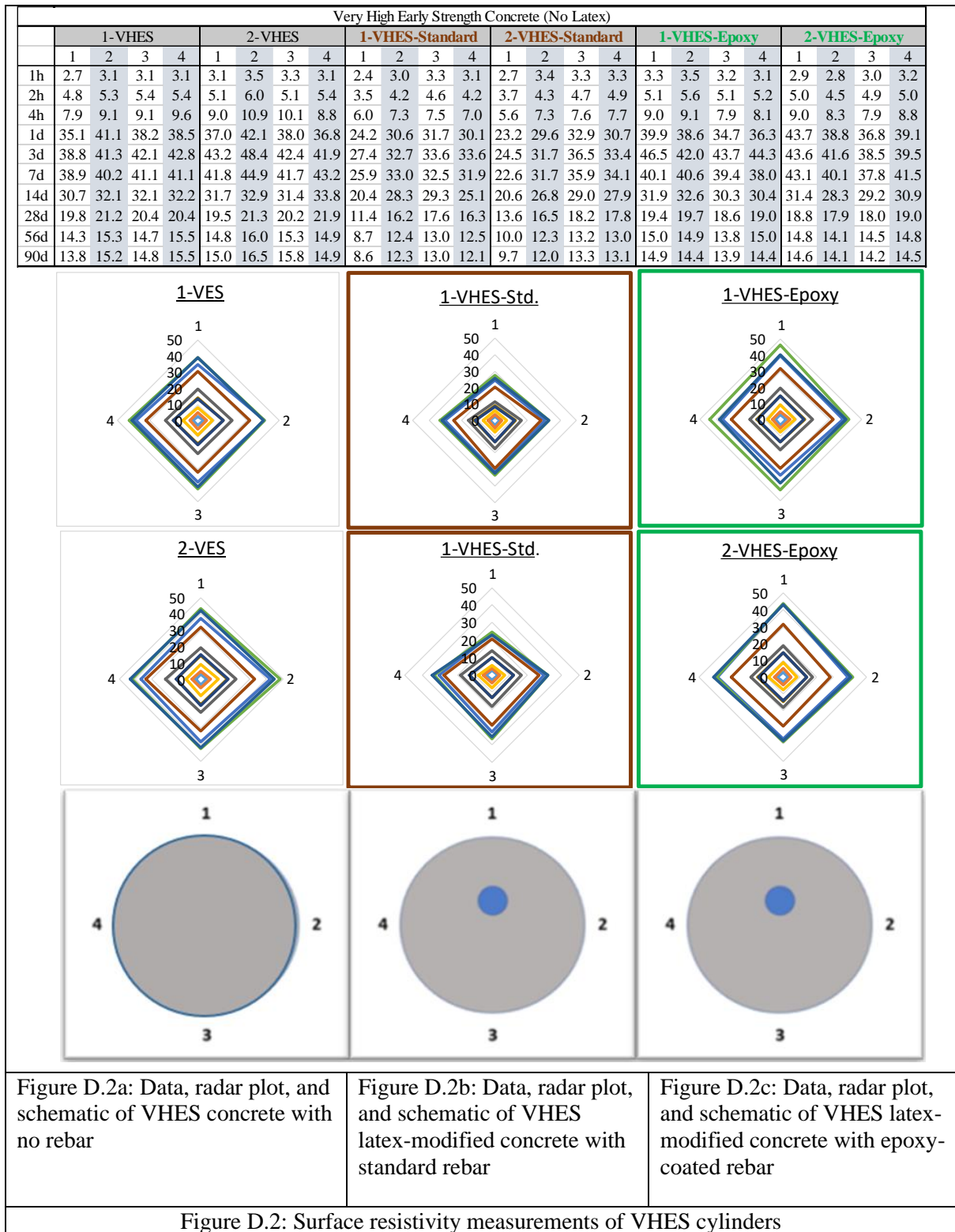
Table C.1 Fresh concrete test results for NCDOT RP 2015-03, RP 2016-06, RP 2018-14, and RP 2020-13

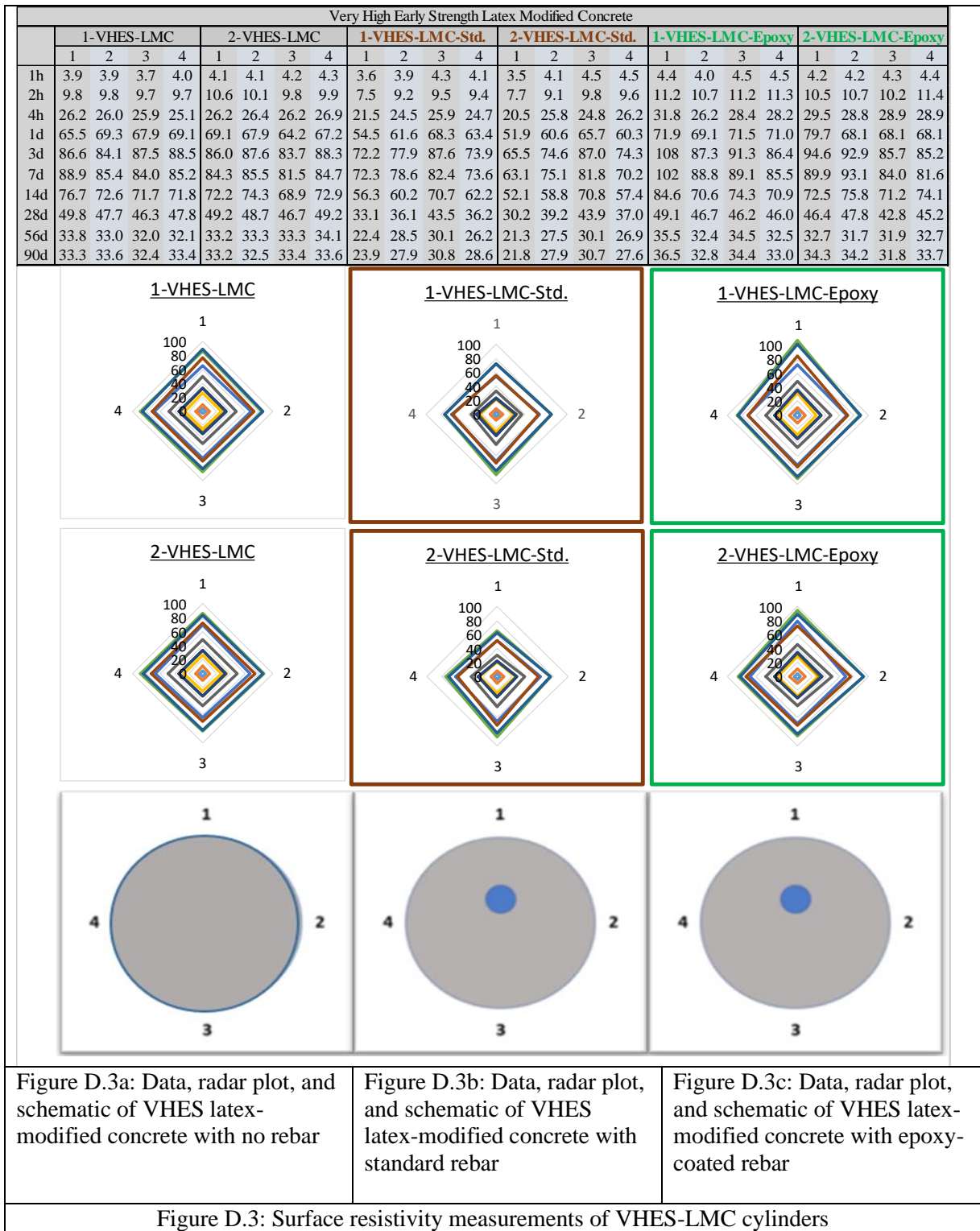
Project ID	Designation	Slump (in.)	Air Content (%)	SAM Number	Unit Weight (pcf)
2015-03	P.A.N.M	1.4	5.4%	0.19	145.0
	P.B.N.M	1.9	6.0%	0.23	143.0
	P.BL.N.M	2.2	5.6%	0.28	144.0
	C.A.N.M	1.1	5.8%	0.80	138.0
	C.B.N.M	1.4	5.6%	0.35	139.0
	C.BL.N.M	1.1	5.5%	0.19	139.0
	M.A.N.M	2.0	5.3%	-	145.0
	M.B.N.M	2.4	5.4%	-	144.0
	M.BL.N.M	2.3	5.1%	-	145.0
	P.A.A.M	2.7	5.7%	0.88	141.0
	P.B.A.M	2.3	5.2%	0.42	142.0
	P.BL.A.M	2.5	5.2%	0.29	142.0
	P.A.B.M	2.4	5.6%	0.29	142.0
	P.B.B.M	2.3	5.7%	0.22	141.0
	P.BL.B.M	2.3	5.6%	0.19	141.0
	P.A.N.N	1.9	5.3%	0.10	143.0
	P.B.N.N	3.3	5.4%	0.27	142.0
	P.BL.N.N	2.8	5.5%	0.19	143.0
2016-06	CC	2.5	5.5%	0.32	144.6
	I1M	2.5	5.3%	0.21	141.0
	I1H	3.2	5.8%	0.24	138.8
	I2H	3.0	5.0%	0.39	139.1
	CF	3.2	6.0%	0.30	140.2
	I1MF	2.0	5.0%	0.25	141.0
	I2MF	2.0	5.0%	0.19	141.0
	I1HF	2.2	5.0%	0.29	139.4
	I2HF	2.0	5.1%	0.27	138.7
	IP	7.5	5.2%	0.30	136.8
	ILA	11.0	10.4%	0.50	127.5
	ILB	3.5	6.2%	0.76	140.2
2018-14	H-700-0	8.0	5.2%	-	137.1
	H-560-140	8.0	5.2%	0.19	136.4
	H-650-0	6.5	6.0%	0.38	141.4
	H-520-130	7.0	5.5%	-	138.0
	H-600-0	2.5	5.8%	-	138.7
	H-480-120	3.0	6.0%	0.28	139.4
	H-420-180	3.8	6.0%	0.22	136.1
	M-700-0	5.0	5.5%	0.25	141.6
	M-560-140	4.3	6.0%	-	136.6
	M-650-0	2.5	5.7%	0.23	142.4
	M-520-130	3.0	5.5%	-	139.7
	M-600-0	1.0	6.0%	-	140.5
	M-480-120	1.5	5.0%	-	139.6
	M-420-180	2.0	6.0%	0.24	138.1
	M-600P-0	0.8	5.5%	-	141.1
	M-480P-120	1.0	5.1%	-	140.5
	M-420P-180	1.5	5.9%	-	137.0
	L-700-0	2.3	6.0%	-	143.9
	L-560-140	1.8	5.0%	-	140.3
	L-650-0	1.0	6.0%	-	141.8

	L-520-130	1.0	5.0%	-	141.6
	L-600-0	1.0	5.5%	0.06	142.6
	L-480-120	0.8	5.5%	-	142.0
	L-420-180	1.0	5.2%	-	142.0
2020-13	H-700*-0	5.0	5.8%	0.29	144.5
	H-560*-140	3.5	5.0%	0.40	142.3
	H-650*-0	5.0	6.0%	0.13	140.9
	H-520*-130	2.2	5.2%	0.30	143.1
	H-600*-0	0.0	6.0%	-	142.2
	H-480*-120	4.0	6.0%	0.18	142.7
	H-420*-180	1.5	5.0%	0.24	142.7
	M-700*-0	3.7	5.5%	0.62	142.9
	M-560*-140	6.0	5.0%	0.74	142.1
	M-650*-0	2.5	6.0%	0.43	144.2
	M-520*-130	1.7	5.0%	0.41	145.8
	M-600*-0	1.0	5.6%	-	142.5
	M-480*-120	1.5	5.9%	0.53	144.4
	M-420*-180	1.0	5.1%	-	145.0
	L-700*-0	1.5	5.9%	0.20	144.5
	L-560*-140	0.5	5.7%	0.39	142.9
	L-650*-0	1.0	6.0%	0.42	144.2
	L-520*-130	0.5	5.3%	0.27	144.1
	L-600*-0	0.0	5.3%	-	142.2
	L-480*-120	0.0	5.6%	0.51	144.0
	L-420*-180	0.5	5.7%	-	144.0
	H-600C-0	2.2	6.0%	0.55	141.8
	M-600C-0	1.0	5.6%	0.38	143.6
	L-600C-0	0.5	6.0%	0.50	142.7

APPENDIX D – SUPPORTING MATERIAL FOR USE OF SURFACE RESISTIVITY METER TO EVALUATE BRIDGE DECK OVERLAYS (Chapter 5)







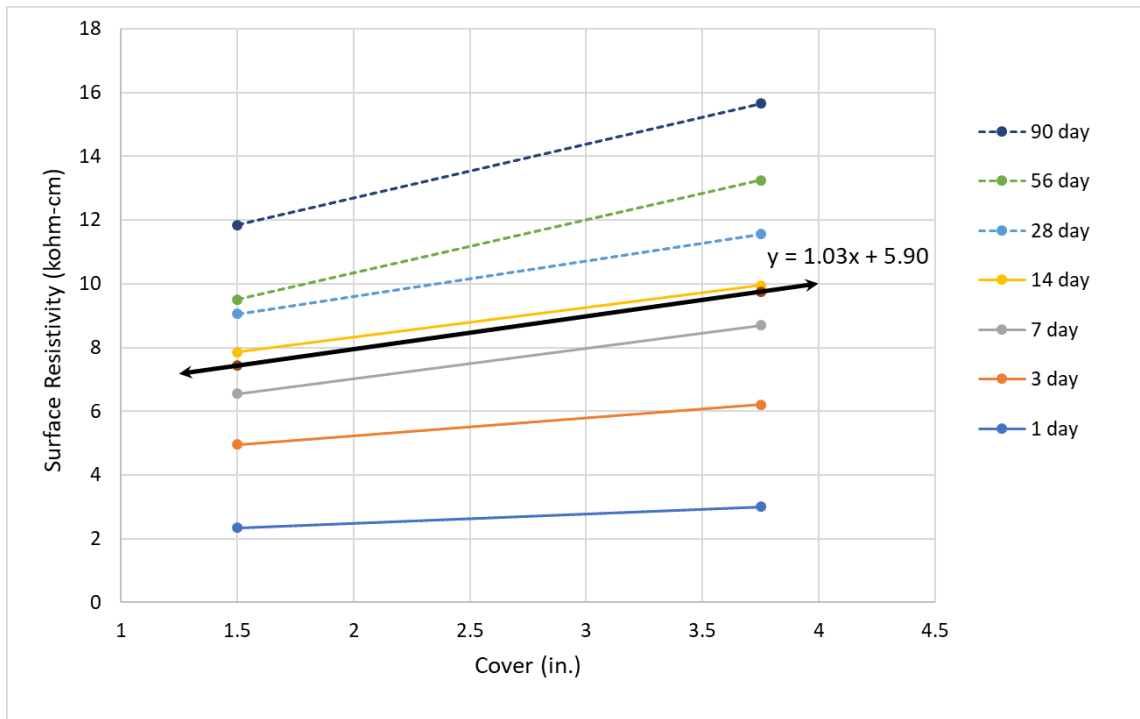


Figure D.4: Surface resistivity vs. concrete cover at selected concrete ages for the LMC cylinders

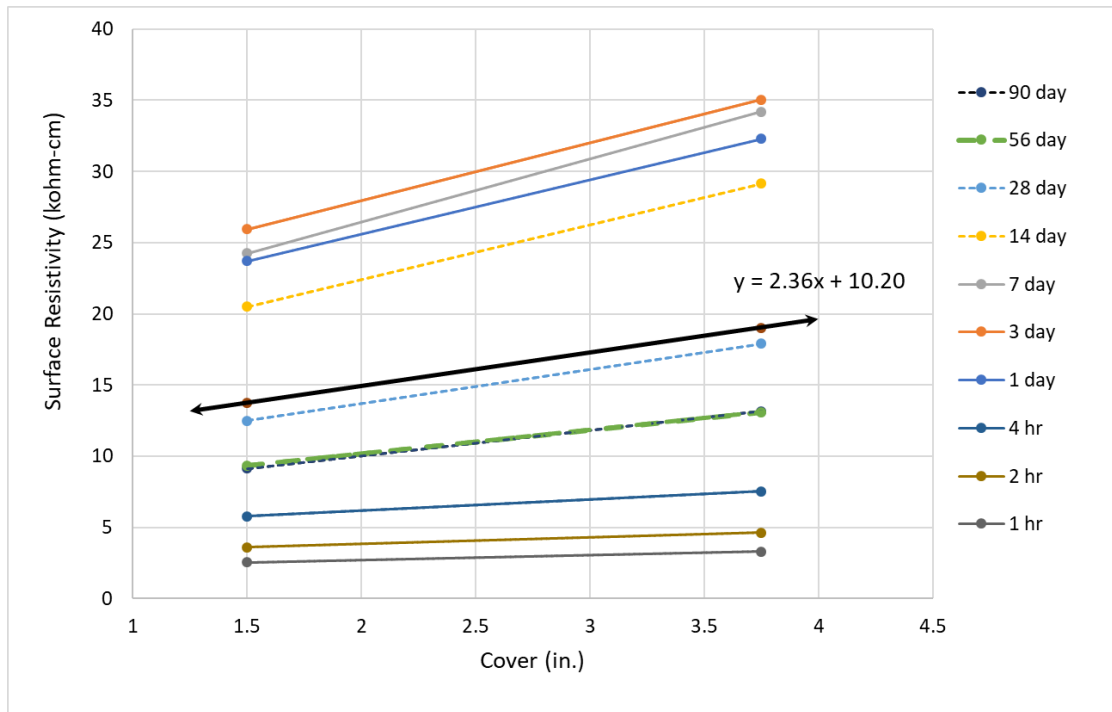


Figure D.5: Surface resistivity vs. concrete cover at selected concrete ages for the VHES cylinders

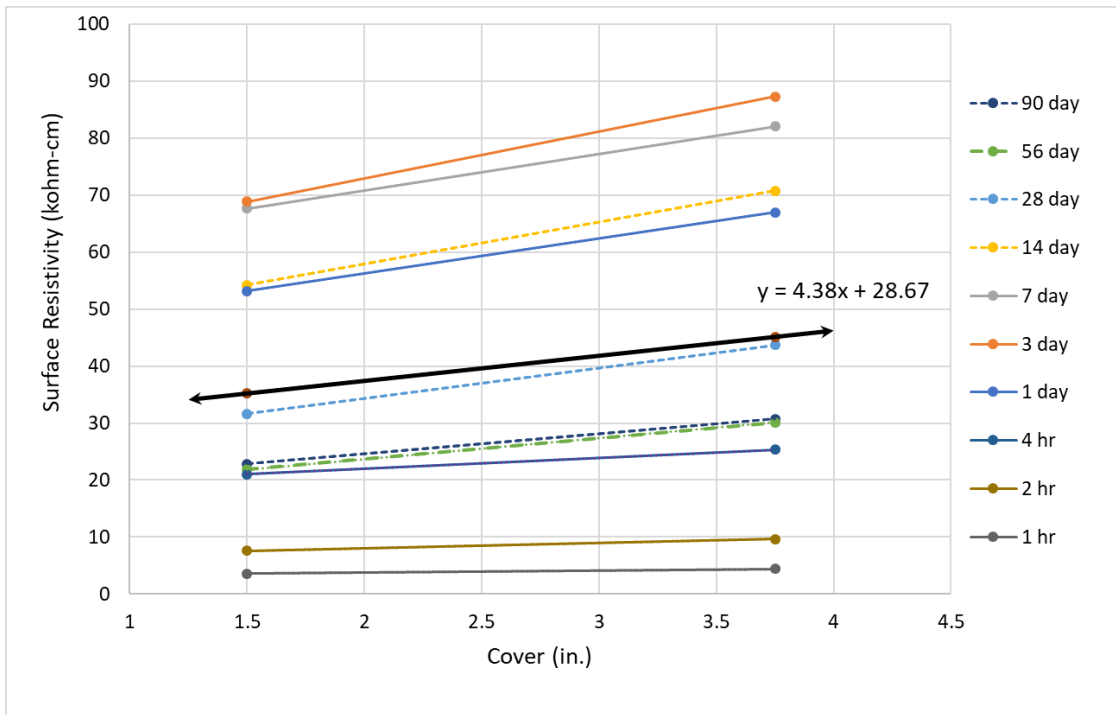


Figure D.6: Surface resistivity vs. concrete cover at selected concrete ages for VHES-LMC cylinders

Table D.1: Equation of the line for each age and mixture (X = cover, Y = surface resistivity)

Age	CC Figure 4.6	LMC Figure 4.7	VHES Figure 4.8	VHES-LMC Figure 4.9
1 hour			$y = 0.33x + 2.1$	$y = 0.33x + 3.0$
2 hour			$y = 0.46x + 2.9$	$y = 0.91x + 6.2$
4 hour			$y = 0.78x + 4.6$	$y = 1.9x + 18$
1 day	$y = 0.22x + 2.1$	$y = 0.29x + 1.9$	$y = 3.8x + 18$	$y = 6.1x + 44$
3 day	$y = 0.47x + 3.0$	$y = 0.56x + 4.1$	$y = 4.01x + 20$	$y = 8.2x + 56$
7 day	$y = 0.42x + 3.8$	$y = 0.96x + 5.1$	$y = 4.4x + 18$	$y = 6.4x + 58$
14 day	$y = 0.60x + 4.1$	$y = 0.93x + 6.5$	$y = 3.8x + 15$	$y = 7.4x + 43$
28 day	$y = 0.84x + 4.7$	$y = 1.1x + 7.4$	$y = 2.4x + 8.9$	$y = 5.4x + 24$
56 day	$y = 0.84x + 5.2$	$y = 1.7x + 7.0$	$y = 1.67x + 6.9$	$y = 3.7x + 16$
90 day	$y = 1.0x + 6.3$	$y = 1.7x + 9.3$	$y = 1.8x + 6.5$	$y = 3.5x + 18$

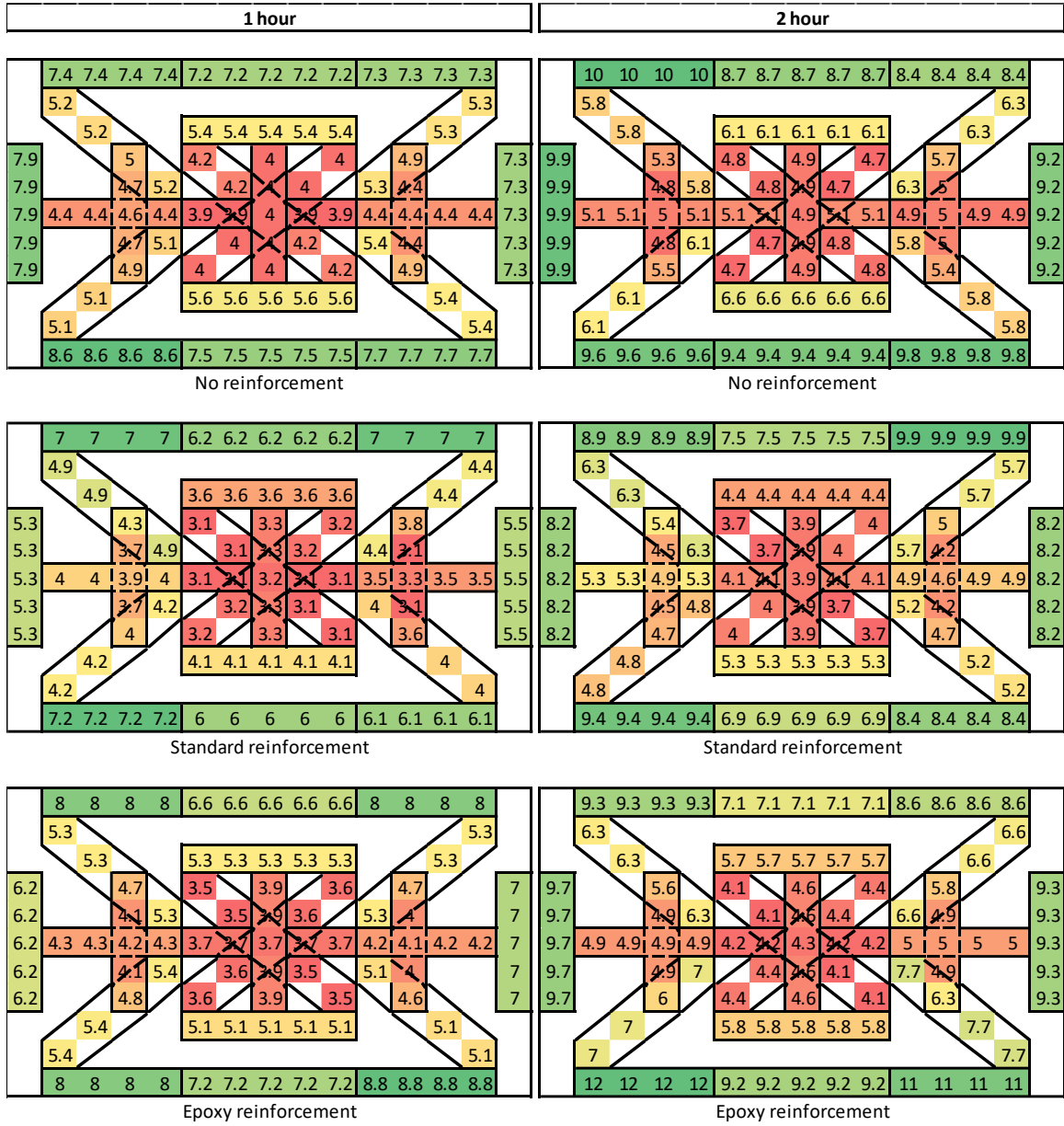


Figure D.7: VHES miniature slabs – 1 and 2 hour surface resistivity measurements

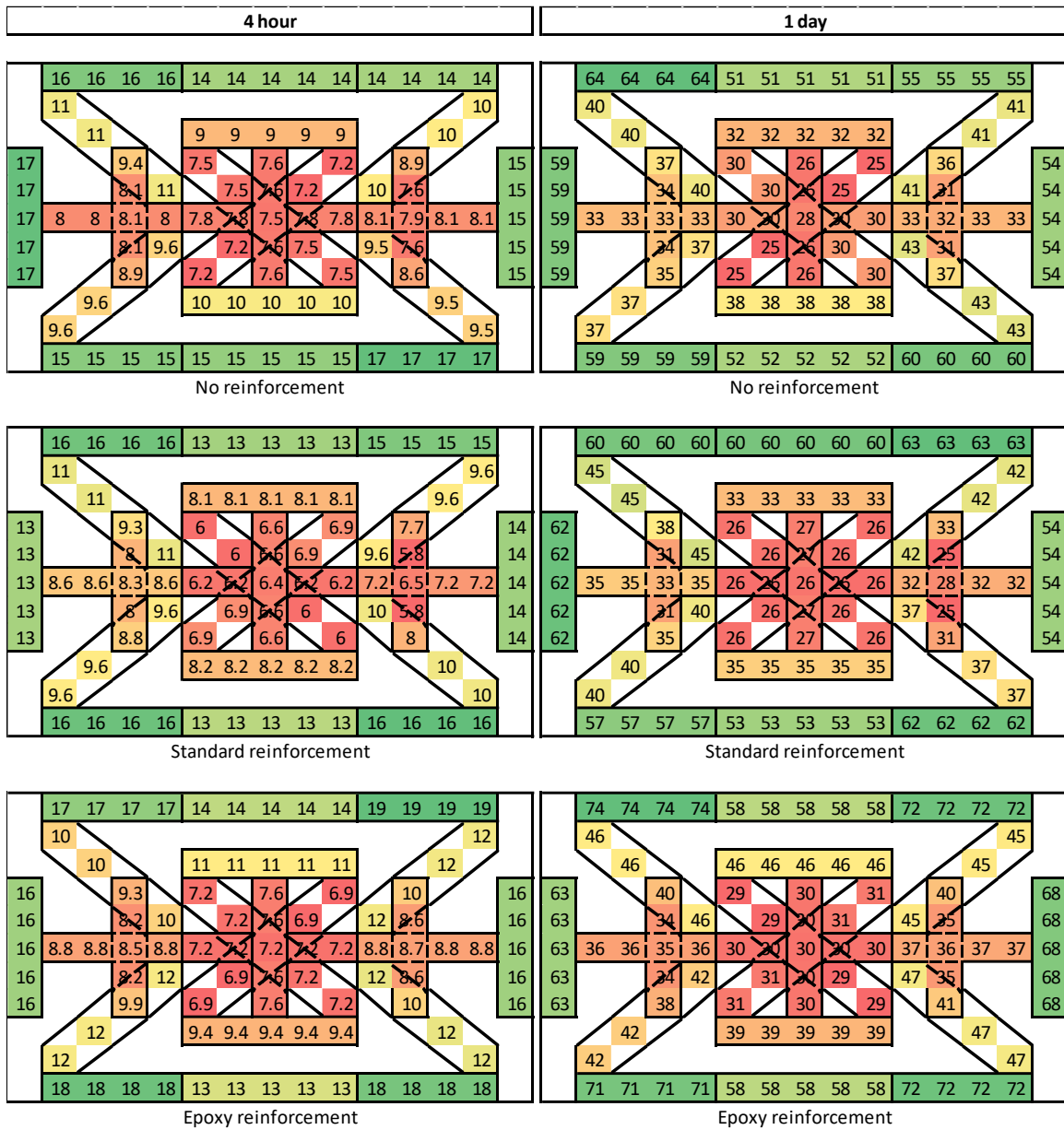


Figure D.8: VHES miniature slabs - 4 hour and 1 day surface resistivity measurements

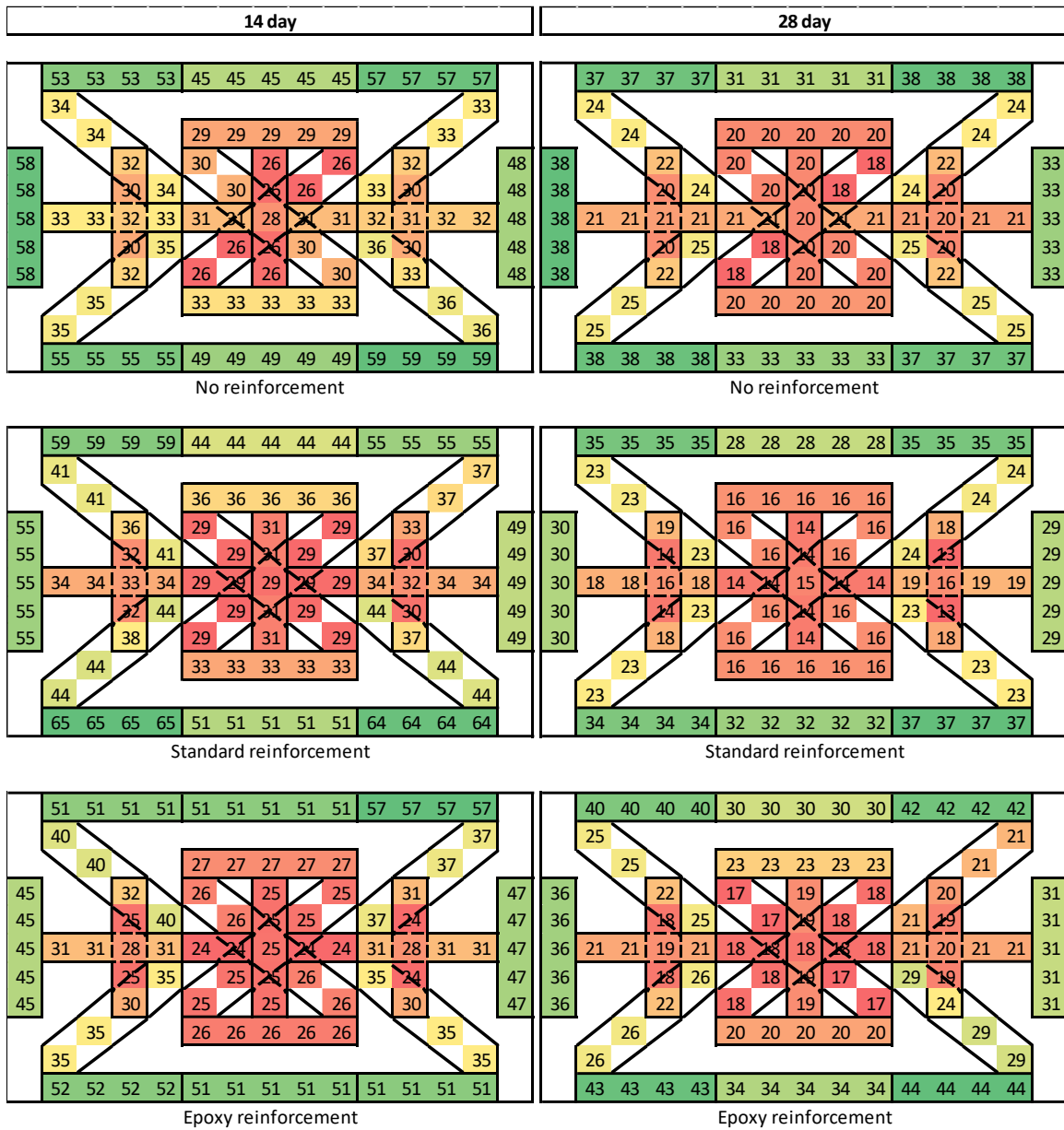


Figure D.10: VHS miniature slabs - 14 and 28 day surface resistivity measurements

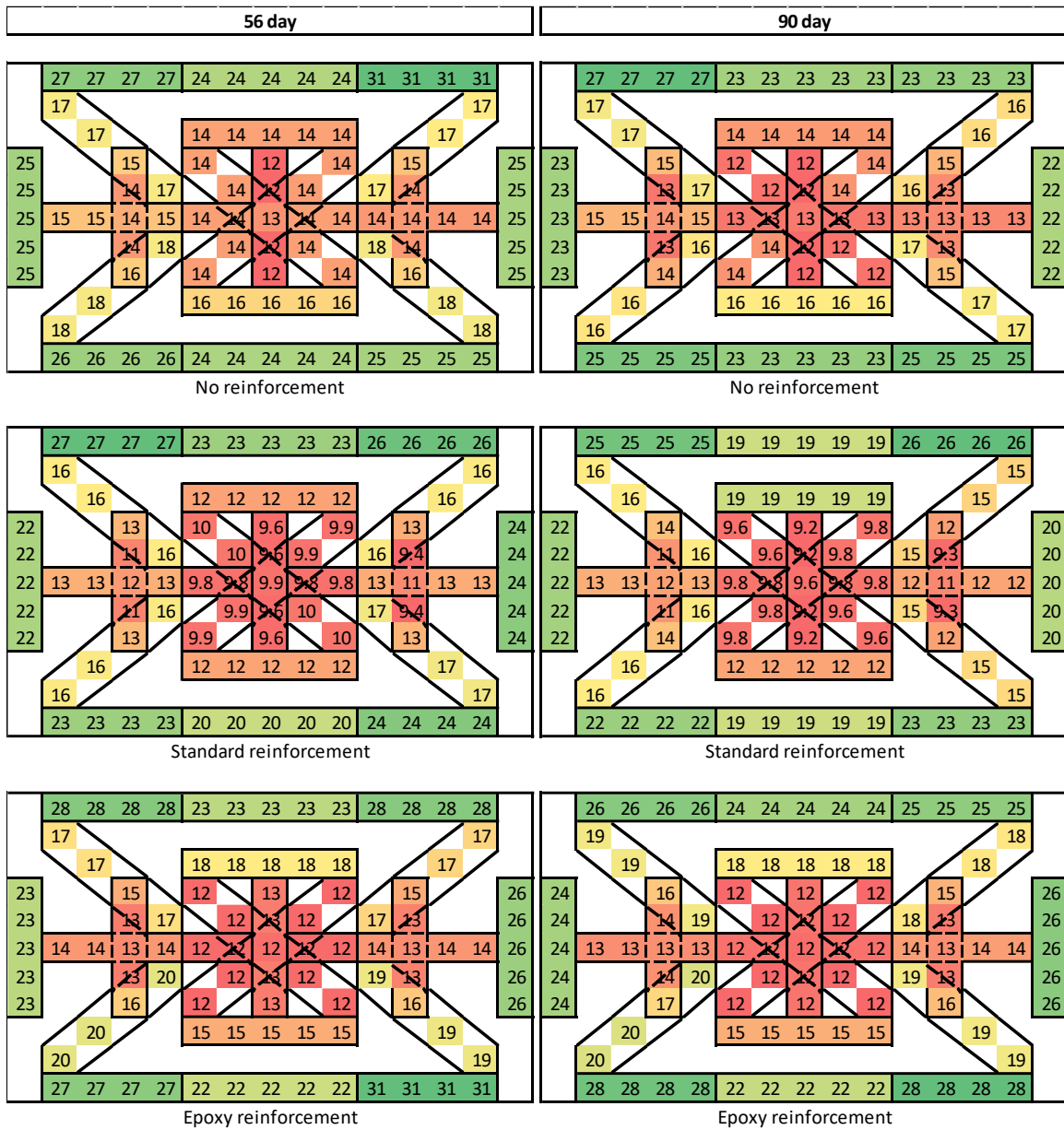


Figure D.11: VHES miniature slabs data - 56 and 90 day surface resistivity measurements

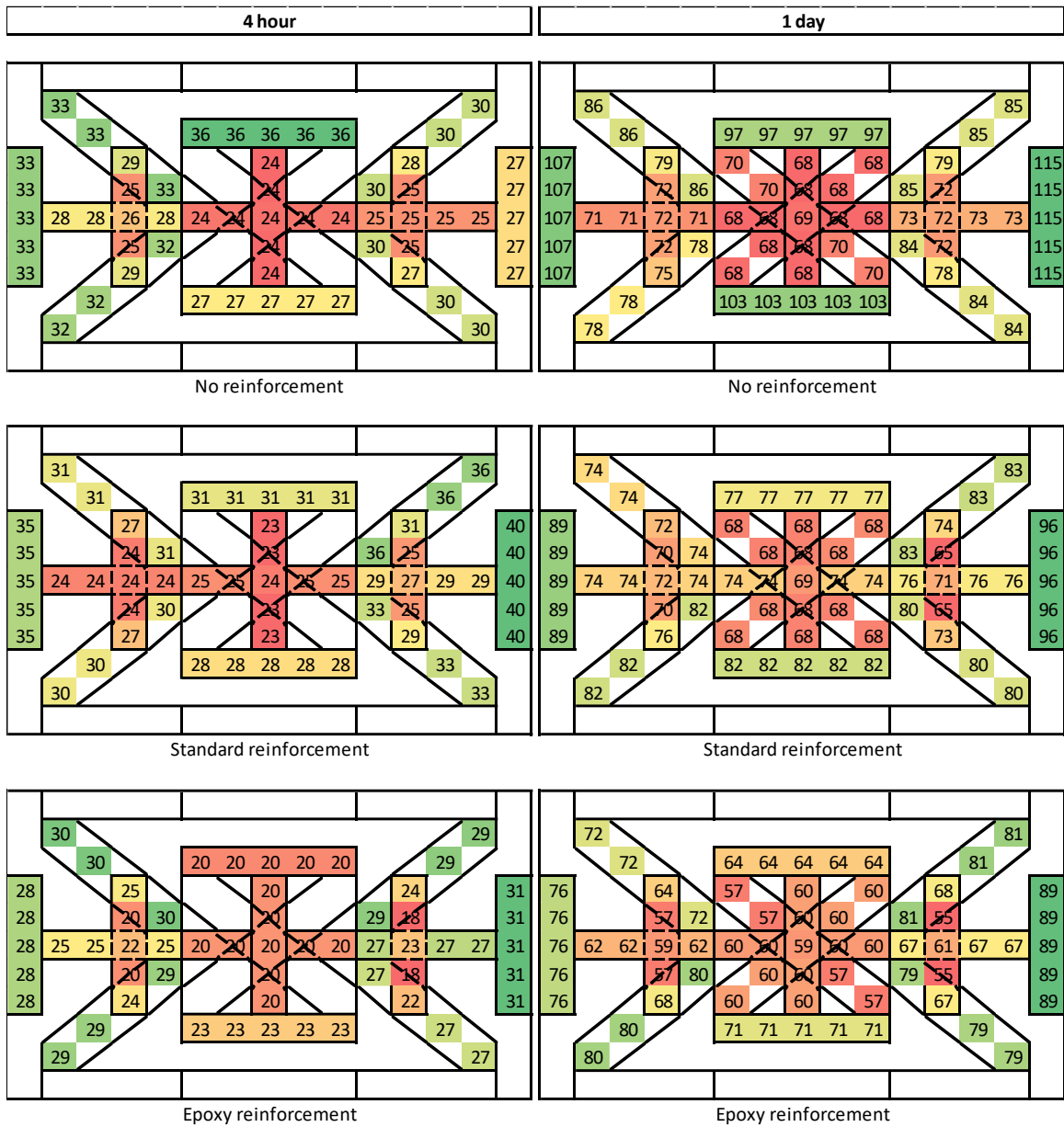


Figure D.12: VHES-LMC miniature slabs - 4 hour and 1 day surface resistivity measurements

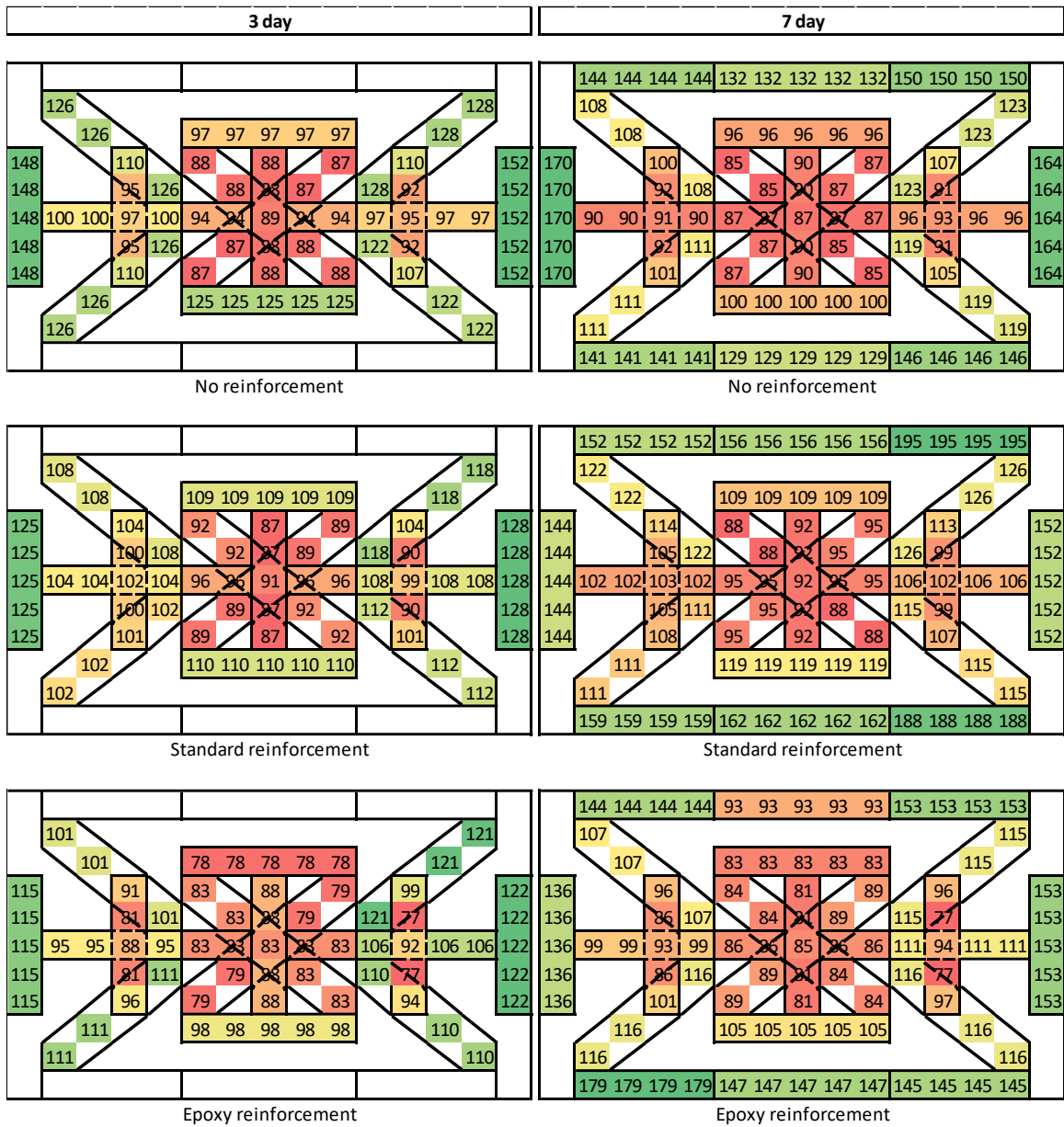


Figure D.13: VHES-LMC miniature slabs - 3 and 7 day surface resistivity measurements

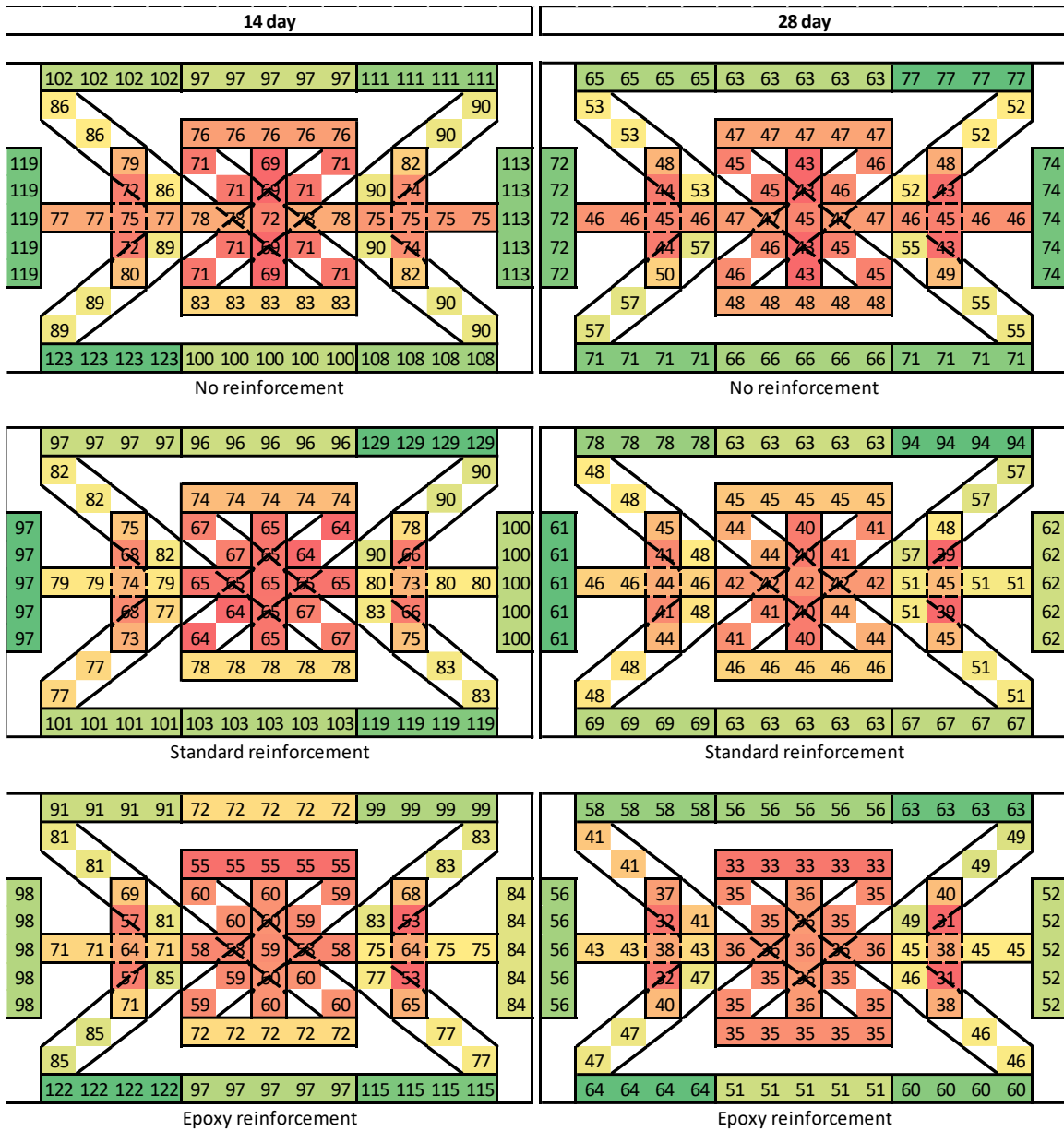


Figure D.14: VHES-LMC miniature slabs - 14 and 28 day surface resistivity measurements

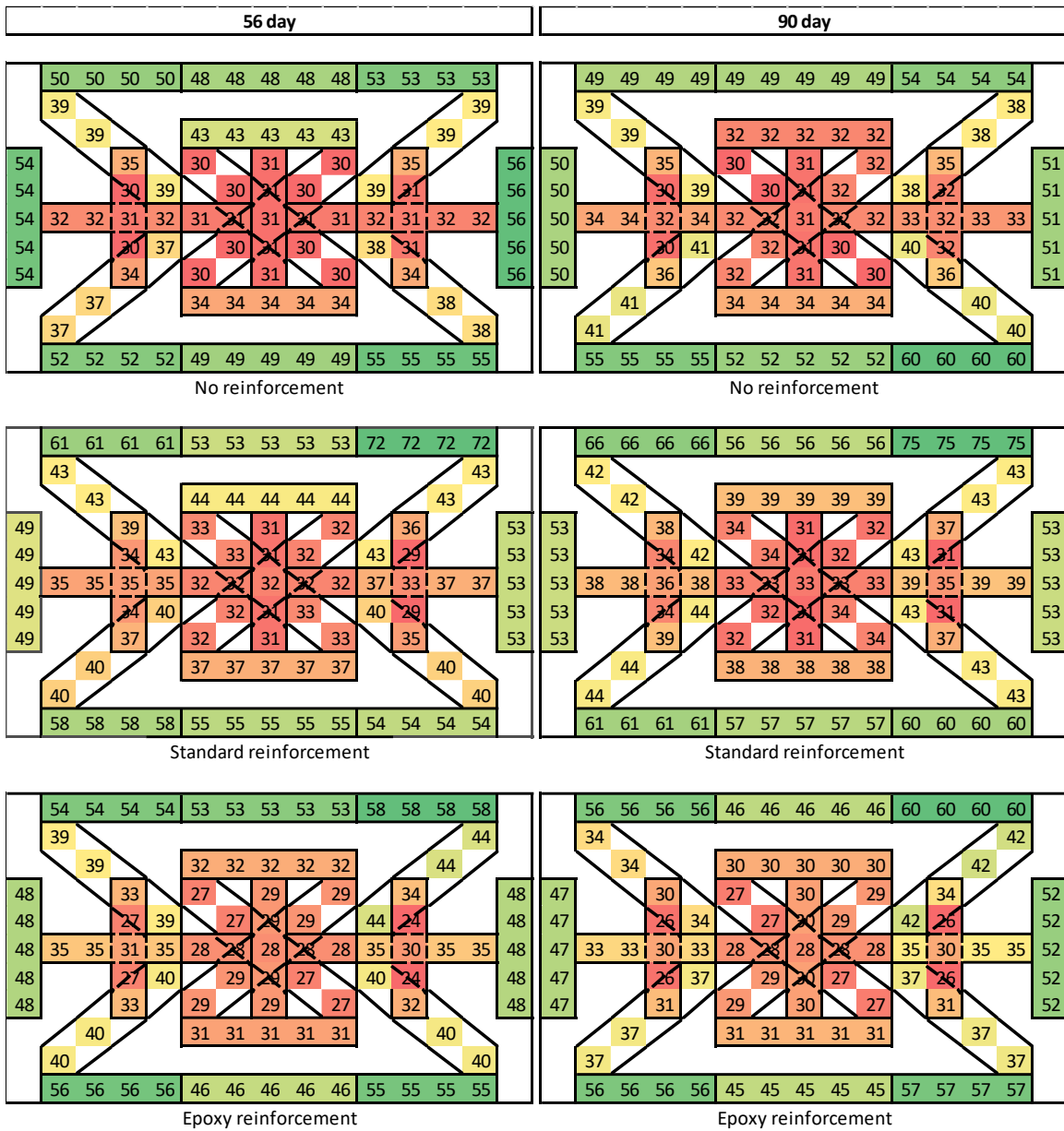


Figure D.15: VHES-LMC miniature slabs - 56 and 90 day surface resistivity measurements

Edge distance (in.)	Horizontal Orientation									Average
	1	2	3	4	5	6	7	8	9	
10	15	16	17	18	17	15	18	20	18	17.1
9	16	17	18	17	15	16	16	18	17	16.5
8	16	17	18	18	18	16	15	16	19	17.0
7	17	18	18	18	18	19	21	17	20	18.2
6	18	19	17	18	19	19	18	21	21	18.8
5	19	18	19	17	17	18	19	18	18	18.1
4	20	21	18	19	21	17	18	19	24	19.6
3	19	21	19	20	19	23	20	21	23	20.6
2	21	21	22	24	23	22	24	24	25	22.8
1	24	26	23	26	28	30	31	30	30	27.6

Edge distance (in.)	Diagonal Orientation									Average
	1	2	3	4	5	6	7	8	9	
10	18	18	19	18	18	16	17	18	19	17.9
9	17	19	17	18	16	16	16	18	17	17.0
8	18	18	16	18	18	16	19	17	20	17.8
7	18	18	17	19	16	19	16	18	18	17.6
6	18	18	18	19	17	19	18	18	14	17.8
5	19	17	19	17	16	16	17	17	15	17.0
4	18	19	19	19	18	17	20	16	19	18.2
3	18	18	18	18	19	20	18	17	20	18.4
2	20	21	22	18	19	21	21	20	22	20.4
1	20	21	21	21	21	24	23	23	25	22.2

Edge distance (in.)	Vertical Orientation									Average
	1	2	3	4	5	6	7	8	9	
10	17	18	17	18	17	17	19	19	19	17.8
9	18	18	17	17	19	17	15	19	18	17.6
8	17	18	16	17	17	16	20	17	16	17.0
7	17	18	16	17	16	16	18	18	16	16.8
6	17	19	18	18	19	16	16	18	17	17.4
5	18	18	17	15	18	17	20	16	17	17.3
4	18	19	16	17	16	17	17	18	18	17.2
3	19	20	17	19	21	17	18	20	18	18.6
2	19	19	19	16	21	17	21	19	17	18.6
1	19	22	21	20	18	20	23	21	22	20.5

Figure D.16: Edge effects on surface resistivity measurements in each orientation

Diagonal													
	Rebar										No Rebar		
Reading #	1	2	3	4	5	6	7	8	9	10	11	12	13
1	3.6	3	3	3.6	3.5	3.5	3.7	3.6	3.6	3.6	3.6	3.2	3.7
2	3.1	3.1	3.6	3	3.1	3.3	3.5	3.7	4.1	3.2	3.2	3.3	3.7
3	3.1	3.1	3.5	3.1	2.9	3.1	2.8	3.3	3.6	3.2	3.2	3.3	4
4	3.4	3.3	3.4	3.2	3	3.1	3.3	3.4	3.5	3.6	3.3	3.1	3.3
5	3.4	3.2	3.6	3.8	2.9	3.1	3.3	3.3	3.4	3.8	3	3.1	3.4
6	3	3.2	3.4	3.3	3.6	3.5	3.4	2.9	3.4	2.9	3.2	3.3	3.7
7	3.3	3.4	3.1	3.6	3.3	3.3	3.1	2.7	3.3	3	3	3.2	3.9
8	3.4	3.1	3.4	3.6	3.3	3.4	3.1	3.3	3.6	3.3	3.1	3	3.6
9	3.3	3.1	3.2	2.9	3.4	3.7	3.7	3.9	3.1	3.4	3.2	2.9	3.7
10	3.1	3.1	3.2	2.9	3.4	2.9	3.6	3.4	3.3	3.4	3	3.3	3.4
11	3.2	3.4	3.4	2.7	3.1	3.1	3.3	3.7	3	3.5	3.2	3.3	3.3
12	3.3	3.6	3.2	3.2	3.3	3	3.7	3.7	3.1	3.2	3.5	3.1	3.4
13	3.6	3.7	3.6	3.2	3.5	3.4	3.7	3.9	3.4	3.5	3.1	3.3	3.6
											Row Average		
											All points	No vert. rebar	
											3.48	3.49	
											3.38	3.45	
											3.25	3.30	
											3.30	3.29	
											3.33	3.26	
											3.29	3.38	
											3.25	3.28	
											3.33	3.31	
											3.35	3.31	
											3.23	3.29	
											3.25	3.23	
											3.33	3.33	
											3.50	3.48	
											3.327	3.337	

Figure D.17: Control mockup – diagonal orientation 7 day surface resistivity reading

Horizontal													
	Rebar										No Rebar		
Reading #	1	2	3	4	5	6	7	8	9	10	11	12	13
1	3.3	3.3	3.5	3.7	3.3	3.3	2.9	3.1	3.5	3.6	3.4	3.2	3.7
2	3.2	3.3	3.3	3.5	3.1	3.2	3.3	3	3.5	3.3	3.5	3	3.7
3	3.4	3.1	3.4	3.6	3.1	2.9	3.4	3.6	3.4	3.3	3.3	2.9	3.7
4	3.6	3.2	3	3.2	3	3.2	3.3	3.6	3.3	3.3	3.3	3.6	3.6
5	4	3.5	3.8	3.7	3.2	3.3	3.4	3.6	3.3	3.3	3	3.1	3.7
6	3.7	3.6	3.3	3.2	2.8	3	3.4	2.8	3.3	3.1	3	2.9	3.6
7	3.3	3.1	3.4	3.1	3.3	3.6	3	3.1	3.2	3.1	2.9	3.3	3.7
8	3.4	3.3	3.3	3.7	3.1	3.1	3.4	3.9	3.7	3.6	3.3	3.5	3.7
9	3.7	3.2	2.9	3.2	3	3.3	3.5	3.6	3.4	3.3	2.9	2.9	4
10	3.5	3.3	3.3	2.9	3.3	3.3	3.1	3.6	3.8	3.3	3.5	3.6	4.2
11	3.5	3.4	3.4	3.6	3.4	3.5	3.1	3.3	3.7	3.4	3.1	3.4	3.6
12	3.4	3.6	3.1	2.9	3.4	3.5	3.4	3.3	3	3.3	3.4	3.2	3.6
13	4	3.4	3.6	3.4	3.3	3.4	3	3.7	3.5	3.3	3.1	2.9	3.3
											Row Average		
											All points	No vert. rebar	
											3.37	3.35	
											3.30	3.33	
											3.32	3.33	
											3.32	3.34	
											3.45	3.44	
											3.21	3.25	
											3.24	3.26	
											3.46	3.43	
											3.30	3.29	
											3.44	3.54	
											3.42	3.40	
											3.32	3.31	
											3.38	3.34	
											3.347	3.353	

Figure D.18: Control mockup – horizontal orientation 7 day surface resistivity reading

Vertical													
Reading #	Rebar										No Rebar		
	1	2	3	4	5	6	7	8	9	10	11	12	13
1	3.6	3.5	3.4	3.7	3.6	4	3.6	3.3	4	3.6	3.5	3.2	4.1
2	3.5	3.5	3.5	3.2	3	3.4	3.8	3.5	3.6	3.6	3.2	3.1	3.8
3	3.4	3.3	2.8	3.1	3.5	3	3.7	3.5	3.7	3.4	3.2	3.2	3.8
4	3.1	3.5	3.5	3.4	2.9	3	3.7	3.4	3.2	3.9	3.3	3.4	3.6
5	3.4	3.6	3.7	3.9	2.9	3.5	2.9	3.4	3.1	3.3	3.3	3.3	3.3
6	3.6	3.3	3.3	3.6	3.1	3.6	3.1	3.4	3.4	2.9	2.8	3.3	3.8
7	3.3	3.5	3.3	3.7	3.3	3.3	3.9	3.3	3.4	3.7	3.2	3.6	4
8	3.3	3.1	3.2	3.3	3.3	3.2	3.4	3.3	3.3	3.6	3.1	3.3	3.5
9	3.3	3.1	3.1	3	3.3	3.2	3.3	3.7	3.5	3.5	3.2	3.1	3.7
10	3.1	3.2	3.1	3.2	3.1	3.4	3.4	3.3	3.5	3	3.1	3.3	3.8
11	3.3	2.9	3.2	2.9	3.1	3.6	3.6	3.1	3.6	2.9	3.1	3.3	3.8
12	3.4	3.5	3.5	3.2	3.2	3.5	3.1	3.1	3.2	3.4	3.5	3.3	3.4
13	4.1	4.1	3.5	4.1	3.1	3.4	3.7	3.8	3.7	3.7	3.6	3.7	3.4
												3.394	3.389

Figure D.19: Control mockup – vertical orientation 7 day surface resistivity reading

Average													
Reading #	Rebar										No Rebar		
	1	2	3	4	5	6	7	8	9	10	11	12	13
1	3.5	3.3	3.3	3.7	3.5	3.6	3.4	3.3	3.7	3.6	3.5	3.2	3.8
2	3.3	3.3	3.5	3.2	3.1	3.3	3.5	3.4	3.7	3.4	3.3	3.1	3.7
3	3.3	3.2	3.2	3.3	3.2	3	3.3	3.5	3.6	3.3	3.2	3.1	3.8
4	3.4	3.3	3.3	3.3	3	3.1	3.4	3.5	3.3	3.6	3.3	3.4	3.5
5	3.6	3.4	3.7	3.8	3	3.3	3.2	3.4	3.3	3.5	3.1	3.2	3.5
6	3.4	3.4	3.3	3.4	3.2	3.4	3.3	3	3.4	3	3	3.2	3.7
7	3.3	3.3	3.3	3.5	3.3	3.4	3.3	3	3.3	3.3	3	3.4	3.9
8	3.4	3.2	3.3	3.5	3.2	3.2	3.3	3.5	3.5	3.5	3.2	3.3	3.6
9	3.4	3.1	3.1	3	3.2	3.4	3.5	3.7	3.3	3.4	3.1	3	3.8
10	3.2	3.2	3.2	3	3.3	3.2	3.4	3.4	3.5	3.2	3.2	3.4	3.8
11	3.3	3.2	3.3	3.1	3.2	3.4	3.3	3.4	3.4	3.3	3.1	3.3	3.6
12	3.4	3.6	3.3	3.1	3.3	3.3	3.4	3.4	3.1	3.3	3.5	3.2	3.5
13	3.9	3.7	3.6	3.6	3.3	3.4	3.5	3.8	3.5	3.5	3.3	3.3	3.4
												3.356	3.360

Figure D.20: Control mockup –average of orientations 7 day surface resistivity reading

Standard Deviation													
	Rebar										No Rebar		
Reading #	1	2	3	4	5	6	7	8	9	10	11	12	13
1	0.2	0.3	0.3	0.1	0.2	0.4	0.4	0.3	0.3	0	0.1	0	0.2
2	0.2	0.2	0.2	0.3	0.1	0.1	0.3	0.4	0.3	0.2	0.2	0.2	0.1
3	0.2	0.1	0.4	0.3	0.3	0.1	0.5	0.2	0.2	0.1	0.1	0.2	0.2
4	0.3	0.2	0.3	0.1	0.1	0.1	0.2	0.1	0.2	0.3	0	0.3	0.2
5	0.3	0.2	0.1	0.1	0.2	0.2	0.3	0.2	0.2	0.3	0.2	0.1	0.2
6	0.4	0.2	0.1	0.2	0.4	0.3	0.2	0.3	0.1	0.1	0.2	0.2	0.1
7	0	0.2	0.2	0.3	0	0.2	0.5	0.3	0.1	0.4	0.2	0.2	0.2
8	0.1	0.1	0.1	0.2	0.1	0.2	0.2	0.3	0.2	0.2	0.1	0.3	0.1
9	0.2	0.1	0.2	0.2	0.2	0.3	0.2	0.2	0.2	0.1	0.2	0.1	0.2
10	0.2	0.1	0.1	0.2	0.2	0.3	0.3	0.2	0.3	0.2	0.3	0.2	0.4
11	0.2	0.3	0.1	0.5	0.2	0.3	0.3	0.3	0.4	0.3	0.1	0.1	0.3
12	0.1	0.1	0.2	0.2	0.1	0.3	0.3	0.3	0.1	0.1	0.1	0.1	0.1
13	0.3	0.4	0.1	0.5	0.2	0	0.4	0.1	0.2	0.2	0.3	0.4	0.2

Figure D.21: Control mockup – standard deviation of 7 day surface resistivity readings

2.9	3.0	3.3	3.3	3.5	4.0	3.5
2.8	3.0	2.9	3.1	3.0	3.3	3.4
2.0	2.6	2.6	2.8	2.9	3.1	3.2
1.6	2.3	2.6	2.6	2.7	2.7	2.5
1.6	2.1	2.3	2.3	2.3	2.1	2.2
1.5	1.7	1.9	2.0	1.8	1.5	1.8
1.2	1.0	1.2	1.3	1.4	1.2	1.3

Figure D.22: LMC mockup overlay thickness measurements

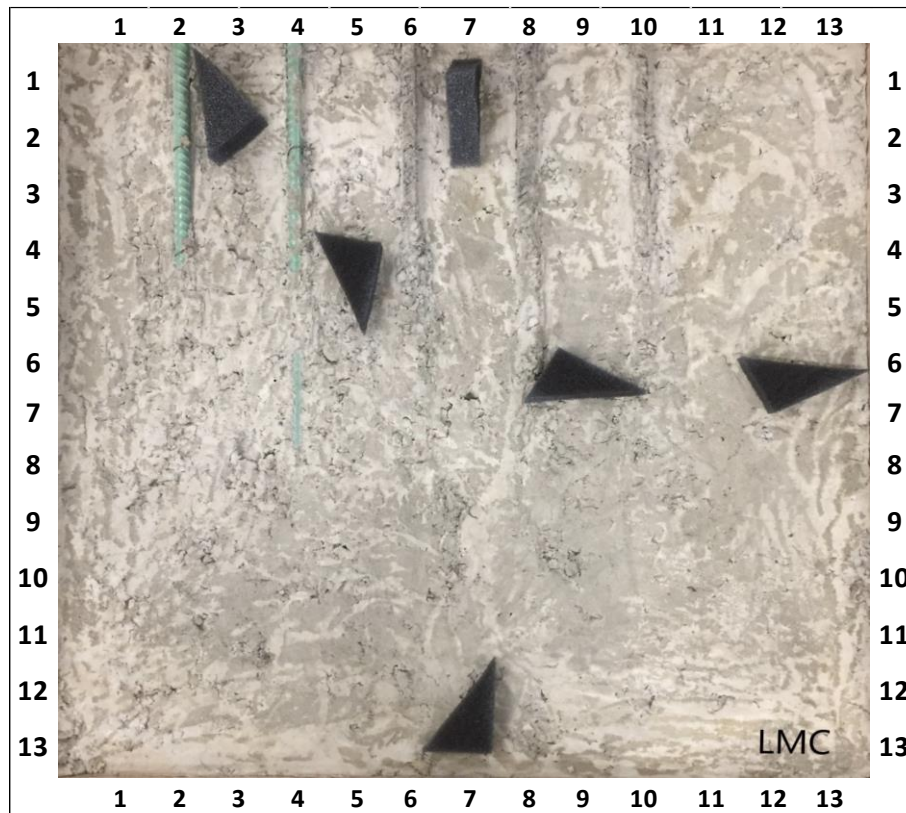


Figure D.23: LMC mockup void locations

Diagonal														Row Average		
	Rebar										No Rebar			All Points	No vert bar	No vert bar/void
	1	2	3	4	5	6	7	8	9	10	11	12	13			
1	6.5	6.6	6.7	6.6	6.3	6.1	6.4	5.7	6.2	5.6	5.8	6.2	6.3	6.231	6.300	6.286
2	6.7	5.9	5.9	5.8	5.8	5.4	5.7	6.6	5.6	5.8	5.6	5.7	5.3	5.831	5.788	5.788
3	6.6	6.5	5.6	5.9	5.6	5.5	5.3	5	5.8	5.7	5.8	5.6	6.4	5.792	5.838	5.838
4	5.6	5.4	5.5	5.7	6.3	5.7	5.7	5.7	5.3	5.9	5.7	5.9	6	5.723	5.750	5.750
5	6.2	6.1	5.9	5.7	5.5	5.9	5.7	5.4	5.2	5.3	5.7	5.7	6	5.715	5.738	5.771
6	6.3	5.7	5.6	5.3	4.8	5.8	5.5	5.5	5.4	5.3	5.1	6.1	6.6	5.615	5.675	5.614
7	6.4	5.7	6	5.1	5.2	5.3	5.3	5.5	5.2	5.4	5.5	5.8	6.5	5.608	5.738	5.817
8	6.7	6	5.9	5.4	5.3	5.2	5.5	5.3	5	5.3	5	5.5	5.9	5.538	5.600	5.600
9	6.8	5.9	5.7	5.4	5.2	5.2	5.3	5.3	5.1	5.3	5.3	5.7	5.9	5.548	5.625	5.625
10	6.9	5.9	5.5	5.3	5.2	5.7	5.6	5.1	4.8	5	5.3	5.5	5.6	5.492	5.550	5.550
11	6.7	6.1	5.3	5.4	5	5.2	5.3	4.9	5.2	5.3	5.7	5.9	6.1	5.548	5.650	5.650
12	6.7	5.9	5.7	5.7	5.7	5.7	6	5.4	5.3	5.7	5.7	5.7	6.6	5.831	5.925	5.925
13	7.1	6.4	6	6.5	5.9	5.8	6.5	5.5	5.9	5.9	6	6.7	7.4	6.277	6.438	6.429
														5.750	5.816	5.819

Figure D.24: LMC overlay mockup – surface resistivity diagonal orientation at 7 days

Horizontal														Row Average		
	Rebar										No Rebar			All Points	No vert bar	No vert bar/void
	1	2	3	4	5	6	7	8	9	10	11	12	13			
1	6.5	6	6.5	6.1	5.7	4.9	5.8	5.9	5.8	5.6	5.3	6	6.1	5.862	5.963	5.986
2	7.3	6.6	6	6.2	6.1	5.6	5.7	5.5	5.4	5.8	5.8	5.9	6.5	6.031	6.088	6.088
3	7	6.4	6.2	5.9	5.7	5.6	6	5	5.3	5.9	5.7	6.1	6.7	5.962	6.088	6.088
4	5.9	6.3	5.9	5.4	5.5	5.8	5.5	5.6	5.5	5.9	5.8	6.1	6.6	5.831	5.850	5.850
5	6.4	6.1	6.1	5.8	5.3	5.9	5.9	6	5.6	5.6	5.8	6	6.5	5.923	5.950	6.043
6	6.3	5.8	5.9	5.5	5.8	5.6	5.7	5.8	5.5	5.6	5.5	6	7.6	5.892	6.038	6.043
7	6.5	6	5.8	5.5	5.3	5.4	5.4	5.5	5.3	5.4	5.8	5.7	6.3	5.685	5.763	5.850
8	6.3	5.8	5.9	5.5	5.4	5.3	5.4	5.4	4.9	5.3	5.3	5.5	6.2	5.554	5.613	5.613
9	7.2	6.1	5.5	5.6	5.6	5.7	5.3	5.4	5	5.3	5.4	5.5	6.3	5.685	5.725	5.725
10	6.9	6	5.7	5.6	5	5.4	5.7	5.4	4.8	5.2	5.5	5.7	5.3	5.554	5.575	5.575
11	7	6	5.6	5.3	5.5	5.4	5.3	5	5.1	5.6	6.1	5.9	6.1	5.685	5.825	5.825
12	7.2	6	5.6	5.8	5.7	5.7	5.9	6.1	5.3	5.5	5.9	6	6.4	5.931	6.000	6.000
13	7.1	6.2	6.5	6.1	5.8	5.7	6.3	5.9	5.4	5.7	5.2	6.2	7.3	6.108	6.225	6.214
														5.823	5.900	5.915

Figure D.25: LMC overlay mockup – surface resistivity horizontal orientation at 7 days

Vertical														Row Average		
	Rebar										No Rebar			All Points	No vert bar	No vert bar/void
	1	2	3	4	5	6	7	8	9	10	11	12	13			
1	7	6.5	6.8	6.5	6.4	5.1	5.3	6	5.9	5.8	5.4	6	6.4	6.087	6.154	6.271
2	6.6	6.3	6.1	6.1	5.9	5.5	5.7	5.4	5.7	5.5	5.7	6	6.5	5.923	6.025	6.025
3	6.2	6.3	5.9	5.6	5.5	5.3	5.2	5.4	5.7	5.6	6	5.8	6.9	5.800	5.900	5.900
4	6.6	6.6	5.8	5.7	6	5.4	5.6	5.8	5.7	5.8	6.3	5.8	6.4	5.962	6.025	6.025
5	6.9	6	5.9	5.7	5.9	5.7	5.6	5.6	5.6	5.6	6	6.3	6.5	5.946	6.088	6.114
6	5.4	5.7	6	5.9	5.8	5.7	5.5	5.6	5.2	5.3	5.5	6.1	6.6	5.715	5.763	5.714
7	5.5	6.1	5.9	6.2	5.7	5.6	5.5	5.4	5.4	5.5	5.4	5.7	6.3	5.708	5.675	5.717
8	6.8	5.9	5.9	5.8	5.5	5.3	5.3	5.4	5.3	5.3	5.4	5.7	5.8	5.646	5.713	5.713
9	6.5	6	5.7	5.4	5.3	5.2	5.3	5.4	5.4	5.4	5.6	5.8	5.9	5.608	5.688	5.688
10	6.6	6	5.6	5.4	5	5.3	5.6	5.1	5.2	5.2	5.5	5.8	5.7	5.541	5.625	5.625
11	6.7	6.1	5.5	5.3	5	5.3	5.5	5.2	5.2	5.3	5.6	5.1	5.8	5.508	5.550	5.550
12	6.5	6	5.9	5.6	5.3	5.6	6.2	5.5	5.3	5.8	6	5.6	6.4	5.823	5.900	5.900
13	7.4	6.4	6.5	6.1	6.2	6.3	6.8	6.2	6.4	6.6	6.6	6.6	7.5	6.585	6.750	6.743
														5.835	5.912	5.922

Figure D.26: LMC overlay mockup – surface resistivity vertical orientation at 7 days

Average														Row Average		
	Rebar										No Rebar			All Points	No vert bar	No vert bar/void
	1	2	3	4	5	6	7	8	9	10	11	12	13			
1	6.7	6.4	6.7	6.4	6.1	5.4	5.8	5.9	6	5.7	5.5	6.1	6.3	6.060	6.139	6.181
2	6.9	6.3	6	6	5.9	5.5	5.7	5.8	5.6	5.7	5.7	5.9	6.1	5.928	5.967	5.967
3	6.6	6.4	5.9	5.8	5.6	5.5	5.5	5.1	5.6	5.7	5.8	5.8	6.7	5.851	5.942	5.942
4	6	6.1	5.7	5.6	5.9	5.6	5.6	5.7	5.5	5.9	5.9	5.9	6.3	5.838	5.875	5.875
5	6.5	6.1	6	5.7	5.6	5.8	5.7	5.7	5.5	5.5	5.8	6	6.3	5.862	5.925	5.976
6	6	5.7	5.8	5.6	5.5	5.7	5.6	5.6	5.4	5.4	5.4	6.1	6.9	5.741	5.825	5.790
7	6.1	5.9	5.9	5.6	5.4	5.4	5.4	5.5	5.3	5.4	5.6	5.7	6.4	5.667	5.725	5.794
8	6.6	5.9	5.9	5.6	5.4	5.3	5.4	5.4	5.1	5.3	5.2	5.6	6	5.579	5.642	5.642
9	6.8	6	5.6	5.5	5.4	5.4	5.3	5.4	5.2	5.3	5.4	5.7	6	5.614	5.679	5.679
10	6.8	6	5.6	5.4	5.1	5.5	5.6	5.2	4.9	5.1	5.4	5.7	5.5	5.529	5.583	5.583
11	6.8	6.1	5.5	5.3	5.2	5.3	5.4	5	5.2	5.4	5.8	5.6	6	5.580	5.675	5.675
12	6.8	6	5.7	5.7	5.6	5.7	6	5.7	5.3	5.7	5.9	5.8	6.5	5.862	5.942	5.942
13	7.2	6.3	6.3	6.2	6	5.9	6.5	5.9	5.9	6.1	5.9	6.5	7.4	6.323	6.471	6.462
														5.803	5.876	5.885

Figure D.27: LMC overlay mockup – surface resistivity average of orientations at 7 days

Standard Deviation																
	Rebar										No Rebar					
	1	2	3	4	5	6	7	8	9	10	11	12	13			
1	0.3	0.3	0.2	0.3	0.4	0.6	0.5	0.2	0.2	0.1	0.3	0.1	0.2			
2	0.4	0.4	0.1	0.2	0.2	0.1	0	0.7	0.2	0.2	0.1	0.2	0.7			
3	0.4	0.1	0.3	0.2	0.1	0.2	0.4	0.2	0.3	0.2	0.2	0.3	0.3			
4	0.5	0.6	0.2	0.2	0.4	0.2	0.1	0.1	0.2	0.1	0.3	0.2	0.3			
5	0.4	0.1	0.1	0.1	0.3	0.1	0.2	0.3	0.2	0.2	0.2	0.3	0.3			
6	0.5	0.1	0.2	0.3	0.6	0.1	0.1	0.2	0.2	0.2	0.2	0.1	0.6			
7	0.6	0.2	0.1	0.6	0.3	0.2	0.1	0.1	0.1	0.1	0.2	0.1	0.1			
8	0.3	0.1	0	0.2	0.1	0.1	0.1	0.1	0.2	0	0.2	0.1	0.2			
9	0.4	0.1	0.1	0.1	0.2	0.3	0	0	0.2	0.1	0.2	0.2	0.2			
10	0.2	0.1	0.1	0.2	0.1	0.2	0.1	0.2	0.2	0.1	0.1	0.2	0.2			
11	0.2	0.1	0.2	0.1	0.3	0.1	0.1	0.2	0.1	0.2	0.3	0.5	0.2			
12	0.4	0.1	0.2	0.1	0.2	0.1	0.2	0.4	0	0.2	0.2	0.2	0.1			
13	0.2	0.1	0.3	0.2	0.2	0.3	0.3	0.4	0.5	0.5	0.7	0.3	0.1			

Figure D.28: LMC mockup – surface resistivity standard deviation at 7 days

Average													
	Rebar										No Rebar		
	1	2	3	4	5	6	7	8	9	10	11	12	13
1	6.7	6.4	5.7	6.4	6.1	5.4	5.4	5.9	6	5.7	5.5	6.1	6.3
2	6.9	6.3	6	6	5.9	5.5	5.7	5.8	5.6	5.7	5.7	5.9	6.1
3	6.6	6.4	5.9	5.8	5.6	5.5	5.5	5.1	5.6	5.7	5.8	5.8	6.7
4	6	6.1	5.7	5.6	5.9	5.6	5.6	5.7	5.5	5.9	5.9	5.9	6.3
5	6.5	6.1	6	5.7	5.9	5.8	5.7	5.7	5.5	5.5	5.8	6	6.3
6	6	5.7	5.8	5.6	5.5	5.7	5.6	5.6	5.4	5.4	5.4	6.1	6.9
7	6.1	5.9	5.9	5.6	5.4	5.4	5.4	5.5	5.3	5.4	5.6	5.7	6.4
8	6.6	5.9	5.9	5.6	5.4	5.3	5.4	5.4	5.1	5.3	5.2	5.6	6
9	6.8	6	5.6	5.5	5.4	5.4	5.3	5.4	5.2	5.3	5.4	5.7	6
10	6.8	6	5.6	5.4	5.1	5.5	5.6	5.2	4.9	5.1	5.4	5.7	5.5
11	6.8	6.1	5.5	5.3	5.2	5.3	5.4	5	5.2	5.4	5.8	5.6	6
12	6.8	6	5.7	5.7	5.6	5.7	5.7	5.7	5.3	5.7	5.9	5.8	6.5
13	7.2	6.3	6.3	6.2	6	5.9	6.5	5.9	5.9	6.1	5.9	6.5	7.4

Figure D.29: Voids superimposed on LMC mockup - 7 day average surface resistivity data

3.5	3.3	3.5	3.8	3.8	3.9	4.0
3.2	2.9	3.0	3.0	3.1	3.3	3.7
3.3	2.8	2.9	3.1	2.8	2.9	3.3
3.0	2.6	2.8	2.7	2.6	2.7	3.0
2.5	2.2	2.4	2.3	2.3	2.3	2.5
2.0	1.7	1.8	1.8	1.9	1.7	2.0
1.7	1.5	1.5	1.4	1.3	1.4	1.4

Figure D.30: VHES mockup overlay thickness measurements

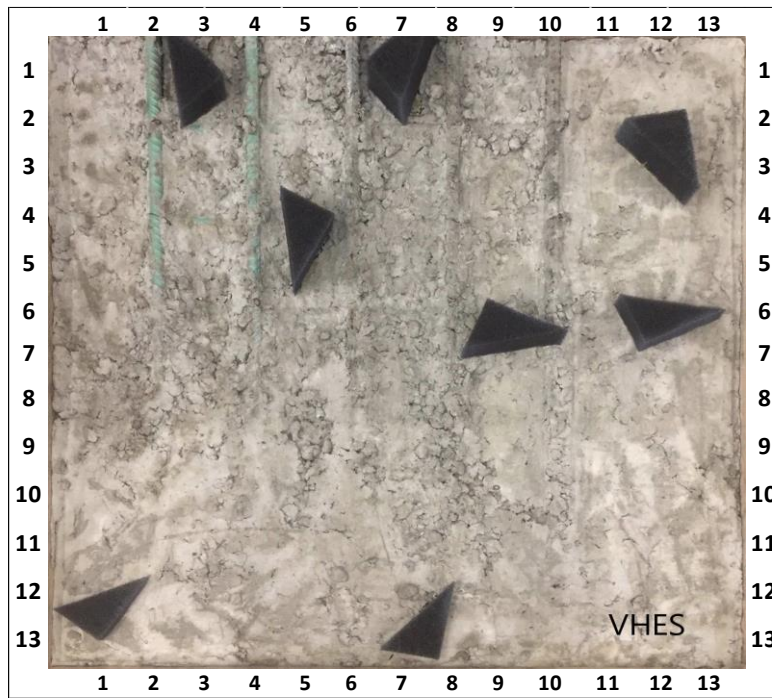


Figure D.31: VHES mockup void locations

Diagonal														Row Average		
	Rebar										No Rebar			All Points	No vert bar	No vert bar/void
	1	2	3	4	5	6	7	8	9	10	11	12	13			
1	11	8.8	9	7.9	8.3	7.9	8.7	7.8	7.5	8	7.9	7.8	8	8.34	8.50	8.50
2	9	8.7	8.1	7.8	9.1	7.9	7.1	7.2	6.9	7.7	7.7	7.6	8.6	7.95	8.01	8.01
3	8.4	8.1	7.5	7.8	7.6	7.6	7.8	7.4	7.7	7.2	8.2	7.6	9.8	7.90	8.08	8.14
4	8.5	8.5	8.3	8.2	7.6	6.6	7.5	7.9	7.9	7.6	8.2	8.2	8.7	7.98	8.11	8.11
5	8.5	8.7	7.6	8.4	8.5	6.5	7.7	8.2	7.9	8.9	8.5	9	9.4	8.29	8.39	8.37
6	9.2	8.3	8.6	8.2	8.2	8.7	8.3	8	7.5	8	9	9.3	9.5	8.52	8.70	8.61
7	9.7	9.6	9.1	8	8.5	8.3	8.6	9.6	9	8.9	8.6	9.1	10	9.03	9.13	8.90
8	8.9	9	8.8	8.8	8.5	8.8	8.8	8.5	9.5	8.7	9	10	10	9.05	9.23	9.23
9	9.3	9.2	8.7	9.3	9.2	9.2	8.8	8.7	8.7	9	10	10	11	9.37	9.55	9.55
10	9.8	9.9	9.3	9.9	9.7	9.2	9.8	9.7	9.4	9.4	11	11	12	9.95	10.15	10.15
11	11	10	9.7	10	10	9.7	10	10	9.1	9.9	11	11	12	10.18	10.33	10.33
12	12	10	9.5	9.8	11	10	9.3	10	9.5	10	11	11	12	10.37	10.54	10.54
13	13	11	11	11	10	9.5	12	11	10	11	11	11	12	10.96	11.27	10.94
														9.068	9.228	9.183

Figure D.32: VHES overlay mockup – surface resistivity diagonal orientation at 7 days

Horizontal														Row Average		
	Rebar										No Rebar			All Points	No vert bar	No vert bar/void
	1	2	3	4	5	6	7	8	9	10	11	12	13			
1	9	8.3	8	7.1	7.3	7.6	7.7	7.8	6.8	6.9	6.3	6.6	9.2	7.58	7.61	7.72
2	8.5	7.4	7	6.5	7.3	7.2	7	6.9	7	7.2	7	7.5	8.9	7.34	7.53	7.53
3	8.7	7.2	7	6.6	7.1	7	7.1	7	6.8	7.5	7.4	7.6	9.2	7.40	7.61	7.61
4	8.6	7.7	7.5	7	7	6.7	7	7.3	7.4	7.6	7.7	7.9	9.6	7.62	7.84	7.84
5	8.2	7.9	6.9	8.1	8.1	7.3	7.3	7.5	7.3	7.8	8.2	8.9	10	7.97	8.13	8.13
6	8.6	7.6	7.3	7	7.1	8.1	7.6	7.3	7.2	7.7	8.4	8.7	9.8	7.88	8.09	8.00
7	9.4	8.2	7.4	6.5	7	8.2	7	8.2	8	7.3	8	8.8	9.6	7.97	8.15	7.76
8	9	7.8	8.3	8.4	7.9	8	8.2	8.9	7.9	8.3	8.4	9.2	10	8.49	8.62	8.62
9	9	8.6	8.2	8.5	8.5	9	8.8	8.8	8.4	9.1	8.9	9.4	10	8.88	8.93	8.93
10	10	9	8.9	8.8	8.8	8.9	8.6	9.2	9.3	9.3	9.8	11	11	9.41	9.64	9.64
11	11	9.4	9	8.9	9.4	9.2	9	9.1	9.2	9.7	10	10	11	9.58	9.78	9.78
12	11	9.5	9.1	9.3	9.7	9.5	9.2	9.5	9.1	9.4	9.5	10	11	9.68	9.84	9.84
13	12	9.7	9.5	9.5	9.1	8.9	9.3	9.4	8.7	9.9	10	10	11	9.82	10.03	9.78
														8.431	8.597	8.551

Figure D.33: VHES overlay mockup – surface resistivity horizontal orientation at 7 days

Vertical														Row Average		
	Rebar										No Rebar			All Points	No vert bar	No vert bar/void
	1	2	3	4	5	6	7	8	9	10	11	12	13			
1	9.1	8.3	8	7.3	7.8	7.5	8.9	7.3	7.4	8	7.4	7.7	8.2	7.92	8.06	7.98
2	7.5	7.7	7.4	6.5	6.8	6.7	6.8	6.6	6.4	6.5	6.7	6.7	7.9	6.94	7.03	7.03
3	7.6	7.6	6.4	6.5	6.7	6.7	6.8	7	6.8	7	7	7.4	8.4	7.07	7.14	7.10
4	7.2	7.6	7.2	7.3	7.3	5.8	7.1	7.1	7	6.9	7	7.9	8.3	7.21	7.38	7.38
5	7.6	8.1	6.9	7.7	7.8	5.6	7.1	7	6.9	6.7	7.7	8.4	8.7	7.40	7.64	7.61
6	8.4	8.1	7.7	7.8	7.8	7.4	6.4	7.7	6.9	8.1	7.8	9	9.1	7.86	7.89	7.73
7	7.9	7.8	8.1	7.1	7.6	7.6	7.5	7.2	7	6	8.2	9.3	9.4	7.75	8.13	7.86
8	8.2	8	7.9	8.2	8.2	8	8	7.8	7.9	8.6	8.4	8.7	9.2	8.24	8.31	8.31
9	8.5	8.6	8.4	8.5	8.8	8.3	8	7.7	8	7.8	9.1	9.7	9.4	8.53	8.74	8.74
10	9.4	8.7	8.1	8.3	8.7	8.5	8.6	8.5	8.1	8.9	9.4	9.8	10	8.85	9.03	9.03
11	9	9.4	8.9	8.7	9.3	8.4	9.1	8.7	8.2	9.5	9.9	9.8	11	9.22	9.39	9.39
12	9.7	9.3	8.4	8.7	9.2	8.5	9.1	9.2	9.1	9.5	9.8	11	11	9.44	9.69	9.69
13	11	10	9.3	9.5	9.5	9.5	10	9.4	8.9	10	11	11	12	10.06	10.26	10.08
														8.191	8.360	8.302

Figure D.34: VHES overlay mockup – surface resistivity vertical orientation at 7 days

Average														Row Average		
	Rebar										No Rebar			All Points	No vert bar	No vert bar/void
	1	2	3	4	5	6	7	8	9	10	11	12	13			
1	9.6	8.5	8.3	7.4	7.8	7.7	8.4	7.6	7.2	7.6	7.2	7.4	8.5	7.95	8.06	8.07
2	8.3	7.9	7.5	6.9	7.7	7.3	7	6.9	6.8	7.1	7.1	7.3	8.5	7.41	7.52	7.52
3	8.2	7.6	7	7	7.1	7.1	7.2	7.1	7.1	7.2	7.5	7.5	9.1	7.46	7.61	7.62
4	8.1	7.9	7.7	7.5	7.3	6.4	7.2	7.4	7.4	7.4	7.6	8	8.9	7.60	7.78	7.78
5	8.1	8.2	7.1	8.1	8.1	6.5	7.4	7.6	7.4	7.8	8.1	8.8	9.4	7.89	8.05	8.04
6	8.7	8	7.9	7.7	7.7	8.1	7.4	7.7	7.2	7.9	8.4	9	9.5	8.09	8.23	8.11
7	9	8.5	8.2	7.2	7.7	8	7.7	8.3	8	7.4	8.3	9.1	9.8	8.25	8.47	8.17
8	8.7	8.3	8.3	8.5	8.2	8.3	8.3	8.4	8.4	8.5	8.6	9.3	9.8	8.59	8.72	8.72
9	8.9	8.8	8.4	8.8	8.8	8.8	8.5	8.4	8.4	8.6	9.5	9.7	10	8.92	9.07	9.07
10	9.8	9.2	8.8	9	9.1	8.9	9	9.1	8.9	9.2	9.9	10	11	9.40	9.60	9.60
11	10	9.6	9.2	9.2	9.6	9.1	9.4	9.3	8.8	9.7	10	10	11	9.66	9.83	9.83
12	11	9.7	9	9.3	9.8	9.4	9.2	9.6	9.2	9.7	10	11	11	9.83	10.02	10.02
13	12	10	9.8	9.9	9.6	9.3	10	9.9	9.3	10	11	11	12	10.28	10.52	10.27
														8.564	8.728	8.679

Figure D.35: VHES overlay mockup – surface resistivity average of orientations at 7 days

Standard Deviation																
	Rebar										No Rebar					
	1	2	3	4	5	6	7	8	9	10	11	12	13			
1	1	0.3	0.6	0.4	0.5	0.2	0.6	0.3	0.4	0.6	0.8	0.7	0.6			
2	0.8	0.7	0.6	0.8	1.2	0.6	0.2	0.3	0.3	0.6	0.5	0.5	0.5			
3	0.6	0.5	0.6	0.7	0.5	0.5	0.5	0.2	0.5	0.3	0.6	0.1	0.7			
4	0.8	0.5	0.6	0.6	0.3	0.5	0.3	0.4	0.5	0.4	0.6	0.2	0.7			
5	0.5	0.4	0.4	0.4	0.4	0.9	0.3	0.6	0.5	1.1	0.4	0.3	0.7			
6	0.4	0.4	0.7	0.6	0.6	0.7	1	0.4	0.3	0.2	0.6	0.3	0.4			
7	1	0.9	0.9	0.8	0.8	0.4	0.8	1.2	1	1.5	0.3	0.3	0.5			
8	0.4	0.6	0.5	0.3	0.3	0.5	0.4	0.6	0.9	0.2	0.3	0.7	0.6			
9	0.4	0.3	0.3	0.5	0.4	0.5	0.5	0.6	0.4	0.7	0.8	0.3	1			
10	0.4	0.6	0.6	0.8	0.6	0.4	0.7	0.6	0.7	0.3	0.6	0.5	1			
11	0.9	0.3	0.4	0.7	0.4	0.7	0.6	0.7	0.6	0.2	0.3	0.4	0.7			
12	1.1	0.5	0.6	0.6	0.7	0.8	0.1	0.5	0.2	0.4	0.7	0.4	0.2			
13	0.7	0.5	0.6	0.6	0.6	0.3	1.3	0.9	0.9	0.4	0.5	0.6	0.5			

Figure D.36: VHES mockup – surface resistivity standard deviation at 7 days

Average													
	Rebar										No Rebar		
	1	2	3	4	5	6	7	8	9	10	11	12	13
1	9.6	8.5	8.3	7.4	7.8	7.7	8.4	7.6	7.2	7.6	7.2	7.4	8.5
2	8.3	7.9	7.5	6.9	7.7	7.3	6.9	6.8	7.1	7.1	7.1	7.2	8.5
3	8.2	7.6	7	7	7.1	7.1	7.2	7.1	7.1	7.2	7.5	7.5	9.1
4	8.1	7.9	7.7	7.5	7.3	6.4	7.2	7.4	7.4	7.4	7.6	8	8.9
5	8.1	8.2	7.1	8.1	8.1	6.5	7.4	7.6	7.4	7.8	8.1	8.8	9.4
6	8.7	8	7.9	7.7	7.7	8.1	7.4	7.7	7.2	7.9	8.4	9	9.5
7	9	8.5	8.2	7.2	7.7	8	7.7	8.5	8	7.4	8.3	9.1	9.8
8	8.7	8.3	8.3	8.5	8.2	8.3	8.3	8.4	8.4	8.5	8.6	9.3	9.8
9	8.9	8.8	8.4	8.8	8.8	8.8	8.5	8.4	8.4	8.6	9.5	9.7	10
10	9.8	9.2	8.8	9	9.1	8.9	9	9.1	8.9	9.2	9.9	10	11
11	10	9.6	9.2	9.2	9.6	9.1	9.4	9.3	8.8	9.7	10	10	11
12	11	9.7	9	9.3	9.8	9.4	9.2	9.6	9.2	9.7	10	11	11
13	12	10	9.8	9.9	9.6	9.3	10	9.9	9.3	10	11	11	12

Figure D.37: Voids superimposed on VHES mockup - 7 day average surface resistivity data

3.4	3.6	4.0	3.6	4.0	4.2	3.8
3.3	3.1	3.2	3.2	3.1	3.3	3.8
2.8	2.8	2.9	2.9	2.9	2.8	3.3
2.4	2.4	2.6	2.7	2.6	2.7	2.5
2.3	2.4	2.4	2.5	2.4	2.5	2.3
1.8	1.9	2.0	2.0	2.0	1.9	1.8
1.4	1.5	1.8	1.4	1.3	1.4	1.4

Figure D.38: VHES-LMC mockup overlay thickness measurements

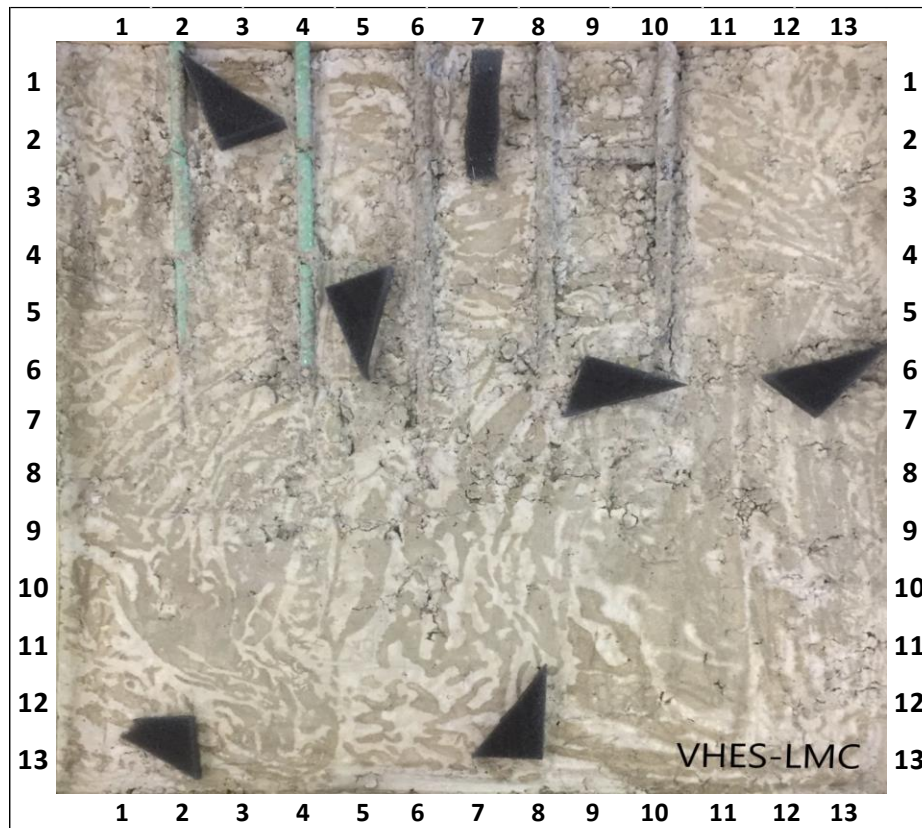


Figure D.39: VHES-LMC mockup void locations

Diagonal														Row Average		
	Rebar										No Rebar			All	No vert	No vert
	1	2	3	4	5	6	7	8	9	10	11	12	13	Points	bar	bar/void
1	16	12	12	13	11	12	12	9.6	11	12	11	11	12	11.877	11.963	11.950
2	13	11	12	10	9.4	10	9.3	9.6	9.8	11	11	11	12	10.762	10.988	10.988
3	13	12	9.6	11	12	12	11	10	10	11	11	11	13	11.223	11.213	11.100
4	13	13	13	12	11	11	11	9.4	11	10	11	12	12	11.469	11.688	11.688
5	13	14	13	12	11	11	11	12	11	11	12	11	13	11.933	11.925	11.920
6	13	14	13	13	12	12	13	12	12	12	12	12	11	12.446	12.363	12.533
7	13	13	14	12	12	12	12	13	13	13	13	13	13	12.823	12.800	12.829
8	15	13	14	13	12	14	13	14	14	14	13	14	14	13.731	13.800	13.800
9	16	14	14	14	14	14	13	14	15	14	14	16	16	14.300	14.575	14.575
10	17	15	15	13	14	13	13	15	15	16	15	15	18	14.885	15.125	15.125
11	16	15	16	16	15	15	14	15	15	16	16	17	19	15.823	16.163	16.163
12	16	17	16	18	17	17	18	17	16	17	17	18	20	17.231	17.250	17.250
13	18	17	16	18	17	17	19	19	18	18	18	18	17	17.708	17.650	17.300
														13.555	13.654	13.632

Figure D.40: VHES-LMC overlay mockup – surface resistivity diagonal orientation at 7 days

Horizontal														Row Average		
											No Rebar			All Points	No vert bar	No vert bar/void
	1	2	3	4	5	6	7	8	9	10	11	12	13			
1	13	13	12	11	11	9.6	10	9.6	10	10	9.6	10	12	10.838	11.013	11.050
2	12	11	11	9.2	9	9.4	8.9	8.7	9.8	9.7	9.5	10	13	10.115	10.413	10.413
3	13	12	10	9.8	10	11	9.1	8.6	9	9.7	10	11	12	10.269	10.413	10.471
4	14	13	12	12	10	9.1	8.9	9.5	10	10	11	11	13	10.933	11.125	11.125
5	12	13	13	12	11	11	11	11	11	12	11	10	13	11.631	11.588	11.660
6	14	14	12	12	12	11	11	12	11	12	12	11	12	11.962	11.925	12.050
7	13	13	13	12	13	12	12	13	12	14	12	12	13	12.477	12.400	12.443
8	15	14	13	13	12	13	12	13	13	14	13	13	14	13.169	13.163	13.163
9	15	15	14	12	13	13	11	14	14	14	13	14	15	13.700	13.700	13.700
10	16	15	14	14	13	13	13	15	14	15	14	15	17	14.469	14.550	14.550
11	17	16	15	15	15	15	14	15	15	16	15	18	20	15.738	16.000	16.000
12	18	16	16	16	17	17	17	16	16	16	15	17	18	16.377	16.688	16.688
13	19	18	16	16	16	16	18	20	17	16	16	18	17	17.200	17.113	16.733
														12.991	13.084	13.080

Figure D.41: VHES-LMC overlay mockup – surface resistivity horizontal orientation at 7 days

Vertical														Row Average		
											No Rebar			All Points	No vert bar	No vert bar/void
	1	2	3	4	5	6	7	8	9	10	11	12	13			
1	13	12	11	11	11	11	11	9.5	11	10	11	11	12	11.069	11.388	11.500
2	13	10	11	9.3	9.4	9.7	9.7	9.8	9.4	9	11	10	11	10.162	10.513	10.513
3	13	11	9.8	9.3	9.8	9.8	9.6	11	9	9.6	10	9.5	11	10.133	10.229	10.290
4	13	12	11	11	9.5	10	9.8	9.8	11	10	10	10	12	10.685	10.700	10.700
5	12	13	12	12	11	12	11	11	11	11	10	11	12	11.277	11.088	11.080
6	13	13	13	12	12	12	11	12	12	11	11	11	10	11.738	11.650	11.950
7	13	13	12	13	11	12	12	12	11	13	12	11	12	12.192	11.838	11.914
8	14	12	13	13	12	13	12	13	13	14	13	13	14	12.846	12.763	12.763
9	15	13	13	12	13	13	12	15	13	13	13	13	14	13.123	13.138	13.138
10	16	15	14	13	13	13	13	15	14	15	14	15	16	14.269	14.338	14.338
11	16	15	15	15	14	14	15	14	15	15	15	16	18	15.138	15.400	15.400
12	16	16	16	17	16	16	15	17	16	15	16	18	19	16.323	16.400	16.400
13	16	17	16	17	16	16	16	18	16	17	17	17	17	16.800	16.563	16.650
														12.750	12.770	12.818

Figure D.42: VHES-LMC overlay mockup – surface resistivity vertical orientation at 7 days

Average														Row Average		
	Rebar										No Rebar			All Points	No vert bar	No vert bar/void
	1	2	3	4	5	6	7	8	9	10	11	12	13			
1	14	12	12	12	11	11	11	9.6	11	11	10	11	12	11.262	11.454	11.500
2	13	11	11	9.6	9.3	9.8	9.3	9.4	9.7	9.8	11	10	12	10.346	10.638	10.638
3	13	12	9.8	9.9	11	11	9.8	9.7	9.3	10	10	11	12	10.542	10.618	10.620
4	13	12	12	12	10	10	10	9.6	11	10	11	11	12	11.029	11.171	11.171
5	12	13	12	12	11	11	11	11	11	11	11	11	13	11.614	11.533	11.553
6	14	13	13	12	12	12	12	12	12	12	11	12	11	12.049	11.979	12.178
7	13	13	13	12	12	12	12	13	12	13	12	12	13	12.497	12.346	12.395
8	15	13	13	13	12	13	12	13	13	14	13	13	14	13.249	13.242	13.242
9	15	14	14	13	13	13	12	14	14	14	13	14	15	13.708	13.804	13.804
10	16	15	14	14	13	13	13	15	14	15	14	15	17	14.541	14.671	14.671
11	16	15	15	15	15	15	14	15	15	15	15	17	19	15.567	15.854	15.854
12	17	16	16	17	17	17	17	16	16	16	16	17	19	16.644	16.779	16.779
13	18	18	16	17	16	17	18	19	17	17	17	18	17	17.236	17.108	16.894
														13.099	13.169	13.177

Figure D.43: VHES-LMC overlay mockup – surface resistivity average of orientations at 7 days

Standard Deviation																
	Rebar										No Rebar					
	1	2	3	4	5	6	7	8	9	10	11	12	13			
1	1.3	0.5	0.2	1.4	0.2	1.2	1.1	0.1	0.6	0.9	0.6	0.6	0.2			
2	0.5	0.6	0.4	0.6	0.2	0.4	0.4	0.6	0.2	0.8	1	0.5	0.9			
3	0.2	0.9	0.3	0.7	1.2	1.2	0.8	1	0.6	0.7	0.3	1	0.7			
4	0.4	0.8	0.8	0.1	0.7	1	1.2	0.2	0.4	0.1	0.6	0.8	0.6			
5	0.3	0.4	0.6	0.3	0.4	0.3	0.4	0.6	0.3	0.3	0.7	0.6	0.9			
6	0.4	0.7	0.5	0.6	0.2	0.6	1.1	0.4	0.6	0.2	0.8	0.6	0.8			
7	0.3	0.2	0.8	0.8	0.8	0.3	0.1	0.2	0.7	0.1	0.7	0.6	0.8			
8	0.9	0.7	0.9	0.1	0.3	0.6	0.7	0.4	1	0.3	0.1	0.9	0.2			
9	0.3	1.1	1	0.8	0.6	0.3	1.2	0.2	1.1	0.7	0.6	1.4	0.7			
10	0.8	0.3	0.4	0.6	0.3	0.2	0.2	0.5	0.4	0.8	0.5	0.2	1			
11	0.6	0.8	0.9	0.2	0.5	0.5	0.5	0.5	0.2	0.3	0.6	1	0.7			
12	0.8	0.8	0.1	0.9	0.8	0.5	1.3	0.6	0.1	1.3	0.8	0.9	1.1			
13	1.2	0.8	0.1	0.8	0.5	0.6	1.4	0.7	0.8	0.9	0.7	0.3	0.5			

Figure D.44: VHES-LMC mockup – surface resistivity standard deviation at 7 days

Average													
	Rebar										No Rebar		
Reading #	1	2	3	4	5	6	7	8	9	10	11	12	13
1	3.5	3.3	3.3	3.7	3.5	3.6	3.4	3.3	3.7	3.6	3.5	3.2	3.8
2	3.3	3.3	3.5	3.2	3.1	3.3	3.5	3.4	3.7	3.4	3.3	3.1	3.7
3	3.3	3.2	3.2	3.3	3.2	3	3.3	3.5	3.6	3.3	3.2	3.1	3.8
4	3.4	3.3	3.3	3.3	3	3.1	3.4	3.5	3.3	3.6	3.3	3.4	3.5
5	3.6	3.4	3.7	3.8	3.3	3.3	3.2	3.4	3.3	3.5	3.1	3.2	3.5
6	3.4	3.4	3.3	3.4	3.3	3.4	3.3	3	3.4	3	3	3.2	3.7
7	3.3	3.3	3.3	3.5	3.3	3.4	3.3	3	3.3	3.3	3	3.4	3.9
8	3.4	3.2	3.3	3.5	3.2	3.2	3.3	3.5	3.5	3.5	3.2	3.3	3.6
9	3.4	3.1	3.1	3	3.2	3.4	3.5	3.7	3.3	3.4	3.1	3	3.8
10	3.2	3.2	3.2	3	3.3	3.2	3.4	3.4	3.5	3.2	3.2	3.4	3.8
11	3.3	3.2	3.3	3.1	3.2	3.4	3.3	3.4	3.4	3.3	3.1	3.3	3.6
12	3.4	3.6	3.3	3.1	3.3	3.3	3.4	3.4	3.1	3.3	3.5	3.2	3.5
13	3.9	3.7	3.6	3.6	3.3	3.4	3.5	3.8	3.5	3.5	3.3	3.3	3.4

Figure D.45: Voids superimposed on VHES-LMC mockup - 7 day average surface resistivity data

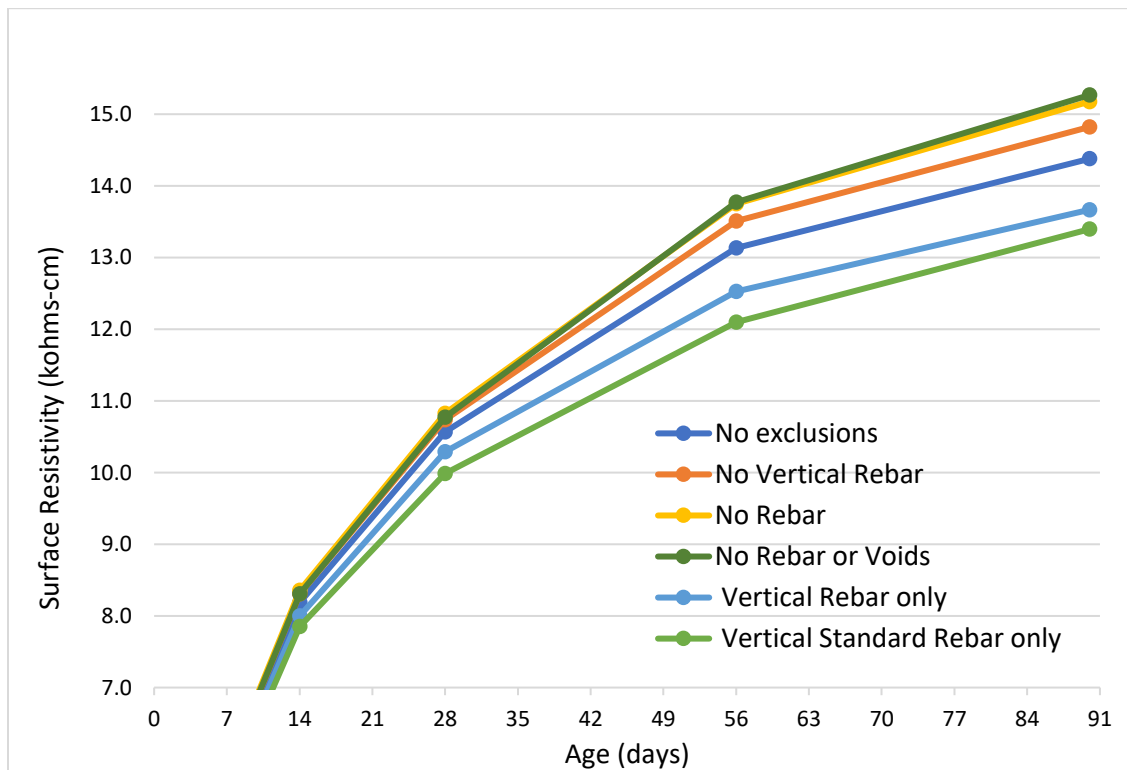


Figure D.46: LMC mockup - surface resistivity diagonal orientation with different exclusions

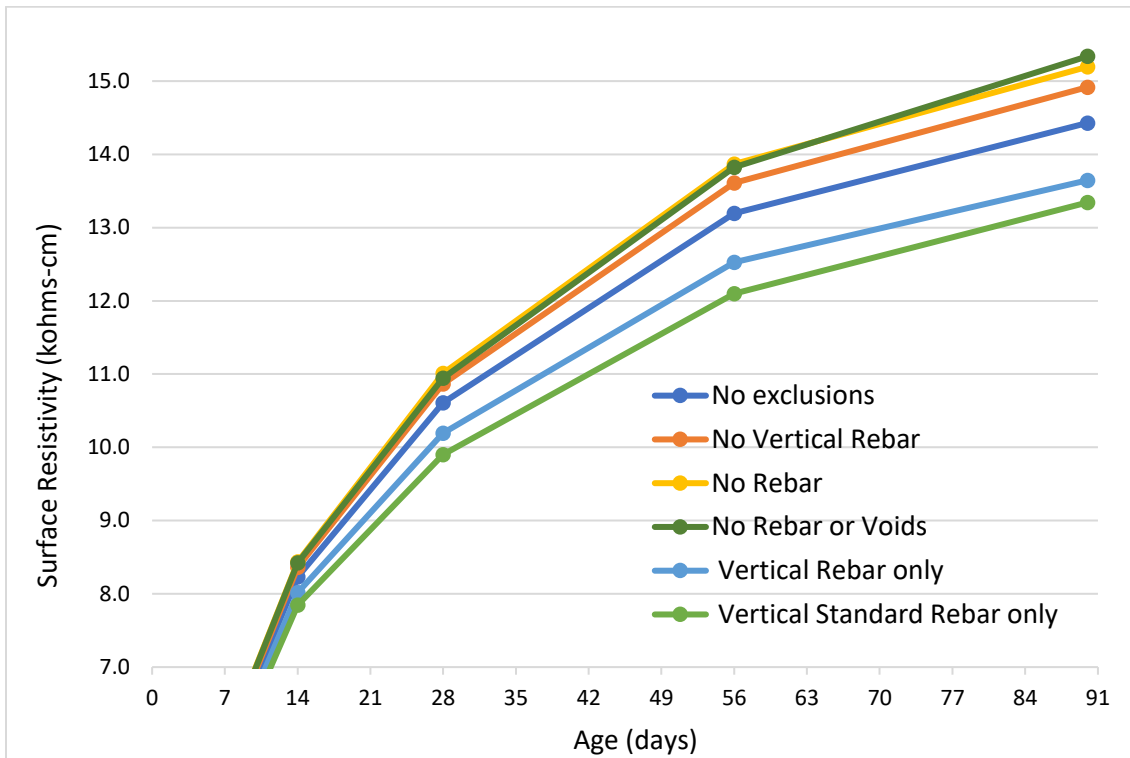


Figure D.47: LMC mockup - surface resistivity horizontal orientation with different exclusions

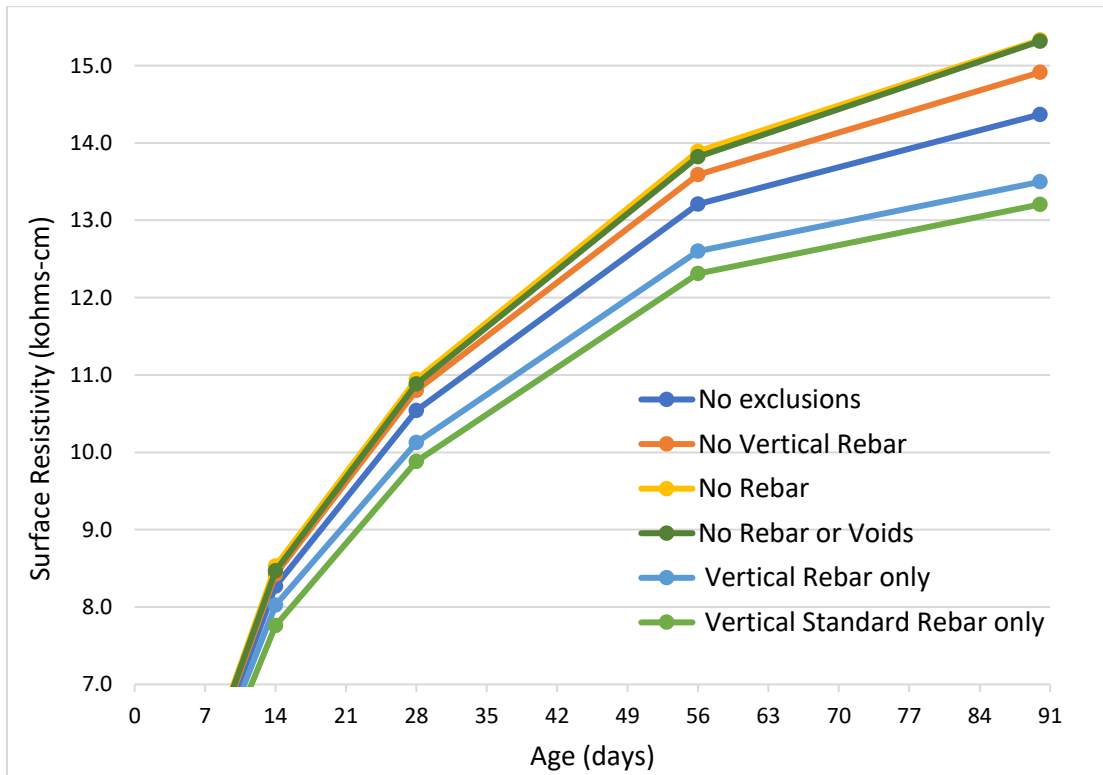


Figure D.48: LMC mockup - surface resistivity vertical orientation with different exclusions

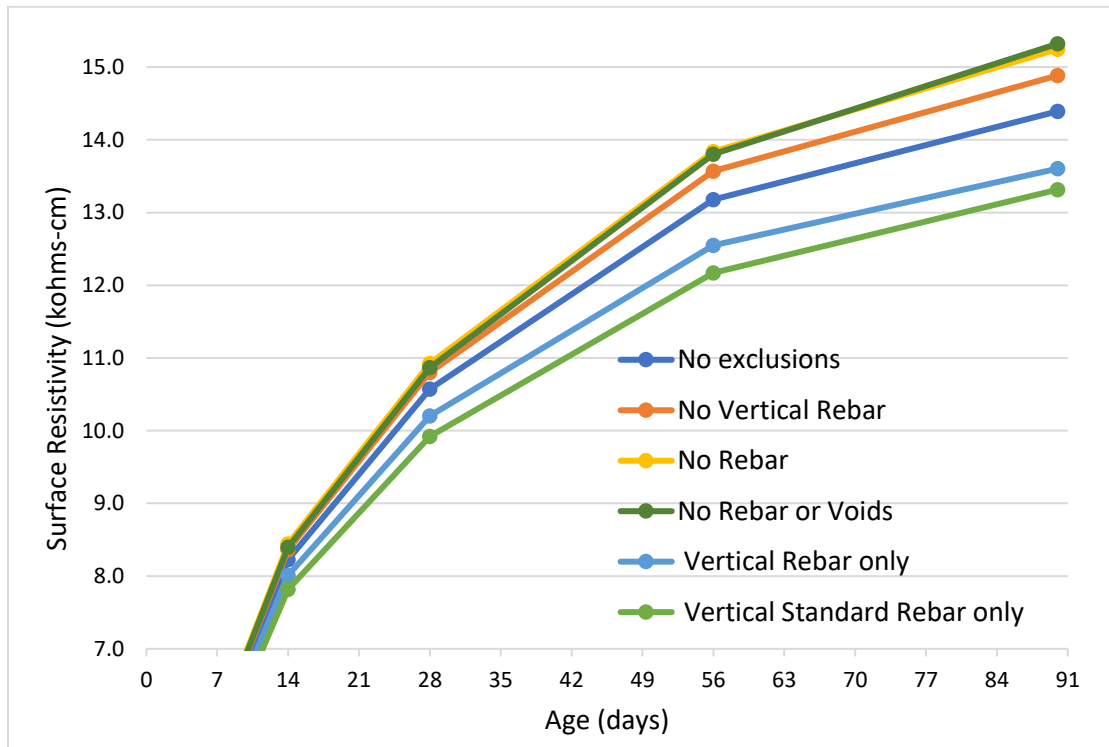


Figure D.49: LMC mockup - surface resistivity average of orientations with different exclusions

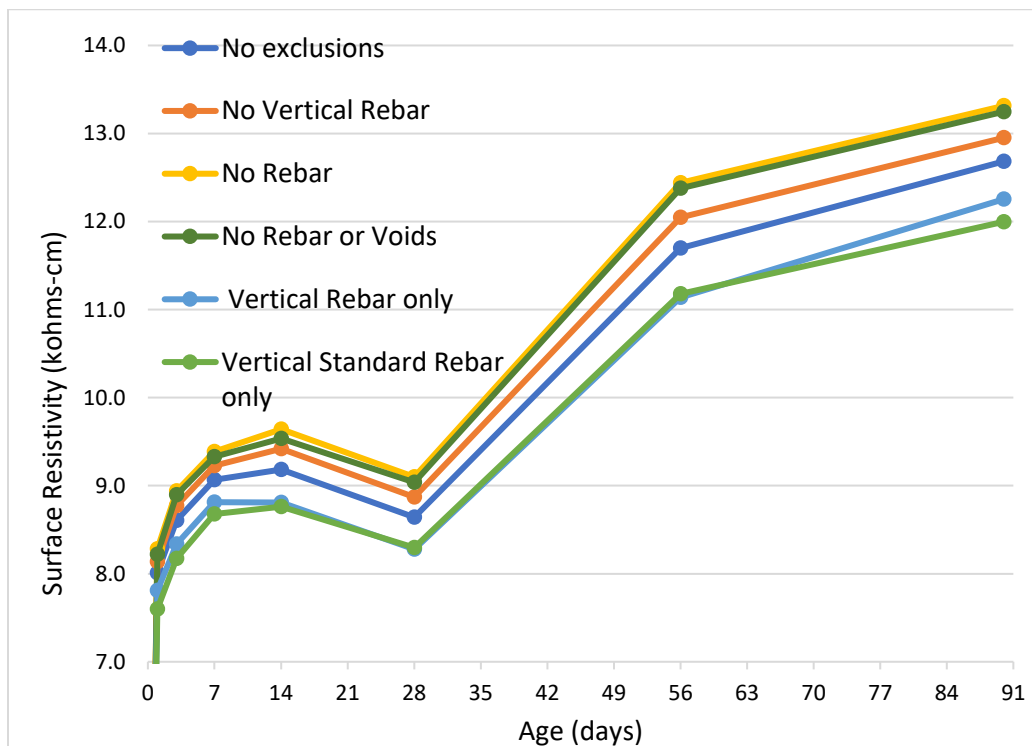


Figure D.1: VHES mockup diagonal orientation with different exclusions

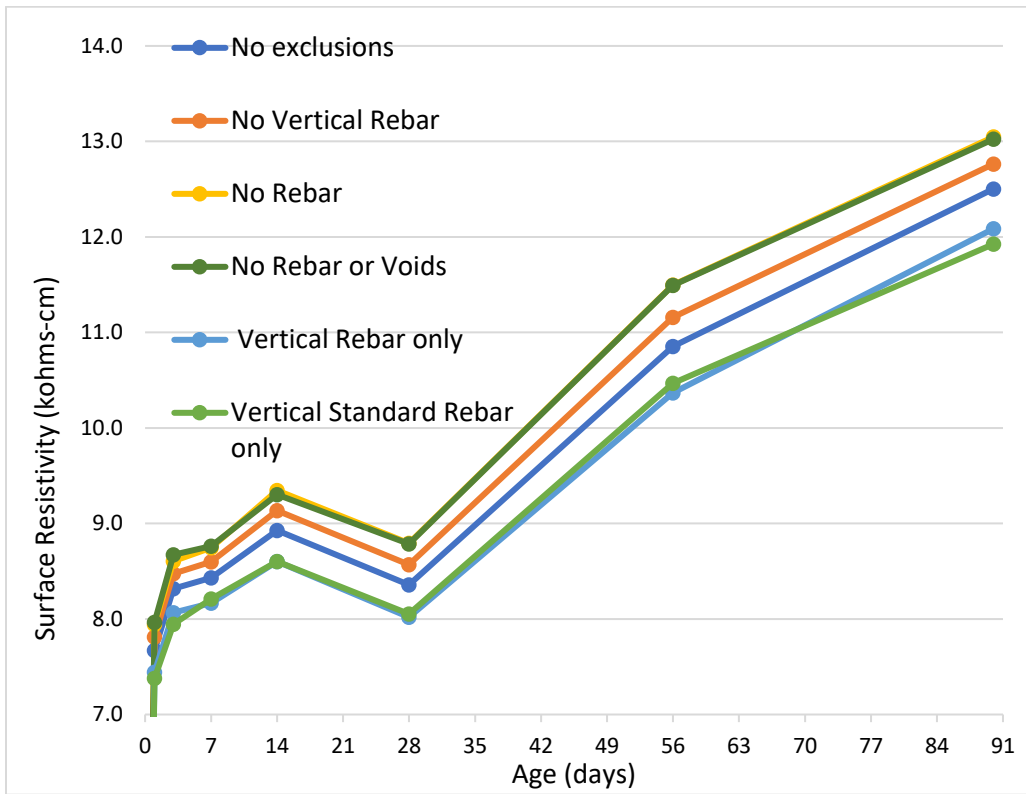


Figure D.2: Vhes mockup horizontal orientation with different exclusions

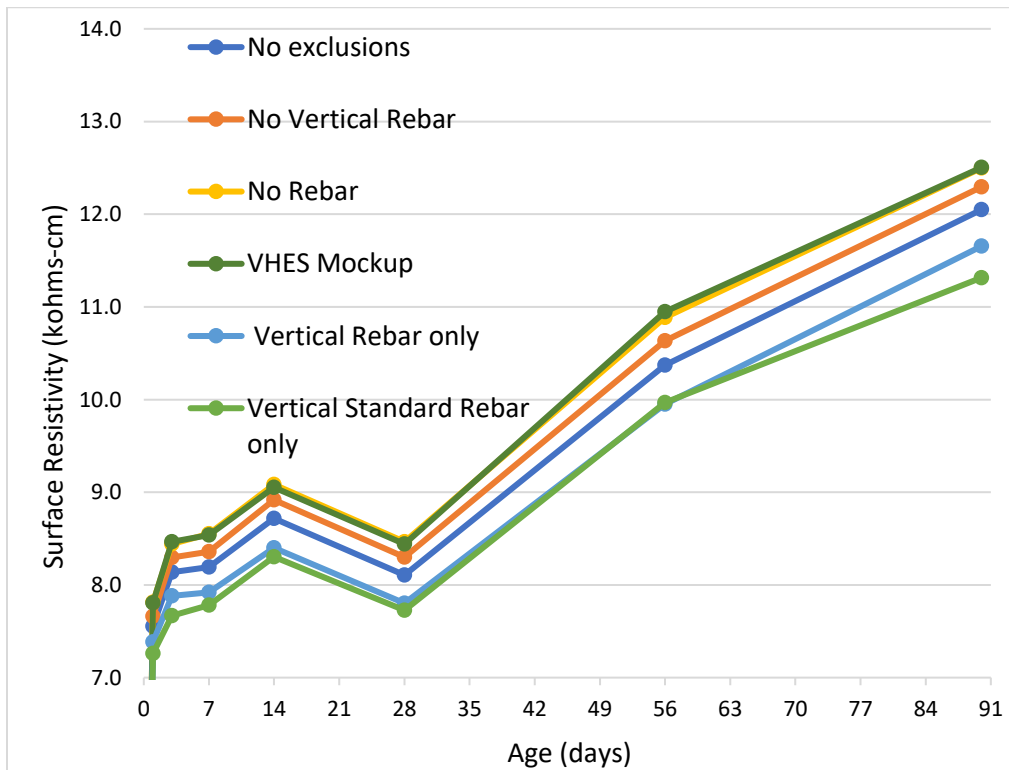


Figure D.3: Vhes mockup vertical orientation with different exclusions

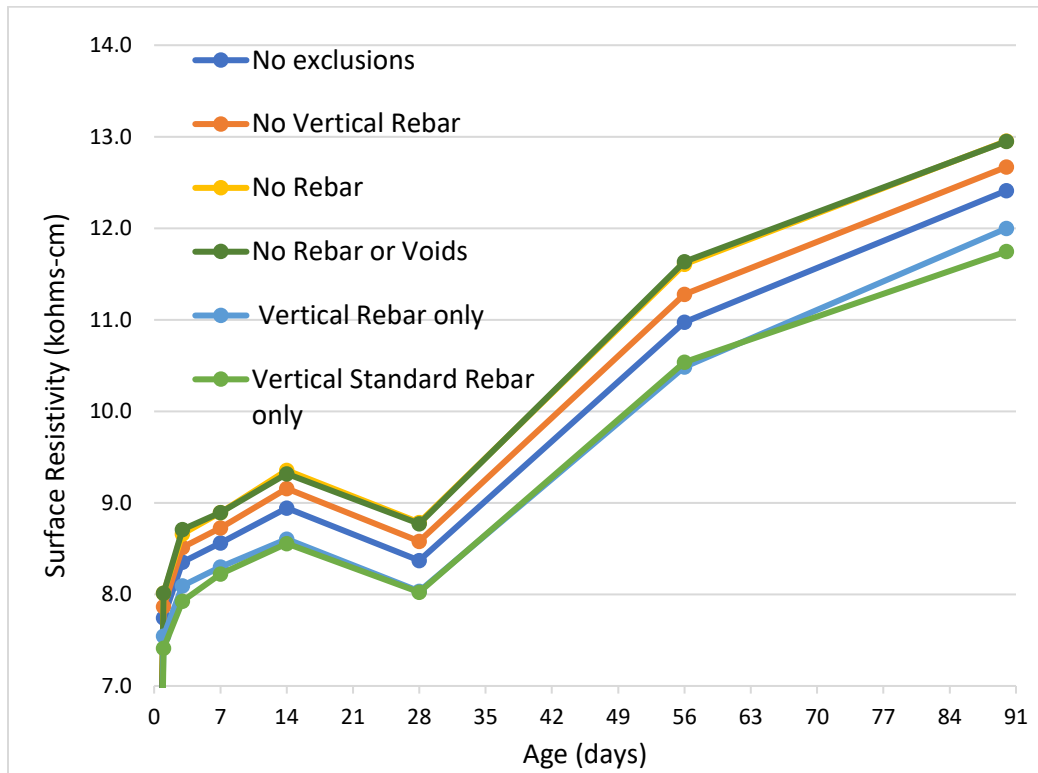


Figure D.4: Vhes mockup average of orientations with different exclusions

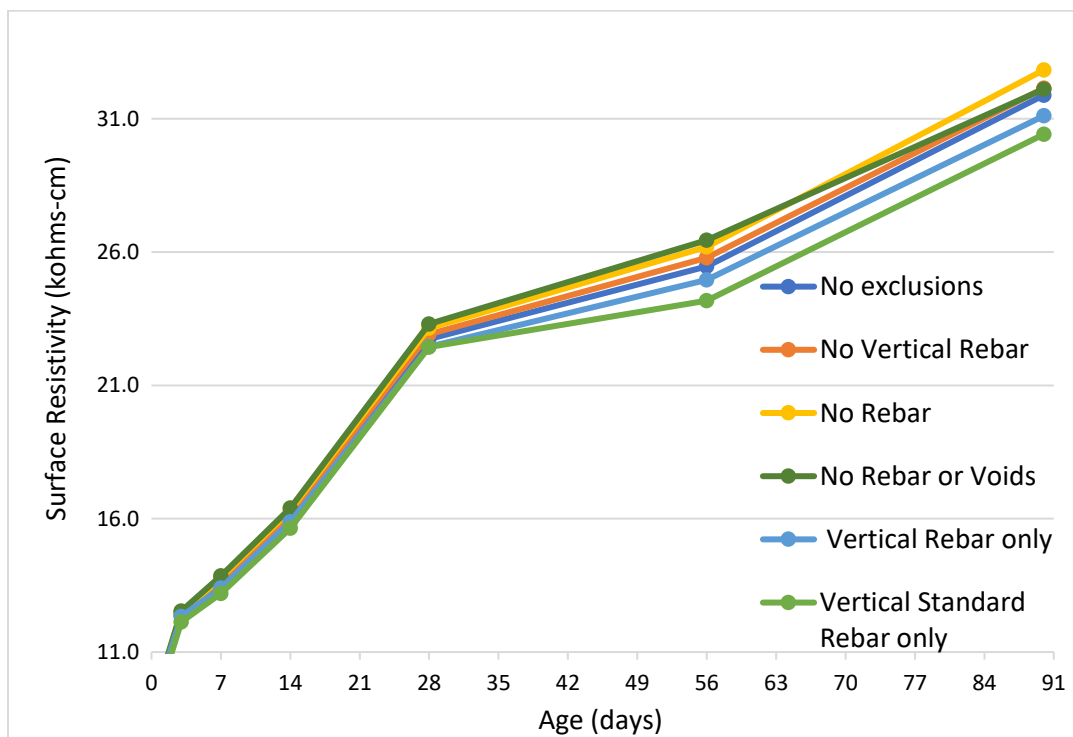


Figure D.54: Vhes-LMC mockup diagonal orientation with different exclusions

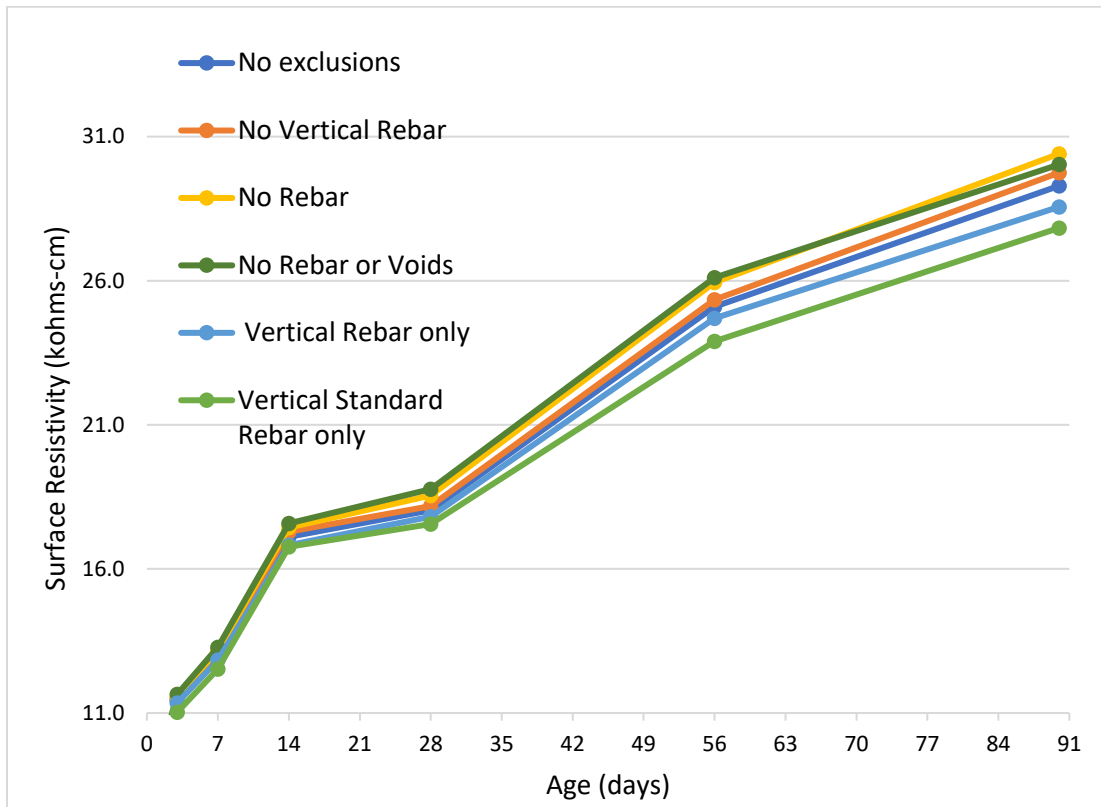


Figure D.55: VHES-LMC mockup horizontal orientation with different exclusions

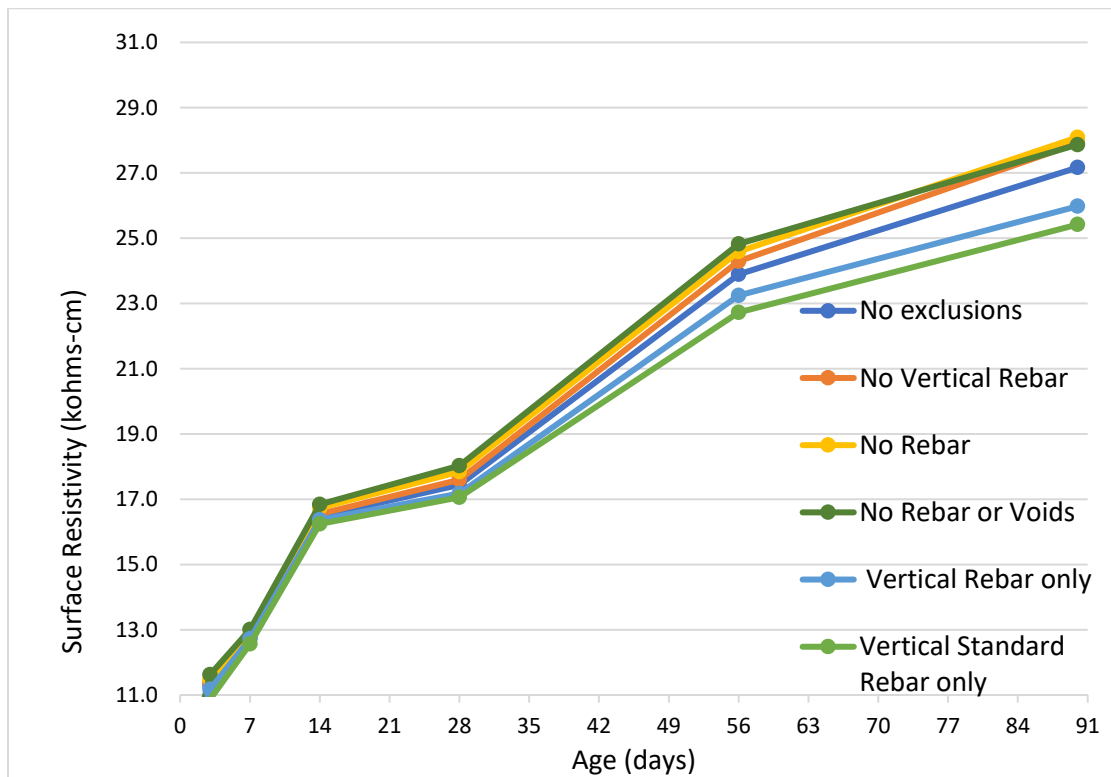


Figure D.56: VHES-LMC mockup vertical orientation with different orientations

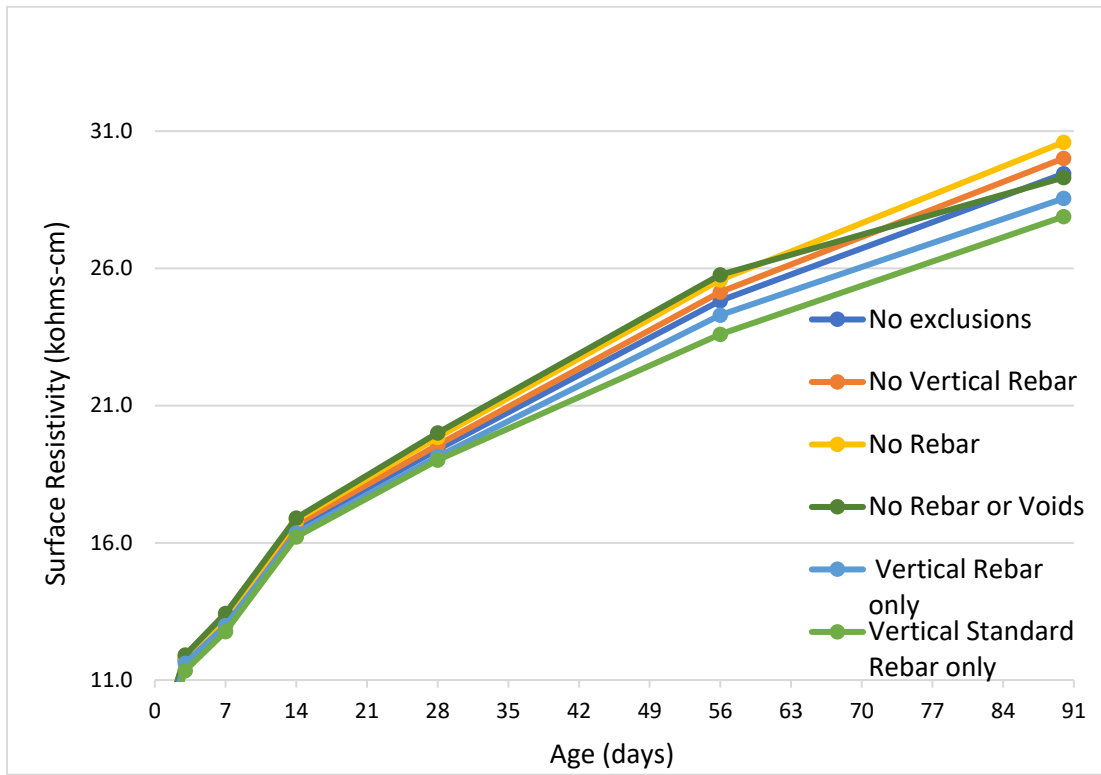


Figure D.57: VHES-LMC mockup average of orientations with different exclusions

APPENDIX E – DRAFT FIELD EVALUATION PROCEDURE FOR USE OF SURFACE RESISTIVITY METER TO EVALUATE BRIDGE DECK OVERLAYS (Chapter 5)

Draft Field Evaluation Procedure Use of Surface resistivity Meter to Evaluate Bridge Deck Overlays

1. Identify area of concern and define perimeter

If the deck overlay area of concern is large, it will need to be analyzed in sections. The section size utilized in this research was a 3.5 ft. by 3.5 ft. area with reinforcement spaced 6 in. on center, although different areas and reinforcement spacings can be investigated. The area to be inspected shall be determined by either by visual inspection, hammer sounding, chain dragging, or as notated during the overlay pour as an area of concern and outline with paint. Hammer sounding and chain dragging should be performed following ASTM D4580 Standard Practice for Measuring Delaminations in Concrete Bridge Decks by Sounding procedure. Clean the testing area, removing debris and any substance that may prohibit the electrical current from making necessary contact with the concrete's pore liquid.

2. Locate the reinforcement

Within the testing perimeter, locate the longitudinal and transverse reinforcement with a reinforcement locating device. Since one orientation of bar is embedded below the other, the use of a depth determining device may assist in improving the results of this evaluation. The location of each rebar should be marked and notated as such based on differing depths. Once marked, the reinforcement mat will act as the datapoint grid for the measurement sequence. Figure A.1 is an example of a bridge deck with 6 in. on-center reinforcement spacing. This spacing should allow for measurements to be taken on top of the reinforcement, as well as centered between two bars. Bridge decks with reinforcement at greater spacing (9 in. on-center) may provide one extra testing point equally spaced between bars so expanding or modifying the grid could be necessary.

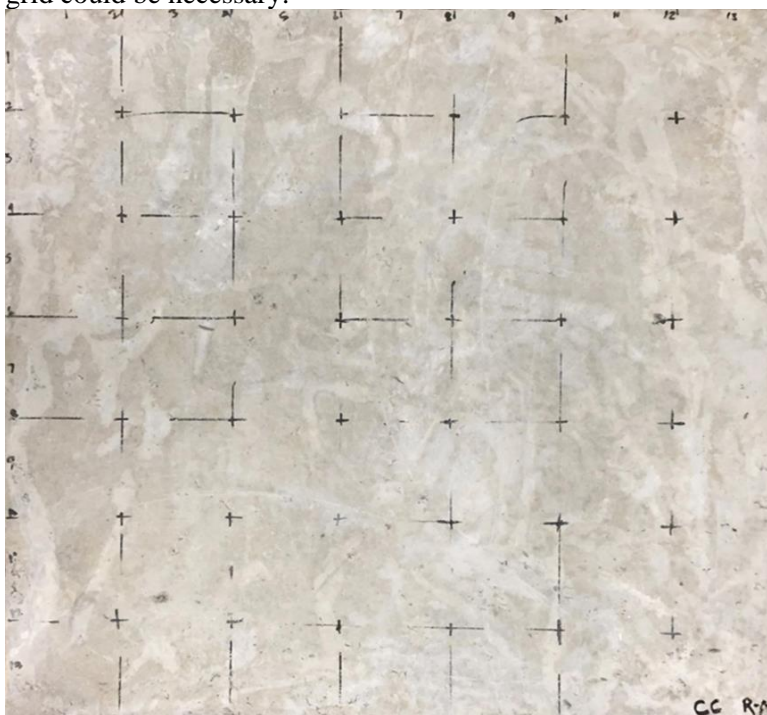


Figure E.1: Bridge deck area to be analyzed

Due to the surface wetting required to support surface resistivity testing, it is important that the markings be made with a durable colorant such as construction marking spray paint, permanent marker, or waterproof paint pen to avoid unintended removal, yet the markings should not be indefinite.

3. Define the desired testing sequence

Utilizing the reinforcement grid that was marked out, create a testing sequence or follow the one provided in Figure A.2, while modifying as appropriate to meet project-specific constraints and the intent of the investigation. Establishing a grid system (rows and columns indicated by numbers) can help with accurate identification of testing locations and recording of the measurements, and the grid system spacing can be tightened or widened to suit the project's specific needs and evaluation objectives. The testing sequence provided in Figure A.2 consists of 169 points spaced 3 in. apart perpendicularly (reinforcement spaced 6 in. on center) illustrated by the dots on the Figure. Testing points will lie between the reinforcement, at reinforcement intersections, and on top of reinforcement mid-spans. It is recommended to analyze one or more test areas of this general size as the data collection, maintenance, and analysis will require less effort. As a general rule of thumb, it is recommended to stay at least 5 in. away from the edge when the parallel or diagonal orientation is used and at least 4 in. away when the perpendicular orientation is being used to avoid edge effects.

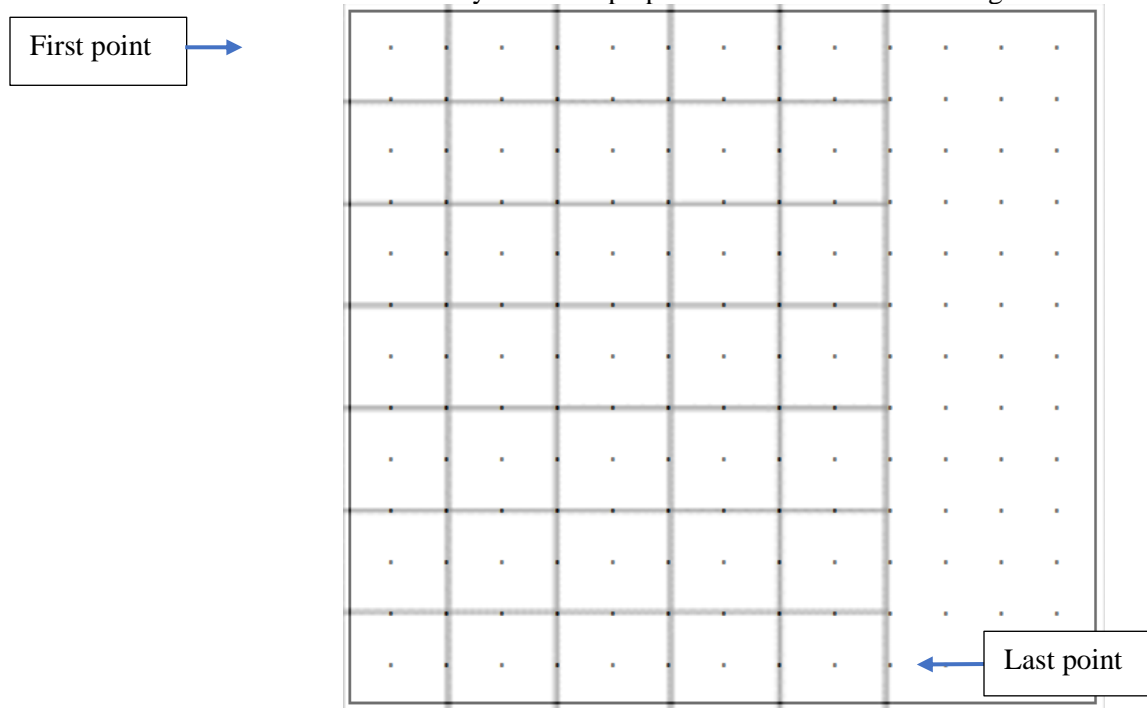


Figure E.2: Proposed testing sequence for surface resistivity of mockups

4. Wetting the testing area

The following wetting protocol is based on an air-conditioned laboratory setting. Depending on environmental conditions such as temperature and humidity, modifications are recommended. The goal of wetting the concrete is to provide ample water so that the current has the ability to be transmitted through the concrete. Excessive ponding must be avoided, since the current can travel across this surface water, affecting the readings. For the testing of slabs performed as part of this study, roughly 1 gallon of water divided into three pours was used to saturate the 3.5 ft. by 3.5 ft. testing area per orientation. Pour enough water onto the surface so that it is fully covered. Allow to absorb then reapply several times accounting for evaporation. The desired saturation is achieved when the surface resistivity measurement no longer drifts and stabilizes at a reasonable magnitude. Once the prewetting procedure has been performed, and the surface appears wet but there is no ponded water, data collection can begin. Note that as the surface dries, the testing area should be continually rewetted by adding water using a sponge or rag, then brushing the surface to remove ponded water.

5. Surface resistivity data collection

Now that each testing point is defined, the surface resistivity can be measured at each point following the defined testing sequence (Figure A.2). It is recommended to test each point with the meter orientated diagonally, transverse, and longitudinal with respect to the bridge centerline. To measure the points, center the surface resistivity meter's four probes

over the desired point and engage, waiting for the result to become stable and document the reading. Each point should be measured twice and averaged. If the surface resistivity value drifts, revisit section 4: wetting the testing area. Test all of the points using one orientation before beginning the following orientation.

From a practical standpoint, this procedure can be performed using either one or two individuals. If two individuals are available, the measurements can be taken by one and called out to the colleague, and he/she can record them into an Excel spreadsheet. If only one individual is available, he or she can call out the measurements to a voice recorder and once all points are measured within an orientation, enter the measurements into the Excel file while listening to the recording.

The surface resistivity meter is a hand-held device and to reduce the influence of being bent over on measurements and to improve ergonomics, an extended handle (PVC pipe, wood block, duct tape, and bungee cord) was attached to the meter for taking measurements in the standing position (shown in Figure E.3).



Figure E.3: Measuring surface resistivity in the standing position

6. Data analysis

As a visual identifier of voids and overlay thickness variation, it is recommended to collect the data in an Excel type grid arrangement using color conditional formatting per cell to create heat maps. If three testing orientations are used, heatmaps could be created for each orientation as well as one for the average of orientation, and one heatmap of the standard deviation (which shows the magnitude of variation between orientations) for a total of five heatmaps. In research to develop this protocol, five heatmaps were created for each age. Of these orientations, the diagonal orientation is the most valuable as it is less influenced by reinforcement, yet it still can detect voids or determine overlay thickness tapering. Often times, an overlay is composed of VHES concrete so, the area of concern within the bridge deck can be tested and analyzed starting at one hour, repeating the process at the desired interval until satisfied.

The heatmaps of the three orientations can be analyzed by direct comparison. For example, the orientation that results in the meter being on top of and parallel to a top reinforcement strand (least amount of cover) is expected to be of the least magnitude. Also, if testing between bars and one of the orientations is much lower than the other two, as signaled by the standard deviation, it is possible that a void exists below that outlier orientation.

Also, the standard deviation can help potentially identify if the measurements were taken without ample moisture of the testing area. Greater discrepancies in orientation results could be interpreted as the reinforcement cover being relatively low, the reinforcement spacing being close to, equal to, or less than that of the surface resistivity meter's current field, or that the concrete has not been saturated sufficiently. The most obvious characteristic indicator was overlay thickness change.

In the study used to develop this protocol, the overlay thickness change was observed in several of the heatmaps. Figure A.4 is an example of the overlay thickness change in the VHES-LMC mockup using data showing the average measurement of three meter orientations. The identification of overlay thickness change is significant and is identified by

the surface resistivity increasing/decreasing magnitude per row or column as a whole. In Figure A.4, the magnitude of the surface resistivity increases from row 1 where the overlay thickness averages 1.3 in. to row 13 where the overlay thickness averages 3.8 in.

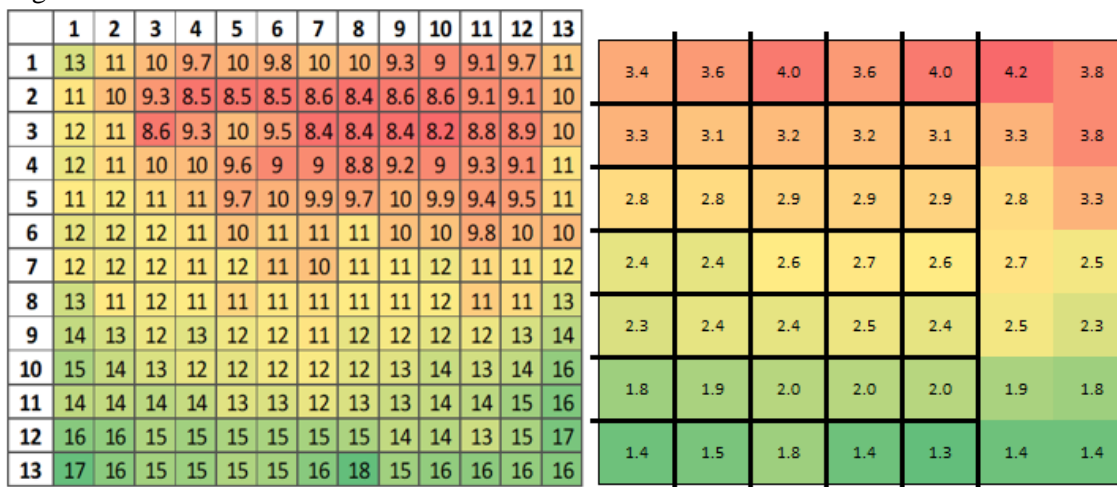


Figure E.4: surface resistivity (left) versus overlay thickness change in inches (right) (VHES-LMC 14 day average orientation)

Surface resistivity can also be measured in areas of known thickness and then used as a benchmark magnitude to evaluate other unknown overlay thickness. The operator must compile multiple surface resistivity measurements at varying (but known) overlay thicknesses in order to determine the rate of change of thickness of a particular overlay/base combination. The benchmark values are used to calibrate or determine the range of expected surface resistivity values within a specific concrete overlay. This method of thickness detection works when the heatmap plotted measurements resemble distinct lines of varying surface resistivity as depicted in Figure A.4. For greater resolution, more particularly in identifying voids, the data should be plotted graphically to help illustrate trends in resistivity and to note obvious inconsistencies that may indicate changes in thickness, voids, or other discontinuities.

APPENDIX F – SUPPORTING MATERIAL FOR PILOT PROJECT (Chapter 7)

Table F.1: Testing program proposed for use on pilot project

Type of Concrete	Test/Method	Sampling Location	Testing Frequency / Number of specimens	Data Collection / Reporting
AA	Shrinkage / ASTM C157	Plant (Concrete Supply)	Once per mixture / 9 beams per mix, divided for testing - 3 beams tested at each NCDOT, WOOD, UNC Charlotte.	Per ASTM C157, initial measurement after demolding and 15 minute soak in limewater. Then 27-day cure in lime water, with initial measurement on day 28. Store in air per ASTM C157, with measurements at 4, 7, 14, and 28 days of air storage. Measurements entered into spreadsheet.
	Resistivity / AASHTO T 358	Plant (Concrete Supply)	Once per mixture / each set of cylinders tested for compressive strength.	Individual measurements on datasheet, average for each cylinder on spreadsheet.
		Field (NCDOT)	Each placement / each set of cylinders tested for compressive strength. Include both 28 day and 56 day cylinders.	Individual measurements on datasheet, average for each cylinder on spreadsheet.
	SAM / AASHTO TP 118	Field (NCDOT)	One test per placement. For pumped concrete, additional tests pre-pump and post pump if time permits. For each test, please make one cylinder for hardened air analysis at UNC Charlotte.	Enter air content from Type B meter, SAM air content, and SAM number into spreadsheet.
Drilled Pier	Shrinkage / ASTM C157	Plant (Concrete Supply)	Once per mixture / 9 beams per mix, divided for testing - 3 beams tested at each NCDOT, WOOD, UNC Charlotte. Due to retarder in mix, consideration will be given to a delay in removal from molds or potentially removing the retarder.	Per ASTM C157, initial measurement after demolding and 15 minute soak in limewater. Then 27-day cure in lime water, with initial measurement on day 28. Store in air per ASTM C157, with measurements at 4, 7, 14, and 28 days of air storage. Measurements entered into spreadsheet.
	Resistivity / AASHTO T 358	Plant (Concrete Supply)	Once per mixture / each set of cylinders tested for compressive strength.	Individual measurements on datasheet, average for each cylinder on spreadsheet.
		Field (NCDOT)	Each placement / each set of cylinders tested for compressive strength. Include both 28 day and 56 day cylinders.	Individual measurements on datasheet, average for each cylinder on spreadsheet.
A	Resistivity / AASHTO T 358	Plant (Concrete Supply)	Once per mixture / each set of cylinders tested for compressive strength.	Individual measurements on datasheet, average for each cylinder on spreadsheet.
		Field (NCDOT)	Each placement / each set of cylinders tested for compressive strength. Include both 28 day and 56 day cylinders.	Individual measurements on datasheet, average for each cylinder on spreadsheet.
	SAM / AASHTO TP 118	Field (NCDOT)	Once per placement. For pumped concrete, additional tests pre-pump and post pump if time permits. For each test, please make one cylinder for hardened air analysis at UNC Charlotte.	Enter air content from Type B meter, SAM air content, and SAM number into spreadsheet.

Table F.2: Surface resistivity data collected by NCDOT regional laboratory personnel for selected structural concrete mixtures

Ticket Number	Mix Type	Mix ID	Date Cast	Plant	Specimen ID	Age of Specimen (days)	Date	Avg	Average Corrected for Curing Condition	Set Average Corrected for Curing Condition
14551	1-A	1055321	10/12/2021	RM385	S-665	7	10/19/2021	5.7	5.69	5.82
14551	1-A	1055321	10/12/2021	RM385	S-665	7	10/19/2021	6.0	5.95	
14422	1-A	1053385	9/22/2021	RM385	S-610	28	10/20/2021	9.8	9.79	9.51
14422	1-A	1053385	9/22/2021	RM385	S-610	28	10/20/2021	9.2	9.23	
14568	2-A	1055727	10/15/2021	RM385	S-670	5	10/20/2021	5.2	5.20	5.34
14568	2-A	1055727	10/15/2021	RM385	S-670	5	10/20/2021	5.5	5.49	
14423	D. Shaft	1053461	9/23/2021	RM519	S-609	28	10/21/2021	5.2	5.18	5.19
14423	D. Shaft	1053461	9/23/2021	RM519	S-609	28	10/21/2021	5.2	5.20	
14431	2-A	1053548	9/23/2021	RM308	S-611	28	10/21/2021	14.0	14.00	13.56
14431	2-A	1053548	9/23/2021	RM308	S-611	28	10/21/2021	13.1	13.11	
14517	1-A	1054956	10/7/2021	RM385	S-661B	14	10/21/2021	8.1	8.10	7.99
14517	1-A	1054956	10/7/2021	RM385	S-661B	14	10/21/2021	7.9	7.89	
14561	2-A	1055531	10/14/2021	RM308	S-656	7	10/21/2021	7.0	7.00	6.93
14561	2-A	1055531	10/14/2021	RM308	S-656	7	10/21/2021	6.9	6.85	
14433	2-A	1053687	9/24/2021	RM308	S-612	28	10/22/2021	13.3	13.34	13.32
14433	2-A	1053687	9/24/2021	RM308	S-612	28	10/22/2021	13.3	13.30	
14592	2-A	1055967	10/19/2021	RM385	S-671	5	10/25/2021	7.0	7.04	6.95
14592	2-A	1055967	10/19/2021	RM385	S-671	5	10/25/2021	6.9	6.86	
14597	1-A	1056065	10/19/2021	RM385	S-672	7	10/25/2021	5.9	5.90	5.89
14597	1-A	1056065	10/19/2021	RM385	S-672	7	10/25/2021	5.9	5.88	
14623	1-A	1056244	10/20/2021	RM519	S-674A	3	10/25/2021	8.5	8.50	8.50
14623	1-A	1056244	10/20/2021	RM519	S-674A	3	10/25/2021	8.5	8.49	
14163	2-A	1056252	10/21/2021	RM385	S-673	5	10/26/2021	6.2	6.16	6.28
14163	2-A	1056252	10/21/2021	RM385	S-673	5	10/26/2021	6.4	6.39	
14452	2-A	1053855	9/28/2021	RM308	S-613	28	10/26/2021	9.3	9.34	9.22
14452	2-A	1053855	9/28/2021	RM308	S-613	28	10/26/2021	9.1	9.10	
14439	D.Pier	1054055	9/28/2021	RM519	S-578	28	10/26/2021	4.4	4.40	4.44
14439	D.Pier	1054055	9/28/2021	RM519	S-578	28	10/26/2021	4.5	4.48	
14440	D.Pier	1054049	9/28/2021	RM519	S-614	28	10/26/2021	4.5	4.50	4.41
14440	D.Pier	1054049	9/28/2021	RM519	S-614	28	10/26/2021	4.3	4.31	
14437	D.Shaft	1054145	9/28/2021	RM519	S-621	28	10/26/2021	4.9	4.85	4.90
14437	D.Shaft	1054145	9/28/2021	RM519	S-621	28	10/26/2021	5.0	4.95	
14438	D.Shaft	1054143	9/28/2021	RM519	S-622	28	10/26/2021	5.8	5.80	5.87
14438	D.Shaft	1054143	9/28/2021	RM519	S-622	28	10/26/2021	5.9	5.94	
14465	D.Shaft	1054072	9/28/2021	RM538	S-618	28	10/26/2021	16.8	16.83	16.63
14465	D.Shaft	1054072	9/28/2021	RM538	S-618	28	10/26/2021	16.4	16.43	
14466	D.Shaft	1054074	9/28/2021	RM538	S-619	28	10/26/2021	12.8	12.80	12.68
14466	D.Shaft	1054074	9/28/2021	RM538	S-619	28	10/26/2021	12.6	12.55	
14467	D.Shaft	1054077	9/28/2021	RM538	S-620	28	10/26/2021	9.9	9.88	9.95
14467	D.Shaft	1054077	9/28/2021	RM538	S-620	28	10/26/2021	10.0	10.03	
14623	1-A	1056244	10/20/2021	RM519	S-674B	7	10/27/2021	6.1	6.10	5.99
14623	1-A	1056244	10/20/2021	RM519	S-674B	7	10/27/2021	5.9	5.89	
14463	2-A	1054081	9/29/2021	RM308	S-584	28	10/27/2021	13.6	13.63	13.09

14463	2-A	1054081	9/29/2021	RM308	S-584	28	10/27/2021	12.6	12.55	
14459	D. Pier	1054304	9/29/2021	RM519	S-615	28	10/27/2021	6.4	6.35	6.54
14459	D. Pier	1054304	9/29/2021	RM519	S-615	28	10/27/2021	6.7	6.74	
14460	D.Pier	1054307	9/29/2021	RM519	S-616	28	10/27/2021	6.7	6.66	6.62
14460	D.Pier	1054307	9/29/2021	RM519	S-616	28	10/27/2021	6.6	6.58	
14461	D.Pier	1054309	9/30/2021	RM519	S-623	28	10/28/2021	6.1	6.11	5.91
14461	D.Pier	1054309	9/30/2021	RM519	S-623	28	10/28/2021	5.7	5.70	
14462	D.Pier	10547305	9/30/2021	RM519	S-624	28	10/28/2021	5.9	5.90	5.83
14462	D.Pier	10547305	9/30/2021	RM519	S-624	28	10/28/2021	5.8	5.76	
14464	2-A	1054302	9/30/2021	RM308	S-585	28	10/28/2021	14.4	14.39	14.38
14464	2-A	1054302	9/30/2021	RM308	S-585	28	10/28/2021	14.4	14.38	
14468	1-A	1054266	9/30/2021	RM308	S-625	28	10/28/2021	11.9	11.89	11.86
14468	1-A	1054266	9/30/2021	RM308	S-625	28	10/28/2021	11.8	11.84	
14639	2-A	1056494	10/25/2021	RM385	S-675	3	10/28/2021	5.4	5.36	5.35
14639	2-A	1056494	10/25/2021	RM385	S-675	3	10/28/2021	5.3	5.34	
14644	1-A	1056649	10/26/2021	RM308	S-677A	2	10/28/2021	3.9	3.89	3.83
14644	1-A	1056649	10/26/2021	RM308	S-677A	2	10/28/2021	3.8	3.78	
14644	1-A	1056649	10/26/2021	RM308	S-677B	3	10/29/2021	5.2	5.16	4.85
14644	1-A	1056649	10/26/2021	RM308	S-677B	3	10/29/2021	4.5	4.54	
14645	1-A	105644	10/26/2021	RM308	S-678A	3	10/29/2021	3.9	3.88	3.71
14645	1-A	105644	10/26/2021	RM308	S-678A	3	10/29/2021	3.5	3.54	
14646	1-A	1056647	10/26/2021	RM308	S-679A	3	10/29/2021	3.6	3.59	3.72
14646	1-A	1056647	10/26/2021	RM308	S-679A	3	10/29/2021	3.9	3.85	
14658	2-A	1056839	10/27/2021	RM35	S-683A	2	10/29/2021	3.4	3.38	3.46
14658	2-A	1056839	10/27/2021	RM35	S-683A	2	10/29/2021	3.5	3.54	
14481	2-A	1054497	10/4/2021	RM385	S-626	28	11/1/2021	14.2	14.15	14.16
14481	2-A	1054497	10/4/2021	RM385	S-626	28	11/1/2021	14.2	14.18	
14483	1-A	1054609	10/4/2021	RM385	S-632	28	11/1/2021	18.9	18.93	18.53
14483	1-A	1054609	10/4/2021	RM385	S-632	28	11/1/2021	18.1	18.14	
14486	D.Pier	1054759	10/4/2021	RM519	S-627	28	11/1/2021	5.1	5.09	5.06
14486	D.Pier	1054759	10/4/2021	RM519	S-627	28	11/1/2021	5.0	5.04	
14487	D.Pier	1054762	10/4/2021	RM519	S-628	28	11/1/2021	6.1	6.09	6.06
14487	D.Pier	1054762	10/4/2021	RM519	S-628	28	11/1/2021	6.0	6.04	
14488	D.Pier	1054763	10/4/2021	RM519	S-629	28	11/1/2021	5.2	5.19	5.17
14488	D.Pier	1054763	10/4/2021	RM519	S-629	28	11/1/2021	5.2	5.15	
14489	D.Shaft	1054764	10/4/2021	RM519	S-630	28	11/1/2021	6.4	6.38	6.27
14489	D.Shaft	1054764	10/4/2021	RM519	S-630	28	11/1/2021	6.2	6.16	
14490	D.Shaft	1054766	10/4/2021	RM519	S-631	28	11/1/2021	5.7	5.69	5.49
14490	D.Shaft	1054766	10/4/2021	RM519	S-631	28	11/1/2021	5.3	5.30	
14491	D.Shaft	1054629	10/4/2021	RM538	S-633	28	11/1/2021	11.1	11.13	11.05
14491	D.Shaft	1054629	10/4/2021	RM538	S-633	28	11/1/2021	11.0	10.98	
14492	D.Shaft	1054631	10/4/2021	RM538	S-634	28	11/1/2021	10.0	9.95	9.88
14492	D.Shaft	1054631	10/4/2021	RM538	S-634	28	11/1/2021	9.8	9.80	
14493	D.Shaft	1054633	10/4/2021	RM538	S-635	28	11/1/2021	10.8	10.76	10.69
14493	D.Shaft	1054633	10/4/2021	RM538	S-635	28	11/1/2021	10.6	10.63	
14494	D.Shaft	1054635	10/4/2021	RM538	S-636	28	11/1/2021	10.3	10.29	10.29
14494	D.Shaft	1054635	10/4/2021	RM538	S-636	28	11/1/2021	10.3	10.29	
14658	2-A	1056839	10/27/2021	RM385	S-683B	5	11/1/2021	5.3	5.30	5.47
14658	2-A	1056839	10/27/2021	RM385	S-683B	5	11/1/2021	5.6	5.64	
14644	1-A	1056649	10/26/2021	RM308	S-677C	7	11/2/2021	4.8	4.84	4.94
14644	1-A	1056649	10/26/2021	RM308	S-677C	7	11/2/2021	5.1	5.05	
14645	1-A	1056644	10/26/2021	RM308	S-678B	7	11/2/2021	4.4	4.41	4.38

14645	1-A	1056644	10/26/2021	RM308	S-678B	7	11/2/2021	4.3	4.34	
14646	1-A	1056647	10/26/2021	RM308	S-679B	7	11/2/2021	4.5	4.45	4.61
14646	1-A	1056647	10/26/2021	RM308	S-679B	7	11/2/2021	4.8	4.78	
14495	D.Shaft	1054711	10/5/2021	RM308	S-645	28	11/2/2021	10.5	10.45	10.29
14495	D.Shaft	1054711	10/5/2021	RM308	S-645	28	11/2/2021	10.1	10.14	
14496	D.Shaft	1054714	10/5/2021	RM308	S-646	28	11/2/2021	10.4	10.38	10.08
14496	D.Shaft	1054714	10/5/2021	RM308	S-646	28	11/2/2021	9.8	9.78	
14497	D.Shaft	1054717	10/5/2021	RM308	S-647	28	11/2/2021	11.9	11.90	11.49
14497	D.Shaft	1054717	10/5/2021	RM308	S-647	28	11/2/2021	11.1	11.09	
14499	D.Pier	1054767	10/5/2021	RM519	S-638	28	11/2/2021	3.9	3.89	3.98
14499	D.Pier	1054767	10/5/2021	RM519	S-638	28	11/2/2021	4.1	4.08	
14500	D.Pier	1054768	10/5/2021	RM519	S-639	28	11/2/2021	5.8	5.78	5.76
14500	D.Pier	1054768	10/5/2021	RM519	S-639	28	11/2/2021	5.8	5.75	
14501	D.Pier	1054769	10/5/2021	RM519	S-640	28	11/2/2021	5.7	5.69	5.71
14501	D.Pier	1054769	10/5/2021	RM519	S-640	28	11/2/2021	5.7	5.73	
14502	D.Pier	1054770	10/5/2021	RM519	S-641	28	11/2/2021	3.8	3.76	3.86
14502	D.Pier	1054770	10/5/2021	RM519	S-641	28	11/2/2021	4.0	3.96	
14503	1-A	1054637	10/5/2021	RM385	S-637	28	11/2/2021	15.6	15.63	15.37
14503	1-A	1054637	10/5/2021	RM385	S-637	28	11/2/2021	15.1	15.11	
14515	D.Shaft	1054689	10/5/2021	RM519	S-643	28	11/2/2021	5.1	5.13	5.08
14515	D.Shaft	1054689	10/5/2021	RM519	S-643	28	11/2/2021	5.0	5.04	
14516	D.Shaft	1054691	10/5/2021	RM519	S-644	28	11/2/2021	5.0	5.01	5.11
14516	D.Shaft	1054691	10/5/2021	RM519	S-644	28	11/2/2021	5.2	5.20	
14504	2-A	1054739	10/6/2021	RM308	S-648	28	11/3/2021	16.6	16.56	16.90
14504	2-A	1054739	10/6/2021	RM308	S-648	28	11/3/2021	17.2	17.24	
14518	D.Pier	1054819	10/6/2021	RM519	S-649	28	11/3/2021	5.7	5.74	5.70
14518	D.Pier	1054819	10/6/2021	RM519	S-649	28	11/3/2021	5.7	5.66	
14519	D.Pier	1054821	10/6/2021	RM519	S-650	28	11/3/2021	5.9	5.86	5.68
14519	D.Pier	1054821	10/6/2021	RM519	S-650	28	11/3/2021	5.5	5.50	
14520	D.Pier	1054822	10/6/2021	RM519	S-651	28	11/3/2021	4.7	4.73	4.73
14520	D.Pier	1054822	10/6/2021	RM519	S-651	28	11/3/2021	4.7	4.73	
14521	D.Shaft	1054970	10/6/2021	RM519	S-652	28	11/3/2021	5.9	5.93	5.83
14521	D.Shaft	1054970	10/6/2021	RM519	S-652	28	11/3/2021	5.7	5.73	
14522	D.Shaft	1054968	10/6/2021	RM519	S-653	28	11/3/2021	6.3	6.30	6.26
14522	D.Shaft	1054968	10/6/2021	RM519	S-653	28	11/3/2021	6.2	6.23	
14485	1-A	1054669	10/5/2021	RM538	S-642	28	11/4/2021	13.0	13.04	12.98
14485	1-A	1054669	10/5/2021	RM538	S-642	28	11/4/2021	12.9	12.91	
14509	D.Shaft	1054952	10/7/2021	RM519	S-586	28	11/4/2021	6.6	6.60	6.76
14509	D.Shaft	1054952	10/7/2021	RM519	S-586	28	11/4/2021	6.9	6.93	
14517	1-A	1054956	10/7/2021	RM385	S-661	28	11/4/2021	14.6	14.56	14.20
14517	1-A	1054956	10/7/2021	RM385	S-661	28	11/4/2021	13.8	13.84	
14529	D. Pier	1054972	10/7/2021	RM519	S-617	28	11/4/2021	6.5	6.46	6.51
14529	D. Pier	1054972	10/7/2021	RM519	S-617	28	11/4/2021	6.6	6.56	
14530	D.Pier	1054974	10/7/2021	RM519	S-654	28	11/4/2021	6.8	6.80	6.76
14530	D.Pier	1054974	10/7/2021	RM519	S-654	28	11/4/2021	6.7	6.71	
14531	D.Pier	1054975	10/7/2021	RM519	S-655	28	11/4/2021	7.6	7.64	7.71
14531	D.Pier	1054975	10/7/2021	RM519	S-655	28	11/4/2021	7.8	7.79	
14534	1-A	1054971	10/7/2021	RM538	S-662	28	11/4/2021	11.2	11.19	11.19
14534	1-A	1054971	10/7/2021	RM538	S-662	28	11/4/2021	11.2	11.19	
14540	D.Shaft	1055178	10/11/2021	RM519	S-663	28	11/8/2021	5.6	5.63	5.56
14540	D.Shaft	1055178	10/11/2021	RM519	S-663	28	11/8/2021	5.5	5.49	
14539	D.Shaft	1055341	10/12/2021	RM519	S-664	28	11/9/2021	5.3	5.25	5.23

14539	D.Shaft	1055341	10/12/2021	RM519	S-664	28	11/9/2021	5.2	5.21	
14551	1-A	1055321	10/12/2021	RM385	S-665	28	11/9/2021	13.7	13.68	13.43
14551	1-A	1055321	10/12/2021	RM385	S-665	28	11/9/2021	13.2	13.18	
14562	D.Shaft	1055446	10/13/2021	RM519/521	S-666	28	11/10/2021	6.6	6.61	6.59
14562	D.Shaft	1055446	10/13/2021	RM519/521	S-666	28	11/10/2021	6.6	6.56	
14565	D.Shaft	1055447	10/13/2021	RM519/521	S-667	28	11/10/2021	5.9	5.88	6.09
14565	D.Shaft	1055447	10/13/2021	RM519/521	S-667	28	11/10/2021	6.3	6.30	
14561	2-A	1055531	10/14/2021	RM308	S-656	28	11/11/2021	13.3	13.34	13.49
14561	2-A	1055531	10/14/2021	RM308	S-656	28	11/11/2021	13.6	13.64	
14566	D.Shaft	1055552	10/14/2021	RM519	S-668	28	11/11/2021	5.9	5.86	5.89
14566	D.Shaft	1055552	10/14/2021	RM519	S-668	28	11/11/2021	5.9	5.93	
14567	D.Shaft	1055553	10/14/2021	RM519	S-669	28	11/11/2021	5.3	5.33	5.33
14567	D.Shaft	1055553	10/14/2021	RM519	S-669	28	11/11/2021	5.3	5.33	
14568	2-A	1055727	10/15/2021	RM385	S-670	28	11/12/2021	14.6	14.55	14.39
14568	2-A	1055727	10/15/2021	RM385	S-670	28	11/12/2021	14.2	14.23	
14592	2-A	1055967	10/19/2021	RM385	S-671	28	11/16/2021	7.0	7.01	7.14
14592	2-A	1055967	10/19/2021	RM385	S-671	28	11/16/2021	7.3	7.26	
14623	1-A	1056244	10/20/2021	RM519	S-674	28	11/17/2021	10.8	10.80	10.81
14623	1-A	1056244	10/20/2021	RM519	S-674	28	11/17/2021	10.8	10.81	
14612	1-A	1056247	10/20/2021	RM538	S-657	28	11/18/2021	14.5	14.50	14.18
14612	1-A	1056247	10/20/2021	RM538	S-657	28	11/18/2021	13.9	13.86	
14613	2-A	1056252	10/21/2021	RM385	S-673	28	11/19/2021	16.2	16.16	15.75
14613	2-A	1056252	10/21/2021	RM385	S-673	28	11/19/2021	15.3	15.34	

Figure F.1: Datasheet for mixture 6011, Class A 3000 psi showing materials, proportions, fresh concrete test results, and compressive strength test results

CONCRETE SUPPLY CO.

Argos Harleyville
CBO
Arrowwood
Hanson Brewer

TRIAL BATCH

55AB

GCP

COMPANY: Concrete Supply Co.

DATE: 4/6/2021

	SPECIFIC GRAVITY	MOISTURE
CEMENT	3.15	
Fly Ash	2.30	
#67 Stone	2.93	0.42%
#78m STONE	2.93	0.36%
#4 Stone	2.80	0.00%
SAND	2.62	4.64%
SAND 2	2.62	0.00%

W/C Ratio	0.42189	749
% FA	0.23097	173

BATCH SIZE	CUBIC FT
2	
FACTOR	0.0741

Sand Vol	Vol Ft^3	% By Vol	F/C
6.60	6.60	100%	100.00%
	0.00	0%	

F / C Ratio	0.388
F / C Weight	0.00
Mortar Volume	40.67
Paste	0.37

ONE YARD WEIGHTS

		WEIGHT	VOLUME
CEMENT	Argos Harleyville	576	2.93
Fly Ash	CBO	173	1.21
#67 Stone	Arrowwood	0	0.00
#78m STONE	Arrowwood	1900	10.39
#4 Stone		0	0.00
Sand	Hanson Brewer	1089	6.60
Sand 2		0	0.00
WATER	37.9	316	5.06
AIR %		3.0%	0.81
	(per cwt)	0.00	27.00
Zyla 640	(per cwt)	2.00	
EXP 950	(per cwt)	3.00	
Daratard 17		3.00	

BATCH WTS		CUMULATIVE TOTAL
42.67	Pounds	42.67
12.81	Pounds	55.48
0.00	Pounds	
141.25	Pounds	
0.00	Pounds	
84.41	Pounds	
0.00	Pounds	
19.16	Pounds	
0.00	Pounds	
0.00	Pounds	
19.16	Pounds	
Oz/CY	(ML)	
0.0	0.0	
15.0	32.8	
22.5	49.2	
22.5	49.2	
	0.000	

WATER (ml) +/-	-350.00
----------------	---------

Theoretical Unit Weight

150.15

ACTUAL WATER	306
ACTUAL W/C	0.408
CONCRETE TEMP	63
SLUMP (inches)	9.00
Air Content %	3.0
ACTUAL UNIT WEIGHT	151.64
Cylinder ID	6013

7 Day	6560	6630
28 Day	8850	8910
56 Day	10220	10520

Time: 1330

Max Water is 40.4 gal or another 672.9 ml for this batch size.
Target 8.5 to 9" slump. May even want to hold water to start.

Average	6600
	8880
	10370

Figure F.2: Datasheet for mixture 6012 (Class AA mixture) showing materials, proportions, fresh concrete test results, and compressive strength test results

Argos Harleyville
CBO
Arrowood
Hanson Brewer

GCP

CONCRETE SUPPLY CO.

TRIAL BATCH

11AB

COMPANY: Concrete Supply Co.

DATE: 4/6/2021

	SPECIFIC GRAVITY	MOISTURE
CEMENT	3.15	
Fly Ash	2.30	
#67 Stone	2.93	0.42%
#78m STONE	2.93	0.36%
#4 Stone	2.80	0.00%
SAND	2.62	4.64%
SAND 2	2.62	0.00%

W/C Ratio	0.3874	744
% FA	0.23118	172

BATCH SIZE FACTOR	CUBIC FT
	2
	0.0741

Sand Vol	Vol Ft^3	% By Vol
6.12	6.12	100%
	0.00	0%

F / C Ratio	0.368
F / C Weight	0.00
Mortar Volume	37.80
Paste	0.38

ONE YARD WEIGHTS

		WEIGHT	VOLUME
CEMENT	Argos Harleyville	572	2.91
Fly Ash	CBO	172	1.20
#67 Stone	Arrowood	1925	10.53
#78m STONE	Arrowood	0	0.00
#4 Stone		0	0.00
Sand	Hanson Brewer	1012	6.12
Sand 2		0	0.00
WATER	34.6	288	4.62
AIR %		6.0%	1.62
	(per cwt)	0.15	27.00
Zyla 640	(per cwt)	2.00	
EXP 950	(per cwt)	0.00	
Daratard 17		3.00	

BATCH WTS

42.37	Pounds
12.74	Pounds
143.19	Pounds
0.00	Pounds
0.00	Pounds
78.44	Pounds
0.00	Pounds
17.27	Pounds
Oz/CY	(ML)
1.1	2.4
14.9	32.6
0.0	0.0
22.3	48.9
	0.000

CUMULATIVE TOTAL
42.37
55.11

WATER (ml) +/-	-350.00
----------------	---------

Theoretical Unit Weight	147.00
-------------------------	--------

ACTUAL WATER	278
ACTUAL W/C	0.373
CONCRETE TEMP	63
SLUMP (inches)	3.75
Air Content %	6.5
ACTUAL UNIT WEIGHT	149.36
Cylinder ID	6012

12:37	
-------	--

Max Water is 36.6 gal or another 560.73 ml for this batch size.

Target 3.5" slump and 6% to 7% air

	Average
7 Day	5170
28 Day	6670
56 Day	7420

Figure F.3: Concrete Supply datasheet for Mixture 6013 (Drilled Shaft Mixture) showing materials, proportions, fresh concrete test results, and compressive strength test results

CONCRETE SUPPLY CO.			
Argos Harleyville CBO Arrowood Hanson Brewer GCP	TRIAL BATCH	55AB	
		COMPANY:	Concrete Supply Co.
		DATE:	4/6/2021

	SPECIFIC GRAVITY	MOISTURE		CUBIC FT	
CEMENT	3.15			BATCH SIZE	2
Fly Ash	2.30			FACTOR	0.0741
#67 Stone	2.93	0.42%			
#78m STONE	2.93	0.36%			
#4 Stone	2.80	0.00%			
SAND	2.62	4.64%			
SAND 2	2.62	0.00%			

	W/C Ratio	749		F / C Ratio	0.388	
% FA	0.23097	173		F / C Weight	0.00	
				Mortar Volume	40.67	
				Paste	0.37	

ONE YARD WEIGHTS					
		WEIGHT	VOLUME		
CEMENT	Argos Harleyville	576	2.93		
Fly Ash	CBO	173	1.21		
#67 Stone	Arrowood	0	0.00		
#78m STONE	Arrowood	1900	10.39		
#4 Stone		0	0.00		
Sand	Hanson Brewer	1089	6.60		
Sand 2		0	0.00		
WATER	37.9	316	5.06		
AIR %		3.0%	0.81		
	(per cwt)	0.00	27.00		
Zyla 640	(per cwt)	2.00			
EXP 950	(per cwt)	3.00			
Daratard 17		3.00			

			BATCH WTS		
			42.67	Pounds	42.67
			12.81	Pounds	55.48
			0.00	Pounds	
			141.25	Pounds	
			0.00	Pounds	
			84.41	Pounds	
			0.00	Pounds	
			19.16	Pounds	
			Oz/CY	(ML)	WATER (ml) +/-
			0.0	0.0	-350.00
			15.0	32.8	
			22.5	49.2	
			22.5	49.2	
				0.000	

Theoretical Unit Weight	150.15	
-------------------------	--------	--

ACTUAL WATER	306	
ACTUAL W/C	0.408	
CONCRETE TEMP	63	
SLUMP (inches)	9.00	
Air Content %	3.0	
ACTUAL UNIT WEIGHT	151.64	
Cylinder ID	6013	

7 Day	6560	6630	Average 6600
28 Day	8850	8910	8880
56 Day	10220	10520	10370

Time: 1330

Max Water is 40.4 gal or another 672.9 ml for this batch size.
 Target 8.5 to 9" slump. May even want to hold water to start.

Table F.3: Surface resistivity data from QC laboratory

Mix ID	Mix Type	Date Cast	Curing Condition (1 = Moist Room, 2 = Limewater Tank)	Age of Specimen (days)	Date	Average	Average corrected for curing condition	Set average corrected for curing condition
6011	A	4/6/2021	2	7	4/13/2021	4.4	4.88	5.07
6011	A	4/6/2021	2	7	4/13/2021	4.7	5.17	
6011	A	4/6/2021	2	7	4/13/2021	4.7	5.16	
6012	AA	4/6/2021	2	7	4/13/2021	6.4	7.07	7.23
6012	AA	4/6/2021	2	7	4/13/2021	6.7	7.38	
6013	DShaft	4/6/2021	2	7	4/13/2021	4.4	4.83	4.87
6013	DShaft	4/6/2021	2	7	4/13/2021	4.5	4.92	
6011	A	4/6/2021	2	28	5/5/2021	14.8	16.31	15.87
6011	A	4/6/2021	2	28	5/5/2021	14.0	15.43	
6012	AA	4/6/2021	2	28	5/5/2021	19.2	21.13	21.44
6012	AA	4/6/2021	2	28	5/5/2021	19.8	21.75	
6013	DShaft	4/6/2021	2	28	5/5/2021	14.4	15.85	15.90
6013	DShaft	4/6/2021	2	28	5/5/2021	14.5	15.95	
6011	A	4/6/2021	2	56	6/1/2021	28.0	30.75	29.73
6011	A	4/6/2021	2	56	6/1/2021	26.1	28.71	
6012	AA	4/6/2021	2	56	6/1/2021	37.9	41.69	41.44
6012	AA	4/6/2021	2	56	6/1/2021	37.5	41.20	
6013	DShaft	4/6/2021	2	56	6/1/2021	28.3	31.10	31.26
6013	DShaft	4/6/2021	2	56	6/1/2021	28.6	31.42	

Table F.4: Surface resistivity data from historical NCDOT projects at low (<0.39) w/cm ratios

Type of Mix	Fly ash %	Surface Resistivity (kΩ-cm)				
		3 day	7 day	28 day	56 day	90 day
Pavement	0	8.0	7.8	10.0	13.4	16.5
Pavement	20	4.8	6.5	12.0	20.5	29.3
Pavement	30	3.9	4.8	10.2	19.7	30.0
Pavement	0	5.7	6.3	9.9	13.7	17.0
Pavement	20	4.9	5.3	9.1	13.9	19.8
Pavement	30	5.1	5.4	8.4	12.0	18.7
Structure	0	5.3	7.5	10.2	12.5	13.7
Structure	20	4.4	5.5	10.6	16.9	25.7
Structure	0	5.8	6.3	9.1	12.1	13.8
Structure	20	4.2	5.3	9.5	18.9	27.2
Structure	0	5.5	6.5	9.3	10.1	15.7
Structure	20	4.5	5.0	12.3	16.1	20.2
Structure	0	6.3	6.9	14.8	17.2	
Structure	20	4.5	5.1	13.1	18.4	23.3
Structure	0	13.3	12.7	16.3		17.9
Structure	23	10.4	11.1	18.1		46.1

Table F.5: Analysis of low (<0.39) w/cm mixtures meeting pavement and Class AA resistivity targets at selected ages

	All	Straight Cement	Fly Ash
Total pavement mixtures	0	2	4
Pavement mixtures ≥ 11.0 by 28 days	0	0	0
Pavement mixtures ≥ 11.0 by 56 days	6	2	4
Pavement mixtures ≥ 11.0 by 90 days	6	2	4
Total AA mixtures	0	5	5
AA mixtures ≥ 15.0 by 28 days	2	1	1
AA mixtures ≥ 15.0 by 56 days	7	2	5
AA mixtures ≥ 15.0 by 90 days	8	3	5
AA mixtures ≥ 16.0 by 28 days	2	1	1
AA mixtures ≥ 16.0 by 56 days	7	2	5
AA mixtures ≥ 16.0 by 90 days	7	2	5

Table F.6: Surface resistivity data from historical NCDOT projects at moderate (0.41 to 0.43) w/cm ratios

Mix ID	w/cm	Type of Mixture	Fly ash %	Surface Resistivity (kΩ-cm)				
				3 day	7 day	28 day	56 day	90 day
M-600-0*	M	Pavement	0	4.8	6.0	8.5	9.2	11.4
M-480-120*	M	Pavement	20	4.3	5.3	7.3	9.6	13.4
M-420-180*	M	Pavement	30	4.2	5.0	8.8	15.7	22.0
M-600-0-1	M	Pavement	0	6.4	7.9	10.0	16.5	22.7
M-480-120-1	M	Pavement	20	4.5	6.3	9.4	14.1	20.3
M-420-180-1	M	Pavement	30	4.7	5.5	6.1	13.8	19.6
M-600P-0-1	M	Pavement	0	7.2	9.0	10.6	17.2	20.0
M-480P-120-1	M	Pavement	20	5.5	6.1	6.6	14.8	19.7
M-420P-180-1	M	Pavement	30	4.7	5.4	6.3	15.3	21.8
M-700-0*	M	Structural	0	5.0	6.1	8.6	10.3	11.5
M-560-140*	M	Structural	20	3.8	4.9	7.5	11.6	16.8
M-650-0*	M	Structural	0	4.8	6.1	8.6	11.3	12.7
M-520-130*	M	Structural	20	3.9	4.8	6.5	9.1	12.8
M-700-0	M	Structural	0	7.1	8.1	10.9	10.9	12.5
M-560-140	M	Structural	20	5.5	6.0	6.4	15.8	
M-650-0	M	Structural	0	7.1	8.0	10.7	11.2	11.9
M-520-130	M	Structural	20	6.1	6.9	12.1	22.4	26.9

Table F.7: Analysis of moderate (0.41 to 0.43) w/cm mixtures meeting pavement and Class AA resistivity targets at selected ages

	All	Straight Cement	Fly Ash
Total pavement mixtures	9	3	6
Pavement mixtures ≥ 11.0 by 28 days	0	0	0
Pavement mixtures ≥ 11.0 by 56 days	7	2	5
Pavement mixtures ≥ 11.0 by 90 days	9	3	6
Total AA mixtures	0	4	4
AA mixtures ≥ 15.0 by 28 days	0	0	0
AA mixtures ≥ 15.0 by 56 days	2	0	2
AA mixtures ≥ 15.0 by 90 days	3	0	3
AA mixtures ≥ 16.0 by 28 days	0	0	0
AA mixtures ≥ 16.0 by 56 days	1	0	1
AA mixtures ≥ 16.0 by 90 days	3	0	3

Table F.8: Surface resistivity data from historical NCDOT projects at high (>0.47) w/cm ratios

Type of Mixture	Fly Ash %	Surface Resistivity (k Ω -cm)				
		3 day	7 day	28 day	56 day	90 day
Pavement	0	4.8	6.1	8.4	9.1	9.6
Pavement	20	4.1	5.2	7.0	9.0	13.5
Pavement	30	3.8	4.8	6.0	10.5	15.9
Pavement	0	6.9	7.3	8.1	11.2	17.6
Pavement	20	5.4	5.8	9.5	12.0	17.1
Pavement	30	4.2	6.9	11.2	16.3	20.7
Pavement	0	3.6	4.3	6.9		8.9
Pavement	0	4.8	5.2	7.3		7.3
Pavement	0	5.0	5.4	7.6		9.1
Pavement	0	4.1	4.9	6.7		9.8
Pavement	0	4.5	5.2	7.0		8.7
Pavement	0	4.8	5.5	6.6		8.1
Pavement	0	3.1	3.7	6.0		7.8
Pavement	0	4.5	4.7	6.7		7.8
Pavement	0	5.9	6.2	7.6		8.5
Pavement	20	3.5	3.6	7.5		24.3
Pavement	20	5.0	5.4	9.8		26.6
Pavement	20	4.8	5.6	12.6		35.3
Pavement	20	3.1	3.6	7.8		26.6
Pavement	20	5.0	5.4	10.5		32.9
Pavement	20	4.6	5.6	12.6		37.4
Pavement	0	4.6	5.4	7.5		9.6
Pavement	0	8.0	8.7	10.7		10.8
Pavement	0	7.1	8.0	9.5		10.3
Pavement	23		7.3	11.0	19.1	31.0
Pavement	23		7.5	11.5	19.5	32.3
Pavement	23		7.8	11.9	19.8	32.8
Structural	0	4.7	5.7	8.0	8.0	8.2
Structural	20	3.9	5.2	7.1	9.3	13.1
Structural	0	4.4	5.5	6.8	7.9	8.1
Structural	20	4.1	4.9	6.2	8.8	12.3
Structural	0	6.1	6.4	7.3	12.1	
Structural	20	5.1	5.7	6.6	14.1	
Structural	0	5.7	6.8	8.7	9.7	9.8
Structural	20	4.8	6.3	10.6	18.0	21.8

Table F.9: Analysis of high (>0.47) w/cm mixtures meeting pavement and Class AA resistivity targets at selected ages.

	All	Straight Cement	Fly Ash
Total pavement mixtures	27	14	13
Pavement mixtures ≥ 11.0 by 28 days	6	0	6
Pavement mixtures ≥ 11.0 by 56 days	10	1	9
Pavement mixtures ≥ 11.0 by 90 days	14	1	13
Total AA mixtures	8	4	4
AA mixtures ≥ 15.0 by 28 days	0	0	0
AA mixtures ≥ 15.0 by 56 days	1	0	1
AA mixtures ≥ 15.0 by 90 days	3	0	3
AA mixtures ≥ 16.0 by 28 days	0	0	0
AA mixtures ≥ 16.0 by 56 days	1	0	1
AA mixtures ≥ 16.0 by 90 days	3	0	3



Figure F.4: Training session for SAM with developer (Jake LeFlore, OSU)

Table F.10: SAM data collected at pilot project

Ticket Number	Mix Type	Mix ID	Structure	Date of Pour	Plant	Truck No.	Slump (in)	Temp (°F)	Air Content from Other Meter (%)	SAM air Content (%)	SAM Number	Operator	Notes
5549330	AA	3082VF11ABLFAPEE	1B - Westinghouse	5/19/2021	Pineville	1	3.00	77	4.70	4.60	0.52	JS	1
5549560	AA	3082VF11ABLFAPEE	1B - Westinghouse	5/19/2021	Pineville	4	3.50	76	4.50	6.00	0.50	JS	1
5549744	AA	3082VF11ABLFAPEE	1B - Westinghouse	5/19/2021	Pineville	8	3.50	80	4.25	5.60	0.38	JS	1
5549943	AA	3082VF11ABLFAPEE	1B - Westinghouse	5/19/2021	Pineville	11	3.50	78	5.00	5.40	0.31	JS	1
5550077	AA	3082VF11ABLFAPEE	1B - Westinghouse	5/19/2021	Pineville	14	3.50	80	3.50	5.60	0.39	JS	2
5550276	AA	3082VF11ABLFAPEE	1B - Westinghouse	5/19/2021	Pineville	19	3.50	79	5.25	7.30	0.29	JS	2
5580194	AA	3852VF11ABAFMQEE	Span A - Elm	6/15/2021	Matthews	1	4.00	84	6.00	5.10	0.26	PG	1
5580351	AA	3852VF11ABAFMQEE	Span A - Elm	6/15/2021	Matthews	4	3.75	84	5.50	5.00	0.27	PG	1
5580542	AA	3852VF11ABAFMQEE	Span A - Elm	6/15/2021	Matthews	7	3.50	85	5.00	5.00	0.31	PG	1
5580699	AA	3852VF11ABAFMQEE	Span A - Elm	6/15/2021	Matthews	10	3.50	85	4.70	4.50	0.31	PG	1
5580888	AA	3852VF11ABAFMQEE	Span A - Elm	6/15/2021	Matthews	14	4.50	85	5.50	4.40	0.29	PG	2
5581035	AA	3852VF11ABAFMQEE	Span A - Elm	6/15/2021	Matthews	17	-	-	5.00	3.70	0.40	PG	2
5581387	AA	3852VF11ABAFMQEE	Span A - Elm	6/15/2021	Matthews	20	-	-	7.30	4.70	0.45	PG	2
5581305	AA	3852VF11ABAFMQEE	Span A - Elm	6/15/2021	Matthews	23	-	-	7.30	3.40	0.42	PG	2
5584235	AA	5382VF11ABLFPBEE	Span B - Elm	6/17/2021	Fort Mill	1	5.00	82	4.60	4.50	0.25	PG	1
5584405	AA	5382VF11ABLFPBEE	Span B - Elm	6/17/2021	Fort Mill	4	3.00	80	4.80	4.40	0.21	PG	1
5584607	AA	5382VF11ABLFPBEE	Span B - Elm	6/17/2021	Fort Mill	7	3.75	81	6.10	5.40	0.17	PG	1
5584707	AA	5382VF11ABLFPBEE	Span B - Elm	6/17/2021	Fort Mill	10	6.25	83	7.30	6.20	0.15	PG	1
5584902	AA	5382VF11ABLFPBEE	Span B - Elm	6/17/2021	Fort Mill	13	5.00	84	6.60	6.10	0.17	PG	2
5585105	AA	5382VF11ABLFPBEE	Span B - Elm	6/17/2021	Fort Mill	16	3.75	75	6.00	5.50	0.26	PG	2
5585178	AA	5382VF11ABLFPBEE	Span B - Elm	6/17/2021	Fort Mill	19	4.00	85	6.10	5.40	0.24	PG	2
5585320	AA	5382VF11ABLFPBEE	Span B - Elm	6/17/2021	Fort Mill	22	2.75	83	5.70	3.70	0.37	PG	2
5590397	AA	5382VF11ABLFPPEE	Bent 1 - Elm	6/23/2021	Fort Mill	1	4.00	83	5.00	6.40	0.06	PG	
5590552	AA	5382VF11ABLFPPEE	Bent 1 - Elm	6/23/2021	Fort Mill	4	3.25	83	4.90	4.90	0.18	PG	
5590756	AA	5382VF11ABLFPPEE	Bent 1 - Elm	6/23/2021	Fort Mill	7	3.00	84	5.30	6.10	0.29	PG	
5591041	AA	3851VF21ACAFMQEE	1A EB1 Cap	6/23/2021	Matthews	3	3.50	78	5.50	7.60	0.25	JS	
5603480	AA	5382VF11ABLFPPEE	Elm EB1 App. Slab	7/1/2021	Fort Mill	1	3.50	76	6.00	5.60	0.16	PG	
5608204	AA	5382VF11ABLFPPEE	Elm EB1 App. Slab	7/1/2021	Fort Mill	5	-	-	4.50	4.90	0.19	PG	
5608707	AA	5382VF11ABLFPPEE	Elm EB1 App. Slab	7/1/2021	Fort Mill	7	-	-	6.50	5.80	0.21	PG	
5604961	AA	5382VF11ABLFPPEE	EB2 Approach Slab	7/6/2021	Fort Mill	1	4.00	75	7.30	7.30	0.35	PG	
5605107	AA	5382VF11ABLFPPEE	EB2 Approach Slab	7/6/2021	Fort Mill	4	4.00	75	6.50	6.60	0.03	PG	
5605286	AA	5382VF11ABLFPPEE	EB2 Approach Slab	7/6/2021	Fort Mill	7	4.00	75	5.60	5.70	0.26	PG	

	AA	3081VF21AHAFAPÉE	Elm Barrier Wall	7/14/2021	Fort Mill	1	3.50		5.50	4.90	0.37	PG	
5615552	AA	3081VF21AHAFAPÉE	Str 6 Bent 1 Column 1	7/14/2021	Pineville	1	3.50	80	6.60	5.70	0.22	PG	
5616955	AA	3852VF13AAAFMQEE	Str 7 Barrier Wall	7/15/2021	Matthews	1	3.50	90	5.80	4.70	0.03	JB	
5619060	AA	3852VF13AAAFMQEE	Str 7 Barrier Wall	7/16/2021	Matthews	1	3.00	88	5.10	4.50	0.15	JB	
	AA	3852VF13AAAFMQEE	Str 7 Barrier Wall	7/19/2021	Matthews	1	3.50	84	6.10	5.40	0.40	JS	
5621073	AA	3852VF13AAAFMQEE	Str 7 Barrier Wall	7/20/2021	Matthews	1	2.50	86	5.10	4.60	0.49	JB	
5622328	AA	3852VF13AAAFMQEE	Str 7 Barrier Wall	7/21/2021	Matthews	1	4.00	85	4.50	4.80	0.23	PG	
5622715	AA	3852VF13AAAFMQEE	Str 7 Barrier Wall	7/21/2021	Matthews	2	4.00	88	4.50	3.80	0.38	PG	
5624240	AA	3852VF13AAAFMQEE	Str 7 Barrier Wall	7/22/2021	Matthews	1	3.50	82	5.60	4.30	0.16	JB	
	A	3081VF21AHAFAPÉE	Str 4 Median Columns	8/18/2021	308	1	5.00	89	5.00	4.60	0.19	JS	1
	B	385BNF33ACAFMQEE	22+60	8/18/2021	385	1	-	74	6.80	6.30	0.16	JS	1
5660919	AA	3852VF11ABAFMQEE	St 9B 647+99.12	8/23/2021	385	1	3.00	87	5.10	4.90	0.39	JS	1
5667908	AA	5382VF11ABFLBEE	EB2 Approach Slab	8/27/2021	538	1	3.50	75	4.20	3.50	0.33	PG	2
5668165	AA	5382VF11ABFLBEE	EB2 Approach Slab	8/27/2021	538	4	3.50	80	5.10	4.50	0.33	PG	2
5668480	AA	5382VF11ABFLBEE	EB2 Approach Slab	8/27/2021	538	7	3.50	79	4.70	4.20	0.38	PG	2
5671844	AA	3852VF11ABAFMQEE	Str 9B deck	8/31/2021	385	1	4.50	76	6.00	5.20	0.23	JS	2
5672037	AA	3852VF11ABAFMQEE	Str 9B deck	8/31/2021	385	4	3.75	79	4.50	4.50		JS	2
5681738	AA	3081VF21AHAFAPÉE	STR 4. FOOTING	9/9/2021	308	1	4.50	84	4.50	4.40	0.03	PG	1
	A	3081VF21AHAFAPÉE	STR. 5 COLUMNS	9/13/2021	308	1	5.00	84	6.20	6.40	0.15	JS	2
5692575	AA	3852VF11ABAFMQEE	STR 1A SPAN A	9/17/2021	385	4	3.50	75	5.00	4.90	0.23	JS	1
5701079	AA	3082VF11ABLFAPEE	STR 9A TILLEY SPAN B	9/28/2021	308	1	4.00	75	6.00	5.50	0.43	JS	2
5701382	AA	3082VF11ABLFAPEE	STR 9A TILLEY SPAN B	9/8/2021	308	4	3.50	78	6.00	4.60	0.12	JS	2
5703793	AA	3082VF11ABLFAPEE	STR. 1A EB2 APP SLAB	9/29/2021	308	1	3.50	76	5.20	4.20	0.31	PG	2
5703793	AA	3082VF11ABLFAPEE	STR. 1A EB2 APP SLAB	9/29/2021	308	4	4.00	79	6.40	5.40	0.23	PG	2
5706000	AA	3082VF11ABLFAPEE	STR 1A EB1 APPROACH	9/30/2021	308	1	3.50	78	5.20	3.60	0.34	PG	2
5706315	AA	3082VF11ABLFAPEE	STR 1A EB1 APPROACH	9/30/2021	308	4	4.00	76	6.00	4.90	0.25	PG	2
5709538	AA	3852VF11ABAFMQEE	STR 9A SPAN C DECK POUR	10/4/2021	385	1	3.50	80	5.70	5.90	0.23	KC	2
5714101	A	3851VF21ACAFMQEE	CULVERT 5	10/7/2021	385	1	3.75	72	5.20	4.90	0.35	JS	1
5718123	A	3851VF21ACAFMQEE	STR 4. EB2 BACKWALL	10/12/2021	385	1	3.50	75	5.20	5.20	0.28	PG	2
5718286	A	3851VF21ACAFMQEE	STR4. EB2 BACKWALL	10/12/2021	385	4	2.50	75	5.20	5.10	0.27	PG	2
	AA	308RVF51ADLFAPEE	STR 1A BARRIER RAIL STG 1	10/14/2021	308	1	1.25	78	4.60	4.60	0.47	JB	1
5724429	AA	3852VF11ABAFMQEE	TILLEY MORRIS 9A EB2 APPROACH	10/15/2021	385	1	3.25	74	5.90	5.10	0.20	JS	1
5726655	A	3851VF21ACAFMQEE	STR 4 EB2 BACK WALL	10/18/2021	385	1	3.25	70	5.75	5.60	0.30	DO	1
5728255	AA	3852VF11ABAFMQEE	TILLEY MORRIS	10/19/2021	385	1	3.25	65	5.90	5.50	0.54	DO	1
5742287	A	5381VF21ACLPPEE	STR 5 B+2B CAP	10/20/2021	538	1	4.00	70	5.00	5.30	0.76	JB	1
5742441	A	5381VF21ACLPPEE	STR 5 B+2B CAP	10/20/2021	538	4	4.00	70	5.00	6.00	0.33	JB	1

5742587	A	5381VF21ACLFPPPEE	STR 5 B+2B CAP	10/20/2021	538	7	4.00	75	5.00	3.70	0.63	PG	1
5736828	AA	3852VF11ABAFMQEE	TILLEY 9B EB1 APPROACH	10/25/2021	385	1	3.25	78	-	5.70	0.05	PG	1
5738656	A	3081VF21ACLFAPPEE	CULVERT 3 TOP	10/26/2021	308	1	-	65	5.20	6.60	0.10	PG	1
5738803	A	3081VF21ACLFAPPEE	CULVERT 3 TOP	10/26/2021	308	4	3.50	70	4.90	7.00	0.10	PG	1
5738885	A	3081VF21ACLFAPPEE	CULVERT 3 TOP	10/26/2021	308	7	3.50	84	5.30	6.20	0.22	PG	1
5739000	A	3081VF21ACLFAPPEE	CULVERT 3 TOP	10/26/2021	308	10	3.50	81	6.50	5.70	0.08	PG	1
5739140	A	3081VF21ACLFAPPEE	CULVERT 3 TOP	10/26/2021	308	13	3.75	84	5.30	3.30	0.36	PG	2
5739354	A	3081VF21ACLFAPPEE	CULVERT 3 TOP	10/26/2021	308	16	3.50	85	5.00	3.10	0.39	PG	2
5741451	AA	3852VF11ABAFMQEE	CULV 4 TOP, WALLS, WINGS	10/27/2021	385	1	3.75	77	7.20	6.90	0.37	JB	1
5755239	A	3081VF21ACLFAPPEE	CULVERT 3	11/9/2021	308	1	6.50	78	6.50	7.80	0.07	PG	1
5755617	A	3081VF21ACLFAPPEE	CULVERT 3	11/9/2021	308	4	4.50	77	5.00	6.90	0.22	PG	1
5755750	A	3081VF21ACLFAPPEE	CULVERT 3	11/9/2021	308	7	3.75	80	6.20	8.90	0.08	PG	1
5755867	A	3081VF21ACLFAPPEE	CULVERT 3	11/9/2021	308	10	4.25	80	6.30	7.20	0.10	PG	1

Notes: 1: Sample taken before pumping
2: Sample taken after pumping

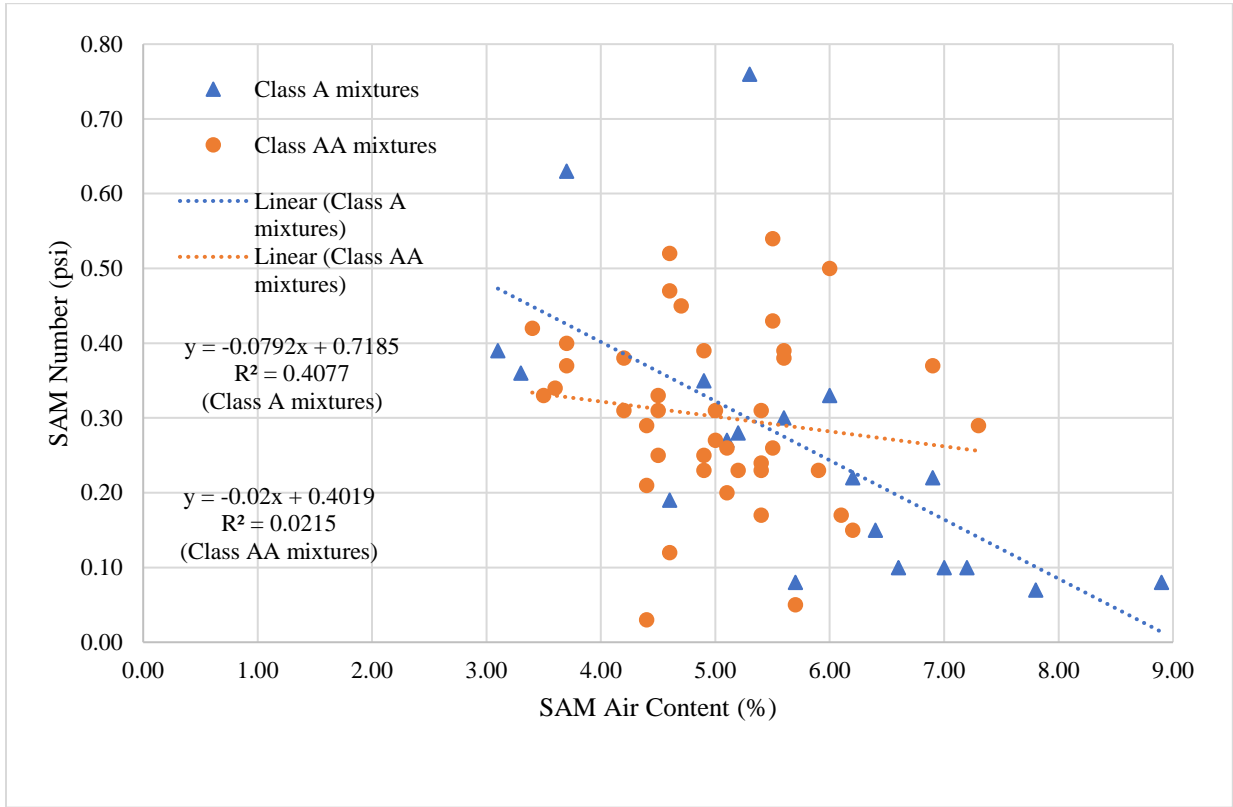


Figure F.5: SAM air content vs. SAM number, comparing test results for Class A and Class AA mixtures